RISK FACTORS OF NONINVASIVE CARDIAC ELECTROPHYSIOLOGY

EDITED BY: Marek Malik, Federico Lombardi, Georg Schmidt and Richard Leonard Verrier

PUBLISHED IN: Frontiers in Physiology

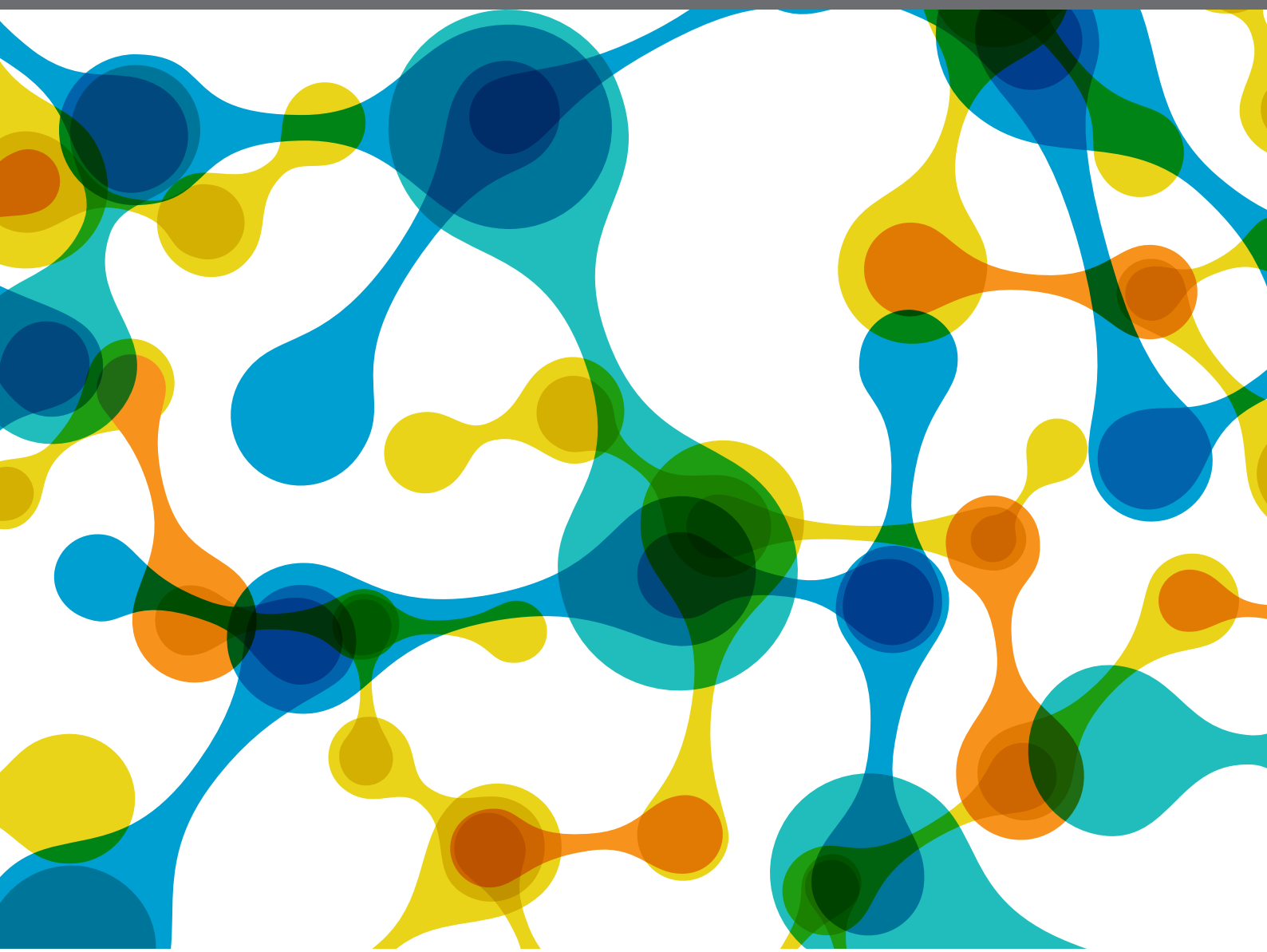

frontiers Research Topics

frontiers

ISSN 1664-8714
ISBN 978-2-88966-970-7
DOI 10.3389/978-2-88966-970-7

About Frontiers

Frontiers is more than just an open-access publisher of scholarly articles: it is a pioneering approach to the world of academia, radically improving the way scholarly research is managed. The grand vision of Frontiers is a world where all people have an equal opportunity to seek, share and generate knowledge. Frontiers provides immediate and permanent online open access to all its publications, but this alone is not enough to realize our grand goals.

Frontiers Journal Series

The Frontiers Journal Series is a multi-tier and interdisciplinary set of open-access, online journals, promising a paradigm shift from the current review, selection and dissemination processes in academic publishing. All Frontiers journals are driven by researchers for researchers; therefore, they constitute a service to the scholarly community. At the same time, the Frontiers Journal Series operates on a revolutionary invention, the tiered publishing system, initially addressing specific communities of scholars, and gradually climbing up to broader public understanding, thus serving the interests of the lay society, too.

Dedication to Quality

Each Frontiers article is a landmark of the highest quality, thanks to genuinely collaborative interactions between authors and review editors, who include some of the world's best academicians. Research must be certified by peers before entering a stream of knowledge that may eventually reach the public - and shape society; therefore, Frontiers only applies the most rigorous and unbiased reviews.
Frontiers revolutionizes research publishing by freely delivering the most outstanding research, evaluated with no bias from both the academic and social point of view. By applying the most advanced information technologies, Frontiers is catapulting scholarly publishing into a new generation.

What are Frontiers Research Topics?

Frontiers Research Topics are very popular trademarks of the Frontiers Journals Series: they are collections of at least ten articles, all centered on a particular subject. With their unique mix of varied contributions from Original Research to Review Articles, Frontiers Research Topics unify the most influential researchers, the latest key findings and historical advances in a hot research area! Find out more on how to host your own Frontiers Research Topic or contribute to one as an author by contacting the Frontiers Editorial Office: frontiersin.org/about/contact

RISK FACTORS OF NONINVASIVE CARDIAC ELECTROPHYSIOLOGY

Topic Editors:
Marek Malik, Imperial College London, United Kingdom
Federico Lombardi, University of Milan, Italy
Georg Schmidt, Technical University of Munich, Germany
Richard Leonard Verrier, Beth Israel Deaconess Medical Center, United States

Effective identification of patients at increased risk of malignant cardiac arrhythmia presently represents a clinically important unmet need. Existing guidelines for the selection of candidates for the prophylactic implantation of cardioverters-defibrillators (ICD) are based solely on the reduction of ventricular haemodynamic performance. Although this guidance is based on statistical results of previously conducted randomized clinical trials, available experience shows that it does not serve clinical needs efficiently. The majority of patients who are implanted with ICDs for prophylactic reasons never utilize the device during its technical longevity whilst, at the same time, many patients who succumb to sudden cardiac death do not have ventricular haemodynamic performance particularly compromised. Recent results also showed that the previous statistical findings of ICD efficacy are not fully reproducible in patients with non-ischemic heart disease and that the reduction of sudden cardiac death after myocardial infarction by external automatic defibrillation vests is lower than expected.

Advances in cardiac electrophysiology are needed for better understanding of the mechanisms that are the basis of different arrhythmic abnormalities. Increased understanding of these mechanisms will allow them to be more effectively classified so that optimum therapeutic options can be offered. Likewise, better understanding of the underlying electrophysiology processes is needed so that novel and more focused randomized clinical trials can be designed. Compared to invasive electrophysiological studies, noninvasive cardiac electrophysiology offers the possibility of screening larger number of patients as well as healthy subjects investigated under different provocations and conditions. To advance the field, broad spectrum of studies is needed together with meta-analyses and reviews facilitating research interactions.

Citation: Malik, M., Lombardi, F., Schmidt, G., Verrier, R. L., eds. (2021). Risk Factors of Noninvasive Cardiac Electrophysiology. Lausanne: Frontiers Media SA. doi: 10.3389/978-2-88966-970-7

Table of Contents

frontiers in Physiology

ORIGINAL RESEARCH
published: 04 December 2018
doi: 10.3389/fphys.2018.01726

Chronic Kidney Disease Increases Atrial Fibrillation Inducibility: Involvement of Inflammation, Atrial Fibrosis, and Connexins

Huiliang Qiu[1,2†], Chunlan Ji[1,3†], Wei Liu[1,2], Yuchi Wu[3], Zhaoyu Lu[3], Qizhan Lin[3], Zheng Xue[4], Xusheng Liu[1,3], Huanlin Wu[1,2,5], Wei Jiang[1,2] and Chuan Zou[1,3*]*

[1] Second Clinical Medical College, Guangzhou University of Chinese Medicine, Guangzhou, China, [2] Department of Cardiology, Guangdong Provincial Hospital of Chinese Medicine, Guangzhou, China, [3] Department of Nephrology, Guangdong Provincial Hospital of Chinese Medicine, Guangzhou, China, [4] Department of Cardiology, Guangzhou Hospital of Traditional Chinese Medicine, Guangzhou, China, [5] Department of internal medicine, Beijing University of Chinese Medicine, Beijing, China

OPEN ACCESS

Edited by:
Marek Malik,
Imperial College London,
United Kingdom

Reviewed by:
Vincenzo Russo,
Università degli Studi della Campania
"Luigi Vanvitelli" Naples, Italy
Sanjay Ram Kharche,
University of Western Ontario, Canada

***Correspondence:**
Wei Jiang
drjiangwei@126.com.
Chuan Zou
doctorzc541888@126.com

[†]These authors have contributed equally to this work

Specialty section:
This article was submitted to Cardiac Electrophysiology, a section of the journal Frontiers in Physiology

Received: 07 September 2018
Accepted: 16 November 2018
Published: 04 December 2018

Citation:
Qiu H, Ji C, Liu W, Wu Y, Lu Z, Lin Q, Xue Z, Liu X, Wu H, Jiang W and Zou C (2018) Chronic Kidney Disease Increases Atrial Fibrillation Inducibility: Involvement of Inflammation, Atrial Fibrosis, and Connexins. Front. Physiol. 9:1726. doi: 10.3389/fphys.2018.01726

Chronic kidney disease (CKD) causes atrial structural remodeling and subsequently increases the incidence of atrial fibrillation (AF). Atrial connexins and inflammatory responses may be involved in this remodeling process. In this study, nephrectomy was used to produce the CKD rat model. Three months post-nephrectomy, cardiac structure, function and AF vulnerability were quantified using echocardiography and electrophysiology methods. The left atrial tissue was tested for quantification of fibrosis and inflammation, and for the distribution and expression of connexin (Cx) 40 and Cx43. An echocardiography showed that CKD resulted in the left atrial enlargement and left ventricular hypertrophy, but had no functional changes. CKD caused a significant increase in the AF inducible rate (91.11% in CKD group vs. 6.67% in sham group, $P < 0.001$) and the AF duration [107 (0–770) s in CKD vs. 0 (0–70) s in sham, $P < 0.001$] with prolonged P-wave duration. CKD induced severe interstitial fibrosis, activated the transforming growth factor-β1/Smad2/3 pathway with a massive extracellular matrix deposition of collagen type I and α-smooth muscle actin, and matured the NLR (nucleotide-binding domain leucine-rich repeat-containing receptor) pyrin domain-containing protein 3 (NLRP3) inflammasome with an inflammatory cascade response. CKD resulted in an increase in non-phosphorylated-Cx43, a decrease in Cx40 and phosphorylated-Cx43, and lateralized the distribution of Cx40 and Cx43 proteins with upregulations of Rac-1, connective tissue growth factor and N-cadherin. These findings implicate the transforming growth factor-β1/Smad2/3, the NLRP3 inflammasome and the connexins as potential mediators of increased AF vulnerability in CKD.

Keywords: chronic kidney disease, atrial fibrillation, fibrosis, transforming growth factor-β1, inflammasome, connexins

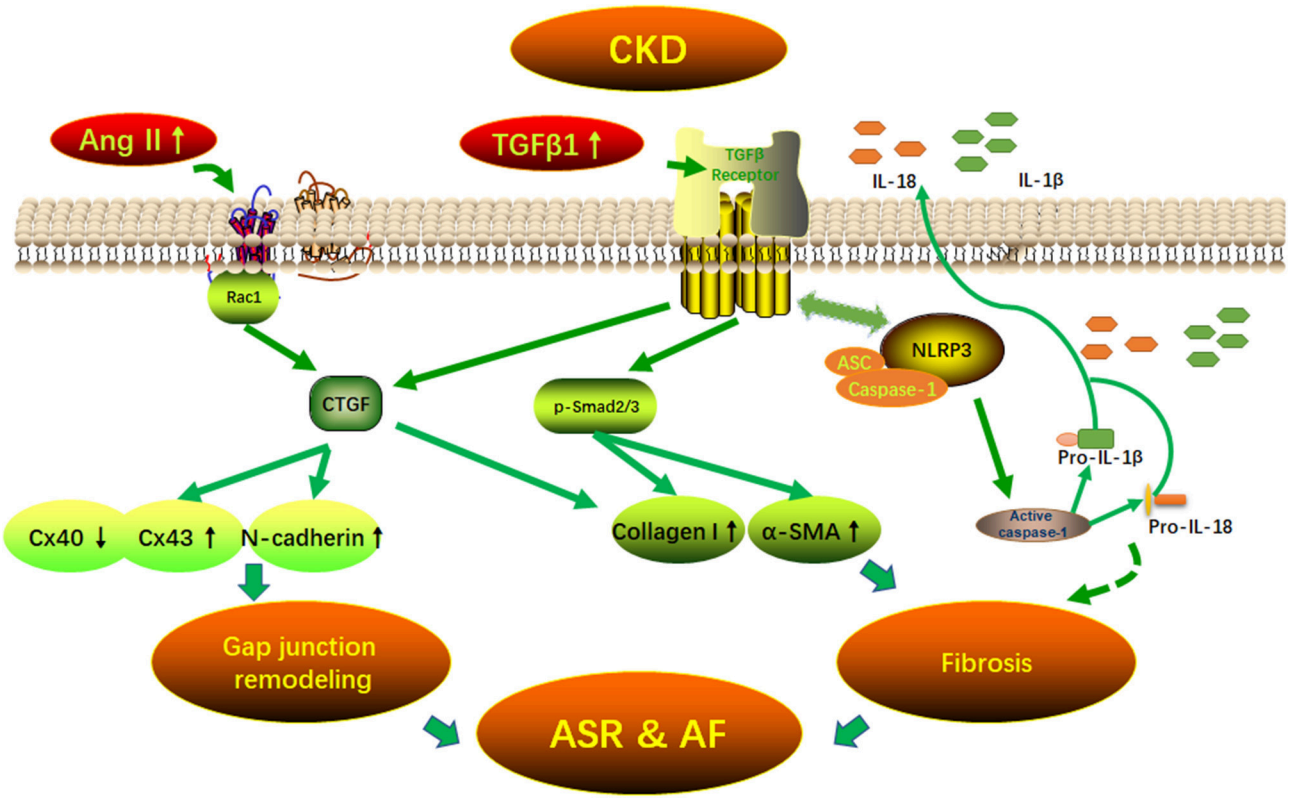

GRAPHICAL ABSTRACT | Potential mechanisms of AF arrhythmogenic substrate in CKD**.** Fibrosis and (connexins) gap junction remodeling are the main pathological substrate in AF development. Our findings suggest that CKD induced-atrial fibrosis may be connected with the activation of TGFβ1/Smads and the NLRP3 inflammasome signaling pathways and the CKD induced-Cx40/43 gap junction remodeling may be connected with Ang II induced-the activation of Rac-1, CTGFand N-cadherin in the atrium. AF, atrial fibrillation; Ang II, angiotensin II; ASC, apoptosis-associated speck-like protein containing a carboxy-terminal CARD; ASR, atrial structural remodeling; α-SMA, α-smooth muscle actin; Collagen I, collagen type I; CTGF, connective tissue growth factor; Cx43, connexin43; IL-1β, interleukin-1β; IL-18, interleukin-18; NLRP3, NLR (nucleotide-binding domain leucine-rich repeat-containing receptor) pyrin domain-containing protein 3; Rac1, Ras-related C3 botulinum toxin substrate 1; TGFβ1, transforming growth factor-β1.

INTRODUCTION

Atrial fibrillation (AF) is the most common arrhythmia and increases the risk of a stroke and heart failure (Kirchhof et al., 2016). Certain factors may increase the risk of AF occurrence. These factors include age, hypertension, heart disease, and other chronic conditions such as chronic kidney disease (CKD) (Soliman et al., 2010; Liao et al., 2015; Kirchhof et al., 2016). The occurrence of AF gradually increases with progressive declines of kidney function (Olesen et al., 2012; Ng et al., 2013; Jun et al., 2015; Gill et al., 2017). The incidence of AF is 6% in elderly people without CKD, 18∼21% in patients with non-dialysis-dependent CKD, and 27% in CKD patients on dialysis (Olesen et al., 2012; Ng et al., 2013; Jun et al., 2015; Gill et al., 2017). Although AF is very frequent in patients with CKD and has gained much attention as a risk factor for stroke and cardiovascular events, the mechanistic pathogenesis of AF in CKD is relatively unexplored.

Atrial structural remodeling (ASR) mainly refers to atrial enlargement and interstitial fibrosis. ASR can result in heterogeneous electrical conduction by forming reentrant activity and is one of the major pathophysiological sources of AF (Everett and Olgin, 2007). Inflammation plays an important role in the development of ASR and AF, partly by stimulating the production of angiotensin II (Ang II), while Ang II can activate inflammatory signaling which in turn acts as a pro-fibrotic factor (Corradi et al., 2008). The transforming growth factor-β1 (TGFβ1) is the main interrelated pathway involved in ASR and in the formation of atrial fibrosis in several disease conditions, including myocardial infarction, heart failure, and hypertension with upregulated Rennin-Angiotensin-Aldosterone System (RAAS) (Hao et al., 2000; Everett and Olgin, 2007; Tsai et al., 2008). TGFβ1 has been reported in the deposition of extracellular matrix through the downstream mediator Smad proteins and pro-fibrotic mediator connective tissue growth factor (CTGF) (Rosin et al., 2013). Recent studies indicate that CKD could cause atrial enlargement and fibrosis, invoke the inducible AF, and is linked to the activation of TGFβ1 (Aoki et al., 2015). However, the mediators linking TGFβ1 to fibrosis have not yet been investigated in CKD. Because of the central role of TGFβ1 in fibrogenesis, it is important to identify its downstream molecules in the atrium for future research and new therapeutic strategies.

NLR (nucleotide-binding domain leucine-rich repeat-containing receptor) pyrin domain-containing protein 3 (NLRP3) inflammasome, is one of the most well-known inflammasomes and widely participates in various immune and cellular death pathways (Gong et al., 2016). It can catalyze the pro-casepase-1 into matured caspase-1 (P10 and P20) and the latter can further mediate the pro-interleukin (IL)-1β and pro-IL-18 into the proinflammatory cytokines of IL-1β and IL-18. The NLRP3 inflammasome may play a crucial role in the development of fibrotic remodeling in organs including the kidney and heart, and can be activated in CKD mice (Gong et al., 2016; Chin et al., 2017). In addition, a Cardiomyocyte (CM)-specific knock-in a murine model (CKI, expressing functional NLRP3 inflammasome in CMs only) developed 100% premature atrial contractions with significantly increased inducible AF, whereas a selective inflammasome inhibitor MCC950 could successfully decrease the inducible AF in CKI mice (Yao et al., 2018), recognizing the NLRP3 inflammasome as a new promotor of fibrogenesis and AF. These studies clearly indicated the vital role of the NLRP3 inflammasome in the pathogenesis of fibrosis and showed that CKD is involved in the activation of the NLRP3 inflammasome in multiple organs. However, it is unclear whether the NLRP3 inflammasome can also be activated in the atrium under the condition of CKD.

ASR not only contributed to the reentrant activity but also influenced the connexins (Giepmans, 2004). Connexins abundantly distributes at the intercalated disk form the cell-to-cell electric conduction propagation that ensures the normal heart rhythm. Connexin (Cx) 40 and Cx43 are two of the mainly functional gap junction subunits in the atria (Ryu et al., 2007; Sawaya et al., 2007; Duffy and Wit, 2008). Any alterations in atrial connexins expression, phosphorylation and distribution are considered proarrhythmogenic. A previous study has demonstrated that the gap junction protein can be restructured by the activation of RAAS and CKD induced the activation of RAAS. Adam et al suggested that an increased Ang II can change the expression of Cx43 by the activation of Rac1 and nicotinamide adenine dinucleotide phosphate (NADPH) oxidase and eventually lead to atrial structural remodeling and AF (Adam et al., 2010). As NADPH oxidase has been implicated as a critical target for the pathogenesis of atrial fibrosis and the inducible AF in the CKD animal model (Fukunaga et al., 2012; Aoki et al., 2015), speculations that Cx43 can also be affected by CKD have been disregarded (Qiu et al., 2018). However, Cx40 must be highlighted, especially as it is one of the most important gap junction proteins in the atrium. The aim of the present study was to investigate the potentially mechanistic pathogenesis in the setting of CKD. We showed that TGFβ1/Smad2/3/CTGF, NLRP3 inflammasome and connexins are potential mediators of increased AF vulnerability in the setting of CKD.

TABLE 1 | Physical and Biochemical characteristics.

Parameters	Sham ($n = 5$)	CKD ($n = 10$)	*P*-values
Body weight, g	566.50 ± 48.00	501.13 ± 28.28	0.001
Urine volume, mL	19.4 ± 12.97	19.13 ± 5.46	0.696
Alb, g/L	50.12 ± 3.14	46.41 ± 1.81	0.004
Urea, mmol/L	8.74 ± 0.29	11.55 ± 0.33	0.000
Cr, umol/L	40.60 ± 1.57	58.40 ± 2.51	0.001
24 h Urine protein, g	0.85 ± 0.55	0.93 ± 0.36	0.691
ALT, U/L	59.60 ± 29.37	42.92 ± 19.29	0.182
AST, U/L	170.20 ± 60.14	172.67 ± 67.03	0.944
ALT/AST	3.04 ± 0.80	4.18 ± 1.22	0.075

Alb, albumin; Cr, creatinine; ALT, alanine transaminase; AST, aspartate transaminase. n = 5 and 10 in Sham and CKD group, respectively.

METHODS

Animals and 5/6 Nephrectomy

Animal experiments in this study were approved under the supervision of the Animal Care Committee of Guangdong Provincial Hospital of Chinese Medicine following the Regulations of Experimental Animal Administrations issued by the State Committee of Science and Technology of the People's Republic of China. Specific pathogen-free grade Sprague Dawley rats (6 weeks old, body weight: 200 ± 10 g) were provided by the Guangdong Provincial Medicinal Laboratory Animal Center [SCXK (Yue) 2013-0002, Guangzhou, China] and housed in a SPF environment. The 5/6 nephrectomy was performed to produce the CKD rat model. Animals were randomly assigned to sham-operated group (Sham, $n = 10$) and 5/6 nephrectomy-induced CKD group (CKD, $n = 15$). 5/6 nephrectomy was performed by the surgical resection of the upper and lower thirds of the left kidney, followed by whole right nephrectomy 7 days later, as previously described (Zeng et al., 2016). Rats in the sham group underwent the same procedure, without nephrectomy. Three months post-surgery, echocardiography, echocardiographic assessment, electrophysiology and AF vulnerability studies, biochemical detection, histology, immunohistochemistry, and atrial proteins expressions were performed as a follow up.

Echocardiographic Assessment

The Visual Sonics Vevo 2100 system (VisualSonics Inc., Toronto, Canada) was used to assess cardiac function and the structure

Abbreviations: AF, atrial fibrillation; ALB, albumin; Ang II, angiotensin II; ASC, apoptosis-associated speck-like protein containing a carboxy-terminal CARD; ASR, atrial structural remodeling; α-SMA, α-smooth muscle actin; CKD, chronic kidney disease; CKI, cardiomyocyte-specific knock-in murine model; CM, cardiomyocyte; Cr, creatinine; CTGF, connective tissue growth factor; Cx, connexin; HR, heart rhythm; IL-1β, interleukin-1β; IL-18, interleukin-18; IVSd, end-diastolic interventricular septum thickness; IVSs, end-systolic interventricular septum thickness; LA, left atrium; LAA, left atrial appendage; LAD, left atrial diameter; LAS, left atrial septum; LVEDD, left ventricular end diastolic diameter; LVEDV, left ventricular end diastolic volume; LVEF, left ventricular ejection fraction; LVESD, left ventricular end systolic diameter; LVESV, Left ventricular end systolic volume; LVFS, left ventricular fractional shortening; LVPWd, end-diastolic left ventricular posterior wall; LVPWs, end-systolic left ventricular posterior wall; NADPH, nicotinamide adenine dinucleotide phosphate; NLR, nucleotide-binding domain leucine-rich repeat-containing receptor; NLRP3, NLR (nucleotide-binding domain leucine-rich repeat-containing receptor) pyrin domain-containing protein 3; P/PR, the ratio of P-wave duration/ PR interval; RAAS, Rennin-Angiotensin-Aldosterone System; SV, stroke volume; TGFβ1, transforming growth factor-β1.

TABLE 2 | Echocardiography.

Parameters	Baseline			Three months post-surgery		
	Sham ($n = 4$)	CKD ($n = 10$)	*P*-values	Sham ($n = 4$)	CKD ($n = 10$)	*P*-values
HR	386.00 ± 11.43	385.50 ± 17.44	0.959	363.99 ± 11.43	373.77 ± 13.47	0.227
LVESD, mm	4.37 ± 0.13	4.34 ± 0.20	0.814	6.09 ± 0.50	5.65 ± 0.82	0.343
LVEDD, mm	7.35 ± 0.22	7.32 ± 0.20	0.820	9.59 ± 0.39	9.06 ± 0.62	0.146
LVESV, μL	94.87 ± 4.29	96.19 ± 9.42	0.795	188.02 ± 35.32	161.39 ± 52.54	0.375
LVEDV, μL	298.45 ± 3.49	296.44 ± 7.64	0.628	515.41 ± 46.07	457.13 ± 68.34	0.147
SV, μL	199.78 ± 7.60	197.06 ± 5.82	0.479	327.39 ± 13.23	295.74 ± 36.46	0.123
LVEF, %	68.56 ± 5.62	66.86 ± 7.73	0.699	63.75 ± 3.72	65.33 ± 7.74	0.708
LVFS, %	39.62 ± 4.33	38.56 ± 5.94	0.754	36.52 ± 2.77	37.85 ± 5.86	0.676
LAD, mm	2.61 ± 0.17	2.67 ± 0.10	0.457	3.38 ± 0.14	4.57 ± 0.55	0.000
IVSs, mm	1.32 ± 0.05	1.28 ± 0.06	0.327	1.36 ± 0.08	1.82 ± 0.22	0.002
IVSd, mm	0.62 ± 0.03	0.60 ± 0.06	0.553	0.63 ± 0.11	0.96 ± 0.16	0.003
LVPWs, mm	1.60 ± 0.04	1.60 ± 0.03	0.919	1.86 ± 0.38	2.56 ± 0.10	0.033
LVPWd, mm	0.81 ± 0.08	0.82 ± 0.07	0.795	0.88 ± 0.17	1.34 ± 0.10	0.000

HR, heart rhythm; LVESD, left ventricular end systolic diameter; LVEDD, left ventricular end diastolic diameter; LVESV, left ventricular end systolic volume; LVEDV, left ventricular end diastolic volume; SV, stroke volume; LVEF, left ventricular ejection fraction; LVFS, left ventricular fractional shortening; LAD, left atrial diameter; IVSs, end-systolic interventricular septum thickness; IVSd, end-diastolic interventricular septum thickness; LVPWs, end-systolic left ventricular posterior wall; LVPWd, end-diastolic left ventricular posterior wall.

TABLE 3 | Serum levels of TGFβ1 and Ang II.

Parameters	Sham ($n = 5$)	CKD ($n = 10$)	*P*-values
TGFβ1, pg/mL	43.96 ± 33.58	138.03 ± 41.20	0.011
Ang II, pg/mL	3.21 ± 1.75	9.83 ± 7.38	0.003

TGFβ1, transforming growth factor-β1; Ang II, angiotensin II.

at the baseline, 3 months after surgery, as described previously (Qiu et al., 2018a,b). Animals were anesthetized with isoflurane (2%). The anterior chest was shaved carefully using an electric razor and depilatory creams (Veet® Hair Removal). Acoustic coupling gel (Guangdong University of Technology, China) was applied. Two- dimensional standard parasternal long-axis views were applied first to acquire the left atrial diameter (LAD) at the level of the aortic valve in M-mode tracing mode. Then, standard parasternal short-axis views at the level of the papillary muscle were applied by rotating the probe ninety degrees clockwise to measure end-systolic interventricular septum thickness (IVSs), end-diastolic interventricular septum thickness (IVSd), end-systolic left ventricular posterior wall (LVPWs), end-diastolic left ventricular posterior wall (LVPWd), heart rhythm (HR), left ventricular end systolic diameter (LVESD), left ventricular end diastolic diameter (LVEDD), left ventricular end systolic volume (LVESV), left ventricular end diastolic volume (LVEDV), left ventricular ejection fraction (LVEF), left ventricular fractional shortening (LVFS), and stroke volume (SV).

Electrophysiology and AF Vulnerability Studies

Animals were anesthetized with 1.4 g/kg urethane (i.p.) and mechanically ventilated. Electrogram morphology was analyzed before AF vulnerability studies. The P-wave duration, PR interval and the ratio of P-wave duration/ PR interval (P/PR) were measured. Transesophageal atrial burst pacing was implemented to test AF vulnerability, as described previously (Qiu et al., 2018a,b). A total of three times pacing was performed for each animal. AF was defined as positive when the duration time of each induced AF was over 5 s. Inducibility and duration time of AF were recorded. In brief, an electrode catheter (four-French, St. Jude Medical Inc., USA) was placed in the esophagus to record the esophageal electrocardiogram and to induce AF. The position of the catheter was adjusted by the height and direction of atrial waves in the esophageal electrocardiogram and determined when clearer, higher, and bi-directional atrial waves were collected. Burst pacing was delivered by a stimulator after measuring the pacing threshold. The scheme of stimuli was set up at a two-fold threshold, with a cycle length of 20 ms, and a pulse width of 5 ms, with a total duration of 30-s.

Biochemical Detection

Twenty-four hour urine samples for urinary protein detection were collected by using metabolic cages. Blood samples were collected from abdominal aorta by using a coagulation-promoting tube after the electrophysiological test. Serum levels of albumin (ALB), urea and creatinine (Cr) were measured by the Clinical Laboratory of Guangdong Provincial Hospital of Chinese Medicine, using an automatic biochemical analyzer (Hitachi 7180). Urine protein was estimated by using a Pierce BCA protein assay kit (Thermo).

Serum Angiotensin II (Ang II) and TGFβ1 Content Assay

Serum Ang II and TGFβ1 were measured by using ELISA kits following the producer's instructions. The Ang-II assay kit was from Cusabio (ref. CSB-E04494r; Wuhan, China), and TGFβ1 from Abcam (ref. BMS623/3).

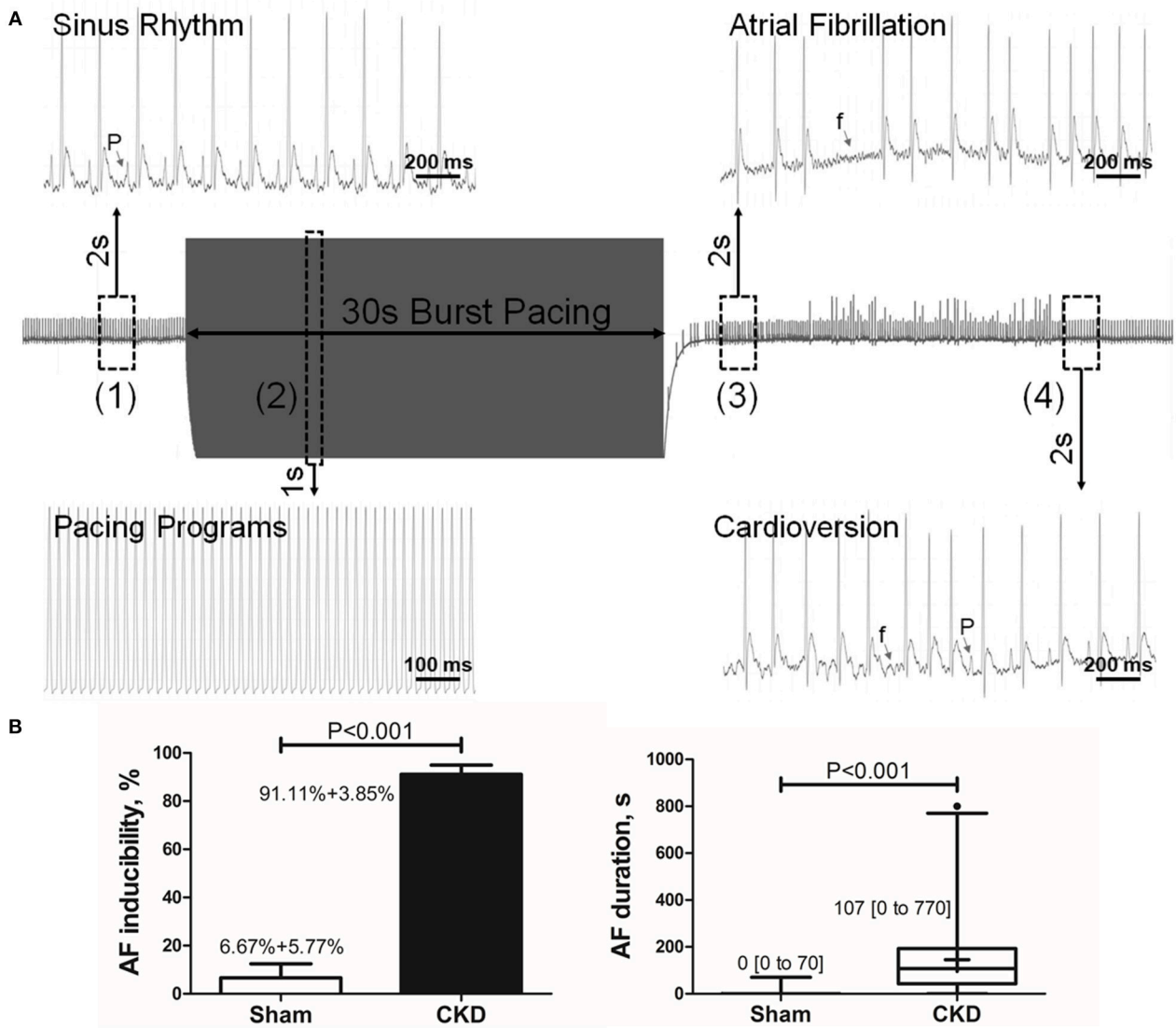

FIGURE 1 | Inducible AF by transesophageal atrial pacing. **(A)** Schematic diagram of AF induction. AF was induced by a 30-s burst pacing protocol at a 20-ms cycle length, 5-ms pulse width, and 50-h frequency. AF was considered as positive if an episode of rapid, quivering atrial beating with an irregular heart rhythm lasting over 5-s, was induced. (1) Before burst pacing, P-waves are clearly distinguishable with a regular heart rhythm; (2) Burst stimuli were delivered; (3) After burst pacing, P-waves were disappeared and replaced by rapid, quivering, and sawtooth-like waves (the f-waves) with an irregular heart rhythm, suggesting an episode of AF; (4) f-waves are dispelled by P-waves, representing the termination of AF and the recovery of sinus rhythm. **(B)** AF inducibility and duration. Data show that CKD results in significant higher AF inducibility and longer AF duration compared with the sham group. AF was induced three times for acquiring the standard deviation of AF inducibility. AF inducibility is shown as mean + SD and the duration is shown as median [2.5–97.5 percentile]. $n = 10$ and 15 in Sham and CKD group, respectively. AF, atrial fibrillation; SR, sinus rhythm.

Histology and Immunohistochemistry

Hearts were dewatered, embedded in paraffin, cut (3 μm thickness), and stained with Sirius red and a fast green counter stain as described previously (Zhang et al., 2014; Qiu et al., 2018,a). The collagen fiber volumes (CVF) of atria were quantified by Image J software (NIH, USA) (Rasband, 1997–2018). The proportion of Sirius red–stained areas relative to the total tissue areas (the non-staining sections in interstitial spaces were excluded from quantification) were counted as CVF. Atrial expression and distribution of Collagen type I (primary antibody: Abcam, ab34710), α-smooth muscle actin (α-SMA, CST, #19245), CTGF (Santa Cruz, sc-101586), N-cadherin (Santa Cruz, sc-59987), Cx40 (Abcam, ab183648) and Cx43 (CST, #3512) were studied using an immunohistochemistry method, as described previously (Qiu et al., 2018,a,b). Sections were incubated with a HRP antibody for 30 min at 37°C. A DAB chromogenic reagent kit (Maxim Biological Technology Development Co., LTD, Fuzhou, China) was used for coloration. Quantification was calculated by Image-Pro Plus 6.0 (Media Cybernetics, USA).

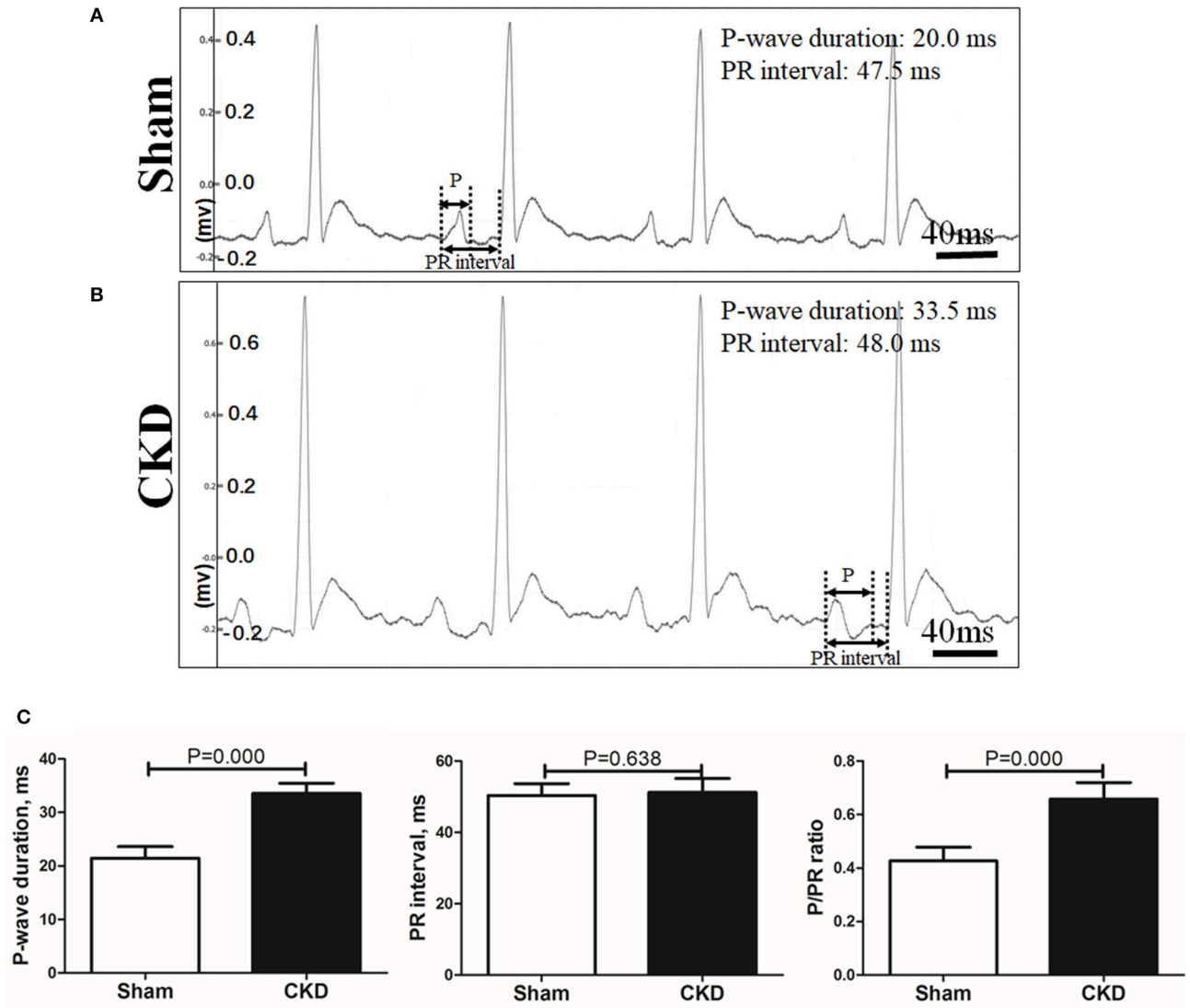

FIGURE 2 | Electrogram morphology. P-wave duration and PR interval were measured from an electrogram (ECG, lead II) before burst pacing. **(A,B)**. Representative ECG recordings from the sham and the CKD group. In the sham group, P-waves are unidirectional whereas P-waves are biphasic and prolonged in CKD group. **(C)** Data suggested that P-wave duration and the ratio of P-wave duration/PR interval (P/PR) are significantly increased in the CKD group than those in the sham group while PR intervals revealed no difference. Data are shown as mean + SD. $n = 8$ and 9 in Sham and CKD group, respectively.

Western Blot Analysis

The left atrium (LA) tissue was lysed in 1 mL RIPA lysis buffer containing a 1 mM PMSF and a 1% phosphatase inhibitor cocktail (Applygen Technologies Inc., Beijing, China). The protein concentration was measured by using a Pierce BCA protein assay kit (Thermo). Twenty-five to fifty micrograms of samples were separated onto 10% SDS–PAGE for protein electrophoresis and wet transferred to polyvinylidene difluoride membrane (EMD Millipore, USA). After blocking with 5% non-fat milk, membranes were incubated with a rabbit anti-rat TGFβ1 antibody (1:1000, Abcam, ab92486), phosphorylated-Smad 2 antibody (1:1000, CST, #3104), a phosphorylated-Smad 3 antibody (1:1000, CST, #9520), a α-SMA antibody (1:1000, CST, #19245), a collagen type I antibody (1:1000, abcam, ab34710), NLRP3 (1:1000, abcam, ab214185), an apoptosis-associated speck-like protein containing a carboxy-terminal CARD (ASC, 1:500, Proteintech group, 10500-1-AP), caspase-1 (1:500, Proteintech group, 22915-1-AP), IL-1β(1:1000, abcam, ab9787), IL-18 (1:1000, abcam, ab191860), Rac-1 (1:1000, abcam, ab33186), Cx40 (1:1000, Abcam, ab183648), total Cx43 (1:1000, CST, #3512); phosphorylated-Cx43 (1:1000, CST, #3511), a β-Tubulin antibody (1:1000, CST, #2146), and a GAPDH antibody (1:1000, CST, #5174), respectively, at 4°C overnight with gentle shaking. Membranes were washed three times and then incubated with a HRP-linked secondary antibody (1:3000, CST, #7074). The immunoreactivity was detected by using

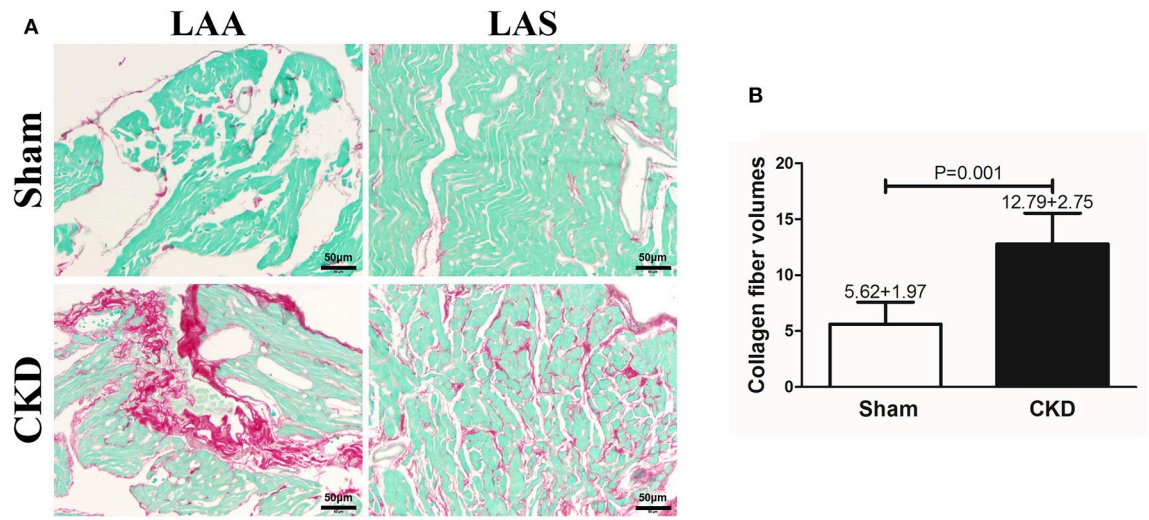

FIGURE 3 | Atrial interstitial fibrosis by Sirius red-fast green counter stain. **(A)** Microscopy (× 200) shows that atrial interstitial fibrosis was dyed red and myocytes dyed green. Atrial myocytes seem to be more diffused and hypertrophic in CKD rats compared with the sham group. **(B)** A marked increase in atrial interstitial fibrosis was found in CKD rats compared with the sham group. Data are shown as mean + SD. $n = 5$ and 6 in Sham and CKD group, respectively. Scale bar = 50 μm. LAA, left atrial appendage; LAS, left atrial septum.

an enhanced chemiluminescence reagent (WBKLS0500, EMD Millipore), and then quantified by Image Lab 5.2.1 software (Bio-Rad, Hercules, USA).

Statistical Analysis

Data were expressed as mean ± standard deviation or median (2.5–97.5 percentile) and were analyzed using the SPSS version 19. The student's independent *t*-test or Mann-Whitney *U*-test was used to analyze the difference between groups after a normal verification and homogeneity of variances analysis. The histograms were produced using the GraphPad Prism version 5 (San Diego, USA). A $P < 0.05$ was accepted as significant.

RESULTS

Physical and Biochemical Characteristics

Three months post-surgery, body weight and ALB were significantly decreased in the CKD group compared to the sham group (**Table 1**). In addition, urea and Cr were significantly increased in the CKD group compared to the sham group. However, 24 h urine volume, urine protein concentration, and 24 h urine protein, were not statistically significant between groups.

Echocardiographic Parameters

At the baseline, no significant differences were found in any of the measured parameters between groups (**Table 2**). Three months after surgery, LAD, IVSs, IVSd, LVPWs, LVPWd were significantly increased in the CKD group compared with the sham group. However, no significant differences in HR, LVESD, LVEDD, LVESV, LVEDV, LVEF, LVFS, and SV were found between groups.

Serum Levels of TGFβ1 and Ang II

Serum concentrations of TGFβ1 and Ang II were significantly increased in the CKD group compared with the sham group (**Table 3**).

AF Inducibility and the Changes in Electrogram Morphology

A representative procedure of AF inducibility is shown in **Figure 1A**. AF inducibility and duration times significantly increased in the CKD group compared with the sham group (**Figure 1B**). The morphology and duration of the P-waves were also analyzed as shown in **Figure 2**. The morphology of the P-wave in the inferior lead II showed biphasic waveforms in CKD rats compared with the sham group rats (**Figures 2A,B**). The results showed that the duration of the P-wave and the ratio of P/PR in the electrogram increased significantly in CKD rats compared with the sham group rats (**Figure 2C**).

Atrial Interstitial Fibrosis

Fibrosis was dyed red by Sirius red and Sirius red staining was used to assess atrial interstitial fibrosis. CVFs were calculated as the percentage of the red-stained area to the whole area except for the blank zone in Image J. As shown in **Supplementary Material 1**, atrial interstitial fibrosis can be accurately identified by using Image J. Representative staining images are shown in **Figure 3A**. The results suggested that fibrosis in both the left atrial appendage (LAA) and the left atrial septum (LAS) was significantly increased in the CKD group compared with the sham group ($P = 0.001$, **Figure 3B**.

Effects of CKD on Atrial Protein Expression

The protein expressions of TGFβ1, p-Smad2, p-Smad3, α-SMA, and collagen type I were markedly upregulated in the

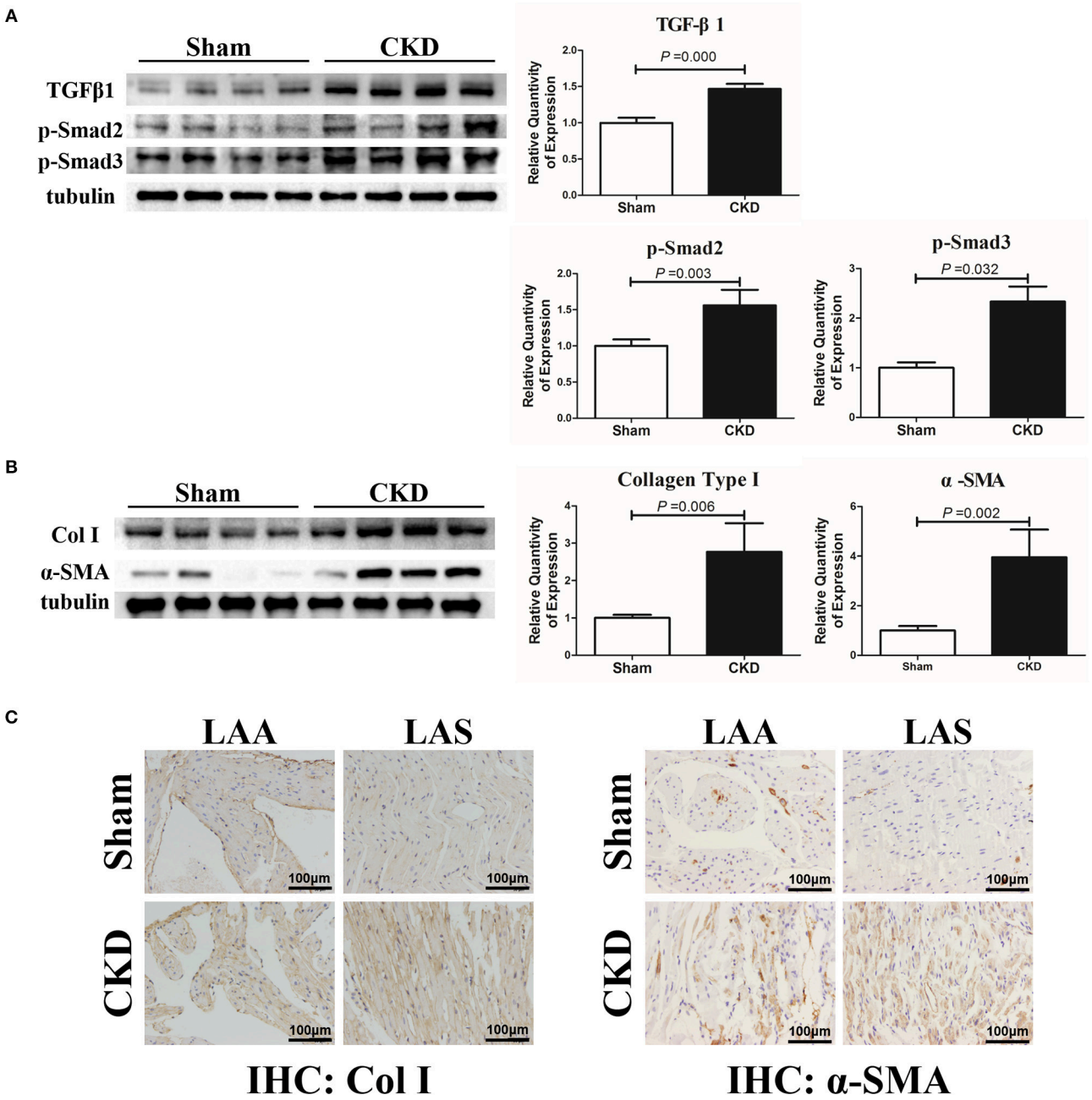

FIGURE 4 | TGFβ1/Smad2/3 signal pathway is activated in CKD rats**. (A)** Expression of TGFβ1, p-Smad2, and p-Smad2, $n = 4$ per group; **(B)** Expression of collagen type I (Col I), α-SMA from fresh left atria tissues, $n = 4$ per group; **(C)** Immunohistochemistry of Col I and α-SMA, $n = 6$ per group, magnifications × 200, scale bar = 100 μm. LAA, left atrial appendage; LAS, left atrial septum.

CKD group compared with the sham group (**Figures 4A,B**). Immunohistochemistry indicated a significant deposition of α-SMA (CKD vs. Sham: 0.20 ± 0.03 vs. 0.15 ± 0.02, $n = 6$ per group, $P = 0.005$) and collagen type I (0.15 ± 0.02 vs. 0.11 ± 0.01, $n = 6$ per group, $P = 0.000$) in the CKD group compared with the sham group (**Figure 4C**).

The protein expressions of NLRP3, ASC and procaspase-1 were significantly higher in the CKD group compared with the sham group, suggesting an upregulated NLRP3 inflammasome (**Figure 5A**). Higher protein expression of cleaved caspase-1 (P10 and P20), IL-1β, and IL18 were also found in the CKD group compared with the sham group (**Figures 5B,C**).

The protein expression of Rac-1 by western blotting (**Figure 6A**), CTGF (0.06 ± 0.01 vs. 0.14 ± 0.04, $n = 6$ per group, $P = 0.001$) and N-cadherin (0.08 ± 0.01 vs. 0.12 ± 0.01, $n = 6$ per group, $P = 0.000$) by immunohistochemistry (**Figures 6B, C**)

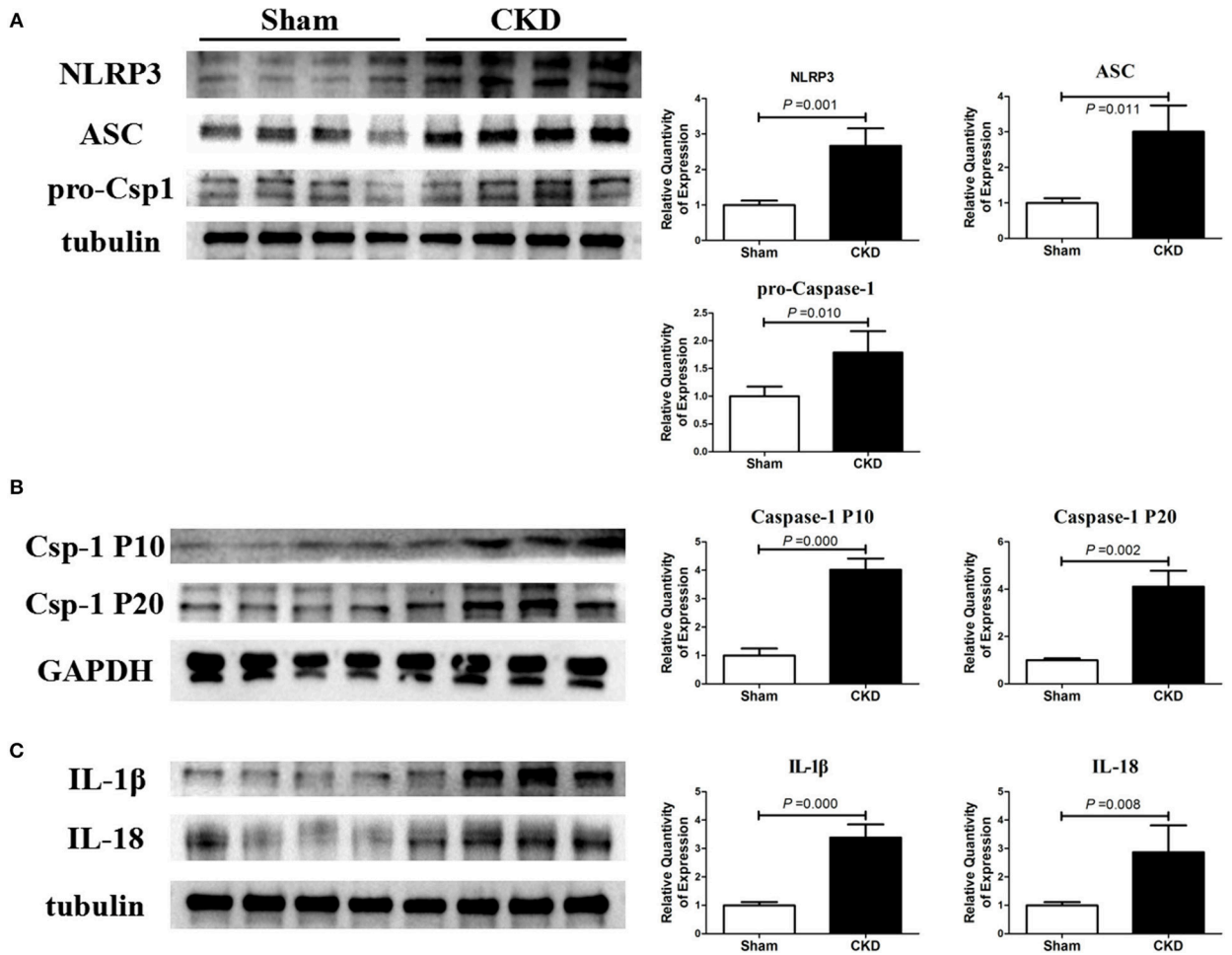

FIGURE 5 | NLRP3 inflammasome/caspase-1/IL-1β and IL18 axis is activated in CKD rats**.** (**A)** Protein expressions of NLRP3, ASC, and pro-caspase-1 (pro-csp1); **(B)** Protein expressions of the matured caspase-1, the P20 and P10; **(C)** Protein expressions of the matured IL-1β and IL-18. Tissue was collected from the left atrium. $n = 4$ per group. ASC, apoptosis-associated speck-like protein containing a carboxy-terminal CARD; Csp-1 P10, active caspase-1 (10 kDa subunit); Csp-1 P20, active caspase-1 (20 kDa subunit); IL-1β, interleukin-1β; IL-18, interleukin-18; NLRP3, NLR (nucleotide-binding domain leucine-rich repeat-containing receptor) pyrin domain-containing protein 3; pro-csp1, pro-caspase-1.

were significantly increased in the CKD group compared with the sham group.

Western blot analysis showed that the total Cx43 was increased significantly whereas Cx40 and p-Cx43 were decreased significantly in the CKD group compared with the sham group (**Figure 7**). Immunohistochemistry showed that both Cx40 and Cx43 became more lateralized with a significantly increased protein content of total Cx43 (0.01 ± 0.01 in CKD vs. 0.15 ± 0.01 in Sham, $n = 6$ per group, $P = 0.000$) and a significantly decreased protein content of Cx40 (0.07 ± 0.01 in CKD vs. 0.12 ± 0.01 in Sham, $n = 6$ per group, $P = 0.000$) in the CKD group compared with the sham group (**Figure 8**).

DISCUSSION

The present study provides evidence for the pathophysiological changes of CKD-enhanced AF. CKD resulted in the left atrial enlargement, interstitial fibrosis, and inducible AF, which may be related to the activation of TGFβ1/Smad2/3 and the NLRP3 inflammasome signaling as well as connexins remodeling. Although the present study was not the first to establish a model of AF associated with CKD in rats, it was the first to investigate the changes of TGFβ1 related-downstream mediators, NLRP3 inflammasome and connexins remodeling in a CKD setting.

In this study, CKD was established by the 5/6 nephrectomy in rats. It is an effective, feasible, and direct method based on the biochemical characteristics and our previous study (Zeng et al., 2016). The echocardiographic results indicated that CKD caused a hypertrophic cardiomyopathy and LA enlargement, without ventricular dysfunction. AF was induced by transesophageal atrial burst pacing, a classic method that was used to assess the vulnerability to AF (Rahmutula et al., 2013; Qiu et al., 2018,a,b). Other methods to induce AF is also be available by implanting a pacemaker for some weeks (Harada et al., 2012).

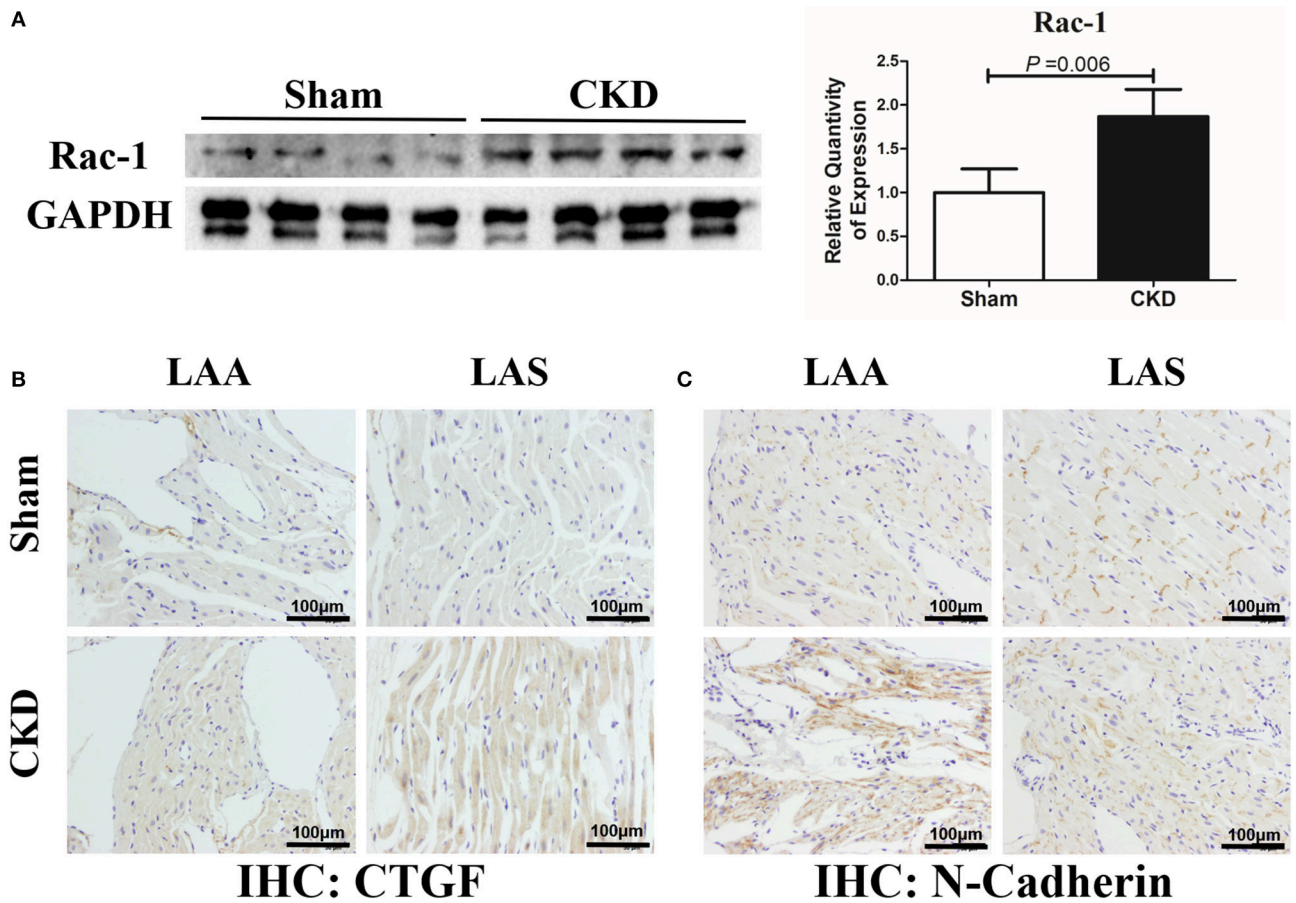

FIGURE 6 | Increased Rac-1, CTGF and N-Cadherin expression in LA of rats with CKD. **(A)** Protein amount of Rac-1, $n = 4$ per group; **(B,C)**. Immunohistochemistry of CTGF and N-cadherin, $n = 6$ per group, magnifications × 200, scale bar = 100 μm. CTGF, connective tissue growth factor; Rac1, Ras-related C3 botulinum toxin substrate 1; LAA, left atrial appendage; LAS, left atrial septum.

Our results showed that the inducibility of AF was 91.11%. This result is much higher than that in our previous study on an animal model of heart failure in the same stimulus protocol (Qiu et al., 2018,a,b). Additionally, our results found that P-waves were extended and biphasic; and the ratio of P/PR was increased in CKD rats. Clinically, these changes can usually be found in Bayés Syndrome, which suggests an advanced interatrial block that mainly results from atrial interstitial fibrosis or connexins remodeling and is highly suggestive of AF in a short-term follow-up (Baranchuk et al., 2018). The ratio of P/PR, also called the Macruz index, provides a clue for heterogeneous electrical conduction (Human and Snyman, 1963).

The progressive deposition of an extracellular matrix creates a structural milieu contributing to the onset and recurrence of AF, by interrupting normal cardiac muscle bundles in their longitudinal orientation. TGFβ1, as an important mediator of atrial fibrosis and AF, is one of the major downstream mediators of Ang II and has been fully elucidated in multiple diseases including heart failure, myocardial infarction, and hypertension, etc., in humans and in animals (Everett and Olgin, 2007; Corradi et al., 2008). TGFβ1 can mediate the phosphorylation of Smad2/3, regulating the profibrotic gene expression. Additionally, Ang II can induce the activation of both TGFβ1/Smads pathway and oxidative stress, acting to produce fibrotic remodeling (Yeh et al., 2011). NAPDH oxidase mediated-oxidative stress plays a role in the pathogenesis of CKD induced-AF which has previously been demonstrated (Fukunaga et al., 2012). However, the critical links between TGFβ1 and atrial fibrosis in CKD remain unclear. Our results revealed that the upregulated TGFβ1 was associated with an activated p-Smad2/3, identifying one of the downstream mediates of TGFβ1 in CKD-induced AF.

CTGF is also a downstream mediator of TGFβ1 and is of vital importance in the regulation of cell mitosis, proliferation and differentiation of fibroblasts and collagen synthesis (Booth and Bishop, 2010). A previous study showed that the serum TGFβ1 can promote CTGF synthesis and induce left atrial enlargement and remodeling, involved in the pathogenesis of AF (Lin et al., 2015). Most importantly, Ang II can also induce fibrosis via CTGF (Rupérez et al., 2003). Our results suggest that CTGF may play a role in CKD induced-atrial fibrosis and AF, due to the increased serum TGFβ1 and Ang II. As CTGF is mainly activated in the final phase of fibrosis, rather than targets in the initial

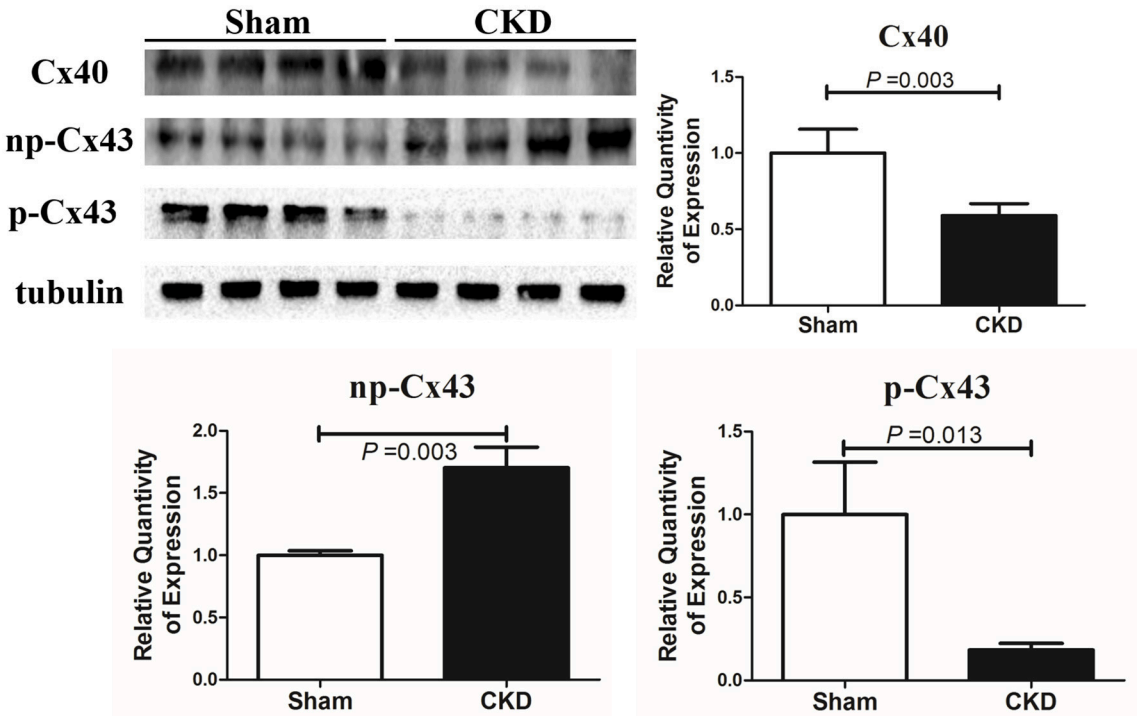

FIGURE 7 | Protein amount of Cx40 and Cx43 by western blot. Shown are protein expressions of Cx40, non-phosphorylated-Cx43 (np-Cx43) and phosphorylated-Cx43 (p-Cx43). These results show that CKD resulted in a decrease in Cx40 and p-Cx43 and an increase in np-Cx43. $n = 4$ per group.

phase like TGFβ1, therefore suggesting that CTGF may be more valuable to intervene with reversing fibrotic remodeling because it has fewer side effects (Rupérez et al., 2003). Further research is needed to investigate its specific mechanism and potential implication.

NLRP3 inflammasome/caspase-1/IL-1β and IL18 axis forms an innate immune response and plays a role in the pathogenesis of fibrosis in multiple organs including the heart, lung, kidney and the liver (Bracey et al., 2014; Rimessi et al., 2015; Cai et al., 2016; Gong et al., 2016; Stout-Delgado et al., 2016; Chin et al., 2017; Romero et al., 2017; Yao et al., 2018). Ang II was found to stimulate the activation of the NLRP3 inflammasome (Cai et al., 2016). Inversely, NLRP3 depletion can inhibit Ang II-induced fibrosis (Cai et al., 2016), block the differentiation of myofibroblasts and reduce the activation of R-Smad in response to TGFβ1 stimulation (Bracey et al., 2014). These data suggest that the NLRP3 inflammasome is critical in the regulation of Ang II-induced fibrosis. Additionally, CKD can also activate the NLRP3 inflammasome/IL-1β/IL-18 axis, contributing to ventricular contractile dysfunction (Chin et al., 2017). However, whether CKD can provoke the activation of the NLRP3 inflammasome and urge inflammatory cascade response in the atrium, remains unknown. Our results showed that CKD increased the activation of the axis in the atrium which was accompanied with increased Ang II and TGFβ1, suggesting a potentially novel therapeutic target involved in CKD enhanced-AF.

Connexins remodeling is an important aspect of Ang II induced-ASR and AF. A previous study reported that Ang II upregulates the protein expression of CTGF via the Rac1 and N-cadherin, contributing to connexins remodeling (Adam et al., 2010). Since an elevated level of Ang II was found, we further investigated whether connexins would be influenced in a CKD setting. The present study showed that CKD increased the expression of np-Cx43, decreased the expression of Cx40 and p-Cx43, and urged the lateralized distribution of Cx43/40 in the atrium, suggesting a connexins remodeling. Normally, connexins are distributed at the adhesion point of intercalated disc, playing a crucial role in maintaining intercellular electrical conduction along the long axis of myocardial fibers. Connexins remodeling including the disorders of expression and distribution are associated with pro-arrhythmic conduction slowing and conduction heterogeneity (Akar et al., 2004), represented as biphasic P-wave and an increased ratio of P/PR in electrocardiogram. Our results showed that the connexins remodeling in the atrium was accompanied with the up-regulation of Rac-1, CTGF and N-cadherin. Rac1 is a small guanosine triphosphate binding protein, a member of the Rho GTPase superfamily of intracellular signal transducers (Satoh et al., 2006). N-cadherin mainly regulates the cell-cell adhesion in the intercalated disc, relating to the intercellular coupling function of connexins gap junction (Rucker-Martin et al., 2006). A previous study has showed that Rac1 can be activated by Ang II and TGFβ1 and then rearrange Cx43 and N-cadherin (Satoh et al., 2006; Tsai et al., 2008; Adam et al., 2010). Therefore, in agreement with the above results, our results showed that a connexins remodeling in CKD may be associated with the activation of Rac1, CTGF and N-cadherin.

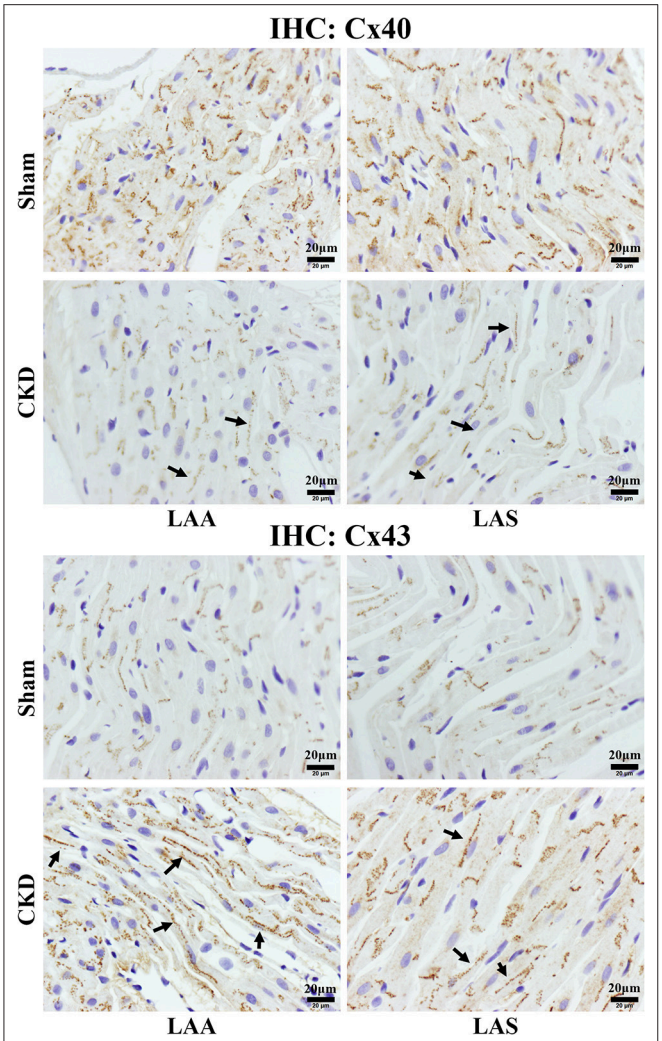

FIGURE 8 | Immunohistochemistry staining of Cx40 and Cx43. The protein level of Cx40 was lower but Cx43 higher in the CKD group compared with the sham group in both LAA and LAS (data are shown in the results section). Additionally, the distribution of both proteins are more lateralized in the CKD group than those in the sham group. Magnifications × 400, scale bar = 20 μm. LAA, left atrial appendage; LAS, left atrial septum. (→) indicates lateralized Cx40 or Cx43.

Excessive atrial interstitial fibrosis, atrial structural alteration and inflammation may break the cytoskeleton network and damage the adhesion proteins that contribute to the normal organization of connexins (Giepmans, 2004; Rucker-Martin et al., 2006). The mechanical deformation of the atrial wall, by chronic hemodynamic overload or by hypertension, both of which are secondary to CKD, could induce Cx40/43 remodeling (Haefliger and Meda, 2000; Severs et al., 2008). It has been demonstrated that exposure to inflammation can reduce Cx40/43 functional expression and change gap junctions in the heart, whereas CKD causes systemic inflammation and activates TGFβ1/Smad2/3 and NLRP3 inflammasome (Sawaya et al., 2007; George et al., 2017). Therefore, taken together with our observation, connexins remodeling is one of pathological changes involved in CKD enhanced-AF.

LIMITATIONS

Our results suggested that the TGFβ1/Smad2/3 signal pathway, the NLRP3 inflammasome and connexins remodeling are involved in CKD enhanced-ASR and AF. These pathological factors, in fact, are interactional. The NLRP3 inflammasome induced-the activation of IL-1β and IL-18 is known to be profibrotic, most importantly it can constitute a positive feedback to the activation of TGF-β1 and exacerbate connexins remodeling (Kolb et al., 2001; Luo et al., 2009; Fix et al., 2011). Inevitably, the present study has shortcomings. Firstly, the specific causes which induced the above pathological changes are unknown. CKD is always complicated with hypertension, heart failure, chronic volume overload, etc., of which alone or together can create the arrhythmogenic substrate for AF initiation. However, it is hard to constitute a model isolating the additional effects of CKD. Secondly, no interventions were taken. The potential effects of antagonist against the activation of RAAS, TGFβ1/Smad2/3, the NLRP3 inflammasome, CTGF and Rac-1 on CKD induced-AF are unknown. The effects of angiotensin converting enzyme inhibitor and angiotensin receptor blocker against Ang II are worthy of further studies as suggested by the present findings. Thirdly, the influences of different periods and different degrees of kidney dysfunction on ASR and AF are not involved. The reason why we chose a CKD rat model of 3 months post-5/6 nephrectomy to investigate the potentially pathological changes was meant to constitute a more stable CKD model based on previous data, and to avoid acute factors, unstable/incomplete kidney failure, and insufficient duration time. Fourthly, the impacts of CKD on atrial electrical remodeling and the functional changes of ion channels were not involved in the present study. Although the characteristics of CKD enhanced-ASR and AF are considered systemic and multifactorial, to validate these pathological changes is important to point out future directions. In short, further studies focused on pathological mechanisms and therapeutic reactions are worthy of investigation.

CONCLUSIONS

Despite upstream therapy that is intended to stop the prevalence of AF by preventing or reversing ASR has been proposed, the prevention of CKD-related AF still has a long way to go due to the lack of a clear understanding of the pathophysiologic mechanisms. In the present study, we investigated the potential pathogenesis of AF in a rat model of CKD established 3 months post-5/6 nephrectomy. Our results showed that CKD led to the left atrial enlargement, increased the vulnerability to AF with prolonged and biphasic P-wave. Pathologically, CKD caused severe atrial interstitial fibrosis and connexins remodeling. Possible mechanisms of ASR and connexins remodeling in CKD should include the TGFβ1/Smad2/3 signaling, NLRP3 inflammasome/caspase-1/IL-1β and IL18 axis, and the changes

of Rac-1, CTGF and N-cadherin. In conclusion, these findings implicate TGFβ1/Smad2/3, the NLRP3 inflammasome and connexins as potential mediators of increased AF vulnerability in CKD.

NEW AND NOTEWORTHY

The present study reports that CKD causes an atrial structural remodeling and inducible AF in a CKD rat model, 3 months post-5/6 nephrectomy. These pathophysiological changes are linked to the activation of TGFβ1/Smad2/3 signaling, NLRP3 inflammasome and connexins remodeling. The present study may produce an effect on the upstream therapy for CKD-enhanced AF.

AUTHOR CONTRIBUTIONS

The conception and design were proposed by HQ, CZ, WJ, YW, ZL, QL, ZX, XL, and HW. Animal and molecular biology experiments were mainly finished by HQ, CJ, and WL. Paper was drafted by HQ and reviewed by CZ and WJ.

FUNDING

This study was supported by the Specific Foundation of Guangdong Hospital of Chinese Medicine (YN2016MJ05, secured by CZ), the National Natural Science Foundation of China (81873142, 81803875, and 81874432, secured by CZ, YW, and WJ, respectively), the MOST/SATCM of the People's Republic of China grant (2013BAI02B04, secured by XL), the Guangdong Provincial Department of Science and Technology funding (809059345141, secured by Dacan Chen, non-authorship).

SUPPLEMENTARY MATERIAL

The Supplementary Material for this article can be found online at: https://www.frontiersin.org/articles/10.3389/fphys.2018.01726/full#supplementary-material

REFERENCES

Adam, O., Lavall, D., Theobald, K., Hohl, M., Grube, M., Ameling, S., et al. (2010). Rac1-induced connective tissue growth factor regulates connexin 43 and N-cadherin expression in atrial fibrillation. *J. Am. Coll. Cardiol.* 55, 469–480. doi: 10.1016/j.jacc.2009.08.064

Akar, F. G., Spragg, D. D., Tunin, R. S., Kass, D. A., and Tomaselli, G. F. (2004). Mechanisms underlying conduction slowing and arrhythmogenesis in nonischemic dilated cardiomyopathy. *Circ. Res.* 95, 717–725. doi: 10.1161/01.RES.0000144125.61927.1c

Aoki, K., Teshima, Y., Kondo, H., Saito, S., Fukui, A., Fukunaga, N., et al. (2015). Role of indoxyl sulfate as a predisposing factor for atrial fibrillation in renal dysfunction. *J. Am. Heart Assoc.* 4:e002023. doi: 10.1161/JAHA.115.002023

Baranchuk, A., Torner, P., and de Luna, A. B. (2018). bayés syndrome: what is it? *Circulation* 137, 200–202. doi: 10.1161/CIRCULATIONAHA.117.032333

Booth, A. J., and Bishop, D. K. (2010). TGF-β, IL-6, IL-17 and CTGF direct multiple pathologies of chronic cardiac allograft rejection. *Immunotherapy* 2, 511–520. doi: 10.2217/imt.10.33

Bracey, N. A., Gershkovich, B., Chun, J., Vilaysane, A., Meijndert, H. C., Wright, J. R., et al. (2014). Mitochondrial NLRP3 protein induces reactive oxygen species to promote Smad protein signaling and fibrosis independent from the inflammasome. *J. Biol. Chem.* 289, 19571–19584. doi: 10.1074/jbc.M114.550624

Cai, S. M., Yang, R. Q., Li, Y., Ning, Z. W., Zhang, L. L., Zhou, G. S., et al. (2016). Angiotensin-(1-7) Improves liver fibrosis by regulating the NLRP3 inflammasome via redox balance modulation. *Antioxid. Redox Signal.* 24, 795–812. doi: 10.1089/ars.2015.6498

Chin, L. H., Hsu, Y. J., Hsu, S. C., Chen, Y. H., Chang, Y. L., Huang, S. M., et al. (2017). The regulation of NLRP3 inflammasome expression during the development of cardiac contractile dysfunction in chronic kidney disease. *Oncotarget*. 8, 113303–113317. doi: 10.18632/oncotarget.22964

Corradi, D., Callegari, S., Maestri, R., Benussi, S., and Alfieri, O. (2008). Structural remodeling in atrial fibrillation. *Nat. Clin. Pract. Cardiovasc. Med.* 5, 782–796. doi: 10.1038/ncpcardio1370

Duffy, H. S., and Wit, A. L. (2008). Is there a role for remodeled connexins in AF? No simple answers. *J. Mol. Cell Cardiol.* 44, 4–13. doi: 10.1016/j.yjmcc.2007.08.016

Everett, T. H. IV., and Olgin, J. E. (2007). Atrial fibrosis and the mechanisms of atrial fibrillation. *Heart Rhythm.* 4(3 Suppl): S24–S27. doi: 10.1016/j.hrthm.2006.12.040

Fix, C., Bingham, K., and Carver, W. (2011). Effects of interleukin-18 on cardiac fibroblast function and gene expression. *Cytokine* 53, 19–28. doi: 10.1016/j.cyto.2010.10.002

Fukunaga, N., Takahashi, N., Hagiwara, S., Kume, O., Fukui, A., Teshima, Y., et al. (2012). Establishment of a model of atrial fibrillation associated with chronic kidney disease in rats and the role of oxidative stress. *Heart Rhythm.* 9, 2023–2031. doi: 10.1016/j.hrthm.2012.08.019

George, S. A., Calhoun, P. J., Gourdie, R. G., Smyth, J. W., and Poelzing, S. (2017). TNFα modulates cardiac conduction by altering electrical coupling between myocytes. *Front. Physiol.* 8:334. doi: 10.3389/fphys.2017.00334

Giepmans, B. N. (2004). Gap junctions and connexin-interacting proteins. *Cardiovasc. Res.* 62:233–245. doi: 10.1016/j.cardiores.2003.12.009

Gill, S., Jun, M., and Ravani, P. (2017). Atrial fibrillation and chronic kidney disease: struggling through thick and thin. *Nephrol. Dial. Transplant.* 32, 1079–1084. doi: 10.1093/ndt/gfw378

Gong, W., Mao, S., Yu, J., Song, J., Jia, Z., Huang, S., et al. (2016). NLRP3 deletion protects against renal fibrosis and attenuates mitochondrial abnormality in mouse with 5/6 nephrectomy. *Am. J. Physiol. Renal Physiol.* 310, F1081–F1088. doi: 10.1152/ajprenal.00534.2015

Haefliger, J. A., and Meda, P. (2000). Chronic hypertension alters the expression of Cx43 in cardiovascular muscle cells. *Braz. J. Med. Biol. Res.* 33, 431–438. doi: 10.1590/S0100-879X2000000400009

Hao, J., Wang, B., Jones, S. C., Jassal, D. S., and Dixon, I. M. (2000). Interaction between angiotensin II and Smad proteins in fibroblasts in failing heart and *in vitro*. *Am. J. Physiol. Heart Circ. Physiol.* 279, H3020–H3030. doi: 10.1152/ajpheart.2000.279.6.H3020

Harada, M., Luo, X., Qi, X. Y., Tadevosyan, A., Maguy, A., Ordog, B., et al. (2012). Transient receptor potential canonical-3 channel-dependent fibroblast regulation in atrial fibrillation. *Circulation* 126, 2051–2064. doi: 10.1161/CIRCULATIONAHA.112.121830

Human, G. P., and Snyman, H. W. (1963). The value of the Macruz index in the diagnosis of atrial enlargement. *Circulation* 27, 935–938. doi: 10.1161/01.CIR.27.5.935

Jun, M., James, M. T., Manns, B. J., Quinn, R. R., Ravani, P., Tonelli, M., et al. (2015). The association between kidney function and major bleeding in older adults with atrial fibrillation starting warfarin treatment: population based observational study. *BMJ* 350:h246. doi: 10.1136/bmj.h246

Kirchhof, P., Benussi, S., Kotecha, D., Ahlsson, A., Atar, D., Casadei, B., Castella, M., et al. (2016). 2016 ESC Guidelines for the management of atrial fibrillation developed in collaboration with EACTS. *Europace* 18, 1609–1678. doi: 10.1093/europace/euw295

Kolb, M., Margetts, P. J., Anthony, D. C., Pitossi, F., and Gauldie, J. (2001). Transient expression of IL-1beta induces acute lung injury and chronic repair leading to pulmonary fibrosis. *J. Clin. Invest.* 107, 1529–36. doi: 10.1172/JCI12568

Liao, J. N., Chao, T. F., Liu, C. J., Wang, K. L., Chen, S. J., Lin, Y. J., et al. (2015). Incidence and risk factors for new-onset atrial fibrillation among patients with end-stage renal disease undergoing renal replacement therapy. *Kidney Int.* 87, 1209–1215. doi: 10.1038/ki.2014.393

Lin, X., Wu, N., Shi, Y., Wang, S., Tan, K., Shen, Y., et al. (2015). Association between transforming growth factor β1 and atrial fibrillation in essential hypertensive patients. *Clin. Exp. Hypertens.* 37, 82–87. doi: 10.3109/10641963.2014.913600

Luo, D. D., Fielding, C., Phillips, A., and Fraser, D. (2009). Interleukin-1 beta regulates proximal tubular cell transforming growth factor beta-1 signalling. *Nephrol. Dial. Transplant* 24, 2655–2665. doi: 10.1093/ndt/gfp208

Ng, K. P., Edwards, N. C., Lip, G. Y., et al. (2013). Atrial fibrillation in CKD: balancing the risks and benefits of anticoagulation. *Am. J. Kidney Dis.* 62, 615–632. doi: 10.1053/j.ajkd.2013.02.381

Olesen, J. B., Lip, G. Y., Kamper, A. L., Hommel, K., Køber, L., Lane, D. A., et al. (2012). Stroke and bleeding in atrial fibrillation with chronic kidney disease. *N. Engl. J. Med.* 367, 625–635. doi: 10.1056/NEJMoa1105594

Qiu, H., Ji, C., Wu, H., and Zou, C. (2018). Chronic kidney disease-induced atrial structural remodeling and atrial fibrillation: more studies on the pathological mechanism are encouraged. *Naunyn Schmiedebergs Arch. Pharmacol.* doi: 10.1007/s00210-018-1494-4. [Epub ahead of print].

Qiu, H., Liu, W., Lan, T., Pan, W., Chen, X., Wu, H., et al. (2018a). Salvianolate reduces atrial fibrillation through suppressing atrial interstitial fibrosis by inhibiting TGF-β1/Smad2/3 and TXNIP/NLRP3 inflammasome signaling pathways in post-MI rats. *Phytomedicine* 51, 255–265. doi: 10.1016/j.phymed.2018.09.238

Qiu, H., Wu, H., Ma, J., Cao, H., Huang, L., Qiu, W., et al. (2018b). DL-3-n-Butylphthalide reduces atrial fibrillation susceptibility by inhibiting atrial structural remodeling in rats with heart failure. *Naunyn Schmiedebergs. Arch. Pharmacol.* 391, 323–334. doi: 10.1007/s00210-017-1457-1

Rahmutula, D., Marcus, G. M., Wilson, E. E., Ding, C. H., Xiao, Y., Paquet, A. C., et al. (2013). Molecular basis of selective atrial fibrosis due to overexpression of transforming growth factor-β1. *Cardiovasc. Res.* 99, 769–79. doi: 10.1093/cvr/cvt074

Rasband, W.S. (1997–2018). *ImageJ, U. S. National Institutes of Health*. Bethesda, ML. Available online at: https://imagej.nih.gov/ij/

Rimessi, A., Bezzerri, V., Patergnani, S., Marchi, S., Cabrini, G., and Pinton, P. (2015). Mitochondrial Ca2+-dependent NLRP3 activation exacerbates the Pseudomonas aeruginosa-driven inflammatory response in cystic fibrosis. *Nat. Commun.* 6:6201. doi: 10.1038/ncomms7201

Romero, C. A., Remor, A., Latini, A., De Paul, A. L., Torres, A. I., and Mukdsi, J. H. (2017). Uric acid activates NRLP3 inflammasome in an *in-vivo* model of epithelial to mesenchymal transition in the kidney. *J. Mol. Histol.* 48, 209–218. doi: 10.1007/s10735-017-9720-9

Rosin, N. L., Falkenham, A., Sopel, M. J., Lee, T. D., and Légaré, J. F. (2013). Regulation and role of connective tissue growth factor in AngII-induced myocardial fibrosis. *Am. J. Pathol.* 182, 714–726. doi: 10.1016/j.ajpath.2012.11.014

Rucker-Martin, C., Milliez, P., Tan, S., Decrouy, X., Recouvreur, M., Vranckx, R., et al. (2006). Chronic hemodynamic overload of the atria is an important factor for gap junction remodeling in human and rat hearts. *Cardiovasc. Res.* 72, 69–79. doi: 10.1016/j.cardiores.2006.06.016

Rupérez, M., Lorenzo, O., Blanco-Colio, L. M., Esteban, V., Egido, J., and Ruiz-Ortega, M. (2003). Connective tissue growth factor is a mediator of angiotensin II-induced fibrosis. *Circulation* 108, 1499–1505. doi: 10.1161/01.CIR.0000089129.51288.BA

Ryu, K., Li, L., Khrestian, C. M., Matsumoto, N., Sahadevan, J., Ruehr, M. L., et al. (2007). Effects of sterile pericarditis on connexins 40 and 43 in the atria: correlation with abnormal conduction and atrial arrhythmias. *Am. J. Physiol. Heart Circ. Physiol.* 293, H1231–H1241. doi: 10.1152/ajpheart.00607.2006

Satoh, M., Ogita, H., Takeshita, K., Mukai, Y., Kwiatkowski, D. J., and Liao, J. K. (2006). Requirement of Rac1 in the development of cardiac hypertrophy. *Proc. Natl. Acad. Sci. U.S.A.* 103, 7432–7437. doi: 10.1073/pnas.0510444103

Sawaya, S. E., Rajawat, Y. S., Rami, T. G., Szalai, G., Price, R. L., Sivasubramanian, N., et al. (2007). Downregulation of connexin40 and increased prevalence of atrial arrhythmias in transgenic mice with cardiac-restricted overexpression of tumor necrosis factor. *Am. J. Physiol. Heart Circ. Physiol.* 292, H1561–H1567. doi: 10.1152/ajpheart.00285.2006

Severs, N. J., Bruce, A. F., Dupont, E., and Rothery, S. (2008). Remodelling of gap junctions and connexin expression in diseased myocardium. *Cardiovasc. Res.* 80, 9–19. doi: 10.1093/cvr/cvn133

Soliman, E. Z., Prineas, R. J., Go, A. S., Xie, D., Lash, J. P., Rahman, M., et al. (2010). Chronic kidney disease and prevalent atrial fibrillation: the Chronic Renal Insufficiency Cohort (CRIC). *Am. Heart J.* 159, 1102–1107. doi: 10.1016/j.ahj.2010.03.027

Stout-Delgado, H. W., Cho, S. J., Chu, S. G., Mitzel, D. N., Villalba, J., El-Chemaly, S., et al. (2016). Age-dependent susceptibility to pulmonary fibrosis Is Associated with NLRP3 Inflammasome activation. *Am. J. Respir. Cell Mol. Biol.* 55, 252–263. doi: 10.1165/rcmb.2015-0222OC

Tsai, C. T., Lai, L. P., Kuo, K. T., Hwang, J. J., Hsieh, C. S., Hsu, K. L., et al. (2008). Angiotensin II activates signal transducer and activators of transcription 3 via Rac1 in atrial myocytes and fibroblasts: implication for the therapeutic effect of statin in atrial structural remodeling. *Circulation* 117, 344–355. doi: 10.1161/CIRCULATIONAHA.107.695346

Yao, C., Veleva, T., Scott, L. Jr, Cao, S., Li, L., Chen, G., et al. (2018). Enhanced Cardiomyocyte NLRP3 Inflammasome Signaling Promotes Atrial Fibrillation. *Circulation*. doi: 10.1161/CIRCULATIONAHA.118.035202. [Epub ahead of print].

Yeh, Y. H., Kuo, C. T., Chan, T. H., Chang, G. J., Qi, X. Y., Tsai, F., et al. (2011). Transforming growth factor-beta and oxidative stress mediate tachycardia-induced cellular remodelling in cultured atrial-derived myocytes. *Cardiovasc. Res.* 91, 62–70. doi: 10.1093/cvr/cvr041

Zeng, Y. Q., Dai, Z., Lu, F., Lu, Z., Liu, X., Chen, C., et al. (2016). Emodin via colonic irrigation modulates gut microbiota and reduces uremic toxins in rats with chronic kidney disease. *Oncotarget* 7, 17468–17478. doi: 10.18632/oncotarget.8160

Zhang, H., Zhong, H., Everett, T. H. IV, Wilson, E., Chang, R., Zeng, D., et al. (2014). Blockade of A2B adenosine receptor reduces left ventricular dysfunction and ventricular arrhythmias 1 week after myocardial infarction in the rat model. *Heart Rhythm.* 11, 101–109. doi: 10.1016/j.hrthm.2013.10.023

Conflict of Interest Statement: The authors declare that the research was conducted in the absence of any commercial or financial relationships that could be construed as a potential conflict of interest.

frontiers in Physiology

ORIGINAL RESEARCH
published: 04 February 2019
doi: 10.3389/fphys.2019.00049

Polyscore of Non-invasive Cardiac Risk Factors

Alexander Steger[1], Alexander Müller[1], Petra Barthel[1], Michael Dommasch[1], Katharina Maria Huster[1], Katerina Hnatkova[2], Daniel Sinnecker[1], Alexander Hapfelmeier[3], Marek Malik[2] and Georg Schmidt[1]*

[1] Klinik für Innere Medizin I, Technische Universität München, Munich, Germany, [2] National Heart and Lung Institute, Imperial College London, London, United Kingdom, [3] Institute of Medical Informatics, Statistics and Epidemiology, Technische Universität München, Munich, Germany

Non-invasive risk stratification of cardiac patients has been the subject of numerous studies. Most of these investigations either researched unique risk predictors or compared the predictive power of different predictors. Fewer studies suggested a combination of a small number of non-invasive indices to increase the accuracy of high-risk group selection. To advance non-invasive risk assessment of cardiac patients, we propose a combination score (termed the Polyscore) of seven different cardiac risk stratifiers that predominantly quantify autonomic cardiovascular control and regulation, namely the slope of heart rate turbulence, deceleration capacity of heart rate, non-invasively assessed baroreflex sensitivity, resting respiration frequency, expiration triggered sinus arrhythmia, post-ectopic potentiation of systolic blood pressure, and frequency of supraventricular and ventricular ectopic beats. These risk stratification tests have previously been researched and their dichotomies defining abnormal results have been derived from previous reports. The Polyscore combination was defined as the number of positive tests among these seven risk predictors, giving a numerical scale which ranges from 0 (all tests normal) to 7 (all tests abnormal). The Polyscore was tested in a population of 941 contemporarily treated survivors of acute myocardial infarction (median age 61 years, 182 females) of whom 72 (7.65%) died during a 5-year follow-up. In these patients, all the risk predictors combined in the Polyscore were assessed during in-hospital 30-min simultaneous non-invasive recordings of high-frequency orthogonal electrocardiogram, continuous blood pressure and respiration. Compared to Polyscore 0 stratum, the hazard ratios of mortality during follow-up increased almost exponentially in strata 1 through 7 (vs. stratus 0, the hazard ratios were 1.37, 1.96, 7.03, 15.0, 35.7, 48.2, and 114, in strata 1 to 7, respectively; $p < 0.0001$). This allowed selecting low-risk (Polyscore $\leq$ 2), intermediate risk (Polyscore 3 or 4) and high-risk (Polyscore $\geq$ 5) sub-groups of the population that differed greatly in the Kaplan–Meier probabilities of mortality during follow-up. Since the Polyscore was derived from recordings of only 30-min duration, it can be reasonably applied in different clinical situations including population-wide screening. We can therefore conclude that the Polyscore is a reasonable method for cardiac risk stratification that is ready for prospective validation in future independent studies.

Keywords: non-invasive autonomic testing, combination of risk factors, electrocardiogram, blood pressure monitoring, resting respiration, survivors of myocardial infarction, all-cause mortality, low-risk and high-risk group separation

OPEN ACCESS

Edited by:
Ademuyiwa S. Aromolaran, SUNY Downstate Medical Center, United States

Reviewed by:
John Pearce Morrow, Columbia University, United States
Leonardo Roever, Federal University of Uberlândia, Brazil

****Correspondence:***
Marek Malik
marek.malik@imperial.ac.uk;
marek.malik@btinternet.com

Specialty section:
This article was submitted to Cardiac Electrophysiology, a section of the journal Frontiers in Physiology

Received: *17 December 2018*
Accepted: *17 January 2019*
Published: *04 February 2019*

Citation:
Steger A, Müller A, Barthel P, Dommasch M, Huster KM, Hnatkova K, Sinnecker D, Hapfelmeier A, Malik M and Schmidt G (2019) Polyscore of Non-invasive Cardiac Risk Factors. Front. Physiol. 10:49. doi: 10.3389/fphys.2019.00049

INTRODUCTION

Non-invasive risk stratification of cardiac patients has been addressed in a broad variety of studies (Josephson et al., 1982; Buxton et al., 1984; Wellens et al., 2014). Repeatedly, different risk factors such as left ventricular ejection fraction (LVEF), late potentials, heart rate variability (HRV), and the presence of non-sustained ventricular tachycardia have been compared with the aim of identifying the most powerful risk factor (Farrell et al., 1991). This led, among others, to the present guidelines for the selection of cardiac patients suitable for prophylactic implantation of automatic defibrillators (ICD) (Al-Khatib et al., 2018). These guidelines are based solely on univariable LVEF assessment and are now understood to be far from optimally effective (Køber et al., 2016). It is now also understood that the disappointment with the ICD guidelines cannot be solved by one single test. Rather, it is now believed that a truly effective risk prediction requires a combination of different risk factors.

Powerful cardiac risk predictions beyond LVEF assessment have previously been shown by different tests related to the autonomic nervous system function (Wellens et al., 2014). These tests quantify cardiovascular control at different levels and scales. Some combinations of such tests, e.g., of heart rate turbulence (HRT) and of deceleration capacity (DC) have already been proposed (Bauer et al., 2009) but these proposals have not reflected the wide scope of autonomic regulation. Having this is mind, we are presenting a Polyscore of seven different autonomic and related tests. The risk prediction performance of this Polyscore was evaluated in a well characterized population of survivors of acute myocardial infarction (AMI).

MATERIALS AND METHODS

Population

The population used in the study was previously described (Barthel et al., 2011). Briefly, between May 2000 and March 2005, 941 consecutive AMI survivors were enrolled at two participating high-volume centers (Klinikum rechts der Isar and Deutsches Herzzentrum München, both Technische Universität München, Munich, Germany). The vast majority of the patients (96.8%) were of European Caucasian origin while the remaining few were of mixed descent (Turkish, Arabic, and Asian).

Acute myocardial infarction was diagnosed based on at least 2 of the following findings: typical chest pain lasting $\geq$20 min, creatine kinase above twice the upper normal limit of the respective laboratory, and admission ST-segment elevation $\geq$0.1 mV in at least 2 contiguous limb leads or $\geq$0.2 mV in at least 2 contiguous precordial leads.

Patients were enrolled if aged $\leq$ 80 years, survived the acute phase of myocardial infarction, were in sinus rhythm, and did not meet the secondary prophylaxis indications for ICD implantation before hospital discharge. The study was approved by the local ethics committee and all participants gave written informed consent.

Clinical Data

Clinical characteristics were assessed during the hospitalization for the index AMI.

Diabetes mellitus was diagnosed if the patient was already on antidiabetic medication or if fasting blood glucose repeatedly exceeded 11 mmol/l.

Left ventricular ejection fraction was assessed either by echocardiography (biplane Simpson's rule, Sonos 5500, Hewlett Packard, Palo Alto, CA, United States) or by left ventricular angiography. In compliance with the current ICD-guidelines (Dagres and Hindricks, 2013), LVEF was dichotomized at 35%.

The GRACE (Global Registry of Acute Coronary Events) score (Eagle et al., 2004), a recognized clinical risk score characterizing acute coronary syndrome patients, combines age, serum creatinine, past myocardial infarction, congestive heart failure, in-hospital percutaneous coronary intervention, resting heart rate, systolic blood pressure, ST segment deviation and positive cardiac enzymes. The score ranges from 1 to 210 points and for the purposes of this study was dichotomized at 120 points (Barthel et al., 2012).

Recordings and Autonomic Tests

During the initial hospitalization and within 2 weeks after the index AMI (median day 7; inter-quartile range 5 to 9 days after the index AMI), simultaneous non-invasive 30-min recordings were performed including an electrocardiogram (1.6 kHz in orthogonal XYZ leads, TMS International, Enschede, Netherlands) and continuous arterial blood pressure by finger photoplethysmographic device (Portapres; TNO-TPD Biomedical Instrumentation, Amsterdam, Netherlands). Respiration was assessed by a piezoelectric thoracic sensor (1.6 kHz, Pro-Tech, Porti system, TMS International). The recordings were made in supine resting position in quiet environment after regular morning medication.

The biosignals were stored digitally and reviewed by experienced technicians blinded to the clinical outcome data. Artifacts were eliminated, and QRS-classifications were manually corrected where necessary.

Polyscore Components

The following seven previously described risk predictors related to autonomous nervous system function were considered:

(1) HRT, that is the development of RR intervals following a ventricular premature contraction, is one of the well-known risk predictors (Schmidt et al., 1999). Of the two HRT components, turbulence slope appears to be a stronger risk predictor compared to turbulence onset. Therefore, it was used in Polyscore design together with the previously established dichotomy of 2.5 ms per RR interval (Bauer et al., 2008).

(2) DC quantifies vagal effects on the heart by measuring and averaging deceleration-related modulations of the heart rate (Bauer et al., 2006). The optimum dichotomy was previously defined at 2.5 ms average beat-to-beat RR-interval prolongation.

(3) Baroreflex is a cardiovascular control mechanism that prevents excessive blood pressure fluctuations. It increases and decreases heart rate and vascular resistance in response to the decrease and increase in the arterial blood pressure, respectively. The extent of the reflex was quantified by studying the heart rate deceleration following a blood pressure rise in the simultaneous ECG and blood pressure recording by bivariate phase-rectified signal analysis. It was expressed by the baroreflex sensitivity measured in ms of RR interval change per mmHg of blood pressure change. The optimum dichotomy was previously defined at 1.58 ms/mmHg (Barthel et al., 2012).

(4) Average respiration rate was measured during the last 10 min of the recordings when the conditions were fully stabilized. The previously suggested dichotomy limit of $\geq$18.6 breaths per minute was used to define abnormally fast resting respiration (Barthel et al., 2013).

(5) Expiration-triggered sinus arrhythmia was assessed by studying the RR interval changes during the early expiration phase by bivariate phase-rectified signal analysis. Dichotomy $\leq$0.19 ms of RR changes was used to define an abnormal heart rate response (Sinnecker et al., 2016).

(6) Systolic blood pressure reaction to single ventricular ectopic beats was expressed by the previously proposed post-ectopic potentiation (PESP). This was quantified by the ratio of the systolic blood pressure of the first post-ectopic beat relative to the systolic pressure values of the following sinus rhythm cycles. Previously published dichotomy of 1.03 was used to define presence or absence of PESP (Sinnecker et al., 2014).

(7) Ectopic beats have long been recognized as a risk factor in its own right (Moss et al., 1979). Since the source recordings of this study were relatively short, the presence of both supraventricular ectopics ($>$7 per 30 min) or ventricular ectopics ($>$29 per 30 min) were considered to signify abnormal substrate. The dichotomy limits were derived in a retrospective analysis by means of long-rank statistics optimization with the aim of establishing a strong mortality predictor.

Polyscore Definition

The seven risk factors described in the previous section were evaluated in each study patient. Using their dichotomy limits, each factor was classified as normal or abnormal. Subsequently, the Polyscore was defined as the number of abnormal factors. This led to 8 possible values ranging between 0 (all risk factors normal) and 7 (all risk factors abnormal).

Follow-Up and Outcome Events

Study patients were followed up with clinical visits every 6 months. In each patient, follow-up was completed after 5 years. Patients who did not attend a scheduled visit were contacted either by letter, telephone or through their general practitioner. In case a patient could not be traced, the population registry was used to identify those who died.

While the follow-up information allowed to classify the death cases into non-cardiac, cardiac non-sudden, and sudden cardiac deaths, total mortality over the 5-year follow-up period was used as the outcome event for the purposes of this study.

Statistics and Data Presentation

The distribution of continuous data is presented as medians with inter-quartile ranges, categorical data are presented as absolute and relative frequencies.

To study the contribution of individual Polyscore components to the total Polyscore, the relative number of patients who had a given risk factor positive within the groups with Polyscore $\varphi = 1, 2, \ldots, 7$ was calculated and displayed graphically.

Univariable Cox regression model was used to calculate hazard ratios (including its 95% confidence intervals) of patients with Polyscore φ vs. Polyscore 0, ranging the value of φ from 1 to 7. These hazard ratios were displayed graphically with the aim of selecting Polyscore cut-off points defining low-risk, intermediate, and high-risk sub-populations.

Using these Polyscore cut-off points, Kaplan–Meier survival curves were calculated for the low-risk, intermediate, and high-risk subpopulations. Log-rank test was used to compare the Kaplan–Meier survival curves. The analysis was subsequently repeated in patients with and without the diagnosis of diabetes mellitus.

Univariable and multivariable Cox regression models were used to compare the strength of risk prediction by LVEF, presence of diabetes mellitus, GRACE score, and the Polyscore. These Cox regression models were used twice, (**a**) using the non-dichotomized values of LVEF, GRACE score and Polyscore (only the presence of diabetes used as a categorical variable) and (**b**) using dichotomized values of all variables.

Kaplan–Meyer survival curves were calculated together with their 95% pointwise confidence intervals using the R statistical package version 3.3.2 (R Core Team, 2018) with the survival package version 2.38 (Therneau, 2018). Other statistical analyses were made using the SPSS package (IBM SPSS Statistics, version 25, Armonk, NY, United States). Hypothesis testing was performed on two-sided 5% significance levels.

RESULTS

Clinical characteristics of the study population are shown in **Table 1**. Of the 941 study patients, 11 (1.2%) were lost during the follow-up period and subsequently censored at the time of last contact.

During the 5-year follow-up period, 72 (7.65%) patients died. In concordance with the observations made in other post-AMI registries (Farrell et al., 1991) the incidence of death was highest during the first year of follow-up. In subsequent years, the incidence of death was practically constant, and the corresponding Kaplan–Meyer curve was almost linear (**Figure 1**).

As expected, the numbers of patients in the different Polyscore strata were decreasing from the low-risk to the high-risk strata. The numbers of patients with Polyscore 0 to 7 were 239 (25.4%), 261 (27.7%), 182 (19.3%), 133 (14.1%), 86 (9.1%), 24 (2.6%), 9 (1.0%), and 7 (0.7%), respectively.

TABLE 1 | Clinical characteristics of the study population.

Number of patients	941
Age (years), median (IQR)	61 (52–69)
Females, n (%)	182 (19.3)
Diabetes mellitus, n (%)	184 (19.6)
Hypertension, n (%)	682 (72.5)
Previous or active smoking, n (%)	488 (51.9)
Family history of CAD or stroke, n (%)	281 (29.9)
History of previous MI, n (%)	90 (9.6)
COPD, n (%)	39 (4.1)
CK max (U/l), median (IQR)	1,302 (647–2,465)
LVEF (%), median (IQR)	53 (45–60)
BMI (kg/m^2), median (IQR)	27 (24–29)
Serum creatinine (md/dl), median (IQR)	1.1 (0.9–1.3)
$eGFR_{(MDRD)} \leq 60$ SI units	201 (21.4)
Cardiogenic shock/CPR, n (%)	41 (4.4)
Intervention	
PCI, n (%)	878 (93.3)
Thrombolysis, n (%)	14 (1.5)
CABG, n (%)	6 (0.6)
Aspirin, n (%)	913 (97.0)
Betablockers, n (%)	897 (95.3)
ACE-inhibitors, n (%)	885 (94.0)
Statins, n (%)	879 (93.4)
Diuretics, n (%)	415 (44.1)

ACE, angiotensine converting enzyme; BMI, body mass index; CAD, coronary artery disease; CABG, coronary artery bypass graft; COPD, chronic obstructive pulmonary disease; CK, serum creatine kinase; CPR, cardiopulmonary resuscitation; eGFR, estimating glomerular filtration rate; IQR, interquartile range; LVEF, left ventricular ejection fraction; MI, myocardial infarction; PCI, percutaneous coronary intervention.

The incidence of mortality in the Polyscore strata was gradually increasing from the low-risk stratum 0 to the high-risk stratum 7. The numbers of patients who died during follow-up in the individual Polyscore strata 0 to 7 were 4 (1.7%), 6 (2.3%), 6 (3.3%), 15 (11.3%), 19 (22.1%), 11 (45.8%), 5 (55.6%), and 6 (85.7%).

Figure 2 shows the contribution of separate risk factors to the individual Polyscore categories. Three groups of risk factors can be distinguished. While the absence of abnormalities in BRS, respiration frequency, and ETA tends to signify overall low risk, the abnormalities in turbulence slope and PESP tend to indicate high risk. These are complemented by DC and ectopic frequency that gradually appear more frequently with increasing Polyscore strata.

This distinction between low-risk and high-risk sub-strata was reflected in the development of univariable hazard ratios of individual Polyscore categories. **Figure 3** shows that from Polyscore stratum 1 to stratum 7, the hazard ratios (in comparison to Polyscore stratum 0) increased almost exponentially, $p < 0.0001$, Wald = 127 (note the logarithmic scale of the vertical axis of the figure). This allowed to select Polyscore dichotomies separated by similar hazard ratio increases. Specifically, hazard ratio of Polyscore 3 (vs. Polyscore 0) was close to 6 (exactly 7.027). Another 6-times hazard increase (to hazard ratio of $6^2 = 36$) was very close to the hazard ratio of Polyscore 5 (exactly 35.71; still vs. Polyscore 0). We have therefore dichotomised Polyscore at ≤ 2 to define a low-risk group, and at ≥ 5 to define a high-risk group. Patients with Polyscore categories 3 and 4 constituted an intermediate risk group.

Kaplan–Meier survival curves of these risk categories are shown in **Figure 4**. The figure shows that the probabilities of death were clearly separated between the low, intermediate, and high-risk groups. This is not surprising since our selection of the sub-groups based on the results shown in **Figure 3** made the differences between these sub-groups positively biased. Hence, although we also calculated the statistical comparison of the Kaplan–Meier curves ($p < 0.0001$, $\chi^2 = 220$) the biased nature of this test needs to be pointed out.

The univariable and multivariable Cox models comparing the predictive power of Polyscore in comparison with LVEF, presence of diabetes mellitus, and GRACE score are shown in **Tables 2**, **3**. In both the non-dichotomized and dichotomized versions of the Cox models, the Polyscore led to the largest χ^2 values and to the largest hazard ratios. In particular, while the Polyscore is predominantly related to the assessment of cardiac autonomic status, the risk prediction by Polyscore was independent of and stronger than that by the presence of diabetes mellitus which is a known source of autonomopathies in cardiac patients (Barthel et al., 2011; May et al., 2018; Yang et al., 2018). This was confirmed by the comparisons of Kaplan–Meier survival curves of dichotomized Polyscrore risk categories in patients with and without diabetes mellitus as shown in **Figure 5**.

DISCUSSION

The study shows that a combination of different non-invasive risk predictors can be combined into a powerful Polyscore that, at least in the data of the present investigation, outperforms other previously established risk stratification techniques. The success of the Polyscore is most likely related to its multifactorial nature. The constituent risk factors characterize different facets at different scales of cardiovascular as well as other regulation and control. Whilst some of these factors are related to the autonomic control of the sinus nodal periodicity, others quantify respiration and its influence on the autonomic (mainly vagal) reflexes, blood pressure regulation, and vascular responsiveness.

The vast majority of previous studies of post-AMI risk stratification were based on HRV and other related autonomic indices and utilized long-term recordings of nominal 24-h duration (Kleiger et al., 1987; Farrell et al., 1991). Such a prolonged period of recording allowed studying not only the day-night differences but also to quantify the autonomic responsiveness of the organism to different environmental stimuli and challenges. For these reasons, it was necessary to reasonably standardize the recording conditions which led to the need of recording the AMI survivors before hospital discharge (Mäkikallio et al., 2005). In truly ambulatory conditions, the differences in the surrounding inputs and activity of different patients resulted in far too substantial inter-subject variability of autonomic measurements (Yoshizaki et al., 2013) which prevented meaningful definitions of low- and high-risk

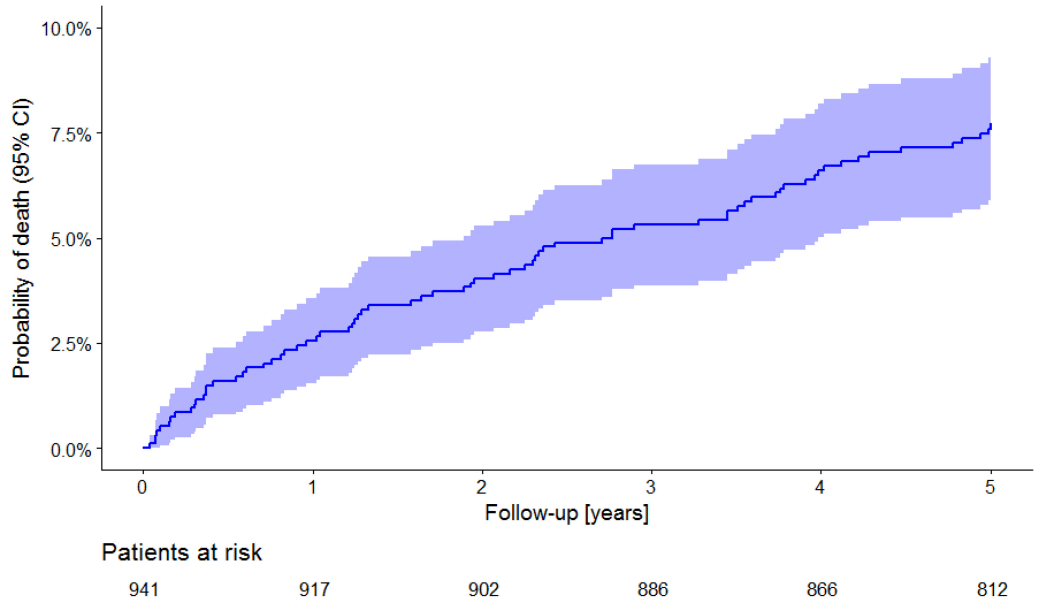

FIGURE 1 | All-cause mortality in the study population. The Kaplan–Meier curve of probability of death is shown together with its 95% confidence intervals. Numbers of patients at risk are shown below the time axis.

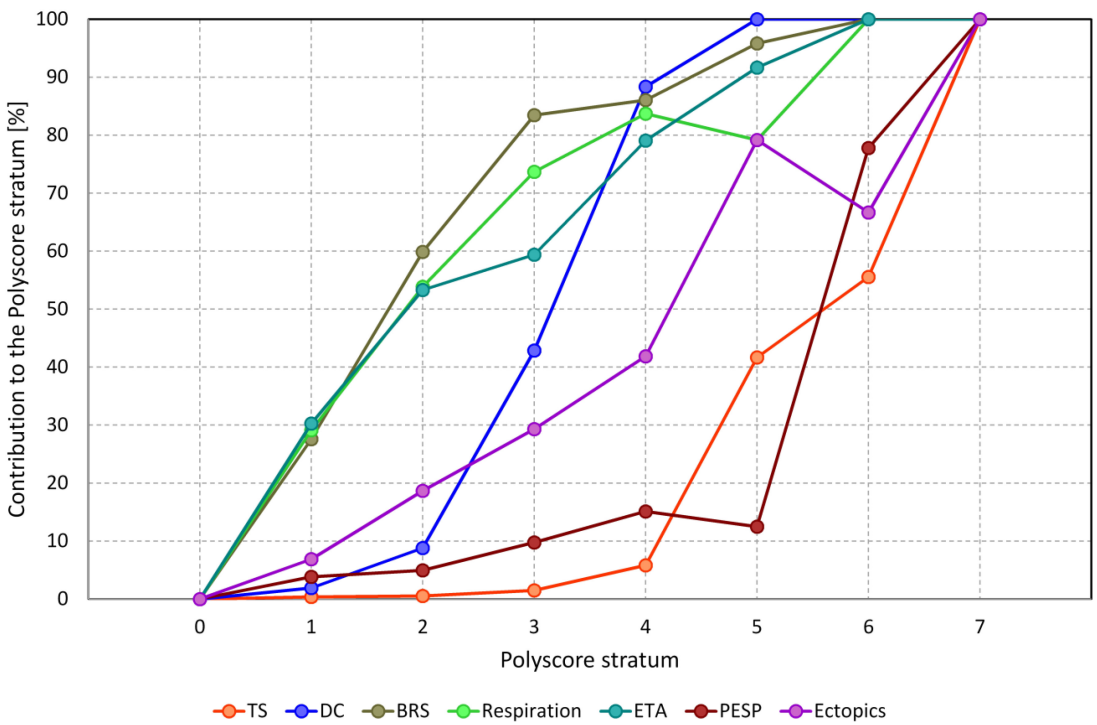

FIGURE 2 | Contribution of individual elements of Polyscore to different Polyscore strata. For each stratum of Polyscore and for each individual risk factor, the graph shows the percentage of patients of the given Polyscore strata in whom this risk factor was positive. Note that the different contribution profiles allow approximate distinction of three groups of risk factors with BRS, respiration frequency, and ETA being more sensitive; TS and PESP being more specific; and DC and ectopic frequency in-between (see the text for further details). TS, turbulence slope; DC, deceleration capacity; BRS, baroreflex sensitivity; Respiration, average respiration frequency; ETA, expiration triggered sinus arrhythmia; PEST, post-ectopic systolic blood pressure potentiation; Ectopics, frequency of ventricular or supraventricular ectopic beats.

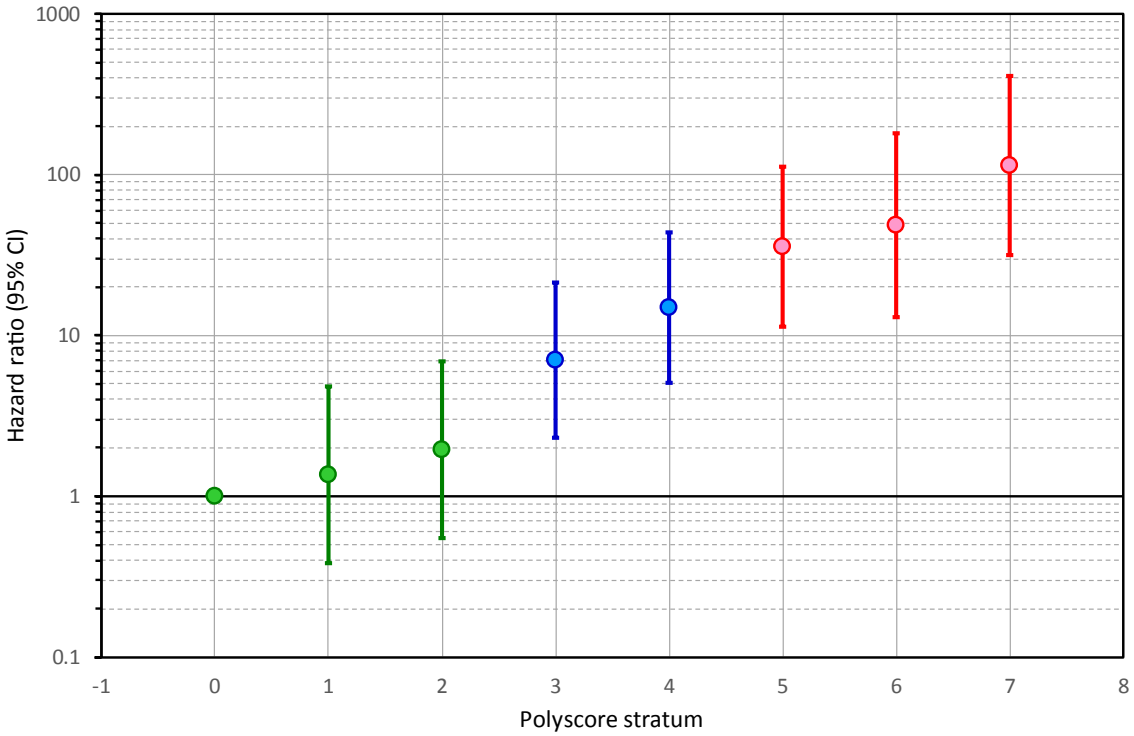

FIGURE 3 | Hazard ratios of individual Polyscore strata. For each stratum 1, 2, . . ., 7, the figure shows the result of a univariable Cox regression model comparing the stratum with the lowest-risk stratum of Polyscore 0. The Hazard ratios are shown together with their 95% confidence intervals. Note the logarithmic scale of the vertical axis. Note also that the development of the hazard ratios allows defining a low-risk group of Polyscore ≤ 2 (shown in green), an intermediate risk group of Polyscore 3 or 4 (shown in blue), and a high-risk group of Polyscore ≥ 5 (shown in red). CI, confidence interval.

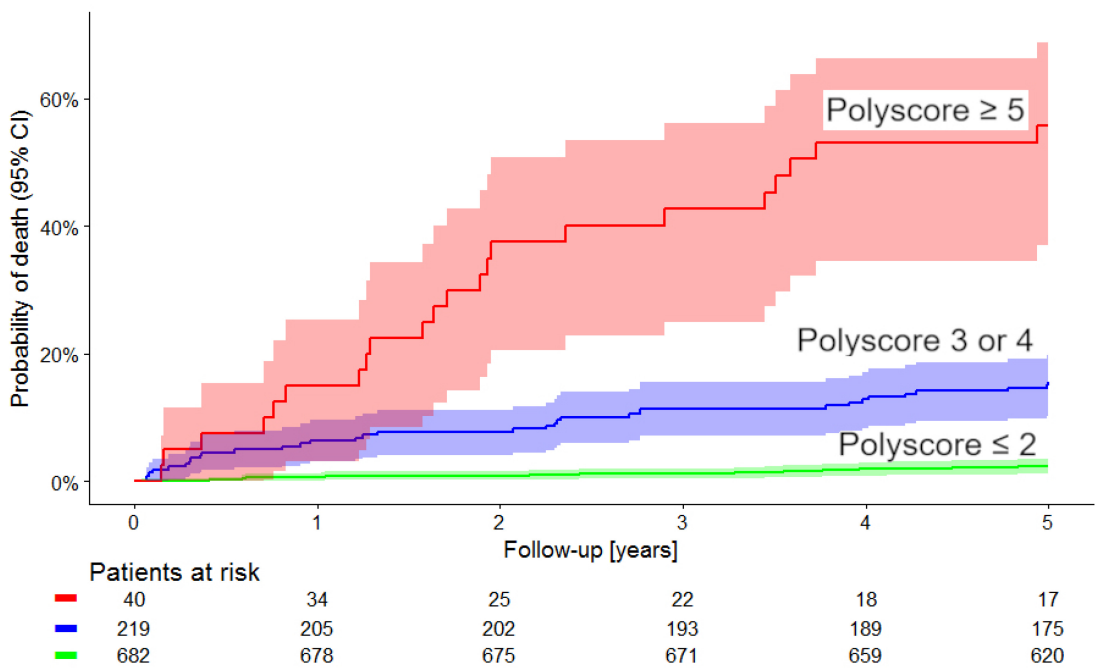

FIGURE 4 | Comparison of Kaplan–Meier probabilities of death in the population sub-groups defined by Polyscore ≤ 2 (green), Polyscore 3 or 4 (blue) and Polyscore ≥ 5 (red). Albeit positively biased (see the text for details) the difference between the probabilities of death in these groups was statistically significant ($p < 0.0001$, $\chi^2 = 220$). Numbers of patients at risk in the individual sub-groups are shown below the time axis.

TABLE 2 | Cox regression model using non-dichotomised variables.

Variable	Univariable model			Multivariable model		
	HR	χ^2	*p*	HR	χ^2	*p*
LVEF (%)	0.96 (0.94 – 0.97)	24.2	<0.0001	0.99 (0.98 – 1.01)	0.5	0.473
Diabetes (yes/no)	2.78 (1.73 – 4.47)	17.9	<0.0001	1.60 (0.99 – 2.60)	3.7	0.473
GRACE score	1.04 (1.03 – 1.05)	65.0	<0.0001	1.02 (1.01 – 1.03)	13.3	<0.0001
Polyscore	2.12 (1.86 – 2.41)	127.1	<0.0001	1.78 (1.53 – 2.07)	55.9	<0.0001

HR, hazard ratio shown together with 95% confidence interval; LVEF, left ventricular ejection fraction.

TABLE 3 | Cox regression model using dichotomised variables.

Variable	Univariable model			Multivariable model		
	HR	χ^2	*p*	HR	χ^2	p
LVEF $\geq$ 35%	4.29 (2.56 – 7.19)	30.6	<0.0001	1.72 (1.00 – 2.96)	3.8	0.050
Diabetes (yes/no)	2.78 (1.73 – 4.47)	17.9	<0.0001	1.73 (1.06 – 2.80)	4.9	0.027
GRACE score $\geq$ 120	5.82 (3.41 – 9.92)	41.9	<0.0001	2.62 (1.47 – 4.66)	10.8	0.001
Polyscore $\geq$ 5	35.71 (11.36 – 112.24)	113.2	<0.0001	15.65 (7.62 – 32.17)	56.0	<0.0001

HR, hazard ratio shown together with 95% confidence interval; LVEF, left ventricular ejection fraction.

subgroups. Subsequently, it became recognized that the necessity of prolonged monitoring of in-patients is a healthcare burden that negatively impacted on the practical utility of HRV and of some associated autonomic risk indicators (Huikuri et al., 2017). This contrasts with the design of the study that provided the data analyzed here. The Polyscore is based on indices derived from controlled 30-min recordings in undisturbed supine position. Thus, little effects of external challenges are involved and the Polyscore reflects the conditions of intra-organism homeostasis control. The limit of 30 min also makes the Polyscore assessment procedures practical for studies in different populations including those of out-patients.

As shown in **Figure 2**, there are differences in the performance of the risk factors that constitute the Polyscore. Although all the contributing risk factors (apart from ectopic frequency) quantify autonomic reflexes and control mechanisms, their different scales and control reflexes allow to combine factors that are differently sensitive to the mortality risk. Consequently, the Polyscore allows definition of both low-risk and high-risk subpopulations that differ very substantially in their outcomes.

Combination of different risk factors including autonomic indices is not entirely new and other possible combinations have previously been attempted. Among others, the DINAMIT study selected patients with reduced LVEF, increased heart rate, and reduced 24-h HRV (Hohnloser et al., 2004). Similar to other studies (Arisha et al., 2013), the design of the REFINE-ICD trial (Perkiömäki et al., 2015) included the combination of abnormal HRT and of T wave alternans (TWA). Our teams have previously showed improved risk stratification based on the combination of HRT and DC (Bauer et al., 2009). Nevertheless, in these and other similar approaches, the number of combined autonomic indices was small, and studies aimed at improving high-risk group predictions rather than developing a system classifying the patients into different risk strata. This possibility of defining separate groups with gradually increasing risk is an obvious advantage of the Polyscore concept. Purposefully, we have therefore selected two dichotomy limits of $\leq$2 and $\geq$5 points of Polyscore since a selection of a singular limit cannot meaningfully define both very low- and very high-risk groups.

Whilst the source data of the study were collected already during the previous decade, the population clinical characteristics shown in **Table 1** demonstrate that the patients received treatment consistent with present standards. Among others, more than 90% of the patients were treated by acute coronary intervention. Similarly, the vast majority received beta-blockers, ACE-inhibitors, aspirin, and statins. The source data thus correspond to the contemporary clinical standards which makes the Polyscore ready for prospective applications.

The strength of the Polyscore in the Cox regression analysis was undoubtedly contributed by the retrospective nature of the study and by using previously optimized dichotomies of the individual constituents. Nevertheless, the gradual increase of the hazard ratios associated with individual Polyscore categories proves the credibility of the concept. Naturally, all retrospective studies are mainly hypothesis generating but the strengths of the Polyscore make it a strong candidate for future prospective testing both in post-AMI patients and in other clinically well-defined clinical populations. The practicality of the Polyscore that we already discussed makes it also suitable for cardiac risk screening in general population especially if a system is set-up allowing computerized evaluation of the individual tests that constitute the Polyscore with no or minimum manual intervention.

Limitations

Several limitations of our data and of the composite of the Polyscore need to be considered. On purpose, we have

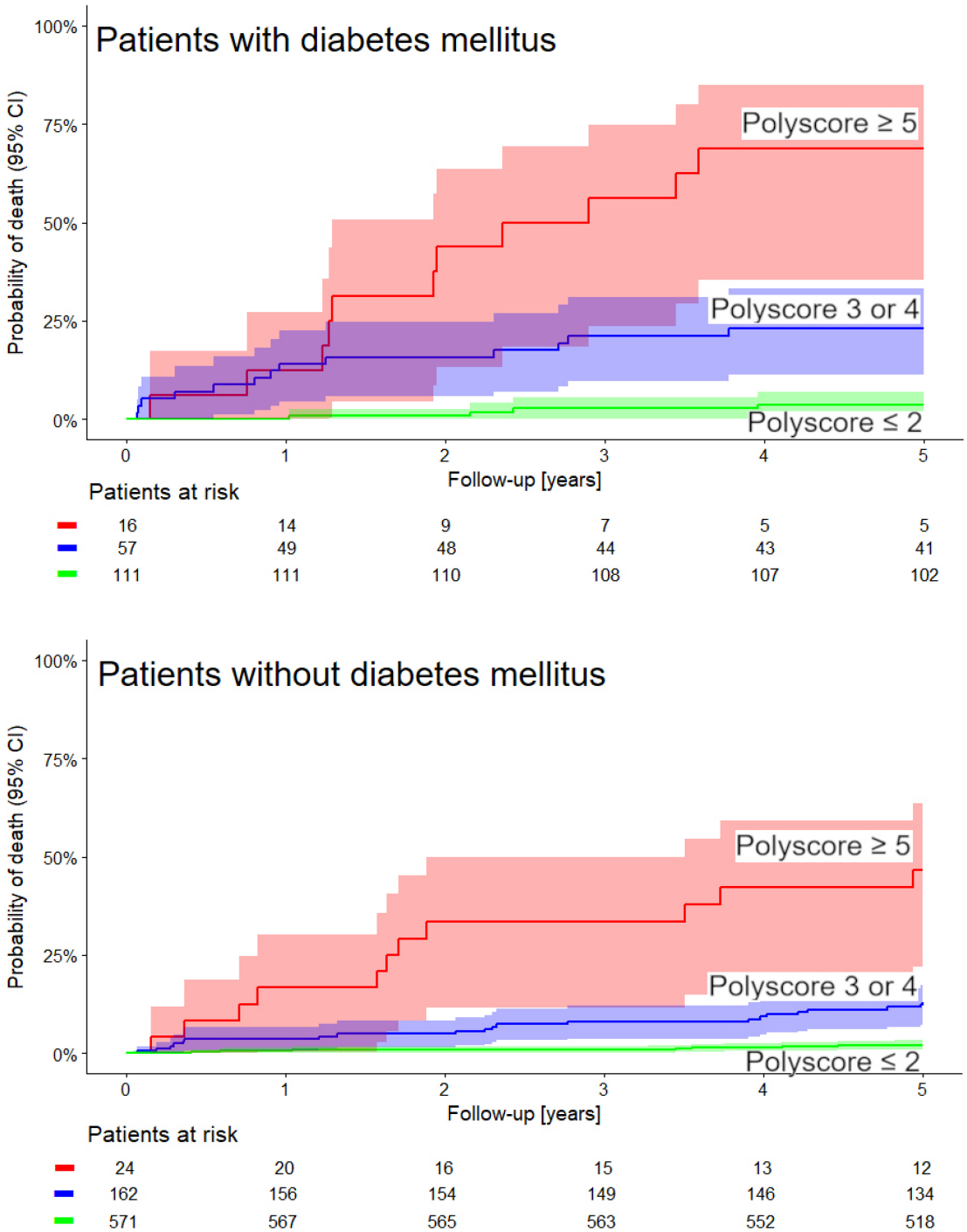

FIGURE 5 | The same comparison of Kaplan–Meier probabilities of death as shown in **Figure 4** repeated separately for patients with the diagnosis of diabetes mellitus (top panel) and for patients without the diagnosis of diabetes mellitus (bottom panel). In both cases, the differences between the probabilities of death in these groups was statistically significant ($\chi^2 = 59$ and $\chi^2 = 123$, respectively, both $p < 0.0001$). Numbers of patients at risk in the individual sub-groups are shown below the time axes.

restricted the Polyscore mainly to autonomic indices that have been previously investigated. Factors of myocardial repolarization abnormality such as TWA, QT interval variability (Baumert et al., 2016), or spatial QRS-T angle (Hnatkova et al., 2018) might also be combined with other risk indices including the autonomic abnormalities. We can only

speculate that the gradual increase of risk in the Polyscore categories would be only marginally improved by adding further factors. The individual risk factors that we combined contributed to the Polyscore equally. It would be possible to optimize their contributions further (e.g., by means of a Cox model) and/or to consider continuous scales of individual Polyscore components. Nevertheless, that would further deepen the retrospective nature of the study. We used all-cause mortality as the primary outcome variable. Other outcomes such as cardiac mortality, reinfarction, stroke, etc., might also be considered in future studies. Since the source population was obtained from a study in AMI survivors, we are unable to comment directly on the strength of the Polyscore in different populations. Nevertheless, because of the general nature of autonomic-related risk predictors, we believe that the concept would be equally applicable to other clinical settings. Intentionally, we restricted the multivariable Cox models to the Polyscore and only three other strong risk factors. Other factors available in the source population and not incorporated in the GRACE score might have also been added (e.g., body mass index, marital/spousal status, post-AMI hypotension). Nevertheless, this might have led to the regression models being overfitted. Finally, since the source population was recorded already during the previous decade, the follow-up period might have been extended, although this might have also weakened the association of the risk factors with the outcome. The mortality probabilities compared over 5 years demonstrate the strength of the Polyscore sufficiently.

CONCLUSION AND FUTURE DIRECTIONS

The newly designed Polyscore categorized AMI survivors into strata with almost exponential step-wise increases in the hazard of death during 5-year follow-up. The study also showed that all the individual constituents of the Polyscore contribute meaningfully to the combination. The individual constituent risk factors are also based on well documented physiologic role of autonomic regulation and homeostasis control. The Polyscore can therefore be proposed for prospective validation in future independent data collections.

AUTHOR CONTRIBUTIONS

PB, AS, MD, DS, and KMH collected the data experiments. PB, AM, and AS contributed to patient follow-up and study database. GS, PB, and MM conceived and designed the study. AM, PB, MM, GS, KMH, and AH analyzed the data. AS, AM, PB, MD, GS, KH, MM, and AH prepared the manuscript. MM, GS, KH, and KMH controlled and finally approved the manuscript.

FUNDING

This work was supported in part by the British Heart Foundation New Horizons Grant NH/16/2/32499.

REFERENCES

Al-Khatib, S. M., Stevenson, W. G., Ackerman, M. J., Bryant, W. J., Callans, D. J., Curtis, A. B., et al. (2018). 2017AHA/ACC/HRS guideline for management of patients with ventricular arrhythmias and the prevention of sudden cardiac death: a report of the american college of cardiology/american heart association task force on clinical practice guidelines and the heart rhythm society. *J. Am. Coll. Cardiol.* 2018, e91–e220. doi: 10.1016/j.jacc.2017.10.054

Arisha, M. M., Girerd, N., Chauveau, S., Bresson, D., Scridon, A., Bonnefoy, E., et al. (2013). In-hospital heart rate turbulence and microvolt T-wave alternans abnormalities for prediction of early life-threatening ventricular arrhythmia after acute myocardial infarction. *Ann. Noninvasive Electrocardiol.* 18, 530–537. doi: 10.1111/anec.12072

Barthel, P., Bauer, A., Müller, A., Huster, K. M., Kanters, J. K., Paruchuri, V., et al. (2012). Spontaneous baroreflex sensitivity: prospective validation trial of a novel technique in survivors of acute myocardial infarction. *Heart Rhythm* 9, 1288–1294. doi: 10.1016/j.hrthm.2012.04.017

Barthel, P., Bauer, A., Müller, A., Junk, N., Huster, K. M., Ulm, K., et al. (2011). Reflex and tonic autonomic markers for risk stratification in patients with type 2 diabetes surviving acute myocardial infarction. *Diabetes Care* 34, 1833–1837. doi: 10.2337/dc11-0330

Barthel, P., Wensel, R., Bauer, A., Müller, A., Wolf, P., Ulm, K., et al. (2013). Respiratory rate predicts outcome after acute myocardial infarction: a prospective cohort study. *Eur. Heart J.* 34, 1644–1650. doi: 10.1093/eurheartj/ehs420

Bauer, A., Barthel, P., Schneider, R., Ulm, K., Müller, A., Joeinig, A., et al. (2009). Improved stratification of autonomic regulation for risk prediction in post-infarction patients with preserved left ventricular function (ISAR-Risk). *Eur. Heart J.* 30, 576–583. doi: 10.1093/eurheartj/ehn540

Bauer, A., Kantelhardt, J. W., Barthel, P., Schneider, R., Mäkikallio, T., Ulm, K., et al. (2006). Deceleration capacity of heart rate as a predictor of mortality after myocardial infarction: cohort study. *Lancet* 367, 1674–1681. doi: 10.1016/S0140-6736(06)68735-7

Bauer, A., Malik, M., Schmidt, G., Barthel, P., Bonnemeier, H., Cygankiewicz, I., et al. (2008). Heart rate turbulence: standards of measurement, physiological interpretation, and clinical use: international society for holter and noninvasive electrophysiology consensus. *J. Am. Coll. Cardiol.* 52, 1353–1365. doi: 10.1016/j.jacc.2008.07.041

Baumert, M., Porta, A., Vos, M. A., Malik, M., Couderc, J. P., Laguna, P., et al. (2016). QT interval variability in body surface ECG: measurement, physiological basis, and clinical value: position statement and consensus guidance endorsed by the european heart rhythm association jointly with the esc working group on cardiac cellular electrophysiology. *Europace* 18, 925–944. doi: 10.1093/europace/euv405

Buxton, A. E., Marchlinski, F. E., Waxman, H. L., Flores, B. T., Cassidy, D. M., and Josephson, M. E. (1984). Prognostic factors in nonsustained ventricular tachycardia. *Am. J. Cardiol.* 53, 1275–1279. doi: 10.1016/0002-9149(84)90078-X

Dagres, N., and Hindricks, G. (2013). Risk stratification after myocardial infarction: is left ventricular ejection fraction enough to prevent sudden cardiac death? *Eur. Heart J.* 34, 1964–1971. doi: 10.1093/eurheartj/eht109

Eagle, K. A., Lim, M. J., Dabbous, O. H., Pieper, K. S., Goldberg, R. J., Van de Werf, F., et al. (2004). A validated prediction model for all forms of acute coronary syndrome: estimating the risk of 6-month postdischarge death in an international registry. *JAMA* 291, 2727–2733. doi: 10.1001/jama.291.22.2727

Farrell, T. G., Bashir, Y., Cripps, T., Malik, M., Poloniecki, J., Bennett, E. D., et al. (1991). Risk stratification for arrhythmic events in postinfarction patients based on heart rate variability, ambulatory electrocardiographic variables and the signal-averaged electrocardiogram. *J. Am. Coll. Cardiol.* 18, 687–697. doi: 10.1016/0735-1097(91)90791-7

Hnatkova, K., Seegers, J., Barthel, P., Novotny, T., Smetana, P., Zabel, M., et al. (2018). Clinical value of different QRS-T angle expressions. *Europace* 20, 1352–1361. doi: 10.1093/europace/eux246

Hohnloser, S. H., Kuck, K. H., Dorian, P., Roberts, R. S., Hampton, J. R., Hatala, R., et al. (2004). Prophylactic use of an implantable cardioverter-defibrillator after acute myocardial infarction. *N. Engl. J. Med.* 351, 2481–2488. doi: 10.1056/NEJMoa041489

Huikuri, H. V., Zabel, M., Lombardi, F., and Malik, M. (2017). Measurement of cardiovascular autonomic function: Where to go from here? *Int. J. Cardiol.* 249, 73–74. doi: 10.1016/j.ijcard.2017.08.076

Josephson, M. E., Simson, M. B., Harken, A. H., Horowitz, L. N., and Falcone, R. A. (1982). The incidence and clinical significance of epicardial late potentials in patients with recurrent sustained ventricular tachycardia and coronary artery disease. *Circulation* 66, 1199–1204. doi: 10.1161/01.CIR.66.6.1199

Kleiger, R. E., Miller, J. P., Bigger, J. T. Jr., and Moss, A. J. (1987). Decreased heart rate variability and its association with increased mortality after acute myocardial infarction. *Am. J. Cardiol.* 59, 256–262. doi: 10.1016/0002-9149(87)90795-8

Køber, L., Thune, J. J., Nielsen, J. C., Haarbo, J., Videbæk, L., Korup, E., et al. (2016). Defibrillator implantation in patients with nonischemic systolic heart failure. *N. Engl. J. Med.* 375, 1221–1230. doi: 10.1056/NEJMoa1608029

Mäkikallio, T. H., Barthel, P., Schneider, R., Bauer, A., Tapanainen, J. M., Tulppo, M. P., et al. (2005). Prediction of sudden cardiac death after acute myocardial infarction: role of holter monitoring in the modern treatment era. *Eur. Heart J.* 26, 762–769. doi: 10.1093/eurheartj/ehi188

May, O., Graversen, C. B., Johansen, M. Ø, and Arildsen, H. (2018). The prognostic value of the frontal QRS-T angle is comparable to cardiovascular autonomic neuropathy regarding long-term mortality in people with diabetes. a population based study. *Diabetes Res. Clin. Pract.* 142, 264–268. doi: 10.1016/j.diabres.2018.05.018

Moss, A. J., Davis, H. T., DeCamilla, J., and Bayer, L. W. (1979). Ventricular ectopic beats and their relation to sudden and nonsudden cardiac death after myocardial infarction. *Circulation* 60, 998–1003. doi: 10.1161/01.CIR.60.5.998

Perkiömäki, J., Exner, D. V., Piira, O. P., Kavanagh, K., Lepojärvi, S., Talajic, M., et al. (2015). Heart rate turbulence and T-wave alternans in patients with coronary artery disease: the influence of diabetes. *Ann. Noninvasive Electrocardiol.* 20, 481–487. doi: 10.1111/anec.12244

R Core Team (2018)). *R: A language and environment for statistical computing*. Vienna: R Foundation for Statistical Computing.

Schmidt, G., Malik, M., Barthel, P., Schneider, R., Ulm, K., Rolnitzky, L., et al. (1999). Heart-rate turbulence after ventricular premature beats as a predictor of mortality after acute myocardial infarction. *Lancet* 353, 1390–1396. doi: 10.1016/S0140-6736(98)08428-1

Sinnecker, D., Dirschinger, R. J., Barthel, P., Müller, A., Morley-Davies, A., Hapfelmeier, A., et al. (2014). Postextrasystolic blood pressure potentiation predicts poor outcome of cardiac patients. *J. Am. Heart Assoc.* 3, e000857. doi: 10.1161/JAHA.114.000857

Sinnecker, D., Dommasch, M., Steger, A., Berkefeld, A., Hoppmann, P., Müller, A., et al. (2016). Expiration-triggered sinus arrhythmia predicts outcome in survivors of acute myocardial infarction. *J. Am. Coll. Cardiol.* 67, 2213–2220. doi: 10.1016/j.jacc.2016.03.484

Therneau, T. M. (2018). *A Package for Survival Analysis in S*. https://CRAN.R-project.org/package=survival

Wellens, H. J., Schwartz, P. J., Lindemans, F. W., Buxton, A. E., Goldberger, J. J., Hohnloser, S. H., et al. (2014). Risk stratification for sudden cardiac death: current status and challenges for the future. *Eur. Heart J.* 35, 1642–1651. doi: 10.1093/eurheartj/ehu176

Yang, Y., Lee, E. Y., Cho, J. H., Park, Y. M., Ko, S. H., Yoon, K. H., et al. (2018). Cardiovascular autonomic neuropathy predicts higher HbA1c variability in subjects with type 2 diabetes mellitus. *Diabetes Metab. J.* 42, 496–512. doi: 10.4093/dmj.2018.0026

Yoshizaki, T., Kawano, Y., Tada, Y., Hida, A., Midorikawa, T., Hasegawa, K., et al. (2013). Diurnal 24-hour rhythm in ambulatory heart rate variability during the day shift in rotating shift workers. *J. Biol. Rhythms* 28, 227–236. doi: 10.1177/0748730413489957

Conflict of Interest Statement: GS owns patents on Heart rate turbulence and on Deceleration capacity.

The remaining authors declare that the research was conducted in the absence of any commercial or financial relationships that could be construed as a potential conflict of interest.

frontiers in Physiology

SYSTEMATIC REVIEW
published: 19 February 2019
doi: 10.3389/fphys.2019.00103

Meta-Analysis of Risk Stratification of SCN5A With Brugada Syndrome: Is SCN5A Always a Marker of Low Risk?

Yihan Yang[1,2†], Dan Hu[3†], Frederic Sacher[4], Kengo F. Kusano[5], Xinye Li[1,2], Hector Barajas-Martinez[6], Mélèze Hocini[4], Yanda Li[1], Yonghong Gao[7], Hongcai Shang[7] and Yanwei Xing[1*]*

[1] Guang'anmen Hospital, Chinese Academy of Chinese Medical Sciences, Beijing, China, [2] Beijing University of Chinese Medicine, Beijing, China, [3] Department of Cardiology and Cardiovascular Research Institution, Renmin Hospital of Wuhan University, Wuhan, China, [4] Hôpital Cardiologique Haut Lévêque, Lyric institute, Université de Bordeaux, Bordeaux-Pessac, France, [5] Division of Arrhythmia and Electrophysiology, Department of Cardiovascular Medicine, National Cerebral and Cardiovascular Center, Osaka, Japan, [6] Global Genetics Corp, Ventura, CA, United States, [7] Key Laboratory of Chinese Internal Medicine of the Ministry of Education, Dongzhimen Hospital Affiliated to Beijing University of Chinese Medicine, Beijing, China

OPEN ACCESS

Edited by:
Federico Lombardi,
University of Milan, Italy

Reviewed by:
Morten Salling Olesen,
Rigshospitalet, Denmark
Gary Tse,
The Chinese University of Hong Kong, China

***Correspondence:**
Hongcai Shang
shanghongcai@126.com
Yanwei Xing
xingyanwei12345@163.com

[†] These authors have contributed equally to this work

Specialty section:
This article was submitted to Cardiac Electrophysiology, a section of the journal Frontiers in Physiology

Received: 09 November 2018
Accepted: 28 January 2019
Published: 19 February 2019

Citation:
Yang Y, Hu D, Sacher F, Kusano KF, Li X, Barajas-Martinez H, Hocini M, Li Y, Gao Y, Shang H and Xing Y (2019) Meta-Analysis of Risk Stratification of SCN5A With Brugada Syndrome: Is SCN5A Always a Marker of Low Risk? Front. Physiol. 10:103. doi: 10.3389/fphys.2019.00103

Background: *SCN5A* with Brugada syndrome (BrS) is not commonly considered as an independent risk marker for subsequent cardiac events. However, the risk of *SCN5A* combined with other clinical characteristics has not been fully investigated.

Objectives: The aim of this study is to investigate and evaluate risk stratification and related risk factors of *SCN5A* in BrS.

Methods: The databases of PubMed, EMBASE, Cochrane Library, MEDLINE, Chinese National Knowledge Infrastructure (CNKI) and Wanfang Data were searched for related studies published from January 2002 to May 2018 followed by meta-analysis. The BrS patients who underwent *SCN5A* gene tests were included. The prognosis and risk stratification of *SCN5A* combined with symptoms and asymptoms diagnosis in BrS, electrophysiology study (EPS) were then investigated and evaluated. Outcomes were defined as ventricular tachycardia/fibrillation (VT/VF), sudden cardiac death (SCD).

Results: Eleven suitable studies involving 1892 BrS patients who underwent *SCN5A* gene tests were identified. *SCN5A* (+) was not considered to be a significant predictor of future cardiac events (95% CI: 0.89–2.11; $P = 0.15$; $I^2 = 0\%$). However, *SCN5A* (+) patients with symptoms at diagnosis revealed a higher prevalence of future VT/VF, SCD compared to *SCN5A* (–) patients with symptoms at diagnosis. (95% CI: 1.06–3.70; $P = 0.03$ $I^2 = 0\%$) Among asymptomatic patients, the risk did not significantly differ between *SCN5A* (+) patients and *SCN5A* (–) patients. (95% CI: 0.51–4.72; $P = 0.45$ $I^2 = 0$ %). In an investigation involving patients in EPS (–) BrS electrocardiogram (ECG), the risk of *SCN5A* (+) is higher than that of *SCN5A* (–) ($P < 0.001$).

Conclusions: In BrS patients with symptoms at diagnosis or EPS (–), the meta-analysis suggests that *SCN5A* (+) are at a higher risk of arrhythmic events than *SCN5A* (–).

Keywords: *SCN5A*, brugada syndrome, electrophysiology study, arrhythmia, sudden cardiac death

INTRODUCTION

BrS is an inheritable arrhythmogenic syndrome in a structurally integrated heart. According to current guidelines, it is the features of an ST segment elevation in the precordial leads which is related to improved danger of SCD (Priori et al., 2013). *SCN5A* gene mutation, as a risk factor for BrS, its prognostic significance in the general population remains controversial. On one hand, the present guideline shows that *SCN5A* mutation status cannot be an independent predictor of future cardiac events (Priori et al., 2013). On the other hand, BrS patients with *SCN5A*-mediated have higher prevalence of incidences of bradyarrhythmia events and conduction abnormalities (Yamagata et al., 2017). Recently, an important study particularly reported that *SCN5A* was the only gene which is clinically associated with BrS among the 21 included genes (Hosseini et al., 2018). Therefore, we initially preformed a comprehensive systematic review and meta-analysis of published data to elucidate the effect on mutations in *SCN5A* with symptoms and EPS, among the patients with BrS.

METHODS

Search Strategy and Inclusion Criteria

A comprehensive literature research on MEDLINE, Embase, CNKI, and Wanfang Data databases was performed by two investigators. We used the query terms "Brugada syndrome" and "*SCN5A* Mutation" to identify and retrieve all potentially relevant studies from January 2002 to May 2018. Only full-size English articles published in peer-reviewed journals were considered for this meta-analysis. Studies were considered to be suitable whether they met the following criteria:

(a) the study was a prospective or retrospective observational study;
(b) inclusion of subjects with BrS were as previously defined;
(c) inclusion of patients who underwent *SCN5A* gene tests;
(d) the follow- up duration was long enough that the arrhythmia events would be observed;
(e) endpoint events [appropriate implantable cardioverter-defibrillator therapy (ICD), VF/VT, and SCD] were clearly defined;
(f) patients with endpoint events were clearly identified if they had *SCN5A* mutations;
(g) risk ratio (RR), hazard ratio (HR), odds ratio (OR), corresponding 95% confidence intervals (CIs), or necessary original data were presented.

In addition, we also contacted several corresponding authors of the studies to obtain more specific experimental data which were not included in the articles. Studies which demonstrated on only compound endpoints but particular data on all-cause mortality or different patient groups were not taken into account. In order to resolve the disagreements or uncertainties between the two investigators, a third investigator was responsible for rechecking the source data and consultation.

Data Extraction

The elements of the extracted data were included in the meta-analysis: (a) publication information: surname of first author, publication year, and location; (b) type of study: multi-center or single-center study; (c) study design; (d) follow-up duration; (f) endpoint events (arrhythmic events were defined as VT/VF, SCD, and the combination of those two during the follow-up); (g) the quality score; (h) the characteristics of the population comprising sample size, gender, age, number of subjects with and without cardiac events, number of subjects with history of sudden cardiac arrest (SCA), syncope and family history of SCD. It also included the number of subjects with ICD, number of subjects with spontaneous type 1 ECG, and non-spontaneous type 1 ECG, number of symptomatic subjects with spontaneous type 1 ECG and non-spontaneous type 1 ECG, number of subjects who underwent EPS, the number of subject with EPS positive and EPS negative, number of EPS positive subjects who underwent ex-stimulation from 1 to 3 times, number of subjects with atrial fibrillation (AF) positive, number of subjects who underwent *SCN5A* gene test, number of subjects with *SCN5A* positive and *SCN5A* negative, number of symptomatic subjects with *SCN5A* positive and *SCN5A* negative during follow-up, number of subjects with Fragmented QRS (f-QRS) positive and f-QRS negative, number of subjects with early repolarization (ER) positive and ER negative; (i) among *SCN5A* (+) subjects with future cardiac events, the number of male subjects and female subjects, the number of subjects with or without family history of SCD, spontaneous type 1 ECG, symptoms and documented AF; (j) among *SCN5A* (–) subjects with future cardiac events, the number of male subjects and female subjects, the number of subjects with or without family history of SCD, spontaneous type 1 ECG, and symptoms and documented AF.

Quality Assessment

The Methodological Index for Non-Randomized Studies (MINORS) was applied used for the Methodological quality to assess all studies. The use of maximum 24 points (each item scored from 0 to 2) was based on the following aspects: aim of the study, inclusion of consecutive patients, prospective data collection, appropriate endpoint to the aim of the study, unbiased evaluation of endpoints, follow-up period appropriate to the end-point, loss to follow-up no more than 5%, comparable control group, contemporary groups, base-line equivalence of groups, prospective calculation of the sample size, and use of adequate statistical analysis. After two independent investigators valued the included publications, the mean MINORS score was assessed as the final result. Studies were considered to be of low quality and high quality according to their MINORS scores of <16 and ≥ 16 points, respectively (Slim et al., 2003).

Statistical Analysis

A series of meta-analysis were performed including an analysis of all the patients who underwent *SCN5A* gene test and 8 subgroups, using Review Manager, version 5.3.5 (Revman; The Cochrane Collaboration, Oxford, U.K.). The concludes of the cardiac events outcome are indicated as ORs with 95% CIs for each study. To assess the heterogeneity among studies, the I^2 value from the

chi-square test was used, which describes the percentage of the variability in effect estimates due to heterogeneity, rather than sampling error. An $I^2 > 50\%$ indicates at least moderate statistical heterogeneity (Higgins et al., 2003).

We extracted data from 3 studies to compare categorical variables applying either a chi-square test or Fisher test (Sacher et al., 2013; Tokioka et al., 2014; Yamagata et al., 2017). TheSPSS 17.0 statistical package (SPSS Inc., IL, USA) was used to perform the analysis. In each analysis, statistical significance for treatment effect was defined at $P < 0.05$.

RESULTS

Study Selection

A flow chart of the data research and study selection is shown in **Figure 1**. We excluded 257 duplicate studies across the number of 687 records that were identified by our research criteria. After screening the titles and abstracts, 408 studies were into the discard since they were categorized as guidelines, editorials, case reports, review articles, animal studies, laboratory studies, or unrelated to the present study. Then, 22 potential relevant studies were retrieved for specific evaluation. Of these, a number of 11 studies were further excluded from further analysis because of the following reasons: 8 studies did not provide RRs, ORs, or HRs or data could be calculated, or the 95% confidence intervals; one study did not clearly define the type of abnormal QRS complex; one did not clearly define the endpoints, and one was only an abstract without full-text.

Eleven studies (six prospective and five retrospective) were ultimately involved in this meta-analysis constituting 1892 patients with BrS in total (**Table 1**) (Gasparini et al., 2002; Juang et al., 2003; Mok et al., 2004; Liang et al., 2006; Yuan et al., 2008; Priori et al., 2012; Sacher et al., 2013; Tokioka et al., 2014; Andorin et al., 2016; Calò et al., 2016; Yamagata et al., 2017). The average age of the BrS patients was from 11 to 53 years old. A spontaneous type 1 ECG pattern of BS was reported in 68.8% of patients and a *SCN5A* gene test was performed on 1075 patients (56.8%). A positive genetic mutation was demonstrated in 248 patients (23.1%). Among these, 41 patients (16.5%) were demonstrated to have symptoms. Whereas, a total of 127 patients (15.4%) out of 827 patients (76.9%) with a negative *SCN5A* gene mutation were symptomatic. The mean follow-up duration ranged from 20 to 77 months. During follow-up, 229 patients (12.1%) suffered an arrhythmia event (syncope, non-sustained VT, aborted sudden cardiac death, and appropriate ICD shocks caused by VT/VF). All involved studies were assessed as high-quality publications (average MINORS score: 15 ± 2.9). In addition, we pursued further analysis to attempt to establish the relationship among *SCN5A*, other clinical features and subsequent cardiac events. The clinical characteristics of the 698 BrS patients from 3 studies are summarized in **Table 2** and **Figure 3** (Sacher et al., 2013; Tokioka et al., 2014; Yamagata et al., 2017). It consists of 660 male patients and 37 female patients. In the *SCN5A*+ and *SCN5A*– patient groups, 23 and 83 individuals experienced subsequent cardiac events, respectively. A total of 161 patients had a family history of SCD. A spontaneous type 1 BrS ECG was demonstrated in 72% of patients and 577 patients underwent EPS in total, with 329 patients displaying positive results. With regard to documented AF, 2 of the 100 AF positive patients and 82 of the 586 AF negative patients had arrhythmia events during follow-up.

As for the symptomatic and asymptomatic BrS patients, we added an extra study based on the results from Andorin et al. and only did the meta-analysis (Andorin et al., 2016). Therefore, a total of 317 patients with symptoms at diagnosis and 456 patients without symptoms at diagnosis were identified. The symptoms were defined as patients with a history of ACA, SCD, or syncope.

SCN5A (+) and SCN5A (–) Groups

Overall, BrS patients with a positive *SCN5A* gene mutation were not proven to be a significant predictor of future cardiac events (OR 1.37, 95% CI: 0.89–2.11, $P = 0.15$; Heterogeneity: $P = 0.52$, $I^2 = 0\%$, **Supplementary Figure 1**).

Symptomatic at Diagnosis and Asymptomatic at Diagnosis Groups

The results of the analysis are presented in **Figures 2**, **3** and **Table 3**. According to the present meta-analysis, 26 (42%) of 62 (20%) *SCN5A* (+) patients and 69 (27%) of 255 (80%) *SCN5A* (–) patients had cardiac events. A total of 6 (5%) in 114 (25%) *SCN5A* (+) patients and 14 (4%) in 342 (75%) *SCN5A* (–) patients experienced future arrhythmic events (**Figure 3**) (Sacher et al., 2013; Tokioka et al., 2014; Andorin et al., 2016; Yamagata et al., 2017). In comparison with the asymptomatic at diagnosis patients (OR: 1,54, 95% CI: 0,51–4,72, $P = 0.45$; Heterogeneity: $P = 0.62$, $I^2 = 0$ %, **Figure 3**), *SCN5A* (+) patients who were symptomatic at diagnosis displayed an increased risk of arrhythmic events. (OR 1,98, 95% CI: 1,06–3,70, $P = 0.03$; Heterogeneity: $P = 0.72$, $I^2 = 0\%$, **Figure 3**) (Sacher et al., 2013; Tokioka et al., 2014; Andorin et al., 2016; Yamagata et al., 2017).

Family History of SCD Group

The results of the analysis are presented in **Figures 2**, **3** and **Table 3**. During follow-up, 5 (13%) of 40 (25%) *SCN5A* (+) patients and 16 (13%) of 121 (75%) *SCN5A* (–) patients had arrhythmic events (Sacher et al., 2013; Tokioka et al., 2014; Yamagata et al., 2017). The meta-analysis result revealed that a family history of SCD had little influence on the incidence of future events among *SCN5A* (+) patients. (OR = 0.95, 95% CI: 0.33–2.80, $P = 0.62$; Heterogeneity: $P = 0.93$, $I^2 = 0\%$, **Figure 3**).

Spontaneous Type 1 BrS ECG Groups

The results of the analysis are presented in **Figure 3** and **Table 3**. Cardiac events were documented, respectively in 22% *SCN5A* (+) and 16% *SCN5A* (–) groups, with no significant difference for patients with spontaneous type 1 BrS ECG patterns (OR = 1.48, 95% CI: 0.83–2.64, $P = 0.18$; Heterogeneity: $P = 0.51$, $I^2 = 0\%$, **Figure 3**) (Sacher et al., 2013; Tokioka et al., 2014; Yamagata et al., 2017). A similar result was demonstrated for the chi-square test as well. ($P = 0.215$ vs. P = 0.691, **Table 3**).

Electrophysiological Study Groups

The results of the analysis are presented in **Figures 2**, **3** and **Table 3**. *SCN5A* (+) and *SCN5A* (–) patients who were

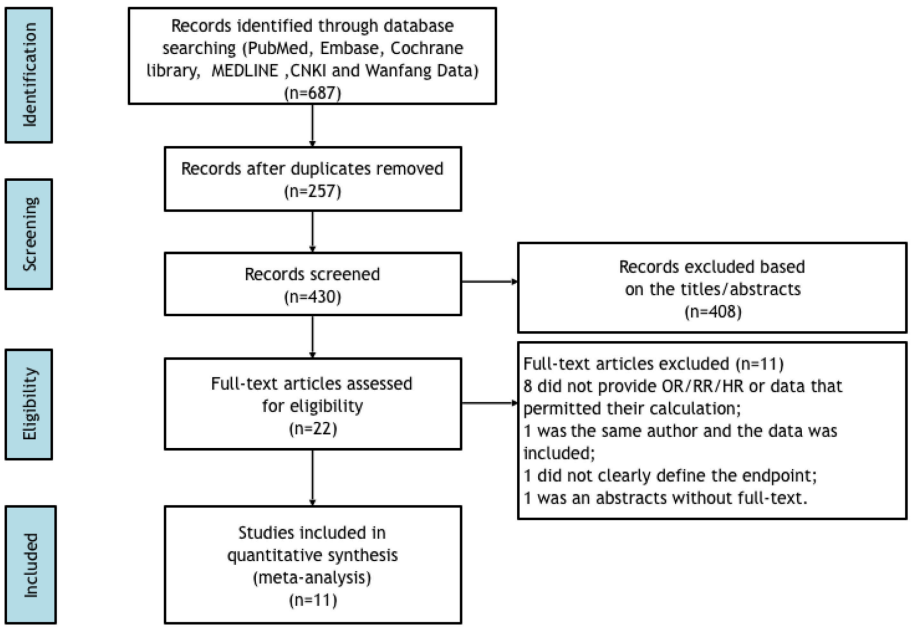

FIGURE 1 | Flow diagram of data search and study selection.

symptomatic during follow-up were presented in 19 and 21%, respectively (**Figure 3**) (Sacher et al., 2013; Tokioka et al., 2014; Yamagata et al., 2017). No statistically significance difference was revealed with respect to the patients with EPS positive between the *SCN5A* (+) group and the *SCN5A* (–) group. (OR = 1.12, 95 % CI: 0.51–2.44, $P = 0.78$; Heterogeneity: $P = 0.50$, $I^2 = 0\%$, **Figure 3**). According to the results from **Table 3**, *SCN5A* (–) BrS patients with positive EPS results had a higher prevalence for future arrhythmia events. ($P = 0.764$ vs. $P < 0.001$). Furthermore, *SCN5A* (+) patients with a negative EPS result had a higher prevalence of cardiac events compared to the case of for *SCN5A* (–) patients. ($P = 0.0.360$ vs. $P < 0.001$).

Documented AF Groups

The results of the analysis are summarized in **Figures 2**, **3** and **Table 3** (Sacher et al., 2013; Tokioka et al., 2014; Yamagata et al., 2017). During follow-up, 6 (31%) of 16 *SCN5A* (+) patients and 17 (23%) of 84 *SCN5A* (−) patients had arrhythmic (OR = 2,10, 95% CI: 0.69–6.39, $P = 0.19$; Heterogeneity: $P = 0.13$, $I^2 = 50$ %, **Figure 3**) (Sacher et al., 2013; Tokioka et al., 2014; Yamagata et al., 2017). In comparison with *SCN5A* (–) patients with AF, no statistically significant difference was observed for *SCN5A* (+) patients with AF. ($P = 0.495$ vs. $P = 0.142$). Based on the results from **Table 3**, *SCN5A* (–) patients with documented AF had a higher rate of cardiac events compared to *SCN5A* (–) patients without AF ($P = 0.021$).

DISCUSSION

The meta-analysis yielded the following main findings: (a) the *SCN5A* gene mutation may not be associated with subsequent cardiac events; (b) *SCN5A* (+) patients with symptoms at diagnosis display a higher risk of arrhythmic events compared to *SCN5A* (–) patients with symptoms at diagnosis (c) Among EPS (–) BrS patients, *SCN5A* (+) patients have a higher prevalence of future cardiac events compared to *SCN5A* (–) patients. Compared with *SCN5A* (–) BrS patients with negative EPS results, *SCN5A* (–) BrS patients with positive EPS results had a higher prevalence for subsequent arrhythmia events.

The *SCN5A* gene locates on chromosome 3p21 and contains 28 exons spanning approximately 80 kb, and encodes α-subunit protein $Na_V1.5$. In most situation, *SCN5A* mutations observed in BrS1 were loss-of-function mutations (Hedley et al., 2009), which results in the reduced availability of sodium channels, either by reducing trafficking and expression of channel on membrane surface, or through changing gate properties of channel (Remme, 2013). Variant mutations in *SCN5A* led to different mechanisms of action. Some mutations resulted in a reduced current density, I_{Na}, while others did not result in a decrease in I_{Na}. In a few cases, the picture was more complicated (Hedley et al., 2009). *SCN5A* gene mutation in particular regions also resulted in a worse outcome during follow-up. For example, pore regions documented by yamagata et al. were identified as being associated with a higher prevalence of future arrhythmia events (Yamagata et al., 2017).

SCN5A (+) and SCN5A (–) Group

The analysis included a total number of 1,075 patients from 11 studies over 10 countries. In accordance with the majority of previous study results, a negative conclusion was obtained. According to the current guideline, a *SCN5A* (+) is not a

TABLE 1 | Study characteristics of 11 studies included in meta-analysis.

Investigator	Location	Type of study	Study of design	Study population	Mean follow-up	Endpoint	Quality score
Gasparini et al., 2002	Italy	SC	PS	Patients with BrS underwent a PES protocol	20 ± 12 months	PES protocol completion/induction of sustained/reproducible nonsustained fast ventricular arrhythmia	15
Juang et al., 2003	Taiwan	MC	RS	Patients with the diagnosis of the BrS	29 ± 17 months	Seizure/syncope/sudden cardiac death	14
Mok et al., 2004	Hong Kong	MC	PS	Patients with type 1 Brugada ECGs	25.8 ± 10.9monthes	Syncope/syncopal ventricular arrhythmia/sudden death/appropriate ICD shock	20
Liang et al., 2006	China	SC	PS	Patients with Brugada ECGs or suspected Brs	NA	Syncope/VT	13
Yuan et al., 2008	China	SC	PS	patients with Brugada ECGs	NA	Syncope/VT	8
Priori et al., 2012	Italy	MC	PS	Patients with type 1 ECGs, without history of cardiac arrest	36 ± 8 months	The occurrence of VF or appropriate ICD interventions	16
Sacher et al., 2013	France	SC	RS	Patients with type 1 Brugada ECGs withimplantable cardioverter-defibrillator	77 ± 42 months	Aborted sudden cardiac arrest/syncope	16
Tokioka et al., 2014	Japan	SC	RS	Patients with a Brugada-type ECG	45.1 ± 44.3 months	VF/SCD	16
Andorin et al., 2016	Europe	MC	RS	Patients with Brugada ECG under 19 years of age	54 months	Sudden death/documented VT or VF/appropriate ICD shock	15
Calò et al., 2016	Italy	MC	PS	Patients with spontaneous type 1 BrS ECG phenotype	48 ± 38.6 months	VF/SCD	16
Yamagata et al., 2017	Japan	MC	RS	Patients with type 1 Brugada ECG pattern	72 months	Documented atrial fibrillation/appropriate ICD interventions	16

BrS, Brugada syndrome; ECG, electrocardiogram; ICD, implantable cardioverter defibrillator; PES, Programmed Electrical Stimulation; MC, multicenter study; NA, not available; n, number; PS, prospective study; RS, retrospective study; SC, single center study; SCD, sudden cardiac death; VF, ventricular fibrillation; VT, ventricular tachycardia.

risk marker for the occurrence of BrS. Genetic testing is not recommended without a diagnostic ECG; unless, there was a successfully genotyped proband observed in family members (Priori et al., 2013). Based on Calò et al. study, patients who developed VF or SCD displayed a lower rate of mutations in *SCN5A* gene (Andorin et al., 2016). The present subgroup analysis indicated a similar result. Also, the EPS results and T waves changes on ECG did not differ significantly between the *SCN5A* (+) patients and the *SCN5A* (–) patients (Tokioka et al., 2014; Tse et al., 2018). On the other hand, the conclusion presented by Andorin et al is that an absent *SCN5A* mutation probably led to a lower risk of subsequent cardiac events (Andorin et al., 2016). Furthermore, *yamagata et al.* demonstrated that *SCN5A* gene mutation positive was an independent risk marker for cardiac events among all probands by applying the Cox proportional hazards model (HR = 1.1, 95% CI: 1.1 to 3.8, $P = 0.02$) (Yamagata et al., 2017).

Symptomatic at Diagnosis and Asymptomatic at Diagnosis Groups

Recently, Yamagata et al. demonstrated that *SCN5A* (+) probands, especially for mutation in the pore region presenting with prior ACA or syncope, were more likely to be associated with future cardiac events compared to *SCN5A* (–) BrS patients. However, no significant difference was revealed between asymptomatic *SCN5A* (+) probands and *SCN5A* (–) probands (Yamagata et al., 2017). In addition, a recent meta-analysis reported that symptomatic male BrS patients were at higher risk than asymptomatic male BrS patients (Yuan et al., 2018). Based on these results, we performed a further subgroup meta-analysis and extracted data from Yamagata et al. and three other studies involving 773 patients who underwent *SCN5A* gene test with either prior ACA or syncope. Interestingly, a significant difference was noted between the *SCN5A* (+) patients with symptoms at diagnosis and the *SCN5A* (–) patients with symptoms at diagnosis. With respect to BrS patients without

TABLE 2 | Patients' characteristics of 11included studies.

	Gasparini et al., 2002	Juang et al., 2003	Mok et al., 2004	Liang et al., 2006	Yuan et al., 2008	Priori et al., 2012	Sacher et al., 2013	Tokioka et al., 2014	Andorin et al., 2016	Calò et al., 2016	Yamagata et al., 2017
Total Patients, *n*	21	10	50	4	7	308	378	246	106	347	415
Male/female, *n*	18/3	10/0	47/3	4/0	7/0	247/61	310/68	236/10	58/48	272/75	403/12
Age (years)	34	46 ± 7	53	40.9	43.6 ± 8.7	47 ± 12	46 ± 13	47.6 ± 13.6	11.1 ± 5.7	45 ± 13.1	46 ± 14
Symptomatic, *n* (%)	0 (0)	3 (30)	30 (60)	4 (100)	4 (57)	14 (4)	46 (12)	24 (10)	10 (9)	32 (9)	62 (15)
History of SCA, *n* (%)	1 (5)	9 (90)	8 (16)	NA	3 (43)	NA	31 (8)	13 (5)	NA	0 (0)	88 (21)
History of sycope, *n* (%)	8 (38)	1 (10)	12 (24)	2 (20)	4 (57)	65 (21)	181 (48)	40 (16)	15 (14)	14 (4)	99 (24)
Asymptomatic, *n* (%)	12 (57)	0 (0)	30 (60)	0 (0)	3 (43)	243 (80)	166 (44)	NA	85 (80)	316 (91)	228 (55)
Family history of SCD, *n* (%)	8 (38)	1 (10)	7 (14)	NA	3 (43)	NA	111 (30)	69 (28)	46 (43)	71 (20)	64 (15)
Patients with ICD, *n* (%)	NA	8 (80)	8 (16)	NA	NA	137 (44)	308 (81)	63 (26)	22 (21)	98 (28)	241 (58)
Spontaneous type1 ECG, *n* (%)	19 (90)	NA	43 (86)	NA	5 (71)	171 (56)	226 (60)	156 (63)	36 (34)	347 (100)	299 (72)
Events, *n* (%)	0 (0)	NA	17 (39)	NA	3 (60)	13 (8)	35 (15)	22 (14)	8 (22)	32 (10)	48 (16)
Non-Spontaneous type1 ECG, *n* (%)	2 (9.5)	NA	7 (14)	NA	0 (0)	NA	152 (40)	90 (37)	70 (66)	0 (0)	116 (28)
Events,*n* (%)	0 (0)	NA	3 (43)	NA	0 (0)	NA	11 (7)	2 (2)	2 (3)	0 (0)	14 (12)
Patients ungergo EPS, *n* (%)	21 (100)	8 (80)	30 (60)	NA	7 (100)	NA	310 (82)	155 (63)	NA	186 (54)	339 (82)
EPS+, (n)	18 (86)	6 (75)	19 (63)	NA	NA	NA	228 (73)	71 (46)	NA	77 (41)	191 (56)
up to 1 ex	0 (0)	NA	2 (10)	NA	NA	NA	NA	NA	NA	NA	NA
up to 2 ex	12 (67)	NA	9 (47)	NA	NA	NA	NA	NA	NA	NA	NA
up to 3 ex	6 (33)	NA	8 (42)	NA	NA	NA	NA	NA	NA	NA	NA
EPS-, *(n)*	3 (14)	2 (25)	11 (37)	NA	1 (14.3)	NA	82 (26)	84 (54)	NA	109 (59)	148 (44)
AF (+), *n* (%)	NA	NA	NA	NA	NA	NA	32 (8)	44 (17)	NA	NA	64
Patients undergo DNA tested, *n* (%)	21 (100)	4 (40)	36 (72)	4 (100)	7 (100)	123 (40)	160 (42)	123 (50)	75 (71)	107 (31)	415 (100)
SCN5A (+), *n* (%)	8 (38)	1 (25)	5 (14)	1 (25)	1 (14)	24 (20)	41 (26)	17 (26)	58 (77)	32 (30)	60 (14)
events, *n* (%)	0 (0)	1 (100)	2 (40)	1 (100)	0 (0)	3 (13)	6 (15)	4 (24)	9 (16)	2 (6)	13 (22)
SCN5A (–), *n* (%)	13 (62)	3 (75)	31 (86)	3 (75)	6 (86)	99 (80)	119 (74)	106 (74)	17 (23)	75 (70)	355 (86)
events, *n* (%)	0 (0)	2 (67)	18 (58)	3 (100)	4 (67)	6 (14)	16 (13)	19 (18)	0 (0)	10 (13)	49 (14)
f-QRS (+), *n* (%)	NA	NA	NA	NA	NA	25 (8)	NA	78 (32)	NA	85 (25)	NA
f-QRS (–), *n* (%)	NA	NA	NA	NA	NA	283 (92)	NA	158	NA	262 (76)	NA
ER (+), *n* (%)	NA	NA	NA	NA	NA	NA	NA	25 (10)	NA	30 (9)	NA
ER (–), *n* (%)	NA	NA	NA	NA	NA	NA	NA	221	NA	317 (91)	NA

Data were presented as mean ± SD, median, or percentage where possible; SCA, sudden cardiac arrest; NA, not available; SCD, sudden cardiac death; ICD, implantable cardioverter defibrillator;ECG, electrocardiogram; EPS, electrophysiological study; n, number; ex, extrastimuli; f-QRS, fragmented QRS; ER, early repolarization.

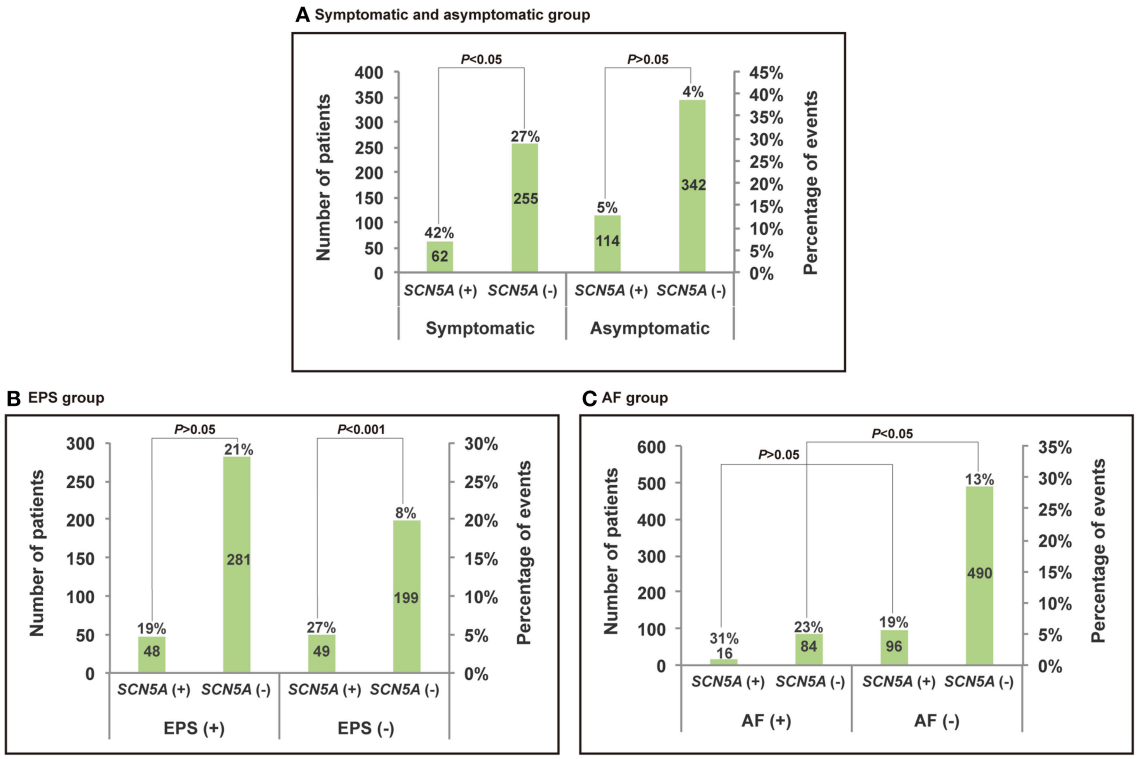

FIGURE 2 | Histogram and broken line for the comparison between events of *SCN5A* (+) and *SCN5A* (–) of subgroups. **(A)** Symptomatic at diagnosis group. **(B)** EPS group. **(C)** AF group.

symptoms at diagnosis, no significant difference was observed. *Sacher et al.* reported on a large multi-center registry on the outcome of BrS patients implanted with an ICD in France (Sacher et al., 2013). Tokioka et al. investigated the combination of ECG markers (depolarization and repolarization abnormalities) on risk assessment of VF in Japan. Both studies indicated that the role of the *SCN5A* mutation was of minor influence (Tokioka et al., 2014). Andorin et al. focused on BrS patients under age 19 at diagnosis in 16 European hospitals and concluded that there was a higher prevalence of *SCN5A* (+) pediatric patients with life-threatening arrhythmias (Andorin et al., 2016).

Some studies have reported that patients with *SCN5A* (+) had a higher prevalence of abnormalities in conduction (longer PQ interval, longer QRS duration, and frequent fragmentation). The decreased of sodium current reduces the action potential upstroke velocity, resulting in atrial and ventricular conduction deceleration accompanied by prolonged PR and QRS intervals (Remme, 2013). Moreover, there was sufficient background for the developed conduction abnormality leading to higher possibilities for arrhythmic events. Furthermore, it was confirmed that an abnormality in a cardiac ion channel may result in cell damage and death in patients with BrS. On this basis, it can be argued that the arrhythmic event may occur when a specific threshold of cell damage is reached, due to the severity of the ion channel protein mutation (Yamagata et al., 2017). The aforementioned facts may explain why *SCN5A* (+) patients with symptoms at diagnosis had a higher risk of arrhythmic events during follow-up in comparison to *SCN5A* (–) patients with symptoms at diagnosis. However, an opposite result was demonstrated by a recent study. It reported that 28 variants in *SCN5A* and other 9 genes in Human Gene Mutation Database were identified to be related to BrS, whereas, neither type 1 BrS ECG pattern nor abnormal J-point elevation in V1 and V2 was observed among genes mutations carriers. Besides, no difference was noted in susceptibility of syncope, ventricular cardiac events, or entirety mortality (Ghouse et al., 2017). On the contrary, Hosseini et al found that *SCN5A* was the only gene which is clinically associated with BrS among 21 included gene (Hosseini et al., 2018), thus, further studies needed to be done.

On the other hand, there was no significant difference between *SCN5A* (+) patients and *SCN5A* (–) patients who were asymptomatic at diagnosis. This may be due to the presence of a BrS-like ECG pattern in some cases including serious coronary events, imbalanced electrolyte, pharmacologic factors, pulmonary embolism, right bundle branch block, arrhythmogenic right ventricular cardiomyopathy, abnormalities in autonomic nervous system, and left ventricular hypertrophy (Shi et al., 2018). According to the specific situation, a certain number of patients might be wrongly diagnosed.

It is worth mentioning that in the meta-analysis, I^2 was zero, which indicates that there was no analytical bias caused

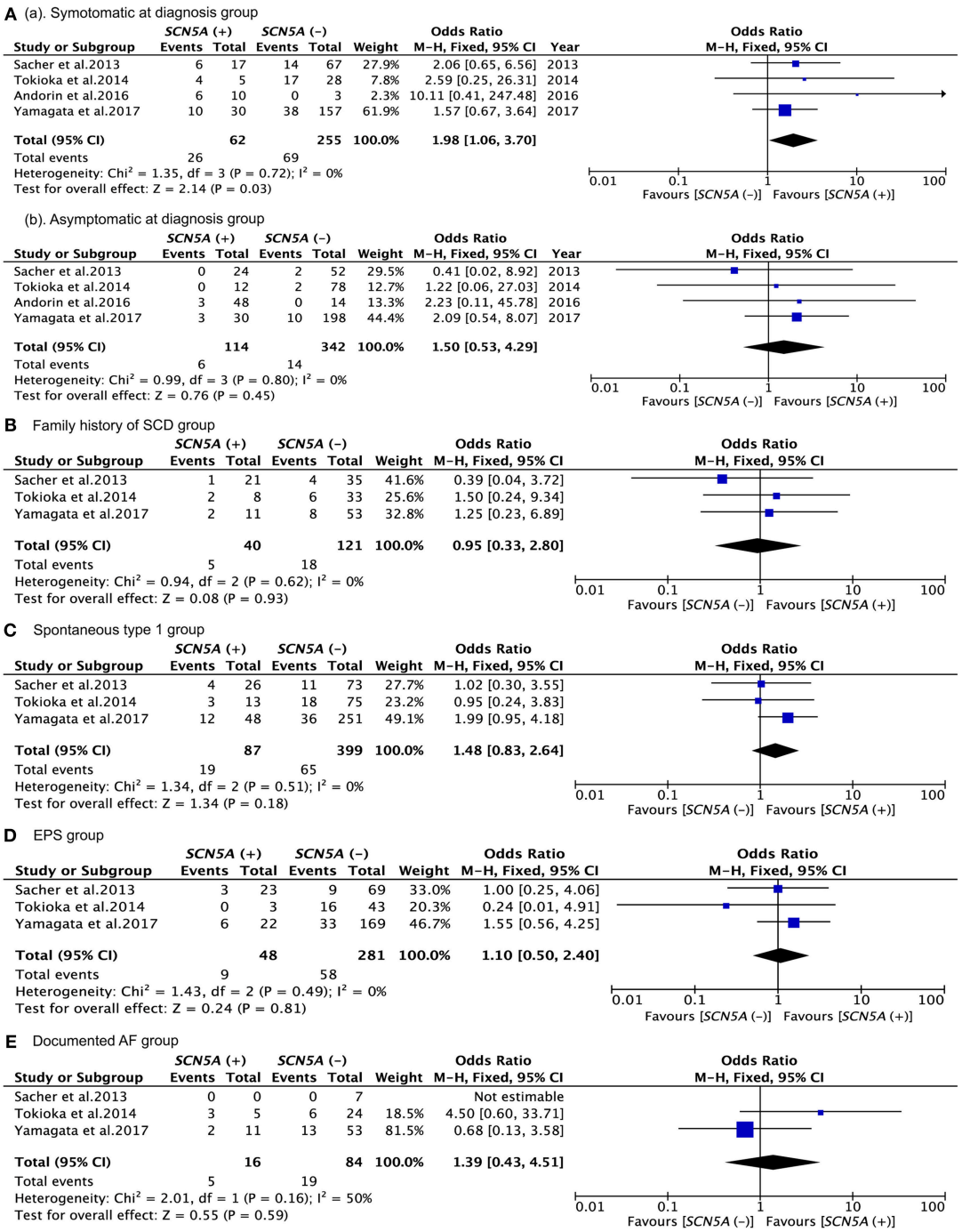

FIGURE 3 | Forest plots comparing outcomes of subgroups. **(Aa)** Comparison between events of *SCN5A* (+) and *SCN5A* (–) in symptomatic at diagnosis group; **(Ab)** comparison between events of *SCN5A* (+) and events of *SCN5A* (–) in asymptomatic at diagnosis group; **(B)** comparison between events of *SCN5A* (+) and *SCN5A* (–) in family history of SCD group; **(C)** comparison between events of *SCN5A* (+) and *SCN5A* (–) in spontaneous type 1 group; **(D)** comparison between events of *SCN5A* (+) and *SCN5A* (–) in EPS group; **(E)** comparison between events of *SCN5A* (+) and *SCN5A* (–) in documented AF group.

by a single dataset. Negative results were obtained according to the original data for each study, but a positive result was obtained when the sample size was expanded. This is the first time that *SCN5A* (+) is reported to increase the risk of future heart events among BrS patients in patients with symptoms at diagnosis.

TABLE 3 | Comparison between subgroup of *SCN5A* (+) group and *SCN5A* (–) group.

			SCN5A (+)	*SCN5A* (–)	*P*-value
EPS status	Positive	Total	48	281	0.764
		Events	9	58	
	Negative	Total	49	199	***<0.001**
		Events	13	15	
		P-value	0.360	***<0.001**	
Spontaneous type 1 ECG	Positive	Total	87	399	0.215
		Events	19	65	
	Negative	Total	31	181	0.691
		Events	4	19	
		P-value	0.281	0.090	
Documented AF status	Positive	Total	16	84	0.495
		Events	5	19	
	Negative	Total	96	490	0.142
		Events	18	64	
		P-value	0.252	***0.021**	

*Bold value means statistically significant (*P < 0.05).*

EPS Groups

According to the 2017 guideline for ventricular cardiac events and SCD, further risk stratification in asymptomatic and spontaneous type 1 patients with EPS following programmed ventricular stimulation using single or double extrastimuli could be considered (Al-Khatib et al., 2018). On the other hand, the current guideline demonstrated that EPS inducibility appeared in a large number of BrS patients who suffered from previous sudden death or syncope (Priori et al., 2013). In addition, PES was of value particularly in patients with previous syncope: in this group, PES aided in the prevention of more than half of unnecessary ICD implants, when there was a follow-up at least within a mean of 30 months (Giustetto et al., 2009).

In the present study, we focused on the relationship between EPS and *SCN5A* gene mutation status. While few studies have investigated this relationship, negative conclusions were noted in Yamagata et al. (2017) and Andorin et al. (2016). Therefore, we performed a related analysis including 554 BrS patients who underwent EPS from three studies and obtained a positive result. The present analysis revealed that *SCN5A* (+) BrS patients with EPS negative probably have a higher prevalence of subsequent arrhythmia events, however, the risk of *SCN5A* (+) was not higher than that of *SCN5A* (–) in patients with EPS (+) BrS. This suggests that *SCN5A* may contribute to the occurrence of future events. According to previous studies, *SCN5A* (+) BrS patients had a longer HV interval during EPS compared to *SCN5A* (–) BrS patients or purely EPS positive BrS patients. This implies that the underlying electrophysiologic mechanisms of conduction block and ventricular arrhythmia are strongly correlated (Giustetto et al., 2009; Yamagata et al., 2017).

STUDY LIMITATION AND CONCLUSIONS

In this study, the number of patients who underwent genetic testing was still limited, probably due to the high cost of the test. Secondly, the inadequacy of the original data prevented further analysis. In addition, *SCN5A* mutations can be variable with presumably differing effects on sodium channel function. Nevertheless, this study shows that positive mutation status is an important determinant of outcomes in particular subgroups described above. Finally, the relationship between BrS patients with symptoms and the higher frequency of future events needs to be further enhanced and additional experiments are required. *SCN5A* (+) as a risk marker of BrS should not be underestimated. *SCN5A* (+) patients with symptoms at diagnosis may have a prognosis significance for BrS. Furthermore, *SCN5A* (+) BrS patients with EPS (−) displayed a higher prevalence of future cardiac events.

AUTHOR CONTRIBUTIONS

All authors listed have made a substantial, direct and intellectual contribution to the work, and approved it for publication.

FUNDING

The current work was supported by the National Natural Science Foundation Project of China (Grant Nos. 81430098 and 81670304), National high-level talent special support plan (No. W02020052), and the National clinical research base of TCM project of the State Administration of traditional Chinese medicine (JDZX2015007).

SUPPLEMENTARY MATERIAL

The Supplementary Material for this article can be found online at: https://www.frontiersin.org/articles/10.3389/fphys.2019.00103/full#supplementary-material

REFERENCES

Al-Khatib, S. M., Stevenson, W. G., Ackerman, M. J., Bryant, W. J., Callans, D. J., Curtis, A. B., et al. (2018). AHA/ACC/HRS Guideline for management of patients with ventricular arrhythmias and the prevention of sudden cardiac death: executive summary: a report of the american college of cardiology/american heart association task force on clinical practice guidelines and the heart rhythm society. *Circulation* 138, e210on iat doi: 10.1161/CIR.0000000000000548

Andorin, A., Behr, E. R., Denjoy, I., Crotti, L., Dagradi, F., Jesel, L., et al. (2016). Impact of clinical and genetic findings on the management of young patients with Brugada syndrome. *Heart Rhythm* 13, 1274–1282. doi: 10.1016/j.hrthm.2016.02.013

Calò, L., Giustetto, C., Martino, A., Sciarra, L., Cerrato, N., Marziali, M., et al. (2016). A New electrocardiographic marker of sudden death in brugada syndrome: the S-Wave in Lead, I. *J. Am. College Cardiol.* 67, 1427–1440. doi: 10.1016/j.jacc.2016.01.024

Gasparini, M., Priori, S. G., Mantica, M., Coltorti, F., Napolitano, C., Galimberti, P., et al. (2002). Programmed electrical stimulation in Brugada syndrome: how reproducible are the results? *J. Cardiovasc. Electrophysiol.* 13, 880–887. doi: 10.1046/j.1540-8167.2002.00880.x

Ghouse, J., Have, C. T., Skov, M. W., Andreasen, L., Ahlberg, G., Nielsen, J. B., et al. (2017). Numerous Brugada syndrome-associated genetic variants have no effect on J-point elevation, syncope susceptibility, malignant cardiac arrhythmia, and all-cause mortality. *Genet. Med.* 19, 521Med. Bdoi: 10.1038/gim.2016.151

Giustetto, C., Drago, S., Demarchi, P. G., Dalmasso, P., Bianchi, F., Masi, A. S., et al. (2009). Risk stratification of the patients with Brugada type electrocardiogram: a community-based prospective study. *Europace* (2009) 11, 507–513. doi: 10.1093/europace/eup006

Hedley, P. L., Jorgensen, P., Schlamowitz, S., Moolman-Smook, J., Kanters, J. K., Corfield, V. A., et al. (2009). The genetic basis of Brugada syndrome: a mutation update. *Hum. Mutat.* 30, 1256–1266. doi: 10.1002/humu.21066

Higgins, J. P., Thompson, S. G., Deeks, J. J., and Altman, D. G. (2003). Measuring inconsistency in meta-analyses. *BMJ* 327, 557–560. doi: 10.1136/bmj.327.7414.557

Hosseini, S. M., Kim, R., Udupa, S., Costain, G., Jobling, R., Liston, E., et al. (2018). Reappraisal of reported genes for sudden arrhythmic death: an evidence-based evaluation of gene validity for brugada syndrome. *Circulation* 138, 1195–1205. doi: 10.1161/CIRCULATIONAHA.118.03507

Juang, J. M., Huang, S. K., Tsai, C. T., Chiang, F. T., Lin, J. L., Lai, L. P., et al. (2003). Characteristics of Chinese patients with symptomatic brugada syndrome in Taiwan. *Cardiology* 99, 182–189. doi: 10.1159/0000 71247

Liang, P., Liu, W., Hu, D., Li, C., Tao, H., and Li, L. (2006). Three new mutations in the SCN5A gene of brugada syndrome. *Chi. J.* 34, 616–619.

Mok, N. S., Priori, S. G., Napolitano, C., Chan, K. K., Bloise, R., Chan, H. W., et al. (2004). Clinical profile and genetic basis of Brugada syndrome in the Chinese population. *Hong Kong Med. J.*. 10, 32–37.

Priori, S. G., Gasparini, M., Napolitano, C., Della Bella, P., Ottonelli, A. G., Sassone, B., et al. (2012). Risk stratification in Brugada syndrome: results of the PRELUDE (PRogrammed ELectrical stimUlation preDictive valuE) registry. *J. Am. College Cardiol.* 59, 37–45. doi: 10.1016/j.jacc.2011. 08.064

Priori, S. G., Wilde, A. A., Horie, M., Cho, Y., Behr, E. R., Berul, C., et al. (2013). HRS/EHRA/APHRS expert consensus statement on the diagnosis and management of patients with inherited primary arrhythmia syndromes: document endorsed by HRS, EHRA, and APHRS in May 2013 and by ACCF, AHA, PACES, and AEPC in June 2013. *Heart Rhythm* 10, 1932–1963. doi: 10.1016/j.hrthm.2013.05.014

Remme, C. A. (2013). Cardiac sodium channelopathy associated with *SCN5A* mutations: electrophysiological, molecular and genetic aspects. *J. Physiol.* 591, 4099–4116. doi: 10.1113/jphysiol.2013.256461

Sacher, F., Probst, V., Maury, P., Babuty, D., Mansourati, J., Komatsu, Y., et al. (2013). Outcome after implantation of a cardioverter-defibrillator in patients with Brugada syndrome: a multicenter study-part 2. *Circulation* 128, 1739–1747. doi: 10.1161/CIRCULATIONAHA.113. 001941

Shi, S., Barajas-Martinez, H., Liu, T., Sun, Y., Yang, B., Huang, C., et al. (2018). Prevalence of spontaneous Brugada ECG pattern recorded at standard intercostal leads: a meta-analysis. *Int. J. Cardiol.* 254, 151–156. doi: 10.1016/j.ijcard.2017.11.113

Slim, K., Nini, E., Forestier, D., Kwiatkowski, F., Panis, Y., and Chipponi, J. (2003). Methodological index for non-randomized studies (minors): development and validation of a new instrument. *ANZ J. Surg.* 73, 712–716. doi: 10.1046/j.1445-2197.2003.02748.x

Tokioka, K., Kusano, K. F., Morita, H., Miura, D., Nishii, N., Nagase, S., et al. (2014). Electrocardiographic parameters and fatal arrhythmic events in patients with Brugada syndrome: combination of depolarization and repolarization abnormalities. *J. Am. College Cardiol.* 63, 2131–2138. doi: 10.1016/j.jacc.2014.01.072

Tse, G., Gong, M., Li, C. K. H., Leung, K. S. K., Georgopoulos, S., Bazoukis, G., et al. (2018). Tpeak-Tend, Tpeak-Tend/QT ratio and Tpeak-Tend dispersion for risk stratification in Brugada Syndrome: a systematic review and meta-analysis. *J. Arrhythmia* 34, 587ythmiadoi: 10.1002/joa3.12118. eCollection 2018

Yamagata, K., Horie, M., Aiba, T., Ogawa, S., Aizawa, Y., Ohe, T., et al. (2017). Genotype-phenotype correlation of *SCN5A* mutation for the clinical and electrocardiographic characteristics of probands with brugada syndrome: a japanese multicenter registry. *Circulation* 135, 2255–2270. doi: 10.1161/CIRCULATIONAHA.117.027983

Yuan, B., Shan, Q., Yang, B., Chen, M., Zou, J., Chen, C., et al. (2008). Detection of gene mutations of *SCN5A* in 7 patients with Brugada syndrome. *Zhonghua Xin Xue Guan Bing Za Zhi* 36, 404a X

Yuan, M., Tian, C., Li, X., Yang, X., Wang, X., Yang, Y., et al. (2018). Gender Differences in Prognosis and Risk Stratification of Brugada Syndrome: A Pooled Analysis of 4,140 Patients From 24 Clinical Trials. *Front. Physiol.* 9:1127. doi: 10.3389/fphys.2018.01127

Conflict of Interest Statement: HB-M was employed by company Global Genetics Corp, Ventura, California, USA.

The remaining authors declare that the research was conducted in the absence of any commercial or financial relationships that could be construed as a potential conflict of interest.

frontiers in Physiology

ORIGINAL RESEARCH
published: 25 February 2019
doi: 10.3389/fphys.2019.00145

QRS-T Angle Predicts Cardiac Risk and Correlates With Global Longitudinal Strain in Prevalent Hemodialysis Patients

*Sofia Skampardoni[1], Darren Green[1], Katerina Hnatkova[2], Marek Malik[2], Philip A. Kalra[1] and Dimitrios Poulikakos[1]**

[1] Department of Renal Medicine, Salford Royal NHS Foundation Trust and The University of Manchester, Manchester, United Kingdom, [2] National Heart and Lung Institute, Imperial College London, London, United Kingdom

OPEN ACCESS

Edited by:
T. Alexander Quinn, Dalhousie University, Canada

Reviewed by:
Maurizio Acampa, Azienda Ospedaliera Universitaria Senese, Italy
Larisa G. Tereshchenko, Oregon Health & Science University, United States

***Correspondence:**
Dimitrios Poulikakos
dimitrios.poulikakos@srft.nhs.uk; dempoulikakos@hotmail.com

Specialty section:
This article was submitted to Cardiac Electrophysiology, a section of the journal Frontiers in Physiology

Received: *13 October 2018*
Accepted: *07 February 2019*
Published: *25 February 2019*

Citation:
Skampardoni S, Green D, Hnatkova K, Malik M, Kalra PA and Poulikakos D (2019) QRS-T Angle Predicts Cardiac Risk and Correlates With Global Longitudinal Strain in Prevalent Hemodialysis Patients. Front. Physiol. 10:145. doi: 10.3389/fphys.2019.00145

Background: Cardiovascular disease is the commonest cause of death in hemodialysis (HD) patients but accurate risk prediction is lacking. The spatial QRS – T angle is a promising electrophysiological marker for sudden cardiac death risk stratification. The aim of this study was to assess the prognostic value of spatial QRS-T angle derived from standard 12 lead electrocardiograms (ECG) and its association with echocardiographic parameters in HD patients.

Methods: This prospective study of 178 prevalent HD patients (aged 67 ± 14 years, 72% men) collected ECG and echocardiographic data on an annual basis. Baseline echocardiograms at study entry were used for cross-sectional comparisons with ECGs. Study endpoints were all-cause mortality, cardiovascular mortality, and major adverse cardiac events (MACE). The QRS – T angle was calculated from standard 10-s ECG as the total cosine R to T (TCRT) using singular value decomposition and expressed in degrees. TCRT above 100° was defined as abnormal.

Results: During a follow-up period of 36 ± 19 months, 74 patients died, including 17 cardiac deaths, and 54 suffered from MACE. In multivariate Cox regression analysis, QRS-T angle by TCRT at baseline was associated with increased cardiovascular mortality both as a continuous value and dichotomized below or above 100° (HR 1.016, $p = 0.029$, CI: 1.002–1.030 and HR 3.506, CI: 1.118–10.995, $p = 0.031$ respectively) and with MACE dichotomized at 100° (HR 1.902, CI: 1.046–3.459; $p = 0.035$). In multivariate regression analysis including baseline parameters, echocardiographic global longitudinal strain (GLS) was significantly correlated with TCRT (F 9.648, $r^2 = 0.192$, standardized $\beta = 0.331$, unstandardized $\beta = 3.567$, $t = 4.4429$, CI: 1.976–5.157, $p < 0.001$).

Conclusion: TCRT correlates with GLS and is independently associated with cardiac deaths and MACE in HD patients.

Keywords: QRS-T angle, TCRT, sudden cardiac death, hemodialysis, cardiovascular, global longitudinal strain

INTRODUCTION

Cardiovascular mortality and morbidity is elevated in End Stage Renal Disease (ESRD) (Caskey et al., 2016). Renal registry data indicate that sudden death or fatal arrhythmia is the documented cause of death in approximately 26% of ESRD patients (United States Renal Data System, 2016). The pathogenesis of cardiac disease associated with sudden death in ESRD is not well understood. Traditional risk stratification models cannot be directly extrapolated to the dialysis population (Poulikakos et al., 2014) and it is speculated that the pathogenetic mechanisms differ compared to cardiac patients and to the general population (Roberts et al., 2006). The identification of high-risk patients so as to intervene to improve outcomes remains an unmet clinical need.

A recent study identified spatial QRS-T angle, an established marker of repolarization heterogeneity in cardiac patients (Zabel et al., 2000) and in the general population (Porthan et al., 2013; Waks et al., 2016), as a strong predictor of cardiovascular mortality and sudden cardiac death in incident HD patients (Tereshchenko et al., 2016). In that study (Tereshchenko et al., 2016), the calculation of the QRS-T angle was derived from signal-averaged ECG orthogonal recordings rather than resting standard 12-lead ECGs that are routinely used in clinical practice.

Amongst the existing methods of calculating the spatial QRS-T angle, (Hnatkova et al., 2017) the Total Cosine R to T (TCRT) (Acar et al., 1999) is a reliable and reproducible descriptor that can be measured from a single standard 12 lead digital ECG. In a recent pilot reproducibility study in 72 HD patients using repeated continuous intradialytic Holter ECG monitoring, abnormal TCRT was associated with major cardiac events (MACE) and mortality (Poulikakos et al., 2018).

Repolarization heterogeneity has been recently associated with structural and functional cardiac abnormalities including global longitudinal strain (GLS) derived from speckle tracking echocardiography in the general population (Biering-Sørensen et al., 2018). GLS is an emerging echocardiographic marker of uremic cardiomyopathy that predicts arrhythmic death (Hensen et al., 2018) and mortality (Waks et al., 2016) but its relationship with repolarization heterogeneity assessed by QRS-T angle has not been evaluated in HD patients.

The purpose of this study was to confirm the predictive value of TCRT calculated from standard 10-s resting ECGs and to examine the association between TCRT and various echocardiographic parameters, including GLS, in HD patients.

MATERIALS AND METHODS

Patient Population and Protocols

Digital ECG recordings collected as part of a recently published prospective study in prevalent hemodialysis patients (Chiu et al., 2016a) that evaluated the predictive value of pulse wave velocity (PWV), left ventricular mass index (LVMI) and GLS on cardiovascular events and mortality, were available for this study. Patient characteristics, selection and recruitment process and protocols for this study have previously been described (Chiu et al., 2016a). This was a substudy of Chronic Renal Insufficiency Standards Implementation Study (CRISIS), an epidemiological study of patients with chronic kidney disease. In brief, recruited prevalent HD patients underwent sequential annual ECG recordings, echocardiography and PWV measurements and blood sampling. After phlebotomy, samples were immediately centrifuged and plasma and serum stored at −80°C. N-terminal pro-brain natriuretic peptide (BNP) and Troponin I were later quantified in batched using electrochemiluminescence (Cobas e601 automate, Roche Diagnostics Indianapolis, IN, United States).

Demographic data were extracted from medical records. Coronary artery disease (CAD) was defined as previous history of myocardial infarction and/or angina.

The study endpoints were all-cause mortality, cardiovascular mortality defined as death due to myocardial infarction, heart failure, arrhythmia or sudden cardiac death, and a composite endpoint of major cardiac events (MACE). MACE included acute coronary syndrome, coronary revascularization, hospitalization due to heart failure or arrhythmia, and sudden cardiac death. Sudden cardiac death was defined as sudden and unexpected death occurring within an hour of the onset of symptoms, or presumably due to a cardiac arrhythmia occurring in previously asymptomatic patients found dead within 24 h of last clinical contact (Al-Khatib et al., 2017). Follow up was calculated from the date of baseline ECG. All participants provided written informed consent prior to enrolment in the study. The study was approved by North West - Greater Manchester South Research Ethics Committee (15/NW/0818).

Echocardiography and Pulse Wave Velocity

Transthoracic two-dimensional echocardiographic imaging and PWV measurements and 12-lead ECGs were obtained on single visits during a mid-week non-dialysis day. The detailed protocol of echocardiographic and PWV measurement has been described elsewhere (Chiu et al., 2016a). In brief, transthoracic echocardiography was performed using Philips Medical Systems (Philips UK Ltd., United Kingdom) with 3.5-MHz transducers. Echocardiographic measurements were in accordance with published guidance (Lang et al., 2015). The Philips Xcelera R4.1 image management system was used for offline analysis. Measurements of left ventricular volumes and left ventricular ejection fraction were performed with the biplane Simpson's method. GLS was calculated from speckle-tracking echocardiography from apical 4- and 2-chamber views using the Philips QLAB version 9 software. Analysis was performed after the anonymization of the echocardiographic images. The GLS was calculated as average over all segmental strains of all 17 segments. M mode left ventricular (LV) mass was calculated using the Devereux formula: LV mass = 0.8 * [1.04 ((LV internal diameter + septal wall thickness + posterior wall thickness) 3 – LV internal diameter 3) + 0.6 g]. LV mass was indexed to height 2.7 (LVMI/HT 2.7). PWV was measured with the Vicorder TM device (Skidmore Medical Ltd., Bristol, United Kingdom) using

a neck and femoral cuff that were inflated to 65 mm Hg and the obtained oscillometric signal was used to calculate the pulse time delay between the two sites and consequently the aortic PWV. The mean result of two consecutive measurements was used for the analysis.

Electrocardiographic Acquisition and Analysis

All 12-lead ECGs were recorded at a sampling rate of 500 Hz in a recumbent position and with standard lead placement (Phillips Pagewriter TC 20 electrocardiograph). Automated measurements by Phillips measurement algorithm of heart rate and ECG intervals for QRS and QT were used in the analysis. QTc was calculated using the Fridericia's formula: $QTcF = QT/\sqrt[3]{RR}$. Software conversion routines were programmed allowing the signal to be exported from the XML Schiller format to a format suitable for further computer processing with a custom developed software. The calculation of TCRT has been previously described in detail (Acar et al., 1999). In brief, the software decomposes the ECG signal into a minimum dimensional space and reconstructs the electrical activity as a three-dimensional moving vector forming a loop during depolarization (QRS) and repolarization (T wave). The angle between the principal orientations of the QRS complex and the T wave loop (QRS –T angle) was calculated as total cosine R to T (Acar et al., 1999) and converted to degrees (**Figure 1**). Analysis of the digital ECG recordings was performed in a blinded manner using a purpose designed software package written in C++ and the TCRT calculations were returned to the clinical investigators for statistical analysis.

Statistical Analysis

Analyses were performed with IBM SPSS Statistics version 22.0. Continuous variables were expressed as means ± standard deviation or as median and interquartile range if normally or non-normally distributed, respectively. *T*-test and Mann–Whitney *U* test were used for comparisons of parametric and non-parametric data as appropriate. The chi-squared test was used for categorical values where appropriate. Pearson's correlation coefficient was used to measure the relationship between the variables and TCRT. Variables found to be significantly associated were entered into linear regression analysis to determine independent relationship with TCRT. Univariate Cox Regression analysis was used to calculate the effect of variables upon the time to outcome. TCRT and all other statistically significant variables in the univariate analysis, apart from those which correlated with TCRT in linear regression analysis, were included in multivariate Cox regression analysis to determine associations between the endpoints and variables. In the Cox regression analysis, TCRT was entered as a continuous value as well as also dichotomized at 100° based on previously published cut–off values for risk stratification for sudden cardiac death in the general population (Porthan et al., 2013). The cumulative probability of events between patient groups stratified by TCRT above and below 100° was compared by the log-rank test.

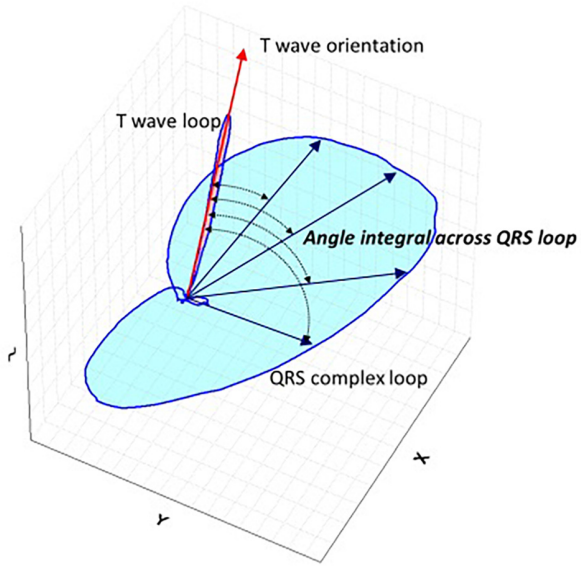

FIGURE 1 | Schematic representation QRS-T angle. Schematic spatial representation of QRS and T vector loops. Main vector of T wave loop is depicted by red arrow and main vectors of QRS loop are depicted with blue straight arrows. Total Cosine R to T is the average of cosines of the angles between the three-dimensional T wave and QRS loop vectors and measures the vectorial deviation between depolarization and repolarization waves. For the three-dimensional reconstruction of the cardiac electrical signal from the surface 12 lead digital ECG, the eight independent leads are subjected to singular value decomposition to yield a system of 3 independent orthogonal leads that contain 99% of the ECG energy.

For the longitudinal analysis, the difference (Δ) between baseline TRCT and first available follow up TRCT was calculated as ΔTCRT = TCRT (follow up)-TCRT (baseline). Paired sample *t*-tests were used to compare baseline and follow up TCRT values. Analysis was performed for the total population and repeated in groups of patients with baseline TCRT below and above 100°. *P*-values < 0.05 were considered statistically significant.

RESULTS

Baseline Characteristics and Associations of TCRT With Biomarkers and Echocardiographic Parameters

From 220 haemodialysis patients recruited to the original study digital ECGs were available and TCRT calculated in 179 and 98 patients at baseline and at follow up, respectively. Comparison of patient groups with TCRT above and below 100° showed significant differences in sex, ethnicity, diastolic BP, biplane left ventricular Ejection Fraction, GLS and $LVMIht^{2.7}$ (**Table 1**). Male patients had higher baseline TCRT values than females (93 ± 41 vs. 80 ± 34°, $p = 0.036$) consistent with previous physiologic observations (Smetana et al., 2002).

On univariate analysis TCRT correlated with GLS ($r = 0.398$, $p < 0.001$), $LVMIht^{2.7}$ ($r = 0.212$, $p = 0.005$), systolic BP ($r = 0.155$, $p = 0.043$) and diastolic BP ($r = 0.172$,

TABLE 1 | Baseline characteristics of the study participants according to TCRT.

Characteristic	All (*N* = 178)	TCRT < 100° *N* = 104	TCRT > 100° *N* = 74	*P*-value
Age, years	67 ± 14	68 ± 14	66 ± 13	0.410
Men, N (%)	128 (71.9)	67 (65)	61 (83)	0.008
Diabetes Mellitus, N (%)	52 (29.2)	23 (25.8)	29 (32.6)	0.853
South Asian, N (%)	31 (17.4)	14 (13.5)	17 (21.3)	0.042
Black, N (%)	5 (2.8)	1 (1.0)	4 (4.5)	
Caucasian, N (%)	142 (79.8)	89 (85.6)	53 (74.2)	
History of Smoking	44 (24.7)	24 (23.1)	20 (27.0)	0.536
CAD, N (%)	42 (23.5)	22(21.2)	20(27)	0.363
Dialysis vintage (months)	36 ± 40	37 ± 46	34 ± 31	0.601
Heart rate, beats/min	73 ± 14	74 ± 13	74 ± 16	0.872
QRS, ms	107 ± 14	107 ± 16	108 ± 13	0.638
QTc, ms	98 ± 14	98 ± 16	406 ± 40	0.858
SBP, mmHg	141 ± 24	138 ± 20	145 ± 26	0.071
DBP, mmHg	70 ± 11	69 ± 10	72 ± 12	0.014
EDV, ml	109 ± 38	104 ± 34	117 ± 41	0.017
Biplane Ejection fraction	62 ± 13	64 ± 13	60 ± 14	0.048
LVMIht^{2,7}g/m	50 ± 20	46 ± 19	56 ± 21	0.002
GLS, %	−12.9 ± 3.8	−14.3 ± 3.3	−11.2 ± 3.7	<0.0001
Troponin I ng/L	30 ± 56	28 ± 49	32 ± 70	0.670
BNP pg/mL	347 ± 520	322 ± 460	382 ± 593	0.224
PWV, m/s	8.9 ± 2.2	8.8 ± 2.0	9.0 ± 2.4	0.424

Values are expressed as mean ± SD or N (%). BNP, N-terminal pro-brain natriuretic peptide; CAD, coronary artery disease; DBP, diastolic blood pressure; EDV, end diastolic volume; GLS, global longitudinal strain; LVMIht$^{2.7}$, left ventricular mass indexed to Ht$^{2.7}$; PWV, pulse wave velocity; QTc, QTc Fridericia; SBP, systolic blood pressure; TCRT, total cosine of R to T (in degrees). Statistically significant differences are highlighted with shaded areas.

p = 0.024). On multivariate linear regression analysis including LVMIht$^{2.7}$, systolic BP, diastolic BP and GLS, only GLS remained significantly correlated with TCRT in the model explaining 19% of the variance (F 9.648, r^2 = 0.192, standardized β = 0.331, unstandardized β = 3.567, t = 4.4429, CI: 1.976–5.157, $p < 0.001$). The relationship between GLS and TCRT is shown in **Figure 2**.

Outcomes

During a mean follow up period of 36 ± 19 months, there were 74 deaths including 17 cardiovascular deaths (9 due to myocardial infarction, 7 were sudden cardiac deaths and 1 was secondary to heart failure), 54 MACE and 32 subjects received a kidney transplant. TCRT values according to outcomes are presented in **Table 2**.

All-Cause Mortality

On univariate Cox regression analysis, the factors associated with increased all-cause mortality were: age, history of CAD, QRS duration, QTc duration, End Diastolic Volume, BNP, Systolic Blood Pressure and PWV. TCRT was found not to have a statistically significant association with all-cause mortality. On multivariate analysis, only age and PWV maintained an association with all-cause mortality. Results of univariate and multivariate Cox regression analysis for all-cause mortality are presented in **Table 3**.

Cardiovascular Mortality

On univariate analysis, variables associated with cardiovascular deaths were TCRT used as a continuous variable as well as dichotomized at 100°, GLS, Troponin I and history of CAD. Patients with TCRT greater than 100° had higher cardiovascular mortality (p = 0.004 by log-rank, **Figure 3A**). In multivariate analysis GLS was not included in the same model with TCRT because GLS and TCRT were correlated with each other. On multivariate analysis only TCRT remained as a significant predictor both as a continuous value and when greater than 100°. Multivariate analysis including GLS and excluding TCRT did not reveal any significant associations. Results of univariate and multivariate Cox regression analysis for cardiovascular mortality are presented in **Table 4**.

Major Cardiac Events

On univariate Cox regression analysis, the factors associated with MACE were TCRT used as a continuous variable and dichotomized at 100°, PWV, GLS, BNP, and history of CAD. Patients with TCRT greater than 100° had higher cumulative probability of MACE (p = 0.002 by log-rank, **Figure 3B**). Because of the significant association between TCRT and GLS we did not include GLS and TCRT in the multivariate model. Using multivariate Cox regression analysis TCRT dichotomized at 100° and PWV remained independent predictors of MACE. TCRT as a continuous variable did not remain significant in the multivariate analysis. Results of univariate and multivariate Cox regression analysis for MACE are presented in **Table 5**. On multivariate analysis including GLS and excluding TCRT, PWV, and CAD remained significant but not GLS.

Longitudinal Changes in TCRT

There were 98 analyzable follow up ECGs. Median time interval from baseline to follow up ECG was 13 (IQR 7) months. There were 31 MACE events, 9 cardiovascular deaths and 40 all-cause deaths in this patient sub-group. From the 31 MACE events, 20 MACE events occurred after the follow up ECG. TCRT increased from baseline to follow up (86 ± 41° vs. 94 ± 41°, p = 0.016). There was no significant increase in TCRT at follow up in the group with baseline TCRT > 100° (128 ± 17° vs. 127 ± 27°, p = 0.794) as opposed to the group with baseline TCRT < 100° (58 ± 24° vs. 72 ± 34°, p = 0.004). Longitudinal changes of TCRT according to baseline values dichotomized at 100° are presented in **Table 6**.

DISCUSSION

In our cohort of prevalent HD patients, QRS – T angle calculated as TCRT from standard surface 12 lead ECGs, carried independent prognostic value for major adverse cardiac events and cardiac mortality. We also observed an association between TCRT and GLS which is a recognized descriptor of uremic cardiomyopathy (Kramann et al., 2014).

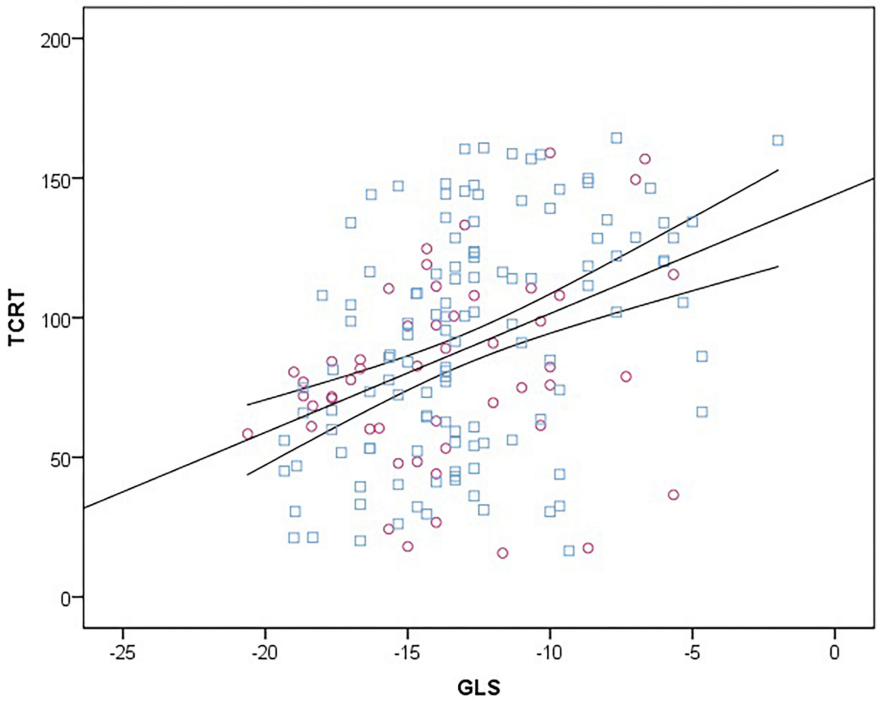

FIGURE 2 | Scatter diagram between TCRT and GLS at baseline. Female subjects are represented with purple circles and male subjects with blue squares. Linear regression line (straight) is plotted with 95% confidence intervals (curved lines). TCRT, total cosine R to T; GLS, global longitudinal strain.

TABLE 2 | TCRT according to end points and to transplant status during follow up.

Outcomes		TCRT	*P*-value
All Cause Deaths, N	Yes (74)	92 ± 38	0.366
	No (104)	87 ± 40	
Cardiac Deaths, N	Yes (17)	114 ± 37	0.006
	No (161)	87 ± 39	
MACE	Yes (54)	98 ± 39	0.043
	No (124)	85 ± 39	
Transplanted	Yes (32)	86 ± 36	0.634
	No (146)	89 ± 40	

Values are expressed as mean ± SD or N. MACE: major cardiac events, TCRT, total cosine of R to T (in degrees). Statistically significant differences are highlighted with shaded areas.

TABLE 3 | Variables associated with increased all-cause mortality by univariate and multivariate Cox regression analysis.

Variables	All-cause Mortality (*N* = 74)	
	HR (95% CI)	*P*-value
	Univariate Cox Regression Analysis	
Age (years)	1.034 (1.014–1.054)	0.001
Diabetes Mellitus	1.650 (1.034–2.634)	0.036
Prevalent CAD	1.679 (1.042–2.707)	0.033
QRS duration	1.017 (1.004–1.031)	0.010
QTc duration	1.017 (1.001–1.034)	0.033
End Diastolic Volume	1.008 (1.002–1.014)	0.010
BNP	1.001 (1.000–1.001)	0.005
Systolic BP (mmHg)	1.010 (1.001–1.019)	0.027
PWV	1.227 (1.128–1.333)	< 0.001
	Multivariate Cox Regression Analysis	
Age (years)	1.038 (1.016–1.059)	0.01
PWV	1.317 (1.180–1.470)	< 0.001

BNP, N-terminal pro-brain natriuretic peptide; BP, blood pressure; CAD, coronary artery disease; CI, confidence interval; PWV, pulse wave velocity; N, number of patients.

QRS-T Angle

Our results, in line with three previously published studies in HD patients (de Bie et al., 2013b; Tereshchenko et al., 2016; Poulikakos et al., 2018) confirm the strong predictive value of the spatial QRS-T angle for cardiac outcomes in HD patients. Tereshchenko et al. (2016) measured the QRS-T angle from signal averaged ECGs in a large cohort of incident HD patients, calculated as the angle between the mean QRS vector and the peak T vector, and identified optimal cut off prognostic value with normal QRS – T angle of 75° for all-cause mortality, cardiovascular mortality and sudden cardiac death. de Bie et al. (2013b) analyzed standard 10 s ECGs in incident HD patients defining the QRS – T angle as the angle between the mean vectors of the QRS and T and used a cut off value of 130° in males and 116° in females for all-cause mortality and sudden cardiac death. The discrepancies between the cut off values quoted in different studies may be explained by the differences in the methods and types of ECG recordings used.

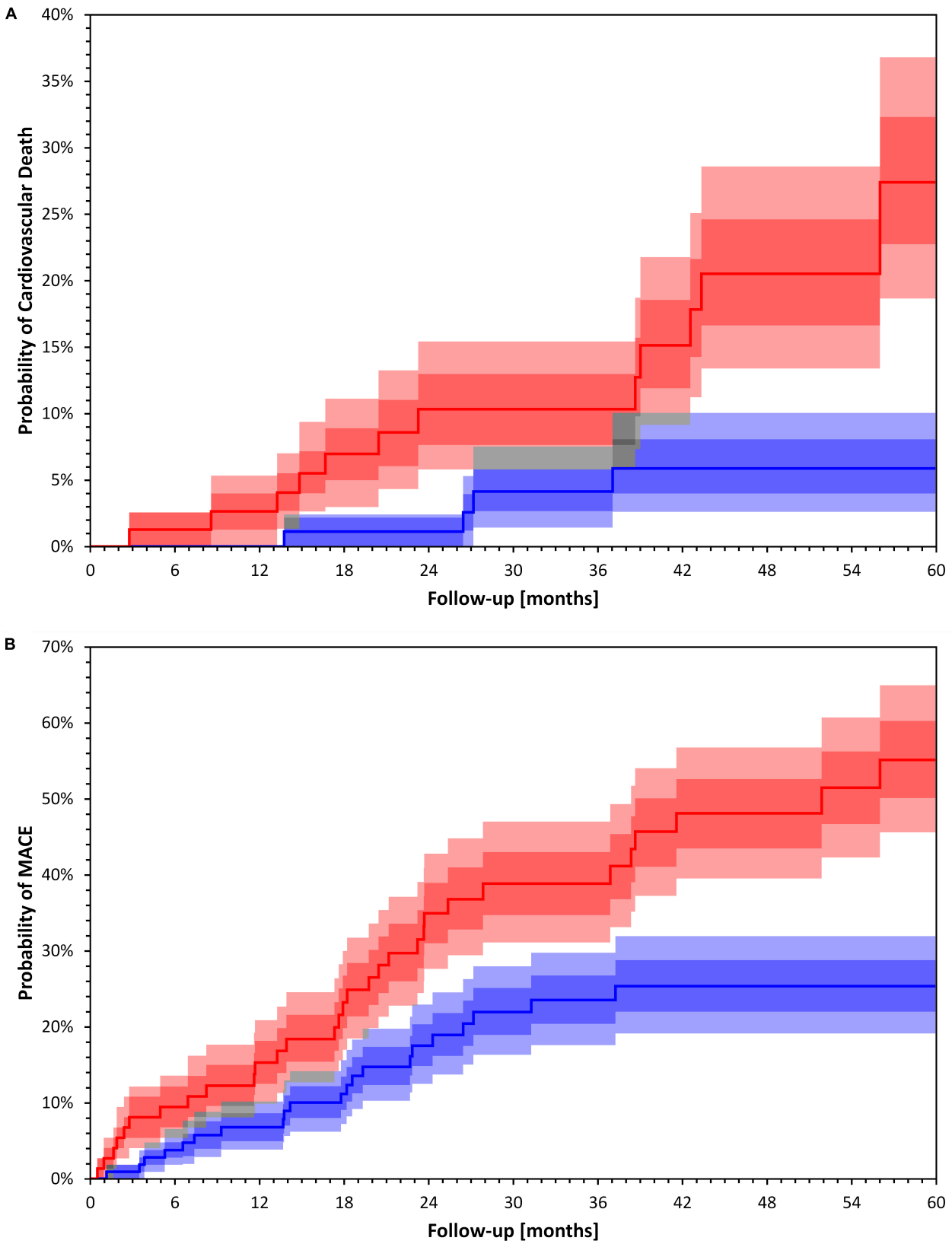

FIGURE 3 | Continued

FIGURE 3 | Kaplan Meier event probability curves for Cardiac Death **(A)** and Major Cardiac Events **(B)**. Kaplan Meier event probability curves for Cardiac Death **(A)** log rank p = 0.004 and Major Cardiac Events **(B)** log rank p = 0.002 for patient groups stratified by a TCRT above and below 100°. Bands represent interquartile ranges (IQR) (darker colors) and 80% percentiles (lighter colors). The gray areas show the overlaps. The dark, middle and light gray correspond to overlaps of IQRs, IQR+80% and 80%+80%, respectively. The bands have been calculated with bootstrap with 10000 random repetitions.

TABLE 4 | Variables associated with increased cardiovascular mortality by univariate and multivariate Cox regression analysis.

Variables		Cardiovascular Mortality (*N* = 17)	
		HR (95% CI)	***P*-value**
		Univariate Cox Regression Analysis	
TCRT	Continuous	1.018 (1.004–1.031)	0.010
	>100°	4.443 (1.447–13.638)	0.009
GLS		1.144 (1.012–1.293)	0.031
Troponin I		1.005 (1.000–1.010)	0.046
Prevalent CAD		2.755 (1.063–7.145)	0.037
		*Multivariate Cox Regression Analysis**	
TCRT	Continuous	1.016 (1.002–1.030)	0.029
	>100°	3.506 (1.118–10.995)	0.031

*CAD, coronary artery disease; CI, confidence interval; GLS, global longitudinal strain; N, number of patients; TCRT, total cosine R to T expressed in degrees. *GLS was not included in the multivariate model together with TCRT due to autocorrelation.*

TABLE 5 | Variables associated with major cardiac events (MACE) by univariate and multivariate Cox regression analysis.

Variables		MACE (*N* = 54)	
		HR (95% CI)	**P value**
		Univariate Cox Regression Analysis	
TCRT	Continuous	1.007 (1.000–1.014)	0.048
	>100°	2.322 (1.328–4.061)	0.008
PWV		1.133 (1.019–1.260)	0.021
GLS		1.115 (1.040–1.196)	0.002
BNP		1.001 (1.000–1.001)	0.011
Prevalent CAD		2.245 (1.280–3.939)	0.005
		Multivariate Cox Regression Analysis model 1 [1]	
TCRT > 100°		1.902 (1.046–3.459)	0.035
PWV		1.141 (1.021–1.276)	0.020
		Multivariate Cox Regression Analysis model 2 [2]	
PWV		1.159 (1.028–1.306)	0.016
Prevalent CAD		1.955 (1.023–1.306)	0.043

BNP, N-terminal pro-brain natriuretic peptide; CAD, history of coronary artery disease; CI, confidence interval; GLS, global longitudinal strain; PWV, pulse wave velocity; HR, hazard ratio; TCRT, total cosine of R to T dichotomized at 100°. [1]Multivariate Cox regression model not including GLS. [2]Multivariate Cox regression model not including TCRT.

In our study, we used TCRT (total cosine of R to T) as an expression of the QRS – T angle. In a recent comparative study between different methods of calculation of the QRS-T angle in cardiac patients and healthy individuals, TCRT was found to be more reliable for risk prediction in cardiac patients compared to other methods for QRS –T angle calculation (Hnatkova et al., 2017). It has been postulated that in the presence of cardiac abnormalities the complexity of the vectorocardiographic loops increases and their spatial orientation is less clearly determined. Therefore, the TCRT technology, by integrating all possible directions of the vectrocardiographic loops as average cosine of all angles, is likely to reflect more accurately the repolarization heterogeneity aberration and improve the risk assessment.

During follow up, TCRT increased in those patients with baseline values below 100°. Large studies in the general population have reported that abnormal increases (Biering-Sørensen et al., 2018) or rapid worsening of QRS-T angle (Biering-Sørensen et al., 2018) is associated with increased risk of sudden cardiac death. The small number of MACE events in the patients with available follow up ECGs, and the relative large proportion of MACE events in the time interval between the ECGs that may have affected the second ECG, prevented us from analyzing the impact of longitudinal changes on MACE and cardiovascular death in this study. Future prospective studies should examine the potential utility of serial assessments of TCRT to characterize the evolution of uremic cardiomyopathy and identify the transition to high risk profiles.

In contrast to the two previous studies in HD patients (de Bie et al., 2013b; Tereshchenko et al., 2016) we did not find an association between higher values of TCRT and all-cause mortality in this cohort of patients. However the aforementioned studies (de Bie et al., 2013b; Tereshchenko et al., 2016) were performed in incident dialysis patients and these patients are known to suffer from particularly high mortality rates during the first 3 months after dialysis initiation (Poulikakos et al., 2014). The third study (Poulikakos et al., 2018) applied intradialytic ECG recordings during the HD sessions of prevalent HD patients and was therefore able to recruit patients with multiple comorbidities and higher mortality risk who would otherwise find it difficult to participate if they had to attend on a non-dialysis day for study screening. We previously reported that patients recruited to our study had longer survival compared to non-participants (Chiu et al., 2016b); patients that denied consent had an adjusted hazard ratio of 1.70, 95% CI 1.10–2.52 and therefore it is possible that recruitment bias may have affected the overall survival outcomes. Furthermore, our prevalent dialysis patients were followed up annually with detailed cardiovascular and clinical assessment and it is possible that such close cardiovascular monitoring enabled early identification and management of cardiovascular disease.

Repolarization Heterogeneity and Cardiac Function

Two previous studies have explored the association between echocardiographic abnormalities and QRS-T angle in dialysis

TABLE 6 | Longitudinal changes of TCRT according to baseline values dichotomized at 100°.

Variable	Total *N* = 98	Baseline TCRT < 100° *N* = 59			Baseline TCRT > 100° *N* = 39
Baseline TCRT	86 ± 41	58 ± 24			128 ± 17
Follow up TCRT	94 ± 41	72 ± 34			127 ± 27
Follow up TCRT > 100° N(%)		7(12)			34(87)
DTCRT	3.41 (32.91)	7.60(35.10)			0.97(23.18)
Transplanted N (%)	9 (9)	7 (12)			2 (5)
		TCRT progressed > 100°			
		Yes (*N* = 7)	No (*N* = 52)	*p*-value	
MACE, N%	31 (32)	4 (57)	15 (29)	0.048	17 (44)
Cardiac Death N%	9 (9)	1 (14)	6 (11)	0.225	7 (18)
Mortality N%	40 (41)	1 (14)	17 (32)	0.011	17 (44)

TCRT values are expressed as mean ± SD, DTCRT: TCRT (follow up)-TCRT (baseline), Outcomes are presented as number N (%). MACE, major cardiac events; TCRT, total cosine of R to T.

patients. In the study by Tereshchenko et al. (2016) increased QRS-T angle was associated with left ventricular hypertrophy but not with left ventricular ejection fraction. In another study of 94 HD patients (de Bie et al., 2013a) left ventricular ejection fraction and LV dysynchrony were indendent predictors of abnormal QRS-T angle (de Bie et al., 2013a). Speckle tracking echocardiography was not included in either study. To our knowledge, the association between TCRT and GLS in a HD population has not been previously reported. Our results are in line with recent large study in the general population (Biering-Sørensen et al., 2018), showing that the QRS-T angle and other measures of repolarization heterogeneity are associated with subclinical abnormalities in cardiac structure and function. In the study by Biering-Sørensen et al. (2018) QRS-T angle explained 10-20% of the variance of GLS depending on the linear regression model used which is similar to the modest 19% of variance in GLS explained by TCRT in our study. The association between repolarization heterogeneity and cardiac function that we observe in HD patients may represent the epiphenomenon of underlying myocardial fibrosis leading to both electrical and functional aberrations or it may reflect the effect of repolarization heterogeneity on cardiac function via inducing heterogeneity and dysynchrony in mechanical contraction within the different myocardial layers. An association between repolarization heterogeneity and mechanical contraction assessed by GLS, in the absence of underlying myocardial fibrosis, has been shown in observational studies in subjects with long QT syndrome (Haugaa et al., 2010; Leren et al., 2015), a condition that is characterized by loss of function potassium channel mutations leading to prolonged action potential duration (APD). In experimental rat models of chronic kidney disease that used optical mapping techniques, increase in APD and lengthening of pacing cycle thresholds to induce APD alterans were detected in CKD rats compared to controls CKD rats; ventricular fibrillation was induced in 9/12 of CKD rats compared to 2/9 normal rats indicating heightened risk of ventricular arrhythmias (Hsueh et al., 2014). Interestingly, although selected markers of myocardial fibrosis, such as mRNA of TGF-b and micro RNA 21, were upregulated in CKD-rats compared to control rats there was no statistically significant difference in myocardial fibrosis between the two groups. The level of fibrosis observed in diseased animals using this rat model of CKD (rats with autosomal dominant polycystic kidney disease) was lower than previous studies using 5/6 nephrectomy model CKD rats (Koleganova et al., 2009; Kramann et al., 2014). In this animal model the increased vulnerability to arrhythmias preceded the development of fibrosis and this finding supports a causative link between altered electrophysiological properties and malignant arrhythmias independent of myocardial fibrosis. However, the effects of electrophysiological aberrations upon the myocardial mechanics were not assessed in this study.

The potential impact of repolarization heterogeneity on cardiac function is also supported by the observation that changes in repolarization heterogeneity measured by 5 ECG parameters including QRS-T angle typically preceded echocardiographic abnormalities in a recently published large general population study (Biering-Sørensen et al., 2018).

The potential relative contribution of repolarization heterogeneity on cardiac function and its relationship with underlying myocardial fibrosis cannot be established from our observational study. Future research to elucidate the link between repolarization heterogeneity and mechanical dysfunction may have important implications in understanding the pathophysiology of uremic cardiomyopathy and in optimizing risk assessment in HD patients. The QRS-T angle assessed by TCRT and GLS, although interrelated, carry prognostic information that is independent of each other and which should be assessed in combination in risk assessment models.

Limitations

The limitations of this study including the relatively small sized population and recruitment selection bias leading to lower mortality have previously been described (Chiu et al., 2016a,b).

Due to the small number of arrhythmic deaths, we did not have the statistical power to investigate associations of TCRT with sudden cardiac death and cardiac arrest separately. Also, we did not manage to investigate follow up ECGs in a large number of patients for the longitudinal ECG analysis thus limiting the scope of the statistical analysis for the longitudinal changes.

CONCLUSION

In conclusion, our study has demonstrated that QRS-T angle calculated by TCRT, an electrocardiographic marker of repolarization heterogeneity that can be derived from standard 10 s ECGs, carries independent prognostic significance for cardiac mortality risk in our HD cohort and it is correlated with GLS. Further prospective studies with longitudinal cardiovascular monitoring including a combination of electrophysiologic and cardiac structural and functional assessment from patients with earlier stages of chronic kidney disease are required to characterize the determinants of the progression of uremic cardiomyopathy and identify potential opportunities for interventions. In light of the consistently strong risk prediction signal of the QRS-T angle in the renal population we suggest that standardization of the assessment of QRS-T angle is important to enable identification of cut-off points indicating high risk to be used in routine clinical practice.

AUTHOR CONTRIBUTIONS

SS and DG collected, analyzed, and interpreted the data, drafted the article, and contributed to statistical expertise. KH processed ECG signal and drafted the article. MM conceived and designed the study, processed the ECG signal, interpreted the data, and critically revised the article. PK conceived and designed the study, interpreted the data, and critically revised the article. DP conceived and designed the work, analyzed and interpreted the data, contributed to statistical expertise, and critically revised the article.

FUNDING

This study was supported by Kidney Research UK Project grant (RP35/2011) that funded the original study and Kidney Research UK Innovation grant (IN4/2015) that funded the advanced ECG analysis. This study was also supported by British Heart Foundation grant NH/16/2/32499.

REFERENCES

Acar, B., Yi, G., Hnatkova, K., and Malik, M. (1999). Spatial, temporal and wavefront direction characteristics of 12-lead T-wave morphology. *Med. Biol. Eng. Comput.* 37, 574–584. doi: 10.1007/BF02513351

Al-Khatib, S. M., Stevenson, W. G., and Ackerman, M. J. (2017). AHA/ACC/HRS guideline for management of patients with ventricular arrhythmias and the prevention of sudden cardiac death: executive summary: a report of the american college of cardiology/american heart association task force on clinical practice guidelines and the heart rhythm society. *Heart Rhythm* 15, e190–e252. doi: 10.1016/j.hrthm.2017.10.035

Biering-Sørensen, T., Kabir, M., and Waks, J. W. (2018). Global ECG measures and cardiac structure and function: the aric study (atherosclerosis risk in communities). *Circ. Arrhythm Electrophysiol.* 11:e005961. doi: 10.1161/CIRCEP.117.005961

Caskey, F., Castledine, C., Dawnay, A., Farrington, K., Fogarty, D., and Fraser, S. (2016). *18th Annual Report of the Renal Association, UK Renal Registry*. Available at: https://www.renalreg.org/wp-content/uploads/2017/09/19th-Annual-Report_web_book.pdf

Chiu, D., Abidin, N., and Johnstone, L. (2016a). Novel approach to cardiovascular outcome prediction in haemodialysis patients. *Am. J. Nephrol.* 43, 143–152. doi: 10.1159/000444924

Chiu, D., Green, D., and Abidin, N. (2016b). Non-recruitment to and selection bias in studies using echocardiography in hemodialysis patients. *Nephrology* 22, 864–871. doi: 10.1111/nep.12865

de Bie, M. K., Ajmone Marsan, N., and Gaasbeek, A. (2013a). Echocardiographical determinants of an abnormal spatial QRS-T angle in chronic dialysis patients. *Nephrol. Dial. Transplant.* 28, 3045–3052. doi: 10.1093/ndt/gft347

de Bie, M. K., Koopman, M. G., and Gaasbeek, A. (2013b). Incremental prognostic value of an abnormal baseline spatial QRS-T angle in chronic dialysis patients. *Europace* 15, 290–296. doi: 10.1093/europace/eus306

Haugaa, K. H., Amlie, J. P., Berge, K. E., Leren, T. P., Smiseth, O. A., and Edvardsen, T. (2010). Transmural differences in myocardial contraction in long-QT syndrome: mechanical consequences of ion channel dysfunction. *Circulation* 122, 1355–1363. doi: 10.1161/CIRCULATIONAHA.110.960377

Hensen, L. C. R., Goossens, K., and Podlesnikar, T. (2018). Left ventricular mechanical dispersion and global longitudinal strain and ventricular arrhythmias in predialysis and dialysis patients. *J. Am. Soc. Echocardiogr.* 31, 777–783. doi: 10.1016/j.echo.2018.01.010

Hnatkova, K., Seegers, J., and Barthel, P. (2017). Clinical value of different QRS-T angle expressions. *Europace* 20, 1352–1361. doi: 10.1093/europace/eux246

Hsueh, C. H., Chen, N. X., and Lin, S. F. (2014). Pathogenesis of arrhythmias in a model of CKD. *J. Am. Soc. Nephrol.* 25, 2812–2821. doi: 10.1681/ASN.2013121343

Koleganova, N., Piecha, G., Ritz, E., and Gross, M. L. (2009). Calcitriol ameliorates capillary deficit and fibrosis of the heart in subtotally nephrectomized rats. *Nephrol. Dial. Transplant.* 24, 778–787. doi: 10.1093/ndt/gfn549

Kramann, R., Erpenbeck, J., and Schneider, R. K. (2014). Speckle tracking echocardiography detects uremic cardiomyopathy early and predicts cardiovascular mortality in ESRD. *J. Am. Soc. Nephrol.* 25, 2351–2365. doi: 10.1681/ASN.2013070734

Lang, R. M., Badano, L. P., and Mor-Avi, V. (2015). Recommendations for cardiac chamber quantification by echocardiography in adults: an update from the american society of echocardiography and the european association of cardiovascular imaging. *Eur. Heart J. Cardiovasc. Imag.* 16, 233–270. doi: 10.1093/ehjci/jev014

Leren, I. S., Hasselberg, N. E., and Saberniak, J. (2015). Cardiac mechanical alterations and genotype specific differences in subjects with long QT syndrome. *JACC Cardiovasc. Imag.* 8, 501–510. doi: 10.1016/j.jcmg.2014.12.023

Porthan, K., Viitasalo, M., Toivonen, L., Havulina, A. S., Jula, A., Tikkanen, J. T., et al. (2013). Predictive value of electrocardiographic T-wave morphology parameters and T-wave peak to T-wave end interval for sudden cardiac death in the general population. *Circ. Arrhythm Electrophysiol.* 6, 690–696. doi: 10.1161/CIRCEP.113.000356

Poulikakos, D., Banerjee, D., and Malik, M. (2014). Risk of sudden cardiac death in chronic kidney disease. *J. Cardiovasc. Electrophysiol.* 25, 222–231. doi: 10.1111/jce.12328

Poulikakos, D., Hnatkova, K., Banerjee, D., and Malik, M. (2018). Association of QRS-T angle and heart rate variability with major cardiac events and

mortality in hemodialysis patients. *Ann. Noninvasive Electrocardiol.* 23:e12570. doi: 10.1111/anec.12570

Roberts, M. A., Hare, D. L., Ratnaike, S., and Ierino, F. L. (2006). Cardiovascular biomarkers in CKD: pathophysiology and implications for clinical management of cardiac disease. *Am. J. Kidney Dis.* 48, 341–360. doi: 10.1053/j.ajkd.2006.06.005

Smetana, P., Batchvarov, V. N., Hnatkova, K., Camm, A. J., and Malik, M. (2002). Sex differences in repolarization homogeneity and its circadian pattern. *Am. J. Physiol. Heart Circ. Physiol.* 282, H1889–H1897. doi: 10.1152/ajpheart.00962.2001

Tereshchenko, L. G., Kim, E. D., and Oehler, A. (2016). Electrophysiologic substrate and risk of mortality in incident hemodialysis. *J. Am. Soc. Nephrol.* 27, 3413–3420. doi: 10.1681/ASN.2015080916

United States Renal Data System (2016). *USRDS Annual Data Report: Epidemiology of Kidney Disease in the United States*. Bethesda, MD: National Institutes of Health.

Waks, J. W., Sitlani, C. M., Soliman, E. Z., Kabir, M., Ghafoori, E., and Biggs, M. L. (2016). Global electric heterogeneity risk score for prediction of sudden cardiac death in the general population: the atherosclerosis risk in communities (ARIC) and cardiovascular health (CHS) studies. *Circulation* 133, 2222–2234. doi: 10.1161/CIRCULATIONAHA.116.021306

Zabel, M., Acar, B., Klingenheben, T., Franz, M. R., Hohnloser, S. H., and Malik, M. (2000). Analysis of 12-lead T-wave morphology for risk stratification after myocardial infarction. *Circulation* 102, 1252–1257. doi: 10.1161/01.CIR.102.11.1252

Conflict of Interest Statement: The authors declare that the research was conducted in the absence of any commercial or financial relationships that could be construed as a potential conflict of interest.

frontiers in Physiology

REVIEW
published: 25 February 2019
doi: 10.3389/fphys.2019.00144

Sudden Cardiac Death in Dialysis: Arrhythmic Mechanisms and the Value of Non-invasive Electrophysiology

Dimitrios Poulikakos[1,2], Katerina Hnatkova[3], Sofia Skampardoni[1,2], Darren Green[1,2], Philip Kalra[1,2] and Marek Malik[3]*

[1] Renal Department, Salford Royal NHS Foundation Trust, Salford, United Kingdom, [2] Centre for Cardiac Research, Institute of Cardiovascular Sciences, The University of Manchester, Manchester, United Kingdom, [3] National Heart and Lung Institute, Imperial College London, London, United Kingdom

Sudden Cardiac Death (SCD) is the leading cause of cardiovascular death in dialysis patients. This review discusses potential underlying arrhythmic mechanisms of SCD in the dialysis population. It examines recent evidence from studies using implantable loop recorders and from electrophysiological studies in experimental animal models of chronic kidney disease. The review summarizes advances in the field of non-invasive electrophysiology for risk prediction in dialysis patients focusing on the predictive value of the QRS-T angle and of the assessments of autonomic imbalance by means of heart rate variability analysis. Future research directions in non-invasive electrophysiology are identified to advance the understanding of the arrhythmic mechanisms. A suggestion is made of incorporation of non-invasive electrophysiology procedures into clinical practice.

Key Concepts:

- Large prospective studies in dialysis patients with continuous ECG monitoring are required to clarify the underlying arrhythmic mechanisms of SCD in dialysis patients.
- Obstructive sleep apnoea may be associated with brady-arrhythmias in dialysis patients. Studies are needed to elucidate the burden and impact of sleeping disorders on arrhythmic complications in dialysis patients.
- The QRS-T angle has the potential to be used as a descriptor of uremic cardiomyopathy.
- The QRS-T angle can be calculated from routine collected surface ECGs. Multicenter collaboration is required to establish best methodological approach and normal values.
- Heart Rate Variability provides indirect assessment of cardiac modulation that may be relevant for cardiac risk prediction in dialysis patients. Short-term recordings with autonomic provocations are likely to overcome the limitations of out of hospital 24-h recordings and should be prospectively assessed.

Keywords: sudden cardiac death, arrhythmias, dialysis, QRS-T angle, TCRT, heart rate variability, implantable loop recorders

OPEN ACCESS

Edited by:
T. Alexander Quinn, Dalhousie University, Canada

Reviewed by:
Jaap Joles, Utrecht University, Netherlands
Jordan Loyal Holtzman, University of Minnesota Twin Cities, United States

****Correspondence:***
Dimitrios Poulikakos
dimitrios.poulikakos@srft.nhs.uk;
dempoulikakos@hotmail.com

Specialty section:
This article was submitted to Cardiac Electrophysiology, a section of the journal Frontiers in Physiology

Received: *13 October 2018*
Accepted: *07 February 2019*
Published: *25 February 2019*

Citation:
Poulikakos D, Hnatkova K, Skampardoni S, Green D, Kalra P and Malik M (2019) Sudden Cardiac Death in Dialysis: Arrhythmic Mechanisms and the Value of Non-invasive Electrophysiology. Front. Physiol. 10:144. doi: 10.3389/fphys.2019.00144

INTRODUCTION

Chronic kidney disease affects 5–7% of the global population and is associated with a 10-fold increase in cardiovascular mortality. Over 2 million people worldwide are on renal replacement therapy (Couser et al., 2011). Despite technological advances in the field of renal replacement therapy, the long-term survival of patients receiving chronic dialysis remains poor, comparable with survival in some forms of cancer (United States Renal Data System, 2012). Cardiovascular disease and infections account for most of these deaths. SCD accounts for a large proportion of cardiovascular deaths and almost one fourth of the overall mortality in these patients as evidenced from registry data (United States Renal Data System, 2012) and from prospective trials with death adjudication (Cheung et al., 2004; Wanner et al., 2005). High risk of SCD is present even at early stages of CKD but it increases substantially when patients are on HD. This high risk is aggravated by the fluctuations in volume and electrolyte status induced by the intermittent pattern of the treatment (Poulikakos et al., 2014a).

It has been shown that renal dysfunction increases the risk of ventricular arrhythmias in patients with underlying ischaemic heart disease. After a first myocardial infarction, the presence of CKD stage 3 was found to be associated with a sixfold increase in odds of developing VF independently of traditional cardiovascular risk factors (Dalal et al., 2012). Advanced CKD has been shown to be a strong predictor of appropriate delivery of shock therapies for ventricular arrhythmias in implantable cardioverter defibrillator recipients (Robin et al., 2006; Cuculich et al., 2007). In these patients, advanced CKD has also been associated with decreased time to the first appropriate shock (Hreybe et al., 2006). However, the implantation of cardioverter defibrillators based on existing guidance has not been associated with survival benefit in retrospective studies in this high-risk population (Charytan et al., 2011; Pun et al., 2015).

Although CKD often coexists with coronary artery disease (Herzog et al., 2011), SCD is also highly prevalent in dialysis patients without a history of coronary artery disease or impaired left ventricular ejection fraction (Baigent et al., 2011). Possible mechanisms that increase cardiovascular risk related to advanced CKD include the ensuing bone mineral abnormalities and vascular calcification (London et al., 2003), endothelial dysfunction (Poulikakos et al., 2014d), electrolyte fluxes (Wang et al., 2018), chronic inflammation (Nowak and Chonchol, 2018), insulin resistance (Semple et al., 2011), increased levels of FGF 23 (Gutiérrez et al., 2009; Isakova et al., 2011) and autonomic imbalance (Converse et al., 1992b). Based on epidemiological data, it has also been postulated that heritable factors contribute to the risk of cardiac arrest in patients receiving dialysis (Chan et al., 2015). However, the exact pathogenic mechanisms that interlink these factors and lead to the high risk cardiovascular phenotype in CKD remain elusive.

Abbreviations: AF, atrial fibrillation; CKD, chronic kidney disease; ECG, electrocardiogram; HD, hemodialysis; HRV, heart rate variability; IHD, ischemic heart disease; ILR, implantable loop recorder; SCD, sudden cardiac death; TCRT, total Cosine R To T; VF, ventricular fibrillation; VT, ventricular tachycardia.

Furthermore, whereas the increased risk of ventricular arrhythmias due to advanced CKD in the context of severe ischaemic cardiomyopathy has been confirmed (Robin et al., 2006; Cuculich et al., 2007; Dalal et al., 2012; Wan et al., 2014), the underlying arrhythmic mechanisms leading to SCD in dialysis patients with preserved left ventricular function are not well understood. Recent studies that used ILR in small cohorts of asymptomatic HD patients have shown increased rates of bradyarrhythmic events and deaths (Kalra et al., 2018).

Risk stratification strategies to identify dialysis individuals who are at high risk of SCD are lacking. This is despite them attending hospital or satellite facilities for their dialysis treatment three times weekly and having clinical observations and blood tests more often than any other out-patient group. Because of this, it is recognized that non-invasive electrophysiology could serve the unmet clinical need for risk prediction in this population (Skampardoni et al., 2018b). Descriptors of repolarization aberration and autonomic dysregulation can be assessed by applying advanced computerized analysis of snapshot and/or continuous ECGs and can be used for this purpose. There is accumulating evidence that increased QRS-T angle is a good descriptor of the arrhythmogenic myocardial substrate and predicts cardiovascular risk in this population (Skampardoni et al., 2018b). Furthermore, measurements of cardiac autonomic regulation by HRV have also shown promising results in cardiac risk assessment in dialysis patients.

This review summarizes the recent evidence from the use of ILRs in HD patients and electrophysiological studies in animal models of CKD, exploring the potential underlying arrhythmic mechanisms. It also presents the evidence from the use of non-invasive electrocardiography in dialysis patients focusing on QRS-T angle and HRV and concludes with suggestions for future directions of research.

Arrhythmic Patterns in Dialysis Patients. Insight From Studies Involving Continuous ECG Monitoring From Implantable Loop Recorders

Since 2015, five studies using ILR in asymptomatic HD patients have been published (Silva et al., 2015; Wong M.C. et al., 2015; Roberts et al., 2017; Roy-Chaudhury et al., 2018; Sacher et al., 2018) (**Table 1**). Collectively, they included 317 prevalent HD patients with largely preserved left ventricular ejection fraction. The age ranged from 56 ± 12 (Roy-Chaudhury et al., 2018) to 68 ± 12 (Roberts et al., 2017) years and follow up time ranged from 6 (Roy-Chaudhury et al., 2018) to 21 ± 7 (Sacher et al., 2018) months. In total, there were 52 deaths (15%) of which 21 (6.6% of patients, 40% of deaths) were classified as SCD. ILRs revealed bradyarrhythmia or asystole as the terminal rhythm in the majority (13) of SCD deaths. SCD cases in the 5 studies ranged from 83% (Wong M.C.G. et al., 2015) to 25% (Roberts et al., 2017) of all deaths and bradycardia as the terminal SCD rhythm was reported in 42% (Silva et al., 2015) to 100% (Sacher et al., 2018) of SCD cases. On the contrary, there were only 4 cases of sustained VT or VF across the 5 studies. In total 9 patients required pacemaker implantation for bradyarrhythmia

TABLE 1 | Studies using implantable loop recorders in HD patients.

Study	Number	Age (years)	IHD	Follow up (months)	SCD/Total mortality (%)	Brady-arrhythmic SCD	VT-VF	Significant arrhythmic events	Comments
Wong M.C.G. et al., 2015	50	67 ± 11	48%	18 ± 4	8/10 (80%)	6	2	**Pacemaker in 1 patient** Bradycardia 30% Sinus arrest 28% 2nd degree atrioventricular block 4% Non-sustained VT 20% AF 28%	All SCDs and increased rates of arrhythmias during long interdialytic interval.
Silva et al., 2015	100	59 ± 8.8	34%	14 ± 4	7/18 (39%)	3	1	Bradycardia 25% Asystole 4% Non-sustained VT 56% AF 13%	Left Ventricular dilatation associated with higher occurrence of non-sustained VT.
Sacher et al., 2018	71	65 ± 9	NR	21 ± 7	4/16 (25%)	4	–	Conduction Abnormalities 14% (patient years) Non-sustained VT 9% (patient years) AF 37% (20% *de novo*)	
Roberts et al., 2017	30	68 ± 12	22%	18 ± 12	2/8 (25%)	0	1	**Pacemakers in 3 patients** (2 dual chamber pacemakers and 1 biventricular pacemaker)	Increased nocturnal bradycardias.
Roy-Chaudhury et al., 2018	66	56 ± 12	48.5%	6	0	–	–	**Pacemakers in 5 patients** Bradycardia 25.8% Asystolic events* 10.6% Non-sustained Ventricular arrhythmias * 77.3% AF* 40.9% (device detected)	Increased rates of bradyarrhythmic events at the end of long interdialytic interval.

AF, atrial fibrillation; IHD, ischemic heart disease; NR, not reported; SCD, sudden cardiac death; VT, ventricular tachycardia; VF, ventricular fibrillation. Table was modified with permission by Kalra et al. (2018).

across the 5 studies [3/30 patients in the study by Roberts et al. (2017), 5/66 in the study by Roy-Chaudhury et al. (2018), and 1/50 in the study by Wong M.C. et al. (2015)]. The temporal pattern of arrhythmias in the detailed study by Roy-Chaudhury et al. (2018) showed an increased rate of clinically significant bradycardias, defined as rate <40 bpm for ≥6 s, toward the latter stages of the long interdialytic interval. One of the studies (Roberts et al., 2017) reported on the circadian pattern of the bradycardic episodes noting an increased rates during night-time. The proportion of patients with at least one episode of severe bradycardia ranged from 20% (Roy-Chaudhury et al., 2018) to 25% (Silva et al., 2015) and asystolic events ranged from 4% (Silva et al., 2015) to 20% (Wong M.C.G. et al., 2015). The studies reported high rates of AF ranging from 13% (Silva et al., 2015) to 40.9% (Roy-Chaudhury et al., 2018).

Although these studies provide novel information, this should be interpreted with caution. The scarcity of available information about the prevalence of bradyarrhythmias from long-term monitoring in asymptomatic patients need to be taken into consideration.

Previous studies using 24-h recordings in healthy individuals have shown a high prevalence of bradycardias (heart rate 40 beats/min or less) during sleep at 24% in males aged 22–27 years (Brodsky et al., 1977). With advancing age, this decreased to 3% in subjects aged 40–79 years (Bjerregaard, 1983) and 2% in the group aged 60–85 years (Fleg and Kennedy, 1982). ILRs are likely to detect more bradycardic events than 24 h Holter monitors (Simantirakis et al., 2004) but have not been used to study healthy populations.

The participants in the HD ILR studies were not young and, despite the lack of knowledge regarding the normal incidence of bradycardias in HD patients and notwithstanding the small number of relatively low cardiovascular risk participants and the heterogeneity amongst the studies, these investigations show a high burden of bradyarrhythmias in HD patients with preserved ejection fraction. This potentially contributes substantially to the overall burden of SCD. Consistent with the HD ILR studies, a recent epidemiological study that investigated registry data of 28,471 dialysis patients (Wang et al., 2016) showed that HD patients had an almost sixfold increased incidence of requiring pacemaker insertion compared to matched patients with normal renal function.

Pathogenesis of Bradycardia

Elucidating the underlying mechanisms of bradycardias and their relationship to SCD has important clinical implications relating to the required routine screening, to the decisions of potential use of beta blockers, and/or to considerations of potential interventions such as pacemaker insertion.

Electrolyte shifts, especially pre-dialysis hyperkalaemia, have been implicated as potential triggers of bradyarrhythmias particularly at the end of the long interdialytic interval in a typical 3 dialysis session week. The electrophysiological role of hyperkalaemia in triggering bradyarrhythmias is

likely potentiated by the presence of underlying structural abnormalities in the conduction system and/or abnormal cardiac autonomic regulation of the pacemaker activity that prevent adequate heart rate reactions in response to physiological stress. Cardiac valve calcification may affect the cardiac conduction system and has also been implicated in bradyarrhythmias (Mainigi et al., 2012). It is highly prevalent in HD (Matsuo et al., 2018) and peritoneal dialysis (PD) patients (Wang et al., 2003) and has been associated with increased cardiovascular mortality (Wang et al., 2018). In addition, evidence of impaired cardiac autonomic modulation in dialysis patients has been demonstrated in several HRV studies (Poulikakos et al., 2014a).

The potential contribution of obstructive sleep apnoea to bradyarrhythmias in dialysis patients merits attention. Sleep apnoea is typically characterized by episodes of bradycardia (Zwillich et al., 1982) as shown with long term recordings with ILR in this population (Simantirakis et al., 2004). Sleep apnoea is highly prevalent in HD patients occurring in 34.5% (Tada et al., 2007) to 65% (Sakaguchi et al., 2011) of cases. It is commonly underdiagnosed and its severity has been associated with the magnitude of fluid overload (Ogna et al., 2015). Interestingly, bradyarrhythmias due to sleep apnoea do not seem to be potentiated by the administration of beta blockers (Wolf et al., 2016) and can be successfully treated with continuous positive airway pressure treatment (Simantirakis et al., 2004). No information regarding the presence of sleep apnoea was provided in the publications of the HD ILR studies. However, it can be speculated that it was present in a fair proportion of the participants and that sleep apnoea related bradyarrhythmias would tend to increase during periods of increased fluid retention, i.e., at the end of the long interdialytic interval.

Atrial Fibrillation and Sudden Cardiac Death

The high rate of AF in the HD population is another important finding and may be linked to increased risk of SCD. Evidence suggests that AF may be associated with SCD in cardiac patients (Gronefeld et al., 2000; Berton et al., 2009; Pedersen et al., 2006) and in the general population (Chen et al., 2013). Several mechanisms have been suggested linking AF with SCD (Chen et al., 2014). It has been speculated that fast ventricular rate in the context of atrial tachyarrhythmia can reduce ventricular refractoriness (Denes et al., 1974) thus increasing the vulnerability to ventricular arrhythmias. In addition, AF can lead to short-long-short sequences in the ventricular cycle length that in turn predispose to some types of ventricular arrhythmias (Gronefeld et al., 2000).

ARRHYTHMIC MECHANISMS IN ANIMAL MODELS OF CKD

Animal models have been used to investigate the pre-arrhythmic substrate and the mechanisms of arrhythmias in CKD (**Table 2**).

Hsueh et al. (2014) used a rat cystic kidney disease model (Cy/+ rats) characterized by progressive CKD that reaches terminal uraemia in about 40 weeks. They investigated 12 CKD and 9 normal rats at week 35 with detailed electrophysiological studies including optical mapping and a pacing protocol for VF induction. CKD rats showed increased action potential duration and longer cycle length thresholds to induce action potential duration alterans compared to normal rats, indicating increased vulnerability to ventricular arrhythmias. VF was induced in 9/12 (75%) CKD rats compared to 2/9 (22%) normal rats. Examination of the heart tissue following euthanasia revealed upregulation of pro-fibrotic pathways in CKD animals but did not show significant difference in cardiac fibrosis between the two groups.

Lee et al. (2017) used a rat model of mild CKD (unilateral nephrectomy at 8 weeks) and performed electrophysiological studies 8 weeks after the operation, including surface ECG. After euthanasia, cardiomyocytes were isolated for further electrophysiological recordings of ionic currents and membrane potential. CKD rats exhibited prolonged QTc compared to normal rats. Longer action potential duration at 50 and 90% repolarization of paced cardiomyocytes was observed in epicardiac cardiomyocytes in CKD rats compared to normal rats but there was no difference in endocardial cardiomyocytes. The transient outward potassium current I_{to} was reduced in epicardial cardiomyocytes in CKD rats compared to controls, and associated with decreased transmural gradient of I_{to}. Similar to the previous study, increased heterogeneity of repolarization occurred independently of the cardiac fibrosis that was observed at similar levels in CKD and normal rats (Chang et al., 2015).

(Zhao et al. (2016) used the same CKD model as presented by Hsueh et al. (2014) (Cy/+ rats). The animals were implanted with ECG and subcutaneous nerve activity electrode recorders at 35 weeks. Subcutaneous nerve activity has been shown to correlate with the stellate ganglion nerve activity and was thus used to estimate the sympathetic tone (Robinson et al., 2015). All 6 CKD rats died suddenly 23 ± 14 days after the implantation. All SCDs occurred after the development of atrioventricular block. Terminal rhythms were progressive bradycardia and asystole in 3 rats, VF in 2 rats and VT converted to bradycardia in one rat. In contrast to the previous studies, histology showed fibrosis in all CKD rats, especially surrounding the AV node and in the sub-endocardium, and calcification affecting the conduction system. These findings were not present in normal rats. The magnitude of the increase in heart rate corresponding to increase in subcutaneous nerve activity was smaller in CKD rats 5 days prior to death.

Fontes et al. (2015) used two different mouse models of renal impairment. First model included aged mice that received deoxycorticosterone acetate for 8 weeks and a high-salt diet that continued for 35 weeks. Second model dealt with adult mice that underwent 5/6-subtotal nephrectomy and were treated for 11 weeks with a high-salt diet. *Ex vivo* epicardial mapping was used to assess vulnerability to arrhythmias and hearts were assessed for fibrosis and characterized for connexin 43 (Cx43). Both models demonstrated a high incidence of arrhythmias accompanied by increased interstitial fibrosis and decreased Cx43 expression in the heart.

The first two animal investigations (Hsueh et al., 2014; Lee et al., 2017) suggest that electrophysiological aberrations leading to increased repolarization heterogeneity and vulnerability to

TABLE 2 | Electrophysiological studies in animal models of CKD.

Study	Animal model	Electrophysiological study	Time	Fibrosis assessment	Time	Main findings
Hsueh et al., 2014	Cy/+ rats (12) compared to normal rats (9)	Optical mapping Induced VF via pacing	35 weeks	Picrosirius red staining	35 weeks	Longer action potential duration at 80% repolarization and cycle length thresholds to induce alterans in CKD rats. VF induced in 9/12 CKD rats vs. 2/9 normal rats. Electrical remodeling favoring initiation and maintenance of VTs in CKD rats. No difference in cardiac fibrosis.
Lee et al., 2017	Unilateral nephrectomy at 8 weeks rats (6) compared to sham operated rats (6)	Surface ECG Patch-clamp studies	8 weeks after nephrectomy	Trichrome staining and picrosirius red staining* Cellular hypertrophy based on cellular capacitance in ventricular cardiomyocytes	8 weeks post nephrectomy	Prolonged QTc in CKD rats. Epicardial prolongation of action potential duration in CKD rats and decreased transmural gradient in CKD rats compared to controls. Electronegative LDL may underlie downregulation of KChIP2 protein expression. No difference in fibrosis.
Zhao et al., 2016	Cy/+ rats (6) Compared to normal rats (8)	Continuous ECG Subcutaneous nerve activity recordings	Started at 35 weeks and continued for 23 ± 14 days	Trichrome staining H&E staining	40 weeks for normal rats After sudden death at CKD rats (35 weeks+ 23 ± 14 days)	6 deaths due to bradycardia or atrioventricular block. 3 deaths due to VT/VF. Myocardial calcification involving the conduction system. Blunted response of heart rate to subcutaneous nerve activity increase in CKD rats. Sudden death preceded by reduction in subcutaneous nerve activity.
Fontes et al., 2015	Aged mice deoxycorticosterone acetate and high salt diet (n = 7) & 5/6 -subtotal nephrectomy and high salt diet (5) Controls (4)	Programmed electrical stimulation of arrhythmias Conduction velocity from electrocardiograms	68 weeks 11 weeks	Picrosirius red staining	68 weeks 11 weeks	Arrhythmias induced in 86 and 75% in hearts from aged mice and partially nephrectomised mice on high salt diet compared to 0% in control hearts. Cx43 expression was reduced and interstitial fibrosis was increased in both groups with renal dysfunction.

*CKD, chronic kidney disease; Cx43, connexin 43, gap junction protein expressed in the heart; ECG, electrocardiogram; VT, ventricular tachycardia; VF, ventricular fibrillation. *Experiments on cardiac fibrosis were performed in previous study of the same group using the same CKD rat model.*

ventricular arrhythmias occur before the development of overt cardiac fibrosis and calcification which is in turn associated with conduction system disorders and bradyarrhythmias in advanced CKD in rodents. Considering the two studies (Hsueh et al., 2014; Zhao et al., 2016) that used the same Cy/+ CKD models, Hsueh et al. (2014) did not find fibrosis in heart tissue retrieved following euthanasia at 35 weeks whereas Zhao et al. (2016) detected fibrosis and calcification in heart tissue retrieved 3 weeks later (after death), i.e., in animals exposed to CKD for longer.

The observation that the relationship between subcutaneous nerve activity, a surrogate of sympathetic tone, and heart rate was different in CKD rats compared to normal rats is in keeping with human studies describing abnormal autonomic cardiac modulation in CKD.

However, fundamental electrophysiological differences exist between rodents and large mammals (Sallam et al., 2015), making rodents a poor model of human electrophysiology. Furthermore, these animal models did not study the dynamic interactions of the fluctuations in fluid and electrolyte changes. Therefore their contribution in understanding the mechanisms of SCD in dialysis patients is limited. Thus, interpretation and extrapolations from these animal experiments need to be made with caution.

NON-INVASIVE ELECTROPHYSIOLOGY IN DIALYSIS PATIENTS

The standard 12 lead ECG is an essential clinical tool in CKD and dialysis patients (Skampardoni et al., 2018b). It is commonly used for the assessment of the acutely unwell patient. It can also be used as routine investigation for the detection of conduction abnormalities that require clinical intervention such as with medication or dialysis prescription review, further studies and referral for pacemaker implantation. However, the fluctuant fluid and electrolyte status of HD patients may affect the ECG waveform that in turn can influence the automated ECG

interpretations including interval calculations (Poulikakos and Malik, 2016). This influence poses challenges in using automated ECG measurements in risk stratification studies. Furthermore, important repolarization abnormalities usually referred to as "non-specific T wave changes" are only subjectively defined and cannot be studied in a quantifiable manner. Advanced computerized analysis of the ECG has the potential to overcome these limitations.

Repolarization Heterogeneity and the Case for QRS-T Angle Assessment in CKD

The QRS-T angle is an established marker of global repolarization heterogeneity (Waks et al., 2016; Hnatkova et al., 2017) that can be measured from a standard 12 lead ECG (**Figure 1**). It is based on three-dimensional vectorial representation of the electrical activity of the heart, that is not affected by impedance changes due to fluid shifts (Vitolo et al., 1987). The QRS-T angle is calculated numerically, is reproducible (Poulikakos et al., 2013; Hnatkova et al., 2017) and thus suitable for risk stratification purposes. A larger QRS-T angle has been shown to predict SCD (de Bie et al., 2013b; Tereshchenko et al., 2016), cardiovascular mortality (Skampardoni et al., 2018a) and all cause mortality (Tereshchenko et al., 2016; de Bie et al., 2013b; Poulikakos et al., 2018) in different cohorts of predominantly African (Tereshchenko et al., 2016) and Caucasian (Sallam et al., 2015; Poulikakos et al., 2018; Skampardoni et al., 2018a) dialysis patients. However, one study in 325 Taiwanese HD patients (Lin et al., 2007) did not find a significant association between magnitude of QRS-T angle and outcomes. Instead, this study reported that T wave residuum, a descriptor of regional repolarization heterogeneity (Zabel and Malik, 2002), was an independent predictor of cardiovascular mortality and SCD. Studies that have investigated the prognostic value of the QRS-T angle in dialysis patients are summarized in **Table 3**.

An increased QRS-T angle has been associated with echocardiographic left ventricular hypertrophy (Tereshchenko et al., 2016), decreased global longitudinal strain (Skampardoni et al., 2018a), lower left ventricular ejection fraction, and with left ventricular systolic dyssynchrony (de Bie et al., 2013a) in different cohorts of HD patients. It has also been associated with increased coronary artery calcium burden, and elevated Troponin T levels in patients receiving peritoneal dialysis (Jaroszynski et al., 2009). The impact of HD treatment on the QRS-T angle has been variable (Jaroszynski et al., 2010; Poulikakos et al., 2013). The intra-subject stability of the QRS-T angle at the start and the end of dialysis has been demonstrated in a cohort of 72 HD patients who underwent five intra-dialytic Holter ECGs at 2-week intervals (Poulikakos et al., 2013). Studies reporting on associations of the QRS-T angle with echocardiographic characteristics and intradialytic changes are presented in **Table 4**. **Figure 2** shows an example of Kaplan–Meier event probability curves of major cardiac events and overall mortality in 72 HD patients (Poulikakos et al., 2018) stratified by QRS-T angle above and below median value.

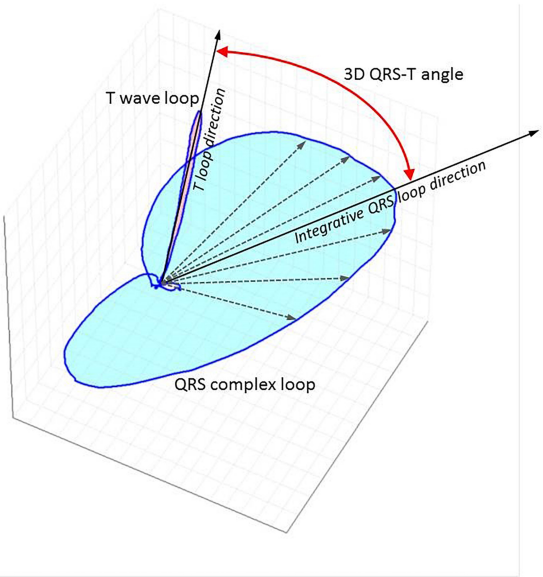

FIGURE 1 | Three-dimensional representation of QRS and T vector loops following computerized analysis of standard 12 lead ECG using singular value decomposition to yield an orthogonal lead system (TCRT method). The little white circle in the middle depicts the loop of the p wave. The curved red line with arrow at both ends depicts the spatial QRS-T angle. The maximal T wave vector magnitude is used for the calculations with this method. TCRT is the averaged cosine of the angles between the T wave vector and all vectors within the QRS complex exceeding a pre-defined level. A different method of QRS-T angle measurement from standard 12 lead digital snapshot ECG uses inverse Dower matrix for vectrographic transformation and calculates the angle between the mean vectors of the QRS and T wave. QRS-T angle has also been calculated from continuous signal averaged ECGs as the angle between the peak QRS vector and the peak T vector.

Methodological Considerations

Different groups have used different methods for the calculation of the QRS-T angle that are summarized in **Table 3**. The methodological differences stem from different approaches in characterizing the spatial deviation between the vectorial loops of depolarization (QRS) and repolarization (T wave). These differences may partially explain the different numerical cut-off values (Hnatkova et al., 2017) used in predicting outcomes in dialysis populations. The challenge lies mainly in the fact that the loops can be irregular and curved in space. It has recently been demonstrated in cardiac patients that the discrepancies between the various methods increase as the angle becomes more abnormal and the distortion of the vectors increases (Hnatkova et al., 2017). In a recent comparative study in cardiac patients, the calculation of the QRS-T angle by the so-called TCRT method was more reliable for cardiac risk prediction. It is thought that the calculation of the sum of the cosines between QRS and T wave vectors increases the ability of depicting the shape and orientation irregularities that accompany increased repolarization heterogeneity.

Racial, and previously described sex differences (Smetana et al., 2002) should also be taken into consideration in studies measuring the QRS-T angle. For example, in the Taiwanese

TABLE 3 | Studies of QRS-T angle for risk prediction in dialysis patients.

Study	Participants	Age (years)	IHD	Calculation	Follow up	Outcome
de Bie et al., 2013b	277 (prevalent) Male 62.1% HD 62.8% Peritoneal dialysis 37.2%	56.3 ± 17.0	24.5%	Inverse Dower matrix from standard 12 lead snapshot ECG. **Measured as angle between mean QRS and T vectors.**	60 months	QRS-T angle independent predictor of all-cause mortality (*N* = 91) and SCD (*N* = 18).
Tereshchenko et al., 2016	358 (incident HD) Male 59% Black 73%	55 ± 13	37%	Calculated from continuous unfiltered averaged *xyz* ECG signal. **Measured as angle between spatial mean QRS vector and spatial peak T vector.**	864.6 person-years of follow-up	QRS-T angle associated with all-cause mortality (*N* = 77) cardiovascular mortality (*N* = 35) and SCD (*N* = 15).
Skampardoni et al., 2018a	178 (prevalent HD) Male 72% Caucasian 80% South Asian 17% Black 3%	67 ± 14	23.5%	Singular value decomposition to standard snapshot 12 lead ECG. **Measured as total cosine R to T.**	36 ± 19 months	TCRT independent predictor of cardiac deaths (*N* = 17) and major cardiac events (*N* = 54).
Poulikakos et al., 2018	72 (prevalent HD) Males 58% Caucasian 44% Black 31% South Asians 25%	61 ± 15	21%	Singular value decomposition to overlapping 10 s segment 12 lead ECGs during continuous monitoring repeated 5 times every 2 weeks. **Measured as total cosine R to T.**	54.8 months	TRCT independent predictor of all-cause mortality (*N* = 16) and major cardiac events (*N* = 9).
Lin et al., 2007	325 (incident) HD Male 44% Taiwanese population	64 ± 13	19%	Singular value decomposition to standard snapshot 12 lead ECG. **Measured as total cosine R to T**	25 ± 22 months	TRCT not associated with all-cause mortality (*N* = 154) cardiovascular mortality (*N* = 79) or arrhythmia related deaths (*N* = 59). T wave residuum independent predictor for all outcomes.

ECG, electrocardiogram; F/up, follow up; HD, hemodialysis; IHD, Ischemic heart disease; SCD, sudden cardiac death; TCRT, Total Cosine R to T.

HD cohort there was no association between QRS-T angle and cardiac outcomes whereas there was with T wave residuum; this may reflect racial differences in repolarization heterogeneity patterns and QRS-T angle. In a previous population study in healthy subjects, the QRS-T angle in Taiwanese individuals was significantly different compared to African, Caucasian and Indian healthy subjects (Elaine and Macfarlane, 2016).

The mechanisms linking abnormal repolarization heterogeneity with clinical outcomes and cardiac structure and function abnormalities remain unclear and will need to be assessed in prospective studies.

Autonomic Dysfunction and Heart Rate Variability in CKD

Sympathetic overactivation has short and long-term proarrhythmogenic effects and may play a role in the pathogenesis of arrhythmic deaths in CKD patients. Sympathetic activation impacts on cellular channel activity increasing repolarization heterogeneity (Vaseghi et al., 2012) and plays a role in the pathogenesis of cardiac fibrosis via α-adrenergic receptor stimulation and via triggering inflammatory responses (Levick et al., 2010). Autonomic imbalance decreases myocardial ability to suppress disorganized electrical activation and may compromise the heart pacemaker response to challenges.

Sympathetic nerve activity, assessed by microneurography of the peroneal nerve, increases with declining renal function (Grassi et al., 2011) and is elevated in patients with end-stage renal disease (Converse et al., 1992b). Potential contributing underlying mechanisms of sympathetic overactivation in CKD (Kaur et al., 2017) include elevated angiotensin 2 levels (Siddiqi et al., 2009) that potentiate norepinephrine release from sympathetic nerve terminals, stimulation of afferent renal nerves and chemoreceptors by adenosine release due to renal ischaemia (Biaggioni et al., 1991; Vallon et al., 2006), and reduced nitric oxide (NO) availability (Jourde-Chiche et al., 2011) potentiated by upregulation of MicroRNA-92a in dialysis patients (Young et al., 2009; Shang et al., 2017).

The baroreflex regulation has also been shown to be impaired in CKD. In dialysis patients, impaired baroreflex sensitivity was shown to be associated with vascular calcification and arterial stiffness (Chesterton et al., 2005) indicating a potential anatomical link between vascular changes and the function of baroreceptors.

Direct measurement of the autonomic system with microneurography poses practical challenges and is not suitable for clinical practice. Nevertheless, indirect measurements are possible by assessing HRV (Task Force of the European Society of Cardiology and North American Society of Pacing and Electrophysiology, 1996). HRV is a non-invasive method based on analysis of tachograms of continuous ECGs. It assesses the cardiac autonomic regulation based on the differences in cardiac pacemaker responses to autonomic activations. HRV can provide an approximation of the cardiac autonomic regulation that integrates multiple feedback systems. In addition to traditional time and frequency domain measurement several different

TABLE 4 | Studies of QRS-T angle reporting on associations with cardiovascular parameters and dialysis procedure.

Study	Participants	Age (years)	IHD	Calculation of QRS-T angle	Findings
de Bie et al., 2013a	101 prevalent Male 76% 66% HD, 44% Peritoneal Dialysis	56.3 ± 17	30%	Inverse Dower matrix from standard 12 lead snapshot ECG. **Measured as angle between mean QRS and T vectors.**	QRS-T angle associated with left ventricular ejection fraction, QRS duration and left ventricular systolic dyssynchrony.
Tereshchenko et al., 2016	358 incident HD Male 59% Black 73%	55 ± 13	37%	Calculated from continuous unfiltered averaged *xyz* ECG signal. **Measured as angle between spatial mean QRS vector and spatial peak T vector.**	QRS-T angle >75° associated with wider QRS and echocardiographic left ventricular hypertrophy defined as left ventricular mass index >51 g/m$^{2.7}$ in men and >47 g/m$^{2.7}$ in women.
Skampardoni et al., 2018a	178 prevalent HD Male 72% Caucasian 80% South Asian 17% Black 3%	67 ± 14	23.5%	Singular value decomposition to standard snapshot 12 lead ECG. **Measured as total cosine R to T.**	QRS-T angle by TCRT correlated with left ventricular mass indexed for height in univariate and Global Longitudinal Strain in multivariate analysis.
Jaroszynski et al., 2009	57 prevalent Peritoneal Dialysis patients 49% male Caucasians	47.7 ± 7.1	Excluded	Inverse Dower matrix from standard 12 lead snapshot ECG. **Measured as angular difference between maximum spatial QRS and T vectors.**	QRS-T angle associated with increased coronary artery calcium burden, atherosclerosis and troponin T elevation.
Jaroszynski et al., 2010	73 prevalent HD 52% male Caucasians	51.5 ± 4.5	Not reported	Inverse Dower matrix from standard 12 lead snapshot ECG. **Measured as angular difference between maximum spatial QRS and T vectors.**	QRS-T angle associated with Troponin T. HD session resulted in increased QRS-T in 59 patients, decreased in 12 patients, and unchanged in 2 patients.
Poulikakos et al., 2013	72 (prevalent HD) Males 70%	61 ± 15	21%	Singular value decomposition to overlapping 10 s segment 12 lead ECGs during continuous monitoring repeated 5 times every 2 weeks. **Measured as total cosine R to T.**	Intra-subject reproducibility confirmed using analysis of variance. Variable effect of HD to TCRT Intradialytic QRS-T change correlated with PTH levels.

ECG, electrocardiogram; HD, hemodialysis; IHD, Ischemic heart disease; TCRT, total Cosine R to T.

methodologies have been developed (Task Force of the European Society of Cardiology and North American Society of Pacing and Electrophysiology, 1996; Sassi et al., 2015).

Many groups have used HRV methodology in dialysis patients. A pubmed search using the terms HRV and dialysis returns 122 studies with the first one published already in 1986 (Forsstrom et al., 1986). Abnormal HRV indices have been associated with all cause (Hayano et al., 1999; Oikawa et al., 2009; Suzuki et al., 2012; Chen et al., 2016; Ng et al., 2017; Poulikakos et al., 2018) and cardiovascular mortality (Hayano et al., 1999; Fukuta et al., 2003; Oikawa et al., 2009; Chen et al., 2016) in east Asian HD patients and in one small study including predominantly Caucasian HD patients (Skampardoni et al., 2018a). Depressed HRV has also been associated with all cause (Pei et al., 2015; Chiang et al., 2016) and cardiovascular (Hayano et al., 1999) mortality in east Asian patients receiving peritoneal dialysis.

Frequent daily HD has been shown to improve components of HRV (Chan et al., 2014). Preserved residual urine output has also been associated with different HRV profiles in peritoneal dialysis patients (Tang et al., 2012) and depressed HRV has been associated with increased PTH (Zhang et al., 2013, 2015; Poulikakos et al., 2014b; Jiang et al., 2016) and FGF 23 levels (Zhang et al., 2015). Depressed HRV has also been associated with increased pulse pressure (Poulikakos et al., 2014c) in patients with end stage renal disease and with increased pulse wave velocity in patients with CKD stages 3–5 (Chandra et al., 2014).

Despite the consistent results confirming the value of HRV in CKD patients, major challenges exist in extrapolating associations from these studies and incorporating HRV measurements into clinical practice. The main challenge is related to the sensitivity of HRV to environmental influences and the need for strict standardization, particularly for 24-h ECG recordings, which is practically impossible when the recording is performed in the outpatient setting.

Short Term HRV Measurements During Autonomic Provocations in HD Patients

For the purposes of standardized assessment, several studies used short term recordings around or during the dialysis procedure, i.e., a period with relatively standardized environment characterized by volume and electrolyte shifts that provoke the autonomic system in a predictable manner. It is known that patients who exhibit excessive intradialytic decline in systolic blood pressure have higher risk of cardiovascular and overall mortality (Chou et al., 2018; Reeves and Mc Causland, 2018). The pathogenesis of intradialytic hypotension is multifactorial (Reeves and Mc Causland, 2018) but it has been postulated that abnormal activation of the sympathetic system plays a central role (Converse et al., 1992a). Some studies have shown that spectral HRV assessment during intradialytic recordings can differentiate patients who are prone to intradialytic hypotension

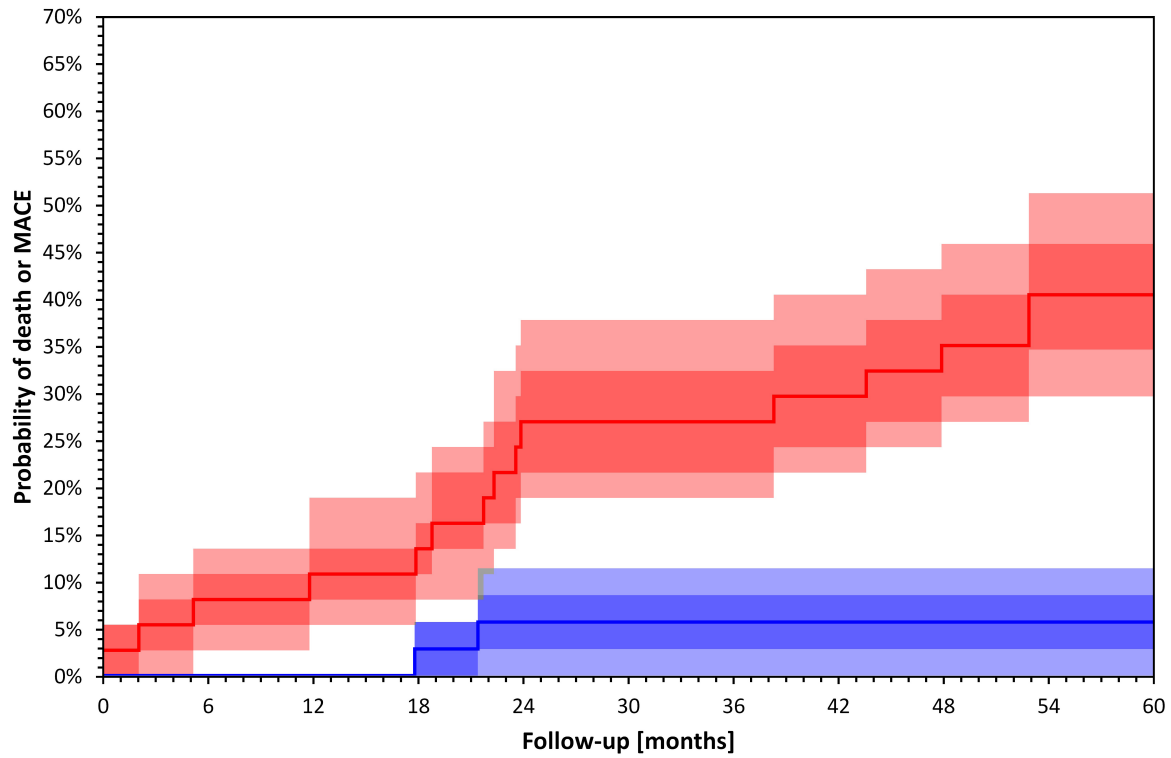

FIGURE 2 | Kaplan–Meier survival curves of total mortality and major cardiac events 72 HD patients included in a recently published study (Poulikakos et al., 2018) stratified by QRS-T angle calculated by TCRT above (red) and below (blue) median value (p = 0.000 Log Rank test). Darker bands depict interquartile ranges and the lighter bands ranges between 10th and 90th percentiles. The calculation of confidence intervals was performed using bootstrap 10,000 repetitions. Major cardiac events were defined as sudden cardiac death, acute coronary syndrome, coronary revascularization or admission due to heart failure or arrhythmia.

(Severi et al., 1997; Hernando et al., 2015). However, Barnas et al. (1999) reported similar intradialytic HRV profiles between hypotension prone and stable patients up to the moment of the hypotensive episode where they observed bradycardia and decline in LF power.

Studies using short term intradialytic ECG monitoring have shown that HRV parameters are influenced by the rate of volume removal during dialysis (Tsuji et al., 2017) and by the dialysis modality between HD and hemofiltration (Genovesi et al., 2007). Two studies also reported associations between short term HRV measurement during dialysis and mortality (Chen et al., 2016; Poulikakos et al., 2018). In a recent study using intradialytic HRV assessment depressed LF/HF over the first hour of treatment predicted overall mortality (Poulikakos et al., 2018). Chen et al. (2016) used spectral HRV assessment before and after HD and showed that decreased difference in LF was associated with increased risk of overall and cardiovascular mortality. **Figure 3** shows an example of Kaplan–Meier event probability curves for major cardiac events and overall mortality in a cohort of 72 HD patients (Poulikakos et al., 2018) stratified by LF/HF ratio above and below median value.

Few studies have used short term HRV assessment during autonomic postural, provocations in HD patients. In the study by Genovesi et al. (2007) postural provocation including 10 min standing before dialysis was performed. Interestingly, whilst active standing was associated with increase in normalized LF and decrease in normalized HF during HD treatment, this was not the case when treatment with hemofiltration was used. Echeverria et al. (2017) showed an increase in LF/HF in response to postural provocations before and after HD treatment.

Genetic differences might contribute to the differences in reported HRV response to autonomic provocations. A recent study in 114 HD patients (Ribas Ribeiro et al., 2018) suggested that genetic polymorphism in the angiotensin converting enzyme, an enzyme that modulates the autonomic system, determines the autonomic response during HD. In this study, an increase in LF and LF/HF through dialysis was observed only in patients with II angiotensin converting enzyme genotype and not in patients with DD genotype. Studies using short term HRV assessment with autonomic provocations are presented in **Table 5**.

Two small studies have reported reasonable reproducibility of HRV measurements from intradialytic recordings (Poulikakos et al., 2014c; da Silva et al., 2016).

CONCLUSION-FUTURE DIRECTIONS

Bradyarrhythmic and Tachyarrhythmic Risk

Recent ILR studies have shown an important relative contribution of bradyarrhythmias to sudden death in

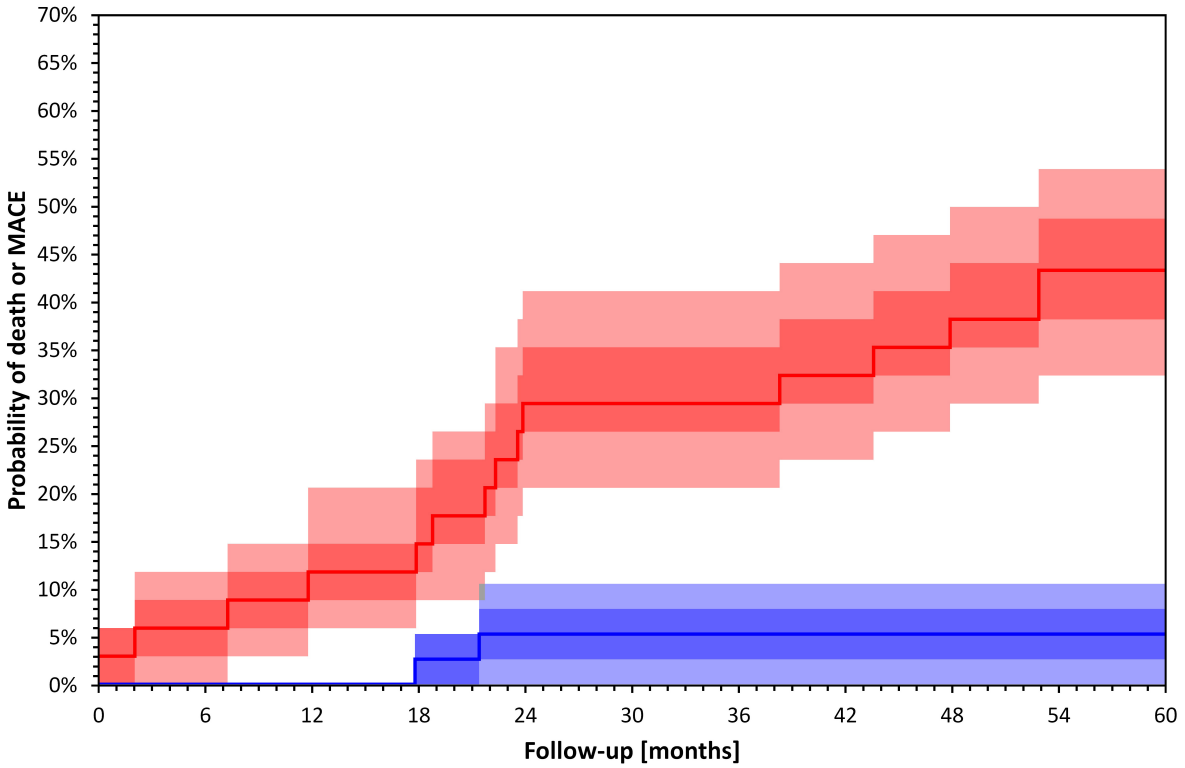

FIGURE 3 | Kaplan–Meier survival curves of total mortality and major cardiac events in 72 HD patients included in a recently published study (Poulikakos et al., 2018) stratified by LF/HF above (blue) and below (red) median value (p = 0.001 Log Rank test). Darker bands depict interquartile ranges and the lighter bands ranges between 10th and 90th percentiles. The calculation of confidence intervals was performed using bootstrap 10,000 repetitions. Major cardiac events were defined as sudden cardiac death, acute coronary syndrome, coronary revascularization or admission due to heart failure or arrhythmia.

dialysis patients. However, these studies did not include incident dialysis patients with high cardiovascular risk that may be more vulnerable to ventricular tachyarrhythmias. Future large studies with long term ECG monitoring in incident dialysis patients are needed to elucidate the precise incidence and underlying arrhythmic mechanisms of SCD. These studies should aim at developing risk stratification strategies for both tachyarrhythmic and bradyarrhythmic risks. Tachyarrhythmic risk is mainly related to static and dynamic ventricular repolarization abnormalities and it is possible that repolarization patterns and changes related dialysis induced fluid and electrolyte shifts prior to the fatal arrhythmias may be important for its prediction. On the contrary, bradyarrhythmic risk is mainly related to cardiac periodicity and is likely to be influenced by autonomic system abnormalities including sleep apnoea.

The ECG signals should be regularly interrogated during the course of such studies and treatment for significant bradyarrhythmias should be offered. Non-invasive surface long term ECG technology with sufficient memory that can record continuous high quality ECG signal could serve the dual purpose of potentially fatal or final rhythm detection and data acquisition for risk profiling for both tachyarrhythmias and bradyarrhythmias. In addition, non-invasive continuous long term ECG monitoring devices that can be attached and exchanged during a dialysis visit may facilitate the recruitment of high risk incident patients who may not wish to attend additional hospital visits or undergo invasive procedures.

Research protocols should include detailed cardiovascular, genetic and sleep disorder phenotyping.

These studies, in addition to clarifying the prevalence of bradyarrhythmias and ventricular arrhythmias, will provide important information about the burden of AF and its potential association with SCD. An association between AF and increased risk of SCD has been shown in cardiac patients (Chen et al., 2014) and may be relevant in the dialysis population given the extremely high burden of AF.

QRS-T Angle-Need for Standardization and Integration Into Clinical Practice

The QRS-T angle assessment has substantial potential to be used as a descriptor of uremic cardiomyopathy. It can also be easily incorporated into clinical practice. In the first instance, the different methodological approaches need to be rigorously tested and compared in existing large ECG databases of CKD and dialysis patients to determine the best methodological approach to the angle expression. This should be based on a multicenter collaboration between clinical

TABLE 5 | Studies using short term Heart Rate Variability assessment with autonomic provocations.

Study	Number of HD patients	Setting	Outcome
Severi et al., 1997	14 stable and 14 hypotension-prone	Spectral HRV from continuous intradialytic ECG.	Spectral HRV different in hypotension prone vs. stable patients.
Hernando et al., 2015	24 patients 52 HD treatment sessions	Spectral HRV from continuous intradialytic ECG and continuous intradialytic arterial BP signal.	Spectral HRV parameters during the first 30 min of the treatment session different in hypotension prone vs. stable patients.
Barnas et al., 1999	11 stable and 9 hypotension prone patients	Spectral HRV from continuous intradialytic ECG and continuous intradialytic arterial BP signal.	No difference in groups up to the point of hypotensive episodes when LF HRV declined
Tsuji et al., 2017	35 patients divided in 3 groups based on UFR	Spectral HRV and approximate entropy from continuous intradialytic ECG.	LF/HF values and approximate entropy increased at the end of HD in patients with UFR >15 ml/h/kg.
Genovesi et al., 2007	10 patients Treated with 6 session of HD and 6 sessions of Hemofiltration	Spectral HRV from continuous ECG during pre-HD postural provocation (10 min rest and 10 min active standing) followed by intradialytic measurements (10 min periods every hour and after the end of treatment) and continuous arterial BP signal.	Normalized LF was higher and HF lower in HF compared to HD. Active standing was associated with increase in normalized LF and decrease in normalized HF in HD but not in Hemofiltration.
Chen et al., 2016	72 patients 5 sessions every 2 weeks	Spectral HRV from continuous intradialytic ECG.	Low LF/HF during the first hour associated with overall mortality. Intrasubject stability of HRV parameters averaged over the first and last hour confirmed by repeated measure ANOVA.
Chen et al., 2016	182 patients	Spectral HRV from 5?min ECG before and 30 min after HD.	Decreased difference in LF associated with increased overall and cardiovascular mortality.
Echeverria et al., 2017	19 stable patients 20 healthy controls	Continuous ECG recording during 16 min in supine position, and during 16 min of active orthostatism pre and post HD treatment for HD patients. Last 5 min of the recording at each position were used for HRV.	Increase in LF/HF and in the short-term scaling exponent (a1) on standing before and after HD.
Ribas Ribeiro et al., 2018	114	HRV from continuous ECG measured for 20 min before, in the second hour and immediately after HD. Assessment of ACE genotypes.	Homozygosity for the II allele of the ACE gene associated with greater increase in LF and LF/HF during HD compared to DD genotype.

ACE, angiotensin converting enzyme; BP, blood pressure; D, deletion; ECG, electrocardiogram; HD, hemodialysis; HF, high frequency; LF, low frequency power; HRV, heart rate variability; I, insertion; UFR, ultrafiltration rate.

research teams and bioengineers. Such collaborative effort can help determine normal reference values and increase our understanding of racial and gender differences in the CKD and dialysis populations.

Furthermore, it is important for the clinical and research community and industry partners in ECG manufacturing to understand the importance of collecting high quality ECGs and storing them in easily accessible formats (Malik et al., 2018) in order to create and maintain open access ECG databases. Such databases would facilitate meaningful research that in turn can inform clinical practice about the possibilities of reducing cardiovascular mortality. The possibility and practical requirements of complementing the existing national and/or international (Goodkin et al., 2001; Perl et al., 2014) renal databases with repositories of routinely collected digital ECG should be explored.

HRV-Methodological Challenges and Clinical Practicality

In the field of HRV and assessment of cardiac autonomic modulation, further research is required to standardize the measurements in dialysis patients. Short-duration tests with autonomic provocations could overcome methodological shortcomings of 24-h outpatient ambulatory ECG recordings. These assessments can be organized around the dialysis treatment in order to minimize a patient's inconvenience and be suitable to be incorporated into regular clinical practice in the future. HRV measurements may be useful for both bradyarrhythmic and tachyarrhythmic risk stratification. The value of cardiac autonomic modulation assessment during standardized autonomic provocations for prediction of significant bradyarrhythmias should be prospectively investigated.

On the other hand, ECG acquisition during autonomic provocations has the potential to yield important prognostic information for tachyarrhythmias, while at the same time characterizing cardiac autonomic regulation measured by HRV and by dynamic repolarization profiles. Short duration continuous ECG measurements with standardized controlled provocations can be used to assess dynamic changes of the QRS-T angle during different stages of cardiac autonomic status; this has been shown to strengthen risk prediction in cardiac patients (Kentta et al., 2012). This type of measurement has the potential to shed more light on the links between autonomic status and cardiac electrical activity and explore the value of combined electrophysiological assessment in this group of patients.

Non-invasive electrophysiology has an important role in CKD patients. Close collaboration across the disciplines of biomedical engineering, clinical cardiology and nephrology is required to bridge the gaps between available

technological tools, research efforts and clinical translation in arrhythmic complications of CKD.

AUTHOR CONTRIBUTIONS

DP: concept, design, drafting article, and critical revision of article. KH and SS: critical revision of article. DG and PK: concept and critical revision of article. MM: concept, design, and critical revision of article.

FUNDING

This study was supported by British Heart Foundation Grant NH/16/2/32499 and Kidney Research UK Grant (IN4/2015).

REFERENCES

Baigent, C., Landray, M. J., Reith, C., Emberson, J., Wheeler, D. C., Tomson, C., et al. (2011). The effects of lowering LDL cholesterol with simvastatin plus ezetimibe in patients with chronic kidney disease (Study of Heart and Renal Protection): a randomised placebo-controlled trial. *Lancet* 377, 2181–2192. doi: 10.1016/S0140-6736(11)60739-3

Barnas, M. G., Boer, W. H., and Koomans, H. A. (1999). Hemodynamic patterns and spectral analysis of heart rate variability during dialysis hypotension. *J. Am. Soc. Nephrol.* 10, 2577–2584.

Berton, G., Cordiano, R., Cucchini, F., Cavuto, F., Pellegrinet, M., and Palatini, P. (2009). Atrial fibrillation during acute myocardial infarction: association with all-cause mortality and sudden death after 7-year of follow-up. *Int. J. Clin. Pract.* 63, 712–721. doi: 10.1111/j.1742-1241.2009.02023.x

Biaggioni, I., Killian, T. J., Mosqueda-Garcia, R., Robertson, R. M., and Robertson, D. (1991). Adenosine increases sympathetic nerve traffic in humans. *Circulation* 83, 1668–1675. doi: 10.1161/01.CIR.83.5.1668

Bjerregaard, P. (1983). Mean 24 hour heart rate, minimal heart rate and pauses in healthy subjects 40-79 years of age. *Eur. Heart J.* 4, 44–51. doi: 10.1093/oxfordjournals.eurheartj.a061370

Brodsky, M., Wu, D., Denes, P., Kanakis, C., and Rosen, K. M. (1977). Arrhythmias documented by 24 hour continuous electrocardiographic monitoring in 50 male medical students without apparent heart disease. *Am. J. Cardiol.* 39, 390–395. doi: 10.1016/S0002-9149(77)80094-5

Chan, C. T., Chertow, G. M., Daugirdas, J. T., Greene, T. H., Kotanko, P., Larive, B., et al. (2014). Effects of daily hemodialysis on heart rate variability: results from the Frequent Hemodialysis Network (FHN) Daily Trial. *Nephrol. Dial. Transplant.* 29, 168–178. doi: 10.1093/ndt/gft212

Chan, K. E., Newton-Cheh, C., Gusella, J. F., and Maddux, F. W. (2015). Heritability of risk for sudden cardiac arrest in ESRD. *J. Am. Soc. Nephrol.* 26, 2815–2820. doi: 10.1681/ASN.2014090881

Chandra, P., Sands, R. L., Gillespie, B. W., Levin, N. W., Kotanko, P., Kiser, M., et al. (2014). Relationship between heart rate variability and pulse wave velocity and their association with patient outcomes in chronic kidney disease. *Clin. Nephrol.* 81, 9–19. doi: 10.5414/CN108020

Chang, K. C., Lee, A. S., Chen, W. Y., Lin, Y. N., Hsu, J. F., Chan, H. C., et al. (2015). Increased LDL electronegativity in chronic kidney disease disrupts calcium homeostasis resulting in cardiac dysfunction. *J. Mol. Cell. Cardiol.* 84, 36–44. doi: 10.1016/j.yjmcc.2015.03.016

Charytan, D. M., Patrick, A. R., Liu, J., Setoguchi, S., Herzog, C. A., Brookhart, M. A., et al. (2011). Trends in the use and outcomes of implantable cardioverter-defibrillators in patients undergoing dialysis in the United States. *Am. J. Kidney Dis.* 58, 409–417. doi: 10.1053/j.ajkd.2011.03.026

Chen, L. Y., Benditt, D. G., and Alonso, A. (2014). Atrial fibrillation and its association with sudden cardiac death. *Circ. J.* 78, 2588–2593. doi: 10.1253/circj.CJ-14-0814

Chen, L. Y., Sotoodehnia, N., Buzkova, P., Lopez, F. L., Yee, L. M., Heckbert, S. R., et al. (2013). Atrial fibrillation and the risk of sudden cardiac death: the atherosclerosis risk in communities study and cardiovascular health study. *JAMA Intern. Med.* 173, 29–35. doi: 10.1001/2013.jamainternmed.744

Chen, S. C., Huang, J. C., Tsai, Y. C., Hsiu-Chin Mai, R. N., Jui-Hsin Chen, R. N., Kuo, P. L., et al. (2016). Heart rate variability change before and after hemodialysis is associated with overall and cardiovascular mortality in hemodialysis. *Sci. Rep.* 6:20597. doi: 10.1038/srep20597

Chesterton, L. J., Sigrist, M. K., Bennett, T., Taal, M. W., and McIntyre, C. W. (2005). Reduced baroreflex sensitivity is associated with increased vascular calcification and arterial stiffness. *Nephrol. Dial. Transplant.* 20, 1140–1147. doi: 10.1093/ndt/gfh808

Cheung, A. K., Sarnak, M. J., Yan, G., Berkoben, M., Heyka, R., Kaufman, A., et al. (2004). Cardiac diseases in maintenance hemodialysis patients: results of the HEMO Study. *Kidney Int.* 65, 2380–2389. doi: 10.1111/j.1523-1755.2004.00657.x

Chiang, J. Y., Huang, J. W., Lin, L. Y., Chang, C. H., Chu, F. Y., Lin, Y. H., et al. (2016). Detrended fluctuation analysis of heart rate dynamics is an important prognostic factor in patients with end-stage renal disease receiving peritoneal dialysis. *PLoS One* 11:e0147282. doi: 10.1371/journal.pone.0147282

Chou, J. A., Streja, E., Nguyen, D. V., Rhee, C. M., Obi, Y., Inrig, J. K., et al. (2018). Intradialytic hypotension, blood pressure changes and mortality risk in incident hemodialysis patients. *Nephrol. Dial. Transplant.* 33, 149–159. doi: 10.1093/ndt/gfx037

Converse, R. L. Jr., Jacobsen, T. N., Jost, C. M., Toto, R. D., Grayburn, P. A., Obregon, T. M., et al. (1992a). Paradoxical withdrawal of reflex vasoconstriction as a cause of hemodialysis-induced hypotension. *J. Clin. Invest.* 90, 1657–1665.

Converse, R. L. Jr., Jacobsen, T. N., Toto, R. D., Jost, C. M., Cosentino, F., Fouad-Tarazi, F., et al. (1992b). Sympathetic overactivity in patients with chronic renal failure. *N. Engl. J. Med.* 327, 1912–1918.

Couser, W. G., Remuzzi, G., Mendis, S., and Tonelli, M. (2011). The contribution of chronic kidney disease to the global burden of major noncommunicable diseases. *Kidney Int.* 80, 1258–1270. doi: 10.1038/ki.2011.368

Cuculich, P. S., Sánchez, J. M., Kerzner, R., Greenberg, S. L., Sengupta, J., Chen, J., et al. (2007). Poor prognosis for patients with chronic kidney disease despite ICD therapy for the primary prevention of sudden death. *Pacing Clin. Electrophysiol.* 30, 207–213. doi: 10.1111/j.1540-8159.2007.00651.x

da Silva, D. M., Macedo, M. C., Lemos, L. B., Vieira, F. C., Pirôpo, U. S., Andrade, H. B., et al. (2016). Reliability analysis of the heart autonomic control parameters during hemodialysis sessions. *Biomed. Tech.* 61, 623–630. doi: 10.1515/bmt-2015-0239

Dalal, D., de Jong, J. S., Tjong, F. V., Wang, Y., Bruinsma, N., Dekker, L. R. C., et al. (2012). Mild-to-moderate kidney dysfunction and the risk of sudden cardiac death in the setting of acute myocardial infarction. *Heart Rhythm* 9, 540–545. doi: 10.1016/j.hrthm.2011.11.014

de Bie, M. K., Ajmone Marsan, N., Gaasbeek, A., Bax, J. J., Delgado, V., Rabelink, T. J., et al. (2013a). Echocardiographical determinants of an abnormal spatial QRS-T angle in chronic dialysis patients. *Nephrol. Dial. Transplant.* 28, 3045–3052. doi: 10.1093/ndt/gft347

de Bie, M. K., Koopman, M. G., Gaasbeek, A., Dekker, F. W., Maan, A. C., Swenne, C. A., et al. (2013b). Incremental prognostic value of an abnormal baseline spatial QRS-T angle in chronic dialysis patients. *Europace* 15, 290–296. doi: 10.1093/europace/eus306

Denes, P., Wu, D., Dhingra, R., Pietras, R. J., and Rosen, K. M. (1974). The effects of cycle length on cardiac refractory periods in man. *Circulation* 49, 32–41. doi: 10.1161/01.CIR.49.1.32

Echeverria, J. C., Infante, O., Perez-Grovas, H., Gonzalez, H., Jose, M. V., and Lerma, C. (2017). Effects of orthostatism and hemodialysis on mean heart period and fractal heart rate properties of chronic renal failure patients. *Artif. Organs* 41, 1026–1034. doi: 10.1111/aor.12887

Elaine, C., and Macfarlane, P. W. (2016). "Comparison of spatial QRS-T angle in different healthy racial groups," in *Paper Presented at the 2016 Computing in Cardiology Conference*, Vancouver.

Fleg, J. L., and Kennedy, H. L. (1982). Cardiac arrhythmias in a healthy elderly population: detection by 24-hour ambulatory electrocardiography. *Chest* 81, 302–307. doi: 10.1378/chest.81.3.302

Fontes, M. S., Papazova, D. A., van Koppen, A., de Jong, S., Korte, S. M., Bongartz, L. G., et al. (2015). Arrhythmogenic remodeling in murine models of deoxycorticosterone acetate-salt-induced and 5/6-subtotal nephrectomy-salt-induced cardiorenal disease. *Cardiorenal Med.* 5, 208–218. doi: 10.1159/000430475

Forsstrom, J., Heinonen, E., Valimaki, I., and Antila, K. (1986). Effects of haemodialysis on heart rate variability in chronic renal failure. *Scand. J. Clin. Lab. Invest.* 46, 665–670. doi: 10.3109/00365518609083729

Fukuta, H., Hayano, J., Ishihara, S., Sakata, S., Mukai, S., Ohte, N., et al. (2003). Prognostic value of heart rate variability in patients with end-stage renal disease on chronic haemodialysis. *Nephrol. Dial. Transplant.* 18, 318–325. doi: 10.1093/ndt/18.2.318

Genovesi, S., Bracchi, O., Fabbrini, P., Luisetto, E., Viganò, M. R., Lucini, D., et al. (2007). Differences in heart rate variability during haemodialysis and haemofiltration. *Nephrol. Dial. Transplant.* 22, 2256–2262. doi: 10.1093/ndt/gfm125

Goodkin, D. A., Mapes, D. L., and Held, P. J. (2001). The dialysis outcomes and practice patterns study (DOPPS): how can we improve the care of hemodialysis patients? *Semin. Dial.* 14, 157–159. doi: 10.1046/j.1525-139X.2001.00043.x

Grassi, G., Quarti-Trevano, F., Seravalle, G., Arenare, F., Volpe, M., Furiani, S., et al. (2011). Early sympathetic activation in the initial clinical stages of chronic renal failure. *Hypertension* 57, 846–851. doi: 10.1161/HYPERTENSIONAHA.110.164780

Gronefeld, G. C., Mauss, O., Li, Y. G., Klingenheben, T., and Hohnloser, S. H. (2000). Association between atrial fibrillation and appropriate implantable cardioverter defibrillator therapy: results from a prospective study. *J. Cardiovasc. Electrophysiol.* 11, 1208–1214. doi: 10.1046/j.1540-8167.2000.01208.x

Gutiérrez, O. M., Januzzi, J. L., Isakova, T., Laliberte, K., Smith, K., Collerone, G., et al. (2009). Fibroblast growth factor 23 and left ventricular hypertrophy in chronic kidney disease. *Circulation* 119, 2545–2552. doi: 10.1161/CIRCULATIONAHA.108.844506

Hayano, J., Takahashi, H., Toriyama, T., Mukai, S., Okada, A., Sakata, S., et al. (1999). Prognostic value of heart rate variability during long-term follow-up in chronic haemodialysis patients with end-stage renal disease. *Nephrol. Dial. Transplant.* 14, 1480–1488. doi: 10.1093/ndt/14.6.1480

Hernando, D., Sornmo, L., Sandberg, F., Laguna, P., Llamedo, M., and Bailon, R. (2015). Identification of patients prone to hypotension during hemodialysis based on the analysis of cardiovascular signals. *Med. Eng. Phys.* 37, 1156–1161. doi: 10.1016/j.medengphy.2015.10.003

Herzog, C. A., Asinger, R. W., Berger, A. K., David, M. C., Javier, D., Robert, G. H., et al. (2011). Cardiovascular disease in chronic kidney disease. A clinical update from Kidney Disease: improving Global Outcomes (KDIGO). *Kidney Int.* 80, 572–586. doi: 10.1038/ki.2011.223

Hnatkova, K., Seegers, J., Barthel, P., Novotny, T., Smetana, P., Zabel, M., et al. (2017). Clinical value of different QRS-T angle expressions. *Europace* 20, 1352–1361. doi: 10.1093/europace/eux246

Hreybe, H., Ezzeddine, R., Bedi, M., Barrington, W., Bazaz, R., Ganz, L. I., et al. (2006). Renal insufficiency predicts the time to first appropriate defibrillator shock. *Am. Heart J.* 151, 852–856. doi: 10.1016/j.ahj.2005.06.042

Hsueh, C. H., Chen, N. X., Lin, S. F., Chen, P. S., Gattone, V. H., Allen, M. R., et al. (2014). Pathogenesis of arrhythmias in a model of CKD. *J. Am. Soc. Nephrol.* 25, 2812–2821. doi: 10.1681/ASN.2013121343

Isakova, T., Xie, H., Yang, W., Xie, D., Anderson, A. H., Scialla, J., et al. (2011). Fibroblast growth factor 23 and risks of mortality and end-stage renal disease in patients with chronic kidney disease. *JAMA* 305, 2432–2439. doi: 10.1001/jama.2011.826

Jaroszynski, A., Czekajska-Chechab, E., Drelich-Zbroja, A., Zapolski, T., and Ksiazek, A. (2009). Spatial QRS-T angle in peritoneal dialysis patients: association with carotid artery atherosclerosis, coronary artery calcification and troponin T. *Nephrol. Dial. Transplant.* 24, 1003–1008. doi: 10.1093/ndt/gfn581

Jaroszynski, A., Wysokiński, A., Bednarek-Skublewska, A., Głowniak, A., Książek, P., Sodolski, T., et al. (2010). The effect of a single dialysis session on spatial QRS-T angle in haemodialysis patients. *Nephrol. Dial. Transplant.* 25, 3723–3729. doi: 10.1093/ndt/gfq247

Jiang, Y., Shen, Z., Zhang, J., Xing, C., Zha, X., Shen, C., et al. (2016). Parathyroidectomy increases heart rate variability and leptin levels in patients with stage 5 chronic kidney disease. *Am. J. Nephrol.* 44, 245–254. doi: 10.1159/000449018

Jourde-Chiche, N., Dou, L., Cerini, C., Dignat-George, F., and Brunet, P. (2011). Vascular incompetence in dialysis patients–protein-bound uremic toxins and endothelial dysfunction. *Semin. Dial.* 24, 327–337. doi: 10.1111/j.1525-139X.2011.00925.x

Kalra, P. A., Green, D., and Poulikakos, D. (2018). Arrhythmia in hemodialysis patients and its relation to sudden death. *Kidney Int.* 93, 781–783. doi: 10.1016/j.kint.2017.12.005

Kaur, J., Young, B. E., and Fadel, P. J. (2017). Sympathetic overactivity in chronic kidney disease: consequences and mechanisms. *Int. J. Mol. Sci.* 18:1682. doi: 10.3390/ijms18081682

Kentta, T., Viik, J., Karsikas, M., Seppänen, T., Nieminen, T., Lehtimäki, T., et al. (2012). Postexercise recovery of the spatial QRS/T angle as a predictor of sudden cardiac death. *Heart Rhythm* 9, 1083–1089. doi: 10.1016/j.hrthm.2012.02.030

Lee, A. S., Chen, W. Y., Chan, H. C., Chung, C. H., Peng, H. Y., Chang, C. M., et al. (2017). Electronegative LDL-mediated cardiac electrical remodeling in a rat model of chronic kidney disease. *Sci. Rep.* 7:40676. doi: 10.1038/srep40676

Levick, S. P., Murray, D. B., Janicki, J. S., and Brower, G. L. (2010). Sympathetic nervous system modulation of inflammation and remodeling in the hypertensive heart. *Hypertension* 55, 270–276. doi: 10.1161/HYPERTENSIONAHA.109.142042

Lin, C. Y., Lin, L. Y., and Chen, P. C. (2007). Analysis of T-wave morphology from the 12-lead electrocardiogram for prediction of long-term prognosis in patients initiating haemodialysis. *Nephrol. Dial. Transplant.* 22, 2645–2652. doi: 10.1093/ndt/gfm238

London, G. M., Guérin, A. P., Marchais, S. J., Métivier, F., Pannier, B., and Adda, H. (2003). Arterial media calcification in end-stage renal disease: impact on all-cause and cardiovascular mortality. *Nephrol. Dial. Transplant.* 18, 1731–1740. doi: 10.1093/ndt/gfg414

Mainigi, S. K., Chebrolu, L. H., Romero-Corral, A., Mehta, V., Machado, R. R., Konecny, T., et al. (2012). Prediction of significant conduction disease through noninvasive assessment of cardiac calcification. *Echocardiography* 29, 1017–1021. doi: 10.1111/j.1540-8175.2012.01752.x

Malik, M., Buxton, A. E., Huikuri, H., Lombardi, F., Schmidt, G., and Zabel, M. (2018). Noninvasive electrophysiology in risk assessment and screening. *Heart Rhythm* 15, 803–804. doi: 10.1016/j.hrthm.2018.03.014

Matsuo, H., Dohi, K., Machida, H., Takeuchi, H., Aoki, T., Nishimura, H., et al. (2018). Echocardiographic assessment of cardiac structural and functional abnormalities in patients with end-stage renal disease receiving chronic hemodialysis. *Circ. J.* 82, 586–595. doi: 10.1253/circj.CJ-17-0393

Ng, H. Y., Hsueh, S. K., Lee, Y. T., Chiou, T. T., Huang, P. C., and Lee, C. T. (2017). Synergic impact of vascular calcification and low autonomic tone in mortality of hemodialysis patients. *Nephron* 137, 91–98. doi: 10.1159/000477827

Nowak, K. L., and Chonchol, M. (2018). Does inflammation affect outcomes in dialysis patients? *Semin. Dial.* 31, 388–397. doi: 10.1111/sdi.12686

Ogna, A., Forni Ogna, V., Mihalache, A., Pruijm, M., Halabi, G., Phan, O., et al. (2015). Obstructive sleep apnea severity and overnight body fluid shift before and after hemodialysis. *Clin. J. Am. Soc. Nephrol.* 10, 1002–1010. doi: 10.2215/CJN.08760914

Oikawa, K., Ishihara, R., Maeda, T., Yamaguchi, K., Koike, A., Kawaguchi, H., et al. (2009). Prognostic value of heart rate variability in patients with renal failure on hemodialysis. *Int. J. Cardiol.* 131, 370–377. doi: 10.1016/j.ijcard.2007.10.033

Pedersen, O. D., Abildstrom, S. Z., Ottesen, M. M., Rask-Madsen, C., Bagger, H., Køber, L., et al. (2006). Increased risk of sudden and non-sudden cardiovascular death in patients with atrial fibrillation/flutter following acute myocardial infarction. *Eur. Heart J.* 27, 290–295. doi: 10.1093/eurheartj/ehi629

Pei, J., Tang, W., Li, L. X., Su, C. Y., and Wang, T. (2015). Heart rate variability predicts mortality in peritoneal dialysis patients. *Ren. Fail.* 37, 1132–1137. doi: 10.3109/0886022X.2015.1061729

Perl, J., Robinson, B., and Davies, S. On behalf of the International Society for Peritoneal Dialysis, Arbor Research Collaborative, and the PDOPPS investigators (2014). Update on the peritoneal dialysis outcomes and practice patterns study (PDOPPS). *Perit. Dial. Int.* 34:332. doi: 10.3747/pdi.2014.00162

Poulikakos, D., Banerjee, D., and Malik, M. (2014a). Risk of sudden cardiac death in chronic kidney disease. *J. Cardiovasc. Electrophysiol.* 25, 222–231. doi: 10.1111/jce.12328

Poulikakos, D., Malik, M., and Banerjee, D. (2014b). Parathyroid hormone and heart rate variability in haemodialysis patients. *Nephron Clin. Pract.* 126, 110–115. doi: 10.1159/000360542

Poulikakos, D., Malik, M., and Banerjee, D. (2014c). Sex-dependent association between heart rate variability and pulse pressure in haemodialysis patients. *Nephron Clin. Pract.* 128, 361–366. doi: 10.1159/000368436

Poulikakos, D., Ross, L., Recio-Mayoral, A., Cole, D., Andoh, J., Chitalia, N., et al. (2014d). Left ventricular hypertrophy and endothelial dysfunction in chronic kidney disease. *Eur. Heart J. Cardiovasc. Imaging* 15, 56–61. doi: 10.1093/ehjci/jet120

Poulikakos, D., Banerjee, D., and Malik, M. T. (2013). wave morphology changes during hemodialysis. *J. Electrocardiol.* 46, 492–496. doi: 10.1016/j.jelectrocard.2013.07.006

Poulikakos, D., Hnatkova, K., Banerjee, D., and Malik, M. (2018). Association of QRS-T angle and heart rate variability with major cardiac events and mortality in hemodialysis patients. *Ann. Noninvasive Electrocardiol.* 23:e12570. doi: 10.1111/anec.12570

Poulikakos, D., and Malik, M. (2016). Challenges of ECG monitoring and ECG interpretation in dialysis units. *J. Electrocardiol.* 49, 855–859. doi: 10.1016/j.jelectrocard.2016.07.019

Pun, P. H., Hellkamp, A. S., Sanders, G. D., Middleton, J. P., Hammill, S. C., Al-Khalidi, H. R., et al. (2015). Primary prevention implantable cardioverter defibrillators in end-stage kidney disease patients on dialysis: a matched cohort study. *Nephrol. Dial. Transplant.* 30, 829–835. doi: 10.1093/ndt/gfu274

Reeves, P. B., and Mc Causland, F. R. (2018). Mechanisms, clinical implications, and treatment of intradialytic hypotension. *Clin. J. Am. Soc. Nephrol.* 13, 1297–1303. doi: 10.2215/CJN.12141017

Ribas Ribeiro, L., Flores de Oliveira, J., Bueno Orcy, R., Castilho Barros, C., Damé Hense, J., Santos, F., et al. (2018). Exploring the complexity: the interplay between the angiotensin-converting enzyme insertion/deletion polymorphism and the sympathetic response to hemodialysis. *Am. J. Physiol. Heart Circ. Physiol.* 315, H1002–H1011. doi: 10.1152/ajpheart.00162.2018

Roberts, P. R., Zachariah, D., Morgan, J. M., Yue, A. M., Greenwood, E. F., Phillips, P. C., et al. (2017). Monitoring of arrhythmia and sudden death in a hemodialysis population: the CRASH-ILR study. *PLoS One* 12:e0188713. doi: 10.1371/journal.pone.0188713

Robin, J., Weinberg, K., Tiongson, J., Carnethon, M., Reddy, M., Ciaccio, C., et al. (2006). Renal dialysis as a risk factor for appropriate therapies and mortality in implantable cardioverter-defibrillator recipients. *Heart Rhythm* 3, 1196–1201. doi: 10.1016/j.hrthm.2006.06.013

Robinson, E. A., Rhee, K. S., Doytchinova, A., Kumar, M., Shelton, R., Jiang, Z., et al. (2015). Estimating sympathetic tone by recording subcutaneous nerve activity in ambulatory dogs. *J. Cardiovasc. Electrophysiol.* 26, 70–78. doi: 10.1111/jce.12508

Roy-Chaudhury, P., Tumlin, J. A., Koplan, B. A., Costea, A. I., Kher, V., Williamson, D., et al. (2018). Primary outcomes of the monitoring in dialysis study indicate that clinically significant arrhythmias are common in hemodialysis patients and related to dialytic cycle. *Kidney Int.* 93, 941–951. doi: 10.1016/j.kint.2017.11.019

Sacher, F., Jesel, L., Borni-Duval, C., De Precigout, V., Lavainne, F., Bourdenx, J.-P., et al. (2018). Cardiac rhythm disturbances in hemodialysis patients: early detection using an implantable loop recorder and correlation with biological and dialysis parameters. *JACC Clin. Electrophysiol.* 4, 397–408. doi: 10.1016/j.jacep.2017.08.002

Sakaguchi, Y., Shoji, T., Kawabata, H., Niihata, K., Suzuki, A., Kaneko, T., et al. (2011). High prevalence of obstructive sleep apnea and its association with renal function among nondialysis chronic kidney disease patients in Japan: a cross-sectional study. *Clin. J. Am. Soc. Nephrol.* 6, 995–1000. doi: 10.2215/CJN.08670910

Sallam, K., Li, Y., Sager, P. T., Houser, S. R., and Wu, J. C. (2015). Finding the rhythm of sudden cardiac death: new opportunities using induced pluripotent stem cell-derived cardiomyocytes. *Circ. Res.* 116, 1989–2004. doi: 10.1161/CIRCRESAHA.116.304494

Sassi, R., Cerutti, S., Lombardi, F., Huikuri, H. V., Peng, C. K., Schmidt, G., et al. (2015). Advances in heart rate variability signal analysis: joint position statement by the e-Cardiology ESC Working Group and the European Heart Rhythm Association co-endorsed by the Asia Pacific Heart Rhythm Society. *Europace* 17, 1341–1353. doi: 10.1093/europace/euv015

Semple, D., Smith, K., Bhandari, S., and Seymour, A. M. (2011). Uremic cardiomyopathy and insulin resistance: a critical role for akt? *J. Am. Soc. Nephrol.* 22, 207–215. doi: 10.1681/ASN.2009090900

Severi, S., Cavalcanti, S., and Avanzolini, G. (1997). Heart rate variability spectral indices for haemodynamic classification of haemodialysis patients. *Physiol. Meas.* 18, 339–353. doi: 10.1088/0967-3334/18/4/007

Shang, F., Wang, S. C., Hsu, C. Y., Miao, Y., Martin, M., Yin, Y., et al. (2017). MicroRNA-92a mediates endothelial dysfunction in CKD. *J. Am. Soc. Nephrol.* 28, 3251–3261. doi: 10.1681/ASN.2016111215

Siddiqi, L., Joles, J. A., Grassi, G., and Blankestijn, P. J. (2009). Is kidney ischemia the central mechanism in parallel activation of the renin and sympathetic system? *J. Hypertens.* 27, 1341–1349. doi: 10.1097/HJH.0b013e32832b521b

Silva, R. T., Martinelli Filho, M., Peixoto Gde, L., Lima, J. J., Siqueira, S. F., Costa, R., et al. (2015). Predictors of arrhythmic events detected by implantable loop recorders in renal transplant candidates. *Arq. Bras. Cardiol.* 105, 493–502. doi: 10.5935/abc.20150106

Simantirakis, E. N., Schiza, S. I., Marketou, M. E., Chrysostomakis, S. I., Chlouverakis, G. I., Klapsinos, N. C., et al. (2004). Severe bradyarrhythmias in patients with sleep apnoea: the effect of continuous positive airway pressure treatment: a long-term evaluation using an insertable loop recorder. *Eur. Heart J.* 25, 1070–1076. doi: 10.1016/j.ehj.2004.04.017

Skampardoni, S., Green, D., Hnatkova, K., Malik, M., Kalra, P. A., and Poulikakos, A. D. (2018a). QRS-T angle predicts Cardiac Risk and correlates with Global Longitudinal Strain in Prevalent Hemodialysis Patients. *Front. Physiol.* 10:145. doi: 10.3389/fphys.2019.00145

Skampardoni, S., Poulikakos, D., Malik, M., Green, D., and Kalra, P. A. (2018b). The potential of electrocardiography for cardiac risk prediction in chronic and end-stage kidney disease. *Nephrol. Dial. Transplant.* doi: 10.1093/ndt/gfy255 [Epub ahead of print].

Smetana, P., Batchvarov, V. N., Hnatkova, K., Camm, A. J., and Malik, M. (2002). Sex differences in repolarization homogeneity and its circadian pattern. *Am. J. Physiol. Heart Circ. Physiol.* 282, H1889–H1897. doi: 10.1152/ajpheart.00962.2001

Suzuki, M., Hiroshi, T., Aoyama, T., Tanaka, M., Ishii, H., Kisohara, M., et al. (2012). Nonlinear measures of heart rate variability and mortality risk in hemodialysis patients. *Clin. J. Am. Soc. Nephrol.* 7, 1454–1460. doi: 10.2215/CJN.09430911

Tada, T., Kusano, K. F., Ogawa, A., Iwasaki, J., Sakuragi, S., Kusano, I., et al. (2007). The predictors of central and obstructive sleep apnoea in haemodialysis patients. *Nephrol. Dial. Transplant.* 22, 1190–1197. doi: 10.1093/ndt/gfl748

Tang, W., Li, L. X., Pei, J., and Wang, T. (2012). Heart rate variability in peritoneal dialysis patients: what is the role of residual renal function? *Blood Purif.* 34, 58–66. doi: 10.1159/000338184

Task Force of the European Society of Cardiology and North American Society of Pacing and Electrophysiology (1996). Heart rate variability: standards of measurement, physiological interpretation and clinical use. *Circulation* 93, 1043–1065.

Tereshchenko, L. G., Kim, E. D., Oehler, A., Meoni, L. A., Ghafoori, E., and Rami, T. (2016). Electrophysiologic substrate and risk of mortality in incident hemodialysis. *J. Am. Soc. Nephrol.* 27, 3413–3420. doi: 10.1681/ASN.2015080916

Tsuji, Y., Suzuki, N., Hitomi, Y., Yoshida, T., and Mizuno-Matsumoto, Y. (2017). Quantification of autonomic nervous activity by heart rate variability and approximate entropy in high ultrafiltration rate during hemodialysis. *Clin. Exp. Nephrol.* 21, 524–530. doi: 10.1007/s10157-016-1305-5

United States Renal Data System (2012). *USRDS Annual Data Report: Epidemiology of Kidney Disease in the United States*. Bethesda, MD: National Institutes of Health.

Vallon, V., Muhlbauer, B., and Osswald, H. (2006). Adenosine and kidney function. *Physiol. Rev.* 86, 901–940. doi: 10.1152/physrev.00031.2005

Vaseghi, M., Lux, R. L., Mahajan, A., and Shivkumar, K. (2012). Sympathetic stimulation increases dispersion of repolarization in humans with myocardial infarction. *Am. J. Physiol. Heart Circ. Physiol.* 302, H1838–H1846. doi: 10.1152/ajpheart.01106.2011

Vitolo, E., Madoi, S., Palvarini, M., De Maria, R., Ciró, E., Colombo, A. E., et al. (1987). Relationship between changes in R wave voltage and cardiac volumes. A vectorcardiographic study during hemodialysis. *J. Electrocardiol.* 20, 138–146. doi: 10.1016/S0022-0736(87)80103-6

Waks, J. W., Sitlani, C. M., Soliman, E. Z., Kabir, M., Ghafoori, E., Biggs, M. L., et al. (2016). Global electric heterogeneity risk score for prediction of sudden cardiac death in the general population: the atherosclerosis risk in communities (ARIC) and cardiovascular health (CHS) studies. *Circulation* 133, 2222–2234. doi: 10.1161/CIRCULATIONAHA.116.021306

Wan, C., Herzog, C. A., Zareba, W., and Szymkiewicz, S. J. (2014). Sudden cardiac arrest in hemodialysis patients with wearable cardioverter defibrillator. *Ann. Noninvasive Electrocardiol.* 19, 247–257. doi: 10.1111/anec.12119

Wang, A. Y., Wang, M., Woo, J., Lam, C. W., Li, P. K., Lui, S. F., et al. (2003). Cardiac valve calcification as an important predictor for all-cause mortality and cardiovascular mortality in long-term peritoneal dialysis patients: a prospective study. *J. Am. Soc. Nephrol.* 14, 159–168. doi: 10.1097/01.ASN.0000038685.95946.83

Wang, I. K., Lin, K. H., Lin, S. Y., Lin, C. L., Chang, C. T., Yen, T. H., et al. (2016). Permanent cardiac pacing in patients with end-stage renal disease undergoing dialysis. *Nephrol. Dial. Transplant.* 31, 2115–2122. doi: 10.1093/ndt/gfw302

Wang, Z., Jiang, A., Wei, F., and Chen, H. (2018). Cardiac valve calcification and risk of cardiovascular or all-cause mortality in dialysis patients: a meta-analysis. *BMC Cardiovasc. Disord.* 18:12. doi: 10.1186/s12872-018-0747-y

Wanner, C., Krane, V., März, W., Olschewski, M., Mann, J. F., Ruf, G., et al. (2005). Atorvastatin in patients with type 2 diabetes mellitus undergoing hemodialysis. *N. Engl. J. Med.* 353, 238–248. doi: 10.1056/NEJMoa043545

Wolf, J., Drozdowski, J., Czechowicz, K., Winklewski, P. J., Jassem, E., Kara, T., et al. (2016). Effect of beta-blocker therapy on heart rate response in patients with hypertension and newly diagnosed untreated obstructive sleep apnea syndrome. *Int. J. Cardiol.* 202, 67–72. doi: 10.1016/j.ijcard.2015.08.139

Wong, M. C., Kalman, J. M., Pedagogos, E., Toussaint, N., Vohra, J. K., Sparks, P. B., et al. (2015). Temporal distribution of arrhythmic events in chronic kidney disease: highest incidence in the long interdialytic period. *Heart Rhythm* 12, 2047–2055. doi: 10.1016/j.hrthm.2015.06.033

Wong, M. C. G., Kalman, J. M., Pedagogos, E., Toussaint, N., Vohra, J. K., Sparks, P. B., et al. (2015). Bradycardia and asystole is the predominant mechanism of sudden cardiac death in patients with chronic kidney disease. *J. Am. Coll. Cardiol.* 65, 1263–1265. doi: 10.1016/j.jacc.2014.12.049

Young, C. N., Fisher, J. P., Gallagher, K. M., Whaley-Connell, A., Chaudhary, K., Victor, R. G., et al. (2009). Inhibition of nitric oxide synthase evokes central sympatho-excitation in healthy humans. *J. Physiol.* 587(Pt 20), 4977–4986. doi: 10.1113/jphysiol.2009.177204

Zabel, M., and Malik, M. (2002). Practical use of T wave morphology assessment. *Card. Electrophysiol. Rev.* 6, 316–322. doi: 10.1023/A:1016353714372

Zhang, J., Yu, X., Sun, B., Bai, J., Wei, Y., Zha, X., et al. (2013). Parathyroidectomy and heart rate variability in patients with stage 5 CKD. *Clin. J. Am. Soc. Nephrol.* 8, 1378–1387. doi: 10.2215/CJN.10381012

Zhang, L. N., Yang, G., Cheng, C., Shen, C., Cui, Y. Y., Zhang, J., et al. (2015). Plasma FGF23 levels and heart rate variability in patients with stage 5 CKD. *Osteoporos. Int.* 26, 395–405. doi: 10.1007/s00198-014-2862-7

Zhao, Y., Chen, N. X., Shirazi, J. T., Shen, C., Lin, S. F., Fishbein, M. C., et al. (2016). Subcutaneous nerve activity and mechanisms of sudden death in a rat model of chronic kidney disease. *Heart Rhythm* 13, 1105–1112. doi: 10.1016/j.hrthm.2015.12.040

Zwillich, C., Devlin, T., White, D., Douglas, N., Weil, J., and Martin, R. (1982). Bradycardia during sleep apnea. Characteristics and mechanism. *J. Clin. Invest.* 69, 1286–1292. doi: 10.1172/JCI110568

Conflict of Interest Statement: The authors declare that the research was conducted in the absence of any commercial or financial relationships that could be construed as a potential conflict of interest.

frontiers in Physiology

ORIGINAL RESEARCH
published: 18 June 2019
doi: 10.3389/fphys.2019.00635

Errors of Fixed QT Heart Rate Corrections Used in the Assessment of Drug-Induced QTc Changes

*Katerina Hnatkova[1], Jose Vicente[2], Lars Johannesen[2], Christine Garnett[2], Norman Stockbridge[2] and Marek Malik[1]**

[1] National Heart and Lung Institute, Imperial College London, London, United Kingdom, [2] Division of Cardiovascular and Renal Products, Office of New Drugs, Center for Drug Evaluation and Research, U.S. Food and Drug Administration, Silver Spring, MD, United States

The accuracy of studies of drug-induced QTc changes depends, among others, on the accuracy of heart rate correction of QT interval. It has been recognized that when a drug leads to substantial heart rate changes, fixed universal corrections cannot be used and that alternative methods such as subject-specific corrections established for each study participant need to be considered. Nevertheless, the maximum heart rate change that permits use of fixed correction with reasonable accuracy has not been systematically investigated. We have therefore used full QT/heart-rate profiles of 751 healthy subjects (mean age 34.2 ± 9.6, range 18–61 years, 335 females) and compared their subject-specific corrections with 6 fixed corrections, namely Bazett, Fridericia, Framingham, Hodges, Rautaharju, and Sarma formulae. The comparison was based on statistical modeling experiments which simulated clinical studies of $N = 10$ or $N = 50$ female or male subjects. The experiments compared errors of ΔQTc intervals calculated as differences between QTc intervals at an initial heart rate (in the range of 40 to 120 beats per minute, bpm) and after a heart rate change (in the range from −20 to +20 bpm). The experiments also investigated errors due to spontaneous heart rate fluctuation and due to omission of correction for QT/RR hysteresis. In each experiment, the absolute value of the single-sided 90th percentile most remote from zero was used as the error estimate. Each experiment was repeated 10,000 times with random selection of modeled study group. From these repetitions, median and upper 80th percentile was derived and graphically displayed for all different combinations of initial heart rate and heart rate change. The results showed that Fridericia formula might be reasonable (with estimated errors of ΔQTc below 8 ms) in large studies if the heart rate does not change more than ± 10 bpm and that the errors by fixed corrections and the errors due to omission of QR/RR hysteresis are additive. Additionally, the results suggest that the variability introduced into QTc data by not correcting for the underlying heart rate accurately might have a greater impact in smaller studies. The errors by Framingham formula were practically the same as with the Fridericia formula. Other investigated fixed heart rate corrections led to larger ΔQTc errors.

Keywords: drug safety, drug-induced QTc changes, heart rate correction of QT interval, Fridericia QTc formula, Framingham QTc formula, subject-specific QTc corrections

OPEN ACCESS

Edited by:
Jiashin Wu,
University of South Florida,
United States

Reviewed by:
Vincent Jacquemet,
Université de Montréal, Canada
Alain Vinet,
Université de Montréal, Canada

****Correspondence:***
Marek Malik
marek.malik@btinternet.com;
marek.malik@imperial.ac.uk

Specialty section:
This article was submitted to Cardiac Electrophysiology, a section of the journal Frontiers in Physiology

Received: *23 March 2019*
Accepted: *06 May 2019*
Published: *18 June 2019*

Citation:
Hnatkova K, Vicente J, Johannesen L, Garnett C, Stockbridge N and Malik M (2019) Errors of Fixed QT Heart Rate Corrections Used in the Assessment of Drug-Induced QTc Changes. Front. Physiol. 10:635. doi: 10.3389/fphys.2019.00635

INTRODUCTION

The possibility of proarrhythmic potential of novel pharmaceutical compounds is well recognized (Guidance to industry, 2005; Vicente et al., 2016) and related considerations are an integral part of regulatory process of the approval of new drugs (Zhang et al., 2015). While novel approaches to these considerations are presently discussed (Darpo et al., 2014; Vicente et al., 2018), the assessment of drug-induced QTc interval prolongation remains a principal test to identify compounds that require further evaluation of their propensity of triggering Torsade de Pointes (TdP) tachycardia. The accuracy of the evaluation of drug-induced QTc interval prolongation depends on a number of factors including the quality of electrocardiogram (ECG) recordings, precision of their measurement and validity of pharmacokinetic / pharmacodynamic modeling (Garnett et al., 2008). When a drug changes heart rate, the assessment of QTc changes also crucially depends on the validity of methods used to correct the QT interval for the underlying heart rate (Garnett et al., 2012).

Practically since the invention of electrocardiography, the relationship between the QT interval duration and the underlying heart rate has been a subject of a large number of studies that proposed a variety of mathematical formulae to describe the relationship and to correct the QT interval for heart rate (Malik, 2002). More recently, it has been recognized that the QT/heart-rate relationship differs among subjects (Batchvarov et al., 2002; Malik et al., 2002) and that consequently, all fixed formulae are inaccurate to a greater or lesser extent (Malik, 2002). This is also reflected in recommendations in a white paper suggesting that in the presence of obvious underlying heart rate changes, fixed formulae cannot be relied on and that the individuality of the QT/heart-rate relationship needs to be taken into account (Garnett et al., 2012).

Nevertheless, the extent of the drug-induced heart rate changes that still allows fixed correction formulae to be used has not been systematically investigated. Discussions of whether alternative methods to account for changes in heart rate need to be used once the heart rate changes on average by some number of beats per minute (bpm) are not based on a systematic analysis of data. Having this knowledge gap in mind, we have conducted a statistical modeling study that compared a battery of previously proposed fixed heart rate correction formulae with individual QT/heart-rate profiles in a large population of healthy subjects.

In these statistical modeling experiments, we considered not only the absolute errors of fixed heart rate corrections but also errors of ΔQTc values representing the QTc changes for different heart rates since when calculation QTc changes, absolute correction errors in QTc estimates on baseline and on active treatment might partially cancel each other. Fixed corrections also only consider how much the QT interval changes at different heart rates but do not deal with the so-called QT/RR hysteresis, that is the assessment of how quickly QT interval changes after heart rate changes (Malik et al., 2008b; Gravel et al., 2018). We have therefore also included modeling experiments that combined the ΔQTc errors due to heart rate change with errors caused by the omission of QT/RR hysteresis correction.

MATERIALS AND METHODS

As explained further in more detail, of all the different previously published correction formulae, we selected 6 that were most representative of different types of QT/heart-rate curvatures. We compared their correction performance with that of the curvilinear models of intra-subject QT/heart-rate relationship (Malik et al., 2013). We obtained these subject-specific data from a previously published population healthy subjects in whom repeated accurate ECG measurements were available (Malik et al., 2016). In the statistical modeling experiments, we also used previously published data to estimate spontaneous heart rate instability and QT/RR hysteresis effects.

Fixed QT Heart Rate Corrections

Although the QT interval duration depends on the underlying heart rate rather than on the duration of the preceding cardiac cycle (Franz et al., 1988), it became customary to correct the QT interval duration for the duration of the RR interval representing the underlying heart rate. Therefore, our study also used the conversion of heart rate changes into RR interval changes allowing to employ previously published corrections in their original form.

The following six correction formulae were selected:

Bazett (Bazett, 1920)
$$QTc = QT/\sqrt{RR}$$

Fridericia (Fridericia, 1920)
$$QTc = QT/\sqrt[3]{RR}$$

Framingham (Sagie et al., 1992)
$$QTc = QT + 0.154\,(1 - RR)$$

Hodges (Hodges et al., 1983)
$$QTc = QT + 0.00175\,(HR - 60)$$

Rautaharju (Rautaharju et al., 1990)
$$QTc = QT + 0.24251 - 0.434 * e^{-0.0097 * HR}$$

Sarma (Sarma et al., 1984)
$$QTc = QT - 0.04462 + 0.664 * e^{-2.7 * RR}$$

where QTc, QT, and RR are ECG intervals measured in seconds and HR is the heart rate in bpm.

The Bazett and Fridericia formulae were selected because of their frequent use, the Framingham and Hodges formulae relate QT interval linearly to the RR interval and to the heart rate, and similarly, the Sarma and Rautaharju formulae relate QT interval exponentially to the RR interval and to the heart rate. Examples of the curvatures of these formulae are shown in the top panel of **Figure 1**.

For the purposes of describing the experiments with these fixed formulae, we shall use the symbol $QTc_{\blacksquare}$(QT,HR) which will mean the results of a fixed formula applied to QT interval corrected for heart rate HR. Where necessary, we use subscripts B, F, Fm, H, R, and S to denote formulae from Bazett to Sarma, respectively.

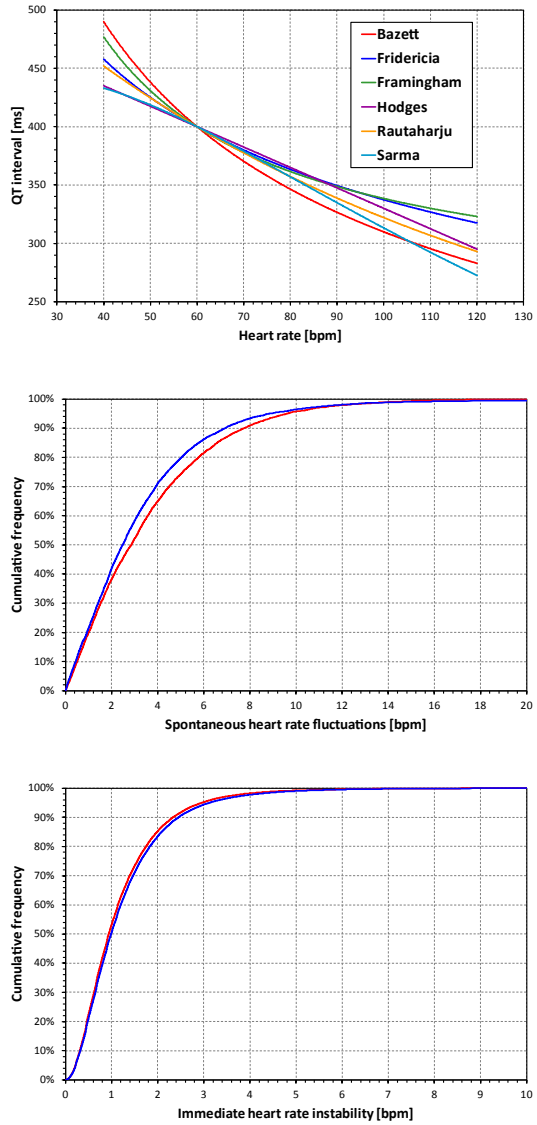

FIGURE 1 | The top panel shows curvatures QT/heart-rate assumed by the six fixed heart rate correction formulae for a subject in whom QT = 400 at heart rate of 60 bpm. The middle and the bottom panel show the cumulative distribution of spontaneous heart rate fluctuations and of immediate heart rate instability, respectively (see the text for details). The red and blue lines correspond to female and male subjects, respectively. Note that the observed distributions of both spontaneous heart rate fluctuations and of immediate heart rate instability were symmetrical in terms of showing the corresponding distributions of both positive and negative values. Therefore, for simplicity, only one half of the distributions is presented showing the positive values.

Population Data

The study used data that have previously been used in conceptually different investigations (Malik et al., 2016). In brief, the data originated from 7 thorough QT studies. Pooled together, these studies investigated 751 individuals, mean ± standard deviation (SD) age 34.18 ± 9.56 years, range 18–61, 335 females. All were healthy subjects with normal physical investigation and normal screening ECG. The source studies were all approved by relevant ethics authorities and all subjects gave written informed consent in accordance with the Helsinki declaration and giving permission for their data to be used in scientific research. The original studies investigated different novel pharmaceuticals, but since we used only anonymised drug-free data, the character of the investigated drugs is irrelevant. For the same reason, no separate ethics clearance of the present investigation was required as per the local legislation.

In each subject, the source studies obtained repeated daytime 12-lead Holter recordings. During drug-free days, multiple QT interval and hysteresis-corrected RR intervals were measured scanning broad ranges of heart rates in each subject. A total of 897,570 ECG measurements (QT interval + hysteresis corrected RR interval, range 321–1560 measurements per subject) were made. Using previously described procedures (Malik et al., 2008a, 2012) the QT interval measurements were made in representative median complexes derived from 10-s ECG segments. The accuracy of each measurement was ensured by repeated visual verifications and, where necessary, manual corrections.

Individual QT/RR Patterns

In the pooled study population, the heart rates (corresponding to hysteresis corrected RR intervals (Malik et al., 2008b)) at which QT interval were measured ranged between 32.0 and 164.3 bpm, (33.9–164.3 bpm in females, 32.0–151.3 bpm in males). The within-subject ranges (max–min) of heart rates at which QT intervals were measured were (mean ± SD) 61.1 ± 12.7 bpm and 57.8 ± 12.9 bpm wide in females and males, respectively.

Using previously published technique (Malik et al., 2013), an individual-specific QT/RR curvilinear regression in the form

$$QT = \alpha + \frac{\beta}{\gamma}\left(RR^{\gamma} - 1\right) + \varepsilon$$

was fitted to the QT and RR interval data in each subject. In this form, QT and RR intervals are in seconds (RR representing the hysteresis-corrected underlying heart rate at which the QT interval was measured), ε are normally distributed zero-centered errors, and parameters α, β, and γ represent the individual-specific values of the central rate-independent QT value, and of the slope and curvature of the QT/RR relationship, respectively. This regression formula leads to individual-specific QT correction in the form:

$$QTc = QT + \frac{\beta}{\gamma}\left(1 - RR^{\gamma}\right)$$

These curvilinear regressions fitted the individual data tightly. The mean regression residuals (i.e., the standard deviations of the individually corrected QTc values) were (mean ± SD) 5.68 ± 1.10 ms and 5.33 ± 1.10 ms in females and males, respectively.

The RR intervals representing the hysteresis-corrected underlying heart rate at which the QT interval was measured were obtained using the previously published exponential decay model (Malik et al., 2008b): If QT interval reading is preceded by RR interval sequence $\{RR_i\}_{i=0}^{N}$ (RR_0 closest to the QT

measurement), and $\Lambda(k) = \sum_{i=0}^{k} RR_i$, the exponential hysteresis model suggests correcting the QT interval for $RR' = \sum_{i=0}^{N} \omega_i RR_i$, where for each $j = 0, \cdots, N$,

$\sum_{i=0}^{j} \omega_i = \left(1 - e^{-\lambda \Lambda(j)/\Lambda(N)}\right) / \left(1 - e^{-\lambda}\right)$ where the coefficient λ characterizes the subject-specific time constant, i.e., the speed with which QT interval adapts to a change in the underlying heart rate. In the data available for the experiments described here, 5-min histories of all QT interval measurements were available, that is $\Lambda(N) \cong 300$s.

The curvilinear QT/RR regression modeling allowed us to estimate reliably the QT interval value for different heart rates. That is, for any given heart rate, the representative RR interval could be calculated and, together with parameters α, β, and γ, turned into the QT interval in the given subject at the given heart rate. For the purposes of describing the computations made in this study, we shall use the symbol $QT(\mathrm{HR})$ meaning the QT interval in a given subject at heart rate HR (i.e.,

$$QT(\mathrm{HR}) = \alpha + \frac{\beta}{\gamma}[(60/\mathrm{HR})^{\gamma} - 1],$$

where the coefficients α, β, and γ correspond to the given subject and the heart rate value HR is in bpm). This means that for every subject and every heart rate HR, the individual-specific correction formula applied to QT (HR) always leads to the same constant value ($= \alpha$). Indeed, this is the basic principle of individual-specific heart rate correction (Garnett et al., 2012; Malik, 2018). In the description of the computations, we shall denote this constant value by $QTcI$.

Basic Evaluation of Fixed Heart Rate Corrections

A simple evaluation of the accuracy of fixed corrections can be based on the comparison of their results with the results of the individual-specific corrections. That is, for different values of heart rate fi, we evaluated the differences between $QTcI$ and $QTc_{\blacksquare}(\mathrm{QT(fi)},\mathrm{fi})$ in each study subject. Subsequently, for each fixed correction formula, these differences were statistically summarized over the complete study populations. In these summaries, we distinguished female and male study subjects because of the known sex differences in the QT/heart-rate patterns (Linde et al., 2018).

The differences $QTc_{\blacksquare}(\mathrm{QT(fi)}, \mathrm{fi}) - \mathrm{QTcI}$ were evaluated for fi between 40 and 120 bpm in 0.1 bpm steps.

Statistical Modeling Experiments

The errors of fixed corrections at different heart rates evaluated over the complete population are potentially misleading in several ways. For the purposes of a more appropriate assessment, we performed three sets of statistical modeling experiments.

Experiments Evaluating QTc Errors Due to Heart Rate Instability

The first problem of the simple evaluation of the differences between fixed corrections and $QTcI$ is the assumption that the very same heart rate might be considered in all subjects. This does not correspond to the reality of clinical studies in which, even during baseline conditions, subjects show short-term variable heart rates. Therefore, using previously published data of 73 thorough QT studies in which 747,912 ECGs were measured in 6,786 healthy subjects (Malik et al., 2016), we obtained a distribution of inter-subject heart rate differences at the same study time-points. That is, in all these studies and subjects, we considered drug-free time-points of each study when the ECGs were measured under the same conditions (e.g., supine, resting, and fasting). In each subject and at each time-point, heart rate measurements were made. Subsequently, we obtained the distribution of heart rate changes between different (drug-uninfluenced) time-points within the same subject. This distribution is shown in the middle panel of **Figure 1**. We shall call this the distribution of the spontaneous heart rate fluctuations. It shows how much the heart rate fluctuates in the same subject between time-points of the same character (e.g., when the subject is placed repeatedly into supine resting position during fasting morning hours of the same day).

Subsequently, in the first type of statistical models, we considered a sub-population of N subjects and for each of these subjects and for different values of heart rate fi, we evaluated the differences between $QTcI$ and

$$QTc_{\blacksquare}(\mathrm{QT(fi} + \varepsilon), \mathrm{fi} + \varepsilon)$$

where ε was a random number derived from the distribution the spontaneous heart rate fluctuations (different random numbers from the distribution were used in different individual comparisons).

If the QTc values were accurate (i.e., if the individual-specific heart rate corrections were used instead of fixed corrections) each the differences would be equal to zero. Therefore, to characterize the results of the comparison in N subjects, we calculated the largest absolute difference $|QTcI - QTc_{\blacksquare}(\mathrm{QT(fi+\varepsilon)},\mathrm{fi+\varepsilon})|$ after excluding the lowest and highest 10% of the $QTcI - QTc_{\blacksquare}(\mathrm{QT(fi+\varepsilon)},\mathrm{fi+\varepsilon})$ differences.

Experiments Evaluating QTc Errors Due to Drug-Induced Heart Rate Changes

The accuracy of fixed corrections also needs to consider situations of heart rate changes. As explained previously, in each individual, the subject-specific heart rate correction results in the same value of $QTcI$ when correcting QT(fi) for the heart rate fi irrespective of the value of fi. Hence, if the heart rate changes, there would be no difference in subject-specific heart rate correction between QT(fi) corrected for fi and QT(fi+δ) corrected for fi+δ. It is therefore appropriate to investigate the difference in fixed QTc values for the same scenario.

In addition to this, the considerations of spontaneous heart rate fluctuations also need to be incorporated. We therefore considered a sub-population of N subjects and for each of these

subjects, evaluated the difference

$$QTc_{\blacksquare}(QT(\text{fi}+\varepsilon_1), \text{fi}+\varepsilon_1) - QTc_{\blacksquare}(QT(\text{fi}+\delta+\varepsilon_2), \text{fi}+\delta+\varepsilon_2)$$

where fi is an initial heart rate, δ is a (drug-induced) heart rate change, and ε_1 and ε_2 are random numbers derived from the distribution the spontaneous heart rate fluctuations. (Note that ε_1 and ε_2 may be positive or negative, independently of each other).

Similar to the previous type of statistical experiments, we have characterized the result of this calculation in *N* subjects by evaluating the largest absolute difference among the $QTc_{\blacksquare}$ values after excluding the lowest and highest 10% of the differences.

Experiments Evaluating QTc Errors Due to QT/RR Hysteresis Omission

Finally, the effects of QT/RR hysteresis also need to be considered. The previous type of experiments corresponds to the situation where each QT interval is corrected for a stable underlying heart rate. In practice, HR shows short-term variability, and the adaptation of QT to HR is not instantaneous, resulting in QT/RR hysteresis (Malik et al., 2016).

This error is worst when the QT interval duration is corrected for the preceding RR interval, and underlying heart rate can only be fully assessed over periods much longer than typical 10-s ECG recordings. Similar to the distribution of the spontaneous heart rate fluctuations, we have estimated the differences between the heart rate underlying the QT interval and the simultaneously measured heart rate by studying the heart rate differences between closely coupled replicate QT/RR measurements of the same time-points in the previously published data of 73 thorough QT studies (Malik et al., 2016). That is, in all these studies and subjects, we considered study drug-free time-points corresponding the same condition (e.g., supine, resting, and fasting). In each subject and at each time-point, multiple heart rate (or RR interval) measurements were made and we obtained the distribution of heart rate discrepancies between the repeated heart rate measurements within the same subject and within the same (drug-uninfluenced) time-point. The distribution of these data is shown in the bottom panel of **Figure 1** and we shall call it the distribution of immediate heart rate instability. It shows how much heart rate fluctuates between measurements during the same time-point (e.g., within the same minute while the subject is in supine resting position for the duration of the same study time-point).

Using these data, we have investigated the combined effect of fixed correction formulae together with the omission of QT/RR hysteresis correction in the following experiments: Considering a sub-population of *N* subjects, we evaluated, for each of these subjects, the difference

$$QTc_{\blacksquare}(QT(\text{fi}+\varepsilon_1), \text{fi}+\varepsilon_1+\vartheta_1) - QTc_{\blacksquare}(QT(\text{fi}+\delta+\varepsilon_2), \text{fi}+\delta+\varepsilon_2+\vartheta_2)$$

where fi is an initial heart rate, δ is heart rate change, $\varepsilon_1$and ε_2 are random numbers derived from the distribution of the spontaneous heart rate fluctuations, and ϑ_1 and ϑ_2 are random numbers derived from the distribution of immediate heart rate instability. Hence, the coefficients ϑ_1 and ϑ_2 represent the differences between the heart rates that underlie the QT intervals and the heart rates for which the QT interval is corrected. (Note that again, ε_1 and ε_2 and similarly ϑ_1 and ϑ_2 may be positive or negative, independently of the other parameters).

To characterize the result of this calculation in *N* subjects, we have again used the largest absolute difference among the $QTc_{\blacksquare}$ values after excluding the lowest and highest 10% of the $QTc_{\blacksquare}$ differences.

Organization of Experiments

All the experiments were performed by varying the value of fi from 40 bpm to 120 bpm in 0.1 bpm steps. The experiments that included the modeled heart rate changes were performed by additionally varying the value of δ from −20 to +20 bpm, again in 0.1 bpm steps (that is, in the experiments of modeled heart rate changes, we used 801 × 401 = 321,201 combinations of fi and δ-values).

All experiments were also repeated for $N = 50$ and $N = 10$, to approximate the situations of standard thorough QT studies (Zhang and Machado, 2008) and of small early clinical investigations that have also been proposed for the assessment of drug-induced QTc changes (Darpo et al., 2014).

For both $N = 50$ and $N = 10$, we repeated the selection of the sub-populations 10,000 times, each time selecting the sub-population randomly from the pool of study subjects, repeating the same process for both female and male study populations. In each repetition of each experiment and in each setting of different fi and δ-values, the coefficients $\varepsilon_1$and ε_2, and, in the last type of experiments, the coefficients ϑ_1 and ϑ_2 were repeatedly randomly generated from the relevant distributions. Mersenne twister pseudorandom number generator was used for all random selections (Matsumoto and Nishimura, 1998).

Statistical Summaries and Results Presentation

As stated, the basic evaluations of the fixed corrections, i.e., those based on differences $QTc_{\blacksquare}(\text{QT}(\text{fi}),\text{fi}) - QTcI$, were performed for female and male subjects separately. For each value of fi, and for each sex-group, we calculated the median, the inter-quartile range, and ranges between 10th and 90th, and between 5th and 95th percentiles of the differences in the complete sex-group. The results were presented graphically.

For each set of experiments of QTc errors due to heart rate instability, i.e., for experiments with $N = 50$ and $N = 10$ of female and male subjects, the repetition of random subject selections provided 10,000 experiment characteristics for each heart rate value of fi. Of these, we again calculated the median, the inter-quartile range, and ranges between 10th and 90th, and between 5th and 95th percentiles. There dependencies on fi were again presented graphically.

Similarly, the repetitions of experiments of QTc errors due to drug-induced heart rate changes and due to QT/RR hysteresis omission provided 10,000 experiments characteristics for each

TABLE 1 | The table shows the summaries (mean ± standard deviation) of QT/RR characteristics of the population used in the computational experiments.

	Female	Male
N	335	416
QTcI interval (ms)	420 ± 14	401 ± 12
QT/RR hysteresis constant (95% adaptation) (s)	112 ± 20	117 ± 21
QT/RR slope (parameter β)	0.161 ± 0.033	0.141 ± 0.026
QT/RR curvature (parameter γ)	0.571 ± 0.703	0.730 ± 0.728

QT/RR hysteresis time constants λ were recalculated into the time intervals needed for the QT interval to reach 95% adaptation after a heart rate change. Note that while the QTcI values and slope and curvature parameters β and γ were used in the computational experiments, the hysteresis time constants λ were only used during the intra-subject optimization of the slope and curvature parameters.

experiment setting and for each combination of initial heart rates ﬁ and heart rate changes δ. Of these, we calculated the median and, for the purposes of power sample estimates, also the 80th percentile. The values of these medians and 80th percentiles were used to generate color contour maps. The values of these medians and 80th percentiles were also averaged for different regions of ﬁ and δ combinations.

RESULTS

The characteristics of the subject-specific QT/RR curvilinear models that were used in the computational experiments are summarized in **Table 1**.

Altogether, with all parameter combinations, the study involved more than 7.71×10^{10} experiments with random selections of 10 or 50 subjects.

Population Performance of the Correction Formulae

Population errors of the different fixed correction formulae are shown in **Figure 2**. By definition, all the formulae as well as the subject-specific corrections do not make any distinction between the uncorrected QT interval and corrected QTc interval at heart rate of 60 bpm. No errors of fixed formulae are therefore found at this heart rate. Nevertheless, the more the heart rate differs from 60 bpm the wider spread of errors is seen.

The median errors of QTc_{F} and QTc_{Fm} are reasonably close to zero (especially in the sub-population of male subjects) but even for these formulae, substantial over- and under-correction is seen at both slow and fast heart rates. Also, the median value of the error might correspond to different subjects at different heart rates. Similarly, the lower and higher percentiles are bound to be derived from different subjects at different heart rates.

Similar results are seen in **Figures 3**, **4** that show the evaluation of experiments evaluating QTc errors due to heart rate instability. Since heart rate instability makes the heart rates in a group of subjects always at least partially different from 60 bpm, the absolute error characteristics of these experiments are always positive. Again, the figures show that the more remote the heart rate is from 60 bpm, the more substantial absolute errors are noted. Also, not surprisingly, while the profile of the error characteristics is similar for $N = 50$ and $N = 10$, the width of the percentile bands is wider if fewer subjects are investigated (that is, the fewer subjects in the experiment, the greater possibility of more substantial errors of the fixed corrections applied to the experiment population).

Correction Accuracy Without QT/RR Hysteresis Influence

The results of modeling experiments evaluating QTc errors due to drug-induced heart rate changes but assuming that the effects of QT/RR hysteresis have been fully covered in the heart rate data are shown in **Figures 5–8**. **Figures 5**, **6** show the medians of error characteristics, **Figures 7**, **8** show their upper 80th percentiles.

Superficially, it might seem surprising that for all fixed formulae, the areas of minimum error characteristics are somewhat remote from the initial heart rate of 60 bpm. This is because the experiments investigated errors of QTc changes rather than errors of QTc values. In other words, if both

$$QTc_{\blacksquare}(QT(\text{ﬁ}), \text{ﬁ}) \text{ and } QTc_{\blacksquare}(QT(\text{ﬁ} + \delta), \text{ﬁ} + \delta)$$

are polluted by similar error from the true *QTcI* value, this error will cancel out when investigating the QTc effects of the heart rate change from ﬁ to ﬁ+δ. For this reason, the ΔQTc errors found in these experiments are mainly influenced by the QT/heart-rate curvatures expected by the fixed formulae. Note in **Figure 2** that while the median lines are 0 at 60 bpm, they are most "flat" at somewhat different heart rates. Thus, the errors of QTc changes depend not only of the underlying heart rate change but also of the position of ﬁ and ﬁ+δ on the curvature of the correction formula.

For the same reason, the images in **Figures 5–8** show rhombus-like shapes of which the long axes correspond to the values ﬁ+δ for which the curvature of the fixed formula is least departing from the true QT/heart-rate curvatures of the investigated subjects. Also, in experiments with $\delta = 0$, it is only the combination of spontaneous heart rate fluctuations ε_1 and ε_2 that drive the modeled errors.

Correction Accuracy Including QT/RR Hysteresis Influence

The results of experiments that investigated the experiments combining the effect of heart rate changes with the effect of the omission of QT/RR hysteresis are shown in **Figures 9–12**. **Figures 9**, **10** show the medians of error characteristics, **Figures 11**, **12** show their upper 80th percentiles.

Comparison of these figures with **Figures 5–8** shows that practically irrespective of the combination of heart rate values ﬁ and ﬁ+δ, the omission of the QT/RR hysteresis adds further inaccuracy. This corresponds to previously published observations (Malik et al., 2018). When investigating the effects of omitting QT/RR hysteresis (using the same distribution data as used here) on subject-specific corrections, we observed uniform errors in the region of 3 to 7 ms for different ﬁ and δ combinations (results not shown).

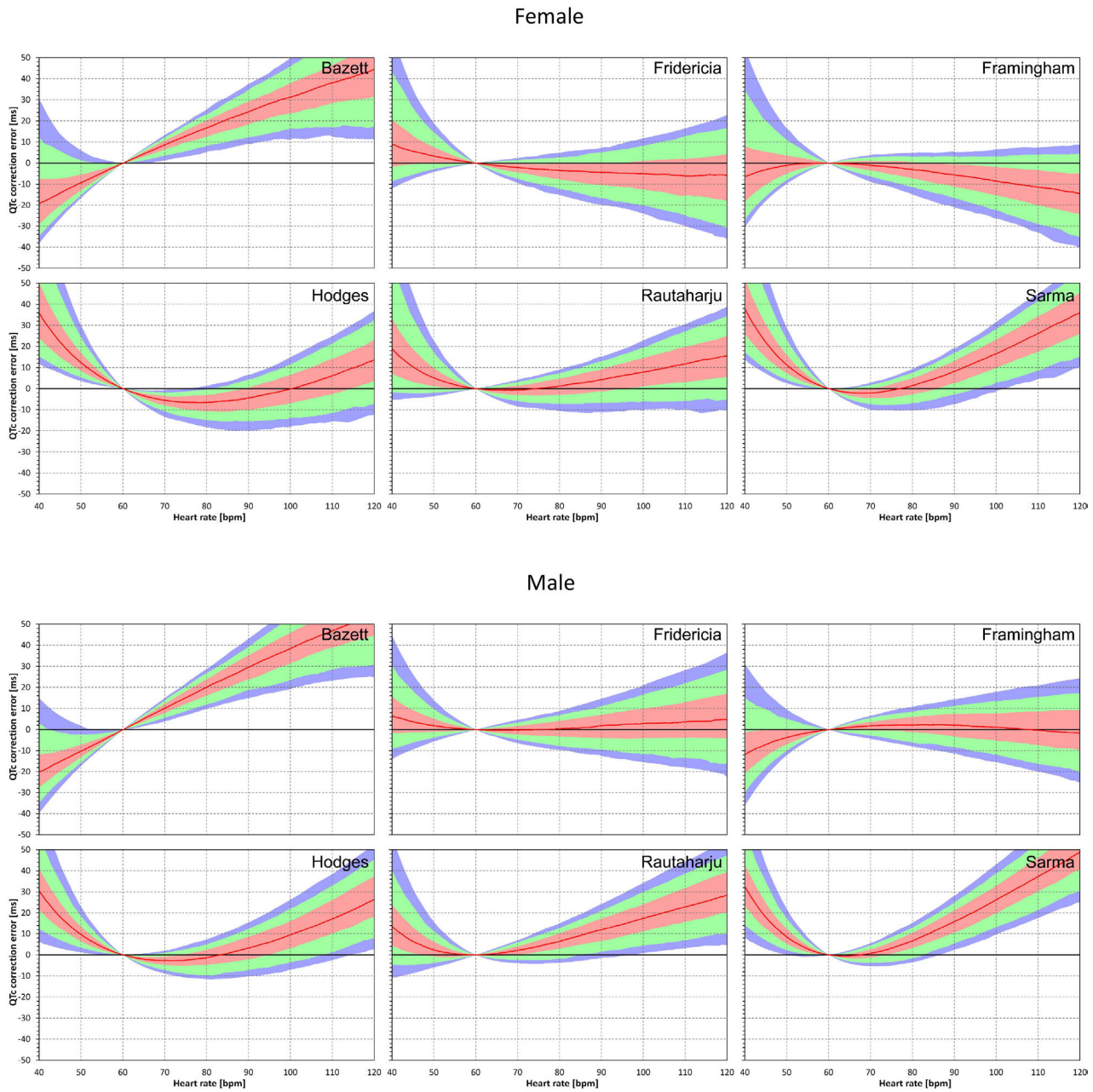

FIGURE 2 | Population QTc errors of fixed heart rate correction formulae. For each formula and for each heart rate 40 to 120 bpm, the figure shows the distribution of the differences between QTc by the formula and subject-specific QTcI values. The red lines are the population medians. The pink, light green, and light blue bands show the inter-quartile ranges, and the ranges 10th to 90th, and 5th to 95th population percentiles, respectively. The top and bottom parts of the figure show the results in female and male subjects, respectively.

Summary of Results

To summarize the findings in **Figures 5–12**, **Table 2** shows the averaged error characteristics (taking female and male subjects together) over the heart rate range $\hat{\imath}$ = 50 to 80 bpm, and for bands of heart rate changes δ bellow $\pm$ 5 bpm, between $\pm$ 5 bpm and $\pm$ 10 bpm, and between $\pm$ 10 bpm and $\pm$ 15 bpm. While the range of $\hat{\imath}$ = 50 to 80 bpm seems to cover reasonably the usual situations of clinical studies in healthy volunteers, very similar results (not shown) were obtained when using different ranges of $\hat{\imath}$.

DISCUSSION

Figures 5–12 and the **Table 2** show that the Fridericia and Framingham corrections lead to lesser errors compared to the other 4 correction formulae. We also found little difference

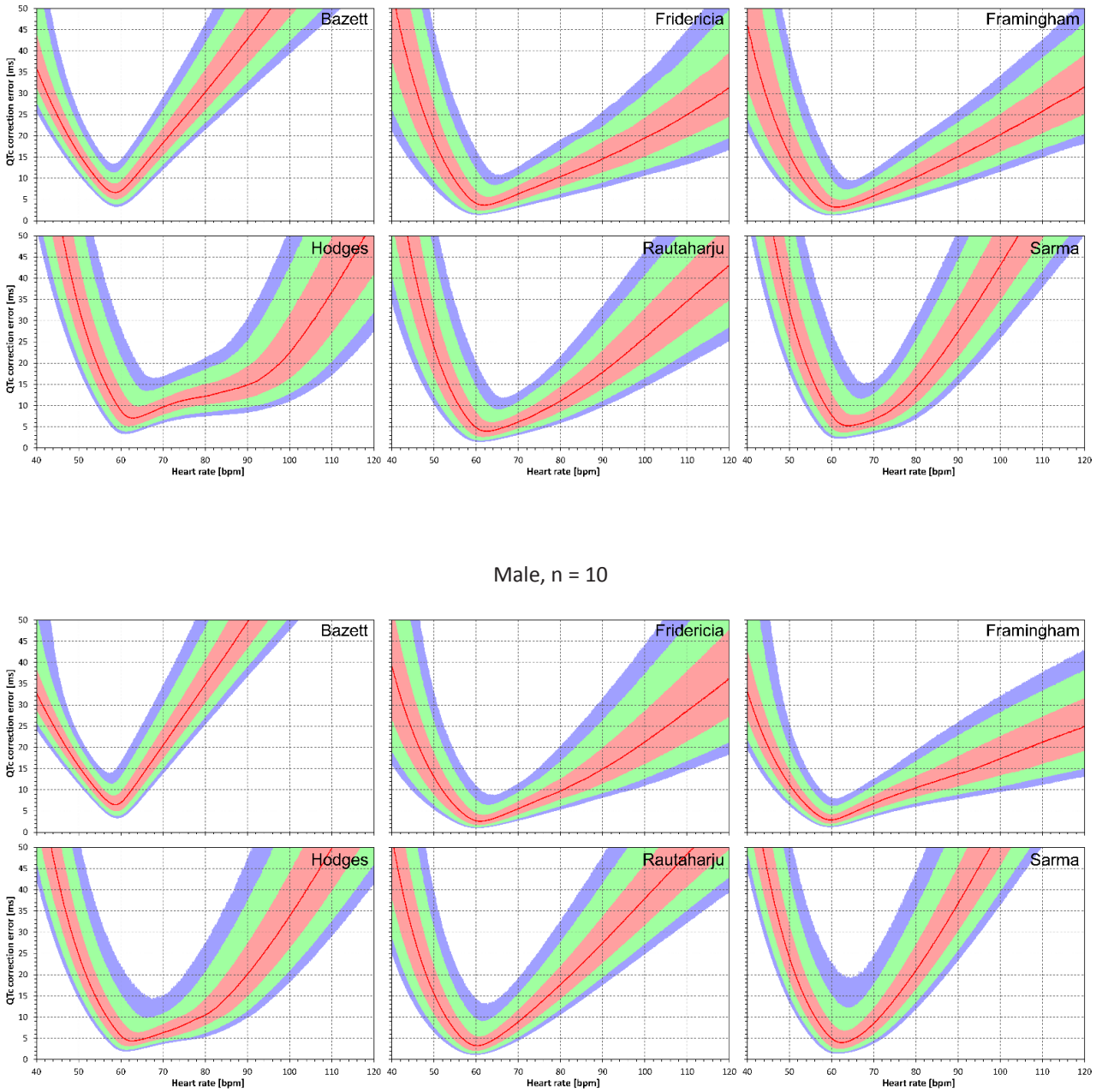

FIGURE 3 | For each of the fixed correction formulae and for each heart rate 40 to 120 bpm, the figure shows the absolute QTc errors due to heart rate instability (see the text for details). The top and bottom part of the figure correspond to experiments with $N = 10$ female and male subjects, respectively. The red lines are the medians of the absolute QTc errors in 10,000 repeated experiments. The pink, light green, and light blue bands show the inter-quartile ranges, and the ranges 10th to 90th, and 5th to 95th percentiles of the repeated experiments, respectively.

between Fridericia and Framingham corrections. It appears that in larger clinical studies, such as those modeled by our experiments with $N = 50$ subjects, these formulae could be reasonably to use if the drug-induced heart rate changes do not exceed $\pm$ 10 bpm. Our results suggest that for smaller studies it might be more important to minimize the variability in QTc introduced by not accounting for QT/RR hysteresis. As already explained, the errors of QTc changes by the fixed correction depend not only on the underlying heart rate change but also on the initial heart rate.

We modeled only errors of ΔQTc data whilst in thorough QT studies, correction of the data for both baseline and

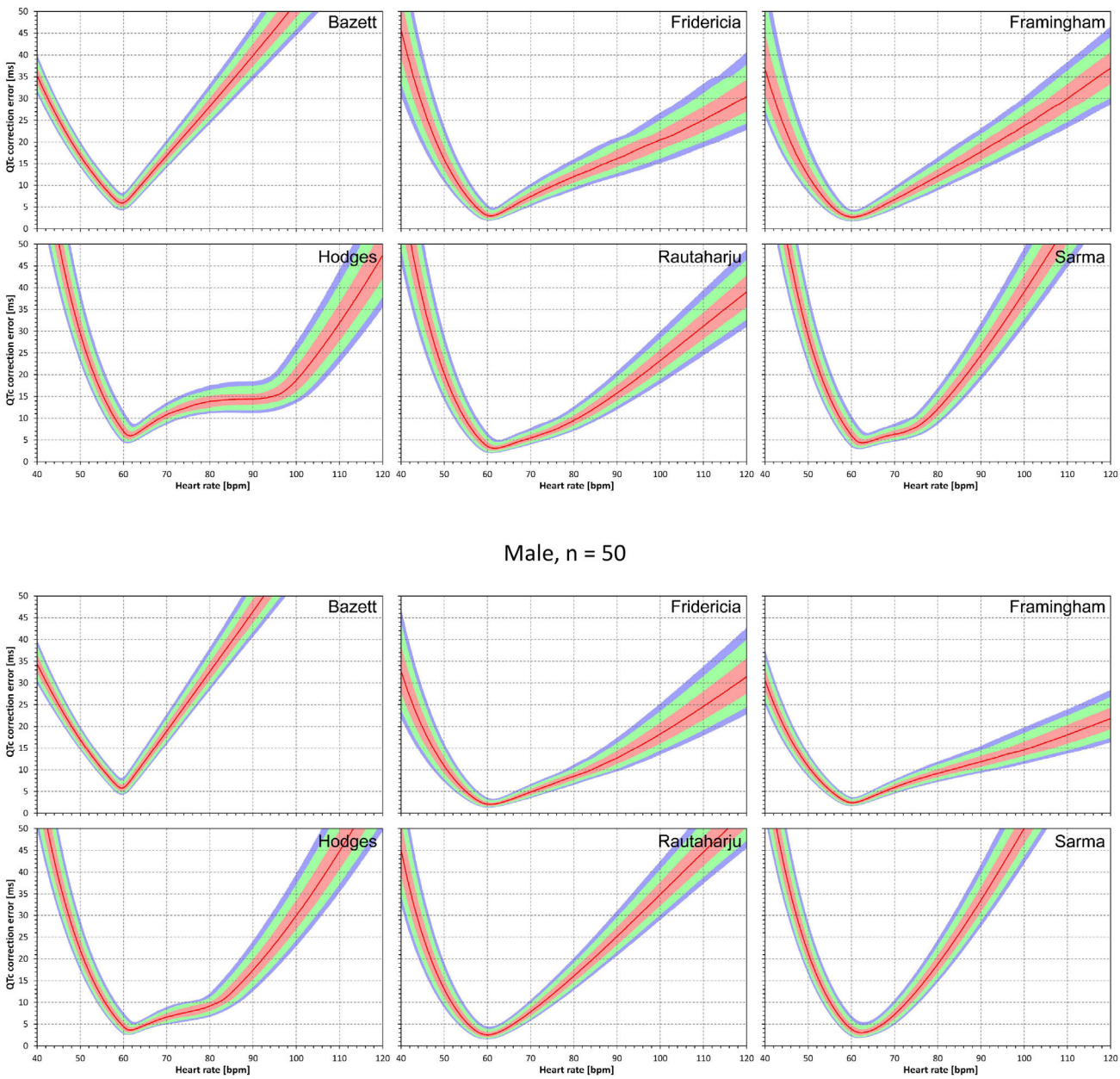

FIGURE 4 | The results of absolute QTc errors due to heart rate instability shown for *N* = 50 female and male subjects. The layout of the figure is the same as in **Figure 3**.

placebo leads to ΔΔQTc values (Guidance to industry, 2005). This means that errors reported by our experiments have somewhat underestimated the errors that might be expected in actual studies. Hence, the greater the mean on-drug heart rate change the more caution is needed when using fixed heart rate corrections.

The method for selecting the characteristics of an individual modeling experiment needs to be discussed. Evaluation of drug-induced QTc changes is not driven by mean changes over an investigated population but by upper confidence intervals, that is, either the upper single-sided 95% confidence intervals of QTc changes in individual study time-points controlled for both baseline and placebo in the so-called intersection union test (Guidance to industry, 2005), or by the same upper confidence interval of QTc change derived from a pharmacokinetic-pharmacodynamic regression model (Garnett et al., 2008). For this reason, we used the exclusion of the low and high 10% of the errors in individual subjects of each

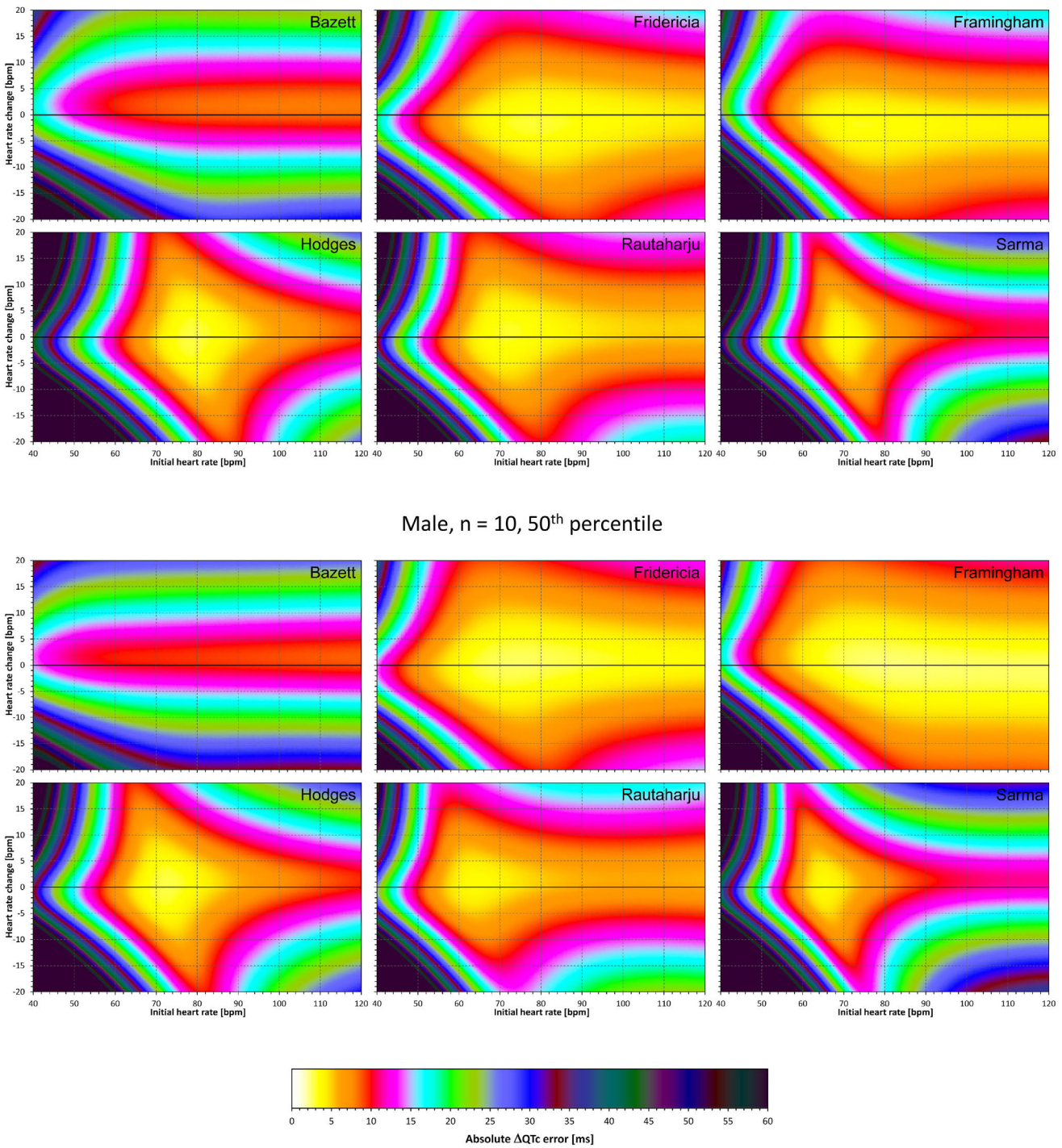

FIGURE 5 | For each of the fixed correction formulae and for each combination of initial heart rate (between 40 and 120 bpm) and each heart rate change (between –20 to +20 bpm), the figure shows the absolute ΔQTc errors due to drug-induced heart rate changes (i.e., the characteristics of the corresponding statistical modeling experiments – see the text for details). The figure shows the median values of the characteristics of 10,000 experiment repetitions with N = 10 female subjects (top part of the figure) and with N = 10 male subjects (bottom part of the figure). The values are color coded according to the scale shown at the bottom of the figure.

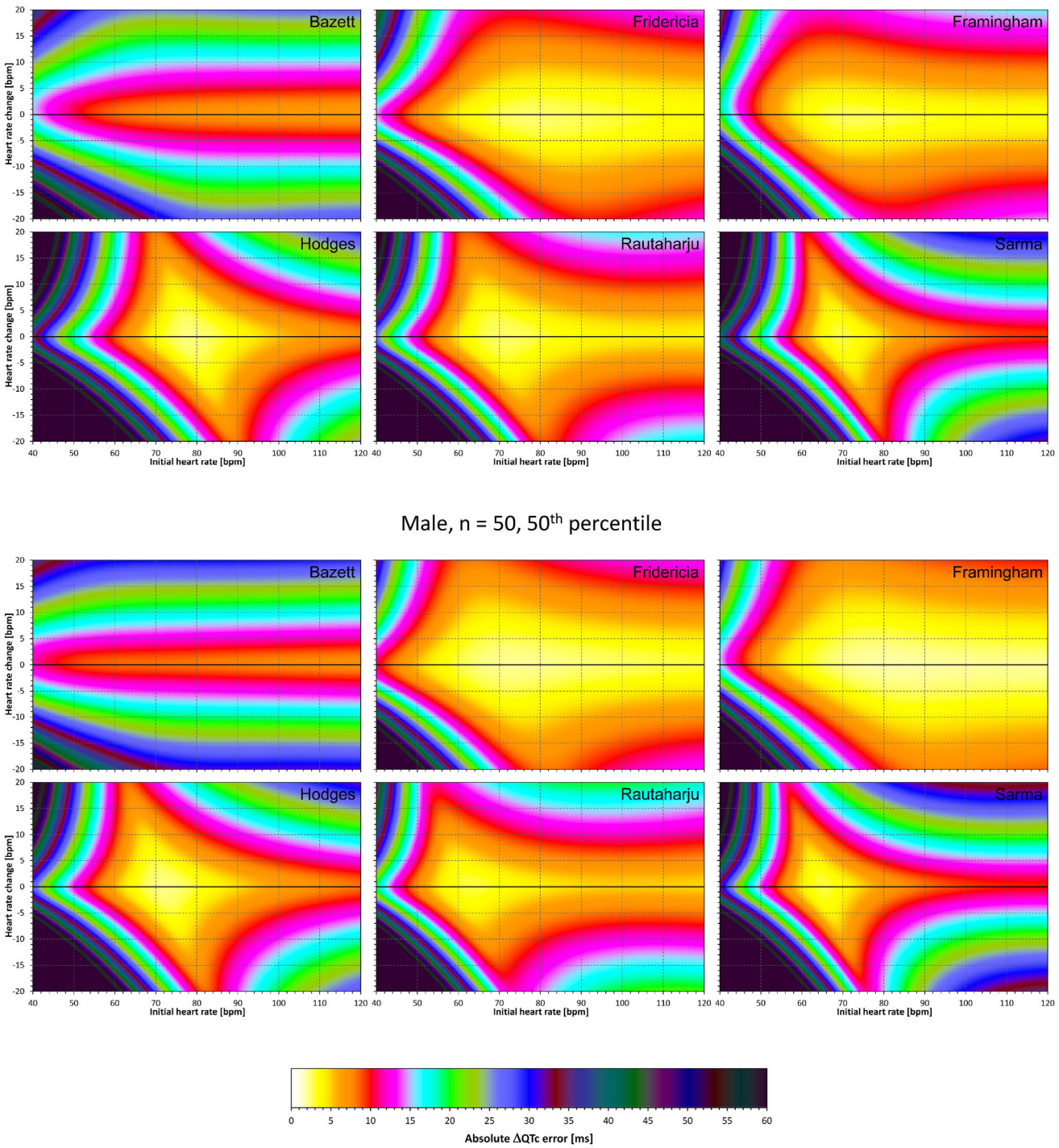

FIGURE 6 | The same results as in **Figure 5** but shown here for experiments with *N* = 50 female subjects (top part of the figure) and with *N* = 50 male subjects (bottom part of the figure). See **Figure 5** for further details.

experiment and considered the maximum absolute error of the modeled data after this exclusion. Hence, this approach approximated the extent in which the inaccurate corrections might influence the interpretation of study results. In each case (i.e., in each fi and δ combination), the distribution of the errors was mostly positioned on one side of the

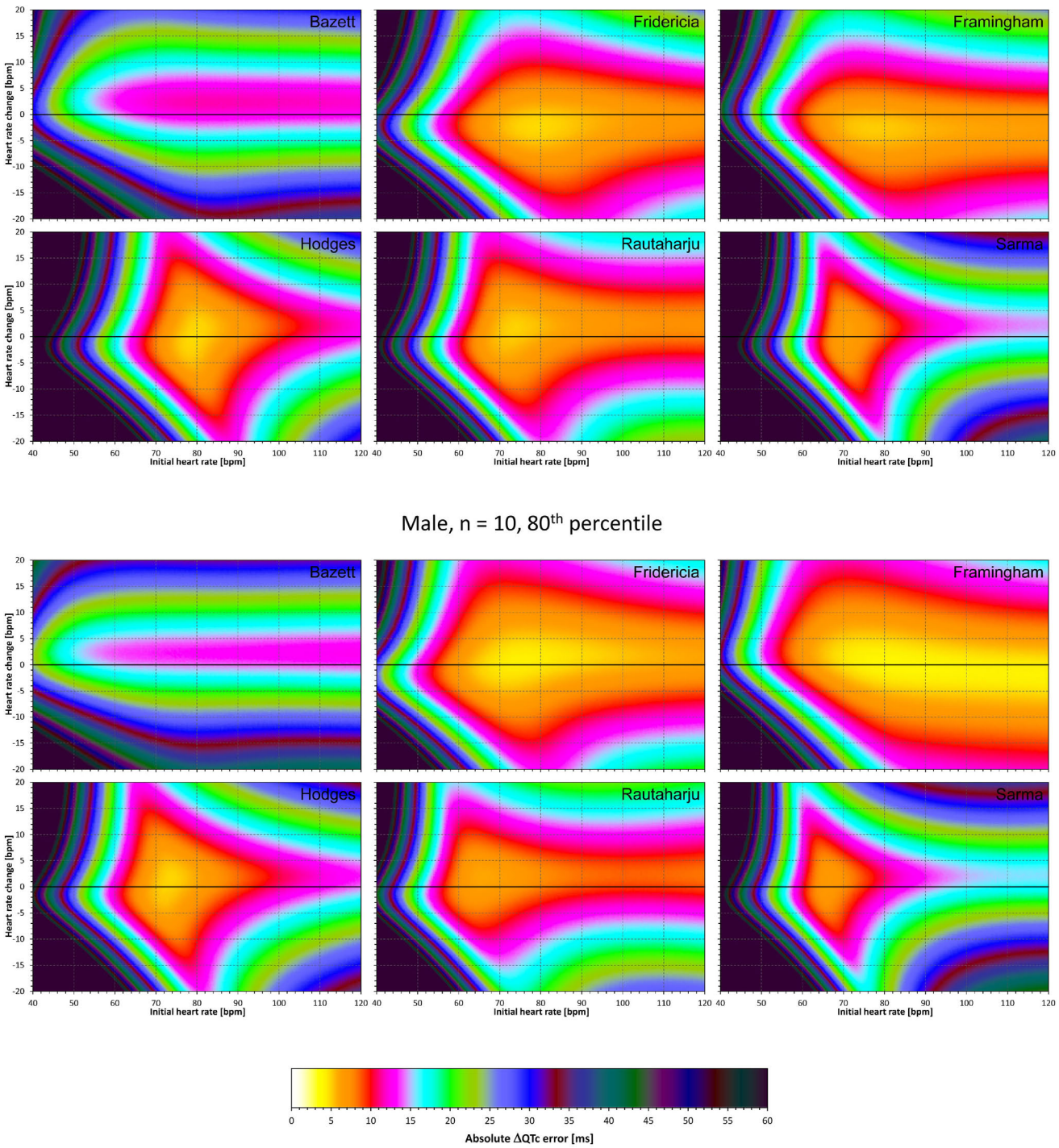

FIGURE 7 | The same results as in **Figure 5** but showing 80th percentile of the characteristics of 10,000 experiment repetitions with *N* = 10 female subjects (top part of the figure) and with *N* = 10 male subjects (bottom part of the figure). See **Figure 5** for further details.

zero line. Therefore, the exclusion of 10% of results on each end and taking the maximum absolute value after the exclusion modeled single-sided 90th percentile of the absolute errors. This reflected the practice of thorough QT study evaluations. (Note that all experiments were set-up in such a way that with accurate subject-specific corrections of heart rate

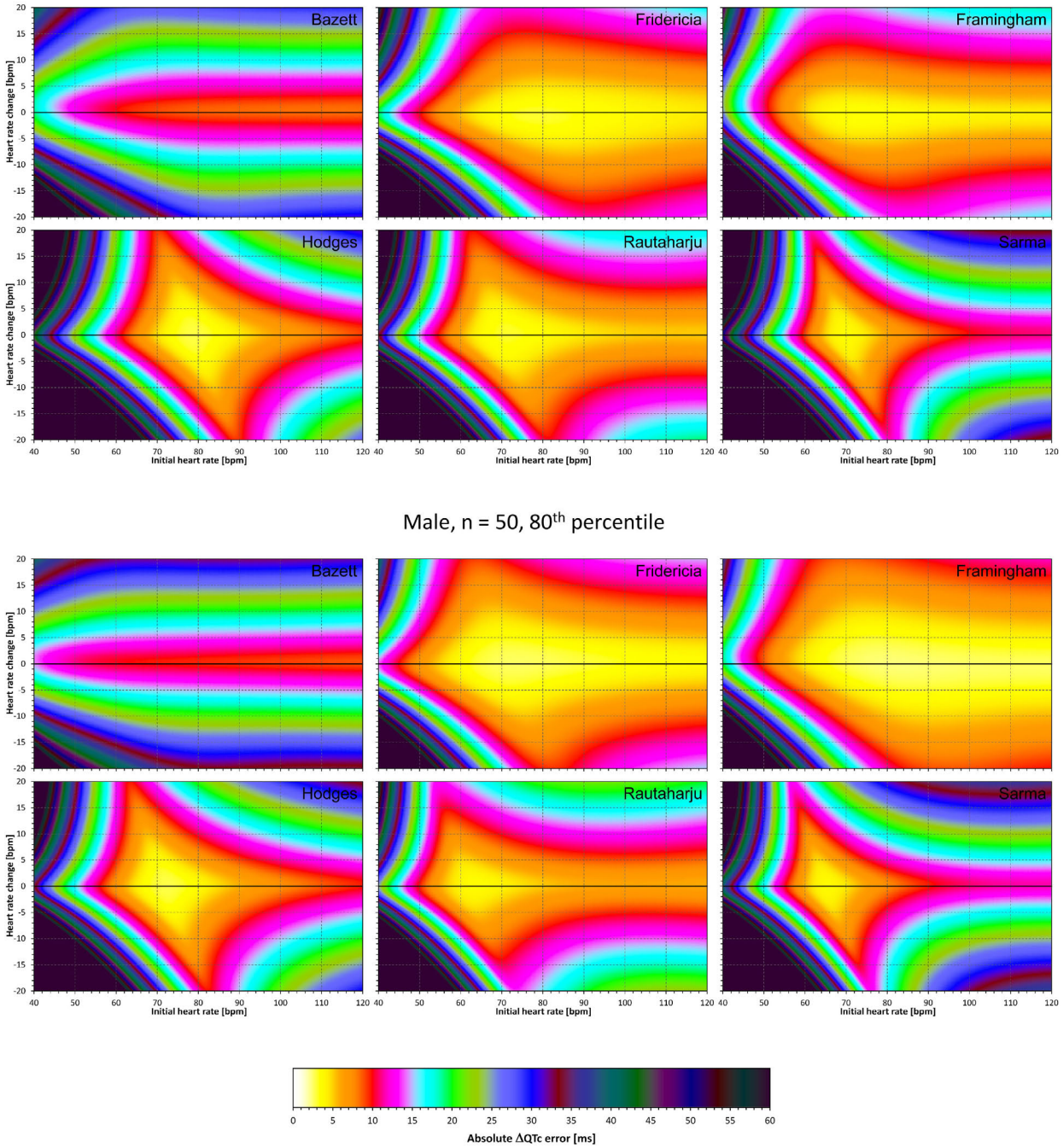

FIGURE 8 | The same results as in **Figure 6** but showing 80th percentile of the characteristics of 10,000 experiment repetitions with *N* = 50 female subjects (top part of the figure) and with *N* = 50 male subjects (bottom part of the figure). See **Figure 5** for further details.

and QT/RR hysteresis influence, all the characteristics would be equal to zero).

The modeling experiments investigated the differences between the fixed corrections and subject-specific QT/heart-rate curvilinear regressions. In other words, the experiments investigated the effects of fixed corrections in comparison of what can be optimally obtained from studying individual QT/heart-rate relationship and QT/RR hysteresis. Nevertheless, the QT and heart rate data that we used to derive the subject-specific regressions showed additional intra-subject QTc variability around 5 ms. This needs to be considered when interpreting the results of the experiments. The errors

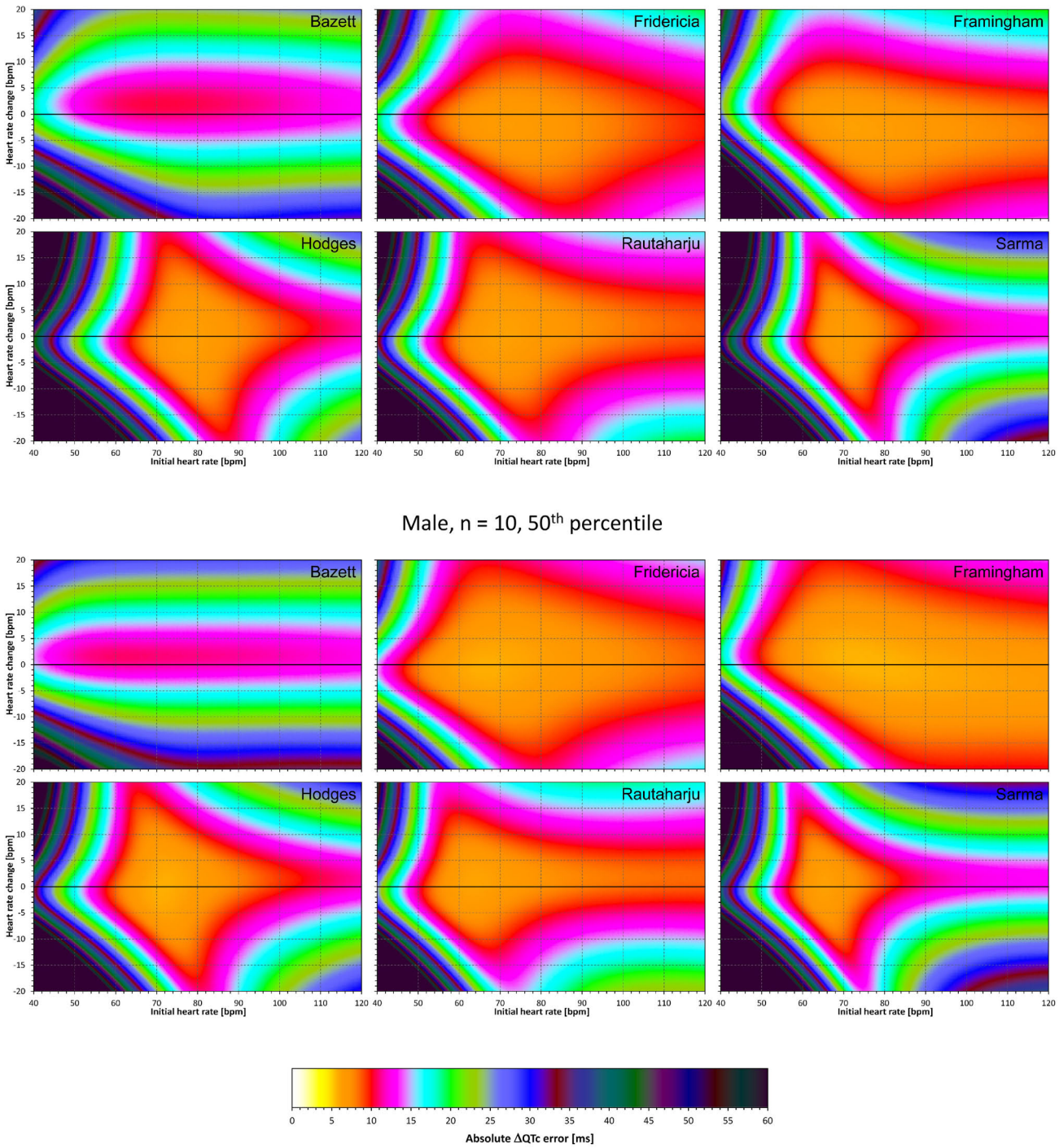

FIGURE 9 | For each of the fixed correction formulae and for each combination of initial heart rate (between 40 and 120 bpm) and each heart rate change (between –20 to +20 bpm), the figure shows the absolute ΔQTc errors due to the combination of drug-induced heart rate changes and omission of QT/RR hysteresis correction (i.e., the characteristics of the corresponding statistical modeling experiments – see the text for details). The figure shows the median values of the characteristics of 10,000 experiment repetitions with *N* = 10 female subjects (top part of the figure) and with *N* = 10 male subjects (bottom part of the figure). The values are color coded according to the scale shown at the bottom of the figure.

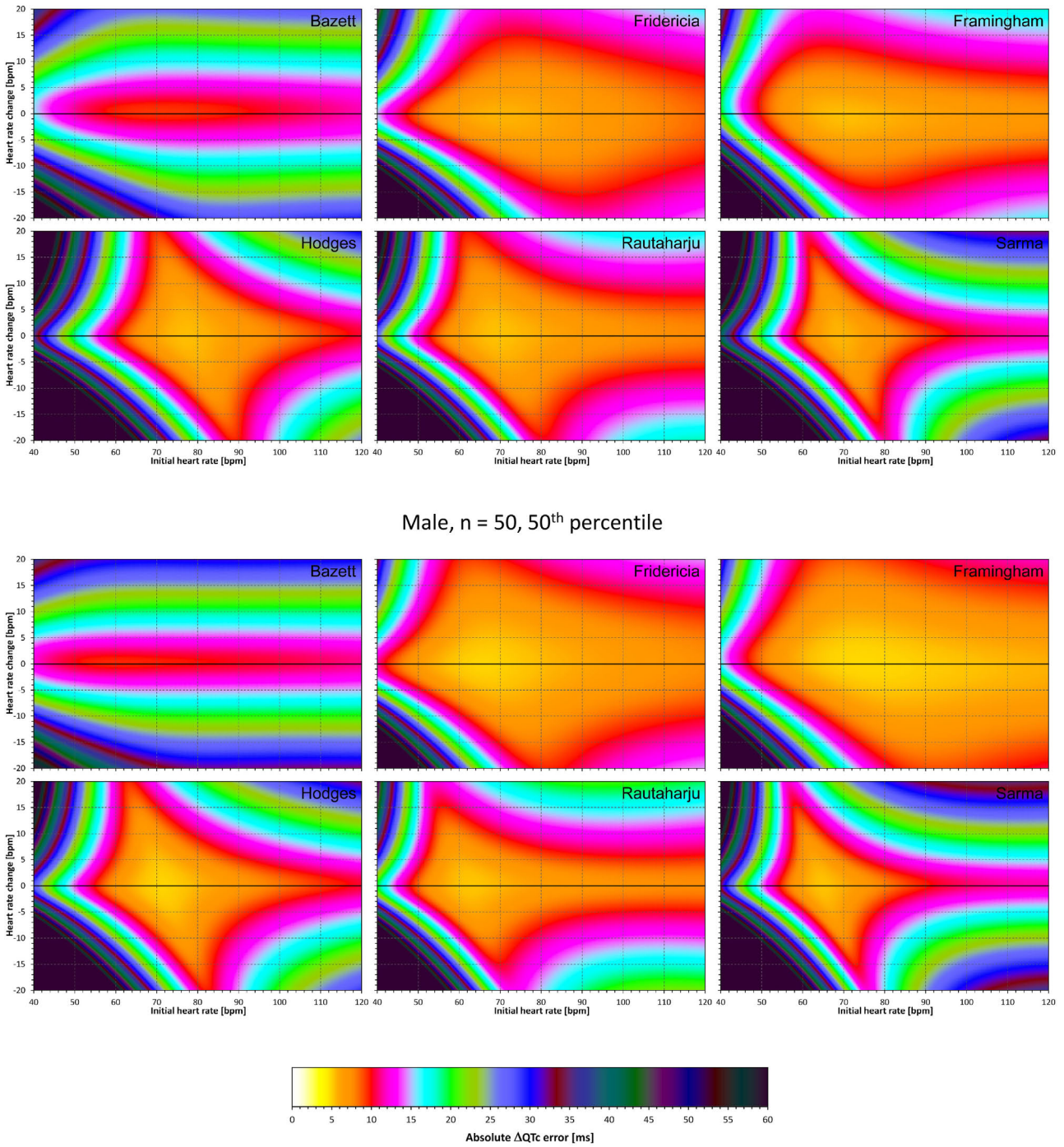

FIGURE 10 | The same results as in **Figure 9** but shown here for experiments with *N* = 50 female subjects (top part of the figure) and with *N* = 50 male subjects (bottom part of the figure). See **Figure 9** for further details.

of QTc investigations based on fixed corrections might have been underestimated.

The differences between the medians and upper 80th percentiles of the experimental results were surprisingly small suggesting that the distribution of the experimental results was rather narrow. It thus seems reasonable to use the 80th percentile data in power calculation projections of our results. In other words, while the

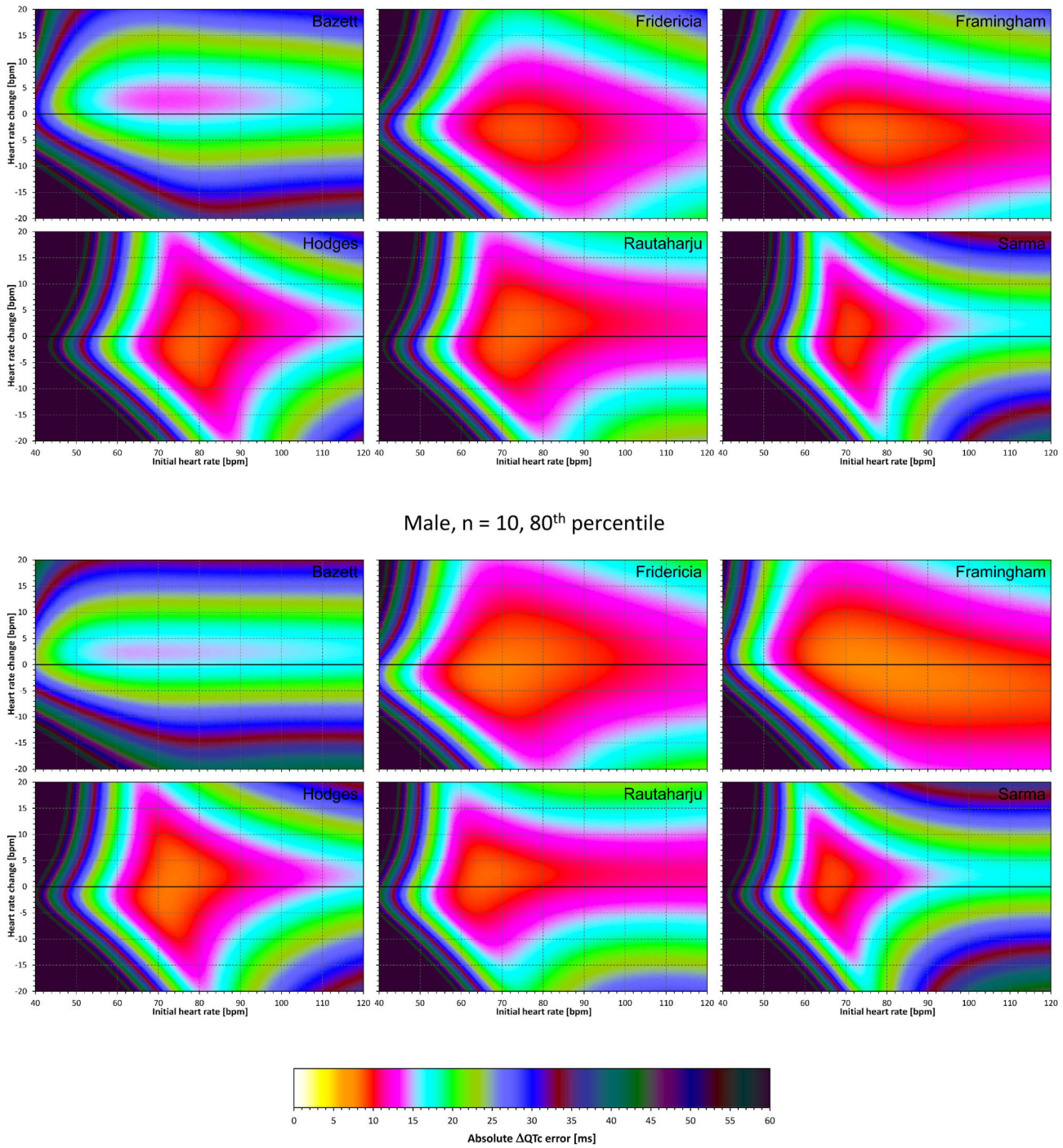

FIGURE 11 | The same results as in **Figure 9** but showing 80th percentile of the characteristics of 10,000 experiment repetitions with *N* = 10 female subjects (top part of the figure) and with *N* = 10 male subjects (bottom part of the figure). See **Figure 9** for further details.

presentation of median results shows the errors that might be expected in "averaged" study situations, the 80th percentile shows the errors that should be considered when designing a new clinical pharmacology study (the percentile reflects the practice of 80% probability of type II error elimination).

It has been previously suggested that physiologically independent processes determine how much QT interval

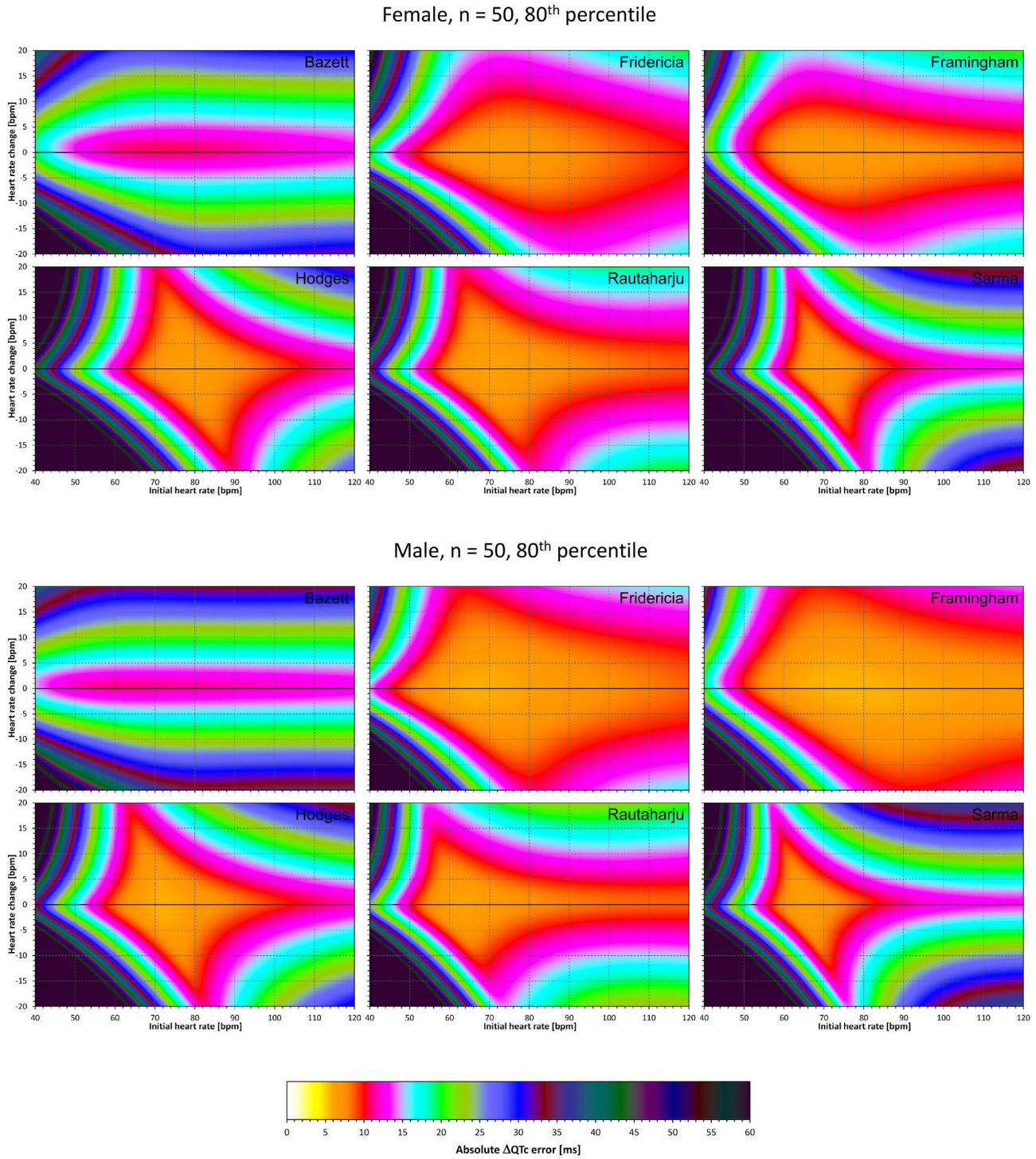

FIGURE 12 | The same results as in **Figure 10** but showing 80th percentile of the characteristics of 10,000 experiment repetitions with *N* = 50 female subjects (top part of the figure) and with *N* = 50 male subjects (bottom part of the figure). See **Figure 9** for further details.

changes in response to the underlying heart rate, and how quickly QT interval adapts to heart rate changes (Malik et al., 2008b). This is the distinction between QT/heart-rate adaptations and QT/RR hysteresis. Surprisingly, whilst the correction of the QT interval for heart rate (i.e., for QT/heart-rate adaptation) is universally accepted, the correction for QT/RR hysteresis is frequently omitted (Malik et al., 2016). At the same time, our results show that neglecting the effects of QT/RR hysteresis

TABLE 2 | The table shows the average values of modeled absolute ΔQTc errors (that is the experiment characteristics obtained with the sex heart rate correction formulae as shown in more detail in **Figures 5–12**).

		0 – ±5 bpm	±5 – ±10 bpm	±10 – ±15 bpm	0 – ±5 bpm	±5 – ±10 bpm	±10 – ±15 bpm	0 – ±5 bpm	±5 – ±10 bpm	±10 – ±15 bpm
N	**Percentile**	**Bazett**			**Fridericia**			**Framingham**		
Effect of QT/RR hysteresis not included										
10	50	11.24	16.21	22.55	4.89	7.41	11.53	5.26	8.32	13.13
50		10.35	16.06	22.37	4.07	7.12	11.18	4.28	7.15	11.48
10	80	15.81	21.14	28.15	8.51	11.87	17.11	8.86	12.99	19.37
50		12.07	18.06	24.66	5.24	8.93	14.18	5.38	8.73	13.70
Effect of QT/RR hysteresis included										
10	50	12.46	17.14	23.3	7.29	9.22	12.52	7.44	9.94	14.33
50		11.48	16.95	23.12	6.33	8.80	12.77	6.35	8.66	12.60
10	80	17.08	22.13	28.96	11.09	13.87	18.64	11.17	14.74	20.72
50		13.23	18.99	25.44	7.59	10.69	15.50	7.51	10.29	14.87
N	**Percentile**	**Hodges**			**Rautaharju**			**Sarma**		
Effect of QT/RR hysteresis not included										
10	50	8.67	12.88	19.53	6.02	9.03	13.94	8.81	13.12	20.17
50		7.75	13.28	21.06	5.18	9.13	15.10	7.86	13.58	21.87
10	80	13.87	18.95	27.41	10.20	14.05	20.65	14.20	19.30	28.08
50		9.51	15.77	24.58	6.55	11.19	18.13	9.67	16.12	25.44
Effect of QT/RR hysteresis included										
10	50	10.47	14.24	20.54	8.03	10.50	15.00	10.45	14.33	21.05
50		9.43	14.54	22.01	7.08	10.49	16.09	9.42	14.72	22.72
10	80	15.78	20.43	28.53	12.28	15.61	21.79	15.86	20.56	29.02
50		11.26	17.10	25.59	8.49	12.58	19.16	11.26	17.30	26.33

*Values are in milliseconds. For each formula, three columns are shown, these show the ΔQTc errors averaged over the area of initial heart rate 50 to 80 bpm and heart rate changes between −5 and +5 bpm (the left column of each formula), between −10 and −5 bpm pooled together with +5 to +10 bpm (middle column), and between −15 to −10 bpm pooled together with +10 to +15 bpm (right column). The averages are repeated for the experiments without QT/RR hysteresis influence (i.e., those shown in **Figures 3–8** – top parts of the table) and for experiment with QT/RR hysteresis influence (i.e., those shown in **Figures 9–12** – bottom parts of the table). The results are shown for the experiments modeling N = 10 and N = 50 study subjects and for each of these, both the averages of median (50th percentile) and of 80th percentile of the ΔQTc errors are shown. The cells with ΔQTc above 10 ms are shown in red, those with ΔQTc between 8 and 10 ms are shown in yellow.*

decreases the accuracy of QTc assessment noticeably. It is also frequently, but falsely believed that QT/RR hysteresis needs to be considered only in cases of abrupt and substantial heart rate fluctuations, e.g., when heart rate change occurs immediately after the drug administration. Whilst in such situations, the necessity of correcting for QT/RR hysteresis is obvious (Malik et al., 2009), the need for it is not restricted to such cases. As we have previously shown, stable heart rate history of QT measurements is rare in clinical studies and thus, correction for QT/RR hysteresis should always be considered. In usual situations, there is only little difference between subject-specific corrections of QT/RR hysteresis (Malik et al., 2008b) and universal hysteresis correction (Malik et al., 2016). The universal hysteresis correction can easily be combined with fixed heart rate correction thus replicating the improvement of data accuracy demonstrated in our experiments. It should also be noted that the distribution of immediate heart rate instability (bottom panel of **Figure 1**) contained rather small values. Still, the modeling experiments show that even such small heart rate instabilities can have a clearly noticeable effect on the QTc data accuracy.

As already explained, absolute differences between correction formulae are potentially misleading when studying drug-induced changes. The ΔQTc values of baseline to on-treatment differences are important. The absolute differences between corrections become only of interest when relating the QTc values to an absolute threshold (e.g., 500 ms) (Fenichel et al., 2004).

Not surprisingly, our experiments with $N = 10$ subjects showed larger errors compared to those with $N = 50$. Indeed, this corresponds to the known experience that in larger studies, the increased number of QTc measurements helps reducing the confidence intervals of the mean QTc changes. Importantly, images in **Figures 9**, **11** show appreciable level of correction errors even in cases with heart rate change δ equal or close to zero. This is because in these cases, the spontaneous heart rate fluctuations are combined with the immediate heart rate instability. This again underlines the need for QT/RR hysteresis correction, particularly in smaller clinical studies (Malik et al., 2018).

We are not aware of other published studies with which we could compare the results of our modeling experiments. Nevertheless, consistent with other reports (Rautaharju et al., 1990), we found the Bazett formula to be the least accurate of all those tested. The experiments with the Fridericia formula

confirmed the previous observations that on average, it is more accurate in males than in females (Malik et al., 2016).

Our results have main prospective value in providing an informed guidance for future investigations including the level on errors that need to be considered in power sample calculations (Zhang and Machado, 2008). Equally importantly, the modeling results identify circumstances in which the fixed corrections become potentially so problematic that it would be difficult to accept them in studies supporting regulatory submissions of new pharmaceuticals or of new treatment applications of existing drugs (Garnett et al., 2012).

Limitations

Limitations of our statistical modeling also need to be considered. We have selected a battery of only 6 formulae while many others have also been proposed (Malik, 2002). Nevertheless, we selected these formulae to represent a wide spectrum of mathematical approaches. Also, since it has also been shown that the subject-specific slopes, curvatures, and central values of QT/heart-rate profiles are highly individual (Batchvarov et al., 2002; Malik et al., 2013), it is doubtful that any other fixed formula would clearly outperform Fridericia and Framingham corrections. The extreme settings of our modeling experiments were obviously not realistic. The broad ranges of the fi and δ coefficients in our experiments were thus used for illustrative purposes. The regions of baseline heart rate and heart rate changes summarized in **Table 2** are more realistic and have indeed been used when interpreting the results of the experiments. The source data we used were derived from recordings of healthy subjects. We cannot comment on the situations in patients in whom the QT/heart-rate profiles are influenced by pathological circumstances. Nevertheless, such circumstances would likely increase the individuality of the profiles and thus, if anything, further decrease the applicability of fixed correction formulae. Finally, the statistical modeling experiments were designed to correspond to cross-over (or partially cross-over) studies in which each subject is also recorded on placebo and serves as her/his own control. Parallel studies that compare different on-treatment and on-placebo populations might require different modeling approach.

Practical Implications

Despite these limitations, we conclude that when investigating drug-induced QTc changes in the presence of drug-related heart rate changes in reasonably sized studies of healthy volunteers, the Fridericia formula might be appropriate if the heart rate change does not exceed ±10 bpm. In smaller studies, such the typical first-in-man investigations, the impact of using fixed heart rate correction as well as the impact of not accounting for QT/RR hysteresis is greater than for larger trials. The same limits of heart rate change appear applicable to Framingham formula while other fixed corrections should be avoided unless independently justified. When the drug-induced heart rate changes exceed ±10 bpm, the use of fixed heart rate QTc corrections becomes problematic and alternative methods such as subject-specific heart rate corrections might need to be considered.

DATA AVAILABILITY

All datasets generated for this study are included in the manuscript.

AUTHOR CONTRIBUTIONS

All authors listed have made a substantial, direct and intellectual contribution to the work, and approved it for publication.

FUNDING

The funding was supported in part by the British Heart Foundation New Horizons Grant NH/16/2/32499.

REFERENCES

Batchvarov, V. N., Ghuran, A., Smetana, P., Hnatkova, K., Harries, M., Dilaveris, P., et al. (2002). QT-RR relationship in healthy subjects exhibits substantial intersubject variability and high intrasubject stability. *Am. J. Physiol. Heart Circ. Physiol.* 282, H2356–H2363.

Bazett, J. C. (1920). An analysis of time relations of electrocardiograms. *Heart* 7, 353–367.

Darpo, B., Garnett, C., Benson, C. T., Keirns, J., Leishman, D., Malik, M., et al. (2014). Cardiac safety research consortium: can the thorough QT/QTc study be replaced by early QT assessment in routine clinical pharmacology studies? Scientific update and a research proposal for a path forward. *Am. Heart J.* 168, 262–272. doi: 10.1016/j.ahj.2014.06.003

Fenichel, R. R., Malik, M., Antzelevitch, C., Sanguinetti, M., Roden, D. M., Priori, S. G., et al. (2004). Drug-induced torsades de pointes and implications for drug development. *J. Cardiovasc. Electrophysiol.* 15, 475–495.

Franz, M. R., Swerdlow, C. D., Liem, L. B., and Schaefer, J. (1988). Cycle length dependence of human action potential duration in vivo. effects of single extrastimuli, sudden sustained rate acceleration and deceleration, and different steady-state frequencies. *J. Clin. Invest.* 82, 972–979. doi: 10.1172/jci113706

Fridericia, L. S. (1920). Die systolendauer im elekrokardiogramm bei normalen menschen und bei herzkranken. *Acta Med. Scand.* 53, 469–486. doi: 10.1111/j.0954-6820.1920.tb18266.x

Garnett, C. E., Beasley, N., Bhattaram, V. A., Jadhav, P. R., Madabushi, R., Stockbridge, N., et al. (2008). Concentration-QT relationships play a key role in the evaluation of proarrhythmic risk during regulatory review. *J. Clin. Pharmacol.* 48, 13–18. doi: 10.1177/0091270007307881

Garnett, C. E., Zhu, H., Malik, M., Fossa, A. A., Zhang, J., Badilini, F., et al. (2012). Methodologies to characterize the QT/corrected QT interval in the presence of drug-induced heart rate changes or other autonomic effects. *Am. Heart. J.* 2012, 912–930. doi: 10.1016/j.ahj.2012.02.023

Gravel, H., Jacquemet, V., Dahdah, N., and Curnier, D. (2018). Clinical applications of QT/RR hysteresis assessment: a systematic review. *Ann. Noninvasive. Electrocardiol.* 23:e12514. doi: 10.1111/anec.12514

Guidance to industry (2005). E14 Clinical evaluation of QT/QTc interval prolongation and proarrhythmic potential for non-antiarrhythmic drugs. *Fed. Regist.* 70, 61134–61135.

Hodges, M., Salerno, D., and Erlien, D. (1983). Bazett's QT correction reviewed: evidence that a linear QT correction for heart rate is better. *J. Am. Coll. Cardiol.* 1983:694.

Linde, C., Bongiorni, M. G., Birgersdotter-Green, U., Curtis, A. B., Deisenhofer, I., Furokawa, T., et al. (2018). ESC scientific document group. Sex differences in cardiac arrhythmia: a consensus document of the european heart rhythm association, endorsed by the heart rhythm society and asia pacific heart rhythm society. *Europace* 20, 1565–1565ao. doi: 10.1093/europace/euy067

Malik, M. (2002). The imprecision in heart rate correction may lead to artificial observations of drug induced QT interval changes. *Pacing Clin. Electrophysiol.* 25, 209–216. doi: 10.1046/j.1460-9592.2002.00209.x

Malik, M. (2018). Methods of subject-specific heart rate corrections. *J. Clin. Pharm.* 58, 1020–1024. doi: 10.1002/jcph.1269

Malik, M., Andreas, J. O., Hnatkova, K., Hoeckendorff, J., Cawello, W., Middle, M., et al. (2008a). Thorough QT/QTc study in patients with advanced Parkinson's disease: cardiac safety of rotigotine. *Clin. Pharmacol. Ther.* 84, 595–603. doi: 10.1038/clpt.2008.143

Malik, M., Hnatkova, K., Novotny, T., and Schmidt, G. (2008b). Subject-specific profiles of QT/RR hysteresis. *Am. J. Physiol. Heart Circ. Physiol.* 295, H2356–H2363. doi: 10.1152/ajpheart.00625.2008

Malik, M., Färbom, P., Batchvarov, V., Hnatkova, K., and Camm, A. J. (2002). Relation between QT and RR intervals is highly individual among healthy subjects: implications for heart rate correction of the QT interval. *Heart* 87, 220–228. doi: 10.1136/heart.87.3.220

Malik, M., Garnett, C., Hnatkova, K., Johannesen, L., Vicente, J., and Stockbridge, N. (2018). Importance of QT/RR hysteresis correction in studies of drug-induced QTc interval changes. *J. Pharmacokinet. Pharmacodyn.* 2018, 491–503. doi: 10.1007/s10928-018-9587-8

Malik, M., Hnatkova, K., Kowalski, D., Keirns, J. J., and van Gelderen, E. M. (2013). QT/RR curvatures in healthy subjects: sex differences and covariates. *Am. J. Physiol. Heart Circ. Physiol.* 305, H1798–H1806. doi: 10.1152/ajpheart.00577.2013

Malik, M., Hnatkova, K., Schmidt, A., and Smetana, P. (2009). Correction for QT/RR hysteresis in the assessment of drug-induced QTc changes - cardiac safety of gadobutrol. *Ann. Noninvasive. Electrocardiol.* 2009, 242–250. doi: 10.1111/j.1542-474X.2009.00304.x

Malik, M., Johannesen, L., Hnatkova, K., and Stockbridge, N. (2016). Universal correction for QT/RR hysteresis. *Drug Saf.* 39, 577–588. doi: 10.1007/s40264-016-0406-0

Malik, M., van Gelderen, E. M., Lee, J. H., Kowalski, D. L., Yen, M., Goldwater, R., et al. (2012). Proarrhythmic safety of repeat doses of mirabegron in healthy subjects: a randomized, double-blind, placebo-, and active-controlled thorough QT study. *Clin. Pharm. Therap.* 92, 696–706. doi: 10.1038/clpt.2012.181

Matsumoto, M., and Nishimura, T. (1998). Mersenne twister: a 623-dimensionally equidistributed uniform pseudo-random number generator. *ACM Trans. Model Comp. Simul.* 1998, 3–30. doi: 10.1145/272991.272995

Rautaharju, P. M., Warren, J. W., and Calhoun, H. P. (1990). Estimation of QT prolongation. A persistent, avoidable error in computer electrocardiography. *J. Elecrocardiol.* 23(Suppl.), 111–117.

Sagie, A., Larson, M. G., Goldberg, R. J., Bengtson, J. R., and Levy, D. (1992). An improved method for adjusting the QT interval for heart rate (the framingham study). *Am. J. Cardiol.* 70, 797–801. doi: 10.1016/0002-9149(92)90562-d

Sarma, J. S. M., Sarma, R. J., Bilitch, M., Katz, D., and Song, S. L. (1984). An exponential formula for heart rate dependence of QT interval during exercise and pacing in humans: reevaluation of Bazett's formula. *Am. J. Cardiol.* 54, 103–108. doi: 10.1016/0002-9149(84)90312-6

Vicente, J., Stockbridge, N., and Strauss, D. G. (2016). Evolving regulatory paradigm for proarrhythmic risk assessment for new drugs. *J. Electrocardiol.* 49, 837–842. doi: 10.1016/j.jelectrocard.2016.07.017

Vicente, J., Zusterzeel, R., Johannesen, L., Mason, J., Sager, P., Patel, V., et al. (2018). Mechanistic model-informed proarrhythmic risk assessment of drugs: review of the "CiPA" initiative and design of a prospective clinical validation study. *Clin. Pharmacol. Ther.* 2018, 54–66. doi: 10.1002/cpt.896

Zhang, J., Chen, H., Tsong, Y., and Stockbridge, N. (2015). Lessons learned from hundreds of thorough QT studies. *Ther. Innov. Regul. Sci.* 49, 392–397. doi: 10.1177/2168479014563549

Zhang, J., and Machado, S. G. (2008). Statistical issues including design and sample size calculation in thorough QT/QTc studies. *J. Biopharm. Stat.* 18, 451–467. doi: 10.1080/10543400802020938

Disclaimer: This article reflects the views of the authors and should not be construed to represent the U.S. FDA's views or policies.

Conflict of Interest Statement: The authors declare that the research was conducted in the absence of any commercial or financial relationships that could be construed as a potential conflict of interest.

frontiers in Physiology

ORIGINAL RESEARCH
published: 26 June 2019
doi: 10.3389/fphys.2019.00809

Renyi Distribution Entropy Analysis of Short-Term Heart Rate Variability Signals and Its Application in Coronary Artery Disease Detection

*Manhong Shi[1,2], Chaoying Zhan[1], Hongxin He[1], Yanwen Jin[1], Rongrong Wu[1], Yan Sun[3] and Bairong Shen[3]**

[1] Center for Systems Biology, Soochow University, Suzhou, China, [2] College of Information and Network Engineering, Anhui Science and Technology University, Fengyang, China, [3] Institutes for Systems Genetics, West China Hospital, Sichuan University, Chengdu, China

Coronary artery disease (CAD) is a life-threatening condition that, unless treated at an early stage, can lead to congestive heart failure, ischemic heart disease, and myocardial infarction. Early detection of diagnostic features underlying electrocardiography signals is crucial for the identification and treatment of CAD. In the present work, we proposed novel entropy called Renyi Distribution Entropy (RdisEn) for the analysis of short-term heart rate variability (HRV) signals and the detection of CAD. Our simulation experiment with synthetic, physiological, and pathological signals demonstrated that RdisEn could distinguish effectively among different subject groups. Compared to the values of sample entropy or approximation entropy, the RdisEn value was less affected by the parameter choice, and it remained stable even in short-term HRV. We have developed a combined CAD detection scheme with RdisEn and wavelet packet decomposition (WPD): (1) Normal and CAD HRV beats obtained were divided into two equal parts. (2) Feature acquisition: RdisEn and WPD-based statistical features were calculated from one part of HRV beats, and student's *t*-test was performed to select clinically significant features. (3) Classification: selected features were computed from the remaining part of HRV beats and fed into K-nearest neighbor and support vector machine, to separate CAD from normal subjects. The proposed scheme automatically detected CAD with 97.5% accuracy, 100% sensitivity and 95% specificity and performed better than most of the existing schemes.

Keywords: coronary artery disease, heart rate variability, renyi distribution entropy, wavelet packet decomposition, classifier

OPEN ACCESS

Edited by:
Marek Malik,
Imperial College London,
United Kingdom

Reviewed by:
Hamido Fujita,
Iwate Prefectural University, Japan
David Cornforth,
The University of Newcastle, Australia

***Correspondence:**
Bairong Shen
bairong.shen@scu.edu.cn

Specialty section:
This article was submitted to Cardiac Electrophysiology, a section of the journal Frontiers in Physiology

Received: *20 March 2019*
Accepted: *07 June 2019*
Published: *26 June 2019*

Citation:
Shi M, Zhan C, He H, Jin Y, Wu R, Sun Y and Shen B (2019) Renyi Distribution Entropy Analysis of Short-Term Heart Rate Variability Signals and Its Application in Coronary Artery Disease Detection. Front. Physiol. 10:809. doi: 10.3389/fphys.2019.00809

INTRODUCTION

Plaque accumulation (fatty and cholesterol substances) in the inner wall of the coronary arteries causes a blockage in the coronary circulation and the reduction of blood supply to the heart muscles, leading to coronary artery diseases (CAD) (Steinberg and Gotto, 1999). Unless treated early, CAD can result in congestive heart failure, ischemic heart disease, myocardial infarction, ischemia, arrhythmias, angina and sudden death (Grech, 2011). In 2012, 7.4 million CAD-related deaths were reported, which accounted for 10% of total fatalities among female population and 16% among male population that year, respectively (World Health Organization, 2015). By 2030, an estimated 37%

increase in CAD-related death is expected in emerging nations (Acharya et al., 2017c). Early CAD detection is therefore the key to prevent further heart function damage and save lives.

The exercise stress test (EST), which monitors various heart status features, is often used for CAD diagnosis. However, not all CAD subjects can achieve the expected heart rate, and many patients may suffer cardiac arrest during EST (Román et al., 1998). Alternatively, measurement of resting ECG signals can be applied as a non-invasive and preferred method for CAD diagnosis. Since no obvious change in the resting ECG signals is detected among ∼70% of CAD subjects, the manual CAD diagnosis is time-consuming and ineffective (Antanavicius et al., 2008). In recent years, computer-aided diagnostic technologies (CADT) for CAD detection have garnered increasing attentions for their ease of operation without the excessive reliance on the personal experience of a doctor, as well as their cost-effectiveness.

Heart rate variability (HRV) extracted from the ECG depicts the variation in time interval between adjacent heartbeats and is vital for autonomic modulation of the heart. CADT-based HRV analyses have been proposed in recent years for CAD diagnosis. Reduced values in the frequency-domain feature of HRV signals is closely related to the severity of CAD (Hayano et al., 1990). For instance, compared to normal subjects, CAD patients exhibit lower circadian rhythms (Huikuri et al., 1994). Power spectral analysis also reveals that the low/high frequency ratio of HRV signals is significantly lower in CAD-affected subjects with panic disorder than in normal subjects (Lavoie et al., 2004). Moreover, CAD patients exhibit lower values in the time domain features of HRV signals, such as NN50 (number of adjacent NNs, which are greater than 50 ms) and pNN50 (NN50 divided by total number of NNs, which is expressed as a percentage), than normal subjects (Acharya et al., 2014). Due to its non-linear and non-stationary nature, the non-linear methods perform better at decoding the invisible complexities and extracting valuable information from HRV signals, compared to the frequency- and time-domain analyses of HRV signals. Applying non-linear methods can also minimize variation and background noise problems that are often associated with the frequency- and time- domain analyses. Many non-linear parameters, including the fractal dimension (Rajendra et al., 2005), the Lyapunov exponents (Acharya et al., 2004), the detrended fluctuation analysis (Peng et al., 1995), and the recurrence quantification analysis (RQA) (Acharya et al., 2014), are calculated from HRV signals in order to separate CAD from normal subjects.

Entropy, the main method of non-linear analysis that measures randomness and complexity of signals, is widely used for HRV signal analyses to detect cardiac abnormalities (Acharya et al., 2014, 2015b; Elias et al., 2014; Rajendra Acharya et al., 2015). Acharya et al. (2014) showed that Approximate Entropy (ApEn) and Sample Entropy (SamEn) are higher in normal subjects than in CAD subjects. Entropy evaluations are highly reliant upon the selection of parameters, including N (data length), r (distance tolerance), and m (embedding dimension) (Pincus, 1991; Mayer et al., 2014). Among these parameters, r has the largest impact on results, as even a small change in its value significantly alters the complexity measurement of a given data set, potentially causing mis-diagnosis (Castiglioni and Rienzo, 2008; Lu et al., 2008; Liu et al., 2011). Li et al. (2015) proposed a new entropy named the Distribution Entropy (DisEn) to measure the distribution property existing in data sets by computing Shannon entropy of the empirical probability density of inter-vector distances. Compared to the effect of r on ApEn and SamEn computations, the parameters M (the number of bins) and m (embedding dimension) have less impact on the stability and consistency of DisEn's performance (Udhayakumar et al., 2016). DisEn excels in analyzing HRV signals with a shorter length (Karmakar et al., 2017). In contrast to the computation of ApEn and SamEn, which requires reconstruction of two adjacent dimension vector spaces, the computation of DisEn only requires reconstruction of the m-dimension vector space. As a result, the amount of DisEn computation is only half that of ApEn or SamEn. Renyi entropy (RenEn) is a generalization and reduction of Shannon entropy as the order parameter q closes to 1. RenEn, highlighting characteristics of multifractality or long-range interactions occurring in biomedical systems, is more sensitive to frequent occurrences when q increases (Liang et al., 2015). RenEn calculated from HRV signals is often used as an important clinical indicator of early cardiac autonomic neuropathy (Cornforth et al., 2013, 2014). Recently, RenEn has also been combined with non-linear decompositions, such as discrete wavelet transform (DWT) (Acharya et al., 2016), wavelet packet decomposition (WPD) (Li and Zhou, 2016), empirical mode decomposition (EMD) (Acharya et al., 2017b; Sridhar et al., 2017) for automated diagnosis of CAD, myocardial infarction, and congestive heart failure.

In our current studies, we propose a new entropy named Renyi Distribution Entropy (RdisEn), which integrates Renyi entropy and distribution entropy. In addition, we have developed an automatic CAD detection scheme (**Figure 1**): CAD and normal HRV beats are each divided into two parts. One part of HRV beats is used to extract features with important clinical information, while the other is used to evaluate classification performance of the CAD detection scheme. The feature extraction consists three steps: (1) CAD and normal HRV beats are subjected to three levels of WPD (2) Statistical features (mean, maximum, and minimum values) are computed from the obtained coefficients of the third decomposition levels, and RdisEn is computed from the HRV beats (3) The resulting WPD-based statistical features and RdisEn are then ranked to extract features with significant information for distinguishing those subjects with CAD from those without. Finally, the extracted features computed from the remaining part of HRV beats are fed into K-nearest neighbor (KNN) and support vector machine (SVM) for automatic CAD detection.

MATERIALS AND METHODS

Data Acquisition

In this study, normal and CAD ECG recordings were downloaded from Fantasia open-access database[1] and St.

[1]https://physionet.org/physiobank/database/fantasia/

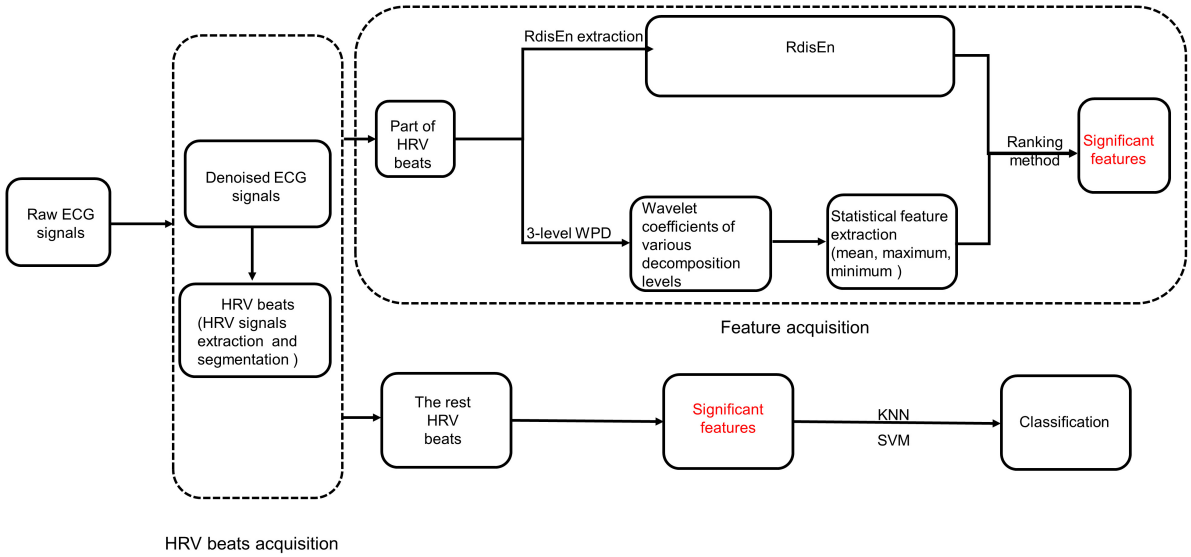

FIGURE 1 | Block diagram of the scheme for CAD detection.

Petersburg Institute of Cardiological Technics 12-lead Arrhythmia Database[2], respectively. Only the lead-II ECG recordings were used for this study. We employed a total of 57 ECG recordings, among which 40 were from normal subjects (20 old: 68 to 85 years, 20 young: 21 to 34 years) and 17 were from 7 CAD patients.

Renyi Distribution Entropy

For a discrete time series $\{x(i), i = 1, 2, \cdots, N\}$, B and m denote bin number and embedding dimension, the RdisEn is computed as follows:

(1) Reconstruction of state space: $(N - m)$vectors $U(i)$ $byU(i) = \{x(i), x(i+1), \cdots, x(i+m-1)\}, 1 \leq i \leq$ N-m.

(2) Construction of the distance matrix: $M = \{d_{i,j}\}$ between vectors $U(i)$ and $U(j)$ for $1 \leq i, j \leq$ N-m, where

$$d_{i,j} = max\left\{\left|x\left(i+k\right) - x\left(j+k\right)\right|, 0 \leq k \leq m-1\right\}$$

. (3) Estimation of probability density: the distances in the matrix M are divided into B bins with equal space, and thus the probability of each bin (t) of the histogram is calculated as

$$p_t = \frac{number\ of\ elements\ in\ the\ t\ bin}{total\ number\ of\ elements\ in\ M}, t = 1, 2, \cdots, B.$$

(4) Calculation: the normalized RdisEn of $x(i)$ is defined as

$$RdisEn\left(B, m, q\right) = \frac{1}{\left(1-q\right) log_2^{(B)}} log_2\left(\sum_{t=1}^{B} p_t^q\right)$$

From the algorithm of RdisEn, it is not difficult to conclude that RdisEn will degenerate to DisEn when $q \to 1$ (Cornforth et al., 2014).

[2]https://www.physionet.org/physiobank/database/incartdb/

Proposed CAD Detection Scheme

In our present study, we developed a combination scheme to separate CAD patients and normal subjects. It consisted of three steps: (1) HRV beats acquisition, (2) RdisEn and WPD-based feature acquisition (3) classification through K-NN and SVM.

HRV Beats Acquisition

The downloaded ECG signals were sampled at 250 HZ for normal group and 257 HZ for CAD group. The normal ECG signals were up-sampled to 257 HZ to maintain uniformity between the two groups. Daubechies wavelet 6 (db6) was used to eliminate unwanted noise (Martis et al., 2013). The ECG signals were subjected to Pan-Tompkin to detect R-peaks (Pan and Tompkins, 2007), and then HRV signals were obtained by calculating the time duration of two consecutive R-peaks (Constant et al., 1999). Finally, each CAD HRV signal was divided into beats (each beat is a segment containing 500 samples), and as a result, 80 HRV beats were acquired from 17 normal ECG signals. In order to keep the dataset balance between the two groups, two normal HRV beats were extracted from each normal HRV signals, and consequently a total of 80 beats were acquired from 40 normal ECG signals.

Feature Acquisition

One hunderd and sixty HRV beats obtained from normal and CAD HRV signals were randomly divided into two parts before feature acquisition, with each part consisting of equal number of beats from the two classes. One part of beats (40 beats for each type of signals) was used for feature acquisition, while the other was utilized to evaluate classification performance.

Feature extraction

As shown in **Figure 1**, RdisEn and WPD-based statistical features were extracted from the HRV beats of the two classes. RdisEn was computed based on the distribution characteristics of inter-vector distances, and parameters on RdisEn evaluation were fixed at

$B = 512, m = 2,\ q = 0.4$ for CAD detection in our proposed scheme (the rationale for the chosen combined parameter is detailed in section "Performance on CAD Detection"). RdisEn was used to extract significant features from each HRV beat to distinguish CAD patients from normal subjects, and WPD-based statistical features were also computed. Briefly, a 3-level WPD was performed on every segmented HRV beat with 500 samples to divide it into a set of sub-bands. WPD, a popular methodology of multiresolution analysis for non-stationary and non-linear signals (Acharya et al., 2015a), can exploit properties of the studied signals in frequency and time domains simultaneously. WPD provides better frequency resolution for the sub-bands than DWT, and it possesses more wavelet sub-bands on the 3rd level WPD of each HRV beat than DWT (8 for WPD and 4 for DWT). Since the obtained wavelet coefficients in each sub-band are related to the wavelet basis selected (Zhang et al., 2018), Daubechies (orders 1–5), Harr, Coiflets (orders 1–3) wavelet function with 3-level decomposition were considered to capture significantly discriminable features for the best classification accuracy for CAD detection. Subsequently, three statistical features, namely mean [*M(k)*], minimum [*Mi(k)*], and maximum [*Ma(k)*] ($k = 1, 2 \cdots 8,$) were evaluated from the wavelet coefficients of the 3rd level wavelet sub-bands.

Feature selection

Not all of the features obtained from the HRV beats exhibited great separation between the two groups, redundant and insignificant features would raise computation cost and impede classification performance. To maximize classification accuracy, feature selection was applied to the original features from extraction, with the least number of features. Student's *t*-test was used as a method of feature selection in our current study (Box, 1987), and features with a *p*-value less than 0.05 were deemed to have significant differences. RdisEn and the top four ranked statistical features were selected.

Classification

Top four ranked statistical features were computed from the remaining part of HRV beats using RdisEN, and fed into classifiers one by one to obtain the highest accuracy with minimum number of features. The two classifiers used in our work are described below.

K-nearest neighbor (KNN)

K-nearest neighbor is a supervised machine learning method widely used in classification, and the class of a testing data is determined by the majority of votes for k training samples with the closest Euclidean distance (González et al., 2016). In this work, $k = 10$ was used.

Support vector machine (SVM)

The SVM classifier divides the training set into two parts by constructing a hyper-plane in the feature space. Features in non-linear separation may be change into linear separation, using kernel functions to map the original data to a feature space with higher dimension (Duda et al., 2012). In this work, an order 1 function kernel was used.

Three evaluation indicators, Accuracy (Acc), Sensitivity (Sen), and Specificity (Spe) were calculated to evaluate the classifiers performance. To ensure unbiasedness and credibility of the classification results, 10 × 10-fold cross validation methodology was implemented, and overall evaluation indicators were calculated.

Feature Assessment

Three statistics methods were used to test the CAD detection performance of these features. The open source R package was used for all the analysis and calculation. First, univariate binary logistic regression method was used to access the statistically significant correlations between CAD and each feature (p-value < 0.05). Second, the correlation between the extracted features was evaluated by using Pearson test (p-value < 0.05, correlation coefficient > 0.5). Finally, multivariate binary logistic regression model without redundant features was established to determine statistically significant feature associated with CAD detection (p-value < 0.05).

RESULTS

Performance of RdisEn on Various Signals

To test the consistency and stability of the RdisEn measurement, we studied the impact of the changing parameter combinations on the RdisEn measurement, using synthetic, physiologic and pathological signals. DisEn was originally introduced to eliminate ApEn and SamEn's excessive dependence on tolerance r. RdisEn proposed in this work was based on DisEn. We therefore compared the performance of RdisEn to that of ApEn, SamEn and DisEn.

Performance of RdisEn on Synthetic Signals by Varying Parameters

The synthetic signals were generated by the Logistic attractor $x_{n+1} = wx_n\,(1 - x_n)$. The constant w was set at 3.5 and 3.8 to obtain periodic and chaotic signals (Pincus, 1991) respectively, which has been widely applied to describe variations of entropy level (Xie et al., 2008; Chen et al., 2009; Karmakar et al., 2017). Twenty realizations were generated from 1000 samples of both signal types, and initial values of the realizations were selected randomly between 0.1 and 0.2 to eliminate the random factors. The mean values of RdisEn with the changing parameter combinations of N (N = 50, 200, 350, 500, 650, 800, 1000), B (B = 100,250,350,500,650,1000,1300,2000) and m (m = 2,3,4,5) for chaotic and periodic signals, as well as the fixed parameter q (q = 0.5), are shown in **Figure 2**. A significant separation between the two signal types was observed, while the traits of the RdisEn values were similar for m = 2, 3, 4, 5 (**Figure 2**).

Performance of RdisEn on Physiologic Signals by Varying Parameters

Next, physiological features were extrapolated from the HRV signals of 20 elderly and 20 young healthy subjects as described in section "HRV Beats Acquisition." For each subject, a HRV signal

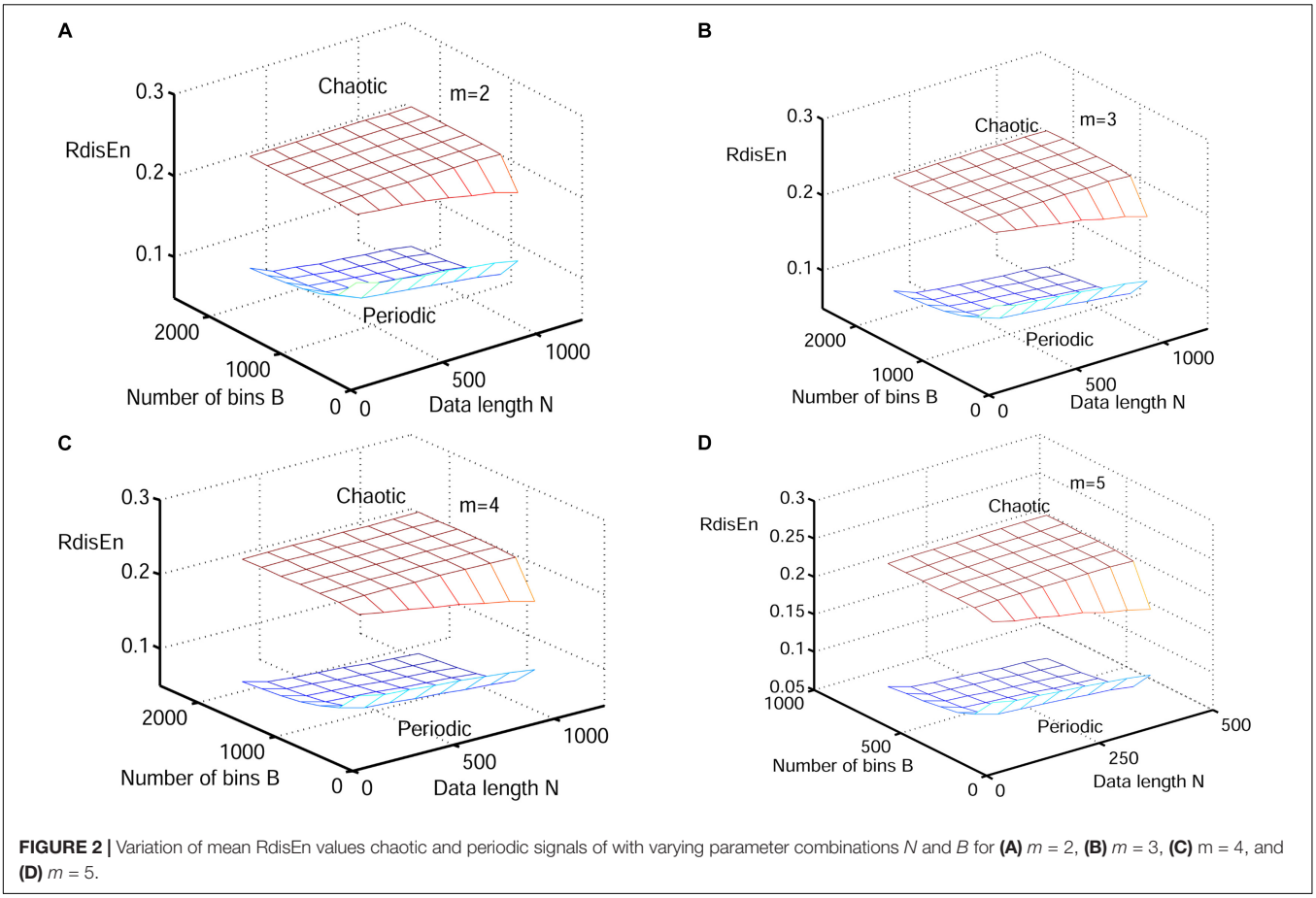

FIGURE 2 | Variation of mean RdisEn values chaotic and periodic signals of with varying parameter combinations *N* and *B* for **(A)** *m* = 2, **(B)** *m* = 3, **(C)** m = 4, and **(D)** *m* = 5.

was selected with varying length (50, 200, 350, 500, 650, 800, and 1000) for RdisEn calculation using the following parameters: N = 50, 200, 350, 500, 650, 800, and 1,000; B = 100, 250, 350, 500, 650, 1,000, 1,300, and 2,000; m = 2, 3, 4, and 5; q = 0.5. As comparison, ApEn and SamEn were also calculated with the following parameters: N = 50, 200, 350, 500, 650, 800, and 1,000; r = 0.1**SD*, 0.2**SD*,· · ·,1**SD*; m = 2, 3, 4, and 5. The results are shown in **Figures 3–5**. The values of ApEn fluctuated widely with different combinations of *N, r,* and *m,* especially for a small data length (**Figure 3**). There was a crossover in ApEn meshes between the HRV signals from the elderly and young subjects, suggesting that ApEn failed to effectively separate the two age groups. The SamEn mesh was sparse in comparison with the ApEn and RdisEn mesh (**Figure 4**), most likely due to the fact that SamEn was not defined for smaller data length, resulting in invalid values. As shown in **Figure 5**, RdisEn could effectively differentiate HRV signals between the two age groups, even for smaller data lengths. In addition, the variation of RdisEn values was small with diverse parameter m. The effects of different parameters N and B or r on entropy measurements (ApEn and RdisEn) for embedding dimension $m \in [2, 5]$ were quantified by the means of the standard deviation across N and B or r (**Table 1**). It was not difficult to find that the change of ApEn measurement with a variation of N was less than that with the change of r. The variation of RdiEn measurement with varying B was higher than that with varying of N for old vs. young subjects. More importantly, compared to ApEn, the variations of RdisEn values with changing parameters B and M were relatively small (**Table 1**).

Performance of RdisEn on Pathological Signals by Varying Parameters

In this work, CAD signals and arrhythmia short-term HRV signals were compared to healthy signals. 40 healthy and 17 CAD short-term HRV signals were acquired from 40 normal and 7 CAD subjects, as described in section "HRV Beats Acquisition." Using the Pan-Tompkin algorithm, 48 arrhythmia short-term HRV signals were obtained from MIT-BIH Arrhythmia Database[3], which contains 48 ECG signals from 47 subjects (25 men: 32 to 89 years, 22 women: 23 to 89 years) (Pan and Tompkins, 2007).

The HRV signals of varying lengths (50, 200, 350, 500, 650, 800, and 1,000) were selected to test ability of RdisEn to separate the two types of pathological signals with changing parameters. ApEn and SampEn were also calculated as references, and the parameters corresponding to the three entropies (RdisEn, ApEn, and SamEn) were set as described in section "Performance of RdisEn on Physiologic Signals by Varying Parameters."

[3]https://physionet.org/physiobank/database/mitdb/

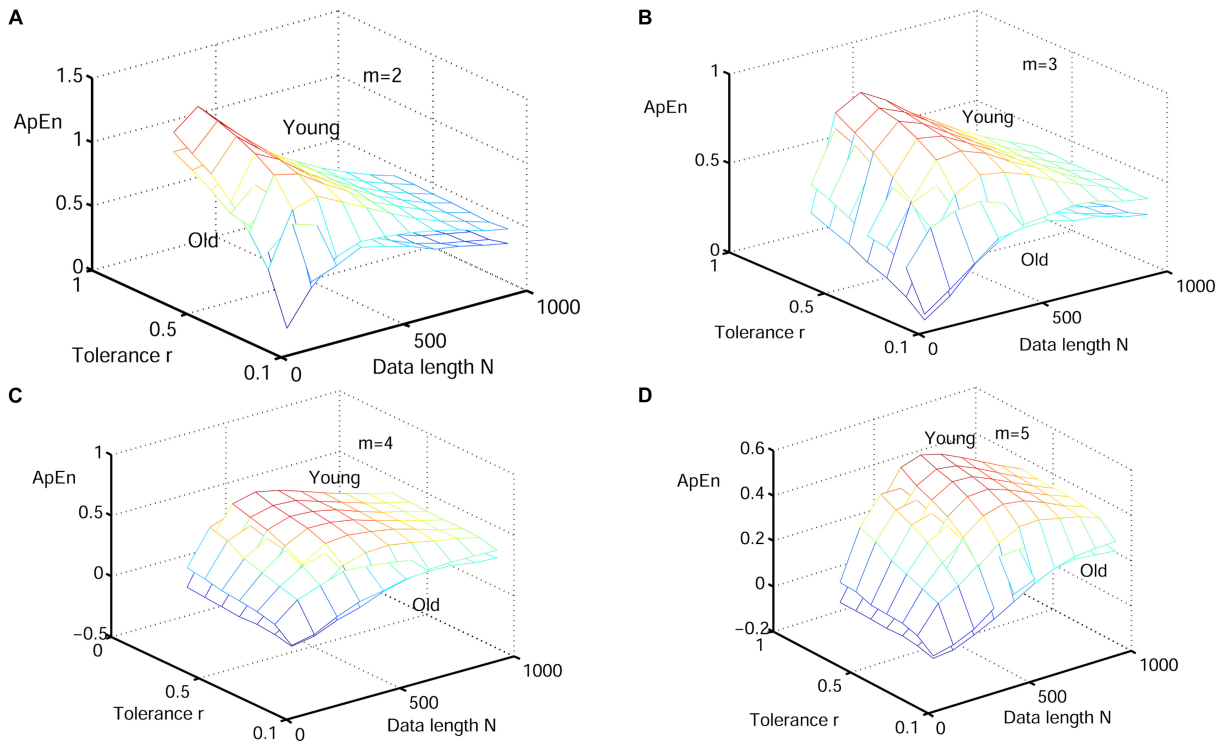

FIGURE 3 | Variation of the mean ApEn value for HRV signals of old and young subjects with varying parameter combinations *N* and *r* for **(A)** $m = 2$, **(B)** $m = 3$, **(C)** $m = 4$, and **(D)** $m = 5$.

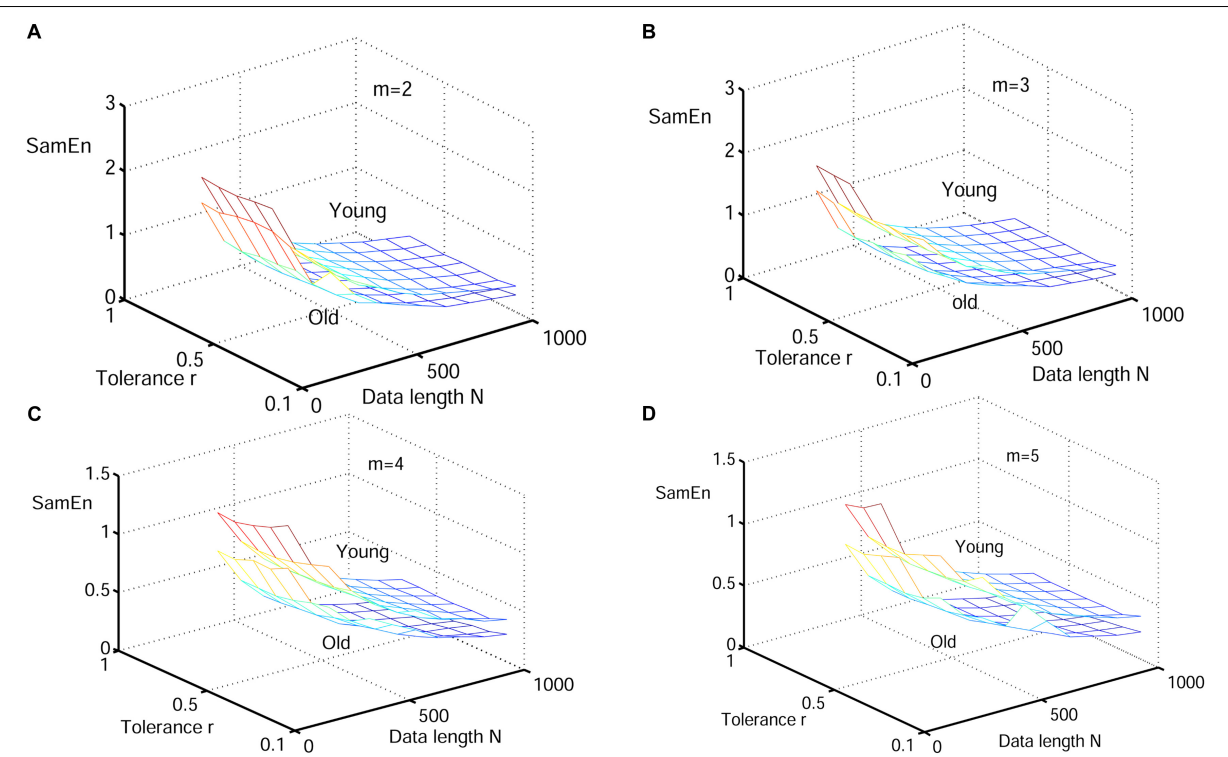

FIGURE 4 | Variation of the mean value for HRV signals of old and young subjects with varying parameter combinations *N* and *r* for **(A)** $m = 2$, **(B)** $m = 3$, **(C)** $m = 4$, and **(D)** $m = 5$.

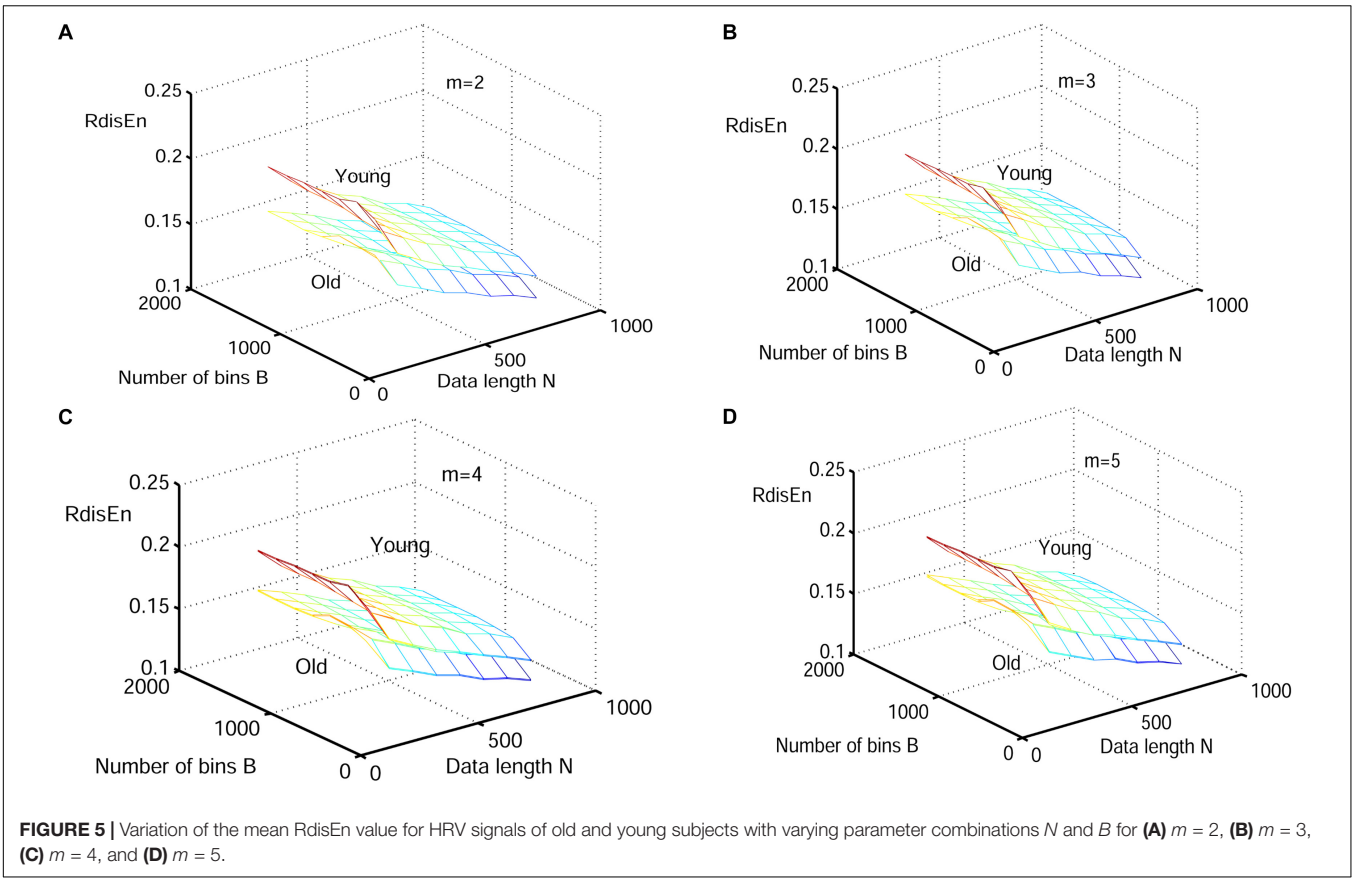

FIGURE 5 | Variation of the mean RdisEn value for HRV signals of old and young subjects with varying parameter combinations *N* and *B* for **(A)** $m = 2$, **(B)** $m = 3$, **(C)** $m = 4$, and **(D)** $m = 5$.

TABLE 1 | Mean of the standard deviation across data length *N* and bin number *B* for RdisEn or tolerance *r* for ApEn.

Entropy	Embedding dimension m	Young		Old		Healthy		CAD		Healthy		Arrhythmia	
		$\overline{\sigma_N}$	$\overline{\sigma_{B/r}}$	$\overline{\sigma_N}$	$\overline{\sigma_{r/B}}$	$\overline{\sigma_N}$	$\overline{\sigma_{r/B}}$	$\overline{\sigma_N}$	$\overline{\sigma_{r/B}}$	$\overline{\sigma_N}$	$\overline{\sigma_{r/B}}$	$\overline{\sigma_N}$	$\overline{\sigma_{r/B}}$
RdisEn	2	0.0043	0.0242	0.0043	0.0217	0.0043	0.0217	0.0067	0.0226	0.004	0.0192	0.0074	0.0196
	3	0.0048	0.0244	0.0049	0.0219	0.0049	0.0219	0.0079	0.0229	0.0051	0.0195	0.0084	0.0199
	4	0.0054	0.0245	0.0054	0.0220	0.0054	0.0220	0.0087	0.0231	0.0057	0.0196	0.0093	0.0200
	5	0.0060	0.0245	0.0060	0.0221	0.0060	0.0221	0.0096	0.0221	0.0062	0.0197	0.0101	0.0201
ApEn	2	0.1302	0.2641	0.0982	0.2527	0.0982	0.2527	0.0404	0.1225	0.0829	0.2481	0.1063	0.2322
	3	0.1114	0.1893	0.0859	0.1599	0.0859	0.1599	0.0401	0.0698	0.0741	0.1487	0.0995	0.1357
	4	0.0983	0.1687	0.0770	0.1314	0.0770	0.1314	0.0447	0.0419	0.0657	0.1122	0.0867	0.11104
	5	0.0875	0.1545	0.0707	0.1172	0.0707	0.1172	0.0447	0.0316	0.0578	0.0941	0.0748	0.0995

Figures 6–8 show the change of mean ApEn, SamEn and RdisEn values with varying parameter combinations for normal and CAD HRV signals. In contrast to ApEn and SamEn, the mean value of RdisEn for CAD HRV signals was higher than that for normal HRV signals, demonstrating the superiority of RdisEn in differentiating CAD and normal subjects. Quantification results on the effect of parameter selections for entropy values (ApEn and RdisEn) for embedding dimension $m \in [2, 5]$, in terms of the means of standard deviation across *N* and *B* or r, are shown in **Table 1**. Our results demonstrated that RdisEn measurement remained relatively stable to parameter selection for very short lengths of HRV signals (**Figures 3–8** and **Table 1**), most likely due to its inherited merits from DisEn (Karmakar et al., 2017). In contrast, a large amount of invalid values was generated in ApEn and SamEn calculation (**Figures 6**, **7**). Moreover, remarkable separation between normal and CAD RdisEn meshes was observed (**Figure 8**). Taken together, these results demonstrated that the RdisEn analysis is the best method to generate stable values with clear separation between normal and CAD groups.

The change of mean RdisEn values with varying parameter combinations for normal and arrhythmia HRV signals was shown in **Figure 9**. The parameter combinations of RdisEn were the same as that described in section "Performance of RdisEn on Physiologic Signals by Varying Parameters." Significant separation between normal and arrhythmia RdisEn

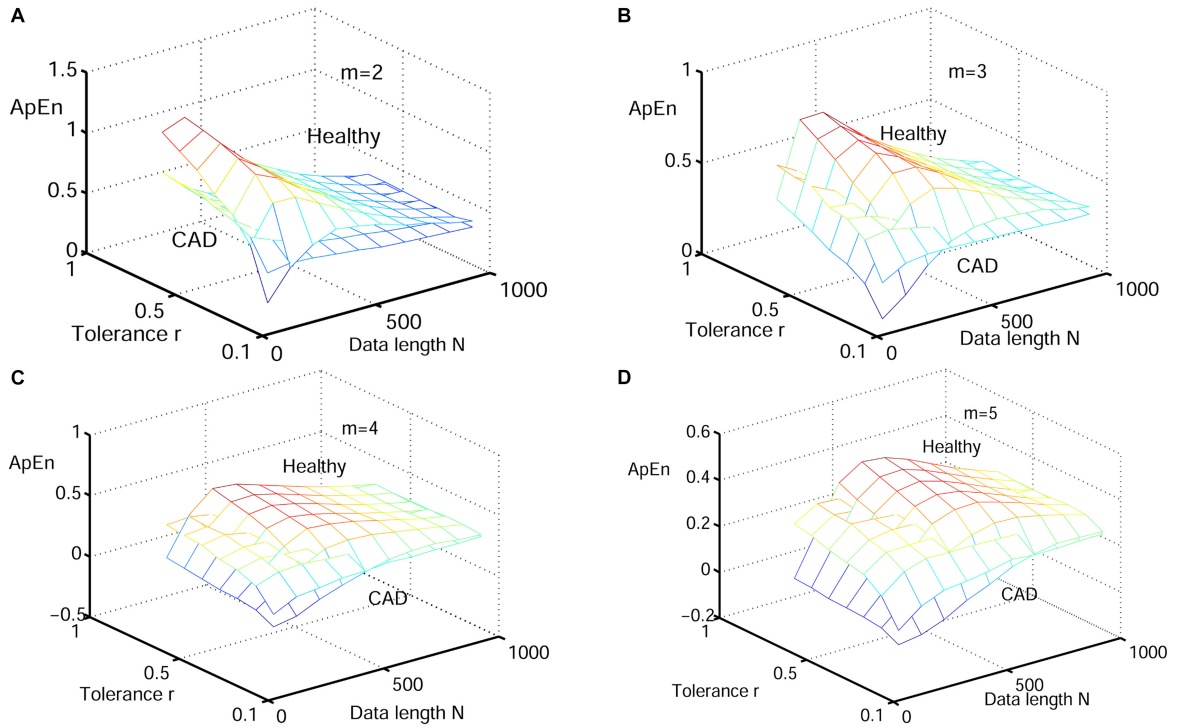

FIGURE 6 | Variation of the mean ApEn value for HRV signals of normal and CAD subjects with varying parameter combinations *N* and *r* for **(A)** *m* = 2, **(B)** *m* = 3, **(C)** *m* = 4, and **(D)** *m* = 5.

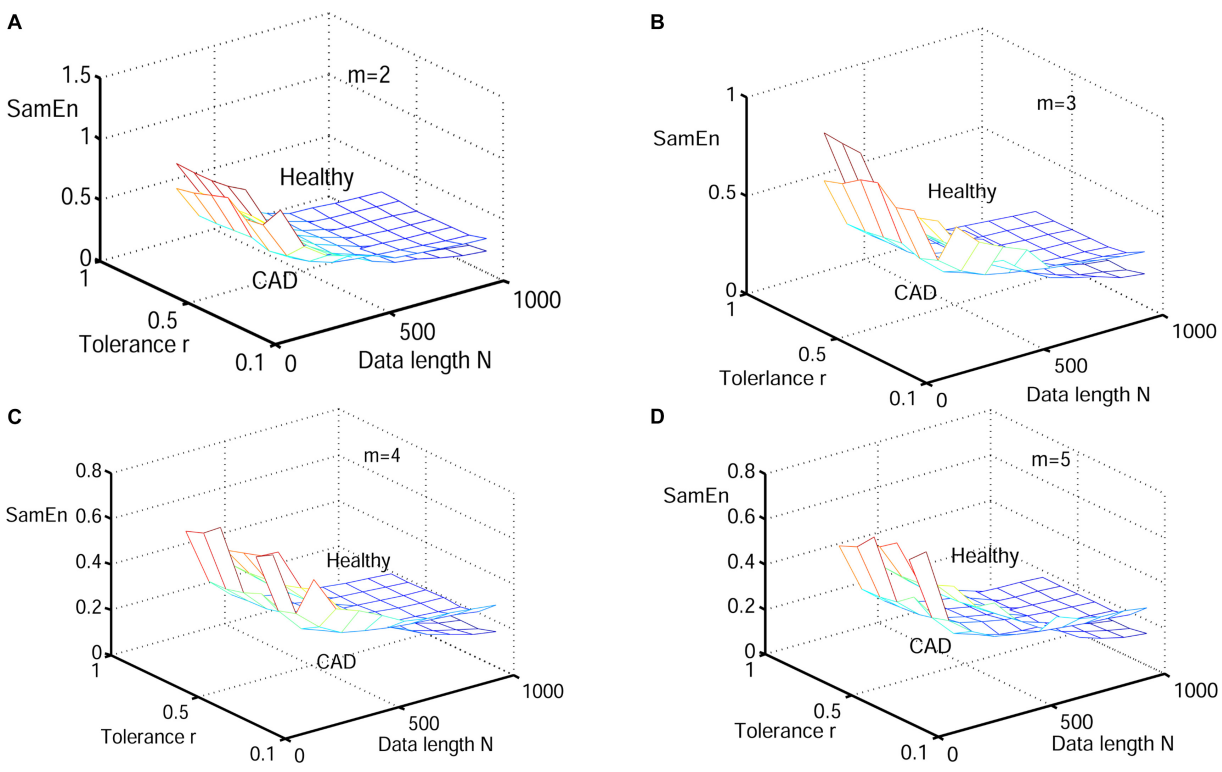

FIGURE 7 | Variation of the mean SamEn value for HRV signals of normal and CAD subjects with varying parameter combinations *N* and *r* for **(A)** *m* = 2, **(B)** *m* = 3, **(C)** *m* = 4, and **(D)** m = 5.

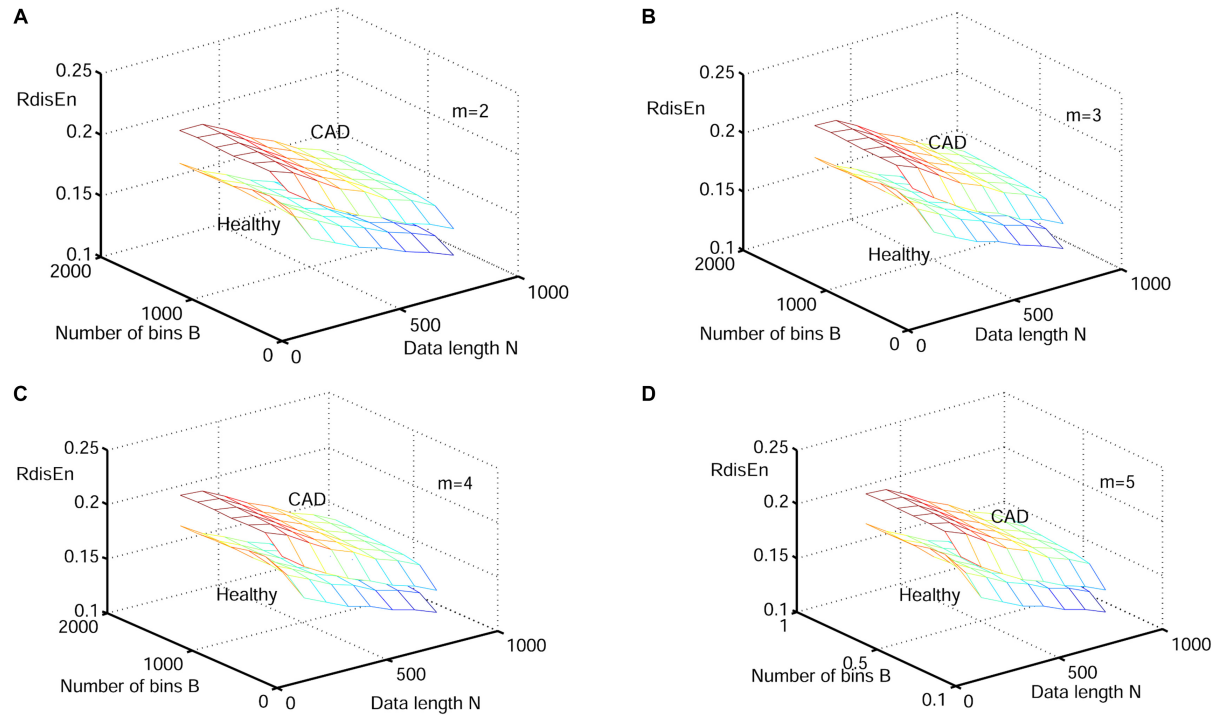

FIGURE 8 | Variation of the mean RdisEn value for HRV signals of normal and CAD subjects with varying parameter combinations *N* and *B* for **(A)** $m = 2$, **(B)** $m = 3$, **(C)** $m = 4$, and **(D)** $m = 5$.

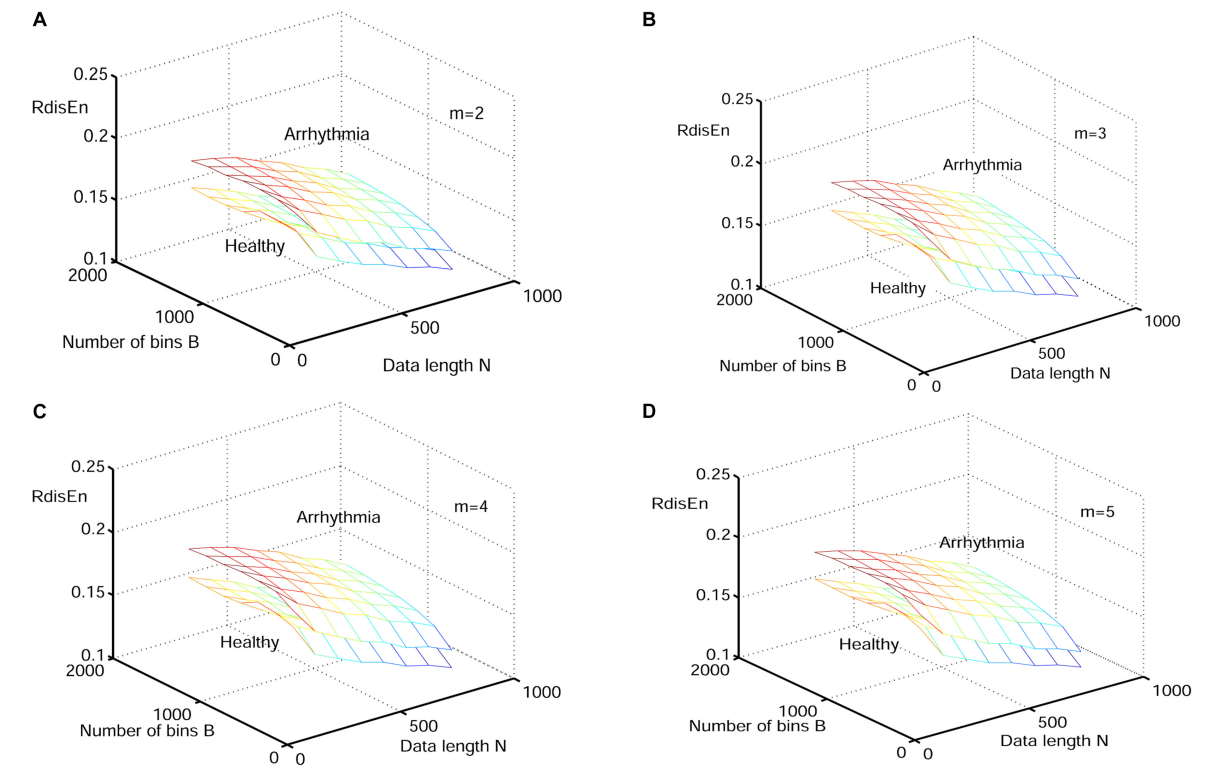

FIGURE 9 | Variation of the mean RdisEn value for HRV signals of normal and arrhythmia subjects with varying parameter combinations *N* and *B* for **(A)** $m = 2$, **(B)** $m = 3$, **(C)** $m = 4$, and **(D)** $m = 5$.

TABLE 2 | AUC values of the fiveentropy measurements with varying lengths for separating healthy from arrhythmia HRV signals.

Entropy	500	800	1000	Mean	SD
ApEn	0.4427	0.4552	0.4583	0.4521	0.0083
SampEn	0.5833	0.5729	0.551	0.5691	0.0165
DisEn	0.7719	0.7677	0.7604	0.7667	0.0058
RenEn	0.5208	0.5104	0.45	0.4937	0.0382
RdisEn	0.7698	0.7698	0.7656	0.7684	0.0024

meshes can be observed (**Figure 9**). In addition, area under the ROC curve (AUC) was used to examine the performance of RdisEn (B = 512, m = 2, q = 0.9) with varying length (500, 800, and 1000) to separate healthy from arrhythmia short-term HRV signals. ApEn (r = 0.2 × SD, m = 2), SamEn (r = 0.2 × SD, m = 2), DisEn (B = 512, m = 2), and RenEn (q = 0.9) were used as references. When AUC equals to 1, the feature distributions belonging to the two classes are completely separated; when AUC equals to 0.5, the feature distributions are similar, suggesting that the closer to 1 the AUC value, the better the discriminatory power of RdisEn (Hanley and McNeil, 1982). RisEn out-performed ApEn, SamEn, DisEn, and RenEn in distinguishing healthy from arrhythmia short-term HRV signals (**Table 2** and **Figure 9**). RdiEn also exhibited good computing stability with varying length, as shown by the SD values (**Table 2**).

Performance on CAD Detection

We repeated the RdisEn analyses using HRV beats obtained via the automated CAD detection scheme from normal and CAD subjects. B = 512 was frequently employed in the analysis of HRV signals with respect to DisEn (Li et al., 2015; Yang et al., 2015), and the selection of m had little effect upon the RdisEn evaluation on the basis of the aforementioned study. Consequently, the related parameters on the RdisEn evaluation were fixed to B = 512 and m = 2 for CAD detection. In addition to the parameter B and m on the DisEn evaluation, another parameter q, which enhances differentiation between normal and CAD HRV beats, requires to be fixed for the RdisEn measurement. To optimize q, we adopted the Student's t-test to assess the performance of RdisEn calculated from one part of normal and CAD HRV beats with varying parameter q ($q \in [0.1, 2]$). As shown in **Table 3**, the two groups exhibited significantly different RdisEn values, regardless of the q parameter variations. The p-value was lowest when q = 0.4, indicative of the optimal condition to differentiate the two groups (RdisEn degenerated into DisEn, as mentioned in section "Renyi Distribution Entropy"). As a result, we computed RdisEn with parameters N = 500, B = 512, m = 2, and q = 0.4. **Table 4** shows the means and SD of RdisEn, as well as the top four statistical features based on WPD with the db1, computed from one part of normal and CAD HRV beats, and their p-values generated by Student's t-test, significant differences were observed between the two groups (**Table 4**).

Five selected features were calculated from the remaining part of normal and CAD HRV beats and then fed into classifiers KNN or SVM one by one to maximize the accuracy with minimal features. As shown in **Table 5**, the proposed scheme for CAD detection achieved the highest mean accuracy of 96.34% with five features (RdisEn and four WPD with db1 d statistical features) in 10 × 10-fold cross validation using KNN. We repeated the CAD detection scheme (**Figure 1**) using RdisEn and WPD with other wavelet-based statistical features, and the results were shown in **Table 5**. We computed the p-values for the correlations between CAD detection with five features, i.e., RdisEn and the top ranked four WPD with coif2 based statistical features [Mi(1), M(1), Ma(1), and Mi(6)] by univariate binary logistic regression method, the corresponding p-values for the five features are 2.5e-6, 0.01, 3.3e-6, 4.6e-6, and 0.02, respectively, which demonstrated that these features statistically significant correlated with CAD detection. As presented in **Table 5**, when the fifth feature was added into the KNN classifier, the CAD detection performed with 97.5% accuracy, 100% sensitivity, 95% specificity, respectively, with no significant improvement compared with the performance of the 4-feature based model (97.37 ± 0.41% accuracy, 99.75 ± 0.79% sensitivity, 95% specificity). This indicated that the fifth feature [Mi(6)] is correlated with the other four features [RdisEn, Mi(1), M(1), and Ma(1)] and therefore includes redundant information. A Pearson test was performed to calculate the correlations between the fifth feature and other four, the correlation coefficient for Mi(6) and RdisEn, fMi(1), M(1), and Ma(1) are −0.26 (p-value = 0.020), −0.073 (p-value = 0.518), 0.218 (p-value = 0.052), and 0.953 (p-value = 4.3e-42), respectively, indicating a significant correlation between the fifth feature [Mi(6)] and Ma(1). At last, the multivariate binary logistic regression model was used to test the relationship between the features and the CAD detection, in which RdisEn and the other three features were entered and their p-values are 0.033, 0.563, 0.089, and 0.501, respectively; it is obvious that RdisEn improved the CAD detection statistically significant.

DISCUSSION

The CAD diagnostic signals can be divided into three major categories: heart sound signals (HSS), ECG signals, and HRV signals. The detailed methods of CAD detection are described in

TABLE 3 | p-Values of RdisEn computed from normal and CAD HRV beats with varying parameter q.

q	0.1	0.2	0.3	0.4	0.5	0.6	0.7	0.8	0.9	1
p-Value	9.68E-5	5.08E-5	3.55E-5	3.15E-5	3.32E-5	3.85E-5	4.68E-5	5.60E-5	7.1E-5	8.86E-5
q	1.1	1.2	1.3	1.4	1.5	1.6	1.7	1.8	1.9	2
p-Value	1.08E-4	1.30E-4	1.54E-4	1.81E-4	2.09E-4	2.39E-4	2.71E-4	3.05E-4	3.39E-4	3.74E-4

TABLE 4 | Mean and SD values of RdisEn and the top five WPD (db1 basis) based statistical features for normal and CAD HRV beats.

Feature	CAD		Normal		*p*-value
	Mean	SD	Mean	SD	
RdisEn	0.2690	0.0363	0.2345	0.0316	3.15E-5
Mi(1)	1.6203	0.3024	2.4613	0.4826	2.37E-14
M(1)	1.9249	0.3958	2.8147	0.5110	3.55E-13
Mi(5)	2.2415	0.4469	3.0369	0.5778	1.29E-9
Ma(6)	0.3315	0.2148	0.0992	0.0995	2.45E-8

Table 6. HRV signals are essential tools widely used for cardiac abnormality detection and CAD diagnosis (Lee et al., 2007, 2008; Dua et al., 2012; Giri et al., 2013; Patidar et al., 2015; Kumar et al., 2016). Lee et al. (2007, 2008) employed linear and non-linear features extracted from HRV signals as indices to distinguish normal subjects from CAD patients, and they achieved a ∼90% accuracy using the SVM classifier. The automatic CAD detection algorithm was proposed by Dua et al. (2012), based on non-linear features (recurrence plots, detrended fluctuation, and three types of entropy) and a principal component analysis method, and achieved an accuracy of 89.5% using multilayer perceptron (MLP) methodology. Giri et al. (2013) used DWT to divide HRV signals into frequency sub-bands. They also applied dimensionality reduction methods such as PCA, independent component analysis (ICA), and linear discriminant analysis (LDA) to the coefficients from the obtained sub-bands to lower the data dimension. With the additional combined method of ICA and Gaussian mixture model (GMM), Giri et al. (2013) reported the highest accuracy for automatically identifying CAD of 96.8%. Patidar et al. (2015) applied a combination of tunable-Q wavelet transform (TQWT), centered correntropy, and the PCA method to achieved an accuracy of 99.72% with HRV signals from the automated diagnosis of CAD. Kumar et al. (2016) developed a CAD detection technique, which consists of the flexible analytic wavelet transform (FAWT) and ranking methods, including receiver operating characteristics (ROC),

TABLE 5 | Classification performance of RdisEn and WPD (various basis) based statistical features by using KNN and SVM classifiers.

Wavelet basis	NoF	KNN			SVM		
		Acc(%)	Sen(%)	Spe(%)	Acc(%)	Sen(%)	Spec(%)
db1	3	96.08 ± 0.38	97.5	94.75 ± 0.79	96.08 ± 0.38	97.25 ± 0.79	95
	4	96.08 ± 0.38	97.5	94.75 ± 0.79	96.06 ± 0.59	97.5 ± 1.79	95.24 ± 0.77
	5	96.34 ± 0.72	97.5	95.25 ± 1.42	95.6 ± 0.85	97.25 ± 0.79	94 ± 1.29
db2	3	96.08 ± 0.38	97.5	94.75 ± 0.79	97.12 ± 0.84	99.25 ± 1.69	95
	4	97.25 ± 0.79	100	94.5 ± 1.58	97.37 ± 0.41	99.75 ± 0.79	95
	5	96.48 ± 0.99	98 ± 1.97	95	96.6 ± 0.86	98.25 ± 1.69	95
db3	3	96.33 ± 0.41	97.75 ± 0.79	95	95.6 ± 0.85	96.5 ± 1.75	94.75 ± 0.79
	4	97.37 ± 0.41	99.75 ± 0.79	95	96.6 ± 0.86	98.5 ± 1.75	94.75 ± 0.79
	5	95.72 ± 0.62	96.5 ± 1.29	95	96.46 ± 0.54	98 ± 1.05	95
db4	3	95.96 ± 0.51	97 ± 1.05	95	95.38 ± 1.31	95.75 ± 2.65	95
	4	97.37 ± 0.41	99.75 ± 0.79	95	96.23 ± 1.17	97.5 ± 2.36	95
	5	97.37 ± 0.41	99.75 ± 0.79	95	95.24 ± 0.95	95.5 ± 1.97	95
db5	3	95.84 ± 0.58	97 ± 1.05	94.75 ± 0.79	95 ± 1.26	95 ± 2.63	95
	4	96.23 ± 1.02	97.75 ± 0.79	94.75 ± 1.84	95.85 ± 0.83	97 ± 1.05	94.75 ± 1.42
	5	96.74 ± 1.22	98.75 ± 1.32	94.75 ± 1.84	95.60 ± 1.34	96.75 ± 1.69	94.50 ± 1.58
db6	3	95.96 ± 0.51	97.50	94.50 ± 1.05	95.97 ± 0.78	97 ± 1.58	95
	4	97.24 ± 0.55	100	94.5 ± 1.05	96.73 ± 0.89	98.50 ± 1.75	95
	5	95.85 ± 0.83	97.50 ± 1.18	94.25 ± 1.21	95.48 ± 0.84	96.50 ± 1.75	94.50 ± 1.05
harr	3	96.08 ± 0.38	97.50	94.75 ± 0.79	96.08 ± 0.38	97.25 ± 0.79	95
	4	96.08 ± 0.38	97.50	94.75 ± 0.79	96.21 ± 0.59	97.50 ± 1.18	95.24 ± 0.77
	5	96.34 ± 0.71	97.50	95.25 ± 1.42	95.60 ± 0.85	97.25 ± 0.79	94 ± 1.23
coif1	3	96.08 ± 0.38	97.50	94.75 ± 0.79	95.84 ± 0.81	97 ± 1.05	94.75 ± 0.79
	4	95.96 ± 0.51	97.50	94.50 ± 1.05	95.85 ± 1.01	97.25 ± 1.42	94.50 ± 1.05
	5	97.24 ± 0.55	99.75 ± 0.79	94.75 ± 0.79	96.24 ± 1.31	98 ± 1.97	94.50 ± 1.05
coif2	3	96.33 ± 0.41	97.75 ± 0.79	95	97.11 ± 0.63	99.25 ± 1.21	95
	4	97.37 ± 0.41	99.75 ± 0.79	95	97.24 ± 0.55	99.5 ± 1.05	95
	5	97.50	100	95	97.24 ± 0.55	100	94.50 ± 1.05
coif3	3	95.96 ± 0.51	97.25 ± 0.79	94.75 ± 0.79	96.98 ± 0.98	97 ± 1.97	95
	4	96.98 ± 0.67	99.25 ± 1.21	94.75 ± 0.79	96.99 ± 0.88	99 ± 1.75	95
	5	95.84 ± 0.58	96.75 ± 1.21	95	95.36 ± 0.58	95.75 ± 1.21	95

NoF, number of features.

TABLE 6 | Studies conducted to distinguish normal from CAD subjects using various signals.

Author	Data used	Method/features	Classifiers	Cross validation	Accuracy
using HSS signals					
Karimi et al., 2005	5 CAD and 5 normal	DWT, WPD (some statistical features)	ANN	No	90%
Zhao and Ma, 2008	40 CAD and 40 normal	EMD, TEO (some statistical features)	BPNN	No	85%
using ECG signals					
Lewenstein, 2001	479 CAD and 297 normal	(slope of an ST segment, blood pressure, load during the test)	Radial basis function neural networks	No	97%
Babaoğlu et al., 2010a	480 CAD	principle component analysis	SVM	5-fold	79.1%
Babaoglu et al., 2010b	480 CAD	binary particle swarm optimization and genetic algorithm	SVM	5-fold	81.46%
Acharya et al., 2017c	7 CAD and 40 normal	Higher-Order Statistics and Spectra (HOS)	KNN,DT	10-fold	98.99%
Kumar et al., 2017	7 CAD and 40 normal	Flexible analytic wavelet transform (cross information potential)	LS-SVM	10-fold	99.6%
Normal and CAD using HRV signals					
Lee et al., 2007	99 CAD, 94 Normal	Linear (time domain, frequency domain) and non-linear methods (Poincare plot, approximation entropy)	Support vector machine (SVM)	10-fold	90%
Lee et al., 2008	99 CAD, 94 Normal	Linear (time domain, frequency domain) and non-linear methods (Poincare plot, the hurst exponent, Detrended fluctuation analysis)	CPAR & SVM:	10-fold	85–90%
Dua et al., 2012	10 CAD and 10 normal subjects	Non-linear methods (recurrence plots, Shannon entropy) and principal component analysis (PCA)	multilayer perceptron (MLP)	5-fold	89.5%
Giri et al., 2013	10 CAD and 15 normal subjects	DWT and Independent Component Analysis (ICA)	Gaussian Mixture Model (GMM)	3-fold	96.8%
Patidar et al., 2015	10 CAD and 10 normal subjects	TQWT and PCA (correntropy)	LS-SVM	3-fold	99.72%
Kumar et al., 2016	10 CAD and 10 normal subjects	FAWT and entropy	LS-SVM	10-fold	100%
In this work	40 normal and 7 CAD subjects	RdisEn and WPD (statistical features)	KNN and SVM	10 times 10-fold	97.5%

entropy and Bhattacharya space algorithm, with a classification accuracy of 100%.

In the current study, we proposed a new entropy called RdisEn based on DisEn. Our simulation experiments with three types of signals showed that RdisEn, as an indicator of the randomness and complexities occurring in the signals, was not overly reliant on parameter selection and remained stable for even very short sequences (**Figures 5**, **8**). It out-performed ApEn and SamEn in separating physiological (old from young) and pathological (healthy from CAD and healthy from arrhythmia) signals (**Figures 3**–**8**). The results indicate that RdisEn is a promising measure to characterize physiological and pathological condition of subjects with short-term HRV signals.

We developed an automatic CAD detection scheme combining RdisEn and WPD-based statistical features to analyze short-term HRV signals. Since the HRV signals used in this work were extracted from standard ECG signals obtained during the rest period instead of exercise, the ECG signal acquisition were harmless to the test subjects. Using only five features with KNN and the 10 × 10-fold cross validation method, the proposed scheme can differentiate normal and CAD affected HRV with 97.5% accuracy, demonstrating that our scheme outperformed other algorithms in automatic CAD detection (**Table 5**). It was worth mentioning that, in feature acquisition, features were extracted from a data set, which was independent of that used for the subsequent evaluation of the classifier in our work. Compared with other CAD detection schemes shown in **Table 6**, our scheme using RdisEn and WPD-based statistical features is more stable, rigorous and efficient. The classification accuracy achieved was significantly higher than that using WPD-based statistical features alone (97.5% vs. 90%) (Karimi et al., 2005). The *p*-values of 2.5e-6 and 0.033 for RdisEn by univariate and multivariable binary logistic regression method, respectively, were obtained in the process of testing the ability of RdisEn as a feature for CAD detection in this work. These indicated that RdisEn made a great contribution in distinguishing normal and CAD affected HRV signals. In the future, RdisEn can be utilized as a quantification index of irregularity within non-linear signals for the diagnosis of other diseases such as fibrillation, myocardial infarction and congestive heart failure (Acharya et al., 2017a, 2018a,b; Fujita and Cimr, 2019).

CONCLUSION AND FUTURE WORK

Coronary artery disease is a serious cardiac abnormality, leading to high fatality. Early diagnosis and treatment of CAD can prevent progression. In this work, we proposed a new important entropy named RdisEn. It can effectively reveal the irregularity

and randomness in HRV beats. A scheme for the automated differentiation between HRV signals from normal and CAD affected people has been developed, using WPD- and RdisEn-based computation, Student's *t*-test selection, and classifiers to yield a classification accuracy of 97.5%, sensitivity of 100% and specificity of 95%. This novel scheme for CAD detection is reproducible, cost-effective, non-invasive, and more accessible than physical examinations such as coronary angiography and cardiac catheterization. In future works, we will apply the proposed scheme for the diagnosis of CAD and test this model in big population samples for future application.

DATA AVAILABILITY

Publicly available datasets were analyzed in this study. This data can be found here: https://www.physionet.org/physiobank/database/incartdb/.

AUTHOR CONTRIBUTIONS

MS and CZ contributed to the majority of writing and conducted major parts of the experiments. YJ, HH, RW, and YS conducted some experiments and contributed to the methodology and writing. BS supervised the project and revised the manuscript.

FUNDING

This study was supported by the National Key Research and Development Program of China (Grant No. 2016YFC1306605), the National Natural Science Foundation of China (Grant No. 31670851), and the Postgraduate Research and Practice Innovation Program of Jiangsu Province (KYCX18_2488), and Natural Science Foundation of Anhui Province (No. 1508085MC55).

REFERENCES

Acharya, U. R., Faust, O., Sree, V., Swapna, G., Martis, R. J., Kadri, N. A., et al. (2014). Linear and nonlinear analysis of normal and CAD-affected heart rate signals. *Comput. Methods Programs Biomed.* 113, 55–68. doi: 10.1016/j.cmpb.2013.08.017

Acharya, U. R., Fujita, H., Oh, S. L., Hagiwara, Y., Tan, J. H., and Adam, M. (2017a). Application of deep convolutional neural network for automated detection of myocardial infarction using ECG signals. *Inf. Sci.* 41, 190–198. doi: 10.1016/j.ins.2017.06.027

Acharya, U. R., Fujita, H., Oh, S. L., Hagiwara, Y., Tan, J. H., Adam, M., et al. (2018a). Deep convolutional neural network for the automated diagnosis of congestive heart failure using ECG signals. *Appl. Intell.* 49, 16–27. doi: 10.1007/s10489-018-1179-1

Acharya, U. R., Fujita, H., Oh, S. L., Raghavendra, U., Tan, J. H., Adam, M., et al. (2018b). Automated identification of shockable and non-shockable life-threatening ventricular arrhythmias using convolutional neural network. *Future Gener. Comput. Syst.* 79, 952–959. doi: 10.1016/j.future.2017.08.039

Acharya, U. R., Fujita, H., Sudarshan, V. K., Bhat, S., and Koh, J. E. W. (2015a). Application of entropies for automated diagnosis of epilepsy using EEG signals: a review. *Knowl. Based Syst.* 88, 85–96. doi: 10.1016/j.knosys.2015.08.004

Acharya, U. R., Fujita, H., Sudarshan, V. K., Ghista, D. N., Lim, W. J. E., and Koh, J. E. W. (2015b). "Automated prediction of sudden cardiac death risk using kolmogorov complexity and recurrence quantification analysis features extracted from HRV signals," in *Proceeding of the 2015 IEEE International Conference on Systems, Man, and Cybernetics*, IEEE, Kowloon.

Acharya, U. R., Fujita, H., Sudarshan, V. K., Shu, L. O., Adam, M., Koh, J. E. W., et al. (2016). Automated detection and localization of myocardial infarction using electrocardiogram: a comparative study of different leads. *Knowl. Based Syst.* 99, 146–156. doi: 10.1016/j.knosys.2016.01.040

Acharya, U. R., Kannathal, N., and Krishnan, S. M. (2004). Comprehensive analysis of cardiac health using heart rate signals. *Physiol. Meas.* 25, 1139–1151. doi: 10.1088/0967-3334/25/5/005

Acharya, U. R., Oh, S. L., Chua, C. K., Fujita, H., Muhammad, A., Chua, K. P., et al. (2017b). Application of empirical mode decomposition (EMD) for automated identification of congestive heart failure using heart rate signals. *Neural Comput. Appl.* 28, 3073–3094. doi: 10.1007/s00521-016-2612-1

Acharya, U. R., Sudarshan, V. K., Koh, J. E. W., Martis, R. J., Tan, J. H., Oh, S. L., et al. (2017c). Application of higher-order spectra for the characterization of coronary artery disease using electrocardiogram signals. *Biomed. Signal Process. Control* 31, 31–43. doi: 10.1016/j.bspc.2016.07.003

Antanavicius, K., Bastys, A., Bluzas, J., Gargasas, L., Kaminskiene, S., Urbonaviciene, G., et al. (2008). Nonlinear dynamics analysis of electrocardiograms for detection of coronary artery disease. *Comput. Methods Programs Biomed.* 92, 198–204. doi: 10.1016/j.cmpb.2008.07.002

Babaoğlu, I., Fındık, O., and Bayrak, M. (2010a). Effects of principle component analysis on assessment of coronary artery diseases using support vector machine. *Expert Syst. Appl.* 37, 2182–2185. doi: 10.1016/j.eswa.2009.07.055

Babaoglu, İ, Findik, O., and Ülker, E. (2010b). A comparison of feature selection models utilizing binary particle swarm optimization and genetic algorithm in determining coronary artery disease using support vector machine. *Expert Syst. Appl.* 37, 3177–3183. doi: 10.1016/j.eswa.2009.09.064

Box, J. F. (1987). Guinness, gosset, fisher, and small samples. *Stat. Sci.* 2, 45–52. doi: 10.1214/ss/1177013437

Castiglioni, P., and Rienzo, M. D. (2008). How the threshold "r" influences approximate entropy analysis of heart-rate variability". *Comput. Cardiol.* 35, 561–564.

Chen, W., Zhuang, J., Yu, W., and Wang, Z. (2009). Measuring complexity using FuzzyEn, ApEn, and SampEn. *Med. Eng. Phy.* 31, 61–68. doi: 10.1016/j.medengphy.2008.04.005

Constant, I., Laude, D., Murat, I., and Elghozi, J. L. (1999). Pulse rate variability is not a surrogate for heart rate variability. *Clin. Sci.* 97, 391–397. doi: 10.1042/cs0970391

Cornforth, D. J., Tarvainen, M. P., and Jelinek, H. F. (2013). Using renyi entropy to detect early cardiac autonomic neuropathy. *Conf. Proc. IEEE Eng. Med. Biol. Soc.* 2013, 5562–5565. doi: 10.1109/embc.2013.6610810

Cornforth, D. J., Tarvainen, M. P., and Jelinek, H. F. (2014). How to calculate renyi entropy from heart rate variability, and why it matters for detecting cardiac autonomic neuropathy. *Front. Bioeng. Biotechnol.* 2:34. doi: 10.3389/fbioe.2014.00034

Dua, S., Du, X., Sree, S. V., and Thajudin Ahamed, V. I. (2012). Novel classification of coronary artery disease using heart rate variability analysis. *J. Mech. Med. Biol.* 12, 1240017-1-19. doi: 10.1142/s0219519412400179

Duda, R. O., Peter, E. H., and David, G. S. (2012). *Pattern Classification*. Hoboken, NJ: Wiley-Interscience.

Elias, E., Mohammad, P., and Ahmad, B. (2014). A novel approach to predict sudden cardiac death (SCD) using nonlinear and time-frequency analyses from HRV signals. *PLoS One* 9:e81896. doi: 10.1371/journal.pone.0081896

Fujita, H., and Cimr, D. (2019). Computer aided detection for fibrillations and flutters using deep convolutional neural network. *Inf. Sci.* 486, 231–239. doi: 10.1016/j.ins.2019.02.065

Giri, D., Rajendra Acharya, U., Martis, R. J., Vinitha Sree, S., Lim, T.-C., Ahamed, T., et al. (2013). Automated diagnosis of coronary artery disease affected patients using LDA, PCA, ICA and discrete wavelet transform. *Knowl. Based Syst.* 37, 274–282. doi: 10.1016/j.knosys.2012.08.011

González, M., Bergmeir, C., Triguero, I., Rodríguez, Y., and Benítez, J. M. (2016). On the stopping criteria for k-nearest neighbor in positive unlabeled time series classification problems. *Inf. Sci.* 328, 42–59. doi: 10.1016/j.ins.2015.07.061

Grech, E. D. (2011). *ABC of Interventional Cardiology*. London: BMJ books.

Hanley, J. A., and McNeil, B. J. (1982). The meaning and use of the area under a receiver operating characteristic (ROC) curve. *Radiology* 143, 29–36. doi: 10.1148/radiology.143.1.7063747

Hayano, J., Sakakibara, Y., Yamada, M., Ohte, N., Fujinami, T., Yokoyama, K., et al. (1990). Decreased magnitude of heart rate spectral components in coronary artery disease. Its relation to angiographic severity. *Circulation* 81, 1217–1224. doi: 10.1161/01.cir.81.4.1217

Huikuri, H. V., Niemela, M. J., Ojala, S., Rantala, A., Ikaheimo, M. J., and Airaksinen, K. E. (1994). Circadian rhythms of frequency domain measures of heart rate variability in healthy subjects and patients with coronary artery disease. *Circulation* 90, 121–126. doi: 10.1161/01.cir.90.1.121

Karimi, M., Amirfattahi, R., Sadri, S., and Marvasti, S. A. (2005). "Noninvasive detection and classification of coronary artery occlusions using wavelet analysis of heart sounds with neural networks," in *Proceedings of the The 3rd IEE International Seminar on Medical Applications of Signal Processing 2005*, London: IET.

Karmakar, C., Udhayakumar, R. K., Li, P., Venkatesh, S., and Palaniswami, M. (2017). Stability, consistency and performance of distribution entropy in analysing short length heart rate variability (HRV) signal. *Front. Physiol.* 8:720. doi: 10.3389/fphys.2017.00720

Kumar, M., Pachori, R. B., and Acharya, U. R. (2016). An efficient automated technique for cad diagnosis using flexible analytic wavelet transform and entropy features extracted from hrv signals. *Int. J.* 63, 165–172. doi: 10.1016/j.eswa.2016.06.038

Kumar, M., Pachori, R. B., and Acharya, U. R. (2017). Characterization of coronary artery disease using flexible analytic wavelet transform applied on ECG signals. *Biomed. Signal Process. Control* 31, 301–308. doi: 10.1016/j.bspc.2016.08.018

Lavoie, K. L., Fleet, R. P., Laurin, C., Arsenault, A., Miller, S. B., and Bacon, S. L. (2004). Heart rate variability in coronary artery disease patients with and without panic disorder. *Psychiatr. Res.* 128, 289–299. doi: 10.1016/j.psychres.2004.06.005

Lee, H. G., Noh, K., and Ryu, K. H. (2008). "A data mining approach for coronary heart disease prediction using hrv features and carotid arterial wall thickness," in *Proceeding of the 2008 International Conference on BioMedical Engineering and Informatics*, Sanya: IEEE.

Lee, H. G., Noh, K. Y., and Ryu, K. H. (2007). *Mining Biosignal Data: Coronary Artery Disease Diagnosis Using Linear and Nonlinear Features of HRV*. Berlin: Springer-Verlag.

Lewenstein, K. (2001). Radial basis function neural network approach for the diagnosis of coronary artery disease based on the standard electrocardiogram exercise test. *Med. Biol. Eng. Comput.* 39, 362–367. doi: 10.1007/BF02345292

Li, P., Liu, C., Li, K., Zheng, D., Liu, C., and Hou, Y. (2015). Assessing the complexity of short-term heartbeat interval series by distribution entropy. *Med. Biol. Eng. Comput.* 53, 77–87. doi: 10.1007/s11517-014-12160

Li, T., and Zhou, M. (2016). ECG classification using wavelet packet entropy and random forests. *Entropy* 18:285. doi: 10.3390/e18080285

Liang, Z., Wang, Y., Sun, X., Li, D., Voss, L. J., Sleigh, J. W., et al. (2015). EEG entropy measures in anesthesia. *Front. Comput. Neurosci.* 9:16. doi: 10.3389/fncom.2015.00016

Liu, C., Liu, C., Shao, P., Li, L., Sun, X., Wang, X., et al. (2011). Comparison of different threshold values r for approximate entropy: application to investigate the heart rate variability between heart failure and healthy control groups. *Physiol. Meas.* 32, 167–180. doi: 10.1088/0967-3334/32/2/002

Lu, S., Chen, X., Kanters, J. K., Solomon, I. C., and Chon, K. H. (2008). Automatic selection of the threshold value R for approximate entropy. *IEEE Trans. Biomed. Eng.* 55, 1966–1972. doi: 10.1109/tbme.2008.919870

Martis, R. J., Acharya, U. R., and Min, L. C. (2013). ECG beat classification using PCA, LDA, ICA and discrete wavelet transform. *Biomed. Signal Process. Control* 8, 437–448. doi: 10.1016/j.bspc.2013.01.005

Mayer, C. C., Bachler, M., Hortenhuber, M., Stocker, C., Holzinger, A., and Wassertheurer, S. (2014). Selection of entropy-measure parameters for knowledge discovery in heart rate variability data. *BMC Bioinformatics* 15(Suppl. 6):S2. doi: 10.1186/1471-2105-15-s6-s2

Pan, J., and Tompkins, W. J. (2007). A real-time QRS detection algorithm. *IEEE Trans. Biomed. Eng.* 32, 230–236. doi: 10.1109/tbme.1985.325532

Patidar, S., Pachori, R. B., and Rajendra Acharya, U. (2015). Automated diagnosis of coronary artery disease using tunable-Q wavelet transform applied on heart rate signals. *Knowl. Based Syst.* 82, 1–10. doi: 10.1016/j.knosys.2015.02.011

Peng, C. K., Havlin, S., Hausdorff, J. M., Mietus, J. E., Stanley, H. E., and Goldberger, A. L. (1995). Fractal mechanisms and heart rate dynamics. Long-range correlations and their breakdown with disease. *J. Electrocardiol.* 28(Suppl.), 59–65. doi: 10.1016/s0022-0736(95)80017-4

Pincus, S. M. (1991). Approximate entropy as a measure of system complexity. *Proc. Natl. Acad. Sci. U.S.A.* 88, 2297–2301. doi: 10.1073/pnas.88.6.2297

Rajendra, A. U., Bhat, P. S., Kannathal, N., Rao, A., and Lim, C. M. (2005). Analysis of cardiac health using fractal dimension and wavelet transformation. *IRBM* 26, 133–139. doi: 10.1016/j.rbmret.2005.02.001

Rajendra Acharya, U., Vidya, K. S., Ghista, D. N., Lim, W. J. E., Molinari, F., and Sankaranarayanan, M. (2015). Computer-aided diagnosis of diabetic subjects by heart rate variability signals using discrete wavelet transform method. *Knowl. Based. Syst.* 81, 56–64. doi: 10.1016/j.knosys.2015.02.005

Román, J. A., San, Vilacosta, I., Castillo, J. A., Rollán, M. J., Hernández, M., et al. (1998). Selection of the optimal stress test for the diagnosis of coronary artery disease. *Heart* 80, 370. doi: 10.1136/hrt.80.4.370

Sridhar, C., Acharya, U. R., Fujita, H., and Bairy, G. M. (2017). "Automated diagnosis of coronary artery disease using nonlinear features extracted from ECG signals," in *Proceedings of the 2016 IEEE International Conference on Systems, Man, and Cybernetics (SMC)*, Budapest: IEEE.

Steinberg, D., and Gotto, A. M. (1999). Preventing coronary artery disease by lowering cholesterol levels: fifty years from bench to bedside. *JAMA* 282:2043. doi: 10.1001/jama.282.21.2043

Udhayakumar, R. K., Karmakar, C., Peng, L., and Palaniswami, M. (2016). "Influence of embedding dimension on distribution entropy in analyzing heart rate variability," in *Proceeding of the 2016 38th Annual International Conference of the IEEE Engineering in Medicine and Biology Society (EMBC)*, Orlando, FL: IEEE.

World Health, and Organization. (2015). Global status report on noncommunicable diseases 2014. *Women* 47, 2562–2563.

Xie, H., He, W., and Liu, H. (2008). Measuring time series regularity using nonlinear similarity-based sample entropy. *Phys. Lett. A* 372, 7140–7146. doi: 10.1016/j.physleta.2008.10.049

Yang, L., Peng, L., Karmakar, C., and Liu, C. (2015). ""Distribution entropy for short-term QT interval variability analysis: a comparison between the heart failure and normal control groups," in *Proceedings of the 2015 Computing in Cardiology Conference (CinC)*, Nice: IEEE.

Zhang, T., Chen, W., and Li, M. (2018). Fuzzy distribution entropy and its application in automated seizure detection technique. *Biomed. Signal Process. Control* 39, 360–377. doi: 10.1016/j.bspc.2017.08.013

Zhao, Z., and Ma, C. (2008). "An intelligent system for noninvasive diagnosis of coronary artery disease with EMD-TEO and BP neural network," in *Education Technology and Training & Geoscience and Remote Sensing*, Vol. 2 (Shanghai: IEEE), 631–635. doi: 10.1109/ETTandGRS.2008.361

Conflict of Interest Statement: The authors declare that the research was conducted in the absence of any commercial or financial relationships that could be construed as a potential conflict of interest.

frontiers in Physiology

ORIGINAL RESEARCH
published: 25 July 2019
doi: 10.3389/fphys.2019.00934

Detection of T Wave Peak for Serial Comparisons of JTp Interval

*Katerina Hnatkova[1], Jose Vicente[2], Lars Johannesen[2], Christine Garnett[2], David G. Strauss[3], Norman Stockbridge[2] and Marek Malik[1]**

[1] National Heart and Lung Institute, Imperial College London, London, United Kingdom, [2] Division of Cardiovascular and Renal Products, Office of New Drugs, Center for Drug Evaluation and Research, U.S. Food & Drug Administration, Silver Spring, MD, United States, [3] Division of Applied Regulatory Science, Office of Clinical Pharmacology, Office of Translational Sciences, Center for Drug Evaluation and Research, U.S. Food and Drug Administration, Silver Spring, MD, United States

Electrocardiogram (ECG) studies of drug-induced prolongation of the interval between the J point and the peak of the T wave (JTp interval) distinguished QT prolonging drugs that predominantly block the delayed potassium rectifier current from those affecting multiple cardiac repolarisation ion channel currents. Since the peak of the T wave depends on ECG lead, a "global" T peak requires to combine ECG leads into one-dimensional signal in which the T wave peak can be measured. This study aimed at finding the optimum one-dimensional representation of 12-lead ECGs for the most stable JTp measurements. Seven different one-dimensional representations were investigated including the vector magnitude of the orthogonal XYZ transformation, root mean square of all 12 ECG leads, and the vector magnitude of the 3 dominant orthogonal leads derived by singular value decomposition. All representations were applied to the median waveforms of 660,657 separate 10-s 12-lead ECGs taken from repeated day-time Holter recordings in 523 healthy subjects aged 33.5 ± 8.4 years (254 women). The JTp measurements were compared with the QT intervals and with the intervals between the J point and the median point of the area under the T wave one-dimensional representation (JT50 intervals) by means of calculating the residuals of the subject-specific curvilinear regression models relating the measured interval to the hysteresis-corrected RR interval of the underlying heart rate. The residuals of the regression models (equal to the intra-subject standard deviations of individually heart rate corrected intervals) expressed intra-subject stability of interval measurements. For both the JTp intervals and the JT50 intervals, the curvilinear regression residuals of measurements derived from the orthogonal XYZ representation were marginally but statistically significantly lower compared to the other representations. Using the XYZ representation, the residuals of the QT/RR, JTp/RR and JT50/RR regressions were 5.6 ± 1.1 ms, 7.2 ± 2.2 ms, and 4.9 ± 1.2 ms, respectively (all statistically significantly different; $p < 0.0001$). The study concludes that the orthogonal XYZ ECG representation might be proposed for future investigations of JTp and JT50 intervals. If the ability of classifying QT prolonging drugs is further confirmed for the JT50 interval, it might be appropriate to replace the JTp interval since with JT50 it appears more stable.

Keywords: JTp interval prolongation, T wave peak measurement, one-dimensional ECG representation, intra-subject stability of rate corrected ECG intervals, normal healthy subjects

OPEN ACCESS

Edited by:
Tobias Opthof, Academic Medical Center (AMC), Netherlands

Reviewed by:
Jan Kors, Erasmus University Medical Center, Netherlands
Ruben Coronel, University of Amsterdam, Netherlands

****Correspondence:***
Marek Malik
marek.malik@btinternet.com;
marek.malik@imperial.ac.uk

Specialty section:
This article was submitted to Cardiac Electrophysiology, a section of the journal Frontiers in Physiology

Received: *17 April 2019*
Accepted: *09 July 2019*
Published: *25 July 2019*

Citation:
Hnatkova K, Vicente J, Johannesen L, Garnett C, Strauss DG, Stockbridge N and Malik M (2019) Detection of T Wave Peak for Serial Comparisons of JTp Interval. Front. Physiol. 10:934. doi: 10.3389/fphys.2019.00934

INTRODUCTION

This article concerns different methodologies for the detection of the peak of the T wave in a 12-lead electrocardiogram (ECG) with the aim of serving serial comparisons of the J to T peak (JTp) interval. By this we mean situations when it needs to be investigated whether the JTp interval was changed during a certain intervention. As explained further, such situations emerge during pharmacologic investigations of repolarisation-active drugs. Nevertheless, other needs for serial JTp comparisons might also emerge, e.g., in physiologic studies of exposure to environmental changes, physical exhaustion, autonomically active provocations, etc. All such situations lead to the comparison of ECGs obtained before and after the intervention. Since the investigated intervention might also change heart rate, stability of the JTp relationship to underlying heart rate is needed which, in turn, might depend of the method for the T peak detection.

Superficially, it might seem that T wave peak is easier to measure compared to the end of the T wave. Nevertheless, this belief is not justified, especially if considering the need for serial comparisons of JTp intervals in ECGs recorded under different conditions. While in physiologic ECGs that do not show any repolarisation abnormality, the end of the T wave is the same in different ECG leads (apart from those leads in which the terminal part of the T wave is projected onto the isoelectric line) (Malik, 2004), T wave peak is determined by lead-specific projection of the vectorcardiographic T wave loop and frequently differs lead to lead (Malik et al., 2018). Moreover, in serial comparisons, constant orientation of the heart in the thorax and thus the same projection of the T wave loop cannot be expected. Therefore, morphological information of different ECG leads need to be combined into a signal matrix that reasonably represents the T wave loop and that allows reproducible and stable detection of the T peak.

Importance in Pharmacological Investigations

The drug-induced QTc interval prolongation is caused by all pharmaceutical compounds that lead to proarrhythmia due to the induction of Torsade de Pointes tachycardia (Fenichel et al., 2004). Therefore, the testing of drug-induced QTc changes belongs to regulatory evaluation of all new pharmaceuticals (Guidance to industry, 2005). However, while the test of torsadogenic toxicity based on QTc prolongation has high sensitivity (i.e., drugs causing Torsade de Pointes also prolong the QTc interval) its specificity is not so high (i.e., not all QTc prolonging drugs are proarrhythmic) (Fenichel et al., 2004).

For this reason, different paradigms of proarrhythmic drug testing are presently being discussed (Vicente et al., 2016, 2018; Strauss et al., 2018). These include classification of drugs along their actions on myocardial ion channels. Among others, differentiation is needed between drugs that cause QTc interval prolongation by predominantly blocking the delayed potassium rectifier current (IKr) and drugs for which the IKr blockade is mitigated by effects on inward currents active during myocardial repolarisation.

In ECG studies of drugs with known effects on myocardial ion channels, it has been observed that drugs that prolong the QT interval in the terminal part of the T wave, i.e., between the peak and the end of the T wave, affect multiple ionic channels whilst drugs that are predominant IKr blockers prolong also the interval between the end of the QRS complex (i.e., the J point) and the peak of the T wave (Johannesen et al., 2014, 2016b; Vicente et al., 2016). This leads to the suggestion that drugs that are found to prolong the QT interval should have their effects on the JTp interval also determined.

Study Design

Based on these considerations, the present study considered several different signal matrices of combination of ECG leads with the aim of determining a matrix that would lead to JTp interval measurements most stable for the purposes of serial comparisons. In practice, serial comparisons are, as already stated, bound to lead to evaluations of ECGs with different underlying heart rate. Therefore, the stability of the measurements was judged by the tightness of the JTp/heart rate relationship. To investigate signal matrices used in the determination of T wave peak, the study used long-term ECG recordings of a large population of healthy subjects. The comparison of the matrices was based on the intra-subject variability of individually heart rate corrected JTp intervals. For serial comparisons of JTp intervals, this intra-subject variability needs to be minimized for the same reasons as the intra-subject variability of QTc intervals needs to be minimized for successful serial comparisons of heart rate corrected QT intervals (Garnett et al., 2012).

Previously, it was also observed that similar distinction between predominant IKr blockers and multichannel blockers was also possible based on the interval between the J point and the center-point of T wave area (Vicente et al., 2017). Therefore, in addition to the JTp intervals, this study also investigated these intervals.

MATERIALS AND METHODS

Population

The available data originated from two clinical pharmacology studies conducted in healthy subjects. Repeated 12-lead day-time Holter recordings were made in all study subjects while they were on no treatment and free of alcohol and/or caffeinated drinks ingestion. All subjects had a normal screening ECG and normal clinical investigation usual in clinical pharmacology studies (ICH Guideline, 2001).

Electrocardiographic Recordings

The 12-lead Holter recordings were obtained using SEER MC (GE Healthcare, Milwaukee, WI, United States) or H12 (Mortara Instrument, Milwaukee, WI, United States) recorders, both using Mason-Likar electrode positions. Using previously

described procedures (Malik et al., 2008a, 2012), multiple ECG interval measurements were made in the day-time portion of each 12-lead Holter recording. The measurements used representative morphologies derived from 10-s portions of the Holter recordings and were sampled at 1000 Hz. J point was defined as the global QRS offset, i.e., the latest QRS offset in any of the 12 leads. Likewise, QRS onset (Q point) was defined as the earliest QRS onset and T wave end as the latest T wave offset in all 12 leads. Both points were determined based on the superimposition of representative morphologies of all 12-leads superimposed on the same isoelectric axis.

In more detail (Malik et al., 2008a, 2012), the continuous 12-lead Holters were divided into 10-s segments. In each segment and each ECG lead, baseline wander was removed, and representative complex constructed by sample-by-sample medians of superimposed P-QRS-T morphological patterns of different beats. Using a combination of threshold, tangent, and pattern recognition algorithms, an automatic identification of the Q, J, and T offset points was made. In each 10-s ECG segment, these measurement points were visually checked and, where necessary, manually corrected by two independently working cardiologists. In case of their disagreement, the measurement point positions were reconciled by a senior cardiologist.

Subsequently, in each subject, published pattern matching algorithms (Hnatkova et al., 2009) were also used to ensure that similar morphologies of the QRS and T wave offset were measured similarly. As previously described (Malik et al., 2012), multiple measurements were made in each recording using ECG samples preceded by both stable and variable heart rates. The measurements were made when the subjects were supine and also during free daily activity and during postural provocations. This leads to substantial heart rate spans in each subject.

For each ECG measurement, a 5-min history of RR intervals preceding the J point and T end measurements was also obtained.

T Wave Signal Representations

As explained, to determine the T wave peak position reasonably applicable to different ECG leads, a one-dimensional representation of T wave is needed so that it can subsequently be used for the peak detection. Individual ECG leads can also be used for the peak detection, but since each lead projects the vectorcardiographic T wave loop from a different direction, individual ECG leads are not representative of complete myocardial mass.

To investigate possibilities of one-dimensional T wave representation, the following seven matrices were investigated:

1. **XYZ:** The conceptually simplest way of reconstructing the T wave loop is by obtaining orthogonal ECG system. Hence, orthogonal XYZ representation of the ECG was obtained by previously published transformation that was optimized for recordings with Mason-Likar electrode positions (Guldenring et al., 2015). That is, at each sample of the original ECG between the J point and T end, algebraically independent leads $E_{1,8} = \{I, II, V_1, V_2, \cdots, V_6\}$ were multiplied by a transformation matrix $T_{8,3}$, obtaining a set of three orthogonal leads $O_{1,3} = E \times T = \{X, Y, Z\}$. Using these, the orthogonal vector magnitude was obtained and used as the one-dimensional ECG representation. That is:

$$\varepsilon_{\mathbf{XYZ}} = \left(X^2 + Y^2 + Z^2\right)^{1/2}$$

2. **RMS:** Other possibility of combining different ECG leads into a unidimensional representation is by studying their distribution. All 12 leads were thus combined by calculating their root mean square, that is, at each sample of the original ECG, the one-dimensional characteristic was obtained as:

$$\varepsilon_{\mathbf{RMS}} = \left(\frac{1}{12}\sum\nolimits_{L\in\{I,II,III,aVR,aVL,aVF,V_1\cdots,V_6\}} L^2\right)^{1/2}$$

3. **RMS(8):** Of the 12 ECG leads, 4 leads (i.e., leads III, aVR, aVL, and aVF) are not independent and only algebraically derived from leads I and II. Therefore, the root mean square calculation of all 12 leads is potentially biased toward the signal of limb leads I and II. Therefore, the approach of root mean square was separately evaluated using only the 8 algebraically independent leads; that is:

$$\varepsilon_{\mathbf{RMS(8)}} = \left(\frac{1}{8}\sum\nolimits_{L\in\{I,II,V_1\cdots,V_6\}} L^2\right)^{1/2}$$

4. **Quasi-orthogonal:** Repeated discussions (Cortez et al., 2014; Ray et al., 2017) suggested that instead of orthogonal algebraic reconstruction, vectorcardiographic loops might be obtained from standard ECG leads oriented in approximately perpendicular directions. Therefore, instead of the orthogonal XYZ leads obtained from the transformation, vector magnitude was calculated using the quasi-orthogonal leads II, V_2, and V_5, that is:

$$\varepsilon_{\mathbf{Quasi\text{-}orthogonal}} = (II^2 + V_2^2 + V_5^2)^{1/2}$$

5. **Precordial:** To incorporate the suggestion that the distinction between the T wave upslope and downslope concerns mainly the left precordial leads, vector magnitude was calculated from leads V4, V5, and V6, i.e.,

$$\varepsilon_{\mathbf{Precordial}} = \left(V_4^2 + V_5^2 + V_6^2\right)^{1/2}$$

6. **SVD(QT):** Orthogonal XYZ reconstruction by a fixed transformation assumes the same relationship between the standard 12-leads and the XYZ leads in different subjects which seems rather unlikely. Therefore, singular value decomposition was applied to the matrix of the 8 algebraically independent leads between the QRS onset and T end (Acar and Köymen, 1999). For a given ECG pattern, this provided optimized orientation of an orthogonal system of derived leads S_i^{QT}, $i = 1, 2, \cdots, 8$. Subsequently, vector magnitude was calculated from the three most dominant derived leads, i.e.,

$$\varepsilon_{\mathbf{SVD(QT)}} = ((S_1^{QT})^2 + (S_2^{QT})^2 + (S_3^{QT})^2)^{1/2}$$

7. **SVD(JT):** Since the singular value decomposition of the complete QT interval is substantially influenced by the power distribution within the QRS complex (Acar and Köymen, 1999), the same procedure was repeated by applying the decomposition only to the interval between the J point and the T wave offset.

$$\varepsilon_{\mathbf{SVD(JT)}} = ((S_1^{JT})^2 + (S_2^{JT})^2 + (S_3^{JT})^2)^{1/2}$$

T Peak and T Median Measurements

In each ECG, each of the seven characteristics $\varepsilon_{\blacksquare}$ (ranging from $\varepsilon_{\mathbf{RMS}}$ to $\varepsilon_{\mathbf{SVD(JT)}}$) was processed, between the J point and T end point, by the previously published algorithm to detect the peak of the T wave (Johannesen et al., 2016a). This resulted in seven different estimates of the JTp interval.

Subsequently, the area under each of the $\varepsilon_{\blacksquare}$ characteristic between the J point and the T end point was divided into two halves with identical areas (Hnatkova et al., 2017; Vicente et al., 2017). That is, the T wave "median" point T50 was found for which $\int_J^{T50} \varepsilon_{\blacksquare}(t)\mathrm{d}t = \int_{T50}^{Tend} \varepsilon_{\blacksquare}(t)\mathrm{d}t$. This resulted in seven different estimates of the JT50 interval (**Figure 1**).

Heart Rate Correction

For each estimate of JTp and JT50 intervals and for each study subject, all the measurements made in the given subject were related to the underlying heart rate using the previously published curvilinear regression model (Malik et al., 2013):

$$\Im_i = \alpha + \frac{\delta}{\gamma}(\overline{RR_i}^{\gamma} - 1) + \epsilon_i$$

where $\Im_i$ are the JTp or JT50 measurements in seconds, α is a central value of the measurement at underlying heart rate of 60 beats per minute, δ and γ are the slope and the curvature of the model, ϵ_i are zero-centered normally distributed errors, and $\overline{RR_i}$ are hysteresis corrected RR intervals (in seconds) representative of the underlying heart rate. The hysteresis correction of the underlying RR intervals was calculated using the exponential decay model (Malik et al., 2008b) that uses a subject-specific decay time constant λ which represents the time delay of achieving 95% of the adaptation after a heart rate change (Malik et al., 2016). The parameter λ was optimized for each type of interval measurement and for each subject so that the standard deviation of the residual errors ϵ_i was the smallest among all possibilities of λ values.

The same approach was used to obtain subject-specific relationship of the QT and JT intervals to the underlying heart rate.

Stability and Intra-Subject Reproducibility

When the curvilinear regression model is used to correct the measured ECG intervals for the underlying heart rate, the standard deviation of the errors ϵ_i represent the regression residual, i.e., the standard deviation of rate-corrected intervals (Malik et al., 2008b).

Since the study used only drug-uninfluenced ECG recordings, the regression residuals are a valid estimate of intra-subject reproducibility of rate corrected intervals used in serial comparisons. Therefore, the comparison of the seven different ECG matrices (and comparison between JTp and JT50 intervals) was based on the value of the curvilinear regression residuals. In other words, to find the most stable JTp and JT50 expressions, this investigation aimed at identifying the ECG matrix that led to the lowest regression residuals among the seven possibilities.

Statistics

Differences between JTp and JT50 intervals obtained from the different ECG matrices were displayed using density plots. The differences between the residuals of the curvilinear JTp/RR and JT50/RR regression were displayed by means of Bland-Altman plots, and their significances were evaluated by paired *t*-test. Paired *t*-test was also used to compare the residuals of JTp/RR and JT50/RR regressions with the residuals of QT/RR and JT/RR regressions, as well as to compare the corresponding hysteresis time constants and the slope and curvature parameters of the curvilinear regressions.

Data are presented as mean ± standard deviation. In addition to the total study population, separate evaluation was made for female and male subjects. Nevertheless, the principal outcome of the study, i.e., the identification of the optimal ECG matrix, was made based on the complete study population. A *p*-value below 0.05 was considered statistically significant without adjustment for multiplicity.

RESULTS

Population

Holter ECG recordings were obtained in 523 healthy subjects aged 33.5 ± 8.4 years (range 18.1–55.4 years). Of these, 254 (48.6%) were females. A total of 236 (45.1%) and 259 (49.5%) study subjects identified themselves as of Black/African origin or White/Caucasians, respectively. The remainder classified themselves as Asian, Polar region natives, or "Other" race.

ECG Data

In the Holter recordings, altogether 660,657 ECG measurements of the J point to T end intervals were made. Of these, technical suitability check based on objective noise assessment (Batchvarov et al., 2002) excluded 3,523 ECGs (0.53%) that were too noise-polluted for reasonable T peak assessment. The remaining 657,134 measurements were accepted for the data analyses. On average, there were 1,256 ± 220 accepted ECG measurements per subject (inter-quartile range 1,058–1,436).

Measurement Comparisons

Not surprisingly, while some large discrepancies of the JTp and JT50 measurements existed among different ECG matrices in noise-polluted ECGs, the overall numerical differences among different matrices were modest, mostly less than 10 milliseconds (**Figures 2**, **3**). The largest differences were found between the measurements based on the precordial matrix and the other possibilities.

The difference between the JTp and JT50 measurements was more substantial. As shown in **Figure 4**, the JTp–JT50 showed

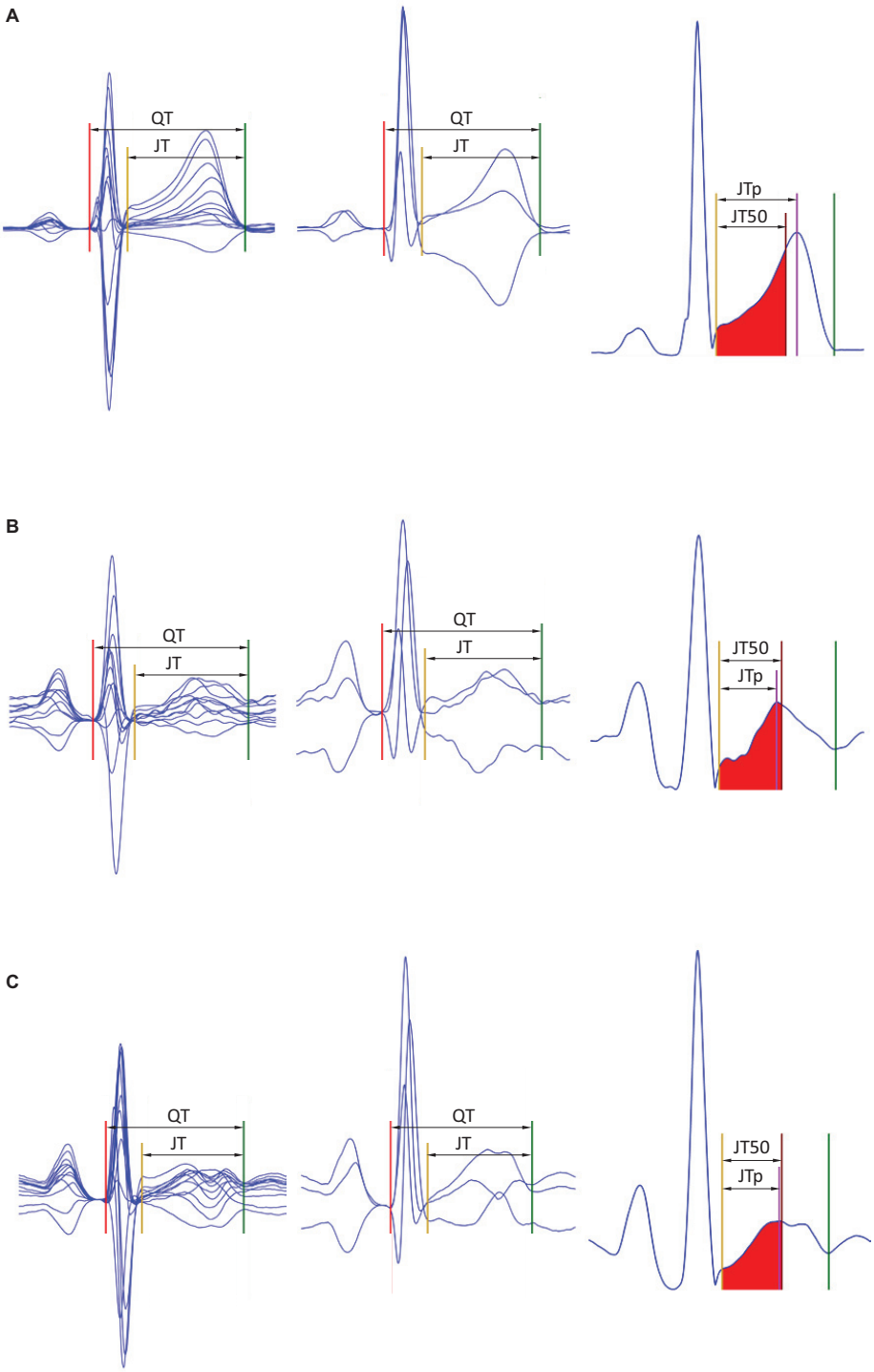

FIGURE 1 | Examples of the JTp and JT50 measurements. The rows **(A–C)** of to three different ECG recordings made in a male (32 years), female (22 years), and female (42 years), respectively. The underlying heart rates were 68, 95, and 96 beats per minute, respectively. In the left panels, representative P-QRS-T complexes are shown for all 12 leads superimposed on the same isoelectric axis, the middle panels show derived orthogonal XYZ leads also on the same isoelectric axis, and the right panels show the vector magnitude of the orthogonal XYZ leads. The horizontal (time) scale of all the panels is the same. The red, yellow, and green lines show the positions of the QRS onset, QRS offset, and T offset points. In the left panels, the violet line shows the T wave peak while the red-filled area (between the yellow and brown lines) is the first middle of the area under the T wave representation (i.e., the brown line divides the area under the T wave between the yellow and green lines into two equal halves). Measurements of the JTp and JT50 intervals are shown in the left panels. Note that JTp > JT50 in panel **(A)** while JTp < JT50 in panels **(B,C)** albeit the difference between JTp and JT50 is minimal in panel **(C)**. Note also that in all three cases, the position of the peak of the T wave is different in different 12 leads as well as in different orthogonal leads.

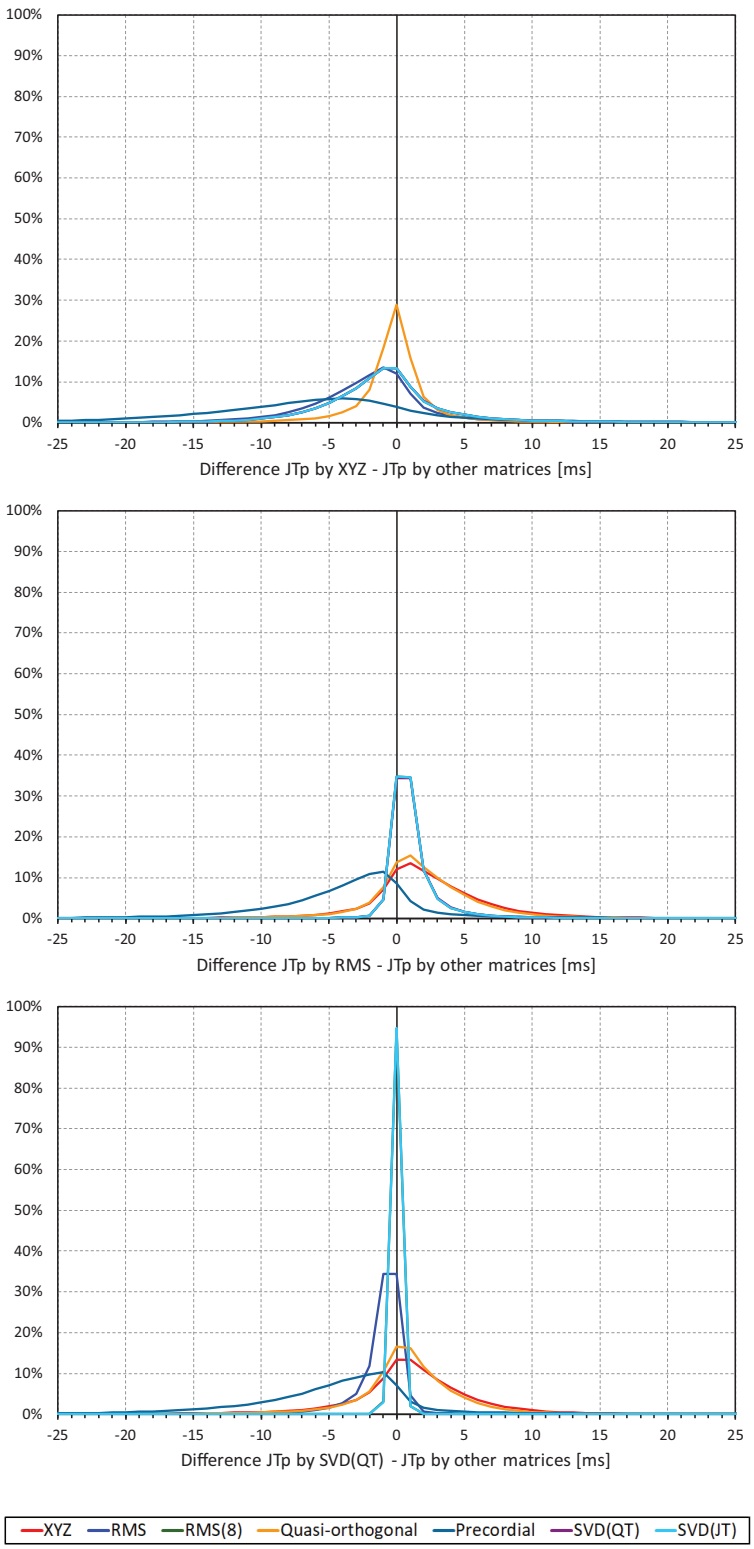

FIGURE 2 | Sample density distributions of the differences between JTp intervals measured based on different one-dimensional matrices in all ECG samples. The top, middle, and bottom panels show the differences between JTp intervals measured based on all other matrices and the measurements based on the XYZ, RMS, and SVD(QT) matrix, respectively. The graphs were constructed using 1 ms bins. Note that in some cases, the lines were superimposed and that some of the graphs might be hidden bellow others – e.g., within the precision of the graphics, the results of RMS(8) were practically identical to those of SVD(JT) which is shown on the top.

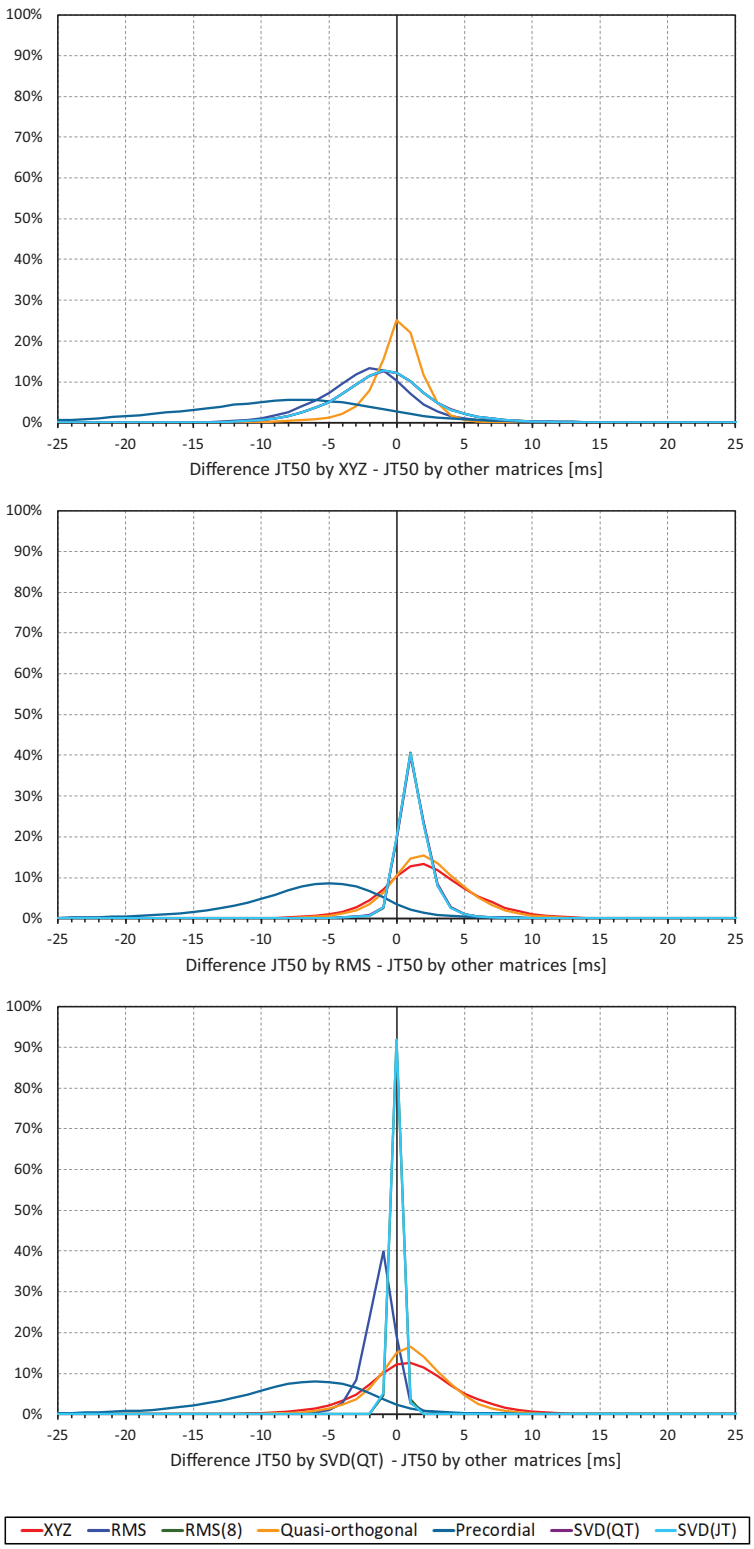

FIGURE 3 | Sample density distributions of the differences between JT50 intervals measured based on different one-dimensional matrices in all ECG samples. The top, middle, and bottom panels show the differences between JT50 intervals measured based on all other matrices and the measurement based on the XYZ, RMS, and SVD(QT) matrix, respectively. The graphs were constructed using 1 ms bins. Note that in some cases, the lines were superimposed and that some of the graphs might be hidden bellow others – e.g., within the precision of the graphics, the results of RMS(8) were practically identical to those of SVD(JT) which is shown on the top.

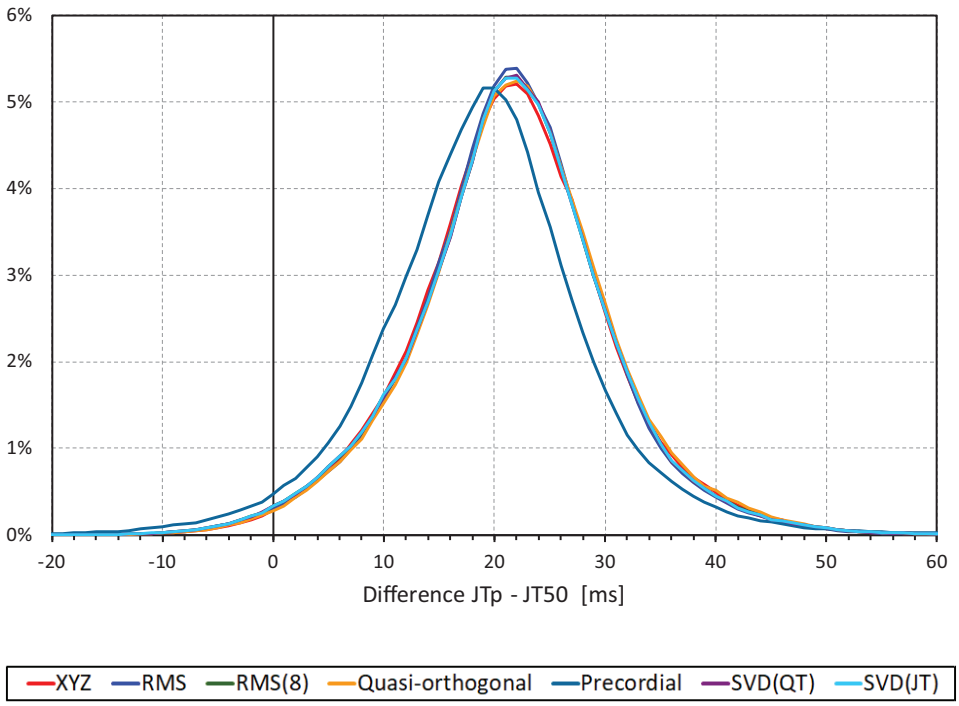

FIGURE 4 | Sample density distributions of the differences between JTp and JT50 intervals measured based on different one-dimensional matrices in all ECG samples. The graphs were constructed using 1 ms bins. Note that in some cases, the lines were superimposed and that some of the graphs might be hidden bellow others – e.g., within the precision of the graphics, the results of RMS(8) were practically identical to those of SVD(JT) which is shown on the top.

a mode slightly above 20 ms for all methods with the exception of the precordial matrix for which the mode was slightly below 20 ms. More importantly, **Figure 5** shows that the JTp–JT50 difference was not without bias. At fast heart rates (when both JTp and JT50 were short), T peak occasionally preceded the T median while at slower heart rates, the relationship was systematically reversed.

Regression Residuals of the Curvilinear Models

Figures 6, **7** show Bland-Altman plots comparing the curvilinear regression of JTp and JT50 measurements based on the XYZ matrix with the interval measurements based on selected other ECG matrices. In all the cases shown in these figures, the measurements based on XYZ ECG representation fitted the curvilinear regression models to heart rate more tightly compared to the other matrices. As shown in **Table 1** and summarized in **Figure 8**, XYZ representation led to higher stability of heart rate dependency of both JTp and JT50 measurements in comparison to all other investigated possibilities.

Although statistically significant, the differences among the JTp regression residuals (and similarly between the JT50 regression residuals) of different ECG matrices were small. This is also demonstrated in **Figure 9** that shows the cumulative distributions of the regression residuals in study subjects.

More importantly, however, the regression residuals of JT50 intervals were non-trivially smaller compared to those of JTp intervals. For all ECG matrices, the differences among the JT50 and JTp residuals shown in **Table 1** were highly statistically significant ($p < 0.0001$ in all cases). This suggests that the measurement of the median point of T wave area was systematically made in a more stable and reproducible way than that of the peak of the T wave.

While the interval measurements based on the XYZ matrix were, in terms of the regression to the underlying heart rate, the most stable in the overall population, this was not necessarily the case in all study subjects considered separately. **Figure 10** shows the distribution of ECG matrices that showed the lowest curvilinear regression residuals in individual subjects. The XYZ ECG matrix led to the lowest residuals of the JTp and JT50 intervals in 191 (36.5%) and 264 (50.5%) subjects, respectively. For the RMS matrix, the corresponding numbers were 132 (25.2%) and 93 (17.8%) subjects while for the Quasi-orthogonal matrix, the numbers were 82 (15.7%) and 96 (18.4%) subjects.

Comparison With QT and JT Intervals

The residuals of the curvilinear regressions between the QT and JT intervals and RR intervals of the underlying heart rate were 5.6 ± 1.1 ms and 5.6 ± 1.2 ms, respectively (no statistical difference between the residuals of the QT and JT intervals).

The residuals of JTp intervals based on the XYZ ECG matrix (see **Table 1**) were statistically significantly larger than those of

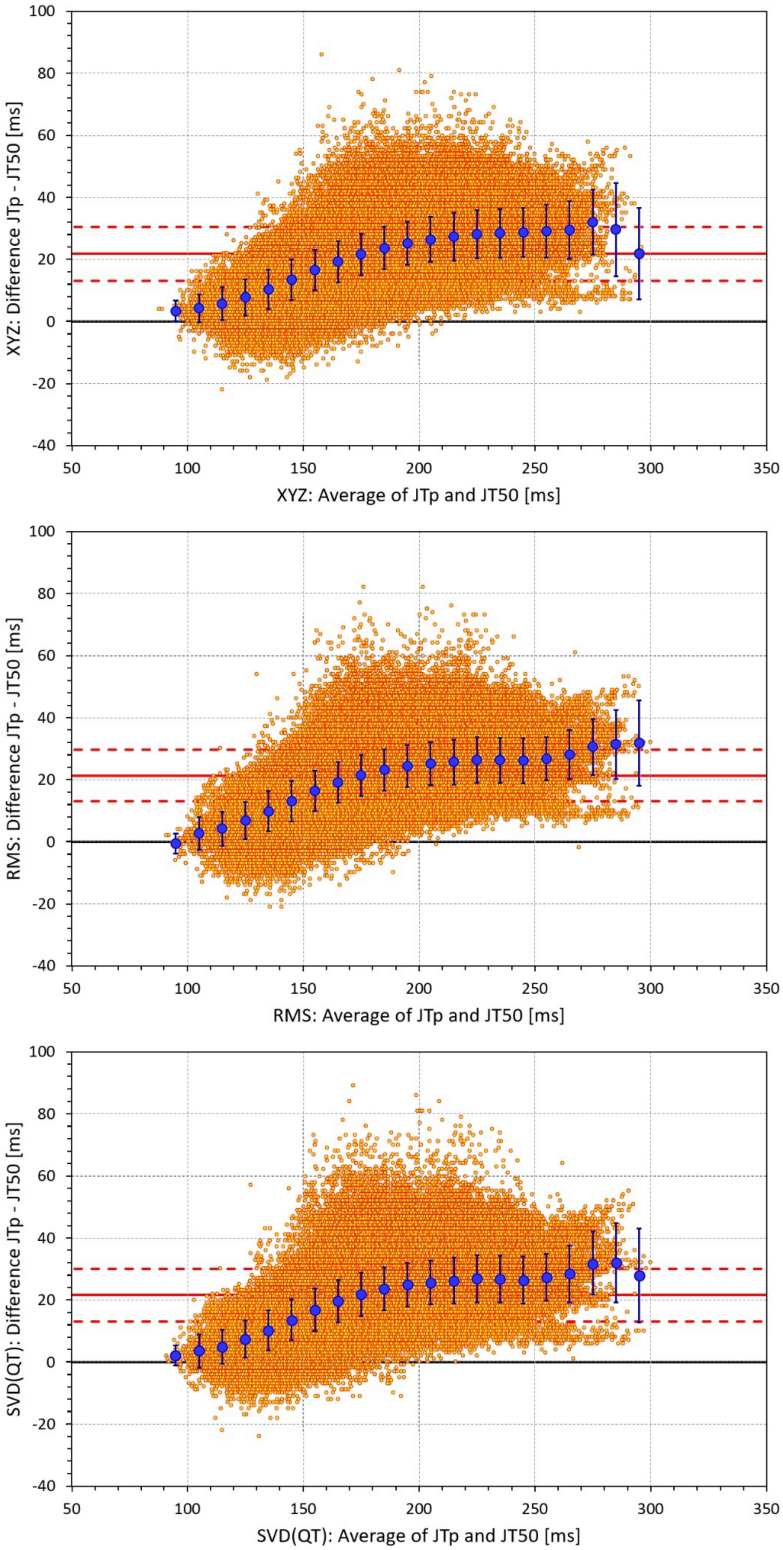

FIGURE 5 | Bland-Altman plots of the individual differences between JTp and JT50 intervals based on XYZ matrix (top panel), RMS matrix (middle panel), and SVD(QT) matrix (bottom panel). In each panel, the bold red line shows the mean difference, the dashed red lines show the mean ± standard deviation. In each panel, the large blue marks show the means of the JTp – JT50 differences in 10-millisecond bins of the JTp and JT50 averages (from 90–100 ms to 290–300 ms); the blue error bars are the standard deviations of the JTp – JT50 differences in these bins.

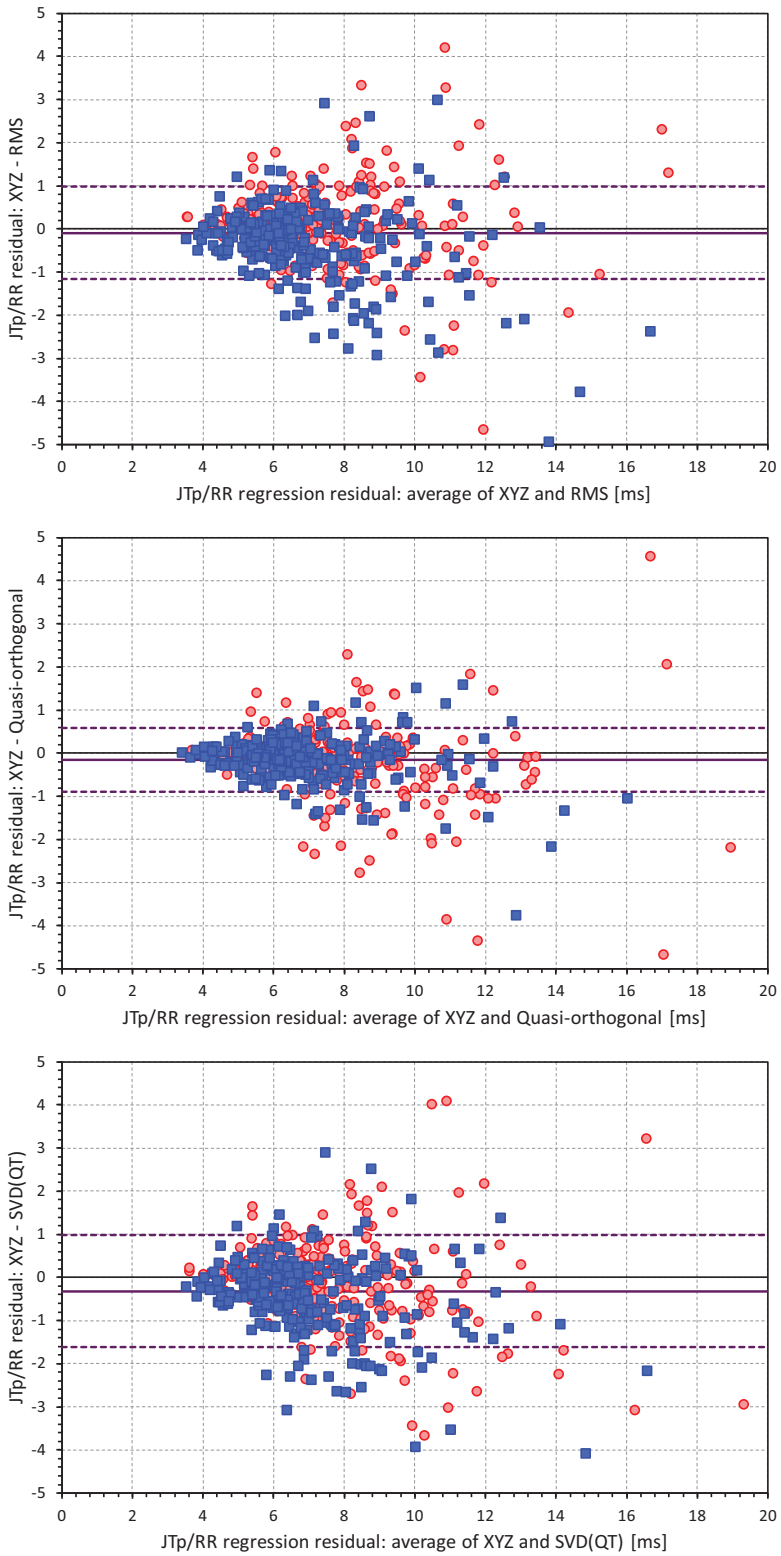

FIGURE 6 | Bland-Altman plots of the differences between curvilinear JTp/RR regression residuals in individual study subjects. The top, middle, and bottom panels show the differences for JTp interval based on XYZ and RMS matrices, XYZ and Quasi-orthogonal matrices, and XYZ and SVD(QT) matrices, respectively. In each panel, the red circles and blue squares show female and male subjects, the bold violet line shows the mean difference and the dashed violet lines show the mean ± standard deviation of the differences.

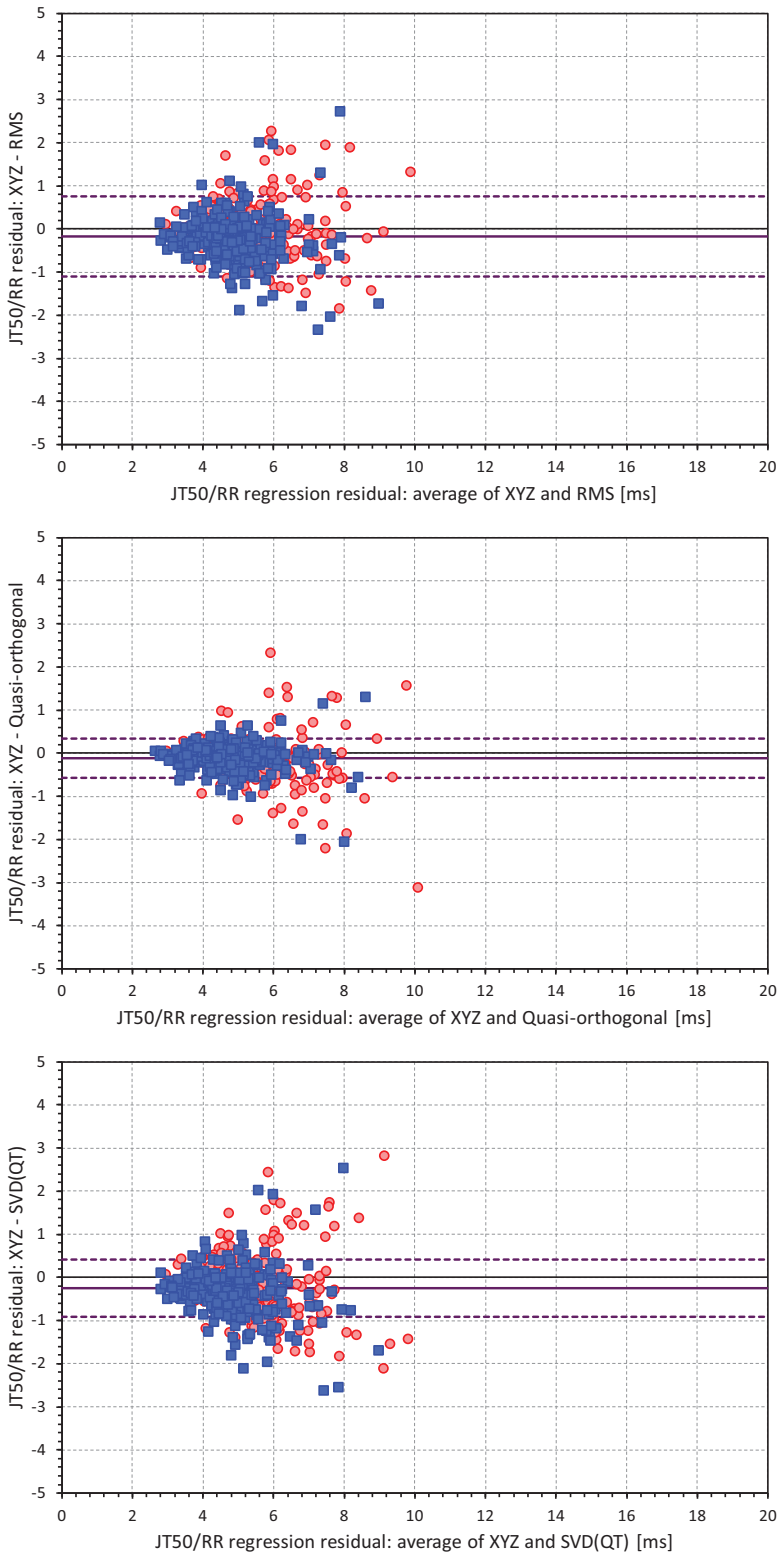

FIGURE 7 | Bland-Altman plots of the differences between curvilinear JT50/RR regression residuals in individual study subjects. The top, middle, and bottom panels show the differences for JT50 interval based on XYZ and RMS matrices, XYZ and Quasi-orthogonal matrices, and XYZ and SVD(QT) matrices, respectively. In each panel, the red circles and blue squares show female and male subjects, the bold violet line shows the mean difference and the dashed violet lines show the mean ± standard deviation of the differences. Compare with **Figure 6** and note the difference in the spread of the data.

TABLE 1 | Curvilinear regression residuals.

Matrix	JTp		JT50	
	Residual (ms)	*p*-value vs. XYZ	Residual (ms)	*p*-value vs. XYZ
XYZ	7.237 ± 2.190		4.940 ± 1.167	
RMS	7.325 ± 2.262	0.0299	5.116 ± 1.357	<0.0001
RMS(8)	7.510 ± 2.402	<0.0001	5.174 ± 1.221	<0.0001
Quasi-orthogonal	7.394 ± 2.344	<0.0001	5.056 ± 1.247	<0.0001
Precordial	8.963 ± 3.775	<0.0001	6.249 ± 2.067	<0.0001
SVD(QT)	7.555 ± 2.491	<0.0001	5.196 ± 1.232	<0.0001
SVD(JT)	7.510 ± 2.401	<0.0001	5.179 ± 1.223	<0.0001

For different ECG matrices, the table shows mean ± standard deviation of the within-subject curvilinear JTp/RR and JT50/RR regression residuals. P-values are shown for the paired comparisons with the residuals of the XYZ matrix. Note that for all matrices, the paired comparisons between the JTp/RR and JT50/RR residuals were highly statistically significant ($p < 0.0001$ for all).

QT and JT intervals. On the contrary, the residuals of JT50 intervals were statistically significantly smaller than those of QT and JT intervals ($p < 0.0001$ for all these comparisons).

The curvilinear slopes (parameters δ of the regression) of the QT, JT, JTp, and JT50 intervals (XYZ matrix) were 0.150 ± 0.029, 0.149 ± 0.030, 0.145 ± 0.070, and 0.121 ± 0.046, respectively. There were no statistical differences among the QT, JT and JTp slopes, but the curvilinear regressions of the JT50 intervals were statistically significantly less steep that those of the other intervals ($p < 0.0001$ for all comparisons).

Differences also existed in the curvatures (parameters γ) of the curvilinear regressions. For the QT, JT, JTp, and JT50 intervals (XYZ matrix) these were 0.72 ± 0.69, 0.71 ± 0.66, 0.52 ± 1.04, and 1.00 ± 1.10, respectively. While the JTp/RR regressions were more curved than all others, the JT50 regressions were less curved than all others and, on average, very close to simple linear regressions ($p < 0.0001$ for all comparisons).

Finally, differences existed in the hysteresis time constants λ, i.e., the delays needed for the intervals to achieve 95% adaptation after a heart rate change. For the QT, JT, JTp and JT50 intervals (XYZ matrix) these were 116.0 ± 21.5, 121.5 ± 23.2, 134.3 ± 32.0, and 105.2 ± 25.0 s, respectively. All their comparisons were statistically significant ($p < 0.0001$ for all), meaning that the JT and JTp intervals adapted more slowly than the QT interval while the adaptation of the JT50 interval was faster compared to the QT interval.

DISCUSSION

The study leads to several conclusions of methodological importance. There were only numerically tiny differences among the JTp and among the JT50 intervals measured using different one-dimensional ECG matrices. The XYZ matrix (Guldenring et al., 2015) that was found to have the lowest regression residuals is easily applicable to all 12-lead ECGs recorded with Mason-Likar electrode positions. Since Mason-Likar configuration is the standard for long-term ECG recordings that are presently used in the majority of pharmaceutical studies, the XYZ matrix may be proposed for future studies of JTp and JT50 intervals. Incidentally, the XYZ matrix was also used in the seminal study that confirmed the importance of JTp interval investigations for the classification of QT prolonging drugs (Johannesen et al., 2016a; Vicente et al., 2016).

This observation of only small differences and of the XYZ matrix preference is potentially surprising. When designing the study, we expected to find the residuals of the individually optimized matrices, i.e., the SVD(QT) or SVD(JT) expression, to suppress the variability of the "universal" expressions substantially. This was not the case probably because singular value decomposition optimizes the rectangular projection for individual ECG samples (Acar and Köymen, 1999) which means that the ECG lead transformations are unlikely constant for all ECGs of the same subject. The within-subject variability of the transformations will lead to unfavorable results compared to a "universal" transformation such as that of the XYZ matrix.

The present study also observed that compared to JTp intervals, the JT50 intervals lead to substantially lower residuals of their intra-subject relationship to heart rate. This is in agreement with the previous observations that also found reduction in data variability when using JT50 intervals (Vicente et al., 2017). Hence, if the importance of JT50 interval for the classification of QT prolonging drugs (Vicente et al., 2017) is confirmed in future studies, the use of this interval would become preferable instead of the JTp interval because of the lower measurement variability. As already explained, the residuals of the intra-subject regression to the underlying RR intervals equal to the standard deviation of individually heart rate corrected intervals. If similar reduction in the variability as we have observed is also found for the variability of placebo-to-baseline differences, power sample calculations would clearly prefer the use of JT50 rather than JTp intervals (Malik et al., 2004; Zhang and Machado, 2008).

In some cases (e.g., all ECGs shown in **Figure 1**), the value of the one-dimensional ECG representation at the J and T offset points is greater than 0. We have therefore also investigated the possibility of measuring the point of the middle of the area between the T wave and the line connecting the ECG representation value at the J and T offset points (leading to JT50' measurements). While the JT50'/RR residuals (results not shown) were still significantly lower than the JTp/RR residuals, they were also significantly larger than the JT50/RR residuals that we present.

In addition to drug-classification studies, JTp interval was also shown to carry prognostic mortality information (O'Neal et al., 2017). It would be interesting to investigate whether similar prognostic information can be obtained using the JT50 interval.

The curvilinear regression residuals, i.e., the heart-rate independent variability, of the JTp intervals were larger than those of the QT intervals. This means that measurement of the T peak is less stable than the measurement of the end of the T wave. While this might be somewhat counterintuitive, it corresponds to the experience of T wave pattern variability due to respiration, meal intake, and other processes that influence the position of the heart within the thorax. On the contrary,

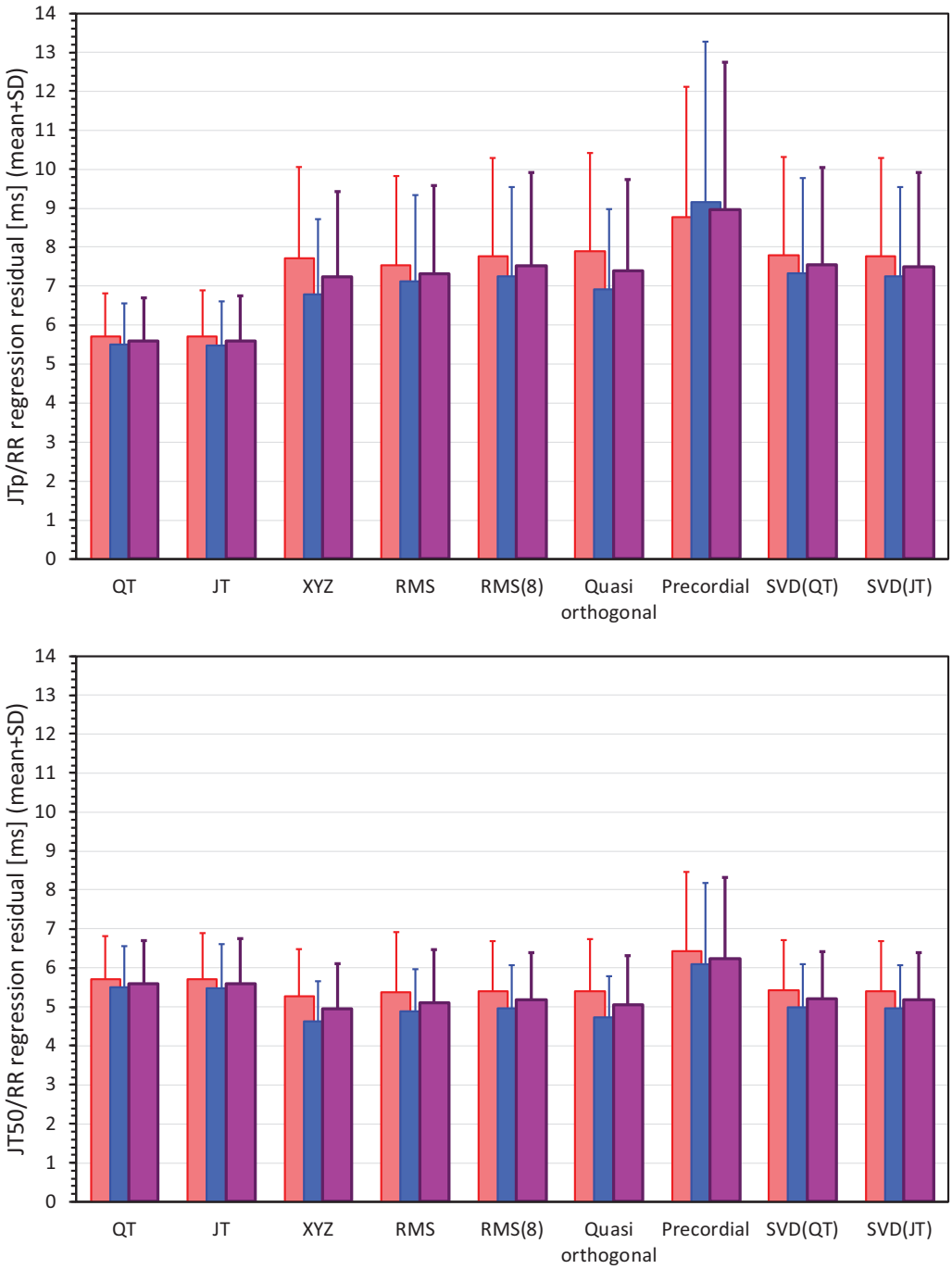

FIGURE 8 | Statistical summaries of the curvilinear JTp/RR (top panel) and JT50/RR (bottom panel) regression residuals for the interval measurements based on different one-dimensional ECG matrices. For comparison, the residuals of the QT/RR and JT/RR regressions are also shown in both panels. The red, blue, and violet bars show the mean values in female, males, and the complete study population, respectively. The errors bars show the corresponding standard deviations.

the residuals of the JT50 intervals were lower than those of the QT interval. This is not surprising since the median point of the area under the one-dimensional representation is little influenced by imprecision at the J point or at the end of the T wave since the voltages are generally rather low at these points.

The increased curvature of the JTp/RR patterns compared to the QT/RR and JT50/RR patterns likely relates to the shifts toward more symmetrical T waves at faster heart rates. The JT50/RR patterns were, on average, practically linear, i.e., less curved compared to the QT/RR patterns. While this, together with the shallower curvilinear slopes, might also be related to the

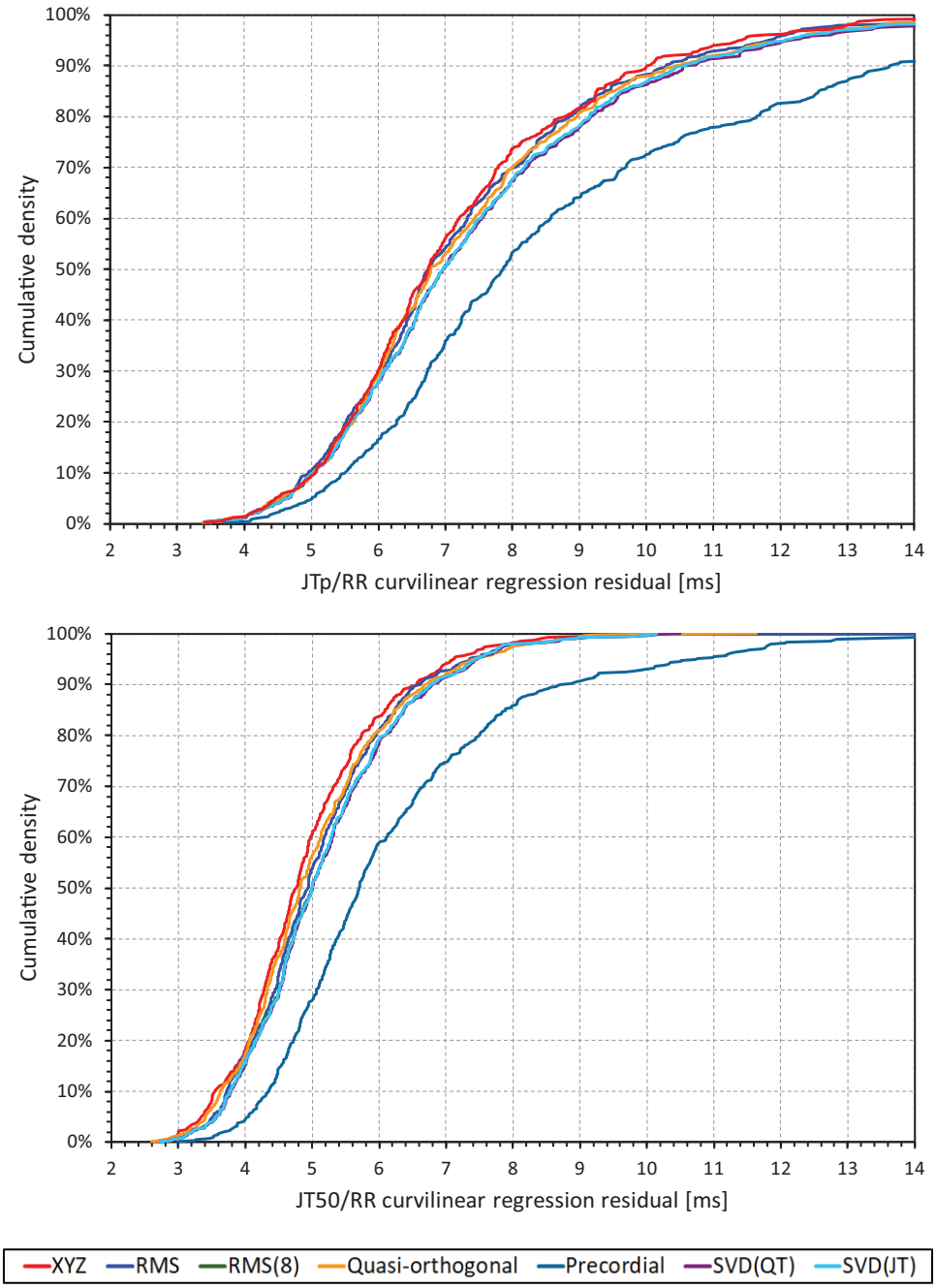

FIGURE 9 | Cumulative sample distributions of the within-subject curvilinear residuals the JTp/RR (top panel) and JT50/RR (bottom panel) regressions superimposed for different ECG matrices. Note that while the red line of the XYZ matrix is on the left side of the other distributions, the differences are not particularly large (apart from the precordial matrix). Note that in some cases, the lines were superimposed and that some of the graphs might be hidden bellow others – e.g., within the precision of the graphics, the results of RMS(8) were practically identical to those of SVD(JT) which is shown on the top.

shifts in the T wave patterns, it needs to be noted that the standard deviation of the curvatures over the investigated population was large and that the population mean values might potentially be misleading in individual cases.

Finally, while the study found statistically significant differences among the RR-interval hysteresis time constants, the numerical differences were small and only little different from 2 min. Hence, unless dealing with situations of substantial and very abrupt heart rate changes [e.g., those seen after administration of some contrast agents (Malik et al., 2009)] the previously proposed universal model of RR-interval hysteresis with the 2-min time constant (Malik et al., 2016) will likely

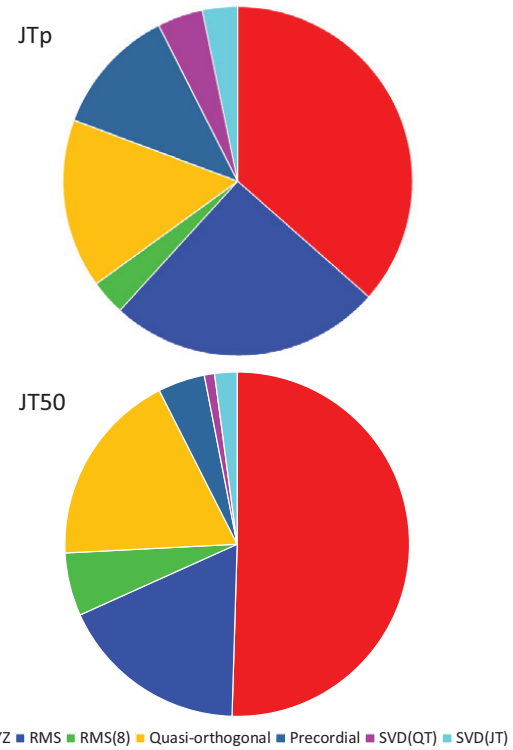

FIGURE 10 | Distribution of the one-dimensional ECG matrices that led to the intra-subject lowest residuals for the JTp/RR (top panel) and JT50/RR (bottom panel) regressions. The pie charts show the proportions of the subjects in whom the given one-dimensional matrix led to the lowest regression residual.

work for JTp/RR and JT50/RR hysteresis equally well as for the QT/RR hysteresis.

Limitations

Limitations of the study also need to be acknowledged. Many other one-dimensional ECG matrices are possible. Nevertheless, since we have found little differences among those tested and since the most stable results were found with "universal" matrix construction, it seems unlikely that some specific matrix would have performed substantially better compared to the XYZ representation. The XYZ matrix was designed for ECGs recorded with Mason-Likar electrode positions. It seems reasonable to propose that for ECGs recorded using other standard electrode positions, corresponding XYZ transformations (Kors et al., 1990) would also show optimal results, but this has not been tested. The study analyzed drug-free data. It may be that different one-dimensional ECG matrices would perform differently in categorizing the effects of different drugs. We are unable to comment on such a possibility. Likewise, we are unable to answer the question of whether these results obtained in healthy and relatively young subjects with normal physiologic ECGs would also be applicable to the elderly or to patients with congenital or other repolarisation abnormalities. Previous studies also related repolarisation ECG intervals to intra-myocardial repolarisation heterogeneity (Brisinda et al., 2004; Meijborg et al., 2017). Since we did not have any independent measurements of intra-myocardial electrophysiology processes available in the healthy subjects of this study, we were unable to study any such relationship. Finally, while the selection of the T wave peak measurement by minimizing the rate-corrected JTp variability is appropriate to the purposes of serial JTp comparisons, it might not be optimal for other applications of the interval measurements such as the beat-to-beat variability if these were eventually found of interest.

CONCLUSION AND PRACTICAL IMPLICATIONS

Searching for optimum ECG representation to be used when categorizing QT prolonging drugs appears unnecessary. The standard ECG conversion into orthogonal leads and calculating vector magnitude or the orthogonal leads appears universally applicable.

Testing of the JT50 interval changes should be carried out in clinical studies that used the JTp interval analyses. If the drug classification possibility of the JT50 interval is confirmed, its lower variability would make it a good replacement of the JTp interval.

DATA AVAILABILITY

All datasets generated for this study are included in the manuscript.

ETHICS STATEMENT

Both the original studies were approved by the relevant ethics boards and all participants gave written informed consent in accordance with the Helsinki declaration. Since only anonymized off-treatment data are presented here, the details of the source studies are of no relevance. For the same reason, no separate ethics clearance of the present investigation was required as per the local legislation.

AUTHOR CONTRIBUTIONS

All authors listed have made a substantial, direct and intellectual contribution to the work, and approved it for publication.

FUNDING

This work was supported by the British Heart Foundation New Horizons Grant NH/16/2/32499.

REFERENCES

Acar, B., and Köymen, H. (1999). SVD-based on-line exercise ECG signal orthogonalization. *IEEE Trans. Biomed. Eng.* 46, 311–321. doi: 10.1109/10.748984

Batchvarov, V., Hnatkova, K., and Malik, M. (2002). Assessment of noise in digital electrocardiograms. *Pacing Clin. Electrophysiol.* 25, 499–503. doi: 10.1046/j.1460-9592.2002.00499.x

Brisinda, D., Meloni, A. M., and Fenici, R. (2004). Magnetocardiographic study of ventricular repolarization in hypertensive patients with and without left ventricular hypertrophy. *Neurol. Clin. Neurophysiol.* 2004:13.

Cortez, D., Sharma, N., Devers, C., Devers, E., and Schlegel, T. T. (2014). Visual transform applications for estimating the spatial QRS-T angle from the conventional 12-lead ECG: Kors is still most Frank. *J. Electrocardiol.* 47, 12–19. doi: 10.1016/j.jelectrocard.2013.09.003

Fenichel, R. R., Malik, M., Antzelevitch, C., Sanguinetti, M., Roden, D. M., Priori, S. G., et al. (2004). Drug-induced Torsades de Pointes and implications for drug development. *J. Cardiovasc. Electrophysiol.* 15, 475–495. doi: 10.1046/j.1540-8167.2004.03534.x

Garnett, C. E., Zhu, H., Malik, M., Fossa, A. A., Zhang, J., Badilini, F., et al. (2012). Methodologies to characterize the QT/corrected QT interval in the presence of drug-induced heart rate changes or other autonomic effects. *Am. Heart J.* 163, 912–930. doi: 10.1016/j.ahj.2012.02.023

Guidance to industry (2005). E14 Clinical evaluation of QT/QTc interval prolongation and proarrhythmic potential for non-antiarrhythmic drugs. *Fed. Regist.* 70, 61134–61135.

Guldenring, D., Finlay, D. D., Bond, R. R., Kennedy, A., McLaughlin, J., Galeotti, L., et al. (2015). The derivation of the spatial QRS-T angle and the spatial ventricular gradient using the Mason-Likar 12-lead electrocardiogram. *J. Electrocardiol.* 48, 1045–1052. doi: 10.1016/j.jelectrocard.2015.08.009

Hnatkova, K., Johannesen, L., Vicente, J., and Malik, M. (2017). Heart rate dependency of JT interval sections. *J. Electrocardiol.* 50, 814–824. doi: 10.1016/j.jelectrocard.2017.08.005

Hnatkova, K., Smetana, P., Toman, O., Bauer, A., Schmidt, G., and Malik, M. (2009). Systematic comparisons of electrocardiographic morphology increase the precision of QT interval measurement. *Pacing Clin. Electrophysiol.* 32, 119–130. doi: 10.1111/j.1540-8159.2009.02185.x

ICH Guideline (2001). Safety pharmacology studies for human pharmaceuticals S7A. *Fed. Regist.* 66, 36791–36792.

Johannesen, L., Vicente, J., Hosseini, M., and Strauss, D. G. (2016a). Automated algorithm for J-Tpeak and Tpeak-Tend assessment of drug-induced proarrhythmia risk. *PLoS One* 11:e0166925. doi: 10.1371/journal.pone.0166925

Johannesen, L., Vicente, J., Mason, J. W., Erato, C., Sanabria, C., Waite-Labott, K., et al. (2016b). Ability of late sodium or calcium current block to balance the ECG effects of potassium current block. *Clin. Pharmacol. Ther.* 99, 214–223.

Johannesen, L., Vicente, J., Mason, J. W., Sanabria, C., Waite-Labott, K., Hong, M., et al. (2014). Differentiating drug-induced multichannel block on the electrocardiogram: randomized study of dofetilide, quinidine, ranolazine, and verapamil. *Clin. Pharmacol. Ther.* 96, 549–558. doi: 10.1038/clpt.2014.155

Kors, J. A., van Herpen, G., Sittig, A. C., and van Bemmel, J. H. (1990). Reconstruction of the Frank vectorcardiogram from standard electrocardiographic leads: diagnostic comparison of different methods. *Eur. Heart J.* 11, 1083–1092. doi: 10.1093/oxfordjournals.eurheartj.a059647

Malik, M. (2004). Errors and misconceptions in ECG measurement used for the detection of drug induced QT interval prolongation. *J. Electrocardiol.* 37(Suppl.), 25–33. doi: 10.1016/j.jelectrocard.2004.08.005

Malik, M., Andreas, J. O., Hnatkova, K., Hoeckendorff, J., Cawello, W., Middle, M., et al. (2008a). Thorough QT/QTc study in patients with advanced Parkinson's disease: cardiac safety of rotigotine. *Clin. Pharmacol. Ther.* 84, 595–603. doi: 10.1038/clpt.2008.143

Malik, M., Hnatkova, K., Novotny, T., and Schmidt, G. (2008b). Subject-specific profiles of QT/RR hysteresis. *Am. J. Physiol. Heart Circ. Physiol.* 295, H2356–H2363. doi: 10.1152/ajpheart.00625.2008

Malik, M., Hnatkova, K., Batchvarov, V., Gang, Y., Smetana, P., and Camm, A. J. (2004). Sample size, power calculations, and their implications for the cost of thorough studies of drug induced QT interval prolongation. *Pacing Clin. Electrophysiol.* 27, 1659–1669. doi: 10.1111/j.1540-8159.2004.00701.x

Malik, M., Hnatkova, K., Kowalski, D., Keirns, J. J., and van Gelderen, E. M. (2013). QT/RR curvatures in healthy subjects: sex differences and covariates. *Am. J. Physiol. Heart Circ. Physiol.* 305, H1798–H1806. doi: 10.1152/ajpheart.00577.2013

Malik, M., Hnatkova, K., Schmidt, A., and Smetana, P. (2009). Correction for QT/RR hysteresis in the assessment of drug-induced QTc changes - cardiac safety of gadobutrol. *Ann. Noninvasive Electrocardiol.* 14, 242–250. doi: 10.1111/j.1542-474X.2009.00304.x

Malik, M., Huikuri, H., Lombardi, F., Schmidt, G., and Zabel, M. (2018). Conundrum of the Tpeak-Tend interval. *J. Cardiovasc. Electrophysiol.* 29, 767–770. doi: 10.1111/jce.13474

Malik, M., Johannesen, L., Hnatkova, K., and Stockbridge, N. (2016). Universal correction for QT/RR hysteresis. *Drug Saf.* 39, 577–588. doi: 10.1007/s40264-016-0406-0

Malik, M., van Gelderen, E. M., Lee, J. H., Kowalski, D. L., Yen, M., Goldwater, R., et al. (2012). Proarrhythmic safety of repeat doses of mirabegron in healthy subjects: a randomized, double-blind, placebo-, and active-controlled thorough QT study. *Clin. Pharmacol. Therap.* 92, 696–706. doi: 10.1038/clpt.2012.181

Meijborg, V. M. F., Belterman, C. N. W., de Bakker, J. M. T., Coronel, R., and Conrath, C. E. (2017). Mechano-electric coupling, heterogeneity in repolarization and the electrocardiographic T-wave. *Prog. Biophys. Mol. Biol.* 130, 356–364. doi: 10.1016/j.pbiomolbio.2017.05.003

O'Neal, W. T., Singleton, M. J., Roberts, J. D., Tereshchenko, L. G., Sotoodehnia, N., Chen, L. Y., et al. (2017). Association between QT-interval components and sudden cardiac death: the ARIC study (Atherosclerosis Risk in Communities). *Circ. Arrhythm. Electrophysiol.* 10:e005485. doi: 10.1161/CIRCEP.117.005485

Ray, D., Hazra, S., Goswami, D. P., Macfarlane, P. W., and Sengupta, A. (2017). An evaluation of planarity of the spatial QRS loop by three dimensional vectorcardiography: its emergence and loss. *J. Electrocardiol.* 50, 652–660. doi: 10.1016/j.jelectrocard.2017.03.016

Strauss, D. G., Gintant, G., Li, Z., Wu, W., Blinova, K., Vicente, J., et al. (2018). Comprehensive in vitro proarrhythmia assay (CiPA) update from a cardiac safety research consortium / health and environmental sciences institute / FDA Meeting. *Ther. Innov. Regul. Sci.* 53, 519–525. doi: 10.1177/2168479018795117

Vicente, J., Hosseini, M., Johannesen, L., and Strauss, D. G. (2017). Electrocardiographic biomarkers to confirm drug's electrophysiological effects used for proarrhythmic risk prediction under CiPA. *J. Electrocardiol.* 50, 808–813. doi: 10.1016/j.jelectrocard.2017.08.003

Vicente, J., Stockbridge, N., and Strauss, D. G. (2016). Evolving regulatory paradigm for proarrhythmic risk assessment for new drugs. *J. Electrocardiol.* 49, 837–842. doi: 10.1016/j.jelectrocard.2016.07.017

Vicente, J., Zusterzeel, R., Johannesen, L., Mason, J., Sager, P., Patel, V., et al. (2018). Mechanistic model-informed proarrhythmic risk assessment of drugs: review of the "CiPA" initiative and design of a prospective clinical validation study. *Clin. Pharmacol. Ther.* 103, 54–66. doi: 10.1002/cpt.896

Zhang, J., and Machado, S. G. (2008). Statistical issues including design and sample size calculation in thorough QT/QTc studies. *J. Biopharm. Stat.* 18, 451–467. doi: 10.1080/10543400802020938

Conflict of Interest Statement: The authors declare that the research was conducted in the absence of any commercial or financial relationships that could be construed as a potential conflict of interest.

frontiers in Physiology

ORIGINAL RESEARCH
published: 02 August 2019
doi: 10.3389/fphys.2019.00994

Individually Rate Corrected QTc Intervals in Children and Adolescents

*Irena Andršová[1], Katerina Hnatkova[2], Kateřina Helánová[1], Martina Šišáková[1], Tomáš Novotný[1], Petr Kala[1] and Marek Malik[2]**

[1] Department of Internal Medicine and Cardiology, University Hospital Brno, Faculty of Medicine, Masaryk University, Brno, Czechia, [2] National Heart and Lung Institute, Imperial College London, London, United Kingdom

Accurate evaluation of the appearance of QTc sex differences during childhood and adolescence is intricate. Inter-subject differences of individual QT/RR patterns make generic heart rate corrections inaccurate because of fast resting heart rates in children. The study investigated 527 healthy children and adolescents aged 4–19 years (268 females, 50.9%). All underwent continuous ECG 12-lead monitoring while performing postural changes during a 70-min investigative protocol to obtain QT interval measurements at different heart rates. On average, more than 1200 ECG measurements (QT interval and its 5-min history of preceding RR intervals) were made in each subject. Curvilinear QT/RR regression involving intra-individual correction for QT/RR hysteresis were calculated in each subject. The projection of the QT/RR regressions to the heart rate of 60 beats per minute defined individually corrected QTc intervals. In males, gradual QTc shortening by about 15 ms appeared during the ages of 13–19 years synchronously with the incidence of secondary sex signs ($p = 0.016$). On the contrary, whilst gradual QTc prolongation by about 10 ms appeared in females, it occurred only during ages 16–19 years and was not related to the incidence of secondary sex signs ($p = 0.18$). The study also showed that in children and adolescents, linear QT/RR models fit the intra-subject data significantly more closely than the log-linear models ($p < 0.001$). The study speculates that hormonal shifts during puberty might be directly responsible for the QTc shortening in males but that QTc prolongation in females is likely more complex since it was noted to follow the appearance of secondary sex signs only after a considerable delay.

Keywords: age, sex differences, individual QT/RR patterns, QT/RR hysteresis, QTc interval, QT/RR slope

OPEN ACCESS

Edited by:
Marcel van der Heyden, University Medical Center Utrecht, Netherlands

Reviewed by:
Wojciech Zareba, University of Rochester, United States
Elise Laura Kessler, University Medical Center Utrecht, Netherlands

****Correspondence:***
Marek Malik
marek.malik@imperial.ac.uk

Specialty section:
This article was submitted to Cardiac Electrophysiology, a section of the journal Frontiers in Physiology

Received: *27 May 2019*
Accepted: *18 July 2019*
Published: *02 August 2019*

Citation:
Andršová I, Hnatkova K, Helánová K, Šišáková M, Novotný T, Kala P and Malik M (2019) Individually Rate Corrected QTc Intervals in Children and Adolescents. Front. Physiol. 10:994. doi: 10.3389/fphys.2019.00994

INTRODUCTION

As recently reviewed in detail (Linde et al., 2018), there are substantial sex differences in many electrophysiology processes and characteristics. While many of the sex differences have important clinical implications, their physiologic origin is frequently insufficiently understood. Among others, as repeatedly observed (Linde et al., 2018), adult pre-menopausal females have higher resting heart rate and longer QTc interval compared to males of the same age. Based on large ECG collections, it was previously suggested that these changes occur during puberty which lead to the conclusion that sex hormones trigger these differences (Rautaharju et al., 1992;

Kurokawa et al., 2016). Indeed, the role of hormones was supported by other studies, e.g., by the observation that the sex of the recipient rather than that of the donor influences QTc sex differences after heart transplant (Novotný et al., 2014).

Nevertheless, the previous studies of the development of QTc interval during childhood and adolescence suffered from the problem of inaccurate heart rate correction. It is well known that in adults, the relationship between QT duration and the underlying heart rate is subject-specific with substantial differences between different individuals (Batchvarov et al., 2002) and that generic heart rate corrections (e.g., Bazett, Fridericia, or Framingham formulae) may lead to noticeable QTc inaccuracy if applied to QT intervals measured at heart rate considerably remote from 60 beats per minute (bpm) (Malik et al., 2002; Garnett et al., 2012). While it is not known whether similar inter-subject differences exist in children, fast resting heart rates are well recognized in young children (Sarganas et al., 2017). Generic QT heart rate corrections may therefore be highly imprecise in individual children (Hnatkova et al., 2019) while normative data obtained from population-based regressions between QT intervals and simultaneously measured heart rates (Rautaharju et al., 2014) might be influenced by substantial correction errors (Malik et al., 2019).

These methodological shortcomings impact not only on the physiologic understanding of the QTc development during childhood but may also lead to difficult judgment of QTc interval in borderline clinical cases. Having these problems in mind, we have designed a physiologic study of healthy school-age children and adolescents and recorded their continuous 12-lead electrocardiograms (ECG) during provocative maneuvers. This allowed us to study individual QT/RR profiles and to investigate their development and sex differences during childhood and adolescence.

MATERIALS AND METHODS

Investigated Population

Per protocol, the study investigated healthy children of school age with the aim of obtaining, in both sexes, uniform age distribution between the ages of 6–19 years. The recruitment was organized at six primary (including preparatory years) and secondary schools in northern and southern Moravia offering ECG-based health check. While every child or adolescent who agreed to participate was investigated, the data used in the analysis presented here excluded those who were on repolarization affecting drugs[1] or on hormonal contraceptives, and those with cardiac abnormality. The study protocol was approved by the Ethics Committee of the University Hospital Brno. All participants (if legally allowed to do so) or their parents or legal guardians gave informed written consent according to the Helsinki declaration.

Standard demographic data were collected in all participants; body mass index was calculated according to the formula W/H^2 where W is the body weight in kilograms and H is body height in meters. Presence of secondary sex characteristics corresponding to recognized standards (Harlan et al., 1979, 1980; Mickey and Brooke, 2019) was detected by a combination of visual inspection and a questionnaire submitted by parents/guardians of the investigated subjects.

Investigative Protocol

Continuous 12-lead ECG (SEER MC version 2, sampled at 1000 Hz) with electrodes in the Mason-Likar position was recorded in each participant during 70-min provocative postural maneuvering that consisted of supine, sitting, standing, supine, standing, sitting, and supine positions (in this order) each of 10-min duration. The sitting and standing positions were maintained without external support and the position changes were accomplished within less than 20 s.

Participants were investigated in the mid-morning hours in groups of up to 20 subjects of similar ages performing the positional changes at the same time. During the investigation, younger children listened to non-exciting age-appropriate stories, others were investigated in quiet noise-free environment.

To make the study practical, the ECG recordings were started before the provocative maneuvering and terminated afterward. Consequently, the duration of the ECG recordings before and after the provocative maneuvering differed in different subjects. During these times, the subjects were engaged in standard school activities excluding physical education. None of the participants smoked before or during the ECG recording.

Electrocardiographic Measurements

For the purposes of the present investigation, all ECGs were divided into 10-s segments with 5-s overlap between adjacent segments. In each segment, QRS complexes were identified, and in each lead, representative P-QRS-T beatform was constructed by calculating sample-by-sample medians of superimposed beats. An algebraic composite of threshold, tangent, wavelet, and polynomial interpolation algorithms that provided pre-review QT assessment in previous studies (Malik et al., 2008a, 2012b) was used to obtain automatic QT interval measurements. The same algorithm of this composite method was used in all recordings of this study; i.e., there were no measurement differences between different study subjects and/or between different ECGs of the same subject. Consistency of QT interval measurements between neighboring (non-adjacent) segments was used to eliminate noise-influenced and other problematic QT values. In each subject, all non-eliminated QT measurements were subsequently adjusted by pattern-matching algorithms (Malik et al., 2004; Hnatkova et al., 2009) to ensure that QRS onset and T wave offset patterns of similar morphology were measured consistently.

For each QT interval measurement, individual RR intervals within the measured 10-s segment and in the preceding 5 min were identified and the sequence of their durations obtained. The accurate QRS detection needed for this purpose was based on a combination of automatic QRS detectors (Kohler et al., 2002;

[1] https://www.crediblemeds.org

Pahlm and Sornmo, 1984; Kors et al., 1986) with visual control and manual corrections where appropriate.

Heart Rate and QT/RR Hysteresis Correction

Using previously published technology (Malik et al., 2008a, 2012b), individual QT/RR patterns were investigated in each study participant including the curvilinear regression of the relationship. Since the QT interval duration depends on the underlying heart rate rather than on the rate of the immediately preceding heartbeat cycle (Franz et al., 1988), QT/RR hysteresis was taken into account. Hence, as previously published (Malik et al., 2012b), the assessment of QT/RR patterns was combined with subject-specific assessment of the QT/RR hysteresis profiles which were modeled using the exponential decay forms (Malik et al., 2008b).

Curvilinear models of the hysteresis-corrected QT/RR patterns were used to estimate the QT interval duration at RR interval of 1 s (i.e., at heart rate of 60 bpm). This was based on averaging individually corrected QT values of all measurements available in the given subject. The result of this averaging is further called the QTcI interval.

To estimate the importance of QT/RR hysteresis correction, QT/RR patterns were also investigated relating the QT interval measurements to the average of 3 RR intervals in the middle of the 10-s ECG segment in which the QT measurement was made as well as to the average of all RR intervals in this segment. The range of heart rates available in each subject (i.e., the "width" of heart-rate data allowing to study the subject-specific QT/RR pattern) was defined as the difference between the maximum and minimum hysteresis corrected heart rates for which the QT measurements were available.

To compare the hysteresis corrected QT/RR patterns between different study subjects, linear and log-linear regression models were further used in the forms $QT_i = \beta_0 + \beta RR_i + \varepsilon_i$ and $\log QT_i = \alpha_0 + \alpha \log RR_i + \varepsilon_i$, respectively. Here QT_i and RR_i are mutually corresponding QT and RR interval measurements (expressed in seconds) in the given subject and in both formulae, ε_i are zero-centered normally distributed errors. The standard deviations or the ε_i errors (i.e., the individual-specific regression residuals) were used to compare the accuracy of both regression models. These models were used since, as well known, they lead to the QT correction formulae $QTc = QT + \beta(1 - RR)$ and $QTc = QT/RR^{\alpha}$.

Statistics and Data Presentation

Numerical data are presented as mean ± standard deviation. Dependency of ECG measurements on age was investigated using linear regression models that were displayed together with the 95% confidence intervals (CI) of the regression lines. When the age dependency appeared non-linear, averages and standard deviations were calculated and compared in separate age bands <8 years, 7–9 years, 8–10 years, etc. up to 16–18 years, and >17 years (the overlaps were used to obtain sufficient case numbers in each band). Intra-subject differences of the QT/RR regression residuals were assessed by the non-parametric Wilcoxon matched-pair test. Differences between females and males, differences between subjects showing and not showing secondary sex signs, and differences between males or females younger and older than a dichotomy age limit were investigated using non-parametric Kolmogorov–Smirnov test. Dichotomy age limits of 10, 11, . . ., 16 years were used. Statistical calculations were made in the SPSS Statistics 64-bit version 25 package (IBM, Armonk, NY, United States). P-values < 0.05 were considered statistically significant.

RESULTS

Population

After the call for participation, 555 subjects (295 females) were enrolled and underwent the investigative protocol. Of these, 27 (4.9%) had to be excluded because of potentially interfering drug therapy, cardiac structural congenital abnormalities (including those with a history of cardiac surgery), cardiac conduction abnormality, and (in one case) sex-transversal procedures. Of the remaining 528 subjects, further one (0.2%) was excluded because of technical failure.

The analysis reported here is thus based on 527 subjects. Of these, 268 were females and 259 were males. Secondary sex signs were observed in 182 (67.9%) and 145 (56.0%) of females and males, respectively. **Table 1** shows the characteristics of the investigated population in individual age groups. **Supplementary Figure 1** shows that, as expected, the body weight and height was similar between sexes of young age. With increasing age, males became taller and heavier compared to females. Body mass index (**Supplementary Figure 2**) was also increasing with advancing age but no significant difference between sexes was observed.

Altogether 19 subjects (3.6% of the investigated populations; 13 females and 6 males) have not completed the investigation protocol because of pre-syncopal episodes, nausea, or vomiting. Nevertheless, in all these subjects, sufficient ECG data were collected before such side-effects occurred. No ECG data potentially influenced by the side-effects were included in the analysis.

The ECG data reported are based on 642,003 measurements of the QT interval and of its 5-min RR interval history. On average, 1218 measurements were made per subject (**Table 1**).

Supplementary Tables 1, **2** summarize electrocardiographic measurements (as presented in subsequent sections in more detail) in individual age groups.

QT/RR Hysteresis

Figure 1 shows examples documenting that the inclusion of QT/RR hysteresis led to substantially more tight relationship between the measured QT intervals and the underlying heart rate. This was verified by the regression residuals. With the incorporation of QT/RR hysteresis, the curvilinear QT/RR regression residuals (i.e., the spread of the QT data around the curvature of the relationship) were 4.59 ± 2.60 ms and 3.87 ± 1.16 ms in females and males, respectively ($p < 0.001$). With the RR intervals averaged from the 10-s ECG segments, these residuals were 7.05 ± 2.40 ms and 6.73 ± 1.64 ms, whilst

TABLE 1 | Investigated population.

Age [years]	Females					Males				
	N	Sign	Height [cm]	Weight [kg]	ECG	*N*	Sign	Height [cm]	Weight [kg]	ECG
≤7	17	0	115.7 ± 5.2	20.5 ± 2.8	868 ± 353	15	0	119.1 ± 6.9	24.7 ± 7.4	1019 ± 348
7–8	14	1	128.1 ± 9.8	26.1 ± 3.9	1113 ± 501	14	0	128.5 ± 6.0	25.9 ± 3.5	1017 ± 389
8–9	23	1	132.5 ± 5.4	28.4 ± 4.1	1012 ± 455	18	0	135.4 ± 5.7	31.9 ± 5.6	1113 ± 301
9–10	15	5	139.2 ± 7.0	33.7 ± 6.3	1459 ± 501	11	0	141.9 ± 7.8	36.1 ± 8.6	1075 ± 442
10–11	23	7	144.2 ± 5.6	36.5 ± 5.6	1548 ± 501	24	1	145.0 ± 7.1	38.0 ± 8.1	1200 ± 489
11–12	15	12	149.9 ± 7.8	38.4 ± 7.5	1365 ± 493	24	9	150.3 ± 6.9	44.6 ± 9.7	1235 ± 431
12–13	22	18	159.1 ± 5.6	48.3 ± 10.3	1181 ± 419	29	20	160.6 ± 10	52.9 ± 12.5	1449 ± 430
13–14	23	22	160.8 ± 8.0	48.2 ± 6.1	1146 ± 401	20	16	163.5 ± 6.6	49.6 ± 9.2	1295 ± 602
14–15	22	22	166.2 ± 5.2	58.3 ± 12.7	1122 ± 435	16	13	173.7 ± 7.3	59.9 ± 10.7	1514 ± 388
15–16	34	34	165.8 ± 5.3	56.7 ± 7.5	1011 ± 448	33	31	177.8 ± 6.9	68.1 ± 9.7	1346 ± 501
16–17	28	28	167.6 ± 5.4	58.3 ± 6.7	1087 ± 340	20	20	180.0 ± 7.7	72.7 ± 8.6	1359 ± 478
17–18	11	11	173.5 ± 4.6	64.3 ± 12.6	1298 ± 672	16	16	182.2 ± 6.4	70.6 ± 9.2	1234 ± 378
>18	21	21	165.9 ± 7.3	57.0 ± 8.3	1054 ± 292	19	19	178.5 ± 6.5	70.4 ± 11.9	1519 ± 511

For each age bin, the table shows the number (N) of investigated females and males, the number of those showing secondary sex signs (Sign), their heights and weights in centimeters and kilograms, respectively, the number of ECG measurement per subject (ECG). Data are shown as mean ± standard deviation.

with the averages of three RR intervals, the residuals increased to 9.34 ± 2.56 ms and 9.04 ± 1.97 ms. All comparisons of these data were highly statistically significant ($p < 0.001$ for all). **Figure 2** shows that the increase of the QT/RR regression residuals from the hysteresis corrected relationship to either RR interval averages over 10 s or RR interval averages over three heart cycles occurred in every study participant.

The top panel of **Figure 3** shows that in both females and males, the QT/RR regression residuals (hysteresis corrected) increased with increasing age. In both sexes, the increase was modest with an increase of 0.11 ms per year in females and 0.06 ms in males (both statistically significant, $p < 0.01$). The bottom panel of **Figure 3** shows cumulative distributions of the QT/RR regression residuals in both sexes and demonstrates that both in females and males, the curvilinear relationship between the QT interval duration and the underlying heart rate was very tight (note that in both sexes, the median QT/RR residual was below 4 ms).

The extent of the QT/RR hysteresis is standardly expressed by its time constant defined as the time interval required for 95% of the adaptation of QT interval to occur after a heart rate change. The dependence of this hysteresis time constant on the age of study subjects is shown in **Figure 4**. The extent of the QT/RR hysteresis was independent of age and, on average, very close to the constant of 2 min.

Since in every subject, QT intervals were more closely related to the hysteresis corrected RR interval values compared to the other possible RR interval expressions, the measurements involving QT/RR hysteresis correction were used in the subsequent parts of the study.

Heart Rate Changes

Figure 5 shows the age-dependency of slowest and fastest heart rates at which the QT intervals were measured as well as of the intra-subject heart rate ranges over which the individual QT/RR patterns were assessed.

As expected, both the slowest and fastest heart rates were higher in younger children compared to adolescents (in both sexes, the minimum heart rates were decreasing by 1.9 bpm per year of age, $p < 0.001$; the decrease of maximum heart rate was approximately 50% shallower but still highly statistically significant, $p < 0.001$). Nevertheless, the bottom panel of **Figure 5** shows that in all study subjects, the heart rate spreads of QT/RR patterns were substantial. The individual QT/RR patterns were thus accurately defined.

QTcI Interval

Figure 6 shows the relationship of QTcI intervals to age which was one of the principal results of the study. In the linear regression analysis (top panel of **Figure 6**), there was significant of QTcI prolongation with advancing age in females (0.70 ms per year, $p = 0.02$) and significant QTcI shortening with advancing age in males (0.64 ms per year, $p = 0.03$).

Nevertheless, as shown in the middle panel of **Figure 6**, the change with age was highly non-linear. No clear differences between the sexes were found up till the age of approximately 12–13 years. From that age on, QTcI interval was gradually decreasing in males. In females, no obvious QTcI change was seen up till the age of approximately 16 years following which, the QTcI interval increased substantially. In the highest age bin of >17 years, the average QTcI differences between the sexes was 24.1 ms.

The surprising late onset of the QTcI change in females was confirmed by the comparison of QTcI distributions in subjects showing and not showing secondary sex signs, as demonstrated in the bottom panel of **Figure 6**. There was no difference between the distributions in females and males without secondary sex signs. The comparison between those with and without secondary sex signs led to only a non-significant trend in females ($p = 0.181$) whilst in males, the same comparison resulted in a clear statistical significance ($p = 0.016$). The sex difference

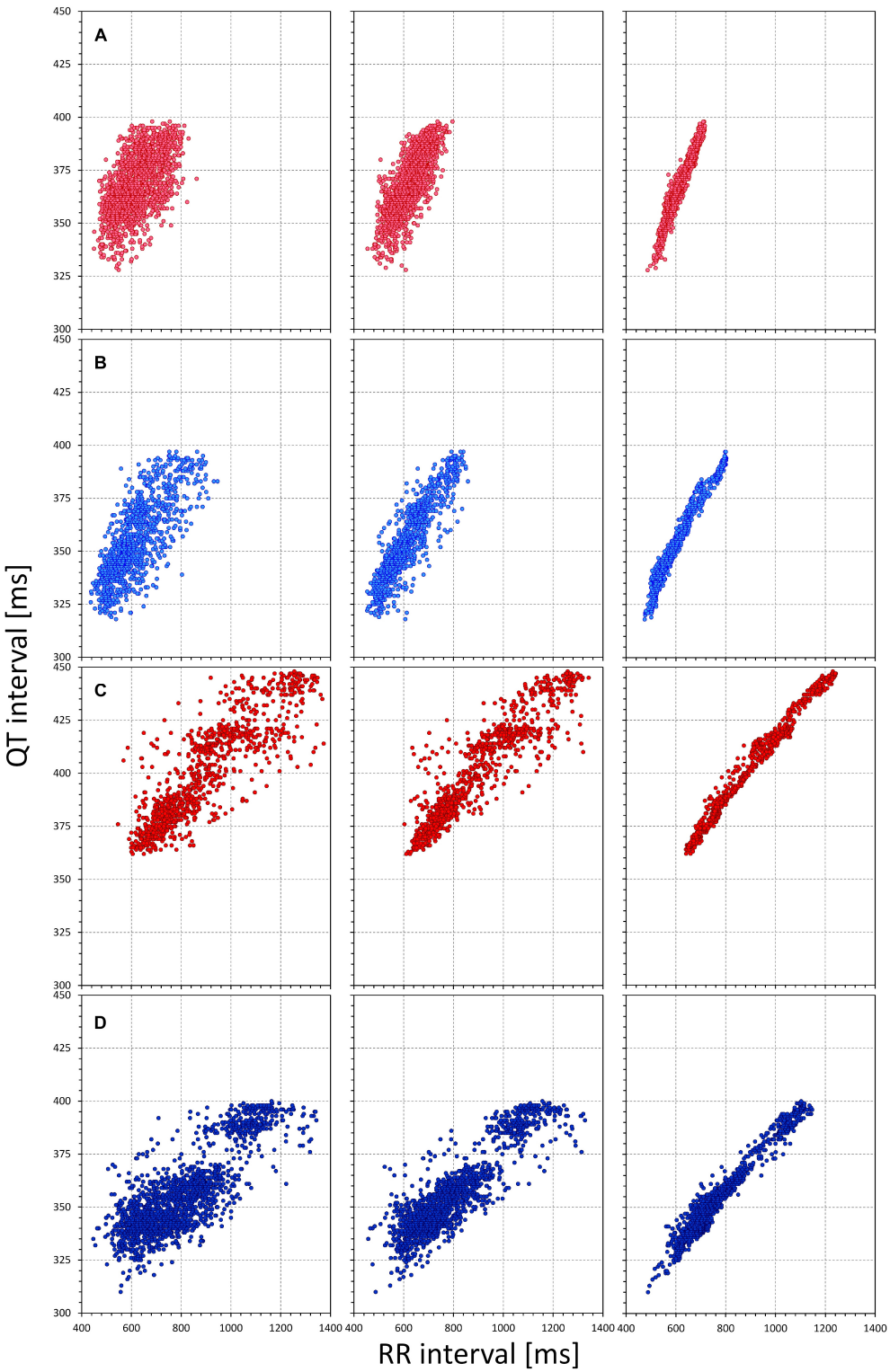

FIGURE 1 | The figure shows examples of comparisons of QT/RR relationship using different RR interval expressions. Each row of panels corresponds to one subject. In each subject, the QT interval measurements are the same but the panels on the left relate the QT intervals to the averages of three RR intervals, the panels in the middle to 10-s RR interval averages, and the panels of the right to the RR interval values obtained from the 5-min histories of the QT interval measurements by individual QT/RR hysteresis profiles. Note the increase of the regression fit from the left panels to the right panels. Cases **(A–D)** correspond to a female aged 7.4 years, a male aged 7.7 years, a female aged 18.7 years, and a male aged 18.7 years, respectively.

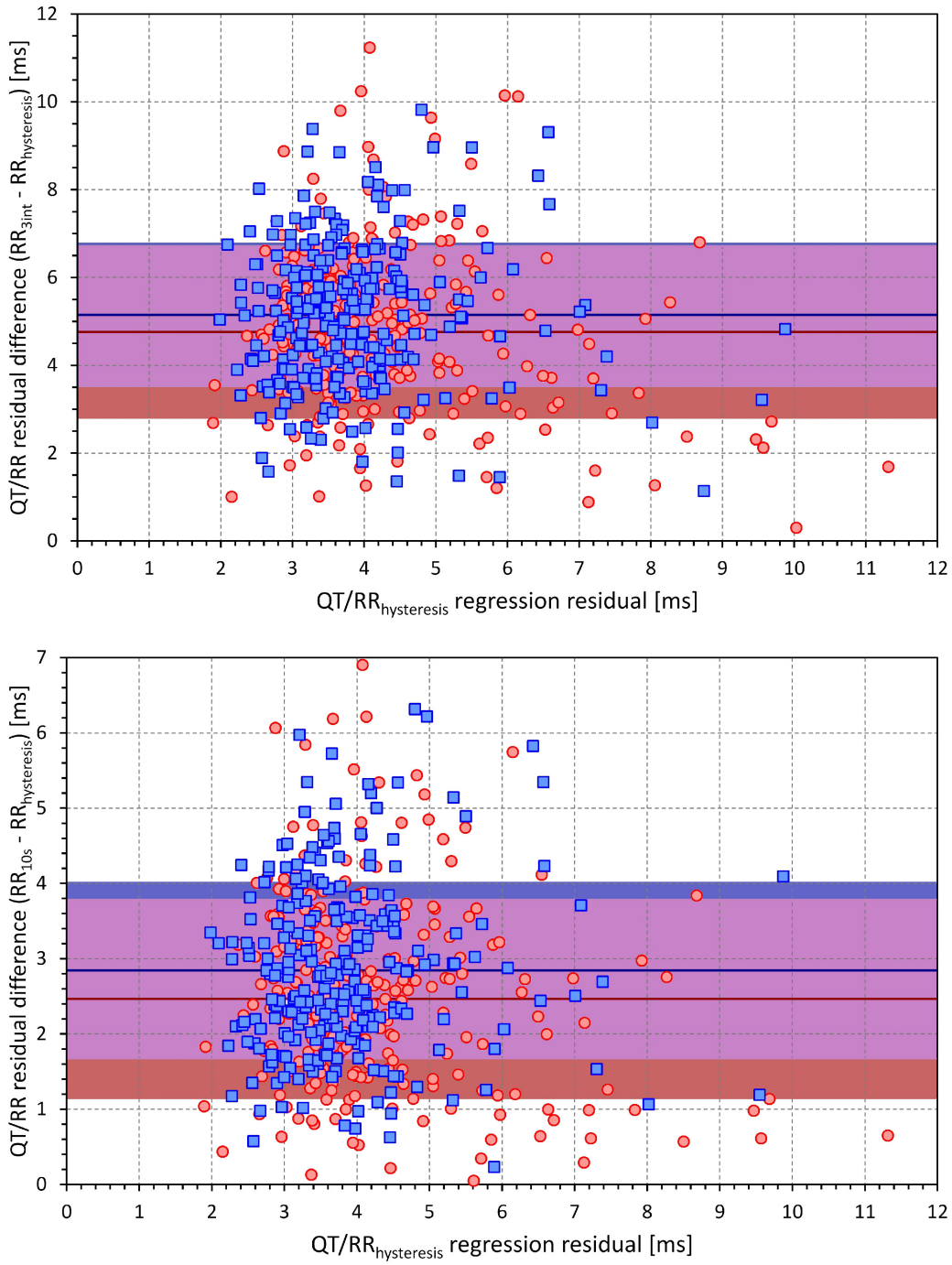

FIGURE 2 | Scatter diagrams between the curvilinear QT/RR regression residuals involving QT/RR hysteresis correction (horizontal axes) and the increases in the residuals when using three RR interval averages **(top)** and 10-s RR interval averages **(bottom)** instead of QT/RR hysteresis correction. Red circles and blue squares correspond to female and male subjects, respectively. Dark red and dark blue lines are means of the residual increase in females and males, respectively. The light red and light blue bands show the intervals of mean ± standard deviation of the sex-specific residual increases. The violet bands are the overlaps between the standard deviation bands of both sexes.

between females and males showing the secondary sex signs was highly significant ($p < 0.001$).

When dichotomizing the population (females and males separately) into those younger and older than 10, 11, 12, . . ., 16 years, the QTcI difference between older and younger males appeared at the dichotomy of 13 years ($p = 0.001$) and was maintained in subsequent dichotomies ($p < 0.001$ for all dichotomies of 14, 15, and 16 years). On the contrary, the QTcI

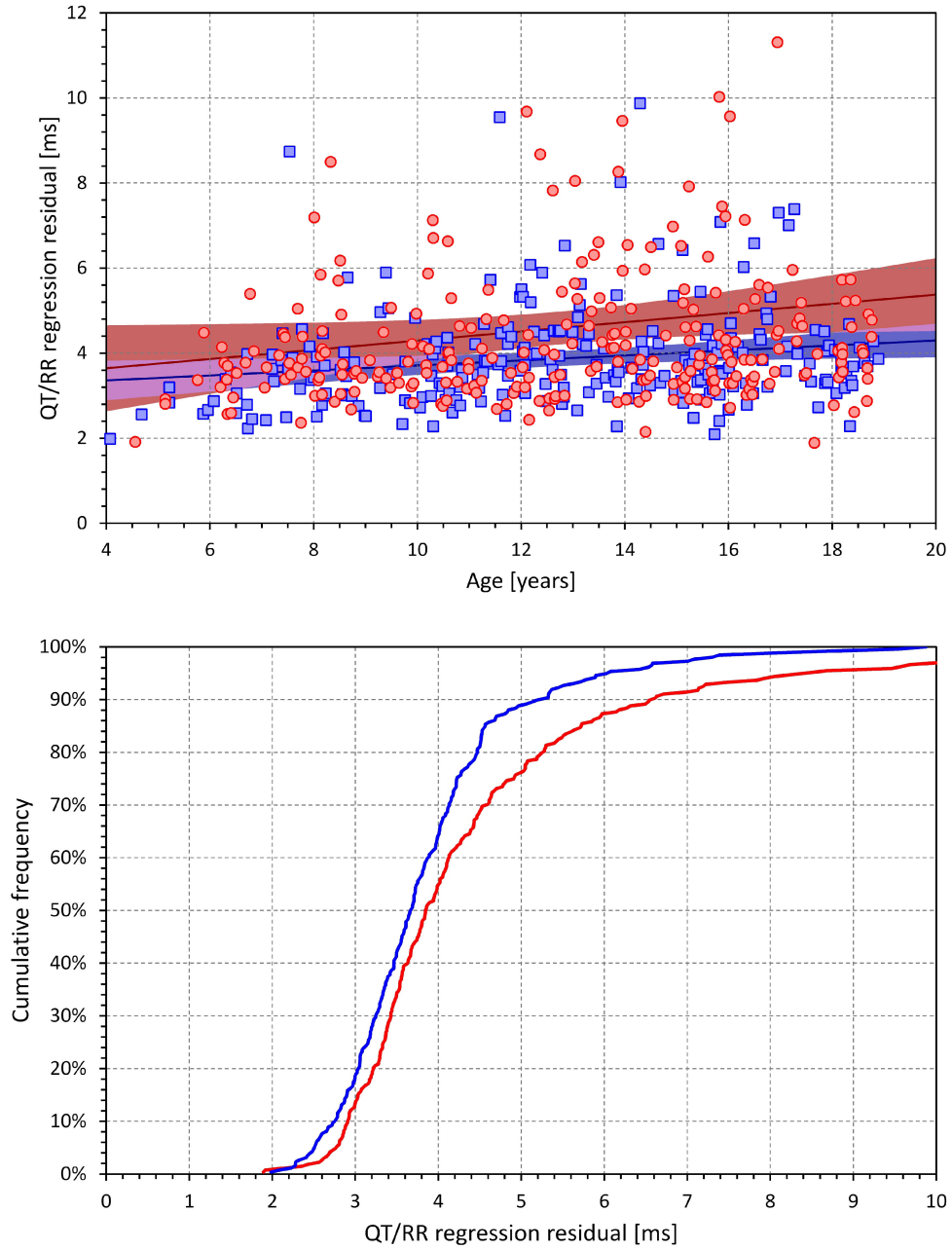

FIGURE 3 | The **(top)** panel show the age dependency of the curvilinear QT/RR regression residuals. The red circles and blue squares correspond to the female and male subjects, respectively. The dark red and dark blue lines are linear regressions in females and males, respectively; the light red and light blue areas are the 95% confidence bands of the sex-specific linear regression lines. The violet areas are the overlaps between the confidence bands of the regression lines of both sexes. The **(bottom)** panel shows the cumulative distributions of QT/RR regression residuals in female (bold red line) and male (bold blue line) subjects.

difference between younger and older females was not significant for all dichotomies 10–15 years and became only significant at the dichotomy of 16 years ($p = 0.014$).

QT/RR Dependency

By definition, both linear and log-linear regressions are bound to lead to larger QT/RR residuals compared to the curvilinear regressions (that is, the linear and log-linear QT/RR regression models cannot fit the data as closely as the curvilinear regressions). Nevertheless, in both sexes, the increases of QT/RR residuals from curvilinear to linear models (0.16 ± 0.30 ms and 0.12 ± 0.24 ms in females and males, respectively) were significantly smaller compared to the residual increases from curvilinear to log-linear models (0.89 ± 0.63 ms and 0.65 ± 0.30 ms in females and males, respectively; $p < 001$ for comparisons in both sexes). The increases of the residuals from

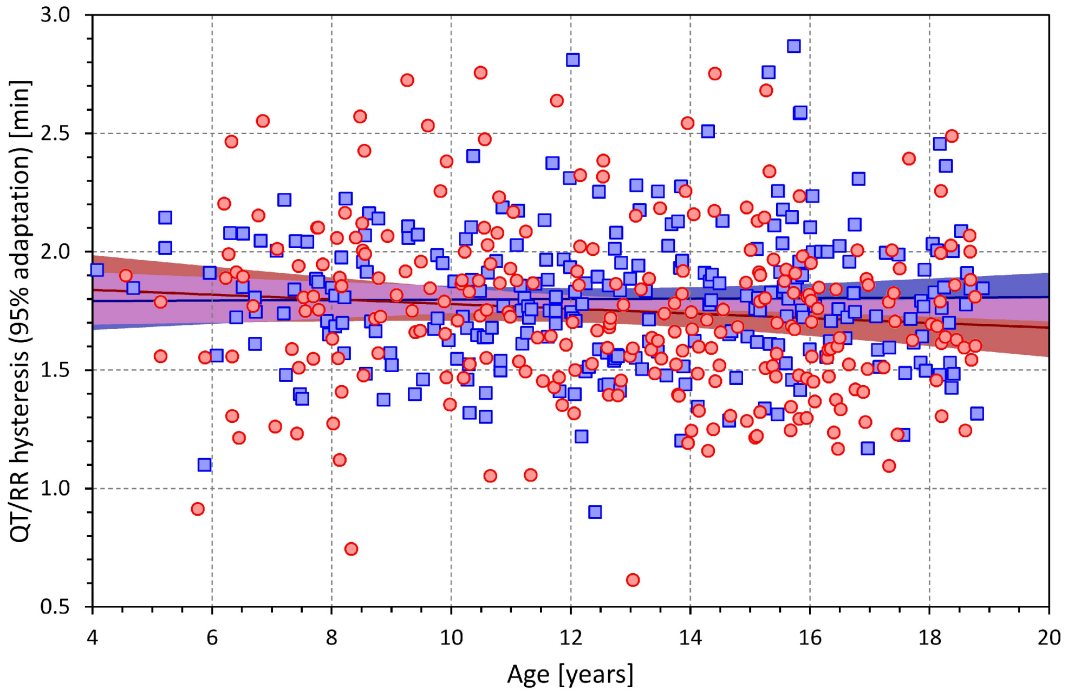

FIGURE 4 | Age dependency of the intra-subject QT/RR hysteresis time constants (i.e., time intervals needed for 95% adaptation of QT interval duration after heart rate change). The layout and symbol definition are the same as in **Figure 3**.

the curvilinear models were also significantly smaller in males compared to females ($p = 0.02$ for linear models, $p < 0.001$ for log-linear models).

Consequently, the linear models described the individual QT/RR relationships better compared to log-linear models and were used in the analysis of age dependency. The corresponding results are shown in **Figure 7**. In both sex groups, the QT/RR patterns became gradually shallower with advancing age (for both sexes $p < 0.005$; linear regression of QT/RR slopes vs. age). The middle panel of **Figure 7** shows that this age effect was again non-linear with the age effect visible in both sexes from approximately 13 years onward. The bottom panel of **Figure 7** shows sex-specific trends to shallower QT/RR slopes in subjects with secondary sex signs (compared to those without the signs) as well as trends to shallower QT/RR slopes in males compared to females (irrespective of the secondary sex signs) but none of these trends was statistically significant.

Corresponding analysis of the log-linear slopes is shown in **Figure 8**. This shows that the log-linear slopes led to erratic results, probably caused by the significantly lesser precision of the log-linear analysis.

DISCUSSION

The results of the study show that during puberty, the known sex difference in QTc interval does not appear at the same time as secondary sex signs. Whilst, as expected, we observed earlier onset of secondary sex signs in females compared to males (Mickey and Brooke, 2019), statistically significant QTc changes in females occurred some 3 years later compared to males (in addition to the statistical tests presented, compare also the middle panel of **Figure 6** with **Figure 9** that shows the development of incidence of secondary sex signs). Purely speculatively, this may suggest that simple hormonal shifts during puberty might be responsible for the QTc shortening in males but are unlikely the principal direct cause of QTc prolongation in females. If our observation is independently confirmed, other mechanisms need to be considered and researched, including the long-term pubertal conditioning, prolonged adaptation to perioding menstruation blood loss, or central and autonomic regulation changes. Indeed, the stability of menstrual cycle appears also after a considerable delay, perhaps similar to the delay that we observed with QTc prolongation, after the appearance of menarche (Lenton et al., 1984; Apter et al., 1987). Thus, while hormonal shifts might still contribute to the QTc prolongation in females, the mechanisms responsible for these repolarization changes are likely more intricate compared to the QTc shortening in males.

The study also shows that with simple postural maneuvering, wide heart rate spans known from clinical studies in adults (Malik et al., 2012b) may also be achieved in relatively young children. This has implications for studying the subject-specific QT/RR profiles that might be helpful when judging borderline cases of QTc interval abnormalities.

While the QT interval and heart rate data of this study might theoretically be also analyzed using previously proposed

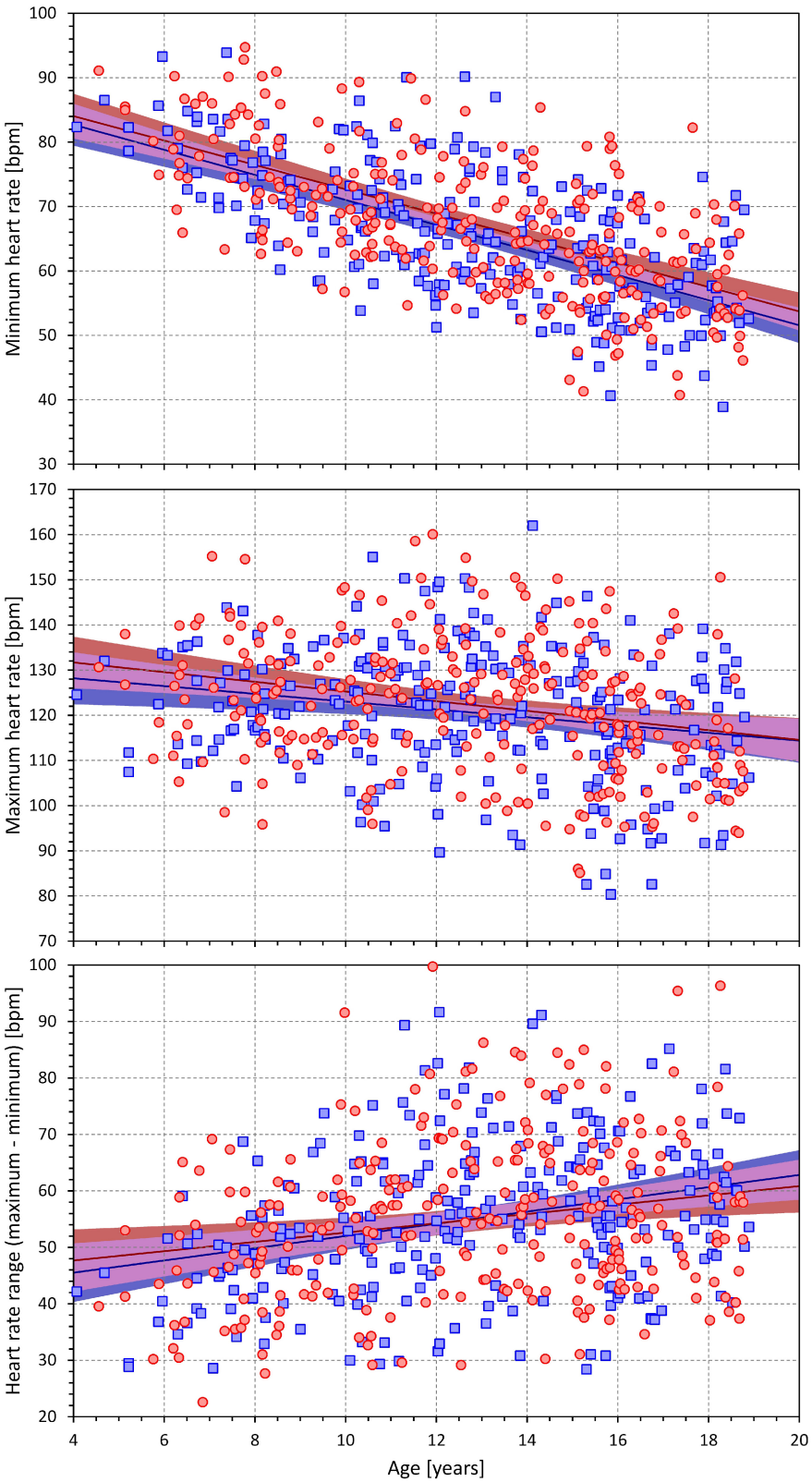

FIGURE 5 | Scatter diagrams between the age and minimum heart rate **(top)** maximum heart rate **(middle)** and the range between the minimum and maximum heart rate **(bottom)**. The layout and symbol definition in each panel are the same as in **Figure 3**.

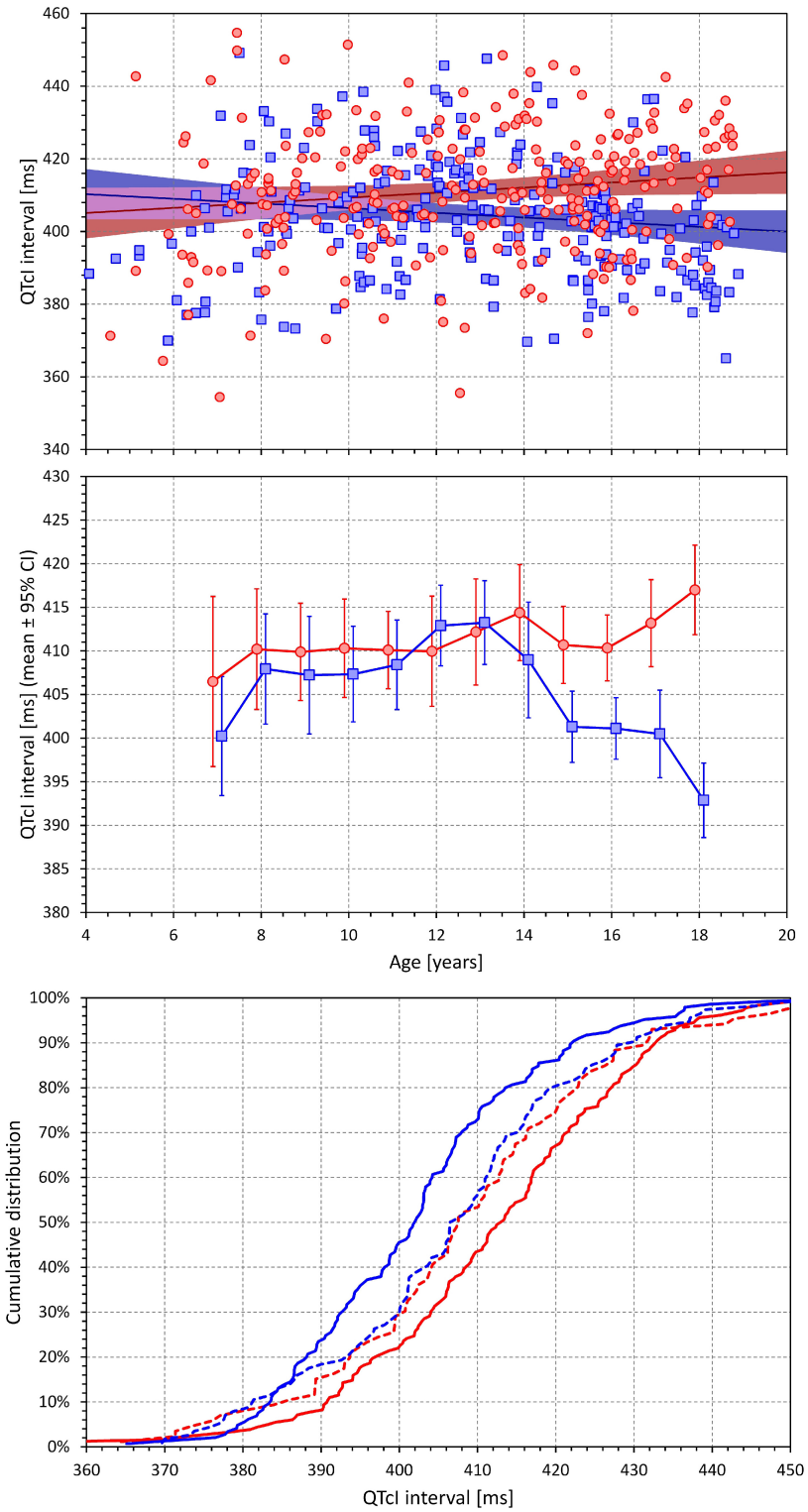

FIGURE 6 | The **(top)** panel shows the scatter diagram between age and QTcI interval (see the legend of **Figure 2** for symbol explanations). The **(middle)** panel shows the averages of QTcI intervals in age bands <8 years, 7–9 years, 8–10 years, etc. up to 16–18 years, and >17 years (each shown approximately at the middle age of the band). The error bars are the corresponding standard deviations. The red and blue marks correspond to the females and males, respectively. The **(bottom)** panel shows the cumulative distributions of QTcI intervals in subjects without (dashed lines) and with (full lines) secondary sex signs. The red and blue lines again correspond to females and males, respectively.

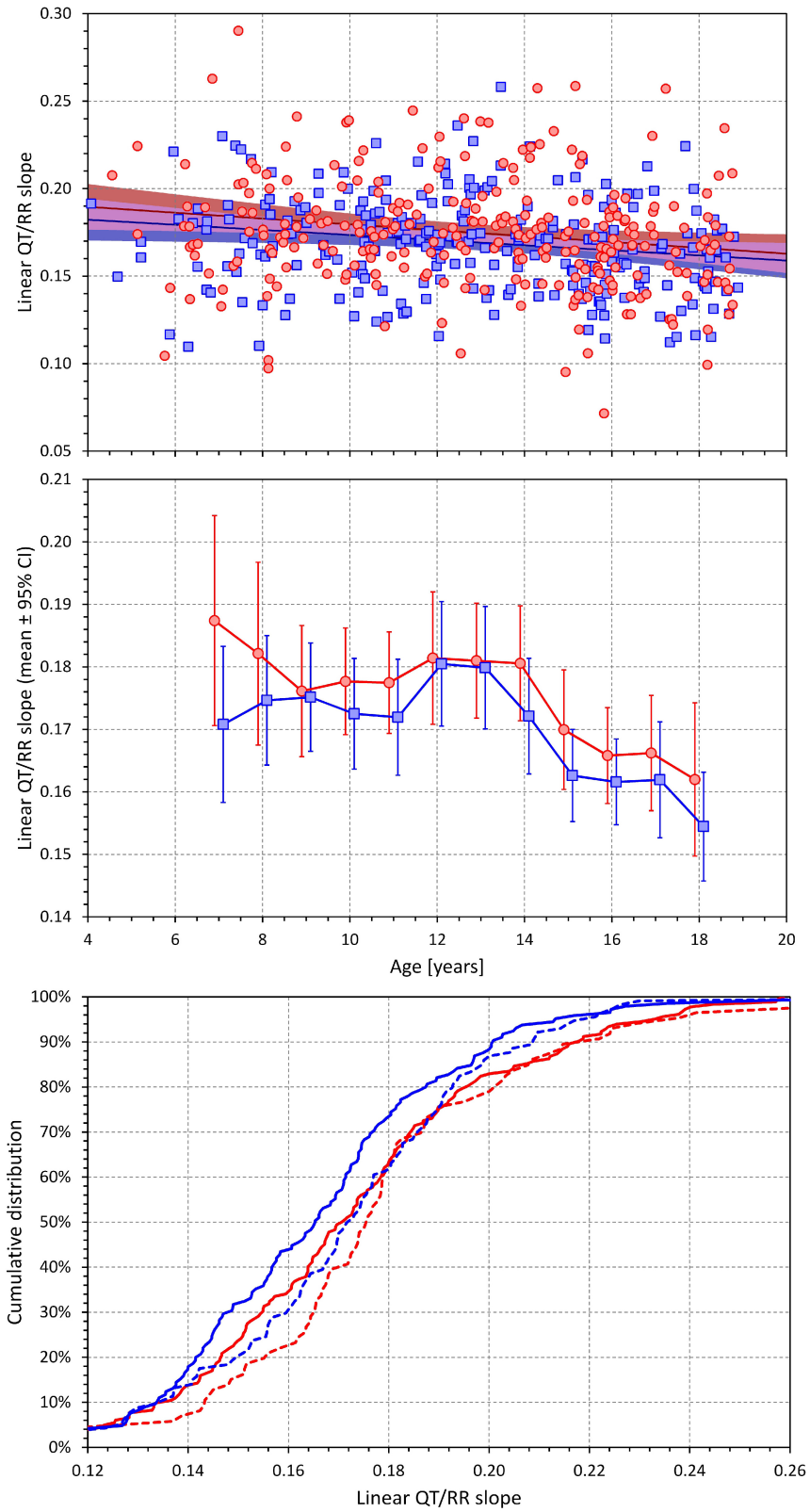

FIGURE 7 | Development of the age dependency of linear QT/RR slopes in both sexes. The layout and meaning of the three panels are the same as the layout and meaning of the three panels of **Figure 6**.

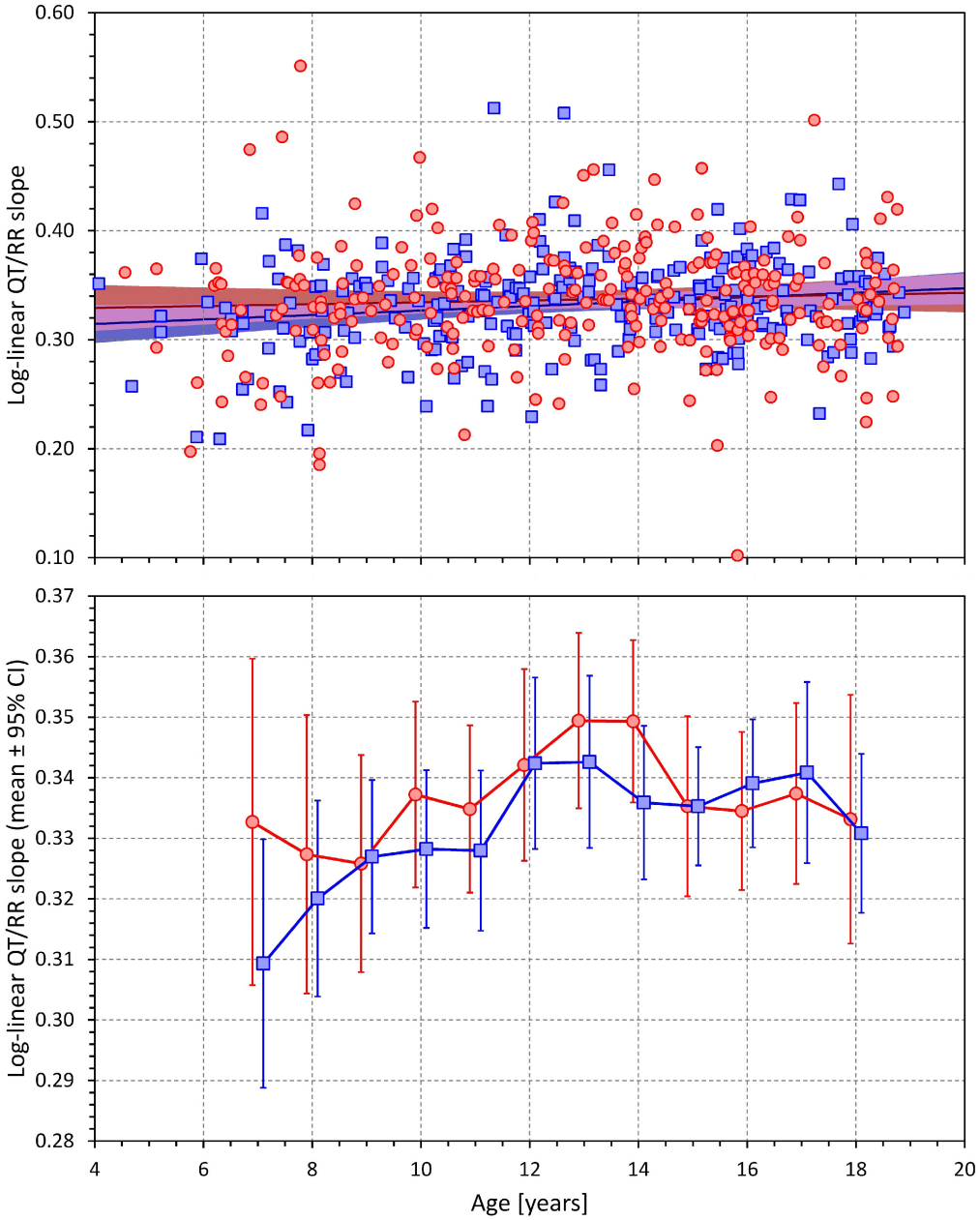

FIGURE 8 | Age dependency of the slopes of the log-linear QT/RR regressions. The layout of the panels is the same as of the top two panels of **Figure 6**.

general correction formulae (e.g., Bazett, Fridericia, Hodges, or Framingham corrections), we have intentionally omitted such analyses since they would not only be inaccurate but potentially also highly misleading. It has recently been demonstrated (Hnatkova et al., 2019) that in the presence of heart rate changes exceeding 10 bpm, the use of fixed heart rate corrections might be substantially erroneous. The individually corrected QTc values that we obtained in this population were derived from averages over heart rate spans that well exceeded this "safety" limit (see **Figure 5**). In addition, the age-related changes in slopes of the QT/RR profiles further suggest that the experience with QTc heart rate correction formulae obtained in adult patients cannot be directly translated to accurate studies and/or clinical evaluations in children. In particular, the significantly worse log-linear regression fits of QT/RR profiles show that formulae based on this type of regression (e.g., Bazett or Fridericia corrections) are potentially highly misleading in individual clinical cases of school-aged children. Also, at fast rates as observed in younger children, the log-linear QT/RR relationship breaks down because the short uncorrected QT interval measurements (Hnatkova et al., 2017) making the use of formulae based on this relationship even more problematic.

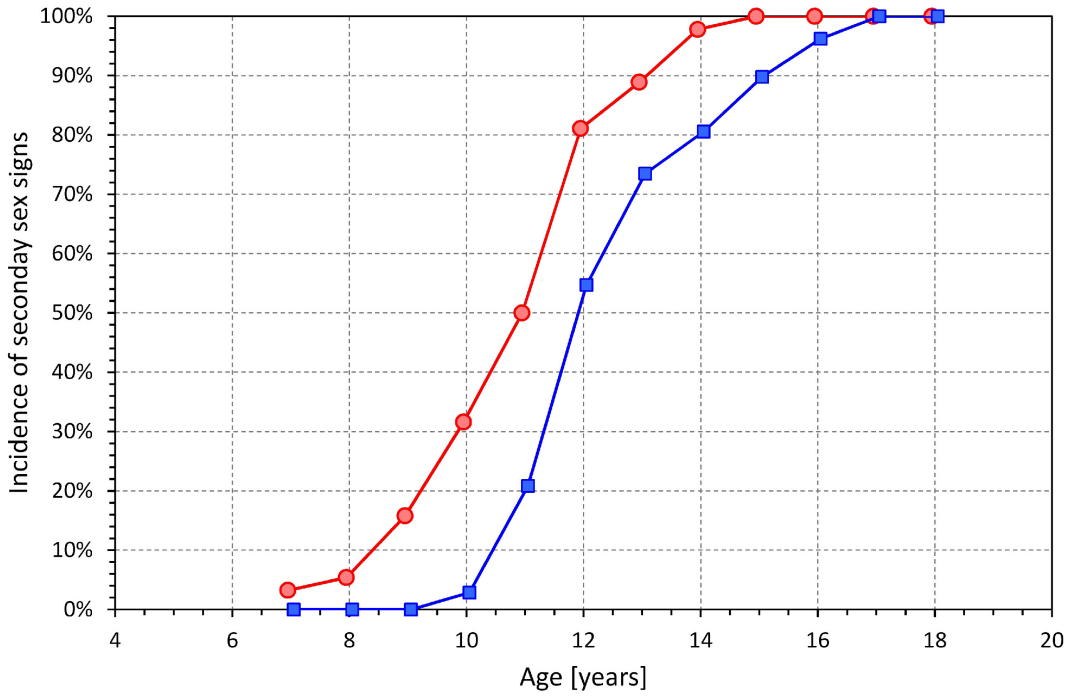

FIGURE 9 | Incidence of secondary sex signs in age bands <8 years, 7–9 years, 8–10 years, etc. up to 16–18 years, and >17 years (each shown approximately at the middle age of the band). Compare with the development of QTcI changes shown in the middle panel of **Figure 6**.

The observation that taking QT/RR hysteresis (Malik et al., 2008b; Gravel et al., 2018) into account decreases the QT/RR residuals and thus increases accuracy of the QTcI assessment is consistent with previous observations in adults. It was previously shown that considerations of QT/RR hysteresis are not only essential during episodes of heart rate changes (Malik et al., 2016; Hnatkova et al., 2019) but also valuable during episodes without any physical activity since psychologically driven fluctuations of heart rate can hardly ever be eliminated (Malik et al., 2016, 2018). In the present study, short-term variability of heart rate, likely influenced by mental reactions, was also present during the individual episodes of the investigative protocol. The observations shown in **Figure 1** were therefore not driven solely by the implications of the postural changes.

In agreement with previously published adult data (Malik et al., 2004, 2012b, 2013), we found only miniscule curvilinear QT/RR residuals (see the bottom panel of **Figure 3**). This means, among others, that in separate study individuals, the individually corrected QTc interval was practically constant during the postural provocations (detailed comparison not shown) and that the minimal variability along the curvilinear QT/RR regressions was only caused by the measurement jitter due to recordings noise. The QTcI values shown in **Figure 6** and **Supplementary Table 2** are thus applicable to different parts of the investigation experiments. Thus, similar to adult data (Malik et al., 2008c, 2013), we found the QT interval duration to be practically exclusively determined by the underlying heart rate (including the considerations of the QT/RR hysteresis) during these experiments in children and adolescents. Note also that the intra-individual QTcI stability was achieved by the sufficiently large intra-individual heart rate ranges over which the QT measurements were made and over which the QT/RR regressions were calculated.

We are not aware of other studies of individual-specific QT/RR profiles in children and adolescents with which we could compare the results of this study. Nevertheless, number of comparisons with adult data are possible. The averaged hysteresis constant close to 2 min is the same as previously reported based on adult investigations (Franz et al., 1988; Malik et al., 2008b). Clinical investigations in young to middle-aged adults found similar spans of minimal to maximal heart rates in response to similar postural maneuvering (Malik et al., 2012b). Like the adult studies, the investigated children and adolescents showed remarkable inter-subject variability of QT/RR profiles (Batchvarov et al., 2002; Malik et al., 2002). The comparison between the linear and log-linear QT/RR regressions is also known to have led to similar conclusions in adult data (Malik et al., 2012a).

Although we do not have detailed measurements of heart sizes available, it is reasonable to expect that as the body enlarges with advancing age (see **Supplementary Figures 1**, **2**) so does the heart and ventricular mass. Nevertheless, this obviously cannot explain the QTc discrepancy between the sexes since with advancing age, the QTc interval changes differently in females and males. Also, while simple heart size might have some physiologic implications

for heart rate, the influence on QTc interval, if it exists, is bound to be more complex and likely multifaceted.

While we observed a slightly higher heart rates in females compared to males (see the top panel of **Figure 5**), the differences were much smaller than the sex distinction known in adult resting heart rates (Linde et al., 2018). The reasons are possibly similar to those for the discrepancy between the secondary sex-sign maturity in females and their QTc prolongation. Prolonged autonomic conditioning in menstruating females might be needed for the autonomic regulatory equilibrium (Smetana and Malik, 2013) responsible for increased heart rates in adult pre-menopausal females.

The QTcI calculation was based on the projection of intra-subject curvilinear QT/RR regressions to predict the QT interval duration at a stable heart rate of 60 bpm. While this projection corresponded to the standard practice of heart rate correction, it required extrapolation of available data in younger children in whom the minimum heart rate was much higher (see the top panel in **Figure 5**). The low regression residuals (obtained when considering QT/RR hysteresis) suggest that this process did not lead to any substantial imprecision but in future studies in pediatric populations, corrections of QT interval to a different heart rate (e.g., 80 bpm) might prove somewhat more reliable.

Limitations

Limitations of the investigation also need to be considered. While we collected demographic data and made sure that only normal subjects without clinically apparent abnormalities were included in the analysis, we were unable (for funding reasons) to subject the participants to further testing such as echocardiography, biochemistry, or detailed anthropometric measurements. For the same reasons, we were unable to collect continuous blood pressure data. Single instance blood pressure measurements were not collected since in children, the "white coat" effects are highly noticeable. This prevents us from considering renin-angiotensin regulation. For ethical reasons, we were also unable to collect any data on mental comprehension that might potentially be important for the development of autonomic conditioning. Nevertheless, as far as we can tell, it was unlikely that cognitions skills among the participants would have shown any sex-related or age-related bias outside the standard expectations of human development. For practicality reasons, it was also impossible to synchronize the investigations with a particular phase of menstrual cycle in menstruating females. Nevertheless, data on the last menstruation were also collected and when it was attempted to analyze the data considering the menstruation cycle, no meaningful influence was found (data not shown). Our observations of a very tight relationship between the QT interval duration and the underlying (hysteresis corrected) heart rate were made during awake state. We cannot comment on the QT/RR relationship in children during sleep which in known to influence QTc duration in adults (Stramba-Badiale et al., 2000; Lanfranchi et al., 2002). Finally, while the accuracy of RR interval histories of QT interval measurements was visually validated and manually corrected where necessary, the measurements of QT intervals relied on automatic computerized processing with exclusion of noise polluted ECG episodes. Nevertheless, the markedly low QT/RR regression residuals showed that the automatic QT interval measurement was fully reliable.

CONCLUSION

Despite these limitations, the study shows that opposite QTc changes occur in both sexes during adolescent years. In the absence of detailed hormone level measurement, we can only speculate that while these QTc changes might be directly maintained by sex hormones in males, pure and direct sex hormone influence in females is less likely. The study also shows that tightly defined QT/RR patterns are achievable in children and adolescents by non-invasive postural testing. Since projection of such patterns may be used to compare the QT interval durations between different subjects, the described technique might be helpful in judging clinical cases of borderline QT interval abnormalities.

DATA AVAILABILITY

All datasets generated for this study are included in the manuscript and/or the **Supplementary Files**.

AUTHOR CONTRIBUTIONS

MM, TN, and IA conceived the study. IA, KHn, TN, and MM designed the study. IA, KHe, MŠ, and TN contributed to the clinical conduct. TN and PK supervised the clinical conduct. KHn and MM analyzed the data. IA, KHn, and MM drafted the manuscript. All authors approved the final manuscript.

FUNDING

This research was supported in part by the British Heart Foundation New Horizons Grant NH/16/2/32499 and the Ministry of Health of the Czech Republic Grant NV19-02-00197.

ACKNOWLEDGMENTS

We are grateful to the investigated subjects and their parents/guardians for their willingness to participate in this study. We are equally grateful for the kind help and support provided by the management and staff of the schools at which the recordings took place, namely Preparatory School Vedlejší, Brno; Preparatory School Údolní, Brno; Primary School Smetanův okruh, Krnov; Primary School Slovanské náměstí, Brno; Secondary and High School Smetanův okruh, Krnov; and Secondary and High School Slovanské náměstí, Brno.

SUPPLEMENTARY MATERIAL

The Supplementary Material for this article can be found online at: https://www.frontiersin.org/articles/10.3389/fphys.2019.00994/full#supplementary-material

REFERENCES

Apter, D., Räisänen, I., Ylöstalo, P., and Vihko, R. (1987). Follicular growth in relation to serum hormonal patterns in adolescent compared with adult menstrual cycles. *Fertil. Steril.* 47, 82–88. doi: 10.1016/s0015-0282(16)49940-1

Batchvarov, V. N., Ghuran, A., Smetana, P., Hnatkova, K., Harries, M., Dilaveris, P., et al. (2002). QT-RR relationship in healthy subjects exhibits substantial intersubject variability and high intrasubject stability. *Am. J. Physiol. Heart Circ. Physiol.* 282, H2356–H2363.

Franz, M. R., Swerdlow, C. D., Liem, L. B., and Schaefer, J. (1988). Cycle length dependence of human action potential duration in vivo. Effects of single extrastimuli, sudden sustained rate acceleration and deceleration, and different steady-state frequencies. *J. Clin. Invest.* 82, 972–979. doi: 10.1172/jci113706

Garnett, C. E., Zhu, H., Malik, M., Fossa, A. A., Zhang, J., Badilini, F., et al. (2012). Methodologies to characterize the QT/corrected QT interval in the presence of drug-induced heart rate changes or other autonomic effects. *Am. Heart J.* 163, 912–930. doi: 10.1016/j.ahj.2012.02.023

Gravel, H., Jacquemet, V., Dahdah, N., and Curnier, D. (2018). Clinical applications of QT/RR hysteresis assessment: a systematic review. *Ann. Noninvasive Electrocardiol.* 23:e12514. doi: 10.1111/anec.12514

Harlan, W. R., Grillo, G. P., Cornoni-Huntley, J., and Leaverton, P. E. (1979). Secondary sex characteristics of boys 12 to 17 years of age: the U.S. health examination survey. *J. Pediatr.* 95, 293–297.

Harlan, W. R., Harlan, E. A., and Grillo, G. P. (1980). Secondary sex characteristics of girls 12 to 17 years of age: the U.S. health examination survey. *J. Pediatr.* 96, 1074–1078. doi: 10.1016/s0022-3476(80)80647-0

Hnatkova, K., Johannesen, L., Vicente, J., and Malik, M. (2017). Heart rate dependency of JT interval sections. *J. Electrocardiol.* 50, 814–824. doi: 10.1016/j.jelectrocard.2017.08.005

Hnatkova, K., Smetana, P., Toman, O., Bauer, A., Schmidt, G., and Malik, M. (2009). Systematic comparisons of electrocardiographic morphology increase the precision of QT interval measurement. *Pacing Clin. Electrophysiol.* 32, 119–130. doi: 10.1111/j.1540-8159.2009.02185.x

Hnatkova, K., Vicente, J., Johannesen, L., Garnett, C., Stockbridge, N., and Malik, M. (2019). Errors of fixed QT heart rate corrections used in the assessment of drug-induced QTc changes. *Front. Physiol.* 10:635. doi: 10.3389/fphys.2019.00635

Kohler, B. U., Henning, C., and Orglmeister, R. (2002). The principles of software QRS detection- Reviewing and comparing algorithms for detecting this important ECG waveform. *IEEE Eng. Med. Biol. Mag.* 21, 42–57.

Kors, J. A., Talmon, J. L., and van Bemmel, J. H. (1986). Multilead ECG analysis. *Comput. Biomed. Res.* 19, 28–46. doi: 10.1016/0010-4809(86)90004-2

Kurokawa, J., Kodama, M., Clancy, C. E., and Furukawa, T. (2016). Sex hormonal regulation of cardiac ion channels in drug-induced QT syndromes. *Pharmacol. Ther.* 168, 23–28. doi: 10.1016/j.pharmthera.2016.09.004

Lanfranchi, P. A., Shamsuzzaman, A. S., Ackerman, M. J., Kara, T., Jurak, P., Wolk, R., et al. (2002). Sex-selective QT prolongation during rapid eye movement sleep. *Circulation* 106, 1488–1492. doi: 10.1161/01.cir.0000030183.10934.95

Lenton, E. A., Landgren, B. M., Sexton, L., and Harper, R. (1984). Normal variation in the length of the follicular phase of the menstrual cycle: effect of chronological age. *Br. J. Obstet. Gynaecol.* 91, 681–684. doi: 10.1111/j.1471-0528.1984.tb04830.x

Linde, C., Bongiorni, M. G., Birgersdotter-Green, U., Curtis, A. B., Deisenhofer, I., Furokawa, T., et al. (2018). Sex differences in cardiac arrhythmia: a consensus document of the european heart rhythm association, endorsed by the heart rhythm society and asia pacific heart rhythm society. *Europace* 20:1565-1565ao.

Malik, M., Andreas, J.-O., Hnatkova, K., Hoeckendorff, J., Cawello, W., Middle, W., et al. (2008a). Thorough QT/QTc study in patients with advanced Parkinson's disease: Cardiac safety of rotigotine. *Clin. Pharm. Therap.* 84, 595–603. doi: 10.1038/clpt.2008.143

Malik, M., Hnatkova, K., Novotný, T., and Schmidt, G. (2008b). Subject-specific profiles of QT/RR hysteresis. *Am. J. Physiol. Heart Circ. Physiol.* 295, H2356–H2363. doi: 10.1152/ajpheart.00625.2008

Malik, M., Hnatkova, K., Schmidt, A., and Smetana, P. (2008c). Accurately measured and properly heart-rate corrected QTc intervals show little daytime variability. *Heart Rhythm* 5, 1424–1431. doi: 10.1016/j.hrthm.2008.07.023

Malik, M., Färbom, P., Batchvarov, V., Hnatkova, K., and Camm, A. J. (2002). Relation between QT and RR intervals is highly individual among healthy subjects: implications for heart rate correction of the QT interval. *Heart* 87, 220–228. doi: 10.1136/heart.87.3.220

Malik, M., Garnett, C., Hnatkova, K., Johannesen, L., Vicente, J., and Stockbridge, N. (2018). Importance of QT/RR hysteresis correction in studies of drug-induced QTc interval changes. *J. Pharmacokinet. Pharmacodyn.* 45, 491–503. doi: 10.1007/s10928-018-9587-8

Malik, M., Garnett, C., Hnatkova, K., Vicente, J., Johannesen, L., and Stockbridge, N. (2019). Implications of individual QT/RR profiles - Part 1: Inaccuracies and problems of population-specific QT/heart rate corrections. *Drug Saf.* 42, 401–414. doi: 10.1007/s40264-018-0736-1

Malik, M., Hnatkova, K., Batchvarov, V., Gang, Y., Smetana, P., and Camm, A. J. (2004). Sample size, power calculations, and their implications for the cost of thorough studies of drug induced QT interval prolongation. *Pacing Clin. Electrophysiol.* 27, 1659–1669. doi: 10.1111/j.1540-8159.2004.00701.x

Malik, M., Hnatkova, K., Kowalski, D., Keirns, J. J., and van Gelderen, E. M. (2012a). Importance of subject-specific QT/RR curvatures in the design of individual heart rate corrections of the QT interval. *J. Electrocardiol.* 45, 571–581. doi: 10.1016/j.jelectrocard.2012.07.017

Malik, M., van Gelderen, E. M., Lee, J. H., Kowalski, D. L., Yen, M., Goldwater, R., et al. (2012b). Proarrhythmic safety of repeat doses of mirabegron in healthy subjects: a randomized, double-blind, placebo-, and active-controlled thorough QT study. *Clin. Pharm. Therap.* 92, 696–706. doi: 10.1038/clpt.2012.181

Malik, M., Hnatkova, K., Kowalski, D., Keirns, J. J., and van Gelderen, E. M. (2013). QT/RR curvatures in healthy subjects: sex differences and covariates. *Am. J. Physiol. Heart Circ. Physiol.* 305, H1798–H1806. doi: 10.1152/ajpheart.00577.2013

Malik, M., Johannesen, L., Hnatkova, K., and Stockbridge, N. (2016). Universal correction for QT/RR hysteresis. *Drug Safety* 39, 577–588. doi: 10.1007/s40264-016-0406-0

Mickey, E., and Brooke, R. B. (2019). *Tanner Stages*. Available at: https://www.ncbi.nlm.nih.gov/books/NBK470280/ (accessed May 13, 2019).

Novotný, T., Leinveber, P., Hnatkova, K., Reichlova, T., Matejkova, M., Sisakova, M., et al. (2014). Pilot study of sex differences in QTc intervals of heart transplant recipients. *J. Electrocardiol.* 47, 863–868. doi: 10.1016/j.jelectrocard.2014.07.015

Pahlm, O., and Sornmo, L. (1984). Software QRS detection in ambulatory monitoring – a review. *Med. Biol. Eng. Comput.* 22, 289–297. doi: 10.1007/bf02442095

Rautaharju, P. M., Mason, J. W., and Akiyama, T. (2014). New age- and sex-specific criteria for QT prolongation based on rate correction formulas that minimize bias at the upper normal limits. *Int. J. Cardiol.* 174, 535–540. doi: 10.1016/j.ijcard.2014.04.133

Rautaharju, P. M., Zhou, S. H., Wong, S., Calhoun, H. P., Berenson, G. S., Prineas, R., et al. (1992). Sex differences in the evolution of the electrocardiographic QT interval with age. *Can. J. Cardiol.* 8, 690–695.

Sarganas, G., Schaffrath Rosario, A., and Neuhauser, H. K. (2017). Resting heart rate percentiles and associated factors in children and adolescents. *J. Pediatr.* 187, 174–181. doi: 10.1016/j.jpeds.2017.05.021

Smetana, P., and Malik, M. (2013). Sex differences in cardiac autonomic regulation and in repolarisation electrocardiography. *Pflugers Arch.* 465, 699–717. doi: 10.1007/s00424-013-1228-x

Stramba-Badiale, M., Priori, S. G., Napolitano, C., Locati, E. H., Viñolas, X., Haverkamp, W., et al. (2000). Gene-specific differences in the circadian variation of ventricular repolarization in the long QT syndrome: a key to sudden death during sleep? *Ital. Heart J.* 1, 323–328.

Conflict of Interest Statement: The authors declare that the research was conducted in the absence of any commercial or financial relationships that could be construed as a potential conflict of interest.

frontiers in Physiology

ORIGINAL RESEARCH
published: 15 January 2020
doi: 10.3389/fphys.2019.01570

Risk Prediction After Myocardial Infarction by Cyclic Variation of Heart Rate, a Surrogate of Sleep-Disordered Breathing Assessed From Holter ECGs

*Xu Cao[1], Alexander Müller[1], Ralf J. Dirschinger[1], Michael Dommasch[1], Alexander Steger[1], Petra Barthel[1], Karl-Ludwig Laugwitz[1,2], Georg Schmidt[1,2] and Daniel Sinnecker[1,2]**

[1] Klinik und Poliklinik für Innere Medizin I, University Hospital Klinikum Rechts der Isar, Technical University of Munich, Munich, Germany, [2] DZHK (German Centre for Cardiovascular Research), Partner Site Munich Heart Alliance, Munich, Germany

OPEN ACCESS

Edited by:
Esther Pueyo,
University of Zaragoza, Spain

Reviewed by:
Frederic Roche,
Université Jean Monnet, France
Óscar Barquero-Pérez,
Rey Juan Carlos University, Spain
Guy Carrault,
University of Rennes 1, France

***Correspondence:**
Daniel Sinnecker
sinnecker@tum.de

Specialty section:
This article was submitted to Cardiac Electrophysiology, a section of the journal Frontiers in Physiology

Received: 15 July 2019
Accepted: 13 December 2019
Published: 15 January 2020

Citation:
Cao X, Müller A, Dirschinger RJ, Dommasch M, Steger A, Barthel P, Laugwitz K-L, Schmidt G and Sinnecker D (2020) Risk Prediction After Myocardial Infarction by Cyclic Variation of Heart Rate, a Surrogate of Sleep-Disordered Breathing Assessed From Holter ECGs. Front. Physiol. 10:1570. doi: 10.3389/fphys.2019.01570

Aims: Sleep-disordered breathing (SDB) is common among cardiac patients, but its role as an independent risk predictor after myocardial infarction (MI) is unclear. SDB causes cyclic variation of heart rate (CVHR). The aim of this study was to score Holter ECGs of a large cohort of MI survivors for SDB-related CVHR to investigate its value for mortality prediction.

Methods: A total of 1590 survivors of acute MI in sinus rhythm were prospectively enrolled and followed for 5-year all-cause mortality. Heart rate (HR) tachograms were generated from nocturnal (00:00–06.00 am) segments of Holter ECGs, and the minutes with CVHR were quantified by a previously developed algorithm. According to a pre-specified cutpoint, SDB was assumed if CVHR was present during ≥72 min.

Results: Seventy-seven patients (4.8%) had flat HR tachograms which prohibited analysis for SDB. Of the remaining 1513 patients, 584 (38.6%) were classified as having SDB. Mortality rates in groups stratified according to ECG-derived SDB did not differ significantly. Taken as a continuous variable, low CVHR duration was associated with increased mortality.

The mortality of patients with flat HR tachograms was significantly increased, even after adjustment for age, sex, LVEF, GRACE score and diabetes mellitus. Mortality prediction by a flat HR tachogram was also independent of heart rate variability (HRV), heart rate turbulence (HRT), and deceleration capacity (DC).

Conclusion: In Holter ECG recordings of survivors of acute MI, signs suggestive of SDB were frequently present, but not associated with mortality. A flat nocturnal HR tachogram was a strong, independent predictor of 5-year all-cause mortality.

Keywords: myocardial infarction, sleep-disordered breathing, cyclic variation of heart rate, risk stratification, heart rate variability

INTRODUCTION

Patients who have survived the acute phase of an acute myocardial infarction (MI) are at increased risk of subsequent mortality within the next years, which may be due to re-infraction, arrhythmias, or progressive heart failure, but also related to co-morbidities. Identification of high-risk MI survivors is a crucial part of subsequent care and secondary prophylactic therapy. Current approaches to assess the mortality risk of these patients include clinical scores (e.g., GRACE risk score) (Eagle et al., 2004) screening for co-morbidities (e.g., diabetes mellitus, renal impairment), measurement of the left-ventricular ejection fraction (LVEF), (Dagres and Hindricks, 2013) or evaluation for parameters of cardiac electric instability or cardiac autonomic dysfunction [e.g., heart rate variability (HRV), (Task Force of the European Society of Cardiology and the North American Society of Pacing and Electrophysiology, 1996) heart rate turbulence (HRT), (Schmidt et al., 1999) deceleration capacity of heart rate (DC), (Bauer et al., 2006) or severe autonomic failure (SAF, a combination of abnormal HRT and abnormal DC) (Bauer et al., 2009)].

Recently, several parameters related to respiration such as the respiratory rate (Barthel et al., 2013) [which can be also measured from Holter ECG recordings as the nocturnal respiratory rate (Dommasch et al., 2014; Sinnecker et al., 2014)] or respiratory sinus arrhythmia (Sinnecker et al., 2016) have been demonstrated to be strong predictors of the mortality risk of MI survivors.

Sleep-disordered breathing (SDB), which is an important risk factor for cardiovascular events such as MI, (Marin et al., 2016) is frequently found in MI survivors (Porto et al., 2017). The question whether the presence of SDB in survivors of acute MI bears implications for the patients' prognosis has been so far investigated in some small clinical studies, with conflicting results (Ludka et al., 2017; Shah et al., 2017). It has been recognized that SDB is accompanied by a typical pattern of heart rate decelerations (during apnea episodes) followed by accelerations (during arousals) which has been termed cyclic variation of heart rate (CVHR), (Guilleminault et al., 1984) and various algorithms have been proposed to assess the likelihood of SDB from standard Holter ECG recordings (Mendonca et al., 2018). Proprietary algorithms to perform this kind of analysis have been also implemented into commercial Holter equipment. Interestingly, a simple method to manually score RR interval tachograms generated from ECG recordings obtained during polysomnography for the presence of CVHR (Stein et al., 2003) was able to predict the presence or absence of SDB (as assessed by standard polysomnography) with a positive and negative predictive accuracy of 86 and 100%, respectively (Stein et al., 2003).

The aim of this work was to assess whether CVHR, assessed with the above mentioned method (Stein et al., 2003) from nocturnal Holter ECG recordings in a large cohort of post-infarction patients, bears prognostic information, and, if so, whether the previously described association of an increased nocturnal respiratory rate with an increased risk of non-sudden cardiac death (Dommasch et al., 2014) is related to SDB.

MATERIALS AND METHODS

Study Cohort

The study is a retrospective analysis of a previously described prospective cohort study (Bauer et al., 2009; Dommasch et al., 2014; Sinnecker et al., 2014) aimed at assessing risk predictors of subsequent mortality in survivors of the acute phase of MI. Patients admitted with acute MI at one of two centers (German Heart Centre and Klinikum rechts der Isar, both in Munich, Germany) were enrolled between May 2000 and March 2005. Inclusion criteria were (i) age $\leq$80 years, (ii) sinus rhythm at admission, (iii) MI within 4 weeks before enrollment, (iv) survival until hospital discharge, and (v) no indication for ICD implantation for secondary prophylaxis at the time of enrolment. Diagnosis of acute MI required two or more findings of: (i) chest pain for $\geq$20 min, (ii) creatine kinase more than twice the upper limit of normal, and (iii) and ST-segment elevation $\geq$0.1 mV in two or more limb leads or $\geq$0.2 mV in two or more contiguous precordial leads on admission. All study subjects underwent Holter ECG recordings during the first days after MI. Patients were followed-up for all-cause mortality for 5 years. The study was approved by the local ethics committee, and informed consent was obtained from all participants.

ECG Analysis

Holter ECG recordings (Oxford Excel Holter system, Oxford instruments; Pathfinder 700, Reynolds Medical; and Mortara Holter system, Mortara Instrument) were performed at a median of 5 days (IQR:4–7 days) after MI, with a median recording period of 21 h (IQR 19–23 h). The recordings were first automatically analyzed to annotate beats. In a second step, each recording was reviewed by a physician who corrected the annotations where necessary and removed segments that were not analyzable due to noise or technical problems.

Assessment of Cyclic Variation of Heart Rate Indicating SDB

Sleep-disordered breathing was assessed from the Holter ECGs using a previously developed method (Stein et al., 2003). Care was taken to faithfully follow the published method, which is based on manual annotation and scoring of tachograms generated from the Holter ECGs. Due to the large number of ECGs in our study, we did not print out the tachograms on paper and marked CVHR episodes with a pen as originally suggested (Stein et al., 2003), but rather inspected the tachograms on a computer screen and annotated the CVHR episodes using a mouse. To this end, a custom-written analysis software was used that plotted the instantaneous heart rate (i.e., the inverse of normal-to-normal intervals) to a computer screen and allowed manual annotation of CVHR episodes, which were stored in a database for further analysis. We restricted the analysis to a nocturnal 6-h segment (00:00–06.00 am) of the recordings, assuming that most of the patients would be asleep during this time. The analysis was performed by a physician with experience in biosignal analysis.

As previously described (Stein et al., 2003), some patients had a flat HR tachogram during the analyzed nocturnal segment,

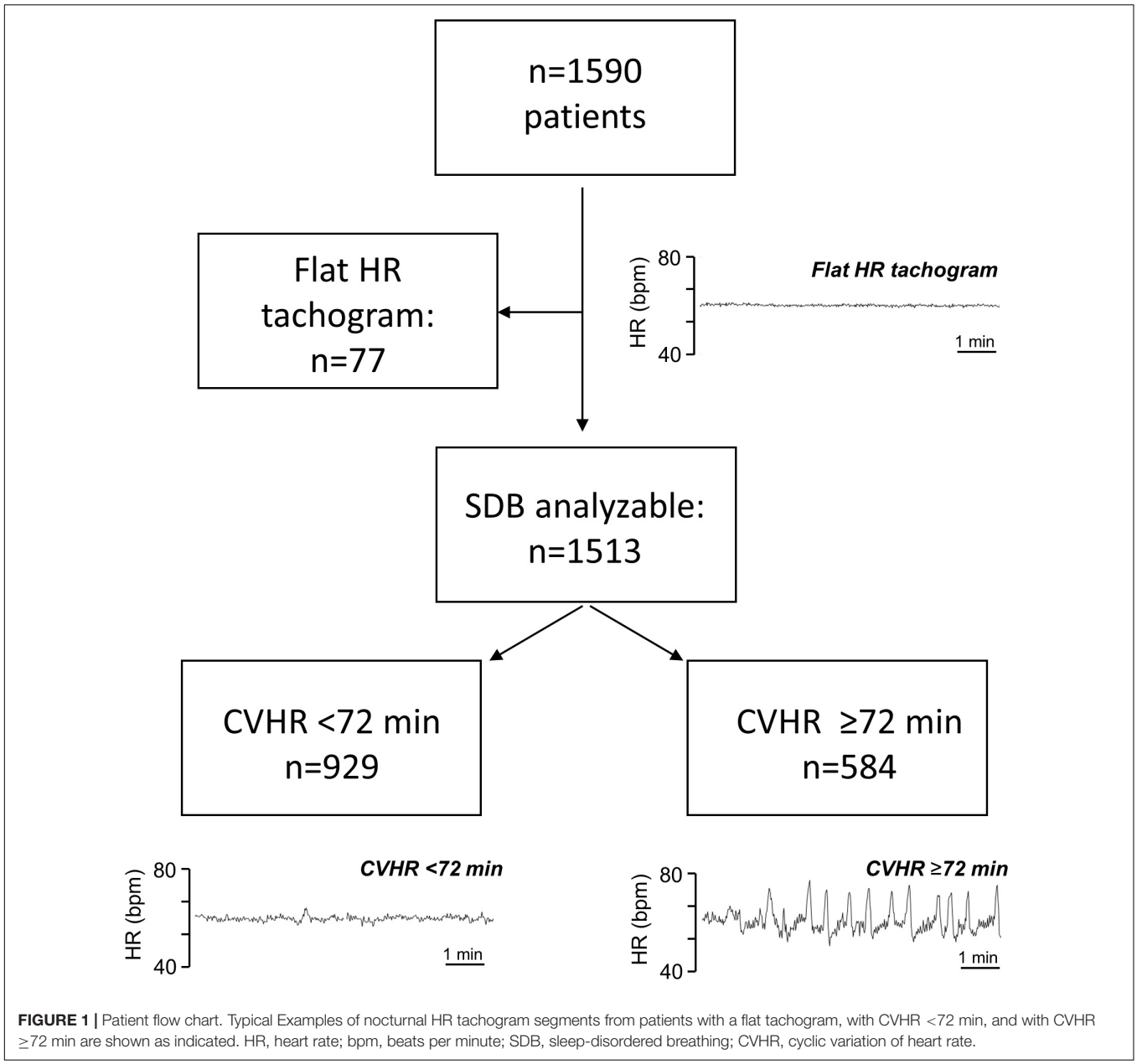

FIGURE 1 | Patient flow chart. Typical Examples of nocturnal HR tachogram segments from patients with a flat tachogram, with CVHR <72 min, and with CVHR ≥72 min are shown as indicated. HR, heart rate; bpm, beats per minute; SDB, sleep-disordered breathing; CVHR, cyclic variation of heart rate.

which was defined as a tachogram having (1) no changes of the instantaneous heart rate exceeding ≥5 beats/min, and (2) no visible respiratory sinus arrhythmia (**Figure 1**). In patients with a flat tachogram, it is not possible to obtain information on the presence of SDB from ECG recordings (Stein et al., 2003). In all recordings not exhibiting any CVHR episodes (see below), the presence or absence of a flat nocturnal tachogram according to the above definition was independently judged by two physicians, and a consensus regarding the presence or absence of a flat nocturnal tachogram was reached in each of these cases. All persons involved in the analysis of the biosignals were blinded to the outcome of the patients.

Recordings with a non-flat tachogram were evaluated for episodes of CVHR, which were defined as previously described (Stein et al., 2003) as ECG segments containing ≥3 successive HR increases (arousals) of at least 6 bpm and at least 10 s duration, with ≤2 min between two successive arousals. The total duration of the CVHR episodes during a recording was calculated based on the manual annotation of CVHR episodes. According to the pre-specified cutpoint, SDB was assumed if CVHR episodes were present in ≥20% of the recording, (Stein et al., 2003) which corresponds to ≥72 min of the nocturnal 6-h segment.

Mean Nocturnal Respiratory Rate

Nocturnal respiratory rate was automatically derived from Holter recordings by a previously described algorithm (Dommasch et al., 2014; Sinnecker et al., 2014) analyzing beat-to-beat changes in QRS amplitudes, QRS vectors, and RR intervals.

TABLE 1 | Baseline characteristics.

Variable	All patients (*n* = 1590)	"Non-flat tachogram" (*n* = 1513)	"Flat tachogram" (*n* = 77)	*p*-Value ("flat" vs."non-flat" tachogram)	"Non-flat tachogram"		*p*-Value (CVHR <72 min vs. CVHR ≥72 min)
					CVHR <72 min (*n* = 929)	CVHR ≥72 min (*n* = 584)	
Age (median [IQR])	59.2 [51.6–66.8]	58.6 [51.2–66.3]	67.2 [59.7–73.3]	<0.001	60.3 [54.0–67.7]	55.9 [48.5–64.1]	<0.001
Females, *n* (%)	327 (20.6)	302 (20.0)	25 (32.5)	0.012	216 (23.3)	86 (14.7)	<0.001
Acute intervention, n (%)				0.051			0.47
PCI	1451 (91.3)	1384 (91.5)	67 (78.0)		840 (90.4)	544 (93.2)	
CABG	33 (2.1)	30 (2.0)	3 (3.9)		22 (2.4)	8 (1.4)	
Thrombolysis	54 (3.4)	53 (3.5)	1 (1.3)		37 (4.0)	16 (2.7)	
None	52 (3.3)	46 (3.0)	6 (7.8)		30 (3.2)	16 (2.7)	
Diabetes mellitus, *n* (%)	270 (17)	249 (16.2)	32 (41.6)	<0.001	158 (17.0)	80 (13.7)	0.099
LVEF (median [IQR])	55 [45–63]	55 [45–63]	48 [39–57]	<0.001	55 [45–63]	56 [46–63]	0.836
GRACE Score [mean (sd)]	96 (80–113)	96 (79–112)	114 (103–125)	<0.001	99 (82–113)	90 (75–108)	<0.001
CK_{max}, U/l (median [IQR])	1140 [569–2478]	1140 [569–2478]	1082 [566–2420]	0.856	1110 [560–2429]	1200 [586–2518]	0.33
Creatinine, mg/dl (median [IQR])	1.1 [0.9–1.3]	1.1 [0.9–1.3]	1.2 [1.0–1.5]	0.002	1.1 [1.0–1.3]	1.1 [0.9–1.2]	0.019

IQR, inter-quartile range; PCI, percutaneous coronary intervention; CABG, coronary artery bypass grafting; LVEF, left-ventricular ejection fraction; GRACE, Global Registry of Acute Coronary Events; CKmax, maximal creatine kinase plasma concentration.

Heart Rate Variability and Severe Autonomic Failure

Parameters assessing HRV (time-domain and frequency-domain parameters, HRT, DC) were determined from the Holter recordings using standard methods (Task Force of the European Society of Cardiology and the North American Society of Pacing and Electrophysiology, 1996; Sassi et al., 2015). According to a previous report, (Bauer et al., 2009) SAF was defined as the combination of both abnormal HRT (slope $\leq$2.5 ms/RR and onset $\geq$0%) and abnormal cardiac DC ($\leq$4.5 ms).

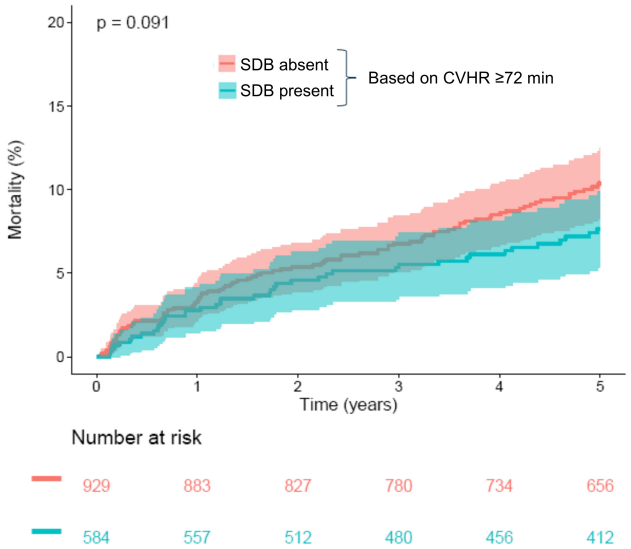

FIGURE 2 | Survival in patients stratified according to CVHR. Kaplan–Meier curves along with 95% confidence intervals are shown for patients with CVHR <72 min ("SDB absent") and ≥72 min ("SDB present"). The numbers of patients at risk in the respective groups are shown below the graph. CVHR, cyclic variation of heart rate; SDB, sleep-disordered breathing.

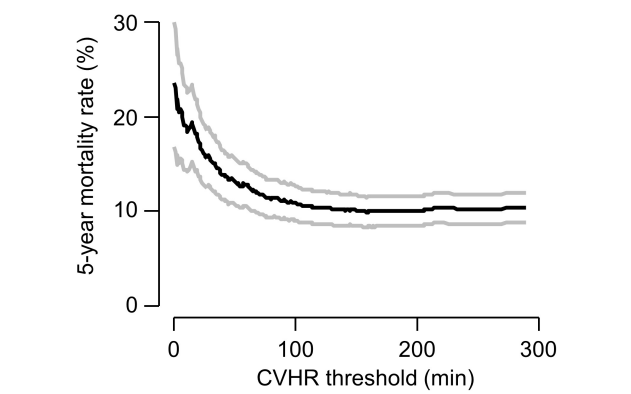

FIGURE 3 | Continuous association of CVHR with mortality. The 5-year mortality rate (black curve) estimated by the Kaplan–Meier method in patients with a non-flat tachogram with a CVHR duration less than or equal to a certain threshold are plotted as a function of this threshold. Gray curves show 95% confidence limits of the mortality estimate.

Left-Ventricular Ejection Fraction

Left-ventricular ejection fraction was measured within 2 weeks after MI by angiography or biplane echocardiography (Sonos 5500, Hewlett Packard) based on Simpson's method.

GRACE Score

The clinical GRACE score to predict the long-term mortality risk was calculated based on age, history of past heart failure and MI, serum creatinine and the cardiac biomarker status at admission, pulse and systolic blood pressure at admission, ST segment deviation and in-hospital percutaneous coronary intervention as described previously (Eagle et al., 2004).

Endpoint of the Study

The primary endpoint was all-cause mortality within 5 years after index MI. Follow-up was conducted with clinical appointments every 6 months. Participants who missed these appointments were contacted by letter, telephone, or through their General Practitioner. If necessary, the local population registry was contacted to obtain the new address in case participants changed residence, or to confirm death in case participants deceased.

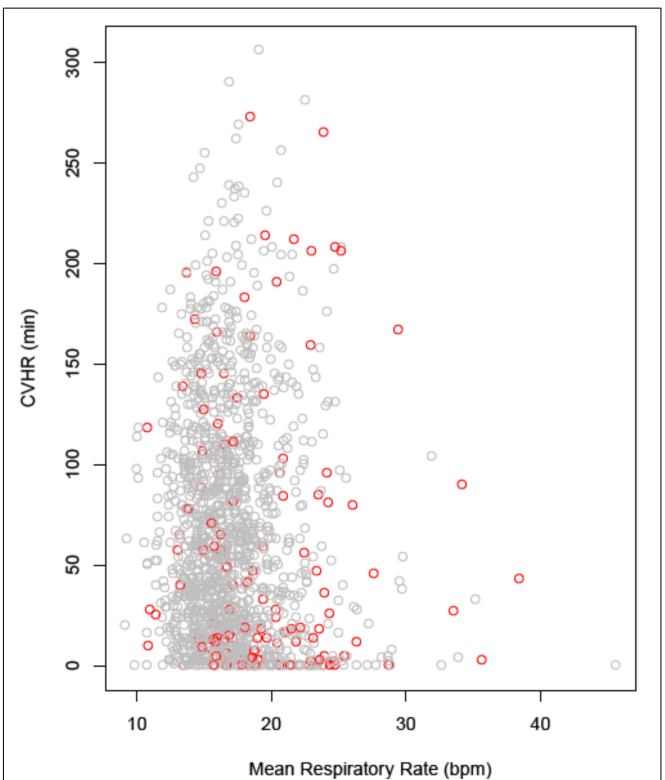

FIGURE 4 | Correlation between nocturnal CVHR and respiratory rate. CVHR is expressed as the number of minutes with CVHR within the nocturnal 6-h segment, respiratory rate as the mean value over the same segment. Data points from patients who were alive at 5 years are printed in gray, data points from deceased patients in red. CVHR, cyclic variation of heart rate; bpm, breaths per minute.

Statistical Analysis

Continuous variables are presented as median and interquartile range (IQR), and categorical data are presented as frequency and percentage.

The linear correlation of two sets of data points was assessed by Pearson correlation coefficient. Survival curves were generated using the Kaplan–Meier method and compared with the log-rank test. Univariable or multivariable Cox analysis was performed to calculate hazard ratios (with 95% confidence intervals) for 5-year all-cause mortality.

R 3.0.1 (R Foundation for Statistical Computing, Vienna, Austria) was used for all statistical calculations. Differences were considered statistically significant if $p < 0.05$.

RESULTS

A total of 1590 patients hospitalized for acute MI met the inclusion criteria and were included in the analysis. Out of these, 1513 patients had a "non-flat tachogram," i.e., it was possible to score the heart rate tachogram for SDB-related CVHR (**Figure 1**). Of these patients, 584 had CVHR episodes in ≥72 min of the analyzed 6-h segment, indicating presence of SDB, while 929 were classified as not having SDB. The remaining 77 patients showed a "flat tachogram" (see **Figure 1**).

The clinical and demographic characteristics of patients with "flat" and "non-flat" HR tachograms are shown in **Table 1**. Patients with a "flat tachogram" were older, more often female, had a higher GRACE score, a lower LVEF, and a higher prevalence of diabetes mellitus. The first part of the section "Results" will focus on the patients with a "non-flat tachogram" to assess the prognostic implications of Holter-derived screening for SDB. The second part will investigate the prognostic implications of a "flat tachogram."

Patients With a "Non-flat Tachogram"

CVHR ≥72 min, indicating presence of SDB, was found in 584/1513 patients (38.6%). Compared to the group with <72 min of CVHR, indicating absence of SDB, these patients were younger, more often male, and had a significantly lower GRACE score, whereas no significant differences were present regarding other risk factors (**Table 1**). Five-year all-cause mortality did not differ significantly between these two groups (**Figure 2**).

As an exploratory analysis, we investigated the effect of the overall duration of CVHR episodes, treated as a continuous variable, on 5-year mortality (**Figure 3**). Interestingly, very short CVHR durations, markedly below the threshold of 72 min that indicates absence of sleep apnea, were associated with substantially increased mortality rates (see **Figure 3**).

There was no substantial correlation between continuous CVHR duration and the nocturnal respiratory rate (NRR) determined from the identical segment of the ECG recording (**Figure 4**; correlation coefficient −0.068). In multivariable Cox regression, NRR (hazard ratio 3.1; $p = < 0.0001$), but not CVHR (hazard ratio 0.99; $p = 0.31$) was a significant mortality predictor in our cohort.

Patients With a "Flat Tachogram"

A comparison of the mortality rates in patients with a "flat tachogram" and in the remaining patients revealed that a "flat tachogram" identifies a high-risk population with a substantially increased 5-year mortality rate [29.1% (95% CI 17.7–38.9) vs. 9.4% (95% CI 7.8–10.9); $p < 0.0001$; **Figure 5**]. This may be partly explained by the above-mentioned differences in baseline risk factors. However, in multivariable Cox analysis considering also age, sex, LVEF, GRACE score, and diabetes mellitus, a "flat tachogram" was independently associated with mortality with a hazard ratio of 1.7 ($p = 0.022$) (**Table 2**).

A "flat tachogram" can be considered indicative of a markedly reduced HRV. It is well-known that reduced HRV signifies an increased risk in cardiac patients (Task Force of the European Society of Cardiology and the North American Society of Pacing and Electrophysiology, 1996; Sassi et al., 2015). To investigate whether the presence of a "flat tachogram" simply signifies reduced HRV that could be captured also by assessing classical HRV parameters (SDNN, HRVTI, SDANN, RMSSD,

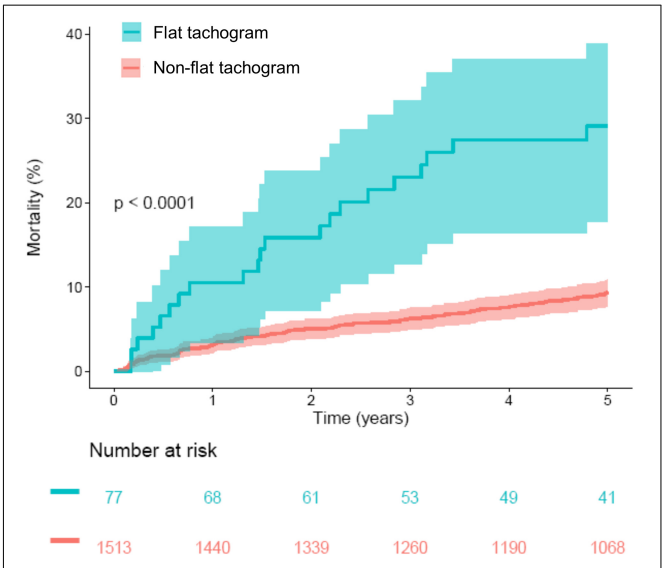

FIGURE 5 | Survival in patients stratified according to presence or absence of a flat heart rate tachogram. Kaplan–Meier curves along with 95% confidence intervals are shown. The numbers of patients at risk in the respective groups are shown below the graph. CVHR, cyclic variation of heart rate; SDB, sleep-disordered breathing.

TABLE 2 | Multivariable Cox analysis.

Variable	Hazard ratio (95% CI)	*p*-Value
Flat HR tachogram	1.73 (1.08–2.78)	0.022
Age (per year)	1.06 (1.03–1.08)	<0.0001
Female sex	0.98 (0.67–1.44)	0.92
LVEF (per %)	0.95 (0.93–0.96)	<0.0001
GRACE score (per point)	1.004 (0.99–1.01)	0.47
Diabetes mellitus	1.66 (1.17–2.35)	0.005

HR, heart rate; LVEF, left-ventricular ejection fraction; GRACE, Global Registry of Acute Coronary Events.

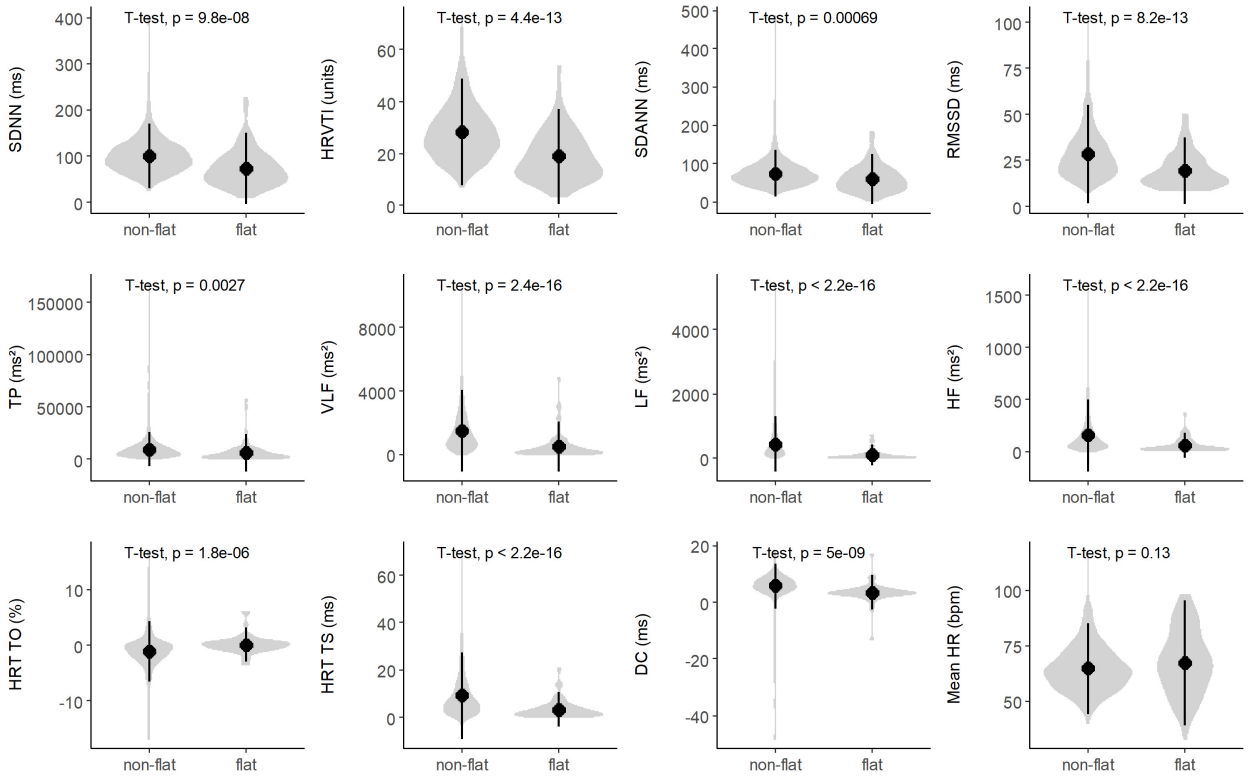

FIGURE 6 | Distribution of heart rate variability (HRV) parameters in patients with non-flat and flat nocturnal tachograms. The gray violin plots illustrate kernel probability density, while the black circles and vertical lines indicate means and 95% confidence intervals, respectively. SDNN, standard deviation of all normal-to-normal intervals; HRVTI, HRV triangular index; SDANN, standard deviation of the averages of NN intervals in 5 min segments; RMSSD, the square root of the mean of the sum of the squares of differences between adjacent NN intervals; TP, total power; VLF, very low frequency; LF, low frequency; HF, high frequency; HRT, heart rate turbulence; TO, turbulence onset; TS, turbulence slope; DC, deceleration capacity; HR, heart rate.

TP, VLF, LF, HF; see legend to **Figure 6** for an explanation of the abbreviations), we first investigated the distribution of these parameters in patients with "flat" and "non-flat" tachograms (**Figure 6**). Indeed, the mean values of all these HRV parameters were significantly lower in the patients with a "flat tachogram." However, the distributions of all these HRV parameters showed a high degree of overlap between patients with "flat" and "non-flat" nocturnal tachograms (see **Figure 6**). In univariable Cox models, each of the parameters shown in **Figure 6** was a significant predictor of 5-year mortality. In pairwise multivariable Cox models considering each of these parameters together with the presence of a "flat nocturnal tachogram," the flat tachogram always remained an independent mortality predictor (data not shown), corroborating that its presence conveys prognostic information not captured by classical HRV parameters. All heart rate variability parameters shown in **Figure 6**, together with mortality status at 5 years, flat nocturnal tachogram status, and the number of minutes with CVHR during the nocturnal segment for all patients are given in **Supplementary Table S1**.

More recently introduced parameters based on the variation of RR intervals such as HRT (Schmidt et al., 1999) or DC (Bauer et al., 2006) provide much stronger risk stratification information than classical HRV parameters (the distribution of these parameters in patients with "non-flat" and "flat" nocturnal tachograms is also shown in **Figure 6**). However, in our cohort, presence of a "flat tachogram" even provided additional prognostic value when added to "severe autonomic failure" (SAF), a parameter combining HRT and DC (Bauer et al., 2009): of the 1590 patients in our cohort, 111 had SAF, and 77 had a "flat tachogram." The overlap between these two groups was small; only 18 patients had both, a "flat tachogram" and SAF. Presence of SAF identified a high-risk group of 111 patients who had a 5-year mortality risk of 40% (**Figure 7**). However, the presence of a "flat tachogram" in patients without SAF identified another high-risk group of 59 patients with an almost similarly high mortality rate (see **Figure 7**). In a multivariable Cox model considering also LVEF and GRACE score, SAF and a "flat tachogram" were independent risk predictors with hazard ratios of 2.9 ($p < 0.001$) and 1.9 ($p = 0.013$), respectively, indicating that the presence of a "flat tachogram" provides additional prognostic information in survivors of acute MI.

DISCUSSION

In this study, we applied a previously developed algorithm to screen nocturnal segments from Holter recordings of a large cohort of survivors of acute MI for SDB based on CVHR. The primary result of our study was that a nocturnal ECG pattern

indicative of SDB did not have prognostic implications regarding 5-year mortality rate in this patient cohort (see **Figure 2**).

Of those patients in whom the algorithm to detect SDB from the ECG could be applied, 38.6% had a nocturnal ECG pattern indicative of SDB in this cohort of post-infarction patients. This fits well with numerous evidence referring to a high prevalence of SDB among cardiac patients [e.g., 30–50% of patients with coronary heart disease (Andreas et al., 1996; Hayano et al., 2017)] and underscores the importance of this disease entity in post-infarction patients.

In some patients (4.8% in our cohort), a "flat" heart rate tachogram does not allow an evaluation for signs of SDB. Considering that reduced HRV, as a sign of cardiac autonomic dysfunction, is a known predictor of adverse outcome, (Task Force of the European Society of Cardiology and the North American Society of Pacing and Electrophysiology, 1996) it might be speculated that the "flat tachogram" is also indicative of cardiac autonomic dysfunction and poor prognosis. Indeed, patients with a "flat tachogram" were characterized by a higher burden of cardiovascular risk factors at baseline (see **Table 1**). In a multivariable logistic regression analysis considering all baseline parameters shown in **Table 1**, only advanced age, presence of diabetes mellitus and reduced LVEF were significantly associated with the presence of a "flat" nocturnal tachogram (data not shown).

Interestingly, however, this "flat tachogram" was a strong risk predictor even after adjustment for baseline risk factors (see **Figure 7** and **Table 2**), providing prognostic information independent from both, "classical" HRV parameters and more recently introduced parameters such as HRT and DC. This unexpected result warrants further investigation. We hypothesize that SDB is a strong stimulus for the sympatho-vagal regulatory circuits influencing the heart rate, and that some of our patients with SDB cannot react to this stimulus (i.e., do not develop CVHR) because of severe impairment of the cardiac autonomic system. The existence of such a mechanism has been demonstrated in a cohort of coronary artery disease patients with preserved (LVEF >50%) and reduced (LVEF ≤35%) left-ventricular function who underwent sleep studies using a Holter ECG and pulse oximetry (Keyl et al., 2017): In patients with preserved LVEF, sleep-apnea-related nocturnal periods of cyclic variations in the oxygen saturation were accompanied by significantly increased HRV and a shift of the sympatho-vagal balance toward sympathetic predominance, whereas in patients with reduced LVEF, this autonomic response to cyclic oxygen desaturations was blunted. Our hypothesis is also in line with a recent report in which the amplitude of the HR fluctuations related to CVHR was investigated by phase-rectified signal averaging (Hayano et al., 2017). This amplitude, rather than the frequency of CVHR episodes, was associated with mortality in different patient cohorts with MI, chronic heart failure, and end-stage renal disease, with a lower amplitude of CVHR indicating an increased mortality risk (Hayano et al., 2017). Interestingly, also in this study, 3.6% of the patients did not have enough CVHR episodes to calculate CVHR amplitude (similar to our 4.8% "flat tachogram" patients, even though the definition of this patient group was slightly different). The mortality risk of this subgroup, however, was not reported.

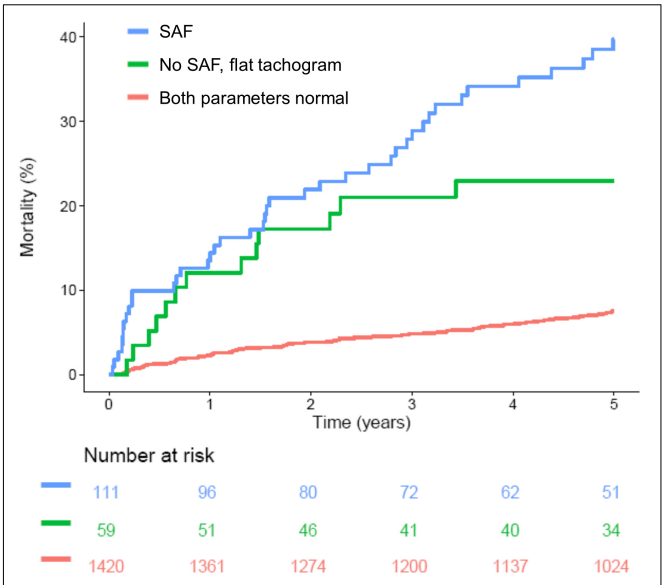

FIGURE 7 | Survival in patients stratified according to presence of a flat heart rate tachogram and severe autonomic failure (SAF). Kaplan–Meier curves are shown for patients without a flat tachogram and SAF ("Both parameters normal"), for patients with SAF regardless of flat tachogram status ("SAF") and for the subgroup of patients without SAF, but with a flat nocturnal HR tachogram ("No SAF, flat tachogram"). The numbers of patients at risk in the respective groups are shown below the graph.

An exploratory analysis of our data was also consistent with the hypothesis that, at least in a substantial fraction of patients, reduced CVHR might signify cardiac autonomic impairment rather than absence of SDB: For the above-reported results, we used the pre-defined cutoff of CVHR in ≥72 min of the analyzed time segment to assume presence of SDB (Stein et al., 2003). However, in our data, there was a continuous association of CVHR duration and increased mortality risk (see **Figure 3**), and the optimal cutpoint with regard to risk stratification would be rather ≤19 min within the 6-h segment. Using this cutpoint, a significant association between CVHR and 5-year mortality was present (data not shown). Notably, a lower CVHR duration was associated with increased risk, i.e., the high-risk group consisted of those patients with CVHR in 19 min or less of the analyzed time segment. We hypothesize that cardiac autonomic impairment, by blunting the heart rate response to CVHR, reduces the number of apnea episodes detectable by CVHR.

Presence of a "flat nocturnal heart rate tachogram" can be easily assessed from standard Holter ECG recordings. It would be interesting to investigate whether its presence provides similar independent prognostic information in other cohorts, or whether the prognostic implications of other ECG-derived parameters profit from only investigating them during a nocturnal time segment.

However, since no polysomnograms were performed in our patients, we do not know how many of the patients actually had SDB. Thus, the study does not allow to make any statement

on whether the presence of SDB (as opposed to "a nocturnal ECG pattern suggestive of SDB") is an independent risk factor in survivors of acute MI. It would be very informative to obtain polysomnogram data from a similar cohort and subsequently follow the patients for endpoints such as mortality, which could answer this question.

Nonetheless, our results suggest that screening for SDB by means of ECG analysis does not provide any meaningful prognostic information in addition to the "classical" risk factors. The fact that the patients with a "flat tachogram" – in whom ECG-based screening for SDB is not possible – are a patient population with an extraordinarily high 5-year mortality risk should raise caution regarding the use of ECG-based SDB detection tools in post-MI patients. If they are used, one should consider performing additional tests, e.g., portable cardiorespiratory polygraphy or polysomnography, in patients with a "flat tachogram" in the Holter ECG to avoid missing possibly important information in a particularly vulnerable patient group. However, even in patients who have a "non-flat" tachogram, one cannot decide, based on the ECG recordings alone, whether a very infrequent occurrence of CVHR solely signifies absence of SDB, or rather severe cardiac autonomic dysfunction.

In our previous study, which revealed that post-MI patients with an increased nocturnal respiratory rate are at increased risk of non-sudden cardiac death (Dommasch et al., 2014; Sinnecker et al., 2014) we could not exclude the possibility that this association is (at least partly) mediated by SDB. Our present study indicates that there is no correlation between SDB and the nocturnal respiratory rate.

Limitations

All the patients enrolled in our study were in sinus rhythm. Thus, we cannot make any statement on the utility of the algorithm in patients with atrial fibrillation. Similarly, we only investigated patients with a recent MI, and it may not be valid to extrapolate our findings to patients with other cardiac conditions.

Since we did not directly measure respiration in our patients, we cannot exclude that SDB that escaped detection by the screening algorithm (possibly in the patients with a "flat tachogram") bears prognostic information after MI. Similarly, since our algorithm does not allow to discriminate between patients with obstructive (OSA) and central (CSA) sleep apnea, we cannot make any statement on differential prognostic implications of these two forms of SDB. It is also possible that part of the observed CVHR arises from sleep fragmentation unrelated to sleep apnea, which is common among hospitalized patients (Macfarlane et al., 2019).

The high-risk group defined by a flat nocturnal tachogram is small (only 4.8% of the whole cohort). This may limit the power of statistical analyses comparing this group to the remaining patients.

CONCLUSION

In survivors of acute MI, Holter recordings suggesting SDB are frequently seen. In our cohort, this specific pattern was not associated with an altered mortality rate. A nocturnal "flat tachogram" — indicating impaired autonomic control of heart rate, and making Holter-based screening for SDB impossible — was a strong and independent mortality predictor after MI. Thus, Holter-based detection methods for sleep apnea should be used with caution in cardiac patients.

DATA AVAILABILITY STATEMENT

The datasets generated for this study are available on request to the corresponding author.

ETHICS STATEMENT

The studies involving human participants were reviewed and approved by the Ethics Committee of the Klinikum rechts der Isar der Technischen Universität München. The patients/participants provided their written informed consent to participate in this study.

AUTHOR CONTRIBUTIONS

DS planned and coordinated the study and performed final data analysis. XC, AM, RD, AS, and MD analyzed the data. GS and PB planned, performed, and supervised the prospective clinical study on which this subanalysis is based. GS and K-LL provided administrative oversight and support. DS and XC wrote the first version of the manuscript, with input from all authors.

FUNDING

This work was supported by the Bundesministerium für Bildung, Wissenschaft, Forschung und Technologie (13N/7073/7), the Deutsche Forschungsgemeinschaft (Si 1747/1-1), and the German Heart Research Foundation (Deutsche Stiftung für Herzforschung, F/19/16). Publication was supported by the German Research Foundation (DFG) and the Technical University of Munich within the funding programme Open Access Publishing.

SUPPLEMENTARY MATERIAL

The Supplementary Material for this article can be found online at: https://www.frontiersin.org/articles/10.3389/fphys.2019.01570/full#supplementary-material

REFERENCES

Andreas, S., Schulz, R., Werner, G. S., and Kreuzer, H. (1996). Prevalence of obstructive sleep apnoea in patients with coronary artery disease. *Coron. Art. Dis.* 7, 541–545.

Barthel, P., Wensel, R., Bauer, A., Müller, A., Wolf, P., Ulm, K., et al. (2013). Respiratory rate predicts outcome after acute myocardial infarction: a prospective cohort study. *Eur. Heart J.* 34, 1644–1650. doi: 10.1093/eurheartj/ehs420

Bauer, A., Barthel, P., Schneider, R., Ulm, K., Müller, A., Joeinig, A., et al. (2009). Improved Stratification of Autonomic Regulation for risk prediction in post-infarction patients with preserved left ventricular function (ISAR-Risk). *Eur. Heart J.* 30, 576–583. doi: 10.1093/eurheartj/ehn540

Bauer, A., Kantelhardt, J. W., Barthel, P., Schneider, R., Mäkikallio, T., Ulm, K., et al. (2006). Deceleration capacity of heart rate as a predictor of mortality after myocardial infarction: cohort study. *Lancet* 367, 1674–1681. doi: 10.1016/s0140-6736(06)68735-7

Dagres, N., and Hindricks, G. (2013). Risk stratification after myocardial infarction: is left ventricular ejection fraction enough to prevent sudden cardiac death? *Eur. Heart J.* 34, 1964–1971. doi: 10.1093/eurheartj/eht109

Dommasch, M., Sinnecker, D., Barthel, P., Müller, A., Dirschinger, R. J., Hapfelmeier, A., et al. (2014). Nocturnal respiratory rate predicts non-sudden cardiac death in survivors of acute myocardial infarction. *J. Am. Coll. Cardiol.* 63, 2432–2433. doi: 10.1016/j.jacc.2014.02.525

Eagle, K. A., Lim, M. J., Dabbous, O. H., Pieper, K. S., Goldberg, R. J., and Van de Werf, F. (2004). A validated prediction model for all forms of acute coronary syndrome: estimating the risk of 6-month postdischarge death in an international registry. *J. Am. Med. Assoc.* 291, 2727–2733.

Guilleminault, C., Connolly, S., Winkle, R., Melvin, K., and Tilkian, A. (1984). Cyclical variation of the heart rate in sleep apnoea syndrome. Mechanisms and usefulness of 24 h electrocardiography as a screening technique. *Lancet* 1, 126–131. doi: 10.1016/s0140-6736(84)90062-x

Hayano, J., Yasuma, F., Watanabe, E., Carney, R. M., Stein, P. K., Blumenthal, J. A., et al. (2017). Blunted cyclic variation of heart rate predicts mortality risk in post-myocardial infarction, end-stage renal disease, and chronic heart failure patients. *Europace* 19, 1392–1400. doi: 10.1093/europace/euw222

Keyl, C., Lemberger, P., Rödig, G., Dambacher, M., and Frey, A. W. (2017). Changes in cardiac autonomic control during nocturnal repetitive oxygen desaturation episodes in patients with coronary artery disease. *J. Cardiovasc. Risk* 3, 221–227. doi: 10.1097/00043798-199604000-00015

Ludka, O., Stepanova, R., Sert-Kuniyoshi, F., Spinar, J., Somers, V. K., and Kara, T. (2017). Differential likelihood of NSTEMI vs STEMI in patients with sleep apnea. *Int. J. Cardiol.* 248, 64–68. doi: 10.1016/j.ijcard.2017.06.034

Macfarlane, M., Rajapakse, S., and Loughran, S. (2019). What prevents patients sleeping on an acute medical ward? An actigraphy and qualitative sleep study. *Sleep Health* 5, 666–669. doi: 10.1016/j.sleh.2019.06.012

Marin, J. M., Carrizo, S. J., Vicente, E., and Agusti, A. G. (2016). Long-term cardiovascular outcomes in men with obstructive sleep apnoea-hypopnoea with or without treatment with continuous positive airway pressure: an observational study. *Lancet* 365, 1046–1053. doi: 10.1016/s0140-6736(05)71141-7

Mendonca, F., Mostafa, S. S., Ravelo-Garcia, A. G., Morgado-Dias, F., and Penzel, T. A. (2018). Review of Obstructive Sleep Apnea Detection Approaches. *IEEE J. Biomed. Health Inform.* doi: 10.1109/JBHI.2018.2823265 [Epub ahead of print].

Porto, F., Sakamoto, Y. S., and Salles, C. (2017). Association between Obstructive Sleep Apnea and Myocardial Infarction: a Systematic Review. *Arq. Bras. Cardiol.* 108, 361–369. doi: 10.5935/abc.20170031

Sassi, R., Cerutti, S., Lombardi, F., Malik, M., Huikuri, H. V., Peng, C. K., et al. (2015). Advances in heart rate variability signal analysis: joint position statement by the e-Cardiology ESC Working Group and the European Heart Rhythm Association co-endorsed by the Asia Pacific Heart Rhythm Society. *Europace* 17, 1341–1353. doi: 10.1093/europace/euv015

Schmidt, G., Malik, M., Barthel, P., Schneider, R., Ulm, K., Rolnitzky, L., et al. (1999). Heart-rate turbulence after ventricular premature beats as a predictor of mortality after acute myocardial infarction. *Lancet* 353, 1390–1396. doi: 10.1016/s0140-6736(98)08428-1

Shah, N., Redline, S., Yaggi, H. K., Wu, R., Zhao, C. G., Ostfeld, R., et al. (2017). Obstructive sleep apnea and acute myocardial infarction severity: ischemic preconditioning? *Sleep Breath* 17, 819–826. doi: 10.1007/s11325-012-0770-7

Sinnecker, D., Dommasch, M., Barthel, P., Müller, A., Dirschinger, R. J., Hapfelmeier, A., et al. (2014). Assessment of mean respiratory rate from ECG recordings for risk stratification after myocardial infarction. *J. Electrocardiol.* 47, 700–704. doi: 10.1016/j.jelectrocard.2014.04.021

Sinnecker, D., Dommasch, M., Steger, A., Berkefeld, A., Hoppmann, P., Müller, A., et al. (2016). Expiration-Triggered Sinus Arrhythmia Predicts Outcome in Survivors of Acute Myocardial Infarction. *J. Am. Coll. Cardiol.* 67, 2213–2220. doi: 10.1016/j.jacc.2016.03.484

Stein, P. K., Duntley, S. P., Domitrovich, P. P., Nishith, P., and Carney, R. M. (2003). A simple method to identify sleep apnea using Holter recordings. *J. Cardiovasc. Electrophysiol.* 14, 467–473. doi: 10.1046/j.1540-8167.2003.02441.x

Task Force of the European Society of Cardiology and the North American Society of Pacing and Electrophysiology (1996). Heart rate variability. Standards of measurement, physiological interpretation, and clinical use. *Eur. Heart. J.* 17, 354–381. doi: 10.1093/oxfordjournals.eurheartj.a014868

Conflict of Interest: The authors declare that the research was conducted in the absence of any commercial or financial relationships that could be construed as a potential conflict of interest.

frontiers in Physiology

ORIGINAL RESEARCH
published: 11 February 2020
doi: 10.3389/fphys.2020.00077

Cardiovascular Mortality Can Be Predicted by Heart Rate Turbulence in Hemodialysis Patients

Matthias C. Braunisch[1†], Christopher C. Mayer[2†], Axel Bauer[3,4], Georg Lorenz[1], Bernhard Haller[5], Konstantinos D. Rizas[3], Stefan Hagmair[2], Lukas von Stülpnagel[3,4], Wolfgang Hamm[3], Roman Günthner[1], Susanne Angermann[1], Julia Matschkal[1], Stephan Kemmner[1], Anna-Lena Hasenau[1], Isabel Zöllinger[1], Dominik Steubl[1], Johannes F. Mann[6,7], Thomas Lehnert[8], Julia Scherf[7], Jürgen R. Braun[9], Philipp Moog[1], Claudius Küchle[1], Lutz Renders[1], Marek Malik[10], Georg Schmidt[11], Siegfried Wassertheurer[2], Uwe Heemann[1] and Christoph Schmaderer[1]**

[1] Abteilung für Nephrologie, Klinikum Rechts der Isar, Fakultät für Medizin, Technische Universität München, Munich, Germany, [2] Center for Health & Bioresources, Biomedical Systems, AIT Austrian Institute of Technology GmbH, Vienna, Austria, [3] Department of Cardiology, Munich University Clinic, German Centre for Cardiovascular Research, Ludwig Maximilian University of Munich, Munich, Germany, [4] University Hospital for Internal Medicine III, Medical University Innsbruck, Innsbruck, Austria, [5] Institut für Medizinische Informatik, Statistik und Epidemiologie, Klinikum Rechts der Isar, Fakultät für Medizin, Technische Universität München, Munich, Germany, [6] Department of Nephrology, University of Erlangen-Nuremberg, Erlangen, Germany, [7] KfH Kidney Center, Munich, Germany, [8] Dialysis Center Munich Nord, Munich, Germany, [9] Praxen Dr. Braun, Dialysis Center, Dingolfing, Germany, [10] National Heart and Lung Institute, Imperial College London, London, United Kingdom, [11] Klinik für Innere Medizin I, Klinikum Rechts der Isar, Fakultät für Medizin, Technische Universität München, Munich, Germany

Background: Excess mortality in hemodialysis patients is mostly of cardiovascular origin. We examined the association of heart rate turbulence (HRT), a marker of baroreflex sensitivity, with cardiovascular mortality in hemodialysis patients.

Methods: A population of 290 prevalent hemodialysis patients was followed up for a median of 3 years. HRT categories 0 (both turbulence onset [TO] and slope [TS] normal), 1 (TO or TS abnormal), and 2 (both TO and TS abnormal) were obtained from 24 h Holter recordings. The primary end-point was cardiovascular mortality. Associations of HRT categories with the endpoints were analyzed by multivariable Cox regression models including HRT, age, albumin, and the improved Charlson Comorbidity Index for hemodialysis patients. Multivariable linear regression analysis identified factors associated with TO and TS.

Results: During the follow-up period, 20 patients died from cardiovascular causes. In patients with HRT categories 0, 1 and 2, cardiovascular mortality was 1, 10, and 22%, respectively. HRT category 2 showed the strongest independent association with cardiovascular mortality with a hazard ratio of 19.3 (95% confidence interval: 3.69–92.03; $P < 0.001$). Age, calcium phosphate product, and smoking status were associated with TO and TS. Diabetes mellitus and diastolic blood pressure were only associated with TS.

OPEN ACCESS

Edited by:
Mark Potse,
Inria Bordeaux – Sud-Ouest Research Centre, France

Reviewed by:
Cristiana Corsi,
University of Bologna, Italy
Phyllis Kravet Stein,
Washington University in St. Louis, United States
Takanori Ikeda,
Toho University, Japan
Josselin Duchateau,
Centre Hospitalier Universitaire (CHU) de Bordeaux, France

***Correspondence:**
Matthias C. Braunisch
Matthias.Braunisch@mri.tum.de
Christoph Schmaderer
Christoph.Schmaderer@mri.tum.de

†These authors have contributed equally to this work

Specialty section:
This article was submitted to Cardiac Electrophysiology, a section of the journal Frontiers in Physiology

Received: *13 September 2019*
Accepted: *23 January 2020*
Published: *11 February 2020*

Citation:
Braunisch MC, Mayer CC, Bauer A, Lorenz G, Haller B, Rizas KD, Hagmair S, von Stülpnagel L, Hamm W, Günthner R, Angermann S, Matschkal J, Kemmner S, Hasenau A-L, Zöllinger I, Steubl D, Mann JF, Lehnert T, Scherf J, Braun JR, Moog P, Küchle C, Renders L, Malik M, Schmidt G, Wassertheurer S, Heemann U and Schmaderer C (2020) Cardiovascular Mortality Can Be Predicted by Heart Rate Turbulence in Hemodialysis Patients. Front. Physiol. 11:77. doi: 10.3389/fphys.2020.00077

Conclusion: Independent of known risk factors, HRT assessment allows identification of hemodialysis patients with low, intermediate, and high risk of cardiovascular mortality. Future prospective studies are needed to translate risk prediction into risk reduction in hemodialysis patients.

Keywords: heart rate turbulence, cardiovascular mortality, baroreflex, mortality risk prediction, hemodialysis

INTRODUCTION

End-stage renal disease patients treated with chronic dialysis are at high mortality risk, frequently succumbing to cardiovascular death (Foley et al., 1998). The incidence of sudden cardiac death is particularly high compared to patients with ischemic heart disease (USRDS, 2014). These patients are often of advanced age and suffer from multiple comorbidities (Ortiz et al., 2011). Standard risk factors including high cholesterol do not predict mortality (Fellström et al., 2009; Chan K.E. et al., 2010). Uremia affects autonomous nervous system in end-stage renal disease, and sympathetic overactivity has consistently been reported (Stenvinkel et al., 2008; Chan C.T. et al., 2010; Rubinger et al., 2013). Consequently, standard autonomic tests, e.g., conventional time- and frequency-domain parameters of heart rate variability (HRV), are blunted in renal patients compared to healthy controls (Celik et al., 2011) but fail to predict mortality in adjusted models (Suzuki et al., 2012). At the same time, cardiovascular and sudden cardiac death risk stratification of end-stage renal patients is presently an important unmet clinical need. Blanket prophylaxis by implantable defibrillators does not improve survival in these patients (Jukema et al., 2019).

Risk stratification of ischemic heart disease patients has been substantially improved by novel autonomic tests including heart rate turbulence (HRT) (Barthel et al., 2003; Bauer et al., 2009). In post-myocardial infarction patients, HRT category 2 was the strongest independent predictor of mortality amongst other risk factors including age $\geq$ 65 years, diabetes mellitus and left ventricular ejection fraction (LVEF) $\leq$ 30% (Barthel et al., 2003). Furthermore, a combination of HRT category 2 and abnormal cardiac deceleration capacity identified high-risk post-myocardial infarction patients with LVEF $>$ 30%. The risk in these patients was nearly as high as the risk in those with LVEF $\leq$ 30% (Bauer et al., 2009).

HRT refers to sinus cycle length fluctuations in response to spontaneous premature ventricular contractions (PVC) (Bauer et al., 2008). Under the condition of normal autonomic function, there is a transient rate acceleration phase of vagal withdrawal immediately after the PVC compensatory pause. This is subsequently followed by a gradual rate deceleration phase due to parasympathetic restoration after sympathetic-mediated gradual increase of arterial resistance. Abnormal autonomic status does not show these HRT variations (Bauer et al., 2009). The components of HRT, namely turbulence onset (TO) and turbulence slope (TS), correlate with baroreflex sensitivity (Wichterle et al., 2002; Iwasaki et al., 2005) thus expressing essential mechanisms of hemodynamic stability maintenance.

Hemodynamic stability during dialysis is important to avoid intradialytic hypotension, which has been associated with impaired sympathovagal balance (Rubinger et al., 2004) and increased mortality (Flythe et al., 2015). In multivariable analysis, an independent association of HRT with all-cause mortality could not be proven in hemodialysis patients (Suzuki et al., 2012). So far, however, HRT-based prediction of cardiovascular mortality has not been reported in hemodialysis patients.

Consequently, the aims of the present study were to examine HRT in a large cohort of unselected, prevalent hemodialysis patients and to study its association with cardiovascular mortality. Specifically, the study reported here hypothesized that HRT is associated with cardiovascular mortality independent of known risk factors. Risk prediction using HRV and HRT parameters was a prospectively defined goal of the study (Schmaderer et al., 2016).

MATERIALS AND METHODS

Study Population

The study investigated the "rISk strAtification in end-stage Renal disease"- (ISAR)-cohort, a multicenter, prospective longitudinal observational cohort study (ClinicalTrials.gov; identifier number: NCT01152892) (Schmaderer et al., 2016). The study protocol, conforming to the ethical guidelines of the Helsinki Declaration, was approved by the Medical Ethics Committee of the Klinikum rechts der Isar of the Technical University Munich and of the Bavarian State Board of Physicians. Patients were recruited from 17 hemodialysis centers in the greater Munich area between April 2010 and January 2014. All participants gave informed written consent. Inclusion criteria were age $\geq$ 18 years and dialysis vintage $\geq$ 90 days (Schmaderer et al., 2016). Patients were excluded if pregnant or if suffering from ongoing infection or malignancy with a life expectancy $\leq$ 24 months (Schmaderer et al., 2016). Out of the 519 patients meeting inclusion criteria, 390 consented to undergo 24 h Holter electrocardiogram (ECG) recording. Out of these patients, 100 had to be excluded (11 and 45 suffered from paroxysmal and permanent atrial fibrillation, respectively, 27 had a pacemaker implanted, and 17 showed $<$ 75% of normal sinus rhythm beats).

Clinical Characteristics

Demographic and clinical data were obtained at baseline. Baseline comorbidities were assessed using an adapted version of the Charlson Comorbidity Index that has been validated for mortality prediction in hemodialysis patients (Liu et al., 2010). The Index assigns numerical weights to the comorbid conditions of atherosclerotic heart disease (1), heart failure (3), cerebrovascular accident/transient ischemic attack (2), peripheral vascular disease (2), dysrhythmia (2), other cardiac disease

(2), chronic obstructive pulmonary disease (2), gastrointestinal bleeding (2), liver disease (2), cancer (2), and diabetes (1). A comorbidity score of a patient is the sum of the assigned numerical weights and ranges between 0 and 21 (Liu et al., 2010). Blood samples were obtained prior to a midweek dialysis session at baseline. Serum chemistry analyses were performed by ISO (International Organization for Standardization) certified local laboratories of the dialysis centers.

Endpoints

Mortality was assessed after a median of 3 years by medical reports, databases of each dialysis center, or by contacting the attending physician or the next of kin. Using this information, the ISAR Endpoint Committee classified the underlying cause of death in each case (Schmaderer et al., 2016). Cardiovascular mortality was considered as the primary endpoint and all-cause mortality as the secondary endpoint.

HRT and HRV Calculation

The 24 h 12-lead ECGs (1000 Hz) were recorded using the Lifecard CF digital Holter recorder (Delmar Reynolds/Spacelabs Healthcare, Nuremberg, Germany) and started before a midweek dialysis session. Reference ECG annotations and RR-interval measurements were performed using the software tools of the equipment (Pathfinder, Delmar Reynolds/Spacelabs Healthcare, Nuremberg, Germany; v.9.027) (Molgaard, 1991). An experienced physician, blinded to the clinical status, visually reviewed and, where appropriate, manually corrected the computerized RR measurements. Calculation of HRT was performed as previously described, if $\geq$ 5 PVCs were present in the complete recording (Bauer et al., 2008). In brief, HRT category 0 was defined as TO (<0%) and TS (>2.5 ms/R-R interval) both normal or fewer than 5 PVCs present (Barthel et al., 2003; Bauer et al., 2009). HRT category 1 was defined as either TO or TS abnormal, and HRT category 2 was defined as both TO and TS abnormal. Traditional HRV parameters of the time-domain and frequency-domain were computed using the 24 h RR interval series according to established standards (Camm et al., 1996). Logarithmic transformation was additionally performed for frequency-domain parameters. Additional non-linear HRV parameters were calculated as previously described (Peng et al., 1995; Penzel et al., 2003; Bauer et al., 2006; Suzuki et al., 2012). Severe autonomic failure (SAF) was assumed if HRT category 2 and abnormal deceleration capacity ($\leq$4.5 ms) were present (Bauer et al., 2009).

Statistical Analysis

Categorical data are presented as absolute and relative frequencies. Continuous variables are expressed as mean $\pm$ standard deviation (SD) for normally distributed variables and as median and interquartile range (IQR) for variables with skewed distribution. Group differences are assessed by χ^2 test for categorical variables and one-way analysis of variance (ANOVA) or Kruskal–Wallis test for continuous variables, as appropriate.

Cumulative incidence functions of the cardiovascular death probability were computed. Cause-specific hazard for cardiovascular mortality were compared between groups by the log-rank test. Median follow-up time was assessed using the reverse Kaplan–Meier method. Univariate Cox proportional hazards regression analysis of HRV parameters was performed for the endpoints. Multivariable Cox proportional hazards model included adjustment variables with previously reported strong links to mortality in hemodialysis patients (Stenvinkel et al., 2008; Herselman et al., 2010; Ortiz et al., 2011; Suzuki et al., 2012). Two multivariable models for the association with cardiovascular mortality were considered: Model 1 included age and albumin, Model 2 included age and the Charlson Comorbidity Index. For all-cause mortality further variables were added to these models. Model 3 added high-sensitivity C-reactive protein (hsCRP) and calcium phosphate product (CaP) to Model 1, comparable to Suzuki et al. (2012). In Model 4, the Charlson Comorbidity Index was added to Model 3. Further, exploratory models were also tested (**Supplementary Tables 4**, **5**).

Multivariable linear regression analysis using backward selection was used to identify factors associated with TO and TS. All variables from **Table 1**, except the Charlson Comorbidity Index (to identify specific associated comorbid conditions) and heart rate, were considered as potential predictors. To retain constant numbers of patients within the Cox regression models, 12 missing hsCRP values were replaced by non-hsCRP values and 3 total calcium values were imputed as dialysis center-specific means.

All statistical tests were two-sided and P-values < 0.05 were considered significant. Statistical analysis was performed using SPSS version 25.0 (SPSS, Inc., Chicago, IL, United States) for Mac and R version 3.4.2. (R Foundation for Statistical Computing, Vienna, Austria).

RESULTS

Patient Characteristics

In total, 290 patients with a 3-year median follow-up were eligible for the analysis (**Figure 1**). The median age was 64 [IQR 51–74] years, 34.5% of the patients were female. Of the 290 patients, 161 patients (55.5%) fell into HRT category 0 (including 108 patients with absent or fewer than 5 PVCs), 88 patients (30.3%) into HRT category 1, and 41 patients (14.2%) into HRT category 2. HRT category 0 and HRT category non-calculable were merged because of no significant difference in the survival probabilities between these patients ($\chi^2 = 0.25$, log-rank $P = 0.62$) (**Supplementary Figure 1**). Age, creatinine, Charlson Comorbidity Index, the intake of antihypertensive medication and comorbidities differed significantly between HRT categories 0 to 2 (**Table 1** and **Supplementary Table 1**). Compared to the excluded patients of the ISAR study cohort, patients in the analyzed population were younger and had relatively fewer comorbidities (see **Supplementary Table 2**).

Association of HRT and Mortality

Twenty patients suffered cardiovascular mortality: sudden cardiac death (n = 7), myocardial infarction (n = 2), heart failure (n = 5), major stroke (n = 2), cardiac surgical

TABLE 1 | Overall baseline characteristics and grouped by categories 0 to 2 of heart rate turbulence (HRT).

Parameter	Total group (*n* = 290)	Heart rate turbulence (HRT) category			*P*
		Category 0 (*n* = 161)	Category 1 (*n* = 88)	Category 2 (*n* = 41)	
Age [years]	63.9 [50.7–73.8]	56.1 [45.4–67.9]	72.0 [62.2–78.3]	70.8 [62.9–75.7]	< 0.001
Gender [male]	190 (65.5)	107 (66.5)	59 (67.0)	24 (58.5)	0.60
Body mass index [kg/m^2]	25.0 [22.4–28.7]	24.5 [22.4–28.2]	26.0 [22.8–29.1]	25.6 [22.4–29.3]	0.096
Dialysis vintage [months]	46.0 [24.0–78.3]	50.0 [21.5–85.5]	45.5 [29.0–75.8]	40.0 [25.0–74.5]	0.73
Ultrafiltration rate [ml/h]	483.0 ± 259.5	495.2 ± 266.9	466.6 ± 246.7	469.8 ± 260.6	0.67
Net ultrafiltration [l]	1.7 ± 1.2	1.8 ± 1.2	1.5 ± 1.1	1.5 ± 1.1	0.16
Kt/V	1.46 [1.21–1.65]	1.45 [1.21–1.74]	1.45 [1.20–1.62]	1.48 [1.31–1.64]	0.68
Systolic blood pressure [mmHg]	137.0 [123.0–149.0]	136.0 [123.0–149.0]	138.5 [122.8–149.3]	137.0 [124.5–151.8]	0.71
Diastolic blood pressure [mmHg]	75.1 ± 14.6	76.2 ± 14.5	73.1 ± 14.3	75.1 ± 15.3	0.29
Heart rate [bpm]	73.7 [65.6–80.9]	74.6 [66.6–81.8]	72.8 [64.6–79.7]	73.4 [65.1–81.1]	0.50
Blood urea nitrogen [mg/dl]	62.8 ± 16.5	64.9 ± 17.0	60.1 ± 16.3	60.5 ± 13.5	0.055
Phosphate [mmol/l]	1.74 ± 0.49	1.73 ± 0.46	1.70 ± 0.49	1.83 ± 0.56	0.40
Total calcium [mmol/l]	2.27 ± 0.18	2.26 ± 0.18	2.28 ± 0.18	2.28 ± 0.18	0.64
Calcium *x* phosphate [mmol^2/l^2]	3.93 ± 1.12	3.90 ± 1.09	3.89 ± 1.14	4.12 ± 1.23	0.49
Creatinine [mg/dl]	8.81 ± 2.83	9.47 ± 2.93	8.02 ± 2.51	7.95 ± 2.41	< 0.001
High-sensitivity CRP [mg/dl]	0.38 [0.16–0.90]	0.31 [0.16–0.77]	0.48 [0.19–1.00]	0.57 [0.16–1.01]	0.023
Albumin [g/dl]	4.02 ± 0.40	4.06 ± 0.41	3.96 ± 0.42	3.96 ± 0.30	0.12
Parathyroid hormone [pg/ml]	238.5 [127.4–402.9]	246.0 [109.0–402.3]	241.5 [128.2–404.3]	232.6 [144.1–387.3]	0.98
Leukocytes [G/l]	6.97 ± 2.06	6.95 ± 2.07	6.64 ± 1.84	7.75 ± 2.34	0.018
Total cholesterol [mg/dl]	177.0 [154.0–207.0]	179.0 [152.8–206.3]	172.0 [148.0–202.0]	181.0 [159.5–222.5]	0.45
Charlson Comorbidity Index [0–21]	2.0 [1.0–5.0]	2.0 [0.0–4.0]	4.0 [2.0–5.0]	4.0 [2.0–6.0]	< 0.001
Diabetes mellitus	99 (34.1)	49 (30.4)	30 (34.1)	20 (48.8)	0.087
History of myocardial infarction	47 (16.2)	17 (10.6)	23 (26.1)	7 (17.1)	0.006
Left ventricular hypertrophy	76 (26.2)	41 (25.5)	23 (26.1)	12 (29.3)	0.89
Heart failure	31 (10.7)	10 (6.2)	16 (18.2)	5 (12.2)	0.013
Peripheral artery disease	55 (19.0)	20 (12.4)	19 (21.6)	16 (39.0)	< 0.001
Hypertension	271 (93.4)	145 (90.1)	86 (97.7)	40 (97.6)	0.034
Coronary heart disease	88 (30.3)	37 (23.0)	35 (39.8)	16 (39.0)	0.010
Cerebral vascular disease	41 (14.1)	12 (7.5)	16 (18.2)	13 (31.7)	< 0.001
Smoking [ever]	79 (27.4)	47 (29.6)	21 (23.9)	11 (26.8)	0.63
Antihypertensive medication	258 (89.0)	137 (85.1)	81 (92.0)	40 (97.6)	0.041
Statin	104 (36.4)	48 (30.2)	38 (44.2)	18 (43.9)	0.052

n (%) for categorical data, mean ± standard deviation or median [interquartile range] for continuous data, as appropriate. CRP, c-reactive protein.

procedure (*n* = 1), aortal dissection (*n* = 1), ruptured aortic aneurysm (*n* = 1), and mesenteric ischemia (*n* = 1). Non-cardiovascular death (*n* = 30) causes included: infectious events (*n* = 16), cancer (*n* = 5), gastrointestinal bleeding (*n* = 1), diabetic coma (*n* = 1), and withdrawal from treatment (*n* = 1). No agreement on cause of death was reached and the cause of death was defined "unknown" in six cases. Patients were censored at the last day of dialysis in case of renal transplantation (*n* = 37) or if lost to follow-up (*n* = 8). Of the seven patients who succumbed to sudden cardiac death, *n* = 1, 3, and 3 showed HRT category 0, 1, and 2, respectively. **Figure 2** shows unadjusted and adjusted hazard ratios of HRT for cardiovascular mortality. In univariate analysis, HRT categories 1 and 2 compared to category 0 were associated with a substantially higher cardiovascular mortality risk. **Supplementary Table 3** shows univariate hazard ratios of baseline parameters. After adjustment in different models, HRT category 1 and 2 remained significantly associated with cardiovascular mortality. The hazard ratio of HRT category 2, with category 0 as reference, ranged from 11.64 to 18.42 depending on the model. Three-year cardiovascular mortality rates were 1.2, 10.2, and 22.0% for those with HRT category 0, 1, and 2, respectively (**Figure 3**). Additional models of adjustment did not materially change the results (**Supplementary Tables 4**, **5**).

None of the traditional HRV parameters of the time-domain and frequency-domain as well as non-linear HRV parameters were related to cardiovascular mortality risk in a univariate or an adjusted model (**Table 2** and **Supplementary Table 6**), except for deceleration capacity that showed an association with cardiovascular mortality in a univariate analysis. Results for SAF are shown in **Supplementary Table 7**. **Table 3** and **Supplementary Table 8** show the median and interquartile ranges of HRV measures.

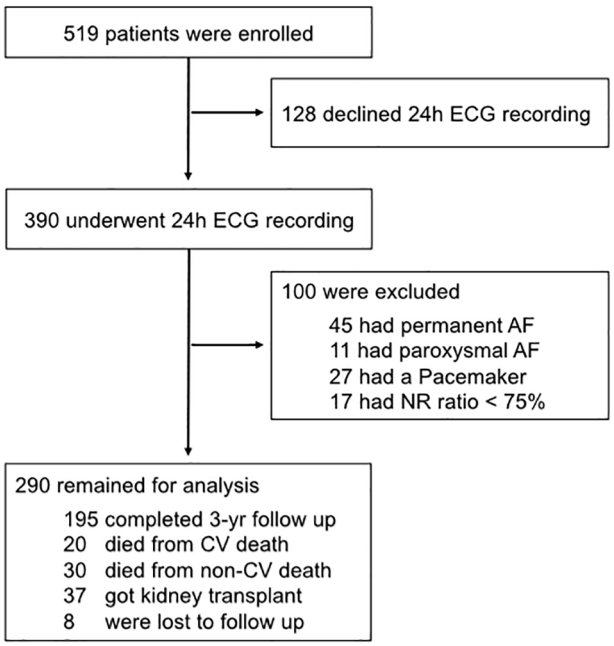

FIGURE 1 | Flowchart of participants. Out of the 519 patients, 390 consented to undergo 24 h Holter electrocardiogram (ECG). Of these, 100 had to be excluded because of atrial fibrillation, a permanent pacemaker implant, or because of having less than 75% of normal sinus rhythm beats. 290 patients remained for the present analysis. AF, arterial fibrillation; CV, cardiovascular; ECG, electrocardiogram; NR, normal rhythm; yr, year.

Table 4 shows the unadjusted and adjusted hazard ratios of HRT for all-cause mortality. In univariate analysis, HRT categories were associated with all-cause mortality. All-cause mortality rates during the first 3 years were 8.7, 26.1, and 31.7% for those with HRT category 0, 1, and 2, respectively ($P < 0.001$, $\chi^2 = 17.6$). After adjustment according to Model 3, HRT category 2, with category 0 as reference, remained significantly and independently associated with all-cause mortality (**Table 4**). However, after adding the Charlson Comorbidity Index to the model (adjusted Model 4), categorical HRT was no longer significantly associated with all-cause mortality risk.

Analysis of Determinants of TO and TS as Factors of HRT

In HRT category 1, 22 (25.0%) patients had an abnormal TO and 66 (75.0%) patients had an abnormal TS. For TO, age, CaP, and smoking status remained in the final model. Age, CaP, smoking status, and diastolic blood pressure were identified as the most relevant determinants for TS (**Table 5**).

DISCUSSION

The results of this observational analysis demonstrate that HRT is independently and strongly associated with cardiovascular mortality in prevalent hemodialysis patients. Approximately one half of the patients of our cohort had HRT category 1 and 2 and displayed an intermediate or high 3-year cardiovascular mortality risk of 10 and 22%, respectively. The other half of the patients with HRT category 0 had a much lower 3-year cardiovascular mortality risk of only 1%. Adding multiple risk variables for mortality in hemodialysis patients to the Cox regression, like age, albumin or multiple comorbidities, the hazard ratio of HRT categories decreased only slightly with HRT category 2 showing the highest hazard ratios. Of particular interest is the subgroup of patients with HRT category 0 who accounted for more than a half of the study population and who displayed a very low risk of cardiovascular mortality over 3 years. It appears that in these patients, examinations and interventions going beyond standard care of dialysis patients to prevent cardiovascular mortality might be unnecessary.

Additionally, we showed independent association between HRT and all-cause mortality. However, similar to previous studies in hemodialysis patients (Suzuki et al., 2012), after adding the Charlson Comorbidity Index for multiple comorbidities to the fully adjusted model, HRT was no longer independently associated with all-cause mortality.

Similar to previous reports (Suzuki et al., 2012), we have not found standard and non-linear HRV parameters helpful in predicting cardiovascular mortality. The observed association of SAF with cardiovascular mortality was attributable mainly to the high hazard ratio of HRT category 2 because deceleration capacity was not predictive in the multivariate models.

Determinants of HRT in Hemodialysis Patients

Since impaired HRT is a consequence of baroreflex dysfunction, our results highlight the importance of complex sympathovagal interaction in the context of cardiovascular mortality risk prediction in hemodialysis patients. Multivariable regression identified an association of age, calcium phosphate product, and smoking status with TO and TS. Diabetes mellitus and diastolic blood pressure were only associated with TS. Both components of HRT, TO and TS, have been previously associated to baroreflex sensitivity (Davies et al., 2001). Autonomic control and parameters of HRT were reported worse in non-hemodialysis patients with older age, diabetes mellitus, hypertension or positive smoking status (Schroeder et al., 2003; Schwab et al., 2005; Bauer et al., 2008; Cagirci et al., 2009). The association of TS and diabetes mellitus is in line with previous publications suggesting that mainly TS is impaired by hyperglycemia mediated cardiac autonomic neuropathy which affects the parasympathetic restoration (i.e., TS) after a PVC (Balcioglu et al., 2007). In post-myocardial infarction patients with and without diabetes mellitus, HRT was associated in both groups with cardiac mortality (Miwa et al., 2011). However, especially in patients with LVEF > 30%, ≥ 65 years of age, the presence of diabetes mellitus and HRT category 2 showed a considerable

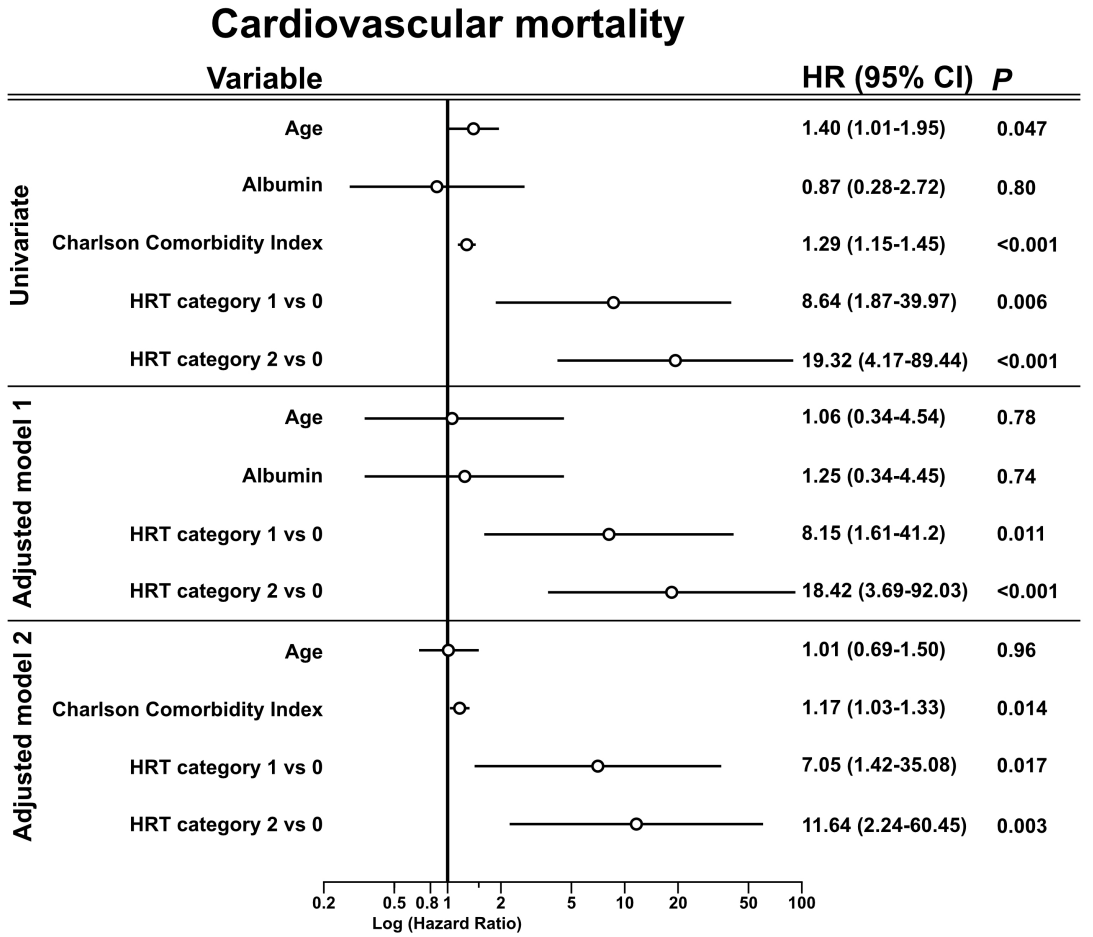

FIGURE 2 | Association of risk variables with cardiovascular mortality in univariate and multivariable analysis. Univariate and multivariable Cox regression analysis for the association of the risk variable and cardiovascular mortality. Unadjusted and adjusted hazard ratios with the respective confidence interval are presented. Age has the unit 10 years. The adjusted Model 1 included age, albumin and HRT. The adjusted Model 2 included age, the Charlson Comorbidity Index and HRT. Units: Age, 10 years; Albumin, 1 g/dl; Charlson Comorbidity Index, 1 point. CI, confidence interval; HR, hazard ratio; HRT, heart rate turbulence.

elevated mortality risk compared to non-diabetic patients (Barthel et al., 2003).

Elevated CaP might be a dialysis-specific parameter with influence on HRT. It has been previously associated with an increased relative risk of death due to cardiac events in hemodialysis patients (Ganesh et al., 2001). Reduced perfusion of vascular macro- and myocardial microcirculation occurs in hemodialysis patients because of increased phosphate and CaP. The association of CaP and the components of HRT may represent an end-organ damage by the disruption of the normal conduction system architecture as well as by vascular obstruction. Furthermore, intradialytic hypotension is considered to be one of the key factors of cardiovascular damage and signifies increased mortality risk in hemodialysis patients (Shoji et al., 2004). However, the association of intradialytic hypotension with HRT is presently unknown.

Although not identified in our cohort, inflammation could be a further determinant of impaired HRT. In hemodialysis patients, chronic inflammation is present (Stenvinkel and Alvestrand, 2002). This could not only aggravate the identified determinants of HRT but also have a separate and additional impact on HRT. An interaction of the inflammatory and autonomous nervous system exists via the cholinergic anti-inflammatory pathway (Pavlov et al., 2003). Vagus nerve afferent sensory fibers are signaling the brain the presence of inflammation (Goehler et al., 2000) which is also impairing autonomous nervous system function via the centrally mediated activation of hypothalamus-pituitary-adrenal axis, increased sympathetic nervous system activity, and direct reduction of parasympathetic nervous system activity (Pavlov et al., 2003). Vagus nerve efferent cardiac fibers might cause HRT displayed baroreflex dysfunction in hemodialysis patients as evident in the HRT findings. However, further studies are needed to evaluate inflammation induced impaired autonomous nervous system in hemodialysis patients before experimental stimulation to enhance parasympathetic activity with an

implantable device might become a therapeutic option (Lohmeier and Iliescu, 2011).

Clinical Implications

The independent association of HRT with cardiovascular mortality addresses the need for risk stratification to deal with the excess cardiovascular mortality in hemodialysis patients. Classifying patients allows more precise clinical decisions independent of age, protein-energy wasting or comorbidities. Interestingly, more than half of the patient (55%, n = 161) with HRT category 0 showed a very low risk of 3-year cardiovascular mortality. This could allow a less stringent monitoring of cardiovascular comorbidities in the subgroup. Therefore, categorization by HRT also allows focused close monitoring of cardiovascular comorbidities in those patients at intermediate or high risk.

In our cohort, 35% (n = 7) of those who succumbed to cardiovascular causes suffered from sudden cardiac death which might be attributed to an arrhythmogenic event and is thus potentially preventable by the implantation of a cardioverter defibrillator (ICD) (Di Lullo et al., 2016). However, a recent randomized controlled trial including dialysis patients with a LVEF $\geq$ 35% showed no advantage of prophylactic ICD implantation (Jukema et al., 2019). One explanation for this result might be provided by recent studies showing that fatal arrhythmias are more frequently related to bradyarrhythmias than to tachyarrhythmias. Although ICDs also have a pacing capability, the brady-/tachyarrhythmia balance might still affect the ICD prophylaxis in hemodialysis patients (Roy-Chaudhury et al., 2018; Sacher et al., 2018; Genovesi et al., 2019). Another reason for the infectivity of ICD implantation in hemodialysis patients includes electrolyte imbalances which increases the risk of ineffective shock therapy. Of our seven patients who succumbed due to sudden cardiac death, only one had a normal HRT. Perhaps the assessment of LVEF $\leq$ 30% and HRT category 2 might help to select the candidates for ICD prophylaxis, reflecting the considerably increased mortality in this subgroup among post-myocardial infarction patients (Barthel et al., 2003). However, as already mentioned, the mode of sudden cardiac death might be different in hemodialysis patients compared to the general population with prevalent heart disease where ventricular arrhythmias are the main cause of sudden cardiac death. Noteworthy, ICD implantation could be more beneficial in secondary than in primary prevention (Genovesi et al., 2019).

Not surprisingly, we found HRT to be influenced by classical determinant of the autonomic nervous system function such as age, diabetes mellitus and smoking status and by factors causing structural cardiovascular damage, such as the CaP and hypertension. Therefore, it might also be important to modulate factors that increase sympathetic or decrease parasympathetic nervous system activity. In high-risk hemodialysis patients, central sympatholytic drugs like clonidine or moxonidine might therefore be beneficial (Rubinger et al., 2013). Whereas ß-blocker therapy had no effect on HRT in patients after myocardial infarction (Lin et al., 2002; Barthel et al., 2003), its anti-arrhythmic properties as well as a tight control of potassium and calcium during hemodialysis treatment may help reducing

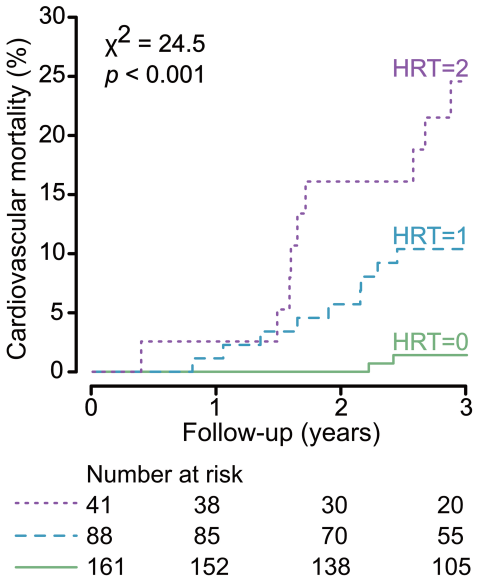

FIGURE 3 | Cumulative cardiovascular mortality curves stratified by heart rate turbulence (HRT). The median follow-up was 3 years. Cause-specific hazards for cardiovascular mortality were compared between groups by the log-rank test. The number of patients of the individual groups involved in the analysis at 1, 2, and 3 years are shown under the graph. 3-Year cardiovascular mortality rates were 1.2, 10.2, and 22.0% for those with HRT category 0, 1, and 2, respectively.

sudden cardiac death risk (Di Lullo et al., 2016). Heavy smokers among hemodialysis patients have an up to 41% increased relative risk for all-cause mortality compared to non-smokers (Li et al., 2018). Smoking cessation might be one modifiable factor to improve autonomic nervous system dysfunction. Furthermore, invasive and therefore limited options to reduce sympathetic overdrive by carotid baroreceptor stimulation during non-dialysis periods or sympathetic denervation of renal arteries have to be evaluated (Grassi et al., 2012; Rubinger et al., 2013). Further larger studies are needed to evaluate if smoking cessation, a precise treatment of diabetes mellitus, arterial hypertension or dialysis specific parameters (e.g., CaP) have an impact on HRT-documented baroreflex dysfunction.

In patients with structural heart disease with left ventricular dysfunction but relatively preserved LVEF, a combination of HRT category 2 and the presence of non-sustained ventricular tachycardia allowed a better prediction of all-cause mortality and fatal arrhythmic events compared to the single parameters (Kinoshita et al., 2019). Further research is warranted to evaluate if ECG based risk prediction might be of use in hemodialysis patients as well.

Limitations

Limitations of the study also need to be considered. First, we only found a small number of 20 cardiovascular death cases. Multivariable adjustment was therefore possible only for a limited number of variables. To avoid the risk of overfitting (Babyak, 2004) and to account for different parameters, two multivariable models for the association with cardiovascular

TABLE 2 | Unadjusted and adjusted hazards ratios of traditional heart rate variability measures (time- and frequency-domain) for cardiovascular mortality.

		Cardiovascular mortality risk					
Parameter	**Unit**	**Univariate**		**Adjusted Model 1**		**Adjusted Model 2**	
		HR (95% CI)	***P***	**HR (95% CI)**	***P***	**HR (95% CI)**	***P***
SDNN	ms	0.99 (0.98 – 1.01)	0.27	0.99 (0.98 – 1.01)	0.38	1.00 (0.98 – 1.02)	0.84
SDANN	ms	0.99 (0.98 – 1.01)	0.38	0.99 (0.98 – 1.01)	0.5	1.00 (0.98 – 1.02)	0.92
RMSSD	ms	0.99 (0.93 – 1.05)	0.66	0.98 (0.92 – 1.04)	0.44	0.99 (0.94 – 1.05)	0.81
pNN50	%	0.97 (0.85 – 1.10)	0.6	0.95 (0.83 – 1.08)	0.41	0.96 (0.84 – 1.10)	0.54
HRVTI		0.96 (0.91 – 1.02)	0.21	0.97 (0.91 – 1.03)	0.36	0.99 (0.94 – 1.05)	0.81
TINN	ms	1.00 (1.00 – 1.00)	0.38	1.00 (1.00 – 1.00)	0.61	1.00 (1.00 – 1.00)	0.93
Total Power	ms^2	1.00 (1.00 – 1.00)	0.18	1.00 (1.00 – 1.00)	0.24	1.00 (1.00 – 1.00)	0.56
ULF	ms^2	1.00 (1.00 – 1.00)	0.22	1.00 (1.00 – 1.00)	0.32	1.00 (1.00 – 1.00)	0.65
VLF	ms^2	1.00 (1.00 – 1.00)	0.11	1.00 (1.00 – 1.00)	0.17	1.00 (1.00 – 1.00)	0.43
LF	ms^2	1.00 (1.00 – 1.00)	0.084	1.00 (1.00 – 1.00)	0.094	1.00 (1.00 – 1.00)	0.21
HF	ms^2	1.00 (1.00 – 1.00)	0.47	1.00 (1.00 – 1.00)	0.26	1.00 (1.00 – 1.00)	0.44
LF/HF		0.71 (0.49 – 1.03)	0.073	0.79 (0.53 – 1.16)	0.23	0.82 (0.58 – 1.15)	0.82
DFA a_1		0.37 (0.08 – 1.71)	0.2	0.66 (0.12 – 3.50)	0.62	0.74 (0.15 – 3.66)	0.71
DFA a_2		7.56 (0.01 – 5465.10)	0.55	1.68 (0.00 – 1618.04)	0.88	0.85 (0.00 – 775.81)	0.96
DC category 1 vs. 0		0.67 (0.27 – 1.69)	0.4	0.70 (0.28 – 1.75)	0.44	0.87 (0.34 – 2.24)	0.77
DC category 2 vs. 0		0.20 (0.04 – 0.92)	<0.05	0.26 (0.05 – 1.24)	0.09	0.44 (0.09 – 2.20)	0.32
AC	ms	1.19 (0.93 – 1.52)	0.16	1.17 (0.91 – 1.50)	0.22	1.06 (0.84 – 1.34)	0.63

Model 1: age, albumin; model 2: age, Charlson Comorbidity Index. CI, confidence interval; SDNN, standard deviation of all NN intervals; SDANN, standard deviation of the averages of NN intervals in all 5-min segments of 24 h recording; RMSSD, square root of the mean square of differences between adjacent NN intervals; pNN50, adjacent NN intervals differing > 50 ms in the total NN intervals; HRVTI, HRV triangular index: number of NN intervals over the number of NN-intervals in the modal bin; TINN, triangular interpolation of NN interval histogram; ULF, ultra-low frequency; VLF, very low frequency; LF, low frequency; HF, high frequency; LF/HF, LF to HF ratio; DFA, detrended fluctuation analysis; DC, deceleration capacity; AC, acceleration capacity.

TABLE 3 | Measures of heart rate variability at baseline in patients overall and grouped by survival state.

Parameter	**Unit**	**Overall**	**Cardiovascular mortality**	
			Survivor (*n* = 270)	**Non-survivor (*n* = 20)**
SDNN	ms	86.8 (69.0 – 105.6)	87.0 (69.1 – 105.9)	85.6 (64.7 – 99.5)
SDANN	ms	77.5 (61.5 – 97.6)	77.6 (62.3 – 98.2)	78.7 (56.1 – 94.1)
RMSSD	ms	13.6 (10.0 – 20.5)	13.6 (10.2 – 20.6)	13.9 (9.2 – 19.7)
pNN50	%	0.86 (0.18 – 3.07)	0.86 (0.18 – 3.14)	0.90 (0.27 – 2.35)
HRVTI		22.5 (17.9 – 27.9)	22.6 (18.0 – 28.1)	21.3 (16.8 – 26.5)
TINN	ms	346.4 (272.0 – 432.1)	347.5 (272.0 – 433.0)	327.7 (264.4 – 414.3)
Total Power	ms^2	7803.3 (4912.0 – 11864.1)	8018.5 (4994.0 – 12065.6)	6893.6 (4396.9 – 10796.9)
ULF	ms^2	6466.3 (3829.6 – 10138.6)	6513 (4014.0 – 10171.6)	5426.0 (3444.7 – 9695.3)
VLF	ms^2	677.0 (383.8 – 1123.6)	682.6 (393.3 – 1154.1)	569.6 (297.3 – 843.4)
LF	ms^2	270.4 (137.2 – 510.7)	285.8 (143.7 – 528.2)	160.6 (130.0 – 274.3)
HF	ms^2	109.7 (51.3 – 254.6)	116.9 (51.1 – 225.9)	89.3 (59.6 – 179.6)
LF/HF		2.1 (1.5 – 3.5)	2.1 (1.5 – 3.5)	1.7 (1.3 – 2.1)
DFA a_1		1.25 (1.06 – 1.48)	1.25 (1.07 – 1.49)	1.18 (0.98 – 1.39)
DFA a_2		1.14 (1.10 – 1.19)	1.14 (1.10 – 1.18)	1.15 (1.10 – 1.21)
DC	ms	3.36 (2.37 – 4.86)	3.48 (2.44 – 5.03)	2.93 (1.76 – 4.10)
AC	ms	−4.17 (− 5.92 to − 3.03)	−4.24 (− 5.95 to − 3.05)	−3.54 (− 4.94 to − 2.40)

Values are expressed as median (interquartile range). SDNN, standard deviation of all NN intervals; SDANN, standard deviation of the averages of NN intervals in all 5-min segments of 24 h recording; RMSSD, square root of the mean square of differences between adjacent NN intervals; pNN50, adjacent NN intervals differing > 50 ms in the total NN intervals; HRVTI, HRV triangular index: number of NN intervals over the number of NN-intervals in the modal bin; TINN, triangular interpolation of NN interval histogram; ULF, ultra-low frequency; VLF, very low frequency; LF, low frequency; HF, high frequency; LF/HF, LF to HF ratio; DFA detrended fluctuation analysis; DC, deceleration capacity; AC, acceleration capacity.

TABLE 4 | Association of risk variables with all-cause mortality in univariate and multivariable analysis.

		Univariate		Adjusted Model 3		Adjusted Model 4	
Variable	**Unit**	**HR (95% CI)**	***P***	**HR (95% CI)**	***P***	**HR (95% CI)**	***P***
Age	10 year	1.56 (1.25 – 1.95)	0.001	1.31 (1.02 – 1.67)	0.033	1.25 (0.97 – 1.60)	0.86
Albumin	1 g/dl	0.23 (0.11 – 0.45)	0.001	0.29 (0.13 – 0.62)	0.002	0.33 (0.15 – 0.74)	0.007
High-sensitivity CRP	1 mg/dl	1.26 (1.13 – 1.39)	0.001	1.20 (1.07 – 1.35)	0.002	1.18 (1.04 – 1.33)	0.008
Calcium *x* phosphate	$mmol^2/l^2$	0.99 (0.77 – 1.27)	0.91	1.01 (0.77 – 1.33)	0.95	0.98 (0.74 – 1.31)	0.91
Charlson Comorbidity Index	1 point	2.14 (1.65 – 2.78)	0.001	–	–	1.20 (1.10 – 1.31)	0.001
HRT category 1 vs. 0		3.13 (1.61 – 6.09)	0.001	1.98 (0.97 – 4.03)	0.061	1.76 (0.87 – 3.56)	0.12
HRT category 2 vs. 0		3.93 (1.85 – 8.36)	0.001	2.86 (1.31 – 6.27)	0.009	1.84 (0.80 – 4.22)	0.15

CI, confidence interval; CRP, c-reactive protein; HR, hazard ratio; HRT, heart rate turbulence.

TABLE 5 | Multivariable linear regression with backward selection to identify determinants of TO and TS.

	Turbulence onset (TO) per 1%		Turbulence slope (TS) per ms	
Parameter	***b* (95% CI)**	***P***	***b* (95% CI)**	***P***
Intercept	−5.14 (– 7.31 to – 2.97)	<0.001	22.23 (14.49 to – 30.00)	<0.001
Age [10 years]	0.46 (0.21 – 0.70)	<0.001	−0.19 (– 2.45 to – 1.28)	<0.001
Calcium *x* phosphate [1 $mmol^2/l^2$]	0.33 (0.01 – 0.65)	0.042	−0.74 (– 1.45 to – 0.03)	0.042
Smoking	0.93 (0.11 – 1.74)	0.026	−2.15 (– 3.95 to – 0.34)	0.020
Diabetes mellitus	–	–	−2.28 (– 3.90 to – 0.67)	0.006
Diastolic blood pressure [1 mmHg]	–	–	−0.06 (– 0.11 to – 0.00)	0.039
Blood urea nitrogen [1 mg/dl]	–	–	0.04 (– 0.01 to 0.09)	0.096

Dependent variables in each model: TO and TS. R^2 (TO model) = 0.09; R^2 (TS model) = 0.24. b, regression coefficient; CI, confidence interval.

mortality were created. We used the Charlson Comorbidity Index to include multiple comorbidities in just one variable. For all-cause mortality, 50 cases existed, thus allowing to add further variables to the models. Second, we had no data on LVEF for model adjustment. Third, the high level of frailty in our cohort limited the number of available ECG recordings because of limited compliance with 24 h recordings, the presence of atrial fibrillation, or pacemaker implant, and low recording quality. Consenting to participate in a 24 h ECG recording and having an analyzable ECG recording may already represent potentially biased and beneficial pre-selection. Fourth, the calculation of HRT based on PVCs already represents certain cardiac impairment. In our cohort, PVC tachograms could not be calculated in 37% of the patients and summarized under HRT category 0 due to similar survival probabilities which is comparable to other studies (Barthel et al., 2003; Suzuki et al., 2012). Although the ECG is a routinely used, inexpensive and non-invasive tool, PVC annotation might be difficult and time consuming, especially in long-term ECG recordings. Therefore, automatic ECG annotation algorithms that allow a more precise identification of PVCs are needed. Finally, participants of the study were from the greater Munich area (i.e., mainly white Caucasians) and represent a younger subgroup with fewer comorbidities from the original ISAR cohort. Generalization of our results to other ethnic groups and populations is consequently potentially problematic.

CONCLUSION

We were able to show that HRT is independently associated with cardiovascular mortality in hemodialysis patients. Patients with HRT category 0, 1, and 2 showed 1, 10, and 22% 3-year cardiovascular mortality rate, respectively. Patients in HRT category 0 who accounted for more than half of the study population had a very low risk of cardiovascular mortality over 3 years. On the other hand, HRT category 2 showed a particularly strong association with cardiovascular mortality. This allows classifying cardiovascular mortality risk of hemodialysis patients into low, intermediate, and high-risk strata. However, lager sample sizes are desired to validate these findings. As HRT displays impaired baroreflex activity, this permits a pathologic explanation for the increased cardiovascular mortality in hemodialysis patients. Identifying patients at intermediate and high risk may allow the development of prevention strategies as well as targeted therapies.

DATA AVAILABILITY STATEMENT

The datasets for this manuscript are not publicly available because written informed consent did not include wording on data sharing. Reasonable requests to access the datasets should be directed to CS, Christoph.Schmaderer@mri.tum.de.

ETHICS STATEMENT

This study involving human participants was reviewed and approved by the Medical Ethics Committee of the Klinikum Rechts der Isar of the Technical University Munich and of the Bavarian State Board of Physicians. The patients/participants provided their written informed consent to participate in this study.

AUTHOR CONTRIBUTIONS

MB, CM, and CS contributed to the research idea and study design. MB, CM, AB, and CS drafted the article. MB, CM, GL, KR, SH, WH, LS, RG, SA, JM, SK, A-LH, IZ, DS, JFM, TL, JS, and JB contributed to the data acquisition. MB, CM, AB, GL, BH, and CS contributed to the data analysis and the data interpretation. MB, CM, and BH contributed to the statistical analysis. AB, PM, CK, LR, MM, GS, SW, UH, and CS contributed to the supervision.

ACKNOWLEDGMENTS

We acknowledge the support and assistance of all participating dialysis centers, hospitals, and patients for making this study possible.

SUPPLEMENTARY MATERIAL

The Supplementary Material for this article can be found online at: https://www.frontiersin.org/articles/10.3389/fphys.2020.00077/full#supplementary-material

REFERENCES

Babyak, M. A. (2004). What you see may not be what you get: a brief, nontechnical introduction to overfitting in regression-type models. *Psychosom. Med.* 66, 411–421. doi: 10.1097/01.psy.0000127692.23278.a9

Balcioglu, S., Arslan, U., Turkoglu, S., Ozdemir, M., and Cengel, A. (2007). Heart rate variability and heart rate turbulence in patients with type 2 diabetes mellitus with versus without cardiac autonomic neuropathy. *Am. J. Cardiol.* 100, 890–893. doi: 10.1016/j.amjcard.2007.03.106

Barthel, P., Schneider, R., Bauer, A., Ulm, K., Schmitt, C., Schomig, A., et al. (2003). Risk stratification after acute myocardial infarction by heart rate turbulence. *Circulation* 108, 1221–1226. doi: 10.1161/01.cir.0000088783.34082.89

Bauer, A., Barthel, P., Schneider, R., Ulm, K., Muller, A., Joeinig, A., et al. (2009). Improved stratification of autonomic regulation for risk prediction in post-infarction patients with preserved left ventricular function (ISAR-Risk). *Eur. Heart J.* 30, 576–583. doi: 10.1093/eurheartj/ehn540

Bauer, A., Kantelhardt, J. W., Barthel, P., Schneider, R., Mäkikallio, T., Ulm, K., et al. (2006). Deceleration capacity of heart rate as a predictor of mortality after myocardial infarction: cohort study. *Lancet* 367, 1674–1681. doi: 10.1016/s0140-6736(06)68735-7

Bauer, A., Malik, M., Schmidt, G., Barthel, P., Bonnemeier, H., Cygankiewicz, I., et al. (2008). Heart rate turbulence: standards of measurement, physiological interpretation, and clinical use: international society for holter and noninvasive electrophysiology consensus. *J. Am. Coll. Cardiol.* 52, 1353–1365. doi: 10.1016/j.jacc.2008.07.041

Cagirci, G., Cay, S., Karakurt, O., Eryasar, N., Kaya, V., Canga, A., et al. (2009). Influence of heavy cigarette smoking on heart rate variability and heart rate turbulence parameters. *Ann Noninvasive Electrocardiol.* 14, 327–332. doi: 10.1111/j.1542-474X.2009.00321.x

Camm, A. J., Malik, M., Bigger, J. T., Breithardt, G., Cerutti, S., Cohen, R. J., et al. (1996). Heart rate variability: standards of measurement, physiological interpretation and clinical use. Task force of the European society of cardiology and the North American society of pacing and electrophysiology. *Circulation* 93, 1043–1065. doi: 10.1161/01.cir.93.5.1043

Celik, A., Melek, M., Yuksel, S., Onrat, E., and Avsar, A. (2011). Cardiac autonomic dysfunction in hemodialysis patients: the value of heart rate turbulence. *Hemodial. Int.* 15, 193–199. doi: 10.1111/j.1542-4758.2011.00529.x

Chan, C. T., Levin, N. W., Chertow, G. M., Larive, B., Schulman, G., and Kotanko, P. (2010). Determinants of cardiac autonomic dysfunction in ESRD. *Clin. J. Am. Soc. Nephrol.* 5, 1821–1827. doi: 10.2215/cjn.03080410

Chan, K. E., Thadhani, R., Lazarus, J. M., and Hakim, R. M. (2010). Modeling the 4D study: statins and cardiovascular outcomes in long-term hemodialysis patients with diabetes. *Clin. J. Am. Soc. Nephrol.* 5, 856–866. doi: 10.2215/CJN.07161009

Davies, L. C., Francis, D. P., Ponikowski, P., Piepoli, M. F., and Coats, A. J. (2001). Relation of heart rate and blood pressure turbulence following premature ventricular complexes to baroreflex sensitivity in chronic congestive heart failure. *Am. J. Cardiol.* 87, 737–742. doi: 10.1016/s0002-9149(00)01493-4

Di Lullo, L., Rivera, R., Barbera, V., Bellasi, A., Cozzolino, M., Russo, D., et al. (2016). Sudden cardiac death and chronic kidney disease: From pathophysiology to treatment strategies. *Int. J. Cardiol.* 217, 16–27. doi: 10.1016/j.ijcard.2016.04.170

Fellström, B. C., Jardine, A. G., Schmieder, R. E., Holdaas, H., Bannister, K., and Beutler, J. (2009). Rosuvastatin and cardiovascular events in patients undergoing hemodialysis. *N. Eng. J. Med.* 360, 1395–1407.

Flythe, J. E., Xue, H., Lynch, K. E., Curhan, G. C., and Brunelli, S. M. (2015). Association of mortality risk with various definitions of intradialytic hypotension. *J. Am. Soc. Nephrol.* 26, 724–734. doi: 10.1681/ASN.2014020222

Foley, R. N., Parfrey, P. S., and Sarnak, M. J. (1998). Epidemiology of cardiovascular disease in chronic renal disease. *J. Am. Soc. Nephrol.* 9(Suppl. 12), S16–S23.

Ganesh, S. K., Stack, A. G., Levin, N. W., Hulbert-Shearon, T., and Port, F. K. (2001). Association of elevated serum PO(4), Ca x PO(4) product, and parathyroid hormone with cardiac mortality risk in chronic hemodialysis patients. *J. Am. Soc. Nephrol.* 12, 2131–2138.

Genovesi, S., Boriani, G., Covic, A., Vernooij, R. W. M., Combe, C., and Burlacu, A. (2019). Sudden cardiac death in dialysis patients: different causes and management strategies. *Nephrol. Dial. Transplant.* gfz182. doi: 10.1093/ndt/gfz182 [Epub ahead of print].

Goehler, L. E., Gaykema, R. P., Hansen, M. K., Anderson, K., Maier, S. F., and Watkins, L. R. (2000). Vagal immune-to-brain communication: a visceral chemosensory pathway. *Auton. Neurosci.* 85, 49–59. doi: 10.1016/s1566-0702(00)00219-8

Grassi, G., Bertoli, S., and Seravalle, G. (2012). Sympathetic nervous system: role in hypertension and in chronic kidney disease. *Curr. Opin. Nephrol. Hypertens.* 21, 46–51. doi: 10.1097/MNH.0b013e32834db45d

Herselman, M., Esau, N., Kruger, J. M., Labadarios, D., and Moosa, M. R. (2010). Relationship between serum protein and mortality in adults on long-term hemodialysis: exhaustive review and meta-analysis. *Nutrition* 26, 10–32. doi: 10.1016/j.nut.2009.07.009

Iwasaki, M., Yuasa, F., Yuyama, R., Mimura, J., Kawamura, A., Motohiro, M., et al. (2005). Correlation of heart rate turbulence with sympathovagal balance in patients with acute myocardial infarction. *Clin. Exp. Hypertens.* 27, 251–257. doi: 10.1081/ceh-200048872

Jukema, J. W., Timal, R. J., Rotmans, J. I, Hensen, L. C. R., Buiten, M. S., and De Bie, M. K. (2019). Prophylactic use of implantable cardioverter-defibrillators in the prevention of sudden cardiac death in dialysis patients: the prospective randomized controlled ICD2 trial. *Circulation* 139, 2628–2638. doi: 10.1161/circulationaha.119.039818

Kinoshita, T., Hashimoto, K., Yoshioka, K., Miwa, Y., Yodogawa, K., and Watanabe, E. (2019). Risk stratification for cardiac mortality using electrocardiographic markers based on 24-hour Holter recordings: the JANIES-SHD study. *J. Cardiol.* 75, 155–163. doi: 10.1016/j.jjcc.2019.07.012

Li, N. C., Thadhani, R. I., Reviriego-Mendoza, M., Larkin, J. W., Maddux, F. W., and Ofsthun, N. J. (2018). Association of smoking status with mortality and hospitalization in hemodialysis patients. *Am. J. Kidney Dis.* 72, 673–681. doi: 10.1053/j.ajkd.2018.04.004

Lin, L. Y., Lai, L. P., Lin, J. L., Du, C. C., Shau, W. Y., Chan, H. L., et al. (2002). Tight mechanism correlation between heart rate turbulence and baroreflex sensitivity: sequential autonomic blockade analysis. *J. Cardiovasc. Electrophysiol.* 13, 427–431. doi: 10.1046/j.1540-8167.2002.00427.x

Liu, J., Huang, Z., Gilbertson, D. T., Foley, R. N., and Collins, A. J. (2010). An improved comorbidity index for outcome analyses among dialysis patients. *Kidney Int.* 77, 141–151. doi: 10.1038/ki.2009.413

Lohmeier, T. E., and Iliescu, R. (2011). Chronic lowering of blood pressure by carotid baroreflex activation: mechanisms and potential for hypertension therapy. *Hypertension* 57, 880–886. doi: 10.1161/HYPERTENSIONAHA.108.119859

Miwa, Y., Miyakoshi, M., Hoshida, K., Yanagisawa, R., Abe, A., Tsukada, T., et al. (2011). Heart rate turbulence can predict cardiac mortality following myocardial infarction in patients with diabetes mellitus. *J. Cardiovasc. Electrophysiol.* 22, 1135–1140. doi: 10.1111/j.1540-8167.2011.02082.x

Molgaard, H. (1991). Evaluation of the reynolds pathfinder II system for 24 h heart rate variability analysis. *Eur. Heart J.* 12, 1153–1162. doi: 10.1093/eurheartj/12.11.1153

Ortiz, A., Massy, Z. A., Fliser, D., Lindholm, B., Wiecek, A., Martinez-Castelao, A., et al. (2011). Clinical usefulness of novel prognostic biomarkers in patients on hemodialysis. *Nat. Rev. Nephrol.* 8, 141–150. doi: 10.1038/nrneph.2011.170

Pavlov, V. A., Wang, H., Czura, C. J., Friedman, S. G., and Tracey, K. J. (2003). The cholinergic anti-inflammatory pathway: a missing link in neuroimmunomodulation. *Mol. Med.* 9, 125–134. doi: 10.1007/bf03402177

Peng, C. K., Havlin, S., Stanley, H. E., and Goldberger, A. L. (1995). Quantification of scaling exponents and crossover phenomena in nonstationary heartbeat time series. *Chaos* 5, 82–87. doi: 10.1063/1.166141

Penzel, T., Kantelhardt, J. W., Grote, L., Peter, J. H., and Bunde, A. (2003). Comparison of detrended fluctuation analysis and spectral analysis for heart rate variability in sleep and sleep apnea. *IEEE Trans. Biomed. Eng.* 50, 1143–1151. doi: 10.1109/tbme.2003.817636

Roy-Chaudhury, P., Tumlin, J. A., Koplan, B. A., Costea, A. I., Kher, V., Williamson, D., et al. (2018). Primary outcomes of the monitoring in dialysis study indicate that clinically significant arrhythmias are common in hemodialysis patients and related to dialytic cycle. *Kidney Int.* 93, 941–951. doi: 10.1016/j.kint.2017.11.019

Rubinger, D., Backenroth, R., and Sapoznikov, D. (2013). Sympathetic nervous system function and dysfunction in chronic hemodialysis patients. *Sem. Dial.* 26, 333–343. doi: 10.1111/sdi.12093

Rubinger, D., Revis, N., Pollak, A., Luria, M. H., and Sapoznikov, D. (2004). Predictors of haemodynamic instability and heart rate variability during haemodialysis. *Nephrol. Dial. Transplant.* 19, 2053–2060. doi: 10.1093/ndt/gfh306

Sacher, F., Jesel, L., Borni-Duval, C., De Precigout, V., Lavainne, F., Bourdenx, J. P., et al. (2018). Cardiac rhythm disturbances in hemodialysis patients: early detection using an implantable loop recorder and correlation with biological and dialysis parameters. *JACC Clin. Electrophysiol.* 4, 397–408. doi: 10.1016/j.jacep.2017.08.002

Schmaderer, C., Tholen, S., Hasenau, A.-L., Hauser, C., Suttmann, Y., and Wassertheurer, S. (2016). Rationale and study design of the prospective, longitudinal, observational cohort study "rISk strAtification in end-stage renal disease" (ISAR) study. *BMC Nephrol.* 17:161.

Schroeder, E. B., Liao, D., Chambless, L. E., Prineas, R. J., Evans, G. W., and Heiss, G. (2003). Hypertension, blood pressure, and heart rate variability: the atherosclerosis risk in communities (ARIC) study. *Hypertension* 42, 1106–1111. doi: 10.1161/01.hyp.0000100444.71069.73

Schwab, J. O., Eichner, G., Shlevkov, N., Schrickel, J., Yang, A., Balta, O., et al. (2005). Impact of age and basic heart rate on heart rate turbulence in healthy persons. *Pacing Clin. Electrophysiol.* 28(Suppl. 1), S198–S201.

Shoji, T., Tsubakihara, Y., Fujii, M., and Imai, E. (2004). Hemodialysis-associated hypotension as an independent risk factor for two-year mortality in hemodialysis patients. *Kidney Int.* 66, 1212–1220. doi: 10.1111/j.1523-1755.2004.00812.x

Stenvinkel, P., and Alvestrand, A. (2002). Inflammation in end-stage renal disease: sources, consequences, and therapy. *Sem. Dial.* 15, 329–337. doi: 10.1046/j.1525-139x.2002.00083.x

Stenvinkel, P., Carrero, J. J., Axelsson, J., Lindholm, B., Heimburger, O., and Massy, Z. (2008). Emerging biomarkers for evaluating cardiovascular risk in the chronic kidney disease patient: how do new pieces fit into the uremic puzzle? *Clin. J. Am. Soc. Nephrol.* 3, 505–521. doi: 10.2215/CJN.03670807

Suzuki, M., Hiroshi, T., Aoyama, T., Tanaka, M., Ishii, H., Kisohara, M., et al. (2012). Nonlinear measures of heart rate variability and mortality risk in hemodialysis patients. *Clin. J. Am. Soc. Nephrol.* 7, 1454–1460. doi: 10.2215/CJN.09430911

USRDS (2014). "United States Renal Data System. 2014 USRDS annual data report: Epidemiology of kidney disease in the United States," in *National Institutes of Health, National Institute of Diabetes and Digestive and Kidney Diseases*, (Bethesda, MD: United States Renal Data System).

Wichterle, D., Melenovsky, V., and Malik, M. (2002). Mechanisms involved in heart rate turbulence. *Card. Electrophysiol. Rev.* 6, 262–266.

Conflict of Interest: JFM reports personal fees from AstraZeneca, Amgen, Braun, ACI, Fresenius, Gambro, Medice, Lanthio, Sanifit, Relypsa, ZS Pharma; grants and personal fees from Celgene, Abbvie, NovoNordisk, Roche, Sandoz; grants from European Union and McMaster University Canada outside the submitted work. The results presented in this manuscript have not been published previously in whole or part, except in abstract format.

The remaining authors declare that the research was conducted in the absence of any commercial or financial relationships that could be construed as a potential conflict of interest.

frontiers in Physiology

ORIGINAL RESEARCH
published: 24 April 2020
doi: 10.3389/fphys.2020.00344

Mechanisms of Arrhythmogenicity in Hypertrophic Cardiomyopathy: Insight From Non-invasive Electrocardiographic Imaging

*Erick A. Perez-Alday[1], Kazi T. Haq[1], David M. German[1], Christopher Hamilton[1], Kyle Johnson[1], Francis Phan[1], Nichole M. Rogovoy[1], Katherine Yang[1,2], Ashley Wirth[1], Jason A. Thomas[1], Khidir Dalouk[1,3], Cristina Fuss[4], Maros Ferencik[1], Stephen Heitner[1] and Larisa G. Tereshchenko[1]**

[1] Department of Medicine, Knight Cardiovascular Institute, Oregon Health & Science University, Portland, OR, United States, [2] Sidney Kimmel Medical College, Philadelphia, PA, United States, [3] Portland VA Medical Center, Portland, OR, United States, [4] Department of Diagnostic Radiology, Oregon Health & Science University, Portland, OR, United States

Background: Mechanisms of arrhythmogenicity in hypertrophic cardiomyopathy (HCM) are not well understood.

Objective: To characterize an electrophysiological substrate of HCM in comparison to ischemic cardiomyopathy (ICM), or healthy individuals.

Methods: We conducted a prospective case-control study. The study enrolled HCM patients at high risk for ventricular tachyarrhythmia (VT) [n = 10; age 61 ± 9 years; left ventricular ejection fraction (LVEF) 60 ± 9%], and three comparison groups: healthy individuals (n = 10; age 28 ± 6 years; LVEF > 70%), ICM patients with LV hypertrophy (LVH) and known VT (n = 10; age 64 ± 9 years; LVEF 31 ± 15%), and ICM patients with LVH and no known VT (n = 10; age 70 ± 7 years; LVEF 46 ± 16%). All participants underwent 12-lead ECG, cardiac CT or MRI, and 128-electrode body surface mapping (BioSemi ActiveTwo, Netherlands). Non-invasive voltage and activation maps were reconstructed using the open-source SCIRun (University of Utah) inverse problem-solving environment.

Results: In the epicardial basal anterior segment, HCM patients had the greatest ventricular activation dispersion [16.4 ± 5.5 vs. 13.1 ± 2.7 (ICM with VT) vs. 13.8 ± 4.3 (ICM no VT) vs. 8.1 ± 2.4 ms (Healthy); P = 0.0007], the largest unipolar voltage [1094 ± 211 vs. 934 ± 189 (ICM with VT) vs. 898 ± 358 (ICM no VT) vs. 842 ± 90 μV (Healthy); P = 0.023], and the greatest voltage dispersion [median (interquartile range) 215 (161–281) vs. 189 (143–208) (ICM with VT) vs. 158 (109–236) (ICM no VT) vs. 110 (106–168) μV (Healthy); P = 0.041]. Differences were also observed in other endo-and epicardial basal and apical segments.

Conclusion: HCM is characterized by a greater activation dispersion in basal segments, a larger voltage, and a larger voltage dispersion through LV.

Clinical Trial Registration: www.clinicaltrials.gov Unique identifier: NCT02806479.

Keywords: hypertrophic cardiomyopathy, electrocardiographic imaging, body surface mapping, conduction velocity, noninvasive

OPEN ACCESS

Edited by:
George E. Billman, The Ohio State University, United States

Reviewed by:
Peter Taggart, University College London, United Kingdom
Ruben Coronel, University of Amsterdam, Netherlands

****Correspondence:***
Larisa G. Tereshchenko
tereshch@ohsu.edu

Specialty section:
This article was submitted to Cardiac Electrophysiology, a section of the journal Frontiers in Physiology

Received: *10 September 2019*
Accepted: *26 March 2020*
Published: *24 April 2020*

Citation:
Perez-Alday EA, Haq KT, German DM, Hamilton C, Johnson K, Phan F, Rogovoy NM, Yang K, Wirth A, Thomas JA, Dalouk K, Fuss C, Ferencik M, Heitner S and Tereshchenko LG (2020) Mechanisms of Arrhythmogenicity in Hypertrophic Cardiomyopathy: Insight From Non-invasive Electrocardiographic Imaging. Front. Physiol. 11:344. doi: 10.3389/fphys.2020.00344

INTRODUCTION

Patients with hypertrophic cardiomyopathy (HCM) are at high risk of life-threatening ventricular arrhythmias and sudden cardiac death (SCD) (Maron et al., 2019). Mechanisms of arrhythmogenicity in HCM are complex and incompletely understood. It was previously shown that the late sodium current is increased in HCM, suggesting the importance of repolarization abnormalities (Coppini et al., 2013). At the same time, cardiac magnetic resonance (CMR) studies have shown that the myocardium in HCM is characterized by increased fibrosis burden, supporting an alternative mechanism for arrhythmogenesis – heterogeneity in electrical activation. The degree of late gadolinium enhancement in HCM is associated with SCD and appropriate implantable cardioverter-defibrillator (ICD) therapy (Mentias et al., 2018). While the presence of a patchy scar in HCM suggests likely similarity with macro-reentrant post-myocardial infarction (MI) ventricular tachycardia (VT) mechanisms, VT ablation in HCM is less successful than in post-infarction VT. In HCM patients who underwent VT ablation, the incidence of VT recurrence, death, and cardiac transplantation at 1 year was one of the highest amongst all non-ischemic cardiomyopathies (NICM) (Vaseghi et al., 2018), even after adjusting for comorbidities. This may be due to anatomic limitations for ablation (predominantly mid-myocardial septal location of the scar), or diffuse nature of cardiomyocyte disarray and interstitial fibrosis that is the histopathological hallmark of HCM (Iles et al., 2008). By and large, the electrophysiological (EP) substrate in HCM is incompletely understood. Recently, the non-invasive electrocardiographic imaging (ECGi), a state-of-the-art technology, became available as a tool to study mechanisms of cardiac arrhythmias (Ramanathan et al., 2004). We designed this study with the goal to describe the EP substrate of HCM, in comparison with the relatively well-understood EP substrate of post-infarction macro-reentrant VT.

METHODS

Study Population: Inclusion and Exclusion Criteria

We conducted a single-center case-control study of high-risk HCM cases with three comparison groups (Clinical Trial Registration – www.clinicaltrials.gov Unique identifier: NCT02806479). The Oregon Health & Science University (OHSU) Institutional Review Board (IRB) approved this study, and all participants signed an informed consent form. Enrollment was performed at OHSU in 2016–2018. Adult (age $\geq$ 18 years) non-pregnant participants were enrolled if the inclusion and exclusion criteria were met, as described below.

Inclusion criteria for HCM group were: (1) a history of resuscitated sudden cardiac arrest, or documented sustained VT, or (2) a maximal left ventricular (LV) wall thickness above 30 mm, or extensive fibrosis on CMR (above 10% of total myocardial volume), or (3) high risk of SCD (>7.5%/5 years) as determined by HCM risk-SCD (O'Mahony et al., 2014) score.

Healthy control group I (*Healthy*) was designed to include individuals who were free from structural heart disease and arrhythmogenic substrate in ventricles. The inclusion criterion required evaluation by a cardiac electrophysiologist for AV nodal reentrant tachycardia. Exclusion criteria were diagnosed structural heart disease, or known risk factors of structural heart disease (Panel, 2002) (history of hypertension, smoking, diabetes, body mass index <18.5 or >30 kg/m^2, and family history of coronary heart disease (CHD) diagnosed at age 50 or younger).

Group II (*post-MI VT-free*) included post-MI VT-free patients as documented by at least one generator life of primary prevention ICD, or medical record.

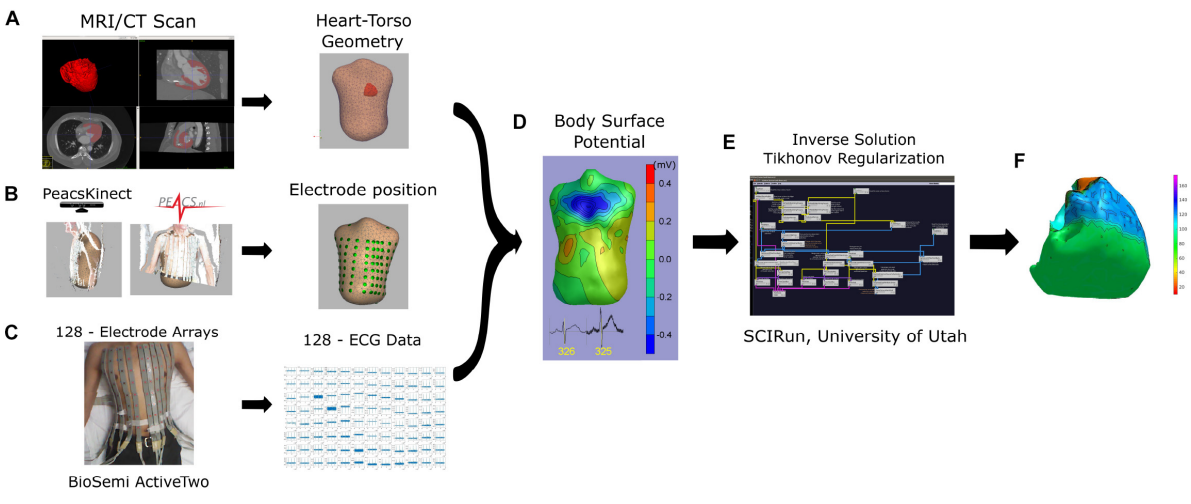

FIGURE 1 | Workflow from data acquisition to data analysis. **(A)** MRI/CT scan to obtain heart and torso 3D meshes; **(B)** electrode position from kinect camera using PeacsKinect, and **(C)** 128-ECG recordings using Biopac system, were used to obtain a **(D)** body surface potential, and calculate **(E,F)** reconstruction of ventricular potential map using SCI-run toolkit **(E)**.

Group III (*post-MI VT*) included post-MI patients with the history of sudden cardiac arrest and implanted secondary prevention ICD, or, if an ICD was implanted for primary prevention of SCD and there was documented sustained (cycle length < 240 ms) VT treated by appropriate ICD shock. MADIT-RIT programming criteria were applied, to avoid inclusion of treated non-sustained VT events. Sudden cardiac arrest due to a transient cause was an exclusion criterion.

In addition, exclusion criteria for all study participants were the age of less than 18y, pregnancy, persistent atrial fibrillation (AF), chronic (above 5%) right ventricular (RV) or biventricular pacing, renal insufficiency with estimated glomerular filtration rate (eGFR) < 30 ml/min, congenital heart disease, and contraindications for CMR or cardiac computed tomography (CT) with contrast. By design, we planned to enroll 10 participants in each group.

Cardiac Imaging and Assessment of Cardiac Structure and Function

Healthy controls underwent non-contrast CMR using a Siemens TIM Trio 3 Tesla with VB17 software and Siemens Prisma Fit 3 Tesla scanner with E11C software. The other three groups underwent prospectively ECG-triggered contrast-enhanced 256-detector row cardiac CT (Philips iCT, Philips Medical Imaging, Cleveland, OH, United States). The images were acquired in mid to end diastole with a slice thickness of 0.6 mm and in-plane resolution of ∼0.5 mm. A cardiologist (DMG) reviewed all cardiac CT and MRI images, and ventricular volumes were obtained in a semiautomatic fashion using commercially available software (IntelliSpace Portal; Philips Healthcare, Redmond, WA, United States; and CVI42; Circle Cardiovascular Imaging Inc., Calgary, Alberta, Canada). The standardized myocardial segmentation and nomenclature (Cerqueira et al., 2002) were used to define 17 segments of LV. For subjects who underwent CMR, left ventricular ejection fraction (LVEF) was calculated from ventricular volume measurements.

Additionally, data from the most recent echocardiogram and CMR was abstracted to provide additional information on baseline cardiac structure and function. LVEF was calculated from the echocardiogram using the biplane Simpson method of discs. Regional LV function was evaluated by the echocardiographic wall motion score index. Motion and systolic thickening in each segment was scored as: normal or

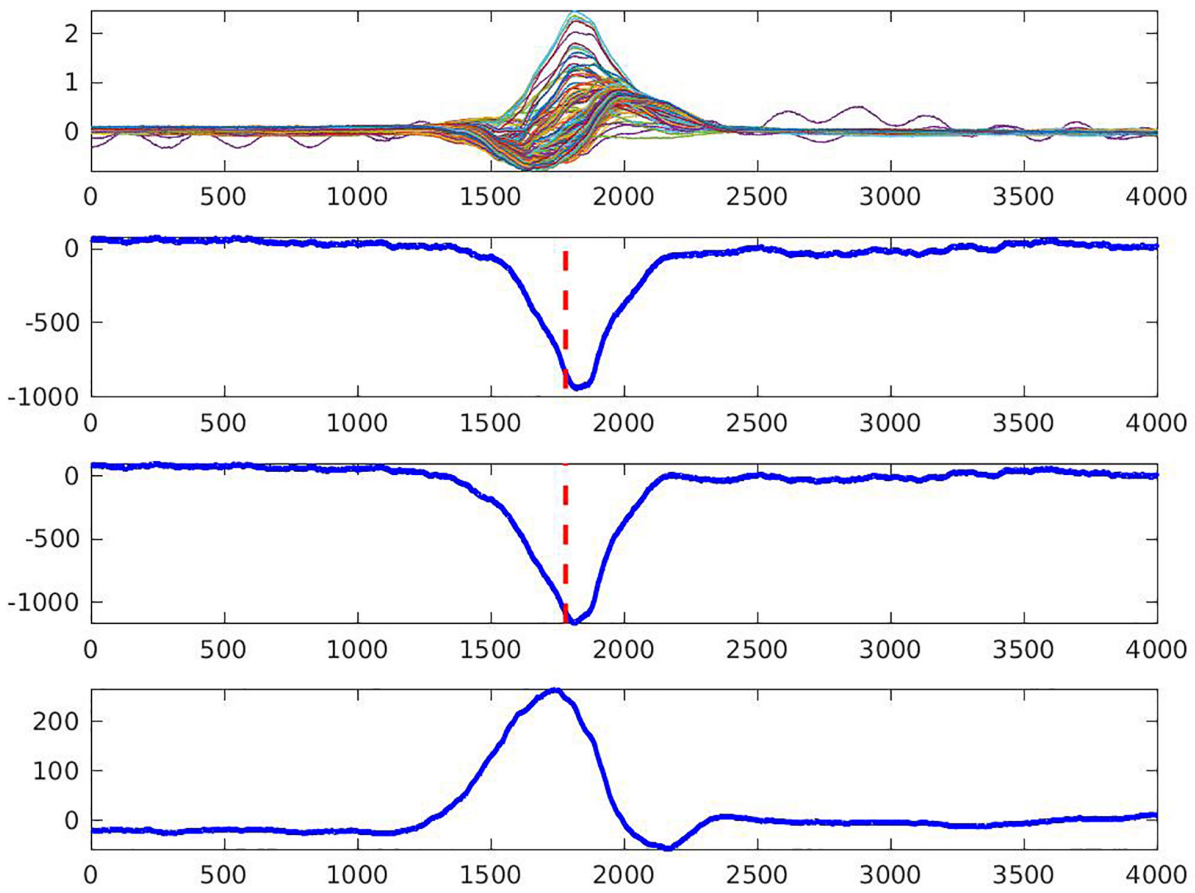

FIGURE 2 | Quality control of the measurement of the steepest downslope of epicardial electrogram (the steepest negative dV/dt, dashed line). Two neighboring unipolar electrograms **(two middle rows)** and bipolar electrogram **(bottom row)** are shown. An upper row shows overlapped 128 body surface electrocardiograms. Local activation time is marked by the dashed line.

hyperkinesis = 1, hypokinesis = 2, akinesis = 3, and dyskinesis (or aneurysmal) = 4. The wall motion score index was calculated as the sum of all scores divided by the number of visualized segments. The resting peak LVOT gradient was calculated for all participants. In addition, HCM participants had peak LVOT gradient measured during Valsalva maneuver and at peak exertion. The location of fibrosis on CMR images was recorded. Age- and sex-specific thresholds were used to define left ventricular hypertrophy (LVH) on cardiac CT and CMR (Juneau et al., 2017).

Body Surface Potentials Recording and ECG Electrodes Localization

A routine clinical resting 12-lead electrocardiogram (ECG) was recorded during the study visit, and ECG metrics were measured by the 12SL algorithm (GE Marquette Electronics, Milwaukee, WI, United States).

Unipolar ECG potentials were recorded on the body surface using the ActiveTwo biopotential measurement system (BioSemi, Amsterdam, the Netherlands) with 128 Ag/AgCL electrodes (4 panels of 32 electrodes; each panel is arranged as four strips of 8-electrodes; diameter of the ECG electrodes 5 mm) (Perez-Alday et al., 2018). The sampling rate of the signal was 16,384 Hz; bandwidth DC-3,200 Hz. ECG electrodes were localized by three-dimensional (3D) photography approach, using a PeacsKinect (Peacs BV, Arnhem, the Netherlands) and Kinect camera (Microsoft, Redmond, WA, United States) (Perez-Alday et al., 2018). For co-registration of torso images, five CMR- or CT- specific markers were placed on each patient's chest to wear during scanning, to mark ECG electrode locations.

Reconstruction of Torso and Heart Meshes

We constructed 3D meshes of a continuous surface of the endocardium (excluding papillary muscles) and epicardium of

TABLE 1 | Demographic and clinical characteristics of the study population.

Characteristic	Healthy (*n* = 10)	Post-MI VT-free (*n* = 10)	Post-MI VT (*n* = 10)	HCM (*n* = 10)
Age (SD), year	28.8 (5.6)	69.3 (9.3)	64.0 (10.5)	61.3 (9.3)
Male, n (%)	4 (40)	10 (100)	10 (100)	8 (80)
White, n (%)	6 (60)	10 (100)	9 (90)	10 (100)
BMI (SD), kg/m^2	23.6 (3.6)	33.0 (6.6)	30.9 (6.9)	30.1 (5.7)
History of hypertension, n (%)	0	9 (90)	9 (90)	6 (60)
History of diabetes, n (%)	0	5 (50)	2 (20)	1 (10)
Chronic kidney disease, n (%)	0	3 (30)	0	0
Class I antiarrhythmics, n (%)	0	0	5 (50)	2 (20)
Beta-blockers, n (%)	0	7 (70)	9 (90)	8 (80)
ACEI/ARB/ARNI	0	6 (60)	8 (80)	2 (20)
Aldosterone antagonists, n (%)	0	4 (40)	2 (20)	0
Diuretics, n (%)	0	8 (80)	2 (20)	0
LVEF (SD), %	65.8 (4.7)	45.8 (15.4)	37.3 (12.7)	60.4 (8.3)
GLS (SD), %	– –	−13.5 (0)	−9.6 (0.4)	−13.2 (0.8)
LVIDd (SD), cm	4.3 (0.4)	5.2 (1.3)	6.1 (1.1)	4.5 (0.7)
LVIDs (SD), cm	2.7 (0.4)	4.2 (0.9)	5.1 (1.4)	2.9 (0.4)
LAVI (SD), ml/m^2	22.3 (3.1)	32.6 (13.9)	33.2 (8.8)	40.1 (12.8)
LVEDVI (SD), ml/m^2	76.7 (13.4)	89.6 (30.0)	100.6 (34.1)	72.2 (12.3)
RVEDVI (SD), ml/m^2	89.0 (20.5)	71.8 (14.4)	76.7 (10.8)	76.3 (13.4)
LV mass index (SD), g/m^2	63.9 (13.9)	76.0 (15.0)	92.2 (25.7)	99.3 (28.9)
LVH, %	0	1	6	6
IVSd (SD), cm	0.8 (0.1)	1.5 (1.4)	1.0 (0.1)	1.5 (0.3)
LVPWd (SD), cm	0.8 (0.1)	1.1 (0.2)	1.0 (0.2)	1.2 (0.3)
E/A ratio	1.7 (0.2)	1.3 (0.8)	0.9 (0.2)	1.0 (0.4)
E/e' ratio	5.9 (1.5)	9.1 (3.4)	11.4 (5.7)	9.5 (4.0)
Peak LVOT gradient (SD), mmHg	4.7 (1.1)	6.2 (2.2)	10.2 (9.0)	77.9 (193)
LVOT diameter (SD), cm	2.2 (0.1)	2.2 (0.2)	2.3 (0.3)	2.2 (0.3)
Wall motion score (SD)	8.8 (8.9)	27.4 (16.6)	18.2 (14.4)	10.3 (8.9)
Resting heart rate (SD), bpm	76.8 (13.7)	74.2 (11.6)	66.9 (15.1)	70.7 (10.5)
QTc interval (SD), ms	408 (24)	398 (32)	444 (23)	424 (37)

LVEF, left ventricular ejection fraction; GLS, global longitudinal strain; LVIDd, Left ventricular internal dimension at end-diastole; LVIDs, Left ventricular internal dimension at end-systole; LVEDV, left ventricular end-diastolic volume; LVEDVI, left ventricular end-diastolic volume index; RVEDV, right ventricular end-diastolic volume; RVEDVI, right ventricular end-diastolic volume index; IVSd, Interventricular septum thickness at end-diastole; LVPWd, Left ventricular posterior wall thickness at end-diastole; LAVI, left atrial volume index; SD, standard deviation; LVH, left ventricular hypertrophy.

both ventricular chambers. The 3D heart and torso meshes were reconstructed using a semi-automatic approach – image growing method of a continuous surface (Alday et al., 2015; Perez-Alday et al., 2018) from CMR/CT images using ITK-snap software (PICSL, United States) (Yushkevich et al., 2006). Each cardiac mesh was manually reviewed to ensure a continuous segmentation of epicardium and endocardium of both ventricular chambers and exclude atria chambers and papillary muscles. Both torso meshes segmented by the 3D photography method and DICOM images were matched using the co-registered CMR/CT markers and electrode position, as previously described (Perez-Alday et al., 2018). The resolution of the cardiac mesh was 3.6 ± 0.5 mm with 3,992 ± 735 nodes.

Inverse Solution and Reconstruction of the Cardiac Activation Map

The workflow is shown in **Figure 1**. One clean normal sinus beat was selected for analysis; an absence of extrasystole before and after the selected beat was verified. We used the open-source SCIRun problem-solving environment developed at the Center for Integrative Biomedical Computing (University of Utah, UT, United States) (Burton et al., 2011; Coll-Font et al., 2014), which was previously used to compute forward and inverse solutions (Babaeizadeh et al., 2006) and reconstruct unipolar epicardial and endocardial electrograms (EGMs). The inverse problem was solved as the potential-based formulation (boundary element method), as a weighted minimum norm problem by applying a Tikhonov L2-norm regularization. The source code and inverse problem SCIRun toolkit with documentation can be found at www.scirun.org.

The steepest downslope of each unipolar EGM was determined automatically, using MATLAB (The MathWorks Inc., Natick, MA, United States) software application. In order to verify the consistency of morphology and the steepest downslope detection, each pair of neighboring unipolar EGMs – together with the resulting bipolar EGM (calculated as their difference) – were reviewed by at least two investigators (AW, KY, NMR, EAPA) who were blinded to the study group assignment (**Figure 2**). In the case of disagreement between all three EGMs, the unipolar EGMs were excluded from further analysis. Recalculation of the steepest downslope was performed in the case of morphology agreement but steepest downslope disagreement. For calculation of the time reference point, the three limb leads (I, II, and III) were used to define the average QRS onset on the surface ECG. Local activation time (LAT) in each node of the mesh was calculated as the time difference between average (surface ECG) QRS onset and the time of the steepest downslope

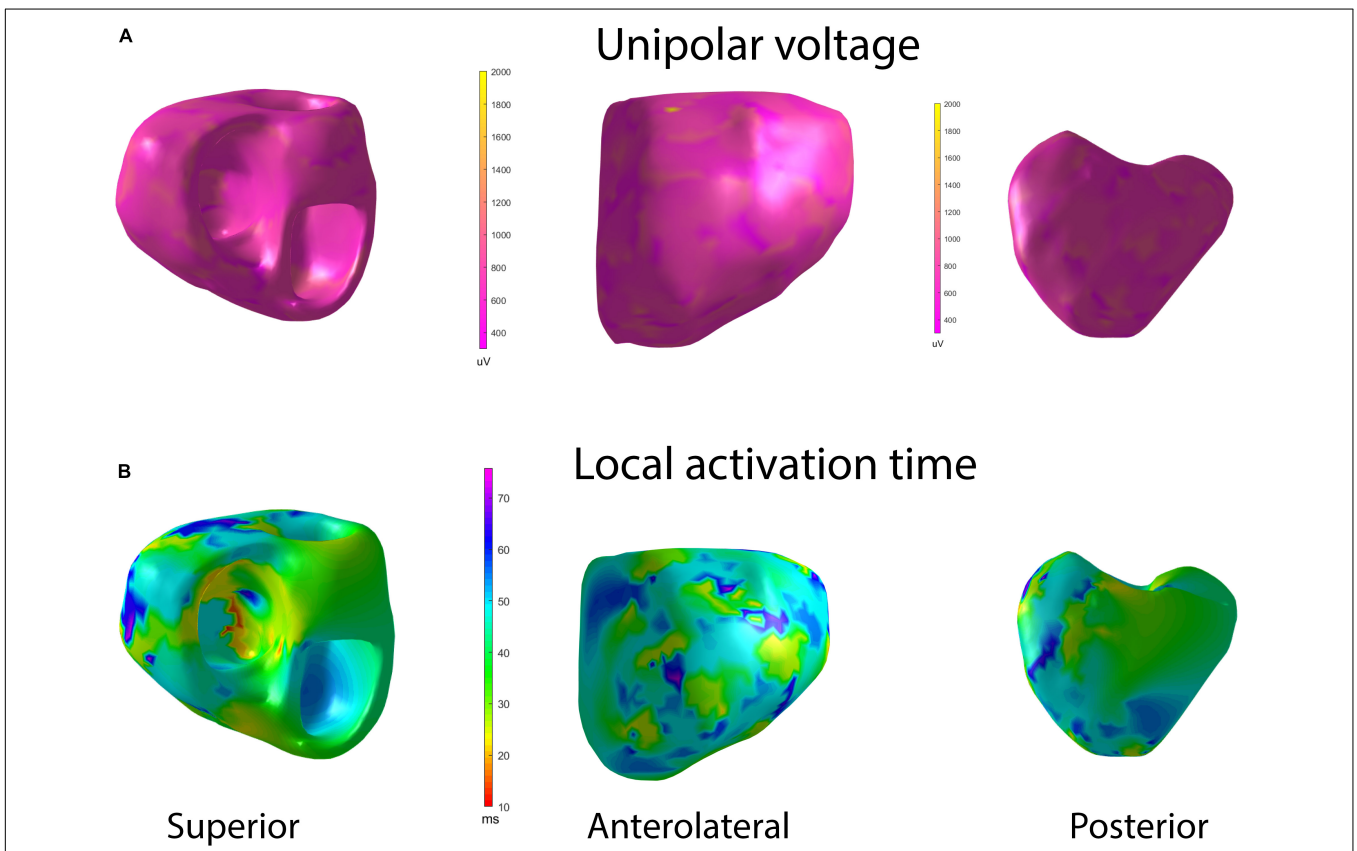

FIGURE 3 | Representative examples of **(A)** unipolar voltage and **(B)** ventricular activation maps in a healthy participant, during sinus rhythm activation. Superior, anterolateral, and a posterior view. The orifices of the aorta and the mitral valve are combined. **Supplementary Movies S1**, **S2** show representative examples of unipolar voltage and ventricular activation maps in a healthy participant, during sinus rhythm activation.

(minimum dV/dt) on a corresponding unipolar EGM. To reconstruct the cardiac activation map on the epicardial and endocardial surface, the LAT was plotted in each epicardial and endocardial node.

Unipolar Voltage Potential Map

Unipolar voltage was measured in each reconstructed EGM, and the unipolar voltage potential maps were constructed. The peak-to-peak voltage on each unipolar EGM was automatically measured using a MATLAB (The MathWorks Inc., Natick, MA, United States) software application. Investigators (AW, KY, NMR, EAPA), blinded to the group assignment, validated the accuracy of the detection of unipolar EGM peaks. We used the standardized myocardial segmentation and nomenclature (Cerqueira et al., 2002) to define 17 segments of the LV. The mean unipolar voltage was calculated for each segment. RV endocardial surface in five segments (basal anteroseptal and inferoseptal, mid-cavity anteroseptal and inferoseptal, and apical septal) served as an "epicardial" surface of the LV. Standard deviation (SD) of unipolar voltage distribution in each segment served as a measure of voltage dispersion within each segment.

Dispersion of Local Activation Time

Mean LAT was calculated for each LV segment (Cerqueira et al., 2002). RV endocardial surface in 5 segments (basal anteroseptal and inferoseptal, mid-cavity anteroseptal and inferoseptal, and apical septal) served as an "epicardial" surface of the LV. The dispersion of activation was measured as SD of LAT in each segment.

Statistical Analysis

Statistics of normally distributed variables are summarized as mean ± SD. Distributions of all variables were reviewed. After verifying the normality of distribution, we tested the hypothesis that the mean voltage is the same across four study groups while removing the assumption of equal covariance matrices. The Wald chi-squared statistic with James's approximation (James, 1954) was used to calculate *P*-values.

TABLE 2 | Mean (SD) unipolar voltage potentials (μ V) in LV endocardial and epicardial, and RV endocardial septal regions.

	Region	Healthy (*n* = 10)	Post-MI VT-free (*n* = 10)	Post-MI VT (*n* = 10)	HCM (*n* = 10)	P_{James}
Endocardial	Basal anterior	802 (108)	853 (281)	982 (230)	1,086 (241)	0.016
	Basal anteroseptal	812 (128)	931 (304)	954 (166)	1,085 (266)	0.043
	Basal inferoseptal	829 (103)	901 (359)	943 (318)	1,121 (239)	0.071
	Basal inferior	823 (106)	804 (275)	942 (241)	1,037 (276)	0.130
	Basal inferolateral	856 (98)	835 (291)	958 (209)	1,081 (286)	0.125
	Basal anterolateral	829 (82)	949 (337)	967 (259)	1,096 (300)	0.023
	Mid-anterior	838 (114)	871 (323)	945 (187)	1,045 (214)	0.090
	Mid-anteroseptal	817 (98)	903 (291)	900 (211)	1,042 (276)	0.136
	Mid-inferoseptal	839 (107)	901 (332)	916 (224)	1,087 (290)	0.135
	Mid-inferior	793 (83)	852 (281)	952 (262)	1,008 (251)	0.071
	Mid-inferolateral	836 (98)	890 (305)	926 (260)	1,111 (297)	0.086
	Mid-anterolateral	837 (94)	936 (414)	984 (238)	1,110 (244)	0.204
	Apical anterior	809 (111)	984 (452)	969 (154)	1,094 (314)	0.036
	Apical septal	810 (133)	898 (450)	941 (205)	1,122 (229)	0.028
	Apical Inferior	835 (97)	863 (282)	902 (233)	1,015 (211)	0.198
	Apical lateral	791 (143)	892 (295)	964 (181)	942 (180)	0.133
Epicardial/RV endocardial	Basal anterior	842 (90)	898 (358)	934 (189)	1,094 (211)	0.023
	RV_{endo} Basal anteroseptal	827 (157)	929 (326)	961 (174)	1,120 (217)	0.028
	RV_{endo} Basal inferoseptal	808 (133)	883 (325)	904 (234)	1,073 (302)	0.251
	Basal inferior	838 (99)	904 (280)	964 (228)	1,053 (177)	0.028
	Basal inferolateral	847 (113)	903 (322)	936 (177)	1,069 (205)	0.064
	Basal anterolateral	855 (131)	937 (355)	996 (166)	1,125 (218)	0.027
	Mid-anterior	856 (118)	901 (307)	942 (182)	1,106 (242)	0.068
	RV_{endo} Mid-anteroseptal	824 (118)	912 (415)	911 (185)	1,068 (288)	0.201
	RV_{endo} Mid-inferoseptal	812 (136)	893 (349)	895 (154)	975 (231)	0.320
	Mid-inferior	838 (88)	920 (335)	966 (229)	1,002 (211)	0.142
	Mid-inferolateral	829 (114)	904 (341)	968 (201)	1,098 (197)	0.013
	Mid-anterolateral	856 (107)	875 (296)	941 (165)	1,076 (215)	0.069
	Apical anterior	825 (102)	883 (288)	950 (195)	1,075 (241)	0.042
	RV_{endo} Apical septal	833 (97)	937 (365)	902 (129)	1,078 (166)	0.008
	Apical Inferior	829 (102)	838 (263)	933 (166)	1,024 (188)	0.068
	Apical lateral	825 (100)	884 (360)	918 (206)	1,082 (266)	0.070
	Apex	840 (94)	888 (320)	935 (182)	1,054 (217)	0.069

We used a Kruskal–Wallis test of the hypothesis that four study groups are from the same population, to compare voltage and LAT dispersions (measured as an SD of LAT and voltage in each of 17 segments; Cerqueira et al., 2002), which have a non-normal distribution. Non-normally distributed variables are summarized as the median and interquartile range (IQR). A *P*-value of less than 0.05 was considered significant. Statistical analyses were performed using STATA MP 15.1 (StataCorp LLC, College Station, TX, United States).

RESULTS

Study Population

The clinical characteristics of the study population are shown in **Table 1**. Most of HCM patients (80%) had previously undergone genetic testing. The definitive, disease-causing *MYHBPC3* mutation was found in two patients. Half of the HCM participants had survived a sudden cardiac arrest, and the other half had a documented history of sustained VT. While half of the HCM patients had a history of severe LVOT obstruction (up to 153 mmHg at peak exertion), they had already undergone surgical myectomy, resulting in vastly improved LVOT gradients (provoked peak LVOT gradient 20 ± 20 mmHg), at the time of enrollment.

Healthy controls had no comorbidities and did not take medications (**Table 1**). Nearly all group II-III participants and HCM patients had hypertension, but only a minority of participants had diabetes and chronic kidney disease. Nearly all post-MI and HCM patients were on beta-blockers. Half of group III participants and 20% of HCM group were taking class I antiarrhythmic medications (amiodarone, sotalol, mexiletine).

In the VT-free post-MI group, the scar was located in the anteroseptal region in 90% of participants. In post-MI VT group, the scar was located in the inferoposterior region in 40% and anteroseptal in 60%. A single-chamber ICD was implanted in ∼50% of patients. The other half had a dual-chamber ICD implanted.

LV systolic function was normal in healthy controls and HCM participants, whereas ischemic cardiomyopathy (ICM) with reduced LVEF was confirmed for both post-MI groups. LVH was equally present in HCM and ICM with VT groups.

Mean Unipolar Voltage and Unipolar Voltage Dispersion

A representative example of voltage maps is shown in **Figure 3**. Mean unipolar voltage (**Table 2** and **Figure 4**) was significantly different across all four study groups in basal anteroseptal and apical septal segments on both sides of septum – LV and RV endocardium. Also, a significant difference in voltage across all four groups was observed on both endocardial and epicardial surfaces of basal anterior and anterolateral segments, the endocardial surface of anterior apical segment, and the epicardial surface of basal inferior and mid-inferolateral segments. Healthy

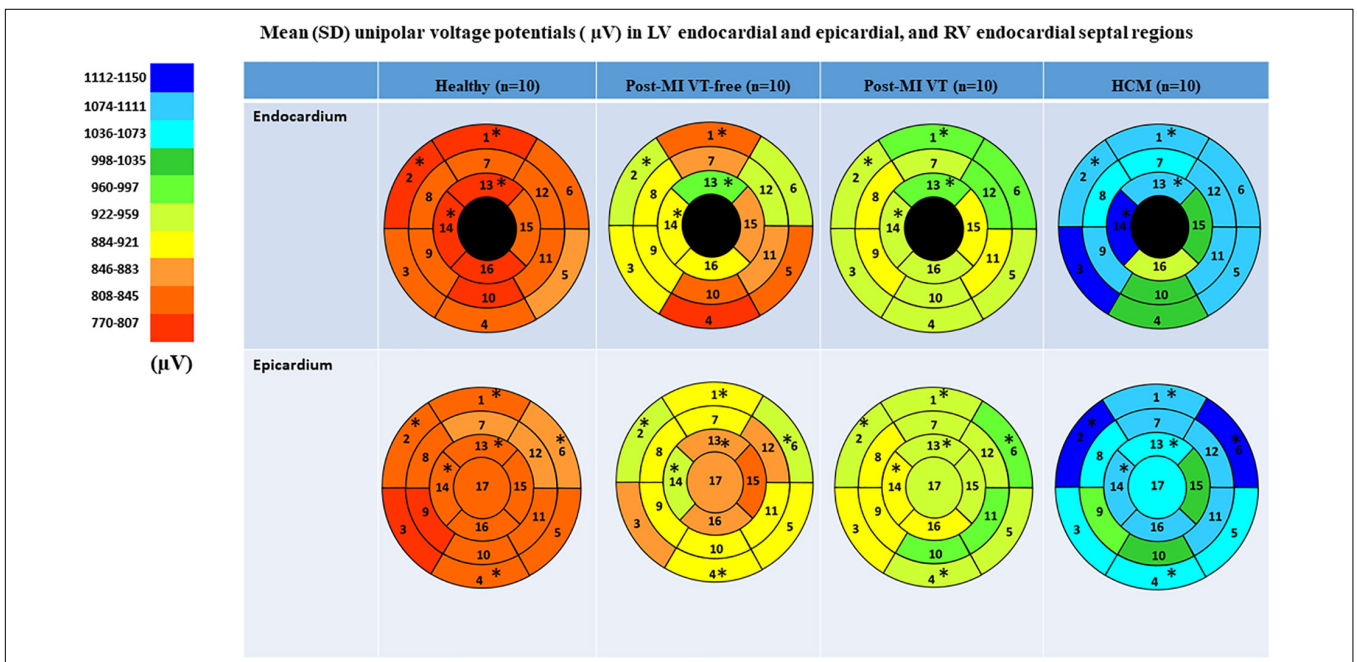

FIGURE 4 | Comparison of mean unipolar voltage in study groups, in 16 LV endocardial and 17 LV epicardial segments. Nomenclature: 1 = basal anterior; 2 = basal anteroseptal; 3 = Basal inferoseptal; 4 = Basal inferior; 5 = Basal inferolateral; 6 = Basal anterolateral; 7 = Mid-anterior; 8 = Mid-anteroseptal; 9 = Mid-inferoseptal; 10 = Mid-inferior; 11 = Mid-inferolateral; 12 = Mid-anterolateral; 13 = Apical anterior; 14 = Apical septal; 15 = Apical Inferior; 16 = Apical lateral; 17 = apex. RV endocardial surface in five segments (basal anteroseptal and inferoseptal, mid-cavity anteroseptal and inferoseptal, and apical septal) served as an "epicardial" surface of the LV. Statistically significant differences are marked with a star.

individuals had the smallest mean unipolar voltage, whereas HCM was characterized by the largest voltage (**Figure 4**). Unipolar voltage in the two post-MI groups was similar, and had intermediate values, as compared to healthy and HCM participants.

Voltage dispersion was significantly smaller in healthy, as compared to the other three groups (**Table 3** and **Figure 5**). Remarkably, in several segments, voltage dispersion in HCM was the highest amongst all four groups, significantly exceeding voltage dispersion in both ICM groups. The unipolar voltage dispersion was significantly different across study groups in both endocardial and epicardial segments of the basal anterior, basal anterolateral and inferolateral, apical inferior, and the epicardial surface of the apex.

Dispersion of Ventricular Activation

A representative example of the activation map is shown in **Figure 3**. In Healthy, we observed a normal activation pattern, which initiated in the septal region and propagated from endocardium to epicardium, with several breakthroughs – near the RV apex and anterior paraseptal aspects of the epicardium in regions adjacent to the left anterior descendent coronary artery. Activation proceeded from apex to the inferior basal area in both RV and LV, with the inferolateral LV base and the region near the right ventricular outflow tract (RVOT) being the latest to activate.

The dispersion of LAT was significantly higher in HCM patients in nearly all epicardial basal segments and basal lateral endocardial segments (**Table 4** and **Figure 6**). A consistent trend in LAT dispersion between groups was observed, with the smallest LAT dispersion in healthy subjects, intermediate LAT dispersion in ICM patients, and the largest LAT dispersion in HCM patients. Furthermore, in ICM and HCM patients there was a trend toward greater LAT dispersion in basal segments, as compared to apical or mid-segments, whereas in healthy controls, small degree of LAT dispersion was homogeneous, without apex-base gradient. In addition, there was a trend of larger LAT dispersion in post-MI patients with VT history, as compared to VT-free post-MI patients.

TABLE 3 | Unipolar voltage dispersion within segments on endocardial and epicardial surface of the left ventricle.

	Region	Healthy (n = 10)	Post-MI VT-free (n = 10)	Post-MI VT (n = 10)	HCM (n = 10)	$P_{Kruskal-Wallis}$
Endocardial	Basal anterior	101 (53 – 147)	161 (102 – 214)	146 (89 – 157)	178 (162 – 276)	0.017
	Basal anteroseptal	73 (42 – 132)	94 (78 – 266)	148 (64 – 227)	223 (166 – 295)	0.053
	Basal inferoseptal	104 (75 – 129)	123 (84 – 199)	130 (59 – 152)	230 (155 – 314)	0.066
	Basal inferior	95 (54 – 126)	126 (79 – 152)	147 (111 – 203)	184 (130 – 267)	0.076
	Basal inferolateral	88 (80 – 117)	114 (89 – 153)	105 (87 – 170)	177 (124 – 252)	0.031
	Basal anterolateral	58 (49 – 117)	153 (128 – 195)	142 (94 – 215)	201 (136 – 224)	0.049
	Mid-anterior	82 (73 – 105)	167 (100 – 241)	127 (80 – 229)	169 (138 – 224)	0.113
	Mid-anteroseptal	50 (36 – 59)	80 (50 – 136)	127 (48 – 171)	112 (47 – 290)	0.345
	Mid-inferoseptal	87 (54 – 117)	84 (36 – 148)	125 (66 – 204)	187 (106 – 227)	0.277
	Mid-inferior	113 (69)	111 (79 – 285)	169 (122 – 180)	183 (72 – 196)	0.752
	Mid-inferolateral	110 (48 – 176)	139 (120 – 282)	158 (112 – 197)	109 (24 – 188)	0.368
	Mid-anterolateral	105 (92 – 121)	112 (83 – 196)	136 (73 – 190)	219 (48 – 335)	0.588
	Apical anterior	67 (18 – 125)	141 (76 – 170)	184 (87 – 224)	248 (102 – 306)	0.160
	Apical septal	107 (106 – 127)	120 (83 – 154)	170 (113 – 233)	180 (110 – 260)	0.222
	Apical Inferior	63 (11 – 109)	151 (97 – 229)	63 (61 – 141)	155 (106 – 199)	0.035
	Apical lateral	66 (34 – 94)	160 (102 – 202)	159 (121 – 221)	63 (23 – 163)	0.097
Epicardial/RV	Basal anterior	110 (106 – 168)	158 (109 – 236)	189 (143 – 208)	215 (161 – 281)	0.041
endocardial	RV Basal anteroseptal	112 (105 – 150)	162 (99 – 233)	152 (91 – 201)	259 (176 – 311)	0.109
	RV Basal inferoseptal	105 (71 – 122)	135 (90 – 229)	202 (106 – 243)	172 (117 – 319)	0.116
	Basal inferior	106 (90 – 131)	179 (146 – 323)	202 (112 – 223)	207 (130 – 311)	0.019
	Basal inferolateral	107 (98 – 121)	151 (131 – 185)	198 (118 – 210)	185 (167 – 290)	0.004
	Basal anterolateral	120 (101 – 147)	145 (135 – 161)	166 (153 – 200)	172 (140 – 268)	0.025
	Mid-anterior	150 (128 – 163)	170 (128 – 235)	195 (166 – 234)	201 (168 – 338)	0.060
	RV Mid-anteroseptal	106 (49 – 134)	180 (119 – 225)	150 (112 – 191)	165 (102 – 280)	0.187
	RV Mid-inferoseptal	90 (69 – 123)	153 (89 – 182)	136 (92 – 167)	89 (59 – 208)	0.338
	Mid-inferior	132 (88 – 155)	178 (116 – 260)	182 (173 – 197)	217 (151 – 277)	0.040
	Mid-inferolateral	79 (75 – 134)	129 (118 – 255)	190 (132 – 228)	180 (150 – 320)	0.024
	Mid-anterolateral	138 (125 – 153)	145 (99 – 144)	167 (117 – 203)	217 (156 – 248)	0.260
	Apical anterior	158 (109 – 182)	163 (124 – 275)	180 (119 – 226)	220 (175 – 244)	0.185
	RV Apical septal	129 (95 – 149)	182 (128 – 261)	194 (161 – 219)	175 (124 – 272)	0.070
	Apical Inferior	127 (106 – 143)	150 (128 – 179)	135 (105 – 198)	222 (152 – 261)	0.047
	Apical lateral	115 (107 – 129)	126 (105 – 207)	146 (106 – 164)	182 (156 – 341)	0.229
	Apex	118 (100 – 129)	166 (123 – 274)	206 (130 – 229)	260 (163 – 315)	0.019

DISCUSSION

Our study revealed the features of the EP substrate in HCM, which differentiate the HCM substrate from the ICM substrate in patients with VT history and post-MI scar located in the same areas (anterior and anteroseptal segments). HCM is characterized by a greater degree of activation dispersion in basal segments, an apex-base gradient in activation dispersion, a larger voltage and a greater voltage dispersion. Dispersion of ventricular activation contributes to the dispersion of total recovery time and facilitates the development and maintenance of reentrant VT (Vassallo et al., 1988). Dispersion of ventricular activation is a well-known mechanism of reentrant VT (Vassallo et al., 1988), which can explain substantial risk of VT and sudden cardiac death in HCM.

EP Substrate and Mechanisms of Arrhythmogenesis in HCM

HCM is the most common monogenic cardiac disease (Semsarian et al., 2015). Diagnosis of HCM is challenging, although some preliminary machine learning studies are promising (Rahman et al., 2015; Green et al., 2019). Prior cellular studies demonstrated that enhanced late sodium current is an important mechanism of arrhythmogenesis in HCM (Coppini et al., 2013). Enhanced late sodium current in HCM cardiomyocytes manifested by action potential prolongation and increased frequency of early depolarizations and delayed afterdepolarizations, suggesting triggered mechanism of VT, similar to that in long QT syndromes. However, the RESTYLE-HCM randomized controlled trial (Olivotto et al., 2018) did not demonstrate a benefit of the late sodium channel blocker ranolazine in symptomatic patients with non-obstructive HCM.

The results of our study suggest explanation to ineffectiveness of pharmacological late sodium current blockade in HCM. In 1988, Vassallo et al. (1988) showed differences between post-infarction scar-related reentrant VT and triggered VT in long QT syndrome. Patients with post-infarction scar and reentrant VT mechanism manifested dispersion of endocardial activation, rather than dispersion of refractoriness. In contrast, patients with long QT syndrome and triggered VT mechanism manifested dispersion of refractoriness, rather than dispersion of activation. The results of our study demonstrated dispersion of activation in HCM patients, supporting the presence of EP substrate of reentrant VT, resembling VT mechanism in post-infarction patients. HCM is characterized by a disorganized sarcomeric alignment, which can augment non-uniform anisotropic conduction, creating a substrate for reentry (both slow conduction and unidirectional block) (Spach and Josephson, 1994). Disorganized bundles of ventricular fibers can lead to asymmetry in conduction. An impulse conducting in one direction meets a different sequence of muscle branching and changes in muscle bundle diameter, as compared to an impulse conducting in the opposite direction. Such asymmetry affects the source-sink relationships (Spach et al., 1981).

We showed a greater degree of voltage dispersion in HCM as compared to post-MI patients in both endocardial and the epicardial segments in basal anterior, basal anterolateral and inferolateral, apical inferior, and the epicardial surface of the apex. This finding may be explained by an underlying phenomenon of diffused interstitial fibrosis in HCM, generating

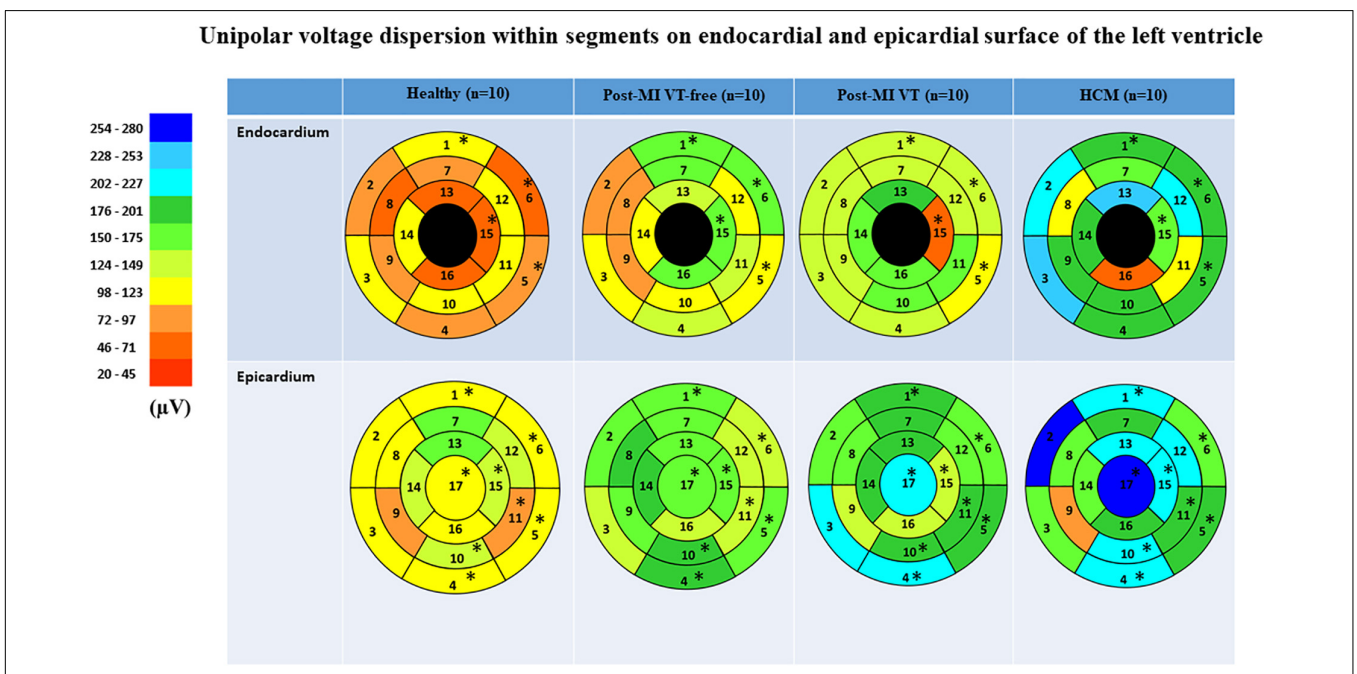

FIGURE 5 | Comparison of unipolar voltage dispersion in study groups, in 16 LV endocardial and 17 LV epicardial segments. Segment nomenclature is described in the **Figure 4** legend. Statistically significant differences are marked with a star.

greater voltage dispersion as compared to patchy post-MI fibrosis. Further MRI studies (Kramer et al., 2015) utilizing late gadolinium enhancement and T1-mapping are needed to evaluate the agreement between voltage dispersion on ECGi voltage maps and imaging-defined type of fibrosis, and their associations with clinical outcomes in HCM patients.

Very few previous studies reported results of electroanatomical mapping in HCM. Reported findings included local conduction delay or conduction block, fractionated electrograms, and reduced voltage (Schumacher et al., 2005). Scattered intramural fibrosis in HCM did not manifest by the low voltage on endocardial, nor epicardial unipolar maps. However, Schumacher et al. (2005) reported reduced bipolar voltage in the septal region in HCM patients. In this study, we observed significantly larger unipolar voltage in HCM as compared to healthy persons or ICM patients, and the difference was especially prominent in HCM-affected regions of the heart: both endocardial and epicardial basal and apical septal segments. The different methodology of voltage mapping (unipolar vs. bipolar) may explain the observed differences between our results and previous contact mapping studies. A previous HCM case report (Ghosh et al., 2008) describing ECGi findings did not provide results of the voltage map from their HCM patient. Consistent with our findings, Yoshida et al. (1986) in 1986 conducted body surface isopotential mapping and showed that HCM patients have significantly larger peak-to-peak voltage than patients with LVH due to essential hypertension.

Non-invasive Mapping of Ventricular Activation

In this study, we used the Forward/Inverse problem toolkit from the SCIRun problem-solving environment, which is used by many investigators in the field (Burton et al., 2011; Coll-Font et al., 2014; Cluitmans et al., 2018; Wang et al., 2018). However, knowing the limitations of the ECGi method (Duchateau et al., 2019), we intentionally limited our analysis by averaged "per segment" data. Duchateau et al. (2019) observed a mean

TABLE 4 | Local activationdispersion in msec (median, interquartile range) on left ventricular endocardial and epicardial surface.

	Region	Healthy (n = 10)	Post-MI VT-free (n = 10)	Post-MI VT (n = 10)	HCM (n = 10)	$P_{Kruskal-Wallis}$
Endocardial	Basal anterior	8.9 (6.9 – 10.9)	9.8 (5.9 – 13.5)	9.5 (5.7 – 16.0)	16.0 (10.7 – 17.2)	0.084
surface	Basal anteroseptal	5.8 (5.2 – 12.0)	10.6 (8.7 – 13.3)	12.6 (11.2 – 15.7)	13.3 (5.2 – 21.1)	0.473
	Basal inferoseptal	7.7 (5.2 – 9.5)	11.8 (9.7 – 17.9)	12.5 (7.7 – 16.2)	15.8 (10.0 – 18.8)	0.053
	Basal inferior	6.4 (4.2 – 9.1)	9.8 (5.9 – 13.4)	12.7 (3.8 – 16.0)	14.6 (11.5 – 15.3)	0.082
	Basal inferolateral	6.9 (6.3 – 11.8)	7.0 (3.2 – 16.0)	12.0 (7.2 – 14.9)	16.5 (14.3 – 20.1)	0.014
	Basal anterolateral	7.0 (6.4 – 9.6)	10.2 (9.0 – 12.3)	10.5 (7.5 – 16.1)	17.3 (12.1 – 22.2)	0.009
	Mid-anterior	8.1 (6.1 – 9.2)	11.0 (5.5 – 16.8)	10.2 (6.1 – 14.9)	11.1 (8.6 – 13.0)	0.402
	Mid-anteroseptal	7.5 (2.7 – 8.8)	8.4 (5.4 – 11.8)	11.6 (6.6 – 14.6)	10.1 (5.7 – 14.7)	0.248
	Mid-inferoseptal	8.9 (5.8 – 13.4)	6.5 (4.8 – 12.3)	9.3 (4.0 – 10.8)	11.0 (6.9 – 11.8)	0.854
	Mid-inferior	11.1 (2.9 – 13.4)	8.9 (5.8 – 12.9)	8.6 (3.4 – 12.2)	9.2 (3.8 – 12.3)	0.924
	Mid-inferolateral	5.5 (4.5 – 9.3)	11.2 (8.6 – 14.1)	6.3 (3.9 – 8.9)	8.5 (1.9 – 13.4)	0.252
	Mid-anterolateral	6.6 (5.3 – 9.2)	7.7 (5.5 – 9.3)	9.7 (3.8 – 16.1)	9.6 (4.8 – 14.0)	0.676
	Apical anterior	4.2 (0.7 – 14.8)	9.0 (5.6 – 11.2)	9.3 (7.6 – 13.4)	9.3 (6.5 – 10.1)	0.507
	Apical septal	5.3 (2.7 – 17.6)	7.8 (5.8 – 14.1)	7.8 (6.2 – 11.3)	10.5 (9.1 – 14.1)	0.727
	Apical Inferior	6.2 (2.1 – 8.4)	11.1 (9.6 – 14.1)	6.9 (2.9 – 14.2)	7.4 (1.2 – 10.1)	0.062
	Apical lateral	7.0 (1.4 – 13.6)	8.8 (1.9 – 12.7)	10.1 (3.4 – 18.2)	4.5 (1.3 – 9.9)	0.454
Epicardial	Basal anterior	8.3 (7.7 – 9.8)	12.8 (11.4 – 15.9)	13.2 (11.9 – 15.1)	13.5 (12.4 – 22.3)	0.0007
	RV Basal anteroseptal	8.1 (7.0 – 11.3)	11.1 (9.3 – 12.8)	14.1 (8.9 – 15.4)	17.7 (14.4 – 22.0)	0.012
	RV Basal inferoseptal	9.8 (7.4 – 12.9)	15.7 (8.3 – 16.5)	10.3 (9.6 – 15.7)	12.7 (9.7 – 18.3)	0.676
	Basal inferior	8.5 (7.7 – 9.9)	12.6 (11.7 – 17.5)	12.5 (11.5 – 14.1)	16.3 (11.4 – 17.5)	0.0008
	Basal inferolateral	11.1 (7.7 – 11.9)	12.6 (10.8 – 13.9)	14.2 (12.2 – 16.6)	17.1 (14.7 – 20.2)	0.006
	Basal anterolateral	9.9 (9.2 – 11.7)	10.7 (9.1 – 14.9)	13.8 (11.1 – 16.0)	17.5 (16.0 – 24.4)	0.002
	Mid-anterior	8.9 (8.3 – 11.0)	10.7 (7.9 – 15.3)	10.2 (8.0 – 12.0)	12.4 (10.1 – 14.2)	0.364
	RV Mid-anteroseptal	8.9 (6.3 – 10.4)	9.1 (7.1 – 12.5)	11.8 (7.3 – 14.6)	11.6 (6.9 – 15.5)	0.720
	RV Mid-inferoseptal	9.4 (3.3 – 11.9)	6.4 (4.7 – 10.9)	9.4 (5.9 – 12.0)	2.7 (0.5 – 8.2)	0.676
	Mid-inferior	9.8 (9.3 – 11.1)	9.3 (7.8 – 11.5)	9.8 (7.9 – 14.8)	9.9 (6.9 – 13.6)	0.977
	Mid-inferolateral	10.5 (7.7 – 11.8)	9.1 (7.3 – 13.8)	11.4 (7.1 – 12.2)	13.6 (8.3 – 16.3)	0.558
	Mid-anterolateral	9.3 (7.3 – 10.6)	9.5 (6.6 – 12.1)	8.4 (7.0 – 13.9)	11.3 (10.3 – 12.8)	0.429
	Apical anterior	8.9 (8.0 – 10.9)	7.9 (7.5 – 9.4)	11.4 (7.9 – 12.4)	9.6 (8.8 – 13.6)	0.257
	RV Apical septal	6.4 (5.3 – 8.5)	7.6 (6.0 – 10.0)	9.4 (6.8 – 13.8)	11.6 (8.9 – 12.2)	0.060
	Apical Inferior	9.9 (8.1 – 10.9)	8.5 (6.4 – 10.7)	10.1 (8.5 – 12.9)	10.0 (9.0 – 14.3)	0.443
	Apical lateral	8.3 (5.4 – 9.6)	8.2 (6.1 – 9.6)	9.0 (7.9 – 10.9)	9.4 (7.1 – 12.1)	0.730
	Apex	8.0 (7.4 – 10.3)	7.3 (7.0 – 8.7)	9.2 (7.1 – 10.0)	11.0 (9.9 – 12.8)	0.051

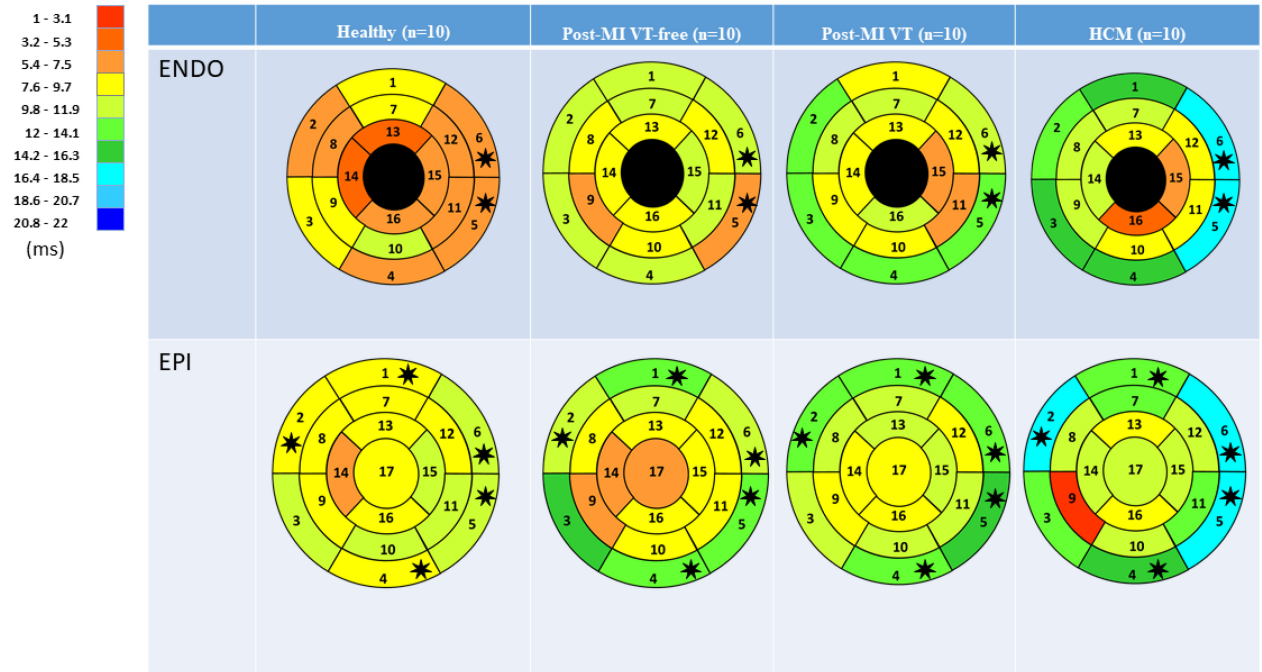

FIGURE 6 | Comparison of ventricular activation dispersion in study participants, in 16 LV endocardial and 17 LV epicardial segments. Segment nomenclature is described in the **Figure 4** legend. Statistically significant differences are marked with a star.

activation time error of ∼20 ms. Nevertheless, in this study, we observed statistically significant differences in ventricular activation dispersion. In the base of LV, dispersion of activation was approximately twice larger in HCM patients, as compared to healthy controls. In spite of limitations, our findings of a higher voltage dispersion through entire LV and an apex-base gradient in increased activation dispersion in HCM provided meaningful insight into mechanisms of arrhythmogenesis in HCM. Further development of ECGi method is needed.

Limitations

A case-control study is susceptible to bias. We selected only high-risk HCM patients, and our HCM case sample may not be representative of all HCM patients. To minimize selection bias, all groups were enrolled in the same single center. Further development of inverse solution non-invasive activation mapping method is needed to enable interpretation of local ventricular activation patterns. The study size was small. Validation of the study findings in larger studies is needed. Because of the high-risk study population, we did not design the discontinuation of medications during the study. It is known that the use of antiarrhythmic medications may affect ventricular conduction and results of the body surface mapping. Nevertheless, our study allowed group comparison of contemporary patient population on guideline-recommended medical therapy. Genetic testing was not performed for all study participants. As the prevalence of HCM gene carriers in the general population was estimated at 0.5% (Semsarian et al., 2015), a low chance exists that group I-III participants carry HCM gene. However, only 10% of group II participants, and no control participants had LVH, which supports the study validity.

DATA AVAILABILITY STATEMENT

The datasets generated for this study are available on request to the corresponding author.

ETHICS STATEMENT

The studies involving human participants were reviewed and approved by Oregon Health & Science University Institutional Review Board. The patients/participants provided their written informed consent to participate in this study.

AUTHOR CONTRIBUTIONS

EP-A run inverse solutions computations and built activation and voltage maps. KH computed mean (SD) LAT and voltage per segment, and prepared figures. DG, CF, and MF helped to design the study and analyzed imaging data. CH, JT, EP-A, and LT collected the study data. KJ, FP, NR, KY, and AW analyzed the ECG and EGM data. KD and SH helped to design the study and facilitated enrollment. LT designed the study, handled the

study funding, directed the study implementation, including quality assurance and control, conducted statistical analyses, and critically revised the manuscript. All authors drafted the study, revised the manuscript, approved the submitted version, and have agreed both to be personally accountable for the author's own contributions and the accuracy and integrity of any part of the work.

FUNDING

The authors declare that this study received funding from Gilead Sciences, Inc. as a physician-initiated study (LT). The funder was not involved in the study design, collection, analysis, interpretation of data, the writing of this article or the decision to submit it for publication. This work was partially supported by 1R01HL118277 and 2R56HL118277 (LT).

ACKNOWLEDGMENTS

We thank the study participants and staff. We thank William Woodward, ARMRIT, for the help with the CMR data acquisition.

SUPPLEMENTARY MATERIAL

The Supplementary Material for this article can be found online at: https://www.frontiersin.org/articles/10.3389/fphys.2020.00344/full#supplementary-material

SUPPLEMENTARY MOVIE 1 | Representative example of unipolar voltage map in a healthy participant, during sinus rhythm activation.

SUPPLEMENTARY MOVIE 2 | Representative example of activation map in a healthy participant, during sinus rhythm activation.

REFERENCES

Alday, E. A., Colman, M. A., Langley, P., Butters, T. D., Higham, J., Workman, A. J., et al. (2015). A new algorithm to diagnose atrial ectopic origin from multi lead ECG systems–insights from 3D virtual human atria and torso. *PLoS Comput. Biol.* 11:e1004026. doi: 10.1371/journal.pcbi.1004026

Babaeizadeh, S., Brooks, D. H., Isaacson, D., and Newell, J. C. (2006). Electrode boundary conditions and experimental validation for BEM-based EIT forward and inverse solutions. *IEEE Trans. Med. Imaging* 25, 1180–1188. doi: 10.1109/tmi.2006.879957

Burton, B. M., Tate, J. D., Erem, B., Swenson, D. J., Wang, D. F., Steffen, M., et al. (2011). A toolkit for forward/inverse problems in electrocardiography within the SCIRun problem solving environment. *Conf. Proc. IEEE Eng. Med. Biol. Soc.* 2011, 267–270. doi: 10.1109/IEMBS.2011.6090052

Cerqueira, M. D., Weissman, N. J., Dilsizian, V., Jacobs, A. K., Kaul, S., Laskey, W. K., et al. (2002). Standardized myocardial segmentation and nomenclature for tomographic imaging of the heart: a statement for healthcare professional from the cardiac imaging committee of the council on clinical cardiology of the american heart association. *Circulation* 105, 539–542. doi: 10.1161/hc0402.102975

Cluitmans, M., Brooks, D. H., MacLeod, R., Dossel, O., Guillem, M. S., van Dam, P. M., et al. (2018). Validation and opportunities of electrocardiographic imaging: from technical achievements to clinical applications. *Front. Physiol.* 9:1305. doi: 10.3389/fphys.2018.01305

Coll-Font, J., Burton, B. M., Tate, J. D., Erem, B., Swenson, D. J., Wang, D., et al. (2014). New additions to the toolkit for forward/inverse problems in electrocardiography within the scirun problem solving environment. *Comput. Cardiol.* 2014, 213–216.

Coppini, R., Ferrantini, C., Yao, L., Fan, P., Del Lungo, M., Stillitano, F., et al. (2013). Late sodium current inhibition reverses electromechanical dysfunction in human hypertrophic cardiomyopathy. *Circulation* 127, 575–584. doi: 10.1161/CIRCULATIONAHA.112.134932

Duchateau, J., Sacher, F., Pambrun, T., Derval, N., Chamorro-Servent, J., Denis, A., et al. (2019). Performance and limitations of noninvasive cardiac activation mapping. *Heart Rhythm* 16, 435–442. doi: 10.1016/j.hrthm.2018.10.010

Ghosh, S., Avari, J. N., Rhee, E. K., Woodard, P. K., and Rudy, Y. (2008). Hypertrophic cardiomyopathy with preexcitation: insights from noninvasive electrocardiographic imaging (ECGI) and catheter mapping. *J. Cardiovasc. Electrophysiol.* 19, 1215–1217. doi: 10.1111/j.1540-8167.2008.01203.x

Green, E. M., van Mourik, R., Wolfus, C., Heitner, S. B., Dur, O., and Semigran, M. J. (2019). Machine learning detection of obstructive hypertrophic cardiomyopathy using a wearable biosensor. *Dig. Med.* 2:57. doi: 10.1038/s41746-019-0130-0

Iles, L., Pfluger, H., Phrommintikul, A., Cherayath, J., Aksit, P., Gupta, S. N., et al. (2008). Evaluation of diffuse myocardial fibrosis in heart failure with cardiac magnetic resonance contrast-enhanced T1 mapping. *J. Am. Coll. Cardiol.* 52, 1574–1580. doi: 10.1016/j.jacc.2008.06.049

James, G. (1954). Tests of linear hypotheses in univariate and multivariate analysis when the ratios of the population variances are unknown. *Biometrika* 41, 19–43. doi: 10.1093/biomet/41.1-2.19

Juneau, D., Erthal, F., Clarkin, O., Alzahrani, A., Alenazy, A., Hossain, A., et al. (2017). Mid-diastolic left ventricular volume and mass: normal values for coronary computed tomography angiography. *J. Cardiovasc. Comput. Tomogr.* 11, 135–140. doi: 10.1016/j.jcct.2017.01.011

Kramer, C. M., Appelbaum, E., Desai, M. Y., Desvigne-Nickens, P., DiMarco, J. P., Friedrich, M. G., et al. (2015). Hypertrophic cardiomyopathy registry: the rationale and design of an international, observational study of hypertrophic cardiomyopathy. *Am. Heart. J.* 170, 223–230. doi: 10.1016/j.ahj.2015.05.013

Maron, M. S., Rowin, E. J., Wessler, B. S., Mooney, P. J., Fatima, A., Patel, P., et al. (2019). Enhanced american college of cardiology/american heart association strategy for prevention of sudden cardiac death in high-risk patients with hypertrophic cardiomyopathy. *JAMA Cardiol.* 4, 644–657. doi: 10.1001/jamacardio.2019.1391

Mentias, A., Raeisi-Giglou, P., Smedira, N. G., Feng, K., Sato, K., Wazni, O., et al. (2018). Late gadolinium enhancement in patients with hypertrophic cardiomyopathy and preserved systolic function. *J. Am. Coll. Cardiol.* 72, 857–870. doi: 10.1016/j.jacc.2018.05.060

Olivotto, I., Camici, P. G., Merlini, P. A., Rapezzi, C., Patten, M., Climent, V., et al. (2018). Efficacy of ranolazine in patients with symptomatic hypertrophic cardiomyopathy. *Circulation* 11:e004124. doi: 10.1161/CIRCHEARTFAILURE.117.004124

O'Mahony, C., Jichi, F., Pavlou, M., Monserrat, L., Anastasakis, A., Rapezzi, C., et al. (2014). A novel clinical risk prediction model for sudden cardiac death in hypertrophic cardiomyopathy (HCM risk-SCD). *Eur. Heart J.* 35, 2010–2020. doi: 10.1093/eurheartj/eht439

Panel, N. E. (2002). Third Report of the National Cholesterol Education Program (NCEP) expert panel on detection, evaluation, and treatment of high blood cholesterol in adults (Adult Treatment Panel III). Final report. *Circulation* 106:278.

Perez-Alday, E. A., Thomas, J. A., Kabir, M., Sedaghat, G., Rogovoy, N., van Dam, E., et al. (2018). Torso geometry reconstruction and body surface electrode localization using three-dimensional photography. *J. Electrocardiol.* 51, 60–67. doi: 10.1016/j.jelectrocard.2017.08.035

Rahman, Q. A., Tereshchenko, L. G., Kongkatong, M., Abraham, T., Abraham, M. R., and Shatkay, H. (2015). Utilizing ECG-Based Heartbeat Classification for Hypertrophic Cardiomyopathy Identification. *IEEE Trans. Nanobiosci.* 14, 505–512. doi: 10.1109/TNB.2015.2426213

Ramanathan, C., Ghanem, R. N., Jia, P., Ryu, K., and Rudy, Y. (2004). Noninvasive electrocardiographic imaging for cardiac electrophysiology and arrhythmia. *Nat. Med.* 10, 422–428. doi: 10.1038/nm1011

Schumacher, B., Gietzen, F. H., Neuser, H., Schummelfeder, J., Schneider, M., Kerber, S., et al. (2005). Electrophysiological characteristics of septal hypertrophy in patients with hypertrophic obstructive cardiomyopathy and moderate to severe symptoms. *Circulation* 112, 2096–2101. doi: 10.1161/CIRCULATIONAHA.104.515643

Semsarian, C., Ingles, J., Maron, M. S., and Maron, B. J. (2015). New perspectives on the prevalence of hypertrophic cardiomyopathy. *J. Am. Coll. Cardiol.* 65, 1249–1254. doi: 10.1016/j.jacc.2015.01.019

Spach, M. S., and Josephson, M. E. (1994). Initiating reentry: the role of nonuniform anisotropy in small circuits. *J. Cardiovasc. Electrophysiol.* 5, 182–209. doi: 10.1111/j.1540-8167.1994.tb01157.x

Spach, M. S., Miller, W. T. III, Geselowitz, D. B., Barr, R. C., Kootsey, J. M., and Johnson, E. A. (1981). The discontinuous nature of propagation in normal canine cardiac muscle. Evidence for recurrent discontinuities of intracellular resistance that affect the membrane currents. *Circ. Res.* 48, 39–54. doi: 10.1161/01.res.48.1.39

Vaseghi, M., Hu, T. Y., Tung, R., Vergara, P., Frankel, D. S., Di Biase, L., et al. (2018). Outcomes of catheter ablation of ventricular tachycardia based on etiology in nonischemic heart disease: an international ventricular tachycardia ablation center collaborative study. *JACC* 4, 1141–1150. doi: 10.1016/j.jacep.2018.05.007

Vassallo, J. A., Cassidy, D. M., Kindwall, K. E., Marchlinski, F. E., and Josephson, M. E. (1988). Nonuniform recovery of excitability in the left ventricle. *Circulation* 78, 1365–1372. doi: 10.1161/01.cir.78.6.1365

Wang, L., Gharbia, O. A., Nazarian, S., Horacek, B. M., and Sapp, J. L. (2018). Non-invasive epicardial and endocardial electrocardiographic imaging for scar-related ventricular tachycardia. *Europace* 20, f263–f272. doi: 10.1093/europace/euy082

Yoshida, H., Imataki, K., Nagahana, H., Ihoriya, F., Nakao, Y., Saito, D., et al. (1986). Cardiac hypertrophy in hypertrophic cardiomyopathy and hypertension evaluated by echocardiography and body surface isopotential mapping. *J. Cardiogr.* 16, 399–406.

Yushkevich, P. A., Piven, J., Hazlett, H. C., Smith, R. G., Ho, S., Gee, J. C., et al. (2006). User-guided 3D active contour segmentation of anatomical structures: significantly improved efficiency and reliability. *Neuroimage* 31, 1116–1128. doi: 10.1016/j.neuroimage.2006.01.015

Conflict of Interest: The authors declare that the research was conducted in the absence of any commercial or financial relationships that could be construed as a potential conflict of interest.

frontiers in Physiology

ORIGINAL RESEARCH
published: 13 August 2020
doi: 10.3389/fphys.2020.00933

Body Surface Mapping of Ventricular Repolarization Heterogeneity: An *Ex-vivo* Multiparameter Study

Marianna Meo[1,2,3], Pietro Bonizzi[4], Laura R. Bear[1,2,3], Matthijs Cluitmans[5], Emma Abell[1,2,3], Michel Haïssaguerre[1,2,3,6], Olivier Bernus[1,2,3] and Rémi Dubois[1,2,3]*

[1] Institute of Electrophysiology and Heart Modeling (IHU Liryc), Foundation Bordeaux University, Pessac-Bordeaux, France, [2] University of Bordeaux, CRCTB, Bordeaux, France, [3] INSERM, CRCTB, U1045, Bordeaux, France, [4] Department of Data Science and Knowledge Engineering, Maastricht University, Maastricht, Netherlands, [5] Department of Cardiology, Cardiovascular Research Institute Maastricht, Maastricht University Medical Center, Maastricht, Netherlands, [6] Bordeaux University Hospital (CHU), Electrophysiology and Ablation Unit, Pessac, France

Background: Increased heterogeneity of ventricular repolarization is associated with life-threatening arrhythmia and sudden cardiac death (SCD). T-wave analysis through body surface potential mapping (BSPM) is a promising tool for risk stratification, but the clinical effectiveness of current electrocardiographic indices is still unclear, with limited experimental validation. This study aims to investigate performance of non-invasive state-of-the-art and novel T-wave markers for repolarization dispersion in an *ex vivo* model.

Methods: Langendorff-perfused pig hearts ($N = 7$) were suspended in a human-shaped 256-electrode torso tank. Tank potentials were recorded during sinus rhythm before and after introducing repolarization inhomogeneities through local perfusion with dofetilide and/or pinacidil. Drug-induced repolarization gradients were investigated from BSPMs at different experiment phases. Dispersion of electrical recovery was quantified by duration parameters, i.e., the time interval between the peak and the offset of T-wave (T_{PEAK}-T_{END}) and QT interval, and variability over time and electrodes was also assessed. The degree of T-wave symmetry to the peak was quantified by the ratio between the terminal and initial portions of T-wave area (*Asy*). Morphological variability between left and right BSPM electrodes was measured by dynamic time warping (DTW). Finally, T-wave organization was assessed by the complexity of repolarization index (CR), i.e., the amount of energy non-preserved by the dominant eigenvector computed by principal component analysis (PCA), and the error between each multilead T-wave and its 3D PCA approximation (NMSE). Body surface indices were compared with global measures of epicardial dispersion of repolarization, and with local gradients between adjacent ventricular sites.

Results: After drug intervention, both regional and global repolarization heterogeneity were significantly enhanced. On the body surface, T_{PEAK}-T_{END} was significantly prolonged and less stable in time in all experiments, while QT interval showed higher variability across the interventions in terms of duration and spatial dispersion. The rising slope of the repolarization profile was steeper, and T-waves were more asymmetric

OPEN ACCESS

Edited by:
Marek Malik, Imperial College London, United Kingdom

Reviewed by:
Pablo Laguna, University of Zaragoza, Spain
Gary Tse, Second Hospital of Tianjin Medical University, China

***Correspondence:**
Marianna Meo
marianna.meo@ihu-liryc.fr;
mariannameo@gmail.com

Specialty section:
This article was submitted to Cardiac Electrophysiology, a section of the journal Frontiers in Physiology

Received: *28 May 2020*
Accepted: *10 July 2020*
Published: *13 August 2020*

Citation:
Meo M, Bonizzi P, Bear LR, Cluitmans M, Abell E, Haïssaguerre M, Bernus O and Dubois R (2020) Body Surface Mapping of Ventricular Repolarization Heterogeneity: An Ex-vivo Multiparameter Study. Front. Physiol. 11:933. doi: 10.3389/fphys.2020.00933

than at baseline. Interventricular shape dissimilarity was enhanced by repolarization gradients according to DTW. Organized T-wave patterns were associated with abnormal repolarization, and they were properly described by the first principal components.

Conclusion: Repolarization heterogeneity significantly affects T-wave properties, and can be non-invasively captured by BSPM-based metrics.

Keywords: sudden cardiac death, ventricular repolarization heterogeneity, body surface potential mapping, T-wave, electrocardiology

INTRODUCTION

Abnormal heterogeneity of ventricular repolarization predisposes to the development of life−threatening ventricular arrhythmias and it is associated with increased mortality in the general population (Antzelevitch, 2007; Prenner et al., 2016).

Global ventricular repolarization dispersion is mainly determined by the heterogeneity of action potential durations (APDs) between different myocardial regions, which can be apical-basal (from apex to base of ventricles), transmural (from endocardium to epicardium) and/or interventricular (left vs. right ventricle), and thus affects T-wave properties from surface electrocardiogram (ECG) (Merri et al., 1989; Vinzio Maggio et al., 2012). Classically, global dispersion of repolarization has been defined as the difference between longest and shortest repolarization time (RT) within a set of measurements at multiple sites without regard to their location (Burton and Cobbe, 2001). On the other hand, regional dispersion of repolarization strongly affects T-wave profile as well, therefore measures of local inhomogeneity have also been introduced to take into account spatial distribution of RTs and their variations across adjacent tissue sites. Patients with long QT syndrome display regions with steep repolarization dispersion caused by localized prolongation of APD and genotype-specific alterations in T- wave morphology (Vijayakumar et al., 2014). In Brugada syndrome, sharp local gradients of repolarization and slow conduction areas can both contribute to increased susceptibility to sustained reentrant excitation and are accompanied by T-wave inversion on the body surface (Zhang et al., 2015).

Both abnormal global and local dispersion of repolarization significantly affect T-wave characteristics. Nevertheless, it is still unclear if T-wave properties are more influenced by one of these two conditions, or if both equally contribute to the electrocardiographic alterations of ventricular recovery. Accordingly, the performance of state-of-the-art ECG markers of T-wave has been questioned in clinics, due to their inability to identify vulnerable substrates and reliably distinguish between healthy and diseased subjects (Malik et al., 2000; Van Huysduynen et al., 2005; Smetana et al., 2011; Marill et al., 2018). Since each ECG electrode summarizes the integrated electrical activity over the entire heart, spatial properties of the cardiac generator are lost, and it was shown that features derived from such a low number of electrodes are unlikely to reflect regional changes in myocardial repolarization (Burnes et al., 2001).

To compensate this intrinsic limitation of ECG, high-density body surface mapping (BSPM) has emerged as a promising tool for the diagnosis of T-wave alterations and risk stratification for sudden cardiac death (SCD) (Taccardi et al., 2007; Korhonen et al., 2009). Several studies have confirmed the ability of this technique to capture non-dipolarities of cardiac electrical activity, and on top of that ECG imaging could localize sites of abnormal recovery (Peeters et al., 1998; Burnes et al., 2001; Vijayakumar et al., 2014; Zhang et al., 2015).

Despite these advances, it is still unclear how regional and global repolarization disparities reflect on body surface, and to which extent they can be inferred from BSPMs, as pre-clinical validation is limited and different invasive metrics are used for validation (Fuller et al., 2000; Burnes et al., 2001).

Our study takes a step further from this background and aims to assess the ability of several state-of-the-art and novel BSPM metrics to describe abnormal dispersion of repolarization in an *ex vivo* torso tank model, for which information about actual heterogeneity of repolarization at the heart level is available, and can be used for validation of body-surface indices.

MATERIALS AND METHODS

Experimental Setup and Database

The experimental protocol was approved by Directive 2010/63/EU of the European Parliament on the protection of animals used for scientific purposes and the local ethical committee. Hearts were excised from pigs (N = 7, 30–40 kg) and perfused in Langendorff setup as previously reported (Bear et al., 2019a,c). The left anterior descending (LAD) artery was cannulated on a separate perfusion. A 108-electrode sock was attached to the free wall epicardial surfaces of the ventricles. After instrumentation, the heart was suspended in a human-shaped 256-electrode torso tank filled with a Tyrode's solution. In 3 hearts, pinacidil (Pin) was injected in increasing concentrations (full dose: 30 μM) into the LAD to locally shorten APD and induce gradients in repolarization with other myocardial regions (Pin Group). In the other 4 hearts, Pin administration with comparable doses was preceded by progressive perfusion of non-LAD coronaries with dofetilide (Dof, full dose: 250 nM) to further enhance regional repolarization heterogeneities

Abbreviations: APD, action potential duration; BA, Bland-Altman; BSPM, body surface potential map; CR, complexity of repolarization; Dof, dofetilide; DTW, dynamic time warping; ECG, electrocardiogram; EGM, electrogram; FIR, finite impulse response; LAD, left anterior descending; LoA, limit of agreement; LV, left ventricle; NMSE, normalized mean square error; Pin, pinacidil; PCA, principal component analysis; RT, repolarization time; RTG, repolarization time gradient; RV, right ventricle; SCD, sudden cardiac death.

(early repolarization in the Pin-area, late in the Dof-area). This second set was referred to as Dof & Pin Group. Only experiments presenting all mentioned phases were assigned to one of these categories, therefore other phases which were not common to all experiments (e.g., drug washout) were not included into our analysis. When more recordings were available at baseline, the first recording was included into our analysis. During drug perfusion, the last recording was generally preferred, in order to have enough time for the drug to make effect.

Signal Preprocessing and Fiducial Point Detection

BSPMs and sock electrograms (EGMs) were simultaneously recorded (BioSemi, Netherlands) at a sampling rate of 2048 Hz during sinus rhythm before and after each drug intervention over $N_b = 10$ beats.

At each beat i, $i = 1, \ldots, N_b$, T-waves from all electrodes were arranged as a $L \times N$ matrix $\boldsymbol{Y}^{(i)} = \left[\boldsymbol{y}(1) \ldots \boldsymbol{y}(N)\right] \in \Re^{L \times N}$, with $L = 256$ equal to the number of tank electrodes, and N to the number of time samples. Since electrodes presenting signals with too high levels of noise and/or low voltage on visual inspection have not been included into our analysis, in some cases we may have $L < 256$. A representative single-lead beat with its characteristic deflections from an experiment from Dof & Pin Group is shown at each drug state in **Figure 1**.

High frequency noise was removed from BSPMs by a low-pass least-squares linear-phase finite impulse response (FIR) filter with cutoff frequency at 40 Hz. Power line interference was suppressed by a discrete Fourier transform-based notch filter. Prior to morphology analysis in section 2.3.3 and 2.3.4, a third-order Savitzky-Golay FIR filter with 50 ms frame length was applied to remove residual noise interferences and further smoothen T-wave profile.

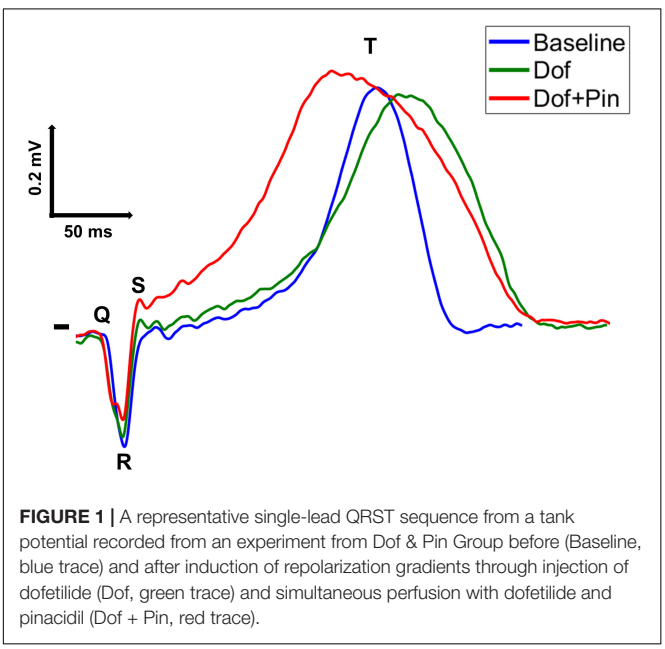

FIGURE 1 | A representative single-lead QRST sequence from a tank potential recorded from an experiment from Dof & Pin Group before (Baseline, blue trace) and after induction of repolarization gradients through injection of dofetilide (Dof, green trace) and simultaneous perfusion with dofetilide and pinacidil (Dof + Pin, red trace).

R-wave peak time occurrences were identified from tank potentials as signal local maxima above a preset threshold equal to the half of the signal maximum amplitude value, and at a minimum time distance of 330 ms, using the MATLAB function *findpeaks*. QRS complex onset and offset were detected using a modified version of the algorithm proposed in Nygårds and Sörnmo (1983). Briefly, the envelope of the input signal was computed as the modulus of its Hilbert transform and denoted x_{env}. In the 60 ms interval preceding each heartbeat, potential candidate QRS onset values $\widetilde{QRS}_{\text{ON}}$ were identified as the local maxima above a fixed threshold equal to $0.2 \times max\left(x'_{\text{env}}\right)$, with $max\left(x'_{\text{env}}\right)$ standing for the maximum value of the numerical gradient of x_{ev}. In this time frame, we computed the curvature of function x_{env} as: $C_{\text{env}} = \frac{x''_{\text{env}}}{\sqrt[3]{1+x'^2_{\text{env}}}}$, with x''_{env} equal to the gradient of x'_{env}. Doing so, the exact time location of each QRS onset QRS_{ON} could be finally determined as that of C_{env} local maximum in the 100 ms interval before the earliest $\widetilde{QRS}_{\text{ON}}$.

An improved version of Woody's method for time delay estimation was applied to each BSPM electrode to detect the offset of T-wave (T_{OFF}) (Cabasson and Meste, 2008). This method introduces an iterative maximum likelihood estimator to analyze variable latency signal. According to this approach, at each instant t a generic signal $x_i(t)$ can be modeled as:

$$x_i(t) = s\left(t - d_i\right) + e_i(t),$$

with $s\left(t - d_i\right)$ defined as the unknown reference wave delayed by d_i and $e_i(t)$ as observation's white Gaussian noise, for i=1, …, N_b. For our application, a fixed-length search window has been used for all electrodes to detect the end of T-wave at each heartbeat, with duration set between 200 and 300 ms depending on signal characteristics. As demonstrated by Cabasson and Meste (2008), each T-wave can be detected under an iterative scheme which determines the time lags $\hat{d}_i$, $i = 1, \ldots, N_b$ as those maximizing the correlation with a template waveform:

$$\hat{d}_i = \arg max_d \left[\sum_t \sum_{i}^{N_b} \sum_{k>i}^{N_b} x_k\left(t + d_k\right) x_i\left(t + d_i\right) \right]$$

Under the constraint that $\sum_i d_i = 0$, and with the template wave equal to the mean of all delayed waves $x_k\left(t + d_k\right)$ except for the one currently examined. The delays $\hat{d}_i$ are finally used to determine the final location of T-wave end T_{OFF} after each R-wave. The algorithm was applied to each electrode separately, but with a fixed search frame.

T-wave peak (T_{PEAK}) was detected from each lead as the time instant of the local maximum (minimum) of T-wave with positive (negative) polarity in the time interval starting 100 ms after the R-wave occurrence and ending at T_{END}. The onset of T-wave (T_{ON}) was finally identified at $0.3 \times T_{\text{FRAME}}$ samples after R-wave peak time instant, with T_{FRAME} equal to the median duration of the R-peak-T-wave offset interval over all leads. The time location of T-wave fiducial points was corrected if possible, otherwise BSPM electrodes associated

with misdetections due to flat repolarization were discarded from our analysis.

Standard and Novel Electrocardiographic Features of Myocardial Repolarization

In this section, we introduce several descriptors of T-wave and we evaluate their ability to non-invasively capture abnormal gradients in repolarization. We investigate to which extent the heterogeneity observed at the level of the tissue can be quantified on body surface, as abnormal dispersion of repolarization is known to strongly affect T-wave characteristics, in terms of: (a) duration; (b) variability duration; (c) shape; (d) spatial complexity, although the mechanistic link is not always clear and findings from previous studies are sometimes in mutual contradiction (Priori et al., 1997; Antzelevitch, 2001; Porthan et al., 2013). Accordingly, moving from previous research we define some markers of duration, morphology and spatial content of T-wave. Since in previous works most of these indices have been merely assessed from one or more beats in single-lead or 12-lead ECGs, we investigated whether equivalent BSPM-derived metrics could provide equally or more detailed information on repolarization abnormalities in our torso-tank model. A brief definition of each BSPM- and EGM-based indices is presented in **Table 1**.

Duration (T_{PEAK}-T_{END}, QT_C)

Time domain descriptors of ventricular electrical recovery were computed from surface potentials at each experimental stage. At each beat and from each electrode, we measured the duration of the time interval between the peak T_{PEAK} and the end of T-wave T_{OFF}, which has been regarded as an index of transmural dispersion of repolarization (Yan and Antzelevitch, 1998; Antzelevitch et al., 1999). For our analysis, the median value of the duration of this interval over all heartbeats was computed from each electrode and denoted T_{PEAK}-T_{END}.

We also investigated the role of QT interval as a marker for impaired electrical recovery, as its abnormal prolongation is known to be proarrhythmic (Straus et al., 2006). Accordingly, at each beat i and in each electrode ℓ the duration $QT_{\ell,i}$ of the interval between the beginning of the QRS complex Q_{ON} and the T-wave offset T_{OFF} was measured and corrected for heart rate using Bazett's formula $QT_{C_\ell,i} = QT_{\ell,i}/(RRm)^{0.5}$, with RRm equal to the mean RR interval. The median of corrected QT values over all beats was computed from each tank electrode (QT_C) and used for subsequent analysis.

Duration Variability [SD(T_{PEAK}-T_{END}), QTD]

The variability of cardiac repolarization was also determined in terms of temporal or beat-to-beat variability. Accordingly, we assessed temporal inhomogeneity of T_{PEAK}-T_{END} duration by computing the standard deviation of the peak-to-end T-wave interval durations across heartbeats from each BSPM electrode and denoted SD(T_{PEAK}-T_{END}), as it is known to be increased in subjects at higher risk for SCD (Piccirillo et al., 2013).

Finally, QTc interval dispersion (QTD) was also calculated as the difference between maximum and minimum QT over BSPM electrodes, being a routine measure of spatial heterogeneity of repolarization in clinics (Baumert et al., 2016).

TABLE 1 | Summary of all EGM- and BSPM-derived metrics of ventricular repolarization investigated in this study.

	Repolarization property	Definition
BSPM index		
T_{PEAK}-T_{END} (ms)	Duration	Median duration of the peak-to-end portion of T-wave per BSPM lead (over heartbeats)
QT_C (ms)	Duration	Median duration of the QT interval corrected for the heart rate (Bazett's formula) per BSPM lead (over heartbeats)
SD(T_{PEAK}-T_{END}) (ms)	Variability of duration (temporal)	Standard deviation of the peak-to-end portion of T-wave per BSPM lead (over heartbeats)
QTD (ms)	Variability of duration (spatial)	Difference between the maximum and the minimum QT_C value at each heartbeat
Asy (a.u.)	Morphology	Median value of the ratio between of the areas of the peak-to-end portion and that between the onset and the peak of T-wave (over heartbeats)
$d_{LV/RV}$ (mV)	Morphology	Cumulative DTW distance between all the possible pairs of electrodes from the right and left sides of the torso tank (associated with the RV and LV, respectively)
CR (%)	Spatial complexity	Ratio of the mean square of the second through L-th eigenvalues to the root mean square of all eigenvalues multiplied by 100
NMSE (%)	Spatial complexity	Average (over electrodes and beats) of the normalized mean square errors between the multilead T-wave at a given heartbeat and its PCA projection onto a 3D subspace from the T-wave at a different heartbeat
EGM index		
RTG_{GLOBAL} (ms)	RT global epicardial dispersion	Absolute difference of the average RTs over sock electrodes from differently perfused epicardial sites (Pin Group: Pin vs. no-Pin; Dof & Pin Group: Dof vs. Pin)
$RTG(LV/RV)_{GLOBAL}$ (ms)	RT global interventricular epicardial dispersion	Absolute difference of the average RTs over sock electrodes from differently perfused epicardial sites (Pin Group: Pin vs. no-Pin; Dof & Pin Group: Dof vs. Pin)
RTG_{LOCAL} (ms/mm)	RT local epicardial dispersion	Temporal average of the maximum absolute differences between RTs from two adjacent epicardial sites, divided by their Euclidean distance

Shape (*Asy*, $d_{LV/RV}$)

As in Di Bernardo and Murray (2000) and Sheridan et al. (2010), in each electrode $\ell = 1, \ldots, L$ and at each heartbeat beat i, $i = 1, \ldots, N_b$, we computed an index of symmetry of T-wave as the ratio between the area of the terminal portion of the repolarization (corresponding with the T_{PEAK}-T_{END} interval) and that between the onset and the peak of T-wave (i.e., the T_{ON}-T_{PEAK} interval):

$$Asy_{\ell,i} = \frac{\int_{T_{PEAK}}^{T_{END}} y_{\ell,i}(t)\,dt}{\int_{T_{ON}}^{T_{PEAK}} y_{\ell,i}(t)\,dt}$$

According to these works, more symmetrical T-waves were associated with increased repolarization heterogeneity, with index values closer to unity. Indeed, normal T waves should have a gradual upstroke with a slightly steeper descending limb, and abnormal dispersion of repolarization seems to alter relative contribution of these two portions. In our study, T-waves were mean-centered and normalized between 0 and 1. Integrals were discretized through the trapezoidal rule. The median of the asymmetry index over all beats was determined from each BSPM electrode and taken as a marker of repolarization dispersion (*Asy*).

T-wave morphology aberrations have been linked to abnormal heterogeneity of ventricular repolarization and increased arrhythmia vulnerability. Right-to-left ventricle dispersion is an important factor contributing to heterogeneous repolarization both in physiological (Hlaing et al., 2005) and pathological conditions (Fish et al., 2004), and it can affect T wave profile (Srinivasan et al., 2019). Dynamic time warping (DTW) has been previously proposed to describe T-wave beat-to-beat morphological changes, assess temporal variability of ventricular recovery from 12-lead ECG and predict SCD risk in chronic heart failure patients (Ramirez et al., 2017). Accordingly, moving from this theory we investigated whether drug-induced repolarization gradients may contribute to interventricular dispersion and be assessed by T-wave shape analysis. Specifically, we split BSPM electrodes into a set of L_{LV} electrodes associated with the left ventricle (LV; from the left side of the heart) and one consisting of L_{RV} electrodes for the right ventricle (RV; from the right side of the heart), and we applied DTW to measure the degree of similarity between waveforms from pairs of tank potentials, each associated with a different ventricle. Algorithm details are reported elsewhere (Müller, 2007). Briefly, this approach aims to find the match between two temporal sequences along an optimal alignment path by minimizing a cost function. In our study we choose the Euclidean distance as a similarity metric. A median T-wave signal was computed over all beats from each electrode and given as input to the algorithm after mean-centering and signal normalization by L2-norm. The cumulative distance $d_{LV/RV}$ minimizing the warping path between the examined pair of signals was used as a T-wave parameter, with higher values of the index denoting higher dissimilarity between the waveforms and increased heterogeneity of the ventricular recovery.

Complexity (CR, NMSE)

Due to its ability to capture inhomogeneities and variability of repolarization, principal component analysis (PCA) has been suggested as a tool to measure the spatial organization of T-wave (Priori et al., 1997; Malik et al., 2000; Zabel and Malik, 2001), under the hypothesis that cardiac activity can be approximated to a 3D electric dipole (Holt et al., 1969), and that components outside the T-wave loops would reflect pathological inhomogeneities and represent an arrhythmic substrate (Okin et al., 2002; Porthan et al., 2013). Accordingly, in line with this research, we assessed body surface electrical organization as follows. At each heartbeat i, $i = 1, \ldots, N_b$, a multi-electrode T-wave matrix $\boldsymbol{Y}^{(i)}$, $i = 1, \ldots, N_b$ was segmented between T_{ON} and the median value of T_{END} over all leads. T-wave matrix was then factorized by singular value decomposition $\boldsymbol{Y}^{(i)} = \boldsymbol{U}\boldsymbol{\Sigma}\boldsymbol{V}^{T}$, with $\boldsymbol{U}$ and $\boldsymbol{V}$ representing the right and left singular vectors, respectively, and $\boldsymbol{\Sigma}$ being a diagonal matrix containing the singular values σ_ℓ, $\ell = 1, \ldots, L$. As in Priori et al. (1997), we measured the relative contribution of the dominant eigenvector over total signal variation by computing the complexity of repolarization (CR) as:

$$CR = \sqrt{\frac{\sum_{\ell=2}^{L} \sigma_\ell^2}{\sum_{\ell=1}^{L} \sigma_\ell^2}}\,100$$

Lower CR values were assumed to describe less complex T-wave patterns and homogeneous repolarization, as one major spatial component (eigenvector) should be able to accurately describe such an organized process. Conversely, spatial repolarization heterogeneities were expected to require a higher number of components for accurate PCA reconstruction, thus yielding higher CR.

Additionally, we used PCA to explore the temporal variability of T-wave spatial components over higher-order spaces. Specifically, after normalization between 0 and 1 and mean-centering, at each beat, $i = 1, \ldots, N_b$ PCA was applied to $\boldsymbol{Y}^{(i)}$ to compute a 3D subspace $\boldsymbol{M}^{(i)}$ onto which every subsequent T-wave $\boldsymbol{Y}^{(j)}$, $j \neq i$, was projected. The normalized mean square error (NMSE) between the input potentials $\boldsymbol{Y}^{(j)}$ and their low-rank PCA approximation was then computed as:

$$NMSE^{(j)} = \frac{\left(\boldsymbol{I} - \boldsymbol{M}^{(i)}\boldsymbol{M}^{(i)\#}\right)\boldsymbol{Y}^{(j)}}{\boldsymbol{Y}^{(j)}}\,100$$

For $j = 1, \ldots, N_b$, $j \neq i$, with $\boldsymbol{M}^{(i)\#} = \left[\boldsymbol{M}^{(i)T}\boldsymbol{M}^{(i)}\right]^{-1}\boldsymbol{M}^{(i)T}$ being the pseudo-inverse of $\boldsymbol{M}^{(i)}$ (Bonizzi et al., 2010; Meo et al., 2013). At each beat, the average NMSE over all tank electrodes was finally considered as a descriptor of T-wave repolarization, assuming that higher reconstruction error would render a higher degree of spatiotemporal dispersion of repolarization.

Validation of Body Surface Signal Processing Algorithms

To confirm whether changes in BSPM parameters across each experiment truly reflected alterations in repolarization characteristics, at each experimental step every non-invasive

index was averaged over all electrodes and/or heartbeats, and their time evolution across the experiment was compared with that of several invasive epicardial markers of repolarization dispersion.

To verify the ability of BSPM-derived features to assess global dispersion of repolarization, at each heartbeat we computed the absolute difference RTG_{GLOBAL} between the spatial average of RTs over sock electrodes from differently perfused epicardial regions, i.e., between mean RT from electrodes in the Pin-area and those in non-perfused sites for Pin Group, and between mean RT from electrodes in the Pin-area and those in the Dof-area for Dof & Pin Group.

Additionally, at each beat we also measured the absolute difference between mean RTs from sock electrodes in contact with LV and those attached to RV ($RTG(LV/RV)_{GLOBAL}$).

We also investigated whether body surface analysis could identify regional repolarization gradients at a smaller scale. Accordingly, for validation at each beat we quantified the local spatial RT gradient RTG_{LOCAL}, i.e., the temporal average of the maximum differences between RTs from two adjacent EGM sites, divided by their Euclidean distance (Vijayakumar et al., 2014). The higher its value, the steeper the local repolarization gradients between neighboring sites. Specifically, for experiments from Pin Group, each invasive and non-invasive parameter was assessed: (1) at the beginning of the experiment, in the absence of drug-induced repolarization gradients ("Baseline"); (2) during LAD coronary perfusion with half concentration of pinacidil (15 μM, "1/2 Pin"); (3) during perfusion of the same site will full concentration of pinacidil (30 μM, "1/1 Pin"). Similarly, we computed all parameters for Dof & Pin Group at three experimental phases as well: (1) "Baseline"; (2) during injection of dofetilide (250 nM) in extra-LAD areas ("Dof"); (3) during injection of pinacidil (between 15 and 30 μM) in the LAD coronary ("Dof + Pin"). While in the Pin Group it has been possible to inject the total drug dose during all interventions, in two hearts (#3 and #4) from the Dof & Pin Group the experiments could not be completed due to some technical problems with LAD cannulation, thus only half dose of pinacidil could be used. Nevertheless, a clear effect of the drug on these additional hearts was observed despite the use of a lower pinacidil concentration, with visible and interpretable impact on repolarization properties, thus all the signal recordings could be eventually used and analyzed. To better understand the ability of each parameter to capture changes in each experimental phase from baseline, we also examined the trend of differences between the value of each feature at a specific experimental stage and that measured at baseline. For Pin Group, interphase variations were referred to as "Δ1/2 Pin" and "Δ1/1 Pin," while for Dof & Pin Group these were labeled as "ΔDof" and "ΔDof + Pin." Variations in body surface parameters were then compared to those in invasive measures of repolarization.

Finally, to verify the agreement of each non-invasive parameter with EGM gradients of repolarization, a Bland-Altman (BA) plot for each BSPM index from all experimental phases was built as follows (Altman and Bland, 1999). After feature standardization, the difference between the examined T-wave marker and the reference invasive metric z_D was displayed against their average z_M. The mean bias was estimated as the average of all differences z_D, to provide an estimate of the average discrepancy between methods. For the same purpose, we also determined the 95% limits of agreement (LoA) of the interval as a measure of confidence. The narrower the interval, and the higher the number of points within it, the higher the degree of agreement between the compared approaches. Confidence bounds were corrected for repeated measures' data, assuming that the true difference value is not constant across observations as in Altman and Bland (1999).

RESULTS

Pin Group

Time evolution of EGM- and BSPM-derived parameters for each experiment from Pin Group is shown in **Figure 2**.

More pronounced differences in electrical recovery timing between perfused and non-perfused regions are globally measured by an increase in RTG_{GLOBAL} in all experiments, except for experiment #3 (**Figure 2A**, left). Pinacidil injection is also responsible for a marked increase in EGM interventricular RT dispersion $RTG(LV/RV)_{GLOBAL}$ in experiments #1 and #2 (**Figure 2A**, middle), whereas RTs become more similar with time in experiment #3. Similar dynamics can be locally retrieved, with higher regional dispersion of repolarization and higher RTG_{LOCAL} in all experiments #1 and #2 during drug injection, although with a more blunted evolution in experiment #3.

As shown in **Figure 2B** (left), the evolution of T_{PEAK}-T_{END} on body surface is consistent with the trend of all epicardial measures of dispersion, namely, an increase in the duration of the ending portion of T-wave can be observed when repolarization is more heterogeneous. Regarding experiment #3, T_{PEAK}-T_{END} prolongation is more pronounced when pinacidil injection has started, and then a drop in the index can be observed, with a time evolution resembling more that of global invasive markers of repolarization dispersion (RTG_{GLOBAL} and $RTG(LV/RV)_{GLOBAL}$) rather than regional measures (RTG_{LOCAL}). On the other hand, a progressive shortening of QT_C duration is observed during pinacidil perfusion throughout all interventions (**Figure 2B**, right), a behavior that has been reported by several experimental studies (Padrini et al., 1992; Extramiana and Antzelevitch, 2004), but in opposition to the time evolution of invasive markers of repolarization dispersion (except for RTG_{LOCAL} in experiment #3).

The $SD(T_{PEAK}$-$T_{END})$ index measures increasing temporal variability of T_{PEAK}-T_{END} in all experiments (**Figure 2C**, right), but with transient fluctuations in parameter values in experiments #1 and #2 that do not always reflect the evolution of EGM metrics when low doses of pinacidil are administered. For experiment #3, temporal increase $SD(T_{PEAK}$-$T_{END})$ does not match the decreasing trend of global markers of epicardial dispersion, while it better captures changes in local recovery heterogeneity RTG_{LOCAL}. Overall, changes between the beginning and the end of all interventions $\Delta SD(T_{PEAK}$-$T_{END})$ are similar to that of the invasive counterparts, thus confirming that enhanced repolarization dispersion at the level of tissue reflects on a less stable temporal distribution of T_{PEAK}-T_{END}

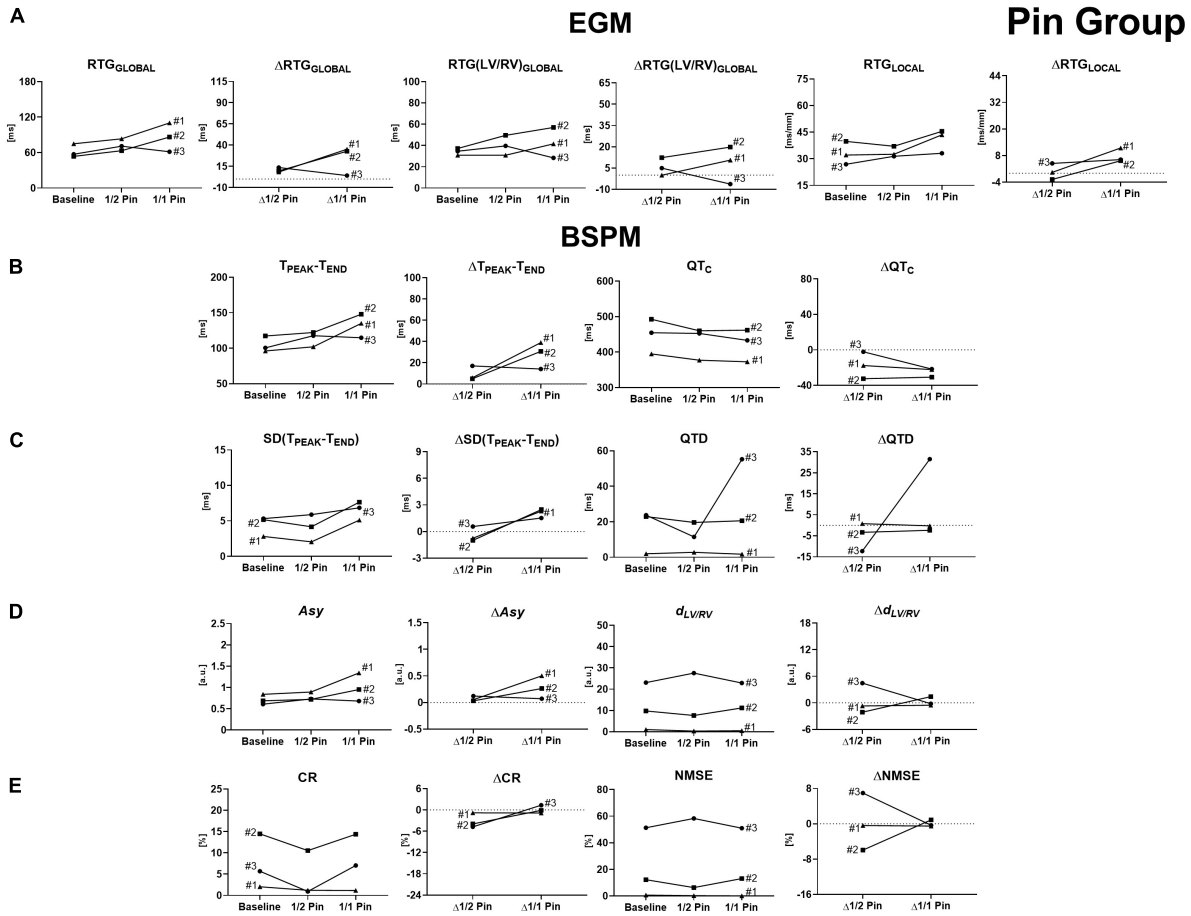

FIGURE 2 | Time evolution of signal features and their variations with respect to baseline conditions for experiments from Pin Group, computed before and during progressive injection with pinacidil. **(A)** Invasive epicardial metrics of heterogeneity of repolarization and changes from baseline computed as global differences in RTs between Pin- and not-Pin sites (RTG_{GLOBAL} and ΔRTG_{GLOBAL}, left), global differences in RTs between LV and RV ($RTG(LV/RV)_{GLOBAL}$ and $\Delta RTG(LV/RV)_{GLOBAL}$, middle), and local RT gradients between neighboring epicardial sock nodes (RTG_{LOCAL} and ΔRTG_{LOCAL}, right). **(B)** BSPM indices and changes from baseline of T-wave duration (T_{PEAK}-T_{END} and ΔT_{PEAK}-T_{END}, left) and corrected QT interval (QT_C and ΔQT_C, right). **(C)** BSPM indices and changes from baseline of temporal variability of T-wave duration [$SD(T_{PEAK}$-$T_{END})$ and $\Delta SD(T_{PEAK}$-$T_{END})$, left] and QT_C spatial dispersion (QTD and ΔQTD, right). **(D)** BSPM indices and changes from baseline of T-wave symmetry (*Asy* and Δ*Asy*, left) and shape ($d_{LV/RV}$ and $\Delta d_{LV/RV}$, right). **(E)** BSPM indices and changes from baseline of T-wave complexity (CR and ΔCR, left, and NMSE and ΔNMSE, right). a.u., arbitrary units.

duration on body surface. Spatial dispersion of QTc (QTD) is overall stable in experiments #1 and #2 (**Figure 2C**, left), while a marked, unexpected increase in QTD is measured during experiment #3, which is in disagreement with all invasive global metrics of dispersion. The same trends were observed without heart rate correction (results not shown).

As reported in **Figure 2D** (left), at baseline T-waves are usually left-skewed, and this characteristic is exacerbated by the introduction of global and regional repolarization gradients in experiments #1 and #2. Concerning experiment #3, T-waves also tend to be more left-skewed since the beginning of the intervention and keep a stable shape in time, as global and interventricular RT gradients from EGMs become more homogeneous. Overall, higher heterogeneity of repolarization seems to be associated with more asymmetric T-waves on body surface, in contrast to previous studies (Di Bernardo and Murray, 2000).

Interventricular differences in T-wave morphology between right and left BSPM electrodes according to DTW processing appear overall modest (**Figure 2D**, right). Drug-induced changes in repolarization properties significantly enhance such differences and lead to an increase in DTW distance $d_{LV/RV}$ only in experiment #2, and this is invasively confirmed by an increase in $RT(LV/RV)_{GLOBAL}$ during pinacidil injection, and by the other epicardial metrics as well. On the contrary, during the other interventions the index tends to have a stable trend, and changes between the initial and the final steps of the experiments are limited, in spite of a marked increase in EGM interventricular RT dispersion.

Unlike previous works (Priori et al., 1997), unexpected patterns of electrical organization are revealed by the dominant PCA spatial direction at low doses of pinacidil, with a drop in CR values when starting the perfusion (**Figure 2E**, left). At the final drug state, CR values are again comparable to those

measured at baseline in all hearts. Similarly, body surface analysis of repolarization complexity according to the NMSE parameter in **Figure 2E** (right) also highlights some variability in its temporal evolution and absolute values across the interventions. In addition, changes in the parameter values from baseline ΔNMSE are modest. Taken together, these findings indicate that the accuracy of T-wave projection onto low-dimension spaces is quite variable and somehow difficult to link with the trend of the reference EGM metrics in this framework.

The agreement between T-wave markers and measures of epicardial RT dispersion is assessed by BA plots in **Figure 3**.

For all T-wave indices, mean difference between non-invasive and invasive analysis (horizontal black line) is close to zero and points are quite scattered above and below zero, suggesting that there is no systematic bias (i.e., the error between BSPM- and EGM-derived parameters z_D does not present any specific trend). The T_{PEAK}-T_{END} index (**Figure 3A**, left) is overall highly consistent both with global (RTG_{GLOBAL}) and local descriptors (RTG_{LOCAL}) of repolarization heterogeneity, as the difference z_D between the measures derived from invasive and non-invasive approaches tends to zero and the band of agreement (LoA) is quite narrow. With regard to the analysis of interventricular dispersion [$RTG(LV/RV)_{GLOBAL}$], scatter points associated with experiment #3 tend to depart from the line $z_D = 0$, but they are still within the LoA bounds. BA analysis of QT interval (**Figure 3A**, right) highlights that points associated with low QT_C values (i.e., late experimental stages) are close to zero, regardless of the EGM marker, whereas longer QT_C characterize points which lie farther from this threshold, although no specific trend can be elucidated from this distribution. Furthermore, the large width of the confidence interval denotes lower certainty with regard to the relation with epicardial RT dispersion at each scale of observation. In **Figure 3B** (left) BA plots for SD(T_{PEAK}-T_{END}) confirm good agreement with all measures of RT gradients, especially with that of global dispersion RTG_{GLOBAL}, with z_D values nearly equal to zero and well separated point clusters (points associated with experiments #1 and #2 are well separated from those related to experiment #3). Similar remarks can be done for the regional analysis of heterogeneity through RTG_{LOCAL}, but with z_D values closer to zero for experiment #3, suggesting that in this heart local dispersion of ventricular recovery was better captured by this index than in the global analysis. The ability to distinguish between distinct drug states is lost when considering spatial dispersion of duration QTD (**Figure 3B**, right), with most of z_D points far from zero and a large LoA interval. The relation between T-wave morphology and epicardial RT heterogeneity is displayed in **Figure 3C**. For the *Asy* index (left panel), BA plot demonstrates accurate agreement with regional and global dispersion of repolarization, and measures acquired from different experiments (i.e., #1 and #2) at the same phase tend to cluster around $z_D = 0$. Measures related to experiment #3 also follow well global EGM metrics, and they are distributed far from each other along $z_D = 0$. Also, the bounds of the interval of agreement are quite narrow. The scatterplots for the $d_{LV/RV}$ index in in **Figure 3C** (right) are more scattered, but at acceptable distance from the zero-threshold and comparable agreement with all EGM parameters. Finally, BA analysis of T-wave complexity according to the CR and NMSE indices (**Figure 3D**, left and right panel, respectively) denotes even lower agreement with invasive RT dispersion, as confirmed by the quite large LoA interval and z_D distribution, with most of the points far from zero.

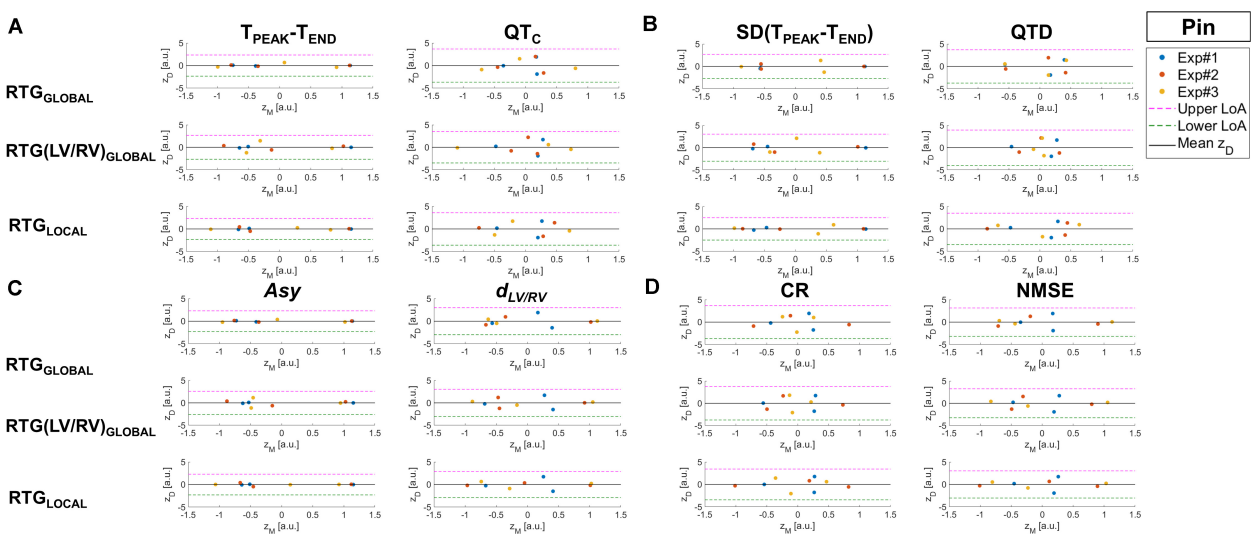

FIGURE 3 | BA plots of the differences z_D between BSPM markers of T-wave and invasive RT dispersion measures vs. their mean z_M for the assessment of the agreement between the two approaches for experiments from Pin Group before and during progressive injection with pinacidil. The mean difference between methods (horizontal continuous black line) and upper and lower 95% LoA (dashed magenta and green lines, respectively) are also displayed. **(A)** BSPM indices and T-wave duration (T_{PEAK}-T_{END}, left) and corrected QT interval (QT_C, right). **(B)** BSPM indices of temporal variability of T-wave duration [SD(T_{PEAK}-T_{END}), left] and QT_C spatial dispersion (QTD, right). **(C)** BSPM indices of T-wave symmetry (*Asy*, left) and shape ($d_{LV/RV}$, right). **(D)** BSPM indices of T-wave complexity (CR, left, and NMSE, right). a.u., arbitrary units.

Dof & Pin Group

The same analysis has been repeated for all experiments from Dof & Pin Group, and the trend of invasive and non-invasive descriptors of ventricular repolarization is reported in **Figure 4**.

In all experiments the injection of dofetilide has favored the onset of global and regional electrical disparities, which are further accentuated by the perfusion with pinacidil later in each experiment. These effects are correctly captured by all EGM metrics (**Figure 4A**), and they are overall stronger than in the setup of Pin Group, due to the combined and opposite effect of the two drugs on the duration of the recovery time.

As for Pin Group, an increasing evolution of T_{PEAK}-T_{END} with the course of time also characterizes experiments from Dof & Pin Group and accurately follows changes in repolarization properties as measured at the level of the epicardium (**Figure 4B**, left). QTc index can also describe electrical recovery alterations (**Figure 4B**, right), although its variations over time are less abrupt than for T_{PEAK}-T_{END} and pinacidil injection seems to have little effect compared with the previous drug state.

Likewise, an increase in temporal variability in the duration of the final portion of T-wave is described by an increase in $SD(T_{PEAK}$-$T_{END})$, which is more evident when both drugs are injected (except for experiment #4, where pinacidil has little effect on the index) (**Figure 4C**, left). Trends of $SD(T_{PEAK}$-$T_{END})$ and its changes from baseline $\Delta SD(T_{PEAK}$-$T_{END})$ closely reflect the appearance of repolarization gradients through pharmacological approach as confirmed by the corresponding evolution of all epicardial measures of RT dispersion with the course of the experiments. Conversely, drug-induced changes

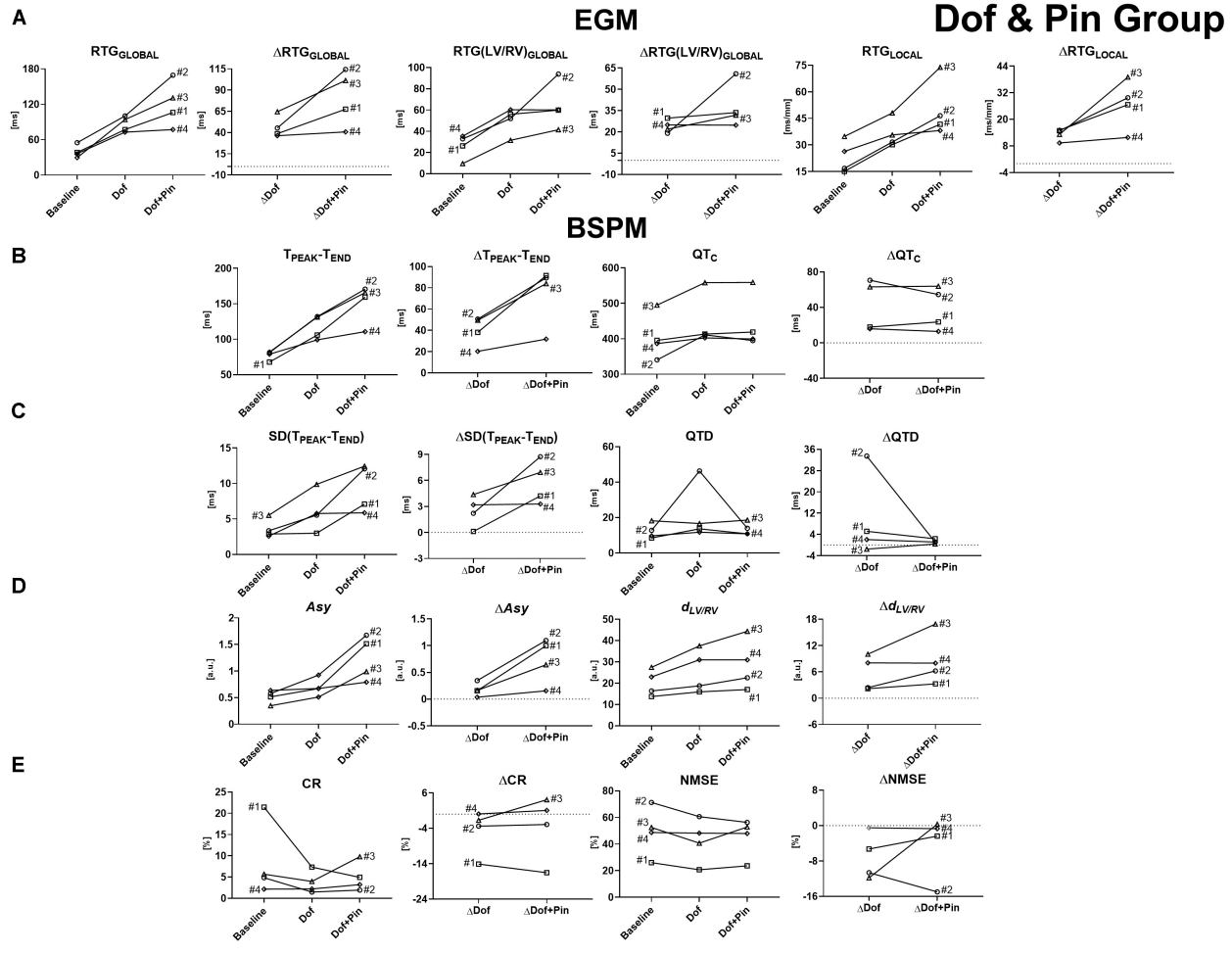

FIGURE 4 | Time evolution of signal features and their variations with respect to baseline conditions for experiments from Dof & Pin Group, computed before and during progressive injection with dofetilide and pinacidil. **(A)** Invasive epicardial metrics of heterogeneity of repolarization and changes from baseline computed as global differences in RTs between Pin- and not-Pin sites (RTG_{GLOBAL} and ΔRTG_{GLOBAL}, left), global differences in RTs between LV and RV ($RTG(LV/RV)_{GLOBAL}$ and $\Delta RTG(LV/RV)_{GLOBAL}$, middle), and local RT gradients between neighboring epicardial sock nodes (RTG_{LOCAL} and ΔRTG_{LOCAL}, right). **(B)** BSPM indices and changes from baseline of T-wave duration (T_{PEAK}-T_{END} and ΔT_{PEAK}-T_{END}, left) and corrected QT interval (QT_C and ΔQT_C, right). **(C)** BSPM indices and changes from baseline of temporal variability of T-wave duration [$SD(T_{PEAK}$-$T_{END})$ and $\Delta SD(T_{PEAK}$-$T_{END})$, left] and QT_C spatial dispersion (QTD and ΔQTD, right). **(D)** BSPM indices and changes from baseline of T-wave symmetry (*Asy* and Δ*Asy*, left) and shape ($d_{LV/RV}$ and $\Delta d_{LV/RV}$, right). **(E)** BSPM indices and changes from baseline of T-wave complexity (CR and ΔCR, left, and NMSE and ΔNMSE, right). a.u., arbitrary units.

in repolarization heterogeneity were not captured by QTD (**Figure 4C**, right), whose values at the end of the perfusion of both drugs were comparable with those measured at baseline, with and without heart rate normalization, and with high variability in its values across the interventions when only dofetilide is injected.

In this set of interventions, T-wave morphology is significantly affected during drug perfusion. Globally, T-wave shape tends to be more triangular/trapezoidal, the ascending slope is steeper and a notched pattern can be frequently observed from BSPMs (see **Figure 1**), compared with Pin Group, at baseline T-waves are either left-skewed or symmetric, with average values of *Asy* inferior to unity (**Figure 4D**, left). Subsequently, late repolarization is prolonged by the injection of dofetilide, thus durations of the starting and final portions are less similar to each other. These differences are further exacerbated by the injection of pinacidil, which drastically shortens the duration of early repolarization and causes a strong increase in *Asy* values. Time evolution of this body surface marker and its changes from baseline closely reflect the trend of the epicardial repolarization dispersion.

Drug-induced repolarization gradients are also responsible for more pronounced differences in T-wave shape between left and right BSPM electrodes according to DTW analysis. As shown in **Figure 4D** (right), a lower degree of similarity between waveforms from left and right side of the torso tank is assessed by DTW during dofetilide perfusion for all interventions, and it is in keeping with the evolution of all EGM measures of RT dispersion. Interventricular differences in T-wave patterns are further emphasized by the injection of pinacidil later in both experiments, and confirmed by EGM analysis.

As for the previous set of interventions, the evolution of PCA-derived features in **Figure 4E** is affected by strong inter-experiment variability, although our findings seem to support the idea that overall higher heterogeneity of the ventricular recovery is better described by low-rank approximations of cardiac repolarization. In all experiments, lower PCA reconstruction errors and a sharp decrease in the CR index are measured during dofetilide perfusion. A further (although more modest) drop in this parameter is observed when adding pinacidil, except for experiment #3. According to NMSE analysis, a decline in spatial complexity with time can be easily appreciated for experiment #2, whereas the other ones are characterized by modest changes from baseline and weak agreement with invasive assessment of repolarization gradients.

In **Figure 5**, BA plots for all BSPM parameters are reported. As for Pin Group, mean bias is negligible for all indices. However, dispersion of point distribution is globally lower than in Pin Group, with z_D values close to zero and no specific pattern in relation to z_M. Specifically, in **Figure 5A** (left), the relation between T_{PEAK}-T_{END} and global and local descriptors of epicardial RT dispersion is displayed. Overall, experimental measures from different phases are even better separated from each other along the z_M horizontal axis than in Pin Group, and their variability at a given phase is low, especially when compared to RTG_{GLOBAL} and RTG_{LOCAL}. Moreover, the LoA interval is quite narrow for all scatterplots, hinting at good agreement with invasive RT gradient metrics, regardless of the scale of observation. Conversely, with regard to QT interval analysis (**Figure 5A**, right), while the interval of agreement has similar bounds and baseline z_D difference values (left side of the scatterplot) tend to zero, then with progressive drug

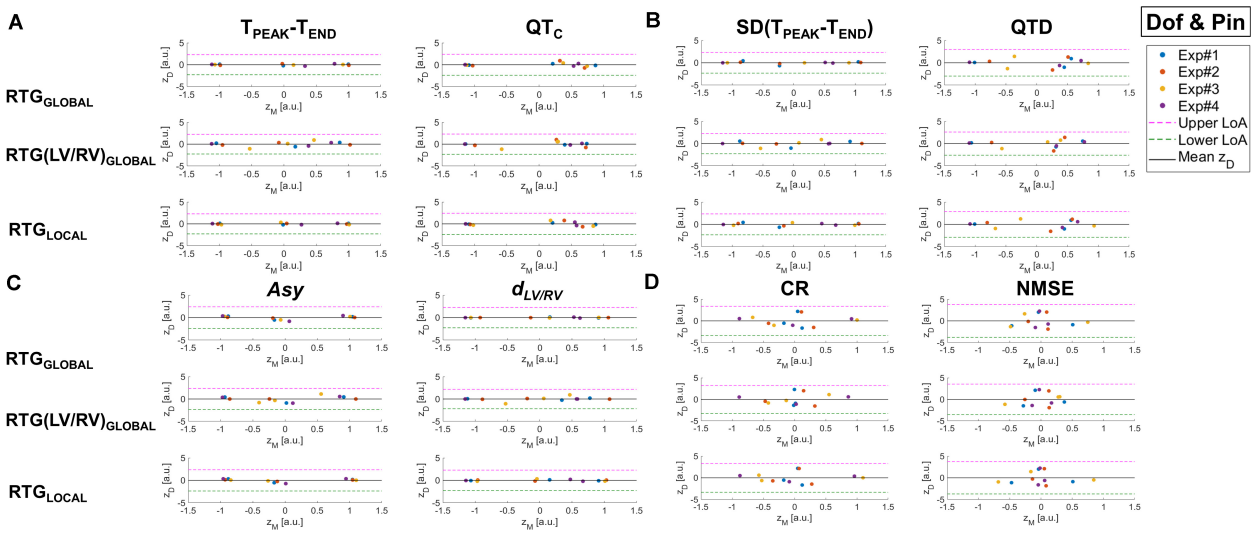

FIGURE 5 | BA plots of the differences z_D between BSPM markers of T-wave and invasive RT dispersion measures vs. their mean z_M for the assessment of the agreement between the two approaches for experiments from Dof & Pin Group before and during progressive injection with dofetilide and pinacidil. The mean difference between methods (horizontal continuous black line) and upper and lower 95% LoA (dashed magenta and green lines, respectively) are also displayed. **(A)** BSPM indices and T-wave duration (T_{PEAK}-T_{END}, left) and corrected QT interval (QT_C, right). **(B)** BSPM indices of temporal variability of T-wave duration [SD(T_{PEAK}-T_{END}), left] and QT_C spatial dispersion (QTD, right). **(C)** BSPM indices of T-wave symmetry (*Asy*, left) and shape ($d_{LV/RV}$, right). **(D)** BSPM indices of T-wave complexity (CR, left, and NMSE, right). a.u., arbitrary units.

administration their distribution appears more scattered around the mean bias, and measures acquired at different drug states tend to form a unique cluster, denoting a lack of sensitivity of the QT_C index and poor discrimination of different drug states (e.g., different degrees of RT heterogeneity). Similar remarks can be done for the indices of variability of body surface repolarization duration (**Figure 5B**), with SD(T_{PEAK}-T_{END}) (left panel) exhibiting closer agreement with all invasive RT gradient parameters at each experimental phase than QTD (right panel). Taken together, these findings suggest that the T-wave final portion is more informative than QT interval with regard to the characterization of distinct levels of repolarization heterogeneity. BA plots for T-wave shape parameters are shown in **Figure 5C**. T-wave asymmetry (left panel) and interventricular DTW distance (right panel) are both more consistent with EGM reference indices than their counterparts from Pin Group, as denoted by all quasi-null z_D values, and confidence intervals are quite tight. Of note, *Asy* values from the same experimental phase tend to form definite clusters, thus denoting lower measure uncertainty and easier phase discrimination than for $d_{LV/RV}$, in particular when compared to RTG_{GLOBAL} and RTG_{LOCAL}. Finally, in **Figure 5D** BA scatterplots for PCA descriptors of spatial complexity are presented. As for Pin Group, the LoA width is larger compared with the other BSPM parameters. Furthermore, point distribution is extremely scattered and BSPM measures associated with distinct intervention steps are difficult to distinguish, with most of z_D values far from zero, hinting at a weaker relation with epicardial RT dispersion, regardless of the metric considered.

DISCUSSION

In this study, we have compared state-of-the-art and novel parameters for the non-invasive assessment of the degree of cardiac repolarization dispersion from BSPMs. The use of an *ex vivo* torso tank model allowed us to test all metrics in a controlled environment and get rid of confounding factors that are typically encountered *in vivo*, e.g., respiration movement, use of anesthetics and lack of control on the mechanisms underlying a certain pathology. Importantly, this model helped us to reproduce global and local repolarization abnormalities due to purely electrical phenomena, which is crucial to understand electrical disorders which may affect structurally normal hearts. In addition, simultaneous invasive mapping of repolarization has enabled a better understanding of the relation between drug-induced changes in repolarization at the level of the tissue and manifestations of these phenomena on body surface as reflected on T-wave characteristics.

T-Wave Duration and Dispersion of Repolarization

As in previous studies, we usually observed a prolongation of the duration of the T_{PEAK}-T_{END} interval when repolarization gradients were created by drug perfusion. Changes in this index have been thought to reflect alterations in transmural dispersion of repolarization (Yan and Antzelevitch, 1998), and be prognostic of arrhythmic risk under a variety of conditions (Antzelevitch et al., 2007). Nevertheless, the ability of T_{PEAK}-T_{END} interval to provide an absolute measure of transmural dispersion *in vivo* is still under debate (Xia et al., 2005), and other studies have supported the idea that this index may rather be a predictor of arrhythmogenesis as the result of increased global dispersion of ventricular recovery (Opthof et al., 2007). Even though we could not fully clarify the precise mechanisms behind this electrocardiographic manifestation (we could not perform endocardial mapping), our findings show that a higher degree of both global and local repolarization heterogeneity subsequent to drug intervention reflects on the lengthening of the terminal part of T-wave on the torso tank. This behavior has also been validated by BA plot analysis, and showed strong consistency with similar formulations for epicardial RT dispersion. In only one case (experiment 3 from Pin Group) a shortening of this interval was measured from EGMs after pinacidil injection. This may be potentially explained by a delayed effect of the drug, which was actually visible only during drug washout (not shown). Concerning the QT interval, different behaviors have been observed depending on the experimental setup. The sole administration of pinacidil in Pin Group caused a shortening of the QT_C interval, in line with previous studies (Padrini et al., 1992; Extramiana and Antzelevitch, 2004) reporting this ECG feature as a consequence of higher transmural dispersion of repolarization. On the contrary, the use of dofetilide led to QT_C prolongation, which may be proarrhythmic (Barrett et al., 2001). Overall, increased epicardial dispersion of repolarization, both local and global, was not reflected by a consistent behavior of QT interval on body surface, thus confirming the lack of specificity of this index, which reflects both the depolarization and repolarization process, thus to be interpreted with caution.

T-Wave Duration Variability and Dispersion of Repolarization

Exacerbation of repolarization gradients was responsible for enhanced beat-to-beat variability of T_{PEAK}-T_{END} duration. This phenomenon has been previously related to increased arrhythmic risk both clinically and experimentally (Pueyo et al., 2011; Piccirillo et al., 2013). Results from computational studies have corroborated the critical role of I_{Ks} and I_{Kr} currents in the temporal modulation of repolarization reserve at the cellular level, both in physiological and pathological conditions (Pueyo et al., 2011). In Piccirillo et al. (2013), temporal myocardial repolarization lability was associated with increased risk for SCD and also potentially correlated with a downregulation of potassium currents, which is typical of patients with congestive heart failure. Importantly, as argued by the same authors, temporal instability of T_{PEAK}-T_{END} duration may be indicative of the presence of tissue areas containing non-homogeneous refractory periods, and under favorable conditions (e.g., ischemia) the recovery of excitability may lag behind the completion of repolarization as well (Burton and Cobbe, 2001). Although the exact cellular mechanisms

could not be elucidated by our investigation, in line with these studies, we also observed that a decline in temporal stability of T_{PEAK}-T_{END} duration during drug perfusion precisely followed changes in RT dispersion on the sock and showed good agreement with the reference invasive metrics, and this phenomenon was observed in all experiments. On the contrary, regional electrical disparities were not accurately identified by the QTD index, whose capability of assessing repolarization heterogeneity has been questioned by previous studies as well (Malik et al., 2000; Prenner et al., 2016). Indeed, QT interval is insensitive to shortening of regional repolarization in the presence of prolonged repolarization elsewhere (Burton and Cobbe, 2001) and its variability is likely the result of the different projections of the heart vector on the body surface, rather than true dispersion of repolarization (Di Bernardo et al., 2000; Malik et al., 2000; Burton and Cobbe, 2001).

T-Wave Morphology and Dispersion of Repolarization

Overall, abnormal dispersion of electrical recovery strongly affected the morphology of T-wave. In our dataset, a decline in T-wave symmetry was found to be associated with higher dispersion of repolarization. This is in contrast to results from simulations presented by Di Bernardo and Murray (2000), who found that T-wave became more symmetrical with increased apico-basal and transmural dispersion. However, other studies presented opposite findings (Van Huysduynen et al., 2005; Vicente et al., 2015), and this may be due to the use of a non-realistic torso-heart model, with too simple geometries, and the lack of granularity in the modulation of action potential initiation at different sites (Di Bernardo and Murray, 2000). In contrast, electrocardiographic manifestations reported by our investigation are closer to those presented by Vicente et al. (2015), although alterations in T-wave profile presented in that study were provoked by other drugs acting on different ionic channels. In our experience, repolarization gradients led to a progressive loss of T-wave symmetry in all experiments, as a result of a steeper T-wave upslope and marked changes in the terminal portion of T-wave, both in terms of duration and area, with strong agreement with invasive measures of dispersion of repolarization. This effect was even clearer during experiments from Dof & Pin Group when both drugs were simultaneously injected, probably because differences between early and late repolarizing sites were more emphasized by the combined use of dofetilide and pinacidil rather than the injection of pinacidil alone and were easier to retrieve on body surface.

According to DTW, creation of repolarization gradients through pharmacological approach highlighted stronger differences in T-wave shape between left and right BSPM electrodes with respect to baseline. Morphological aberrations of T-wave profile as a consequence of repolarization inhomogeneity have been previously documented (Vicente et al., 2015; Ramirez et al., 2017), but mechanisms underlying such alterations are still unclear. Abnormal T-wave patterns have been observed during dofetilide-induced long QT syndrome (type 2) by Meijborg et al. (2015), who reported a correlation between increased interventricular dispersion of repolarization and appearance of notched waveforms on ECG, although shape assessment was rather qualitative. Alterations in ECG T-wave upslope have also been attributed to increased right-to-left RT dispersion from human hearts (Srinivasan et al., 2019). In Ramirez et al. (2017) DTW processing of T-wave accurately assessed risk for SCD in a population of congestive heart failure patients, although that retrospective study was more focused on temporal changes of T-wave rather than spatial aspects. Our research proposed a potential application of DTW processing as a descriptor of T-wave abnormalities in relation to dispersion of repolarization, and its capability of detecting variations in T-wave shape across leads. Interventricular differences in T-wave patterns were easier to appreciate in all experiments from Dof & Pin Group when both drugs were simultaneously injected, as for the *Asy* index. This finding is also confirmed by BA plot, which is characterized by narrower interval of agreement than in Pin Group and quasi-null z_D values, thus confirming good agreement with evidence from invasive recordings.

T-Wave Complexity and Dispersion of Repolarization

PCA has proved to be a suitable tool for the description of cardiac activity from body surface, with prognostic value in SCD prediction (Porthan et al., 2013). Previous studies showed that T-wave non-dipolar components assessed by PCA are associated with increased dispersion of repolarization in a multitude of pathologies (De Ambroggi et al., 1997; Priori et al., 1997). Surprisingly, an inverse correlation between spatiotemporal organization of T-wave and repolarization uniformity was underlined by our analysis, albeit with some variability across the experiments. This unusual result is in line with (Zabel et al., 2000), showing that lower PCA ratios are predictive of post-myocardial infarction arrhythmic events, although with borderline statistical significance. The observed phenomenon may be due to an intrinsic limitation of our *ex vivo* model, as when we inject drug(s) in and outside the LAD artery we artificially create two distinct clusters with distinct recovery timings, with a steep transition at their border. This scenario is simpler than *in vivo* repolarizing tissue, where each myocardial cell differently contributes to the global behavior of the heart, therefore it may be more easily and accurately captured by low-rank PCA approximations rather than in the absence of drugs. Another potential explanation for this phenomenon may come from Van Oosterom's T-wave model (Sassi and Mainardi, 2011; Laguna et al., 2016), which assumes surface T-wave genesis as the result of the counteraction between spatial distribution of RTs across the ventricular tissue and changes in the AP repolarization profile at the level of the single cardiomyocyte in a PCA-based framework. Indeed, according to Van Oosterom's formulation, in substrates with increased heterogeneity of repolarization, at each time instant t surface T-wave $y(t)$ can be decomposed into a weighted sum of

a function T_d (also called the dominant T-wave) and its derivative $\dot{T}_d$:

$$\boldsymbol{Y}(t) \approx \boldsymbol{w}_1 \boldsymbol{T}_d + \boldsymbol{w}_2 \dot{\boldsymbol{T}}_d \approx -\boldsymbol{A}\Delta\boldsymbol{\rho}\dot{d}(t-\bar{\rho}) + \frac{1}{2}\Delta\boldsymbol{\rho}^2\ddot{\boldsymbol{d}}(t-\bar{\rho})$$

With the weights $\boldsymbol{w}_1 = -\boldsymbol{A}\Delta\boldsymbol{\rho}$ and $\boldsymbol{w}_2 = \frac{1}{2}\Delta\boldsymbol{\rho}^2$ dependent on RT dispersion $\Delta\rho$ across the tissue, A a transfer matrix, $d(t-\bar{\rho})$ describing the repolarization phase of the transmembrane potentials of the myocytes of a given region, and $\bar{\rho}$ equal to the spatial average of local RTs over that region. As illustrated in Laguna et al. (2016), the unknown $\boldsymbol{T}_d$ and $\dot{\boldsymbol{T}}_d$ functions can be estimated by SVD of the input BSPM matrix $\boldsymbol{Y}$ as:

$$\boldsymbol{T}_d = c_1\sigma_1\boldsymbol{v_1}^T,\ \boldsymbol{w}_1 = \frac{\boldsymbol{u}_1}{c_1}$$

$$\dot{\boldsymbol{T}}_d = c_2\sigma_2\boldsymbol{v_2}^T,\ \boldsymbol{w}_2 = \frac{\boldsymbol{u_2}}{c_2}$$

Where c_1 and c_2 are scalar constants which can be computed under suitable constraints (Sassi and Mainardi, 2011). This theoretical framework clarifies the simultaneous dependence of the second singular value σ_2 on RT dispersion $\Delta\rho$ and on the AP downstroke velocity $\ddot{d}(t-\bar{\rho})$, which may explain (at least in part) the unexpected trend of PCA features during drug injection. Specifically, in Pin Group the increased spatial heterogeneity of repolarization $\Delta\rho$ with progressive infusion of pinacidil is accompanied by K_{ATP} channel opening, causing shorter APD and steeper downstroke $\ddot{d}(t-\bar{\rho})$ (Fedorov et al., 2011). However, this action is not strong enough to induce a significant change in spatial complexity of T-wave, maybe because a relatively small area (the LAD coronary) is affected by this intervention, thus drug-induced changes in repolarization cannot be correctly captured by high-order PCA approximations, and in particular by the spatial direction $\boldsymbol{u}_2$. Conversely, in Dof & Pin Group, the injection of dofetilide in extra-LAD regions may have caused a more marked reduction in AP downslope velocity $\ddot{d}(t-\bar{\rho})$ compared with RT spatial dispersion $\Delta\boldsymbol{\rho}$ (Vicente et al., 2015), with a stronger effect likely due to the involvement of a higher number of ventricular sites, and partial restoration of the initial conditions during pinacidil injection. Furthermore, other factors may contribute to the complexity of myocardium electrical recovery *in vivo*, including autonomic modulation (Ghuran et al., 2000) or ischemia (Al-Zaiti et al., 2011). To our knowledge, this is the first application of PCA to T-wave analysis in an experimental model, as it has been so far performed only in clinical human patients, with comparisons with invasive measures from explanted hearts performed only indirectly (Zabel et al., 1995). Further investigation is needed to clarify this divergence between experimental and clinical findings.

Limitations and Perspectives

The study was performed on a limited number of hearts, thus the proposed BSPM markers should be tested on a larger dataset to corroborate their descriptive accuracy. However, evolution of BSPM indices was overall consistent across experiments, and deviations from expected trends were linked to experimental conditions (e.g., delayed drug effect, tissue block etc.).

Paucity of data may also have affected the outcome of the BA analysis of signal features, and in particular with respect to the width of confidence intervals and the impossibility to perform a statistical comparison over such a low number of samples. Nevertheless, most of BSPM indices demonstrated good agreement with all indices of epicardial dispersion of repolarization, thus proving that physiologically relevant information about repolarization alterations can be inferred by body surface T-wave analysis at multiple observation scales.

Although the spatial resolution of the signal processing framework presented in this study is not sufficiently high to clearly distinguish different mechanisms of recovery dispersion from body surface and/or localize tissue areas with abnormal timing, the proposed techniques can overall help to non-invasively detect repolarization abnormalities by exclusively exploiting the information provided by BSPMs, with no need for patient's anatomy, requiring the use of more expensive imaging technologies. On the contrary, these tools could be used to detect repolarization anomalies at a larger scale of observation and potentially complement other approaches (e.g., electrocardiographic imaging or contact mapping) to identify diseased ventricular sites with higher precision at a second stage.

Body surface markers for repolarization variability were compared and validated with global and regional measures of epicardial RT gradients. Although reliable, as they straightforwardly account for tissue local properties, these measures should be interpreted with caution. Indeed, the computation of RT-dependent metrics may be affected by experimental maneuvers (e.g., loss of sock electrode contact during LAD cannulation). Additionally, the examined parameters only allow us to describe what happens on the epicardium, thus any unexplained behavior of RT gradient measures may be potentially influenced by other phenomena, either endocardial or transmural. To address this question, in a subset of two hearts from Pin Group (Experiments #2 and #3) we recorded transmural potentials through 8 plunge needles (four electrodes, 3 mm spacing) and we measured the average of the epi-to-endo RT gradients over four needles (two in LAD region, two in the posterior interventricular artery area). Changes in transmural dispersion of repolarization over time were either limited (Experiment #2: Baseline 28 $\pm$ 25 ms vs. 1/2 Pin 24 $\pm$ 25 ms vs. 1/1 Pin 19 $\pm$ 22 ms, repeated-measures one-way ANOVA $p = 0.05$) or absent (Experiment #3: Baseline 20 $\pm$ 14 ms vs. 1/2 Pin 20 $\pm$ 14 ms vs. 1/1 Pin 20 $\pm$ 11 ms, $p = 0.82$). Transmural needle mapping has not been performed on the other hearts due not only this weak evidence, but also to its technical challenges, e.g., the risk for myocardial damage and potential onset of ischemia that could have compromised the accomplishment of the experiments. Furthermore, the low number of needle probes and their uneven positioning were likely responsible for the variability of these results across the experiments and the impossibility to give even a preliminary interpretation of the absence/presence of epi-endo dissociation. As a consequence, future works may rather envisage the inclusion of simultaneous endocardial mapping (e.g., with a

basket catheter) to explore additional mechanisms beyond epicardial repolarization heterogeneity more systematically.

Future research may include the comparison with other invasive features (e.g., from intracardiac or optical mapping), to better elucidate the mechanisms underlying body surface manifestations of repolarization dispersion, as well as their direction. For the same purpose, the use of *in silico* models may help validating BSPM features and possibly link them to specific mechanisms at lower scale.

In both datasets, drug injection provoked marked repolarization gradients, both globally at the level of the whole organ and locally between neighboring, smaller sites, and all examined BSPM parameters exhibited a consistent relation with regional and global invasive RT dispersion gradients. A potential perspective of this research may envision the inclusion of models with different interventions (e.g., to create sharp local/global repolarization gradients with globally/locally homogeneous repolarization, as it partially happened during experiment #3 from Pin Group) to investigate whether and how these forms of electrical unevenness selectively affect body surface potentials.

As explained in section 2, in keeping with (Cabasson and Meste, 2008), a fixed-length search window has been used for all electrodes to detect T-wave offset. While the range of values chosen has allowed for the segmentation of the entire T-wave with no spurious truncation in most of the BSPM leads, in other electrodes the time occurrence of T-wave end may have been slightly overestimated, with some impact on T-wave duration parameters. To overcome this issue, incorrect T_{OFF} time locations were usually fixed after visual inspection when possible, and our analysis confirmed that shifted detections did not affect significantly differences in duration between distinct drug states and explanted hearts.

Measures of QT interval duration and dispersion have been adjusted for heart rate using Bazett's equation, in spite of the lack of a clear consensus on the use of this formula for porcine models. To overcome this limitation, we also analyzed uncorrected values of QT duration and spatial variability, and we concluded that their time evolution was independent of heart rate, which is expected to be stable in explanted perfused hearts.

With regard to PCA assessment of T-wave, in this document we report a detailed analysis of only two PCA-derived indices, although we have investigated a larger number of PCA markers of T-wave from the state-of-the-art (e.g., the relative T-wave spatial residuum, T-wave planarity, total cosine R-to-T; Merri et al., 1989; Malik et al., 2000; Korhonen et al., 2009; Porthan et al., 2013), and evaluated their ability to measure repolarization heterogeneity in our database when using between one and three principal components. In line with the findings presented in section "2.3.4," all indices were characterized by an unexpected inverse correlation between T-wave complexity and ventricular recovery dispersion, therefore we considered it appropriate to include a few of them in this report to avoid redundancy. Moreover, as stated above, to clarify whether and how changes in AP downslope and cell-to-cell coupling affect PCA eigenvalues' extraction during drug injection, meaningful insights could be provided by computational models of cardiac repolarization at the single myocyte level, which may help exploring mechanisms at a lower scale than our epicardial sock (Laguna et al., 2016).

In this work propensity to ventricular arrhythmias was not systematically explored, as we mainly investigated how substrate-dependent repolarization abnormalities reflected on T-wave properties rather than those trigger-related. Preliminary research from our group on a similar dataset has shown that arrhythmia susceptibility is strongly influenced both by the trigger location and timing, but also by the properties of the underlying substrate (Bear et al., 2019b), and that in vulnerable hearts T-waves are longer, flatter and more asymmetric (Meo et al., 2020). However, the potential of electrocardiographic features as a tool for arrhythmogenesis assessment in this model deserves further investigation.

Finally, a systematic comparison with T-wave features from an equivalent 12-lead ECG could not be performed, as in most of the experiments electrodes with noisy/low voltage signals were located close to lead III and precordial leads (especially V5-V6) and removed. This may also be object of future investigation, for potential translation of the proposed T-wave analysis tools into clinical routine, where standard ECG is more commonly used.

CONCLUSION

This study investigated performance of several indices for the non-invasive assessment of different mechanisms of dispersion of ventricular repolarization from BSPMs. Our findings confirm that pathological alterations of cardiac recovery can be studied from body surface, and that a more detailed assessment of such aberrations can be obtained only if we look at multiple properties of T-wave, including duration, morphology and spatiotemporal organization. This research opens promising perspectives in the characterization of repolarization abnormalities, with potential applicability to clinical electrocardiology.

DATA AVAILABILITY STATEMENT

The raw data supporting the conclusions of this article will be made available by the authors, upon reasonable request. Requests to access the datasets should be directed to laura.bear@ihu-liryc.fr. A subset of the experimental data will be made available for the electrocardiographic imaging community, through the EDGAR project (http://www.ecg-imaging.org/), a collaborative effort by the Consortium for ECG Imaging.

ETHICS STATEMENT

The animal study was reviewed and approved by the Directive 2010/63/EU of the European Parliament on the protection of animals used for scientific purposes and the local ethical committee.

AUTHOR CONTRIBUTIONS

MM conceived and designed the study, implemented the signal processing methods, analyzed and interpreted the results, and drafted the manuscript. PB equally contributed to the implementation of the study, methodological considerations, interpretation of results, and manuscript revision. LB and MC designed and performed the experiments, and provided insights into the interpretation of the results. EA also helped with experimental data acquisition. MH and OB provided feedback on the outcome of the study from a clinical and mechanistic point of view, respectively. RD helped with the conception of the study, provided feedback about the implementation of the methods and the interpretation of the results, and revised the manuscript. All authors have significantly contributed to this work.

FUNDING

This study was supported by the French Government as part of the "Investments of the Future" program managed by the National Agency Research (ANR-10-IAHU04-LIRYC), and the Leducq transatlantic network of excellence RHYTHM transatlantic network (16CVD02).

REFERENCES

Altman, D. G., and Bland, J. M. (1999). Measuring agreement in method comparison studies. *Stat. Methods Med. Res.* 8, 135–160. doi: 10.1191/096228099673819272

Al-Zaiti, S. S., Runco, K. N., and Carey, M. G. (2011). Increased T wave complexity can indicate subclinical myocardial ischemia in asymptomatic adults. *J. Electrocardiol.* 44, 684–688. doi: 10.1016/j.jelectrocard.2011.07.017

Antzelevitch, C. (2001). Tpeak-Tend interval as an index of transmural dispersion of repolarization. *Eur. J. Clin. Invest.* 31, 555–557. doi: 10.1046/j.1365-2362.2001.00849.x

Antzelevitch, C. (2007). Heterogeneity and cardiac arrhythmias: an overview. *Heart Rhythm* 4, 964–972. doi: 10.1016/j.hrthm.2007.03.036

Antzelevitch, C., Shimizu, W., Yan, G. X., Sicouri, S., Weissenburger, J., Nesterenko, V. V., et al. (1999). The M cell: its contribution to the ECG and to normal and abnormal electrical function of the heart. *J. Cardiovasc. Electrophysiol.* 10, 1124–1152. doi: 10.1111/j.1540-8167.1999.tb00287.x

Antzelevitch, C., Sicouri, S., Di Diego, J. M., Burashnikov, A., Viskin, S., Shimizu, W., et al. (2007). Does Tpeak-Tend provide an index of transmural dispersion of repolarization? *Heart Rhythm* 4, 1114–1116; author reply 1116–1119.

Barrett, T. D., Hennan, J. K., Fischbach, P. S., O'Neill, B. P., Driscoll, E. M., and Lucchesi, B. R. (2001). Tedisamil and dofetilide-induced torsades de pointes, rate and potassium dependence. *Br. J. Pharmacol.* 132, 1493–1500. doi: 10.1038/sj.bjp.0703967

Baumert, M., Porta, A., Vos, M. A., Malik, M., Couderc, J. P., Laguna, P., et al. (2016). QT interval variability in body surface ECG: measurement, physiological basis, and clinical value: position statement and consensus guidance endorsed by the European heart rhythm association jointly with the ESC working group on cardiac cellular electroph. *Europace* 18, 925–944. doi: 10.1093/europace/euv405

Bear, L. R., Bouhamama, O., Cluitmans, M., Duchateau, J., Walton, R. D., Abell, E., et al. (2019a). Advantages and pitfalls of noninvasive electrocardiographic imaging. *J. Electrocardiol.* 57S, S15–S20.

Bear, L. R., Cluitmans, M., Abell, E., Belterman, C., Roger, J., Labrousse, L., et al. (2019b). A novel index to predict the ventricular locations associated with arrhythmia vulnerability. *Heart Rhythm Soc. Congress* 5S, S426–S521, doi: 10.1016/j.hrthm.2019.04.018

Bear, L. R., Walton, R. D., Abell, E., Coudière, Y., Haissaguerre, M., Bernus, O., et al. (2019c). Optical imaging of ventricular action potentials in a torso tank: a new platform for non-invasive electrocardiographic imaging validation. *Front. Physiol.* 10:146. doi: 10.3389/fphys.2019.00146

Bonizzi, P., De La Salud Guillem, M., Climent, A. M., Millet, J., Zarzoso, V., Castells, F., et al. (2010). Noninvasive assessment of the complexity and stationarity of the atrial wavefront patterns during atrial fibrillation. *IEEE Trans. Biomed. Eng.* 57, 2147–2157. doi: 10.1109/tbme.2010.2052619

Burnes, J. E., Ghanem, R. N., Waldo, A. L., and Rudy, Y. (2001). Imaging dispersion of myocardial repolarization, I: comparison of body-surface and epicardial measures. *Circulation* 104, 1299–1305. doi: 10.1161/hc3601.094276

Burton, F. L., and Cobbe, S. M. (2001). Dispersion of ventricular repolarization and refractory period. *Cardiovasc. Res.* 50, 10–23. doi: 10.1016/s0008-6363(01)00197-3

Cabasson, A., and Meste, O. (2008). Time delay estimation: a new insight into the Woody's method. *IEEE Signal Process. Lett.* 15, 573–576. doi: 10.1109/lsp.2008.2001558

De Ambroggi, L., Aimè, E., Ceriotti, C., Rovida, M., and Negroni, S. (1997). Mapping of ventricular repolarization potentials in patients with arrhythmogenic right ventricular dysplasia: principal component analysis of the ST-T waves. *Circulation* 96, 4314–4318. doi: 10.1161/01.cir.96.12.4314

Di Bernardo, D., Langley, P., and Murray, A. (2000). Dispersion of QT intervals: a measure of dispersion of repolarization or simply a projection effect? *Pacing Clin. Electrophysiol.* 23, 1392–1396. doi: 10.1111/j.1540-8159.2000.tb00968.x

Di Bernardo, D., and Murray, A. (2000). Explaining the T-wave shape in the ECG. *Nature* 403:40. doi: 10.1038/47409

Extramiana, F., and Antzelevitch, C. (2004). Amplified transmural dispersion of repolarization as the basis for arrhythmogenesis in a canine ventricular-wedge model of short-QT syndrome. *Circulation* 110, 3661–3666. doi: 10.1161/01.cir.0000143078.48699.0c

Fedorov, V., Glukhov, A., Ambrosi, C., Kostecki, G., Chang, R., Janks, D., et al. (2011). Effects of KATP channel openers diazoxide and pinacidil in coronary-perfused atria and ventricles from failing and non-failing human hearts. *J. Mol. Cell. Cardiol.* 51, 215–225. doi: 10.1016/j.yjmcc.2011.04.016

Fish, J. M., Di Diego, J. M., Nesterenko, V., and Antzelevitch, C. (2004). Epicardial activation of left ventricular wall prolongs QT interval and transmural dispersion of repolarization: implications for biventricular pacing. *Circulation* 109, 2136–2142. doi: 10.1161/01.cir.0000127423.75608.a4

Fuller, M. S., Sándor, G., Punske, B., Taccardi, B., MacLeod, R. S., Ershler, P. R., et al. (2000). Estimates of repolarization dispersion from electrocardiographic measurements. *Circulation* 102, 685–691. doi: 10.1161/01.cir.102.6.685

Ghuran, A., Batchvarov, V., Dilaveris, P., Färbom, P., Camm, A. J., and Malik, M. (2000). Reflex autonomic modulation of automatically measured repolarization parameters. *Pacing Clin. Electrophysiol.* 23, 1973–1976. doi: 10.1111/j.1540-8159.2000.tb07065.x

Hlaing, T., Guo, D., Zhao, X., DiMino, T., Greenspon, L., Kowey, P. R., et al. (2005). The QT and Tp-e intervals in left and right chest leads: comparison between patients with systemic and pulmonary hypertension. *J. Electrocardiol.* 38, 154–158. doi: 10.1016/j.jelectrocard.2005.06.028

Holt, J. H., Barnard, C. L., Lynn, M. S., and Svendsen, P. (1969). A study of the human heart as a multiple dipole electrical source in normal adult male subjects. *Circulation* 40, 687–696. doi: 10.1161/01.cir.40.5.687

Korhonen, P., Husa, T., Konttila, T., Tierala, I., Mäkijärvi, M., Väänänen, H., et al. (2009). Complex T-wave morphology in body surface potential mapping in prediction of arrhythmic events in patients with acute myocardial infarction and cardiac dysfunction. *Europace* 11, 514–520. doi: 10.1093/europace/eup051

Laguna, P., Martinez Cortes, J. P., and Pueyo, E. (2016). Techniques for Ventricular repolarization instability assessment from the ECG. *Proc. IEEE* 104, 392–415. doi: 10.1109/jproc.2015.2500501

Malik, M., Acar, B., Gang, Y. I., Yap, Y. G., Hnatkova, K., and John Camm, A. (2000). QT dispersion does not represent electrocardiographic interlead heterogeneity of ventricular repolarization. *J. Cardiovasc. Electrophysiol.* 11, 835–843. doi: 10.1111/j.1540-8167.2000.tb00061.x

Marill, K. A., Dorsey, P., Holmes, A., Muthal, K., Miller, E. S., and Xue, J. (2018). Is myocardial repolarization duration associated with repolarization

heterogeneity? *Ann. Noninvasive Electrocardiol.* 23:e12519. doi: 10.1111/anec.12519

Meijborg, V. M. F., Chauveau, S., Janse, M. J., Anyukhovsky, E. P., Danilo, P. R., Rosen, M. R., et al. (2015). Interventricular dispersion in repolarization causes bifid T waves in dogs with dofetilide-induced long QT syndrome. *Heart Rhythm* 12, 1343–1351. doi: 10.1016/j.hrthm.2015.02.026

Meo, M., Bonizzi, P., Bear, L., Cluitmans, M., Abell, E., Haïssaguerre, M., et al. (2020). Relation of surface T-wave to vulnerability to ventricular fibrillation in explanted structurally normal hearts. *Comput. Cardiol.* (in press).

Meo, M., Zarzoso, V., Meste, O., Latcu, D. G., and Saoudi, N. (2013). Catheter ablation outcome prediction in persistent atrial fibrillation using weighted principal component analysis. *Biomed. Signal Process. Control* 8, 958–968. doi: 10.1016/j.bspc.2013.02.002

Merri, M., Benhorin, J., and Alberti, M. (1989). Electrocardiographic quantitation of heterogeneity of ventricular repolarization. *Circulation* 80, 1301–1308. doi: 10.1161/01.cir.80.5.1301

Müller, M. (ed.). (2007). "Dynamic time warping," in *Information Retrieval for Music and Motion*, (Berlin: Springer), 69–84.

Nygårds, M. E., and Sörnmo, L. (1983). Delineation of the QRS complex using the envelope of the e.c.g. *Med. Biol. Eng. Comput.* 21, 538–547. doi: 10.1007/bf02442378

Okin, P. M., Devereux, R. B., Fabsitz, R. R., Lee, E. T., Galloway, J. M., and Howard, B. V. (2002). Principal component analysis of the T wave and prediction of cardiovascular mortality in American Indians: the strong heart study. *Circulation* 105, 714–719. doi: 10.1161/hc0602.103585

Opthof, T., Coronel, R., Wilms-Schopman, F. J. G., Plotnikov, A. N., Shlapakova, I. N., Danilo, P., et al. (2007). Dispersion of repolarization in canine ventricle and the electrocardiographic T wave: Tp-e interval does not reflect transmural dispersion. *Heart Rhythm* 4, 341–348. doi: 10.1016/j.hrthm.2006.11.022

Padrini, R., Bova, S., Cargnelli, G., Piovan, D., and Ferrari, M. (1992). Effects of pinacidil on guinea-pig isolated perfused heart with particular reference to the proarrhythmic effect. *Br. J. Pharmacol.* 105, 715–719. doi: 10.1111/j.1476-5381.1992.tb09044.x

Peeters, H. A. P., Sippensgroenewegen, A., Wever, E. F. D., Grimbergen, C. A., Hauer, R. N. W., and Medina, E. O. R. D. E. (1998). Electrocardiographic identification of abnormal ventricular depolarization and repolarization in patients with idiopathic ventricular fibrillation. *J. Am. Coll. Cardiol.* 31, 1406–1413. doi: 10.1016/s0735-1097(98)00120-x

Piccirillo, G., Rossi, P., Mitra, M., Quaglione, R., Dell'Armi, A., Di Barba, D., et al. (2013). Indexes of temporal myocardial repolarization dispersion and sudden cardiac death in heart failure: any difference? *Ann. Noninvasive Electrocardiol.* 18, 130–139. doi: 10.1111/anec.12005

Porthan, K., Viitasalo, M., Toivonen, L., Havulinna, A. S., Jula, A., Tikkanen, J. T., et al. (2013). Predictive value of electrocardiographic T-wave morphology parameters and T-wave peak to T-wave end interval for sudden cardiac death in the general population. *Circulation* 6, 690–696. doi: 10.1161/circep.113.000356

Prenner, S. B., Shah, S. J., Goldberger, J. J., and Sauer, A. J. (2016). Repolarization heterogeneity: beyond the QT interval. *J. Am. Heart Assoc.* 5:e003607.

Priori, S. G., Mortara, D. W., Napolitano, C., Diehl, L., Paganini, V., Cantù, F., et al. (1997). Evaluation of the spatial aspects of T-wave complexity in the long-QT syndrome. *Circulation* 96, 3006–3012. doi: 10.1161/01.cir.96.9.3006

Pueyo, E., Corrias, A., Virág, L., Jost, N., Szél, T., Varró, A., et al. (2011). A multiscale investigation of repolarization variability and its role in cardiac arrhythmogenesis. *Biophys. J.* 101, 2892–2902. doi: 10.1016/j.bpj.2011.09.060

Ramirez, J., Orini, M., Mincholé, A., Monasterio, V., Cygankiewicz, I., de Luna, A. B., et al. (2017). T-wave morphology restitution predicts sudden cardiac death in patients with chronic heart failure. *J. Am. Heart Assoc.* 6:e005310.

Sassi, R., and Mainardi, L. T. (2011). An estimate of the dispersion of repolarization times based on a biophysical model of the ECG. *IEEE Trans. Biomed. Eng* 58, 3396–3405. doi: 10.1109/tbme.2011.2166263

Sheridan, P. J., Marques, J. L. B., Newman, C. M. H., Heller, S. R., and Clayton, R. H. (2010). Rate-dependent measures of repolarization predict inducibility of ventricular arrhythmias. *Europace* 12, 553–560. doi: 10.1093/europace/euq024

Smetana, P., Schmidt, A., Zabel, M., Hnatkova, K., Franz, M., Huber, K., et al. (2011). Assessment of repolarization heterogeneity for prediction of mortality in cardiovascular disease: peak to the end of the T wave interval and nondipolar repolarization components. *J. Electrocardiol.* 44, 301–308. doi: 10.1016/j.jelectrocard.2011.03.004

Srinivasan, N. T., Orini, M., Providencia, R., Simon, R., Lowe, M., Segal, O. R., et al. (2019). Differences in the upslope of the precordial body surface ECG T wave reflect right to left dispersion of repolarization in the intact human heart. *Heart Rhythm* 16, 943–951. doi: 10.1016/j.hrthm.2018.12.006

Straus, S. M. J. M., Kors, J. A., De Bruin, M. L., Van Der Hooft, C. S., Hofman, A., Heeringa, J., et al. (2006). Prolonged QTc interval and risk of sudden cardiac death in a population of older adults. *J. Am. Coll. Cardiol.* 47, 362–367. doi: 10.1016/j.jacc.2005.08.067

Taccardi, B., Punske, B. B., Lux, R. L., MacLeod, R. S., Ershler, P. R., Dustma, T. J., et al. (2007). Useful lessons from body surface mapping. *J. Cardiovasc. Electrophysiol.* 9, 773–786. doi: 10.1111/j.1540-8167.1998.tb00965.x

Van Huysduynen, B. H., Swenne, C. A., Draisma, H. H. M., Antoni, M. L., Van De Vooren, H., Van Der Wall, E. E., et al. (2005). Validation of ECG indices of ventricular repolarization heterogeneity: a computer simulation study. *J. Cardiovasc. Electrophysiol.* 16, 1097–1103. doi: 10.1111/j.1540-8167.2005.40758.x

Vicente, J., Johannesen, L., Mason, J. W., Crumb, W. J., Pueyo, E., Stockbridge, N., et al. (2015). Comprehensive T wave morphology assessment in a randomized clinical study of dofetilide, quinidine, ranolazine, and verapamil. *J. Am. Heart Assoc.* 4:e001615.

Vijayakumar, R., Silva, J. N. A., Desouza, K. A., Abraham, R. L., Strom, M., Sacher, F., et al. (2014). Electrophysiologic substrate in congenital long QT syndrome: noninvasive mapping with electrocardiographic imaging (ECGI). *Circulation* 130, 1936–1943. doi: 10.1161/circulationaha.114.011359

Vinzio Maggio, A. C., Paula, M., Laciar, E., and David, P. (2012). "Quantification of ventricular repolarization dispersion using digital processing of the surface ECG," in *Advances in Electrocardiograms - Methods and Analysis*, ed. R. M. Millis (London: IntechOpen).

Xia, Y., Liang, Y., Kongstad, O., Liao, Q., Holm, M., Olsson, B., et al. (2005). In vivo validation of the coincidence of the peak and end of the T wave with full repolarization of the epicardium and endocardium in swine. *Heart Rhythm* 2, 162–169. doi: 10.1016/j.hrthm.2004.11.011

Yan, G. X., and Antzelevitch, C. (1998). Cellular basis for the normal T wave and the electrocardiographic manifestations of the long-QT syndrome. *Circulation* 98, 1928–1936. doi: 10.1161/01.cir.98.18.1928

Zabel, M., Acar, B., Klingenheben, T., Franz, M. R., Hohnloser, S. H., and Malik, M. (2000). Analysis of 12-lead T-wave morphology for risk stratification after myocardial infarction. *Circulation* 102, 1252–1257. doi: 10.1161/01.cir.102.11.1252

Zabel, M., and Malik, M. (2001). Predictive value of T-wave morphology variables and QT dispersion for postmyocardial infarction risk assessment. *J. Electrocardiol.* 34, 27–35. doi: 10.1054/jelc.2001.28822

Zabel, M., Portnoy, S., and Franz, M. R. (1995). Electrocardiographic indexes of dispersion of ventricular repolarization: an isolated heart validation study. *J. Am. Coll. Cardiol.* 25, 746–752. doi: 10.1016/0735-1097(94)00446-w

Zhang, J., Sacher, F., Hoffmayer, K., O'Hara, T., Strom, M., Cuculich, P., et al. (2015). Cardiac electrophysiological substrate underlying the ECG phenotype and electrogram abnormalities in brugada syndrome patients. *Circulation* 131, 1950–1959. doi: 10.1161/circulationaha.114.013698

Conflict of Interest: MC was part-time employed by Philips Research.

The remaining authors declare that the research was conducted in the absence of any commercial or financial relationships that could be construed as a potential conflict of interest.

frontiers in Physiology

ORIGINAL RESEARCH
published: 21 August 2020
doi: 10.3389/fphys.2020.01005

Evaluation of a Fully Automatic Measurement of Short-Term Variability of Repolarization on Intracardiac Electrograms in the Chronic Atrioventricular Block Dog

Agnieszka Smoczyńska[1]†, David J. Sprenkeler[1]†, Alfonso Aranda[2], Jet D.M. Beekman[1], Alexandre Bossu[1], Albert Dunnink[1], Sofieke C. Wijers[1], Berthold Stegemann[2], Mathias Meine[3] and Marc A. Vos[1]*

[1]Department of Medical Physiology, University Medical Center Utrecht, Utrecht, Netherlands, [2]Medtronic Bakken Research Center, Maastricht, Netherlands, [3]Department of Cardiology, University Medical Center Utrecht, Utrecht, Netherlands

OPEN ACCESS

Edited by:
Ruben Coronel,
University of Amsterdam,
Netherlands

Reviewed by:
Daniel M. Johnson,
The Open University, United Kingdom
Peter Taggart,
University College London,
United Kingdom

***Correspondence:**
Agnieszka Smoczyńska
a.smoczynska@umcutrecht.nl

†These authors have contributed equally to this work

Specialty section:
This article was submitted to Cardiac Electrophysiology, a section of the journal Frontiers in Physiology

Received: 20 April 2020
Accepted: 23 July 2020
Published: 21 August 2020

Citation:
Smoczyńska A, Sprenkeler DJ, Aranda A, Beekman JDM, Bossu A, Dunnink A, Wijers SC, Stegemann B, Meine M and Vos MA (2020) Evaluation of a Fully Automatic Measurement of Short-Term Variability of Repolarization on Intracardiac Electrograms in the Chronic Atrioventricular Block Dog. Front. Physiol. 11:1005. doi: 10.3389/fphys.2020.01005

Background: Short-term variability (STV) of repolarization of the monophasic action potential duration (MAPD) or activation recovery interval (ARI) on the intracardiac electrogram (EGM) increases abruptly prior to the occurrence of ventricular arrhythmias in the chronic AV-block (CAVB) dog model. Therefore, this parameter might be suitable for continuous monitoring of imminent arrhythmias using the EGM stored on an implanted device. However, 24/7 monitoring would require automatic STV_{ARI} measurement by the device.

Objective: To evaluate a newly developed automatic measurement of STV_{ARI} for prediction of dofetilide-induced torsade de pointes (TdP) arrhythmias in the CAVB-dog.

Methods: Two retrospective analyses were done on data from recently performed dog experiments. (1) In seven anesthetized CAVB-dogs, the new automatic STV_{ARI} method was compared with the gold standard STV_{MAPD} at baseline and after dofetilide administration (0.025 mg/kg in 5 min). (2) The predictive value of the automatic method was compared to currently used STV_{ARI} methods, i.e., slope method and fiducial segment averaging (FSA) method, in 11 inducible (≥3 TdP arrhythmias) and 10 non-inducible CAVB-dogs.

Results: (1) The automatic measurement of STV_{ARI} had good correlation with STV_{MAPD} ($r^2 = 0.89$; $p < 0.001$). Bland-Altman analysis showed a small bias of 0.06 ms with limits of agreement between −0.63 and 0.76 ms. (2) STV_{ARI} of all three methods was significantly different between inducible and non-inducible dogs after dofetilide. The automatic method showed the highest predictive performance with an area under the ROC-curve of 0.93, compared to 0.85 and 0.87 of the slope and FSA methods, respectively. With a threshold of STV set at 1.69 ms, STV_{ARI} measured with the automatic method had a sensitivity of 0.91 and specificity of 0.90 in differentiating inducible from non-inducible subjects.

Conclusion: We developed a fully-automatic method for measurement of STV_{ARI} on the intracardiac EGM that can accurately predict the occurrence of ventricular arrhythmias in the CAVB-dog. Future integration of this method into implantable devices could provide the opportunity for 24/7 monitoring of arrhythmic risk.

Keywords: ventricular arrhythmias, short-term variability of repolarization, automatic measurement, electrogram, activation recovery interval

INTRODUCTION

Sudden cardiac arrest due to ventricular tachyarrhythmias, such as ventricular tachycardia (VT) or ventricular fibrillation (VF), is an important cause of death in patients with structural heart disease, accounting for approximately 50% of all cardiovascular deaths (Al-Khatib et al., 2018). Despite the widespread availability of automatic external defibrillators (AEDs), the prognosis after an out-of-hospital cardiac arrest remains poor, with an estimated survival rate around 10% (Benjamin et al., 2017). Therefore, focus has shifted toward preventive strategies in patients at high risk of sudden cardiac death (SCD).

Multiple randomized controlled trials have shown a survival benefit of the implantable cardioverter-defibrillator (ICD) in the prevention of SCD in patients with ischemic or non-ischemic cardiomyopathy and a reduced left ventricular ejection fraction (LVEF) below 35% (Moss et al., 2002; Bardy et al., 2005). Since the publication of these landmark trials, both European and American guidelines recommend ICD implantation as a class I indication for these patients (Priori et al., 2015; Al-Khatib et al., 2018). Nevertheless, while the ICD is highly effective in the prevention of SCD by termination of sustained ventricular tachyarrhythmias, the device does not prevent the arrhythmia itself from occurring. Despite being potentially life-saving, ICD discharges have also shown to cause severe psychological distress, depression, and anxiety and can reduce the quality of life in ICD recipients (Schron et al., 2002; Bostwick and Sola, 2007). Moreover, recurrent ICD shocks increase the number of hospital admissions and reduce the lifespan of the generator. Therefore, adjunctive therapy such as radiofrequency ablation of the arrhythmogenic substrate or administration of anti-arrhythmic drugs is often necessary to reduce the shock burden (Reddy et al., 2007; Van Herendael et al., 2010). However, both these treatment modalities expose the patient to potential adverse effects. In an ideal situation, the implanted device would not only terminate an arrhythmia that is already occurring but can also monitor if an arrhythmia is imminent and initiate preventive therapy (e.g., temporarily altering pacing rate) before the arrhythmia starts. However, the question remains how the device could predict if an arrhythmia is upcoming.

The chronic complete AV-block (CAVB) dog model is an arrhythmogenic animal model that is often used to evaluate new anti-arrhythmic agents or to study the mechanisms of ventricular tachyarrhythmias, mainly torsade de pointes (TdP) arrhythmias, in the remodeled heart. In this model, it has been shown that beat-to-beat variation of the monophasic action potential duration (MAPD), quantified as short-term variability (STV), increases abruptly a couple of minutes prior to the occurrence of TdP, after these animals are challenged with a pro-arrhythmic drug (Thomsen et al., 2007). Interestingly, the increase in STV was not seen in dogs that did not develop TdP after the same pro-arrhythmic challenge. While STV seems a promising parameter in predicting upcoming arrhythmic events, the use of monophasic action potential (MAP) catheters is not feasible for 24/7 monitoring in a clinical setting. Recently, it has been shown that STV of the activation recovery interval (STV_{ARI}) of the electrogram (EGM) derived from the right ventricular ICD lead can be used as surrogate for the MAPD and accurately reflects arrhythmic risk in the CAVB dog under both anesthetized and awake conditions (Wijers et al., 2018). This would imply that the EGMs stored on the device could be used in the prediction of upcoming arrhythmic events. In the aforementioned study, however, the measurement of STV_{ARI} was done offline by use of semi-automatic custom-made software. In order to integrate continuous STV_{ARI} calculation in an implantable device, an automatic measurement is required that determines STV_{ARI} precisely, consistently, and in real-time without manual correction.

In the present study, we describe a new automatic method for measuring STV_{ARI} and compare this method with the current methodologies used to measure STV. In addition, we evaluate the potential of this automatic method in identifying imminent TdP arrhythmias in the CAVB dog model.

MATERIALS AND METHODS

Animal handling was in accordance with the "Directive 2010/63/EU of the European Parliament and of the Council of 22 September 2010 on the protection of animals used for scientific purposes" and the Dutch law, laid down in the Experiments on Animals Act. The Animal Experiment Committee of the University of Utrecht approved all experiments.

The current study is a retrospective analysis of data obtained during animal experiments performed in our laboratory between 2014 and 2017 and can be divided into two parts. In part 1, three different methods of STV_{ARI} measurement, including the newly developed automatic method, are compared to the golden standard STV_{MAPD}. In part 2, the predictive value of the automatic method in identifying dogs inducible to TdP arrhythmias is evaluated and compared to the methods of STV_{ARI} measurement currently used in our department.

Animal Experiments

The standard experimental procedures have been described in detail previously (Dunnink et al., 2010, 2012). After premedication with

methadone 0.5 mg/kg, acepromazine 0.5 mg/kg, and atropine 0.02 mg/kg i.m., general anesthesia was induced *via* pentobarbital sodium 25 mg/kg i.v., and maintained by isoflurane 1.5% in O_2 and N_2O. During the experiments, 10 surface-ECG leads were recorded. Under aseptic conditions, the femoral artery and vein were dissected and sheaths were inserted. In the initial experiment, complete AV-block was created by radiofrequency ablation of the proximal His bundle. In the dogs included in part 1, a screw-in lead was placed in the right ventricular apex (RVA) *via* the jugular vein and connected to an internal pacemaker (Medtronic, Maastricht, The Netherlands), which was implanted subcutaneously. Subsequently, these dogs were left to remodel for at least 3 weeks during RVA pacing at the lowest captured rate, in the ventricular demand mode of ventricular pacing, sensing, and inhibition of pacing output in response to a sensed ventricular event (VVI). In contrast, the dogs selected for part 2 remodeled for at least 3 weeks on idioventricular rhythm (IVR).

At CAVB, a second experiment was performed to test for TdP susceptibility. Under general anesthesia, left and right ventricular (LV and RV) MAP catheters (Hugo Sachs Elektronik, March, Germany) and/or a duo-decapolar EGM catheter (St. Jude Medical, St. Paul, MN, USA) were inserted and advanced to the apex to record LV and RV MAPD and/or unipolar EGMs. A reference electrode was inserted in a superficial vein of the right hind leg. The I_{Kr} blocker dofetilide (0.025 mg/kg i.v., in 5 min or until the first TdP) was administered to test for inducibility of TdP arrhythmias. TdP was defined as a run of five or more short-coupled (occurring before the end of the T-wave) ectopic beats, with polymorphic twisting of the QRS-axis. If a TdP did not terminate by itself, the dog was defibrillated with 100 J by use of an external defibrillator. When ≥3 TdP's occurred in the first 10 min after the start of infusion, the dog was considered inducible. During baseline and dofetilide challenge, dogs had either IVR or were paced from the RVA by the RV MAP catheter with a cycle length of 1,000 ms.

Part 1 – Comparison of STV_{ARI} With STV_{MAPD}

For part 1, adult mongrel dogs were selected that had both a LV EGM catheter and a LV MAP catheter in place during the experiment and were challenged for TdP inducibility with dofetilide. Since the simultaneous use of both LV EGM and LV MAP catheters is not common practice in our laboratory, only seven dogs (weight 27 ± 3 kg, all females) were included. All these dogs remodeled during RVA pacing at the lowest captured rate (59 ± 9 bpm) and were tested for inducibility at VVI60.

Part 2 – Predictive Value of STV_{ARI} Measurements

For part 2, dogs were selected that had remodeled on IVR, had an LV EGM catheter inserted, and were challenged for TdP inducibility with dofetilide. Of a total of 33 dogs in our database, 12 were excluded for various reasons (**Figure 1**), among which too much ectopy defined as the baseline recording of 10 min containing <2 consecutive minutes without ectopic beats. The 21 included dogs (weight 24.5 ± 3.2 kg, 7 males, 14 females) consisted of 11 inducible (5 tested at IVR, 6 at VVI60, 6 males) and 10 non-inducible dogs (2 tested at IVR, 8 at VVI60, 1 male).

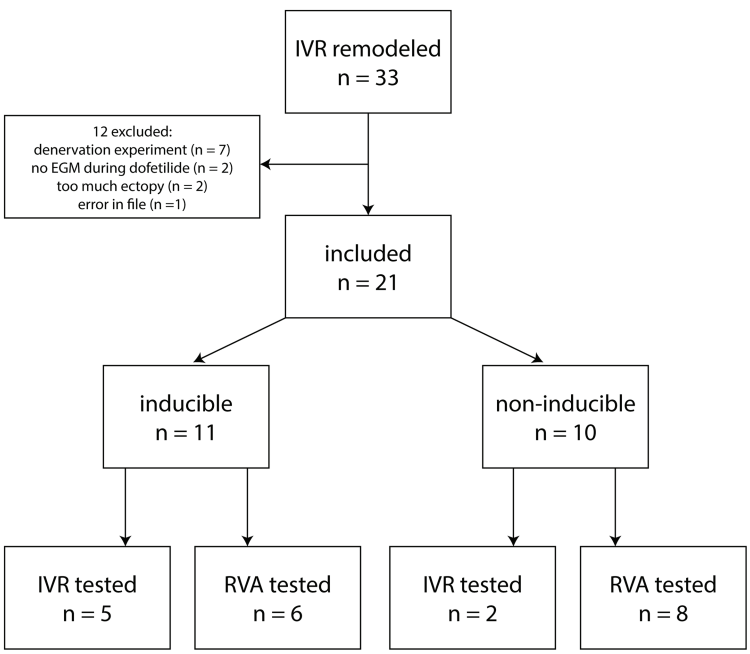

FIGURE 1 | Flowchart of dogs included in part 2.

Data Analysis

Both the surface ECG, LV MAPD, and LV unipolar EGM were recorded with EP Tracer (Cardiotek, Maastricht, The Netherlands) at a sampling frequency of 1,000 Hz. The RR-interval and QT-interval were measured offline with calipers on lead II. QT-interval was corrected for heart rate (QTc) with the van der Water formula (Van de Water et al., 1989). LV MAPD was measured semi-automatically from the initial peak until 80% of repolarization using custom-made software (AutoMAPD, MATLAB, MathWorks, Natick, MA, USA; **Figure 2A**). For comparison of STV_{MAPD} and STV_{ARI}, we chose the EGM electrode that was located most closely to the MAP catheter under fluoroscopy. For calculation of STV_{ARI}, the ARI of consecutive beats was determined by use of three different methods:

- Slope method (**Figure 2B**): ARI of every beat was measured from the minimum dV/dt of the QRS-complex to the maximum dV/dt of the T-wave, irrespectively of the morphology of the T-wave (either positive, negative, or biphasic).
- Fiducial segment averaging (FSA) method (**Figure 2C**): first, two fiducial points were defined, i.e., the minimum dV/dt of the QRS-complex as the ARI onset and the maximum dV/dt of the T-wave as the ARI offset. Using the method of FSA (Ritsema van Eck, 2002), all complexes were aligned separately around the ARI onset (**Figure 2CI**) and ARI offset (**Figure 2CII**) by cross-correlating the individual complex to the average of the other complexes until maximal correlation is achieved. The ARI of every single beat was then defined as the interval between the two fiducial points, taking the amount of shifting into account.
- Automatic method (**Figure 2D**): the obtained EGM signals were injected into an Evera ICD of Medtronic (sampling frequency 256 Hz) equipped with the algorithm to automatically determine STV in real-time. First, a complex was detected with the regular ventricular sensing method of the device (**Figure 2DI**). The QRS-complex was blanked to avoid interference in the T-wave end detection and was set at 140 ms (**Figure 2DII**). Once the QRS-complex was blanked, the first derivative of the resultant signal is calculated over time to detect changes in the slope. This gradient signal was then squared in order to make all data points positive and to emphasize slope changes in the signal (**Figure 2DII**). Finally, the T-wave end was defined as the point at 60% of the area under the curve of the resultant signal. The ARI is defined from the moment of ventricular sensing of the QRS-complex to the T-wave end, derived with this method (**Figure 2DI**).

Short-term variability of MAPD or ARI was calculated over 31 consecutive beats using the formula: $STV = \sum |D_{n+1} - D_n| / \left(30 \times \sqrt{2}\right)$, where D represents MAPD or ARI. For STV calculation, ectopic beats and the first post-extrasystolic beat were excluded from analysis. All measurements were performed both at baseline and after administration

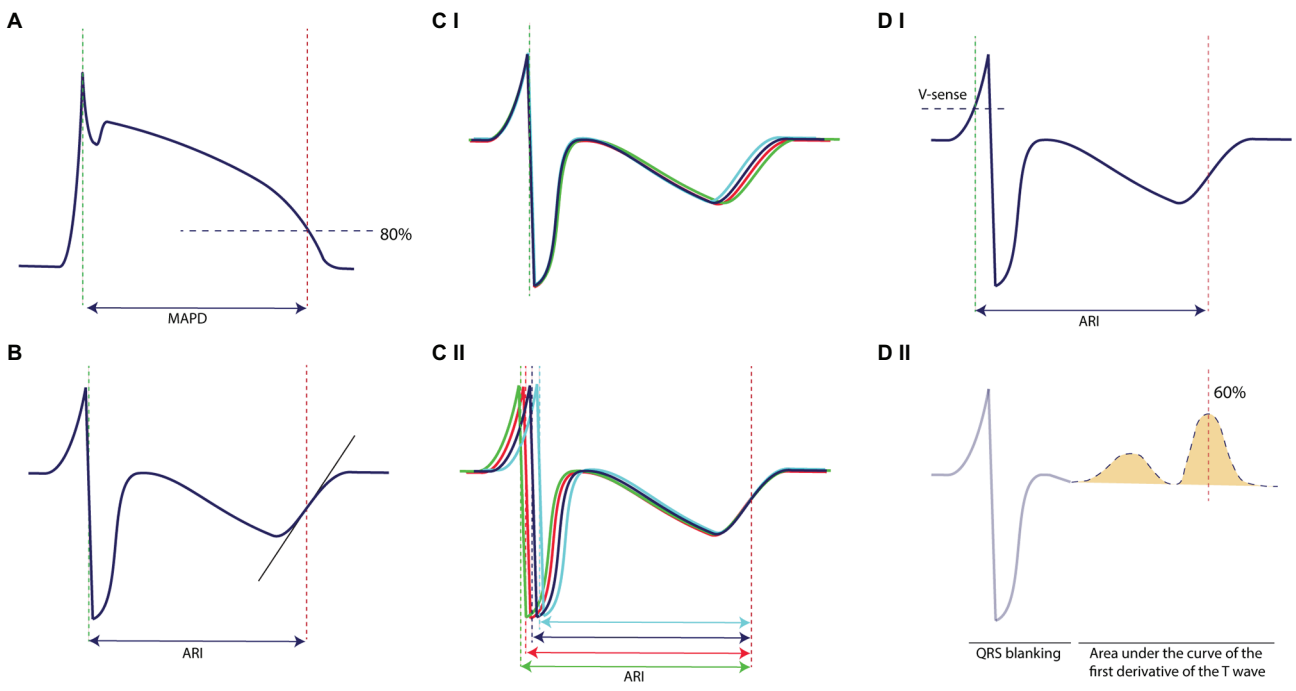

FIGURE 2 | Methodology of measurement on the monophasic action potential and the electrogram. **(A)** STV_{MAPD} is measured from the initial peak until 80% of repolarization. **(B)** STV_{ARI} measured with the slope method from the minimum dV/dt of the QRS-complex to the maximum dV/dt of the T-wave, irrespectively of the morphology of the T-wave. **(C)** (I) STV_{ARI} measured with fiducial segment averaging from the minimum dV/dt of the QRS-complex to (II) the maximum dV/dt of the T-wave, which also form the fiducial points of alignment. **(D)** STV_{ARI} measured with the new automatic method, (I) whereby ventricular sensing by conventional device methodology indicates the start of the determinant of repolarization and (II) the T-wave end is determined as 60% of the area under the curve of the first derivative of the T-wave.

of dofetilide. After dofetilide, parameters were determined just prior to the first ectopic beat. In the non-inducible dogs that did not show any ectopic beats, all parameters were assessed at the same time after start of dofetilide as measured in the inducible subjects.

Statistical Analysis

Numerical values are expressed as mean ± standard deviation (SD). Comparison of serial data was performed with a paired Student's *t*-test. Group comparison was done with an unpaired Student's *t*-test. Group comparison with both a within-subject variable and a between-subject variable was performed with a mixed analysis of variance (ANOVA) with Sidak's correction for multiple comparisons. The relation between the different STV modalities was analyzed by use of simple linear regression. In addition, Bland-Altman analysis was done to assess for systematic bias and limits of agreements. The area under the receiver operator characteristics (ROC) curve was used to evaluate the predictive power of the different STV_{ARI} methods. All statistical analyses were performed with GraphPad Prism 8.0 (GraphPad Software Inc., La Jolla, CA, USA). A value of $p < 0.05$ was considered as statistically significant.

RESULTS

Part 1 – Comparison of STV_{ARI} With STV_{MAPD}

Electrophysiological parameters at baseline and after dofetilide of the seven included animals are summarized in **Table 1**. From these seven animals, two were reproducibly inducible for TdP arrhythmias. All dogs were paced with a cycle length of 1,000 ms. As expected, dofetilide induced an increase in all repolarization parameters compared to baseline, including STV by all four different methods. MAPD and ARI_{slope} were comparable at baseline (251 ± 18 and 263 ± 21 ms, respectively, $p = 0.26$) and showed a similar increase after dofetilide (395 ± 53 and 396 ± 53 ms, respectively, $p = 0.98$). The highest values of STV, both at baseline and after dofetilide, were found when using the slope method (0.74 ± 0.26 and 2.67 ± 1.79 ms, respectively). The automatic method derived the lowest values of STV with a low SD (0.53 ± 0.24 ms at baseline and 1.52 ± 1.26 ms after dofetilide).

Figure 3 shows the regression analysis and Bland-Altman plots of the three different STV_{ARI} methods compared to the gold standard STV_{MAPD}. The slope method had a moderate correlation with STV_{MAPD} (r^2 of 0.68, $p < 0.001$). A systematic bias was found of −0.61 ms with increasing differences between the two methods at higher values. The limits of agreement of the Bland-Altman plot were −2.42 and 1.21 ms. The FSA method had a better correlation with an r^2 of 0.86 ($p < 0.001$). A small bias of −0.20 was found with limits of agreement between −0.99 and 0.62 ms. The new automatic method showed a very good correlation with STV_{MAPD} with an r^2 of 0.89 ($p < 0.001$). A negligibly small systematic bias was seen of 0.06 ms with a narrow bandwidth of agreement between −0.63 and 0.76 ms.

TABLE 1 | Electrophysiological parameters of part 1 ($n = 7$).

	Baseline	Dofetilide
RR (ms)	1,000	1,000
QT (ms)	350 ± 20	499 ± 57*
QTc (ms)	350 ± 20	499 ± 57*
$MAPD_{80}$ (ms)	251 ± 18	395 ± 53*
ARI (ms)	263 ± 21	396 ± 53*
STV_{MAPD} (ms)	0.58 ± 0.22	1.61 ± 1.37*
STV_{ARI} slope (ms)	0.74 ± 0.26	2.67 ± 1.79*
STV_{ARI} FSA (ms)	0.61 ± 0.21	1.97 ± 1.06*
STV_{ARI} automatic (ms)	0.53 ± 0.24	1.52 ± 1.26*

*Data expressed as mean ± SD in ms. *p < 0.05 compared to baseline.*

Part 2 – Predictive Value of STV_{ARI} Measurements

In **Table 2**, the electrophysiological parameters at baseline and after dofetilide of the 21 included dogs are shown, separately analyzed for inducible and non-inducible dogs. No differences were found in RR-interval, QT-interval, QTc-interval, or ARI between inducible and non-inducible dogs, both at baseline and after administration of dofetilide. In addition, at baseline, STV_{ARI} was similar for inducible and non-inducible dogs. After administration of dofetilide, the STV_{ARI} measured by all different methods increased significantly in the inducible dogs, creating a significant difference in STV_{ARI} between inducible and non-inducible subjects after dofetilide. **Figure 4** shows an example of the effect of dofetilide infusion on the three different methods of STV_{ARI} in both inducible and non-inducible dogs. While the non-inducible dog shows only a mild increase of STV_{ARI}, a prominent rise in STV is observed in the inducible dog prior to the occurrence of TdP arrhythmias.

The predictive performance of the three methods was evaluated, i.e., to what extent the different methods of STV_{ARI} were able to distinguish between dogs that were inducible versus those that were not inducible to drug-induced TdP arrhythmias. In **Figure 5**, the STV_{ARI} of the three methods is presented separately for inducible and non-inducible dogs, both at baseline and dofetilide. One can clearly see that, while STV_{ARI} measured with the slope and FSA method partly overlap for some inducible and non-inducible subjects after dofetilide, an almost total separation in STV_{ARI} between the two groups can be found with the new automatic measurement. This is further illustrated in the ROC-curves of the different methods. The automatic method results in the highest area under the curve (AUC) of 0.93 (95% CI 0.79–1.00), compared to an AUC of 0.85 (95% CI 0.69–1.00) and 0.87 (95% CI 0.72–1.00) of the slope method and FSA method, respectively. With a threshold set at 1.69 ms, the automatic method yields a sensitivity of 0.91 (95% CI 0.59–0.99) and a specificity of 0.90 (95% CI 0.55–0.99).

DISCUSSION

In the present study, we evaluated a fully automatic method of STV_{ARI} measurement in the CAVB dog model and compared this new method with the current gold standard STV_{MAPD} and two other methods used in our laboratory to derive STV_{ARI}

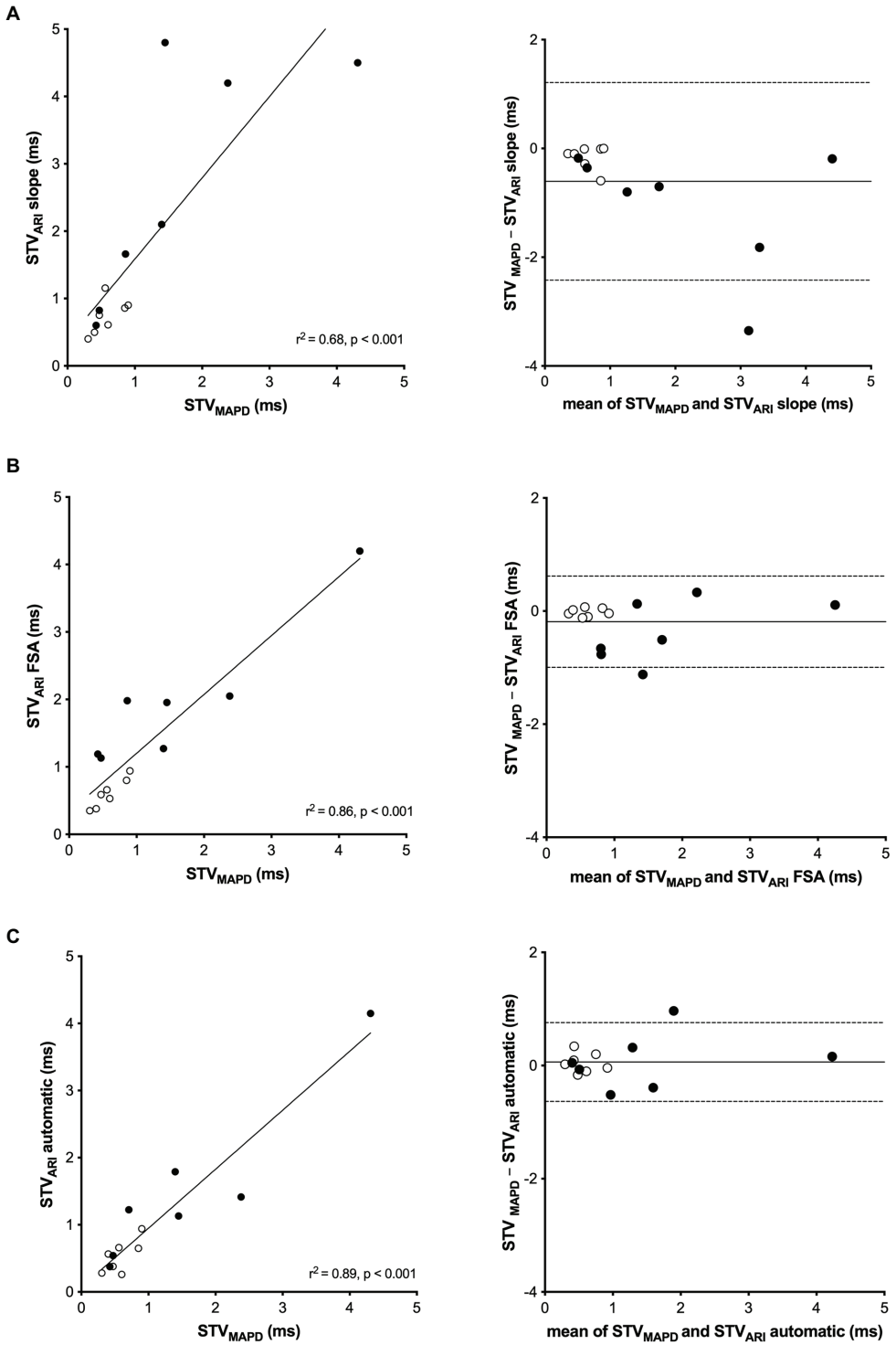

FIGURE 3 | Linear regression and Bland-Altman analysis of STV_{ARI} compared to STV_{MAPD}. **(A)** STV_{MAPD} vs. STV_{ARI} measured with the slope method. **(B)** STV_{MAPD} vs. STV_{ARI} measured with the fiducial segment averaging (FSA) method. **(C)** STV_{MAPD} vs. STV_{ARI} measured with the new automatic method.

from the intracardiac EGM. The results show that (1) STV_{ARI} determined with the automatic method is highly comparable to STV_{MAPD} both under baseline conditions and after dofetilide, (2) the automatically determined STV_{ARI} performs better in predicting imminent TdP arrhythmias after dofetilide administration compared to the current STV_{ARI} methods.

TABLE 2 | Electrophysiological parameters of part 2 (n = 21).

	Baseline			Dofetilide		
	Total (n = 21)	**I (n = 11)**	**NI (n = 10)**	**Total (n = 21)**	**I (n = 11)**	**NI (n = 10)**
RR (ms)	1,186 ± 255	1,263 ± 229	1,102 ± 267	1,197 ± 257	1,274 ± 219	1,111 ± 266
QT (ms)	395 ± 57	403 ± 59	387 ± 56	569 ± 72*	578 ± 76*	560 ± 75*
QTc (ms)	379 ± 59	380 ± 61	378 ± 59	522 ± 70*	554 ± 70*	550 ± 71*
ARI (ms)	296 ± 49	309 ± 52	282 ± 44	411 ± 88*	443 ± 85*	375 ± 80*
STV_{ARI} slope (ms)	1.44 ± 1.04	1.69 ± 1.33	1.15 ± 0.49	3.57 ± 2.75*	5.09 ± 3.07*	1.90 ± 0.64§
STV_{ARI} FSA (ms)	1.14 ± 0.68	1.20 ± 0.88	1.08 ± 0.42	2.41 ± 1.25*	3.11 ± 1.30*	1.63 ± 0.57§
STV_{ARI} automatic (ms)	1.00 ± 0.58	1.02 ± 0.63	0.98 ± 0.54	1.93 ± 0.95*	2.51 ± 0.96*	1.30 ± 0.33§

Data expressed as mean ± SD in ms.
$p < 0.05$ compared to baseline.
§$p < 0.05$ compared to inducible subject after dofetilide administration.*

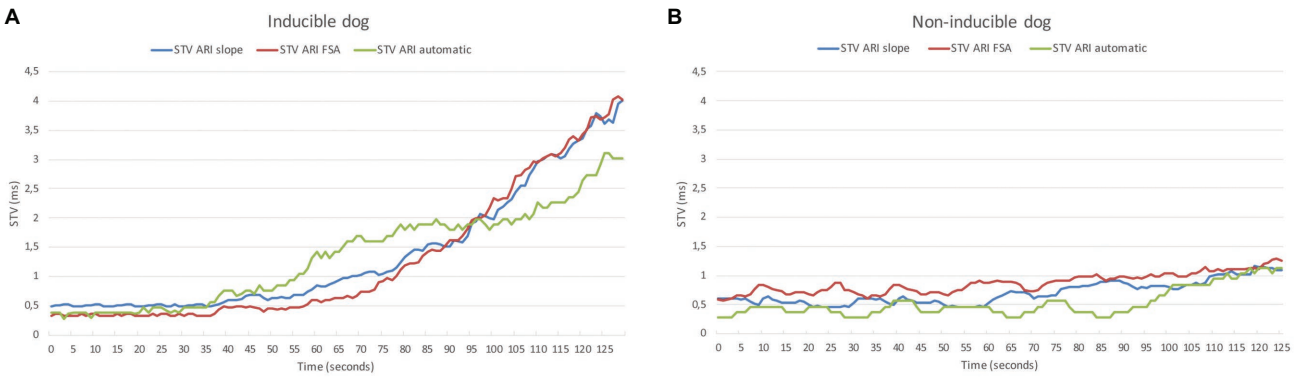

FIGURE 4 | Example of STV_{ARI} in inducible **(A)** and non-inducible dog **(B)** after dofetilide. STV_{ARI} measured with the slope method (blue line), fiducial segment averaging (FSA) method (red line), and automatic method (green line) from the moment of dofetilide infusion at time = 0 s.

STV as a Marker of Arrhythmic Risk

As expected, of all electrophysiological parameters, only STV could distinguish between inducible and non-inducible subjects after dofetilide administration (**Table 2**). Previous studies in the CAVB dog model have well established STV as a better marker of reduced repolarization reserve and arrhythmic risk compared to parameters of repolarization duration (QT, MAPD, or ARI) alone (Thomsen et al., 2004, 2006b). In pro-arrhythmic drug safety testing, STV was able to identify safe from unsafe drugs despite similar QT-prolongation (Thomsen et al., 2006a; Varkevisser et al., 2012). In addition, reduction of STV is highly related to efficacy of anti-arrhythmic agents (Bossu et al., 2017). Furthermore, a dynamic behavior of STV prior to the occurrence of arrhythmias has been demonstrated. Thomsen et al. (2007) observed that after infusion of dofetilide, STV of LV MAPD shows a steep increase just prior to the occurrence of TdP-arrhythmias, which was not present in the non-inducible dogs. The extent of the increase in STV has also been correlated to the severity of the arrhythmic outcome. A more severe arrhythmic outcome requiring >3 defibrillations during the 10 min following dofetilide infusion was preceded by a higher increase in STV of LV MAPD than a moderate arrhythmic outcome consisting of only self-terminating TdP-arrhythmias (Smoczyńska et al., 2019). Therefore, STV dynamics could provide important information about impending arrhythmic events. Since MAP-catheters are rarely used outside the experimental laboratory, recent interest shifted toward measurement of STV on the EGM of chronically implanted ICD-leads (Oosterhoff et al., 2010, 2011; Wijers et al., 2018). These leads have the advantage of recording EGMs 24/7 from a fixed position on the myocardium.

Different Methods of STV_{ARI} Compared to STV_{MAPD}

We demonstrated a moderate to good correlation between STV_{ARI} of the LV EGM with STV of the LV MAPD, with an r^2 ranging from 0.68 to 0.89 for the different methodologies (**Figure 3**). This finding is in line with results of previous studies. Oosterhoff et al. (2010) compared STV LV MAPD and STV LV ARI measured *via* an epicardial inserted screw electrode with a slightly lower sampling rate of 800 Hz. Despite the methodological differences, a similar correlation between STV ARI and STV MAPD was found with an r^2 of 0.71. Recently, Wijers et al. (2018) observed a positive correlation between STV MAPD and STV ARI from the RV EGM. Yet, the correlation was less strong (r^2 = 0.41), possibly due to differences in sampling frequency between the MAP and EGM recording (1,000 Hz for the MAP and 250 Hz, resampled to 400 Hz, for the EGM).

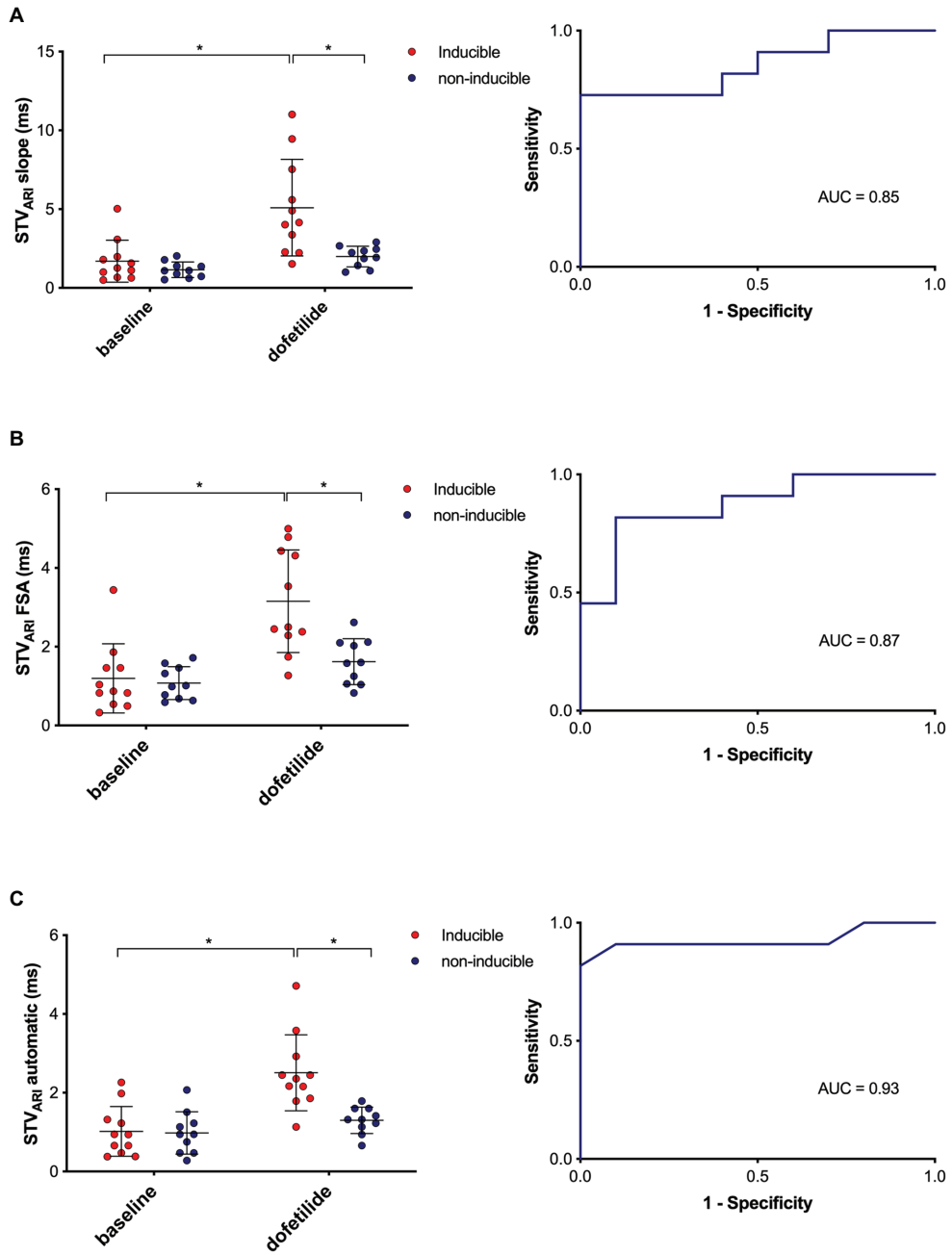

FIGURE 5 | Predictive value of different methods of STV_{ARI}. STV_{ARI} at baseline and after dofetilide in inducible (*red*) and non-inducible dogs (*blue*) measured with the slope method **(A)**, FSA method **(B),** and automatic method **(C)** with the corresponding receiver operating characteristics (ROC) curves. AUC, area under the curve. *$p < 0.05$.

When comparing the three methods of STV_{ARI}, important differences in correlation with STV_{MAPD} are found. The slope method had the weakest correlation with an r^2 of 0.68. This method incorporates the widely used definition of ARI as proposed by Wyatt (1980), who showed that the interval from the minimum dV/dt of the QRS-complex to the maximum dV/dt of the T-wave of the unipolar EGM correlates highly with action potential duration. While there is general consensus on the use of the minimum dV/dt as local depolarization time, a debate exists on whether the maximum or minimum dV/dt of the T-wave should be used as index of local repolarization time, especially when the T-wave is positive or biphasic. However, recent computer simulation and experimental studies have demonstrated that, irrespective of T-wave morphology, the upstroke of the T-wave coincides with repolarization

on the MAP and that the minimum dV/dt of a positive T-wave represents remote repolarization (Coronel et al., 2006; Western et al., 2015). Therefore, we have chosen to use maximal upstroke as index of local repolarization for all T-wave morphologies (negative, positive, or biphasic). Nevertheless, most of the EGMs used for the analysis had negative upsloping T-waves, possibly due to their location in the apex of the heart. Therefore, the definition of ARI offset does not seem the reason for the weak correlation of the slope method with MAPD. While at baseline STV_{ARI} by the slope method is more or less similar to STV_{MAPD}, the discrepancy between the two methods starts to arise after dofetilide (**Figure 3A**). This is further illustrated by the Bland-Altman plot, which shows that the systematic bias of the slope method increases at higher average values. The explanation for this bias is probably related to the inaccuracy of determining maximal dV/dt of the T-wave at longer ARIs. After infusion of dofetilide, the ARI prolongs and the T-wave widens. Hence, the upstroke of the T-wave becomes less steep, making it difficult to determine the exact point of maximal dV/dt for every beat, which introduces measurement error. Since the STV formula uses absolute differences between consecutive ARI, there is no cancellation of measurement error, resulting in a higher STV.

STV_{ARI} measured with the FSA method shows better correlation with STV_{MAPD} and has no clear systematic bias on the Bland-Altman plot. FSA has been developed to accurately determine intervals between certain fiducial points and thus prevents the aforementioned problem of summation of measurement error that is caused by determining ARI for every single beat separately. FSA determines the fiducial points (i.e., ARI onset and the ARI offset) for all complexes at once. After alignment of the complexes around these fiducial points, the individual shifts between the fiducial points are used to calculate the individual ARIs. Therefore, the beat-to-beat variations in ARI are preserved, without introducing repeated measurement error. However, while this method shows improved accuracy in measurement of STV compared to the slope method, the use of FSA for continuous monitoring in an implanted device is problematic, because it requires a lot of computing memory for the calculation to be performed. Therefore, we tried to come up with a new method that is both easy to calculate and will not drain the battery of the device, even when used continuously.

The automatic method of STV_{ARI} shows an excellent correlation with STV_{MAPD} with an r^2 of 0.89 despite the lower sampling frequency of 256 Hz in the device compared to the MAP signal of 1,000 Hz. Oosterhoff et al. (2010) investigated the effect of sampling frequency on measurement of STV of the ARI and MAPD by using computer simulations. The lowest sampling frequency of 250 Hz had the highest SD at low values of STV compared to a higher sampling frequency of 1,000 Hz. However, in the current study, the automatic method of STV_{ARI} yielded lower or similar SDs at the sampling frequency of 250 Hz as the other methodologies at a sampling frequency of 1,000 Hz. The automatic method may be more robust and able to perform well at a lower sampling frequency, because it determines the T-wave end based on the area under the slope of the first derivative of the signal, rather than one exact point in the original signal of the T-wave.

The Performance of STV_{ARI} in Prediction of TdP Arrhythmia

In part 2 of the study, the three different methods were evaluated on their ability to identify a change in STV_{ARI} prior to the occurrence of TdP arrhythmias in the inducible dogs. At baseline, all electrophysiological parameters including STV_{ARI} were similar for inducible and non-inducible dogs (**Table 2**). This is in contrast to the study by Thomsen et al. (2007), which already found a difference in STV_{MAPD} at baseline between inducible and non-inducible subjects. However, since the values of STV are very low at baseline, it is imaginable that you do not find a difference here. Nonetheless, after infusion of dofetilide, all three STV methods showed a significant higher STV_{ARI} in the inducible dogs prior to the occurrence of first ectopic beat compared to a similar timepoint in the non-inducible dogs. While the slope method derived the largest absolute difference of STV_{ARI} between inducible and non-inducible dogs (5.09 vs. 1.90 ms), there was also a high variability, with some dogs showing a very large increase in STV, while others had STV values comparable to the non-inducible subjects. This resulted in a lower predictive capability as seen by a lower AUC of the ROC curve. The same applies for the FSA method. On the other hand, the new automatic method could almost completely separate inducible from non-inducible dogs, resulting in a very high specificity and sensitivity. This would make it possible to define a specific threshold, above which STV_{ARI} predicts, with high accuracy, the occurrence of upcoming arrhythmic events.

Clinical Utility of the Intracardiac EGM

A number of clinical studies have evaluated the use of intracardiac EGMs for the prediction of ventricular tachyarrhythmias. Tereshchenko et al. (2009) analyzed the predictive value of QT variability index (QTVI) on intracardiac EGMs in 298 ICD-patients. The highest quartile of QTVI was an independent predictor of VT/VF and appropriate ICD therapy at a mean follow-up of 16 months. In addition, Sandhu et al. (2008) analyzed intracardiac T-wave alternans on the EGM during an electrophysiological study in 78 patients and found a positive predictive value of only 14% but a high negative predictive value of 95% at 1 year. However, both these studies investigated the use of intracardiac EGM parameters for prediction of sustained arrhythmias during long-term follow-up. Swerdlow et al. (2011) did a prospective multicenter study in 68 ICD-patients and evaluated T-wave alternans and non-alternans T-wave variability (TWA/V) on EGMs preceding spontaneous ventricular tachyarrhythmias. They observed a significantly higher TWA/V immediately before the occurrence of arrhythmias compared to four control recordings. In line with our findings, this study demonstrates that the intracardiac EGM can provide valuable information for the prediction of imminent life-threatening arrhythmias in a clinical setting. However, this information would only be useful if appropriate treatment, such as alternative pacing algorithms, can be initiated in time to prevent the arrhythmia from occurring. Recently, Wijers et al. (2017) demonstrated that temporary accelerated pacing (TAP) initiated just after the first ectopic beat can prevent TdP-arrhythmias in the CAVB-dog.

This is in agreement with clinical studies that show that rate-smoothing pacing algorithms can reduce the number of sustained ventricular tachyarrhythmias in ICD-recipients and patients with long QT-syndrome (Viskin et al., 2000; Wietholt et al., 2003). Therefore, by use of 24/7 automatic measurement of STV_{ARI} in real-time, the device does not have to wait for an ectopic beat to initiate pacing therapy but can already start with treatment when STV rises above a certain threshold value, thereby preventing the arrhythmia and ICD shock.

Limitations

Certain limitations of the current study must be addressed. First, this study had a retrospective study design, therefore, not all variables could be controlled. This resulted in important differences between the dogs used for the analyses of part 1 and part 2. For the comparison of STV_{MAPD} and STV_{ARI} in part 1, we were limited in the number of animals, because the combined use of an LV MAP and LV EGM catheter has only been done in a few experiments, in which dogs remodeled at low rate RVA pacing. It is known from previous (unpublished) data from our laboratory that control of the activation pattern by pacing can influence the course of electrical remodeling and the arrhythmic susceptibility compared to dogs that remodeled on their own IVR. Therefore, for part 2, in which no additional MAP catheter was required, we selected only IVR remodeled dogs to maintain a more homogeneous population. It should also be noted that we included both dogs that had IVR or were RVA paced at VVI60 during the experiment. Since the IVR can be lower than 60/min, these dogs could have longer APD and thus higher STV, which may act as a possible confounder in the differences of STV between inducible and non-inducible dogs. Finally, we should acknowledge that the CAVB dog is a specific animal model sensitive to triggered-activity based TdP arrhythmias. Therefore, extrapolation of the predictive value of STV to other types of ventricular tachyarrhythmias should be done with caution.

Future Directions

The development of a reliable and accurate automatic method of STV measurement on intracardiac EGMs is an important step toward clinical implementation of STV for continuous monitoring. Prospective observational studies in ICD patients should evaluate if the same increase in STV_{ARI} prior to the occurrence ventricular arrhythmias is observed in a clinical setting. Furthermore, in future studies, the detection mode of predicting imminent arrhythmias should be coupled to a fully automatic algorithm for the initiation of preventive pacing therapy, such as TAP. When a sudden increase of STV above a certain threshold value is detected, the device could then automatically start a pacing algorithm, thereby preventing the arrhythmia from occurring.

Conclusion

In conclusion, we have developed a new fully-automatic method of measuring STV_{ARI} on the intracardiac EGM in the CAVB dog model. This method is highly correlated to the gold standard STV_{MAPD} and can accurately identify a pro-arrhythmic rise in STV_{ARI} prior to the occurrence of dofetilide induced TdP-arrhythmias. This technique could be integrated in implantable devices for prediction of imminent ventricular tachyarrhythmias and initiation of preventive pacing therapy.

DATA AVAILABILITY STATEMENT

The raw data supporting the conclusions of this article will be made available by the authors, without undue reservation.

ETHICS STATEMENT

The animal study was reviewed and approved by The Animal Experiment Committee of the University of Utrecht.

AUTHOR CONTRIBUTIONS

AS and DS analyzed data and wrote the manuscript. AA developed the automatic algorithm. DS, JB, AB, AD, and SW did experimental work. BS and MM contributed to experimental concepts and design of the study. MV was responsible for organization of experiments and revised the manuscript thoroughly. All authors contributed to the article and approved the submitted version.

FUNDING

The research leading to these results has received funding from the framework of PREDICT II (Predicting sudden cardiac arrest 2) of the Dutch Cardiovascular Alliance, funded by the Public Private Partnership grant of the Dutch Heart Foundation (grant no. 2018B015).

REFERENCES

Al-Khatib, S. M., Stevenson, W. G., Ackerman, M. J., Bryant, W. J., Callans, D. J., Curtis, A. B., et al. (2018). 2017 AHA/ACC/HRS guideline for management of patients with ventricular arrhythmias and the prevention of sudden cardiac death: a report of the American College of Cardiology/American Heart Association Task Force on Clinical Practice Guidelines and the Heart Rhythm Society. *Heart Rhythm* 15, e73–e189. doi: 10.1016/j.hrthm.2017.10.036

Bardy, G. H., Lee, K. L., Mark, D. B., Poole, J. E., Packer, D. L., Boineau, R., et al. (2005). Amiodarone or an implantable cardioverter-defibrillator for congestive heart failure. *N. Engl. J. Med.* 352, 225–237. doi: 10.1056/NEJMoa043399

Benjamin, E. J., Blaha, M. J., Chiuve, S. E., Cushman, M., Das, S. R., Deo, R., et al. (2017). Heart disease and stroke statistics-2017 update: a report from the American Heart Association. *Circulation* 135, e146–e603. doi: 10.1161/CIR.0000000000000485

Bossu, A., Varkevisser, R., Beekman, H. D. M., Houtman, M. J. C., van der Heyden, M. A. G., and Vos, M. A. (2017). Short-term variability of repolarization is superior to other repolarization parameters in the evaluation of diverse antiarrhythmic interventions in the chronic atrioventricular block dog. *J. Cardiovasc. Pharmacol.* 69, 398–407. doi: 10.1097/FJC.0000000000000488

Bostwick, J. M., and Sola, C. L. (2007). An updated review of implantable cardioverter/defibrillators, induced anxiety, and quality of life. *Psychiatr. Clin. North Am.* 30, 677–688. doi: 10.1016/j.psc.2007.07.002

Coronel, R., de Bakker, J. M., Wilms-Schopman, F. J., Opthof, T., Linnenbank, A. C., Belterman, C. N., et al. (2006). Monophasic action potentials and activation recovery intervals as measures of ventricular action potential duration: experimental evidence to resolve some controversies. *Heart Rhythm* 3, 1043–1050. doi: 10.1016/j.hrthm.2006.05.027

Dunnink, A., Sharif, S., Oosterhoff, P., Winckels, S., Montagne, D., Beekman, J., et al. (2010). Anesthesia and arrhythmogenesis in the chronic atrioventricular block dog model. *J. Cardiovasc. Pharmacol.* 55, 601–608. doi: 10.1097/FJC.0b013e3181da7768

Dunnink, A., van Opstal, J. M., Oosterhoff, P., Winckels, S. K., Beekman, J. D., van der Nagel, R., et al. (2012). Ventricular remodelling is a prerequisite for the induction of dofetilide-induced torsade de pointes arrhythmias in the anaesthetized, complete atrio-ventricular-block dog. *Europace* 14, 431–436. doi: 10.1093/europace/eur311

Moss, A. J., Zareba, W., Hall, W. J., Klein, H., Wilber, D. J., Cannom, D. S., et al. (2002). Prophylactic implantation of a defibrillator in patients with myocardial infarction and reduced ejection fraction. *N. Engl. J. Med.* 346, 877–883. doi: 10.1056/NEJMoa013474

Oosterhoff, P., Tereshchenko, L. G., van der Heyden, M. A., Ghanem, R. N., Fetics, B. J., Berger, R. D., et al. (2011). Short-term variability of repolarization predicts ventricular tachycardia and sudden cardiac death in patients with structural heart disease: a comparison with QT variability index. *Heart Rhythm* 8, 1584–1590. doi: 10.1016/j.hrthm.2011.04.033

Oosterhoff, P., Thomsen, M. B., Maas, J. N., Atteveld, N. J., Beekman, J. D., VAN Rijen, H. V., et al. (2010). High-rate pacing reduces variability of repolarization and prevents repolarization-dependent arrhythmias in dogs with chronic AV block. *J. Cardiovasc. Electrophysiol.* 21, 1384–1391. doi: 10.1111/j.1540-8167.2010.01824.x

Priori, S. G., Blomstrom-Lundqvist, C., Mazzanti, A., Blom, N., Borggrefe, M., Camm, J., et al. (2015). 2015 ESC Guidelines for the management of patients with ventricular arrhythmias and the prevention of sudden cardiac death: The Task Force for the Management of Patients with Ventricular Arrhythmias and the Prevention of Sudden Cardiac Death of the European Society of Cardiology (ESC). Endorsed by: Association for European Paediatric and Congenital Cardiology (AEPC). *Eur. Heart J.* 36, 2793–2867. doi: 10.1093/eurheartj/ehv316

Reddy, V. Y., Reynolds, M. R., Neuzil, P., Richardson, A. W., Taborsky, M., Jongnarangsin, K., et al. (2007). Prophylactic catheter ablation for the prevention of defibrillator therapy. *N. Engl. J. Med.* 357, 2657–2665. doi: 10.1056/NEJMoa065457

Ritsema van Eck, H. J. (2002). Fiducial segment averaging to improve cardiac time interval estimates. *J. Electrocardiol.* 35, 89–93. doi: 10.1054/jelc.2002.37160

Sandhu, R. K., Costantini, O., Cummings, J. E., Poelzing, S., Rosenbaum, D. S., and Quan, K. J. (2008). Intracardiac alternans compared to surface T-wave alternans as a predictor of ventricular arrhythmias in humans. *Heart Rhythm* 5, 1003–1008. doi: 10.1016/j.hrthm.2008.04.003

Schron, E. B., Exner, D. V., Yao, Q., Jenkins, L. S., Steinberg, J. S., Cook, J. R., et al. (2002). Quality of life in the antiarrhythmics versus implantable defibrillators trial: impact of therapy and influence of adverse symptoms and defibrillator shocks. *Circulation* 105, 589–594. doi: 10.1161/hc0502.103330

Smoczyńska, A., Beekman, H. D. M., and Vos, M. A. (2019). The increment of short-term variability of repolarisation determines the severity of the imminent arrhythmic outcome. *Arrhythmia Electrophysiol. Rev.* 8, 166–172. doi: 10.15420/aer.2019.16.2

Swerdlow, C., Chow, T., Das, M., Gillis, A. M., Zhou, X., Abeyratne, A., et al. (2011). Intracardiac electrogram T-wave alternans/variability increases before spontaneous ventricular tachyarrhythmias in implantable cardioverter-defibrillator patients: a prospective, multi-center study. *Circulation* 123, 1052–1060. doi: 10.1161/CIRCULATIONAHA.110.986364

Tereshchenko, L. G., Fetics, B. J., Domitrovich, P. P., Lindsay, B. D., and Berger, R. D. (2009). Prediction of ventricular tachyarrhythmias by intracardiac repolarization variability analysis. *Circ. Arrhythm. Electrophysiol.* 2, 276–284. doi: 10.1161/CIRCEP.108.829440

Thomsen, M. B., Beekman, J. D., Attevelt, N. J., Takahara, A., Sugiyama, A., Chiba, K., et al. (2006a). No proarrhythmic properties of the antibiotics Moxifloxacin or Azithromycin in anaesthetized dogs with chronic-AV block. *Br. J. Pharmacol.* 149, 1039–1048. doi: 10.1038/sj.bjp.0706900

Thomsen, M. B., Oros, A., Schoenmakers, M., van Opstal, J. M., Maas, J. N., Beekman, J. D., et al. (2007). Proarrhythmic electrical remodelling is associated with increased beat-to-beat variability of repolarisation. *Cardiovasc. Res.* 73, 521–530. doi: 10.1016/j.cardiores.2006.11.025

Thomsen, M. B., Verduyn, S. C., Stengl, M., Beekman, J. D., de Pater, G., van Opstal, J., et al. (2004). Increased short-term variability of repolarization predicts d-sotalol-induced torsades de pointes in dogs. *Circulation* 110, 2453–2459. doi: 10.1161/01.CIR.0000145162.64183.C8

Thomsen, M. B., Volders, P. G., Beekman, J. D., Matz, J., and Vos, M. A. (2006b). Beat-to-beat variability of repolarization determines proarrhythmic outcome in dogs susceptible to drug-induced torsades de pointes. *J. Am. Coll. Cardiol.* 48, 1268–1276. doi: 10.1016/j.jacc.2006.05.048

Van de Water, A., Verheyen, J., Xhonneux, R., and Reneman, R. S. (1989). An improved method to correct the QT interval of the electrocardiogram for changes in heart rate. *J. Pharmacol. Methods* 22, 207–217. doi: 10.1016/0160-5402(89)90015-6

Van Herendael, H., Pinter, A., Ahmad, K., Korley, V., Mangat, I., and Dorian, P. (2010). Role of antiarrhythmic drugs in patients with implantable cardioverter defibrillators. *Europace* 12, 618–625. doi: 10.1093/europace/euq073

Varkevisser, R., Wijers, S. C., van der Heyden, M. A., Beekman, J. D., Meine, M., and Vos, M. A. (2012). Beat-to-beat variability of repolarization as a new biomarker for proarrhythmia in vivo. *Heart Rhythm* 9, 1718–1726. doi: 10.1016/j.hrthm.2012.05.016

Viskin, S., Glikson, M., Fish, R., Glick, A., Copperman, Y., and Saxon, L. A. (2000). Rate smoothing with cardiac pacing for preventing torsade de pointes. *Am. J. Cardiol.* 86, 111k–115k. doi: 10.1016/s0002-9149(00)01228-5

Western, D., Hanson, B., and Taggart, P. (2015). Measurement bias in activation-recovery intervals from unipolar electrograms. *Am. J. Physiol. Heart Circ. Physiol.* 308, H331–H338. doi: 10.1152/ajpheart.00478.2014

Wietholt, D., Kuehlkamp, V., Meisel, E., Hoffmann, E., Stellbrink, C., Neuzner, J., et al. (2003). Prevention of sustained ventricular tachyarrhythmias in patients with implantable cardioverter-defibrillators—the PREVENT study. *J. Interv. Card. Electrophysiol.* 9, 383–389. doi: 10.1023/A:1027407829958

Wijers, S. C., Bossu, A., Dunnink, A., Beekman, J. D. M., Varkevisser, R., Aranda Hernandez, A., et al. (2017). Electrophysiological measurements that can explain and guide temporary accelerated pacing to avert (re)occurrence of torsade de pointes arrhythmias in the canine chronic atrioventricular block model. *Heart Rhythm* 14, 749–756. doi: 10.1016/j.hrthm.2017.02.007

Wijers, S. C., Sprenkeler, D. J., Bossu, A., Dunnink, A., Beekman, J. D. M., Varkevisser, R., et al. (2018). Beat-to-beat variations in activation-recovery interval derived from the right ventricular electrogram can monitor arrhythmic risk under anesthetic and awake conditions in the canine chronic atrioventricular block model. *Heart Rhythm* 15, 442–448. doi: 10.1016/j.hrthm.2017.11.011

Wyatt, R. (1980). "Comparison of estimates of activation and recovery times from bipolar and unipolar electrograms to in vivo transmembrane action potential durations" in *Proc IEEE/Engineering Med Biol Soc 2nd Annu Conf*; September 28-30, 1980; Washington, DC, 22–25.

Conflict of Interest: AA and BS were employed by the Bakken Research Center in Maastricht of Medtronic.

The remaining authors declare that the research was conducted in the absence of any commercial or financial relationships that could be construed as a potential conflict of interest.

frontiers in Physiology

ORIGINAL RESEARCH
published: 31 August 2020
doi: 10.3389/fphys.2020.01115

No Association Between T-peak to T-end Interval on the Resting ECG and Long-Term Incidence of Ventricular Arrhythmias Triggering ICD Interventions

Peter Michalek[1], Sasha Benjamin Hatahet[2], Martin Svetlosak[3], Peter Margitfalvi[3], Iveta Waczulikova[4], Sebastian Trnovec[1], Allan Böhm[2,5], Ondrej Benacka[1,3] and Robert Hatala[2,3]*

[1] Faculty of Medicine, Comenius University in Bratislava, Bratislava, Slovakia, [2] Faculty of Medicine, Slovak Medical University in Bratislava, Bratislava, Slovakia, [3] Department of Arrhythmias and Cardiac Pacing, The National Institute of Cardiovascular Diseases, Bratislava, Slovakia, [4] Faculty of Mathematics, Physics and Informatics, Comenius University in Bratislava, Bratislava, Slovakia, [5] Department of Acute Cardiology, The National Institute of Cardiovascular Diseases, Bratislava, Slovakia

OPEN ACCESS

Edited by:
Marek Malik,
Imperial College London,
United Kingdom

Reviewed by:
Gary Tse,
Second Hospital of Tianjin Medical University, China
Tong Liu,
Tianjin Medical University, China

***Correspondence:**
Peter Michalek
peter.michalek@cinre.sk;
pepon1@gmx.net

Specialty section:
This article was submitted to Cardiac Electrophysiology, a section of the journal Frontiers in Physiology

Received: *27 May 2020*
Accepted: *11 August 2020*
Published: *31 August 2020*

Citation:
Michalek P, Hatahet SB, Svetlosak M, Margitfalvi P, Waczulikova I, Trnovec S, Böhm A, Benacka O and Hatala R (2020) No Association Between T-peak to T-end Interval on the Resting ECG and Long-Term Incidence of Ventricular Arrhythmias Triggering ICD Interventions. Front. Physiol. 11:1115. doi: 10.3389/fphys.2020.01115

Background and Objectives: Potential of using the T-peak to T-end (TpTe) interval as an electrocardiographic parameter reflecting the transmural dispersion of ventricular repolarization (TDR) to identify patients (pts.) with higher risk of malignant ventricular arrhythmias (MVA) for better selection of candidates for implantable cardioverter-defibrillator (ICD) in primary prevention (PP) of sudden cardiac death (SCD) remains controversial. The primary objective of this study was to investigate the relationship between the TpTe interval in patient's preimplantation resting 12-lead electrocardiogram (ECG) and the incidence of MVA resulting in appropriate ICD intervention (AI). The secondary objective was to assess its relationship to overall mortality.

Methods: A total of 243 consecutive pts. with severe left ventricular (LV) systolic dysfunction after myocardial infarction (MI) with a single-chamber ICD for PP of SCD from one implantation center were included. Excluded were all pts. with any other disease that could interfere with the indication of ICD implantation. Primarily investigated intervals were measured manually in accordance with accepted methodology. Data on ICD interventions were acquired from device interrogation during regular outpatient visits. Survival data were collected from the databases of health insurance and regulatory authorities.

Results: We did not find a significant relationship between the duration of the TpTe interval and the incidence of MVA (71.5 ms in pts. with MVA vs. 70 ms in pts. without MVA; $p = 0.408$). Similar results were obtained for the corrected TpTe interval (TpTec) and the ratio of TpTe to QT interval (76.3 ms vs. 76.5 ms; $p = 0.539$ and 0.178 vs. 0.181; $p = 0.547$, respectively). There was also no significant difference between the duration of TpTe, TpTec and TpTe/QT ratio in pts. groups by overall mortality (71.5 ms in the deceased group vs. 70 ms in the survivors group; HR 1.01; 95% CI, 0.99–1.02;

p = 0.715, 76.3 ms vs. 76.5 ms; HR 1.01; 95% CI, 0.99–1.02; p = 0.208 and 0.178 vs. 0.186; p = 0.116, respectively).

Conclusion: This study suggests no significant association of overall or MVA-free survival with ECG parameters reflecting TDR (TpTe, TpTec) in patients with systolic dysfunction after MI and ICD implanted for primary prevention.

Keywords: electrocardiography, primary prevention of sudden cardiac death, transmural dispersion of ventricular repolarization, T-peak to T-end, ventricular tachyarrhythmia

INTRODUCTION

Under physiological conditions, the sequence of electrical activation and recovery of the heart is optimally synchronized in order to minimize heterogeneity of repolarization. The heterogeneity of repolarization processes (dispersion of repolarization) creates undesirable potential gradients between individual areas and layers of the myocardium, leading to a potentially proarrhythmogenic milieu.

In 1991, for the first time Sicouri and Antzelevitch described the electrophysiological properties of a hitherto unknown subpopulation of cardiomyocytes located in the deep subepicardial layer in both chambers of canine hearts (Sicouri and Antzelevitch, 1991). These M cells have distinct electrophysiological properties positioning them between cells of the cardiac conduction system and contractile cardiomyocytes. They are therefore a substrate for the existence of transmural dispersion of repolarization (TDR) across the ventricular myocardial wall. The end of the T wave on a resting 12-lead electrocardiogram (ECG) reflects the complete repolarization of the action potential (AP) of M cells, while its peak indicates the terminal phase of epicardial cells AP (Shimizu and Antzelevitch, 1998). Hence, the electrocardiographic parameter reflecting TDR is the interval from the peak of the T wave to its end (T-peak to T-end, TpTe). For the first time in the human heart, the presence of M cells was confirmed by Drouin et al. (1995), but the first clinical research was not conducted until 9 years later, when (Watanabe et al., 2004) demonstrated an association between TpTe prolongation (which reflects TDR accentuation) and a higher incidence of malignant ventricular arrhythmias. In the experiment, several authors described the electrophysiological mechanism of these processes (Antzelevitch et al., 1991; Yan et al., 2001; Gupta et al., 2008; Antzelevitch, 2010).

TpTe parameter subsequently became the subject of clinical research, but its results remain controversial (Lellouche et al., 2007; Letsas et al., 2009; Smetana et al., 2011; Morin et al., 2012; Porthan et al., 2013; Rosenthal et al., 2015). At present, even the very concept of association between TpTe and TDR is being questioned (Srinivasan et al., 2019), which only adds further doubts to its clinical validity (Malik et al., 2019).

Considering practical clinical application, it is most important to specify the potential of ECG measurements of the TpTe interval for the purpose of identifying patients at risk for malignant ventricular arrhythmias. Such a parameter would be desirable for improved patient selection for primary prevention of sudden cardiac death (SCD) using an implantable cardioverter-defibrillator (ICD). The unmet need for more precise patient selection for ICD implantation is not only due to the economic burden (García-Pérez et al., 2014), but also to the multifaceted ethical aspects (Strömberg et al., 2014) and well known complications of ICD therapy (Olde Nordkamp et al., 2016).

The primary objective of this study was to investigate the relationship between the duration of TpTe interval in patient's resting 12-lead ECG and the incidence of malignant ventricular arrhythmias (MVA). A strictly defined population of patients with severe left ventricular systolic dysfunction after myocardial infarction (MI) with an ICD implanted for primary prevention of SCD and who did not require pacing was selected. In this population, the occurrence of malignant ventricular tachyarrhythmias can be very accurately identified by long-term permanent monitoring of heart rhythm by ICD. The secondary objective was to evaluate TpTe's relationship to overall mortality and to analyze other clinical predictors of mortality.

MATERIALS AND METHODS

All consecutive patients who were implanted with an ICD in the years 2006–2015 in the primary prevention of SCD from the ICD register of the National Institute of Cardiovascular Diseases in Bratislava, Slovakia, were selected. Post-MI heart failure (HF) with left ventricular systolic dysfunction with an ejection fraction $\leq$ 35% was the principal inclusion criterion. To minimize the effect of other electrical disorders of the heart on the analyzed ECG parameters, only patients with single-chamber devices were included (as such disorders typically require implantation of dual-chamber or resynchronization ICD systems). Excluded from the analysis were patients:

- with ICD implanted for primary prevention of SCD due to another heart disease,
- with history of any arrhythmia and/or treatment with any antiarrhythmic drugs except beta blockers,
- with need of permanent ventricular pacing,
- with incomplete documentation and/or poor quality ECG recordings.

All patients were indicated and subsequently followed-up by the same team of physicians and the implantation procedure was in most cases performed by a single implanter (PM).

Last available ECG recording made prior to ICD implantation was used for measuring the ECG parameters. Standard 12-lead ECG recordings with a paper speed of 25 mm per second and an amplitude of 10 mm/mV were available and manual measurements of heart rate, QRS complex length, and QT interval were used. The QT interval was measured according to Goldenberg et al. (2006) and the duration of the QRS complex according to Turagam et al. (2013). The TpTe interval was measured from the top of the T wave to its end by the Tangent method (Rosenthal et al., 2017; **Figure 1**). The peak of the T wave was determined to be the most positive or the most negative amplitude from the isoelectric line. The intersection of the tangent with the descending part of the T wave and the isoelectric line was defined as the end of the T wave. All measurements were performed in lead V5 in accordance with the accepted methodology, leads V4 and V6 were used as alternative leads, respectively (Haarmark et al., 2009). The lead was omitted from the measurement if the most positive or negative deflection was less than 1.5 mm. The Bazett's formula (Bazett, 1920) was used to calculate the corrected QT and TpTe intervals. All measurements were performed by single investigator (SBH). All recordings were scanned in high resolution on a Brother MFC-J5335DW scanner and measurements were performed in EP Calipers version 1.19 (EP Studios, Inc., Paris, FR).

Sustained ventricular tachycardia including torsades de pointes and ventricular fibrillation were considered as malignant ventricular arrhythmias. Data on ICD interventions (appropriate and inappropriate) were acquired from device interrogation during regular outpatient visits. All ICD therapies (antitachycardia pacing or shocks) for sustained ventricular tachycardia or ventricular fibrillation were considered as appropriate. Survival data were collected from the databases of health insurance and regulatory authorities.

Statistical Analysis

Clinical and demographic data were analyzed using the methods of descriptive and inferential statistics. In the case of continuous data with a normal distribution tested by the Shapiro-Wilk test, we present the means and standard deviations (SD), the characteristics with an asymmetric distribution are described by the median and the first and third quartiles (IQR). Categorical data are presented as absolute and relative counts (a percentage of the respective total).

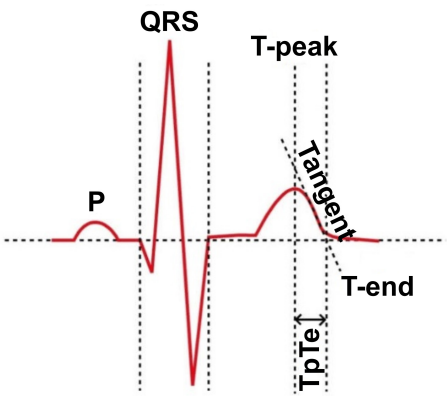

FIGURE 1 | The Tangent method of TpTe measurement, adopted from Yılmaz (2017).

The between-group differences for normally distributed continuous variables were tested by a two-tailed unpaired Student's t test. In the case of a significant deviation from the normal distribution a non-parametric Mann-Whitney test was used. Associations between categorical characteristics were tested by chi-square (χ^2) tests. The effects of predictors on the primary and secondary endpoints are expressed as the respective odds ratios (OR), or hazard ratios (HR, as a form of immediate risk of the event). More precisely, OR (HR) expresses the ratio of a patient's odds of having the observed event (occurrence of malignant ventricular arrhythmias, or death), if the value of the analyzed predictor increases by 1, relative to his/her odds at the original value of the predictor. Consequently, if the OR (HR) > 1, the risk of the event among those in the comparison category ("cases") will increase compared to those in the reference category ("controls"). The ORs (HRs) are presented together with the 95% confidence intervals (95% CI).

Statistical analyses were performed using Microsoft Office Excel 2010 (Microsoft Corporation, Redmond, US) and Stats Direct 3.2.7 (Stats Direct Ltd., Cheshire, United Kingdom). All $P-$values were considered significant at a two$-$tailed $P-$value of < 0.05.

RESULTS

From a total of 243 patients, appropriate ICD interventions were documented in 39.5% of patients, while 10.3% of patients had inappropriate interventions. The median time to first appropriate intervention (AI) was 23 months (IQR 7.5–43.0). The median follow-up was 62.6 months (IQR 41.4–91.6) and 69.5% of patients survived at the end of follow-up. Patients in the group with appropriate ICD interventions had a significantly better 3-year survival (92.7% vs. 82.3%, $P = 0.022$, **Table 1**).

We did not find a significant relationship between the duration of the TpTe interval and the incidence of appropriate ICD interventions when analyzing TpTe differences in patient groups by primary endpoint (71.5 ms, IQR 62.0–80.0 in the group with AI vs. 70.0 ms, IQR 62.0–85.0 in the group without AI, P = 0.408). Similar results were obtained for the corrected TpTe interval (TpTec) and the ratio of TpTe to QT interval (76.3 ms, IQR 65.5–85.4 in the group with AI vs. 76.5 ms, IQR 65.7–91.2 in group without AI, $P = 0.539$ and 0.178 ± 0.037 vs. 0.181 ± 0.040, $P = 0.547$, respectively, **Table 1**). The distribution of TpTec data in both groups is presented in **Figure 2**.

Results of fitting the multinomial logistic regression models to the data did not reveal any significant explanatory variables for the event of appropriate intervention, but gender. We have found male gender to be significantly associated with higher proportion of appropriate ICD interventions on the univariate analysis (HR = 2.29; 95% CI, 1.06–4.94; $P = 0.034$) and this

TABLE 1 | Clinical characteristics and follow-up data of patients grouped by the occurrence of appropriate ICD interventions.

Characteristics	Category (units)	Total	With AI ICD	Without AI ICD	*P*-value
Number of cases	(%)	243 (100%)	96 (39.5%)	147 (60.5%)	n.a.
Age	(Years)	58.8 ± 9.81	59.0 ± 9.39	58.3 ± 10.10	0.557
Gender	Female	30 (12.3%)	7 (7.3%)	23 (15.7%)	0.072
	Male	213 (87.7%)	89 (92.7%)	124 (84.3%)	
BMI	(kg/m^2)	29.0 ± 4.79	29.5 ± 5.07	28.7 ± 4.60	0.184
Smoker	Yes	29 (11.9%)	11 (11.5%)	18 (12.2%)	0.853
	No	214 (88.1%)	85 (88.5%)	129 (87.8%)	
Diabetes mellitus	Yes	76 (31.3%)	27 (28.1%)	49 (33.3%)	0.479
	No	167 (68.7%)	69 (71.9%)	98 (66.7%)	
NYHA II and III	Yes	235 (96.7%)	94 (97.9%)	141 (95.9%)	0.485
	No	8 (3.3%)	2 (2.1%)	6 (4.1%)	
sBP	(mmHg)	126.1 ± 16.02	127.4 ± 15.48	125.3 ± 16.35	0.316
dBP	(mmHg)	79.1 ± 9.74	79.8 ± 9.51	78.6 ± 9.88	0.341
HR	(min^{-1})	68.0 (61.0–77.0)	67.5 (60.5–79.5)	68.0 (61.0–77.0)	0.773
LVEF	(%)	30 (25–32)	30 (25–31.5)	30 (25–32)	0.640
S-CREAT	(μmol/l)	92 (80–104)	94 (81–104)	91 (78–104)	0.643
CKD-EPI GFR	(ml/min/1.73 m^2)	76.2 (64.6–92.5)	76.7 (65.7–91.3)	76.0 (62.9–93.2)	0.889
TpTe	(ms)	71.0 (62.0–83.0)	71.5 (62.0–80.0)	70.0 (62.0–85.0)	0.408
TpTec	(ms)	76.5 (65.6–89.8)	76.3 (65.5–85.4)	76.5 (65.7–91.2)	0.539
TpTe/QT	(ms/ms)	0.180 ± 0.038	0.178 ± 0.037	0.181 ± 0.040	0.547
Median follow-up	(months)	62.6 (41.4–91.6)	80.1 (54.3–99.6)	53.3 (35.1–77.5)	< 0.001
3-year survival rate	Dead	33 (13.6%)	7 (7.3%)	26 (17.7%)	0.022[a]
	Survived	210 (86.4%)	89 (92.7%)	121 (82.3%)	

Continuous data are presented as means ± standard deviations, or as medians with lower – upper quartiles. Categorical data are presented as absolute counts with percent of column total. [a]logrank test from Kaplan-Meier analysis. AI ICD, appropriate intervention(s) of ICD device; BMI, body mass index; NYHA, classification of heart failure symptoms according to New York Heart Association; sBP, systolic blood pressure; dBP, diastolic blood pressure; HR, heart rate; LVEF, left ventricular ejection fraction; S-CREAT, serum creatinine; CKD-EPI GFR, estimated glomerular filtration rate according to Chronic Kidney Disease Epidemiology Collaboration; TpTe, T-peak to T-end interval; TpTec, corrected T-peak to T-end interval; TpTe/QT, T-peak to T-end and QT intervals ratio; n.a., not applicable.

contribution was maintained also on the multivariate analysis (HR = 2.32; 95% CI, 1.06–5.09; $P = 0.035$).

There was also no significant difference between the duration of TpTe, TpTec and TpTe/QT ratio in patient groups by overall mortality (71.5 ms, IQR 62.0–80.0 in the deceased group vs. 70.0 ms, IQR 62.0–85.0 in the survivors group, HR 1.01; 95% CI, 0.99–1.02; $P = 0.715$ and 76.3 ms, IQR 65.5–85.4 vs. 76.5 ms, IQR 65.7–91.2, HR 1.01; 95% CI, 0.99–1.02; $P = 0.208$ and 0.178 ± 0.038 vs. 0.186 ± 0.039; $P = 0.116$ respectively, **Table 2**). From other ECG indices, the only significant difference was observed between the duration of uncorrected QT intervals in patient groups by overall mortality (396.4 ± 43.08 ms in the deceased group vs. 415.0 ± 46.04 ms in the survivors group, $P = 0.003$, **Table 3**).

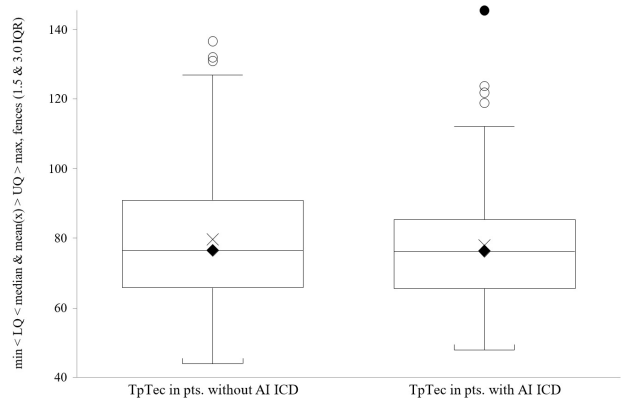

FIGURE 2 | TpTec interval in patients without/with appropriate ICD interventions.

Significant factors affecting mortality included: higher age (HR 1.06; 95% CI, 1.04–1.09; $P < 0.001$), lower ejection fraction of left ventricle (HR 0.93; 95% CI, 0.89–0.97; $P = 0.001$), higher serum creatinine (HR 1.01; 95% CI, 1.01–1.02; $P < 0.001$), lower glomerular filtration rate (HR 0.98; 95% CI, 0.97–0.99; $P < 0.001$), higher heart rate (HR 1.02; 95% CI, 1.00–1.03; $P = 0.024$) and lower BMI (HR 0.94; 95% CI, 0.89–0.98; $P = 0.009$). There was a 1.7-fold higher risk of death in patients with diabetes (HR 1.67; 95% CI, 1.05–2.66; $P = 0.031$). No significant difference in survival between smokers and non-smokers was observed (HR 0.84; 95% CI, 0.40–1.75; $P = 0.642$, **Table 2**).

DISCUSSION

According to our knowledge, this work is the first attempt to analyze the relationship of the TpTe parameter and the incidence of ventricular tachyarrhythmias in a strictly defined population

TABLE 2 | Clinical characteristics and follow-up data of patients grouped by overall survival.

Characteristics	Category (units)	Dead	Survived	HR (95% CI)	*P*-value
Number of cases	(%)	74 (30.5%)	169 (69.5%)	n.a.	n.a.
Age	(Years)	62.7 ± 8.46	56.7 ± 9.82	1.06 (1.04–1.09)	< 0.001
Gender	Female	12 (16.2%)	18 (10.7%)	1.31 (0.70–2.42)[a]	0.399
	Male	62 (83.8%)	151 (89.3%)		
BMI	(kg/m^2)	27.9 ± 5.17	29.5 ± 4.53	0.94 (0.89–0.98)	0.009
Smoker	Yes	8 (10.8%)	21 (12.4%)	0.84 (0.40–1.75)[a]	0.642
	No	66 (89.2%)	148 (87.6%)		
Diabetes mellitus	Yes	30 (40.5%)	46 (27.2%)	1.67 (1.05–2.66)[a]	0.031
	No	44 (59.5%)	123 (72.8%)		
NYHA II and III	Yes	74 (100%)	161 (95.3%)	∞	0.110
	No	0 (0%)	8 (4.7%)		
sBP	(mmHg)	125.5 ± 14.77	126.4 ± 16.57	0.99 (0.98–1.01)	0.229
dBP	(mmHg)	78.3 ± 7.95	79.4 ± 10.43	0.99 (0.96–1.01)	0.194
HR	(min^{-1})	70 (64–86)	67 (60–75)	1.02 (1.00–1.03)	0.024
LVEF	(%)	27.7 ± 4.86	29.8 ± 5.44	0.93 (0.89–0.97)	0.001
S-CREAT	(μmol/l)	96 (81–113)	91 (79–102)	1.01 (1.01–1.02)	< 0.001
CKD-EPI GFR	(ml/min/1.73 m^2)	71.9 (54.3–88.0)	77.7 (67.8–94.5)	0.98 (0.97–0.99)	< 0.001
TpTe	(ms)	71.5 (62.0–80.0)	70 (62.0–85.0)	1.01 (0.99–1.02)	0.715
TpTec	(ms)	76.3 (65.5–85.4)	76.5 (65.7–91.2)	1.01 (0.99–1.02)	0.208
TpTe/QT	(ms/ms)	0.178 ± 0.038	0.186 ± 0.039	n.a.	0.116
Median follow-up	(Months)	38.2 (27.2–63.0)	74.7 (52.1–96.3)	n.a.	< 0.001
Appropriate intervention of ICD device (at least 1)[b]	Yes	28 (37.8%)	68 (40.2%)	0.68 (0.42–1.09)[a]	0.108
	No	46 (62.2%)	101 (59.8%)		
Median time to first appropriate intervention	(Months)	14.6 (5.0–23.0)	27.8 (7.8–48.0)	n.a.	0.007

Continuous data are presented as means ± standard deviations, or as medians with lower – upper quartiles. Categorical data are presented as absolute counts with percent of column total. [a]The ratio of the odds of having an event in the upper row category to the odds of having an event in the lower row category of the predictor variable. [b]At the end of the follow-up. HR, hazard ratio; BMI, body mass index; NYHA, classification of heart failure symptoms according to New York Heart Association; sBP, systolic blood pressure; dBP, diastolic blood pressure; HR, heart rate; LVEF, left ventricular ejection fraction; S-CREAT, serum creatinine; CKD-EPI GFR, estimated glomerular filtration rate according to Chronic Kidney Disease Epidemiology Collaboration; TpTe, T-peak to T-end interval; TpTec, corrected T-peak to T-end interval; TpTe/QT, T-peak to T-end and QT intervals ratio; AI ICD, appropriate intervention(s) of ICD device; n.a., not applicable.

TABLE 3 | Duration of QRS complex and QT(c) intervals in studied patients groups.

Characteristics	Units	Total	With AI ICD	Without AI ICD	*P*-value
Number of cases	(%)	243 (100%)	96 (39.5%)	147 (60.5%)	n.a.
QRS	(ms)	111.7 ± 20.00	113.2 ± 20.48	110.7 ± 19.25	0.328
QT	(ms)	409.3 ± 45.88	404.9 ± 40.80	412.2 ± 48.83	0.228
QTc	(ms)	438.8 ± 35.93	439.4 ± 38.96	437.9 ± 33.93	0.747
Characteristics	**Units**	**Total**	**Dead**	**Survived**	***P*-value**
Number of cases	(%)	243 (100%)	74 (30.5%)	169 (69.5%)	n.a.
QRS	(ms)	111.7 ± 20.00	114.7 ± 20.95	110.3 ± 19.48	0.116
QT	(ms)	409.3 ± 45.88	396.4 ± 43.08	415.0 ± 46.04	0.003
QTc	(ms)	438.8 ± 35.93	434.5 ± 35.69	440.7 ± 35.97	0.215

Continuous data are presented as means ± standard deviations. Categorical data are presented as absolute counts with percent of column total. AI ICD, appropriate intervention(s) of ICD device; n.a., not applicable.

of patients after myocardial infarction with a single-chamber ICD without the need for permanent ventricular pacing. In our analysis, significant differences in the monitored ECG parameters (TpTe, TpTec) as well as in the ratio of TpTe to QT intervals between the patients with and without malignant ventricular arrhythmias were not observed. The occurrence of malignant ventricular arrhythmias was assessed based on the presence of appropriate ICD interventions in the event of such arrhythmias. Differences in ECG parameters between the groups of surviving and deceased patients were also not demonstrated.

The results of this analysis in an exactly defined and monitored patient population did not confirm an association between prolongation of TpTe (which should reflect increased TDR) and a higher incidence of malignant ventricular arrhythmias. Thus,

our work ranks among those who failed to prove any predictive value of the TpTe interval for overall mortality or for better selection of patients with a higher risk for malignant arrhythmias (Smetana et al., 2011; Porthan et al., 2013). In our work we have analyzed only post-MI patients with chronic HF without the need for permanent cardiac pacing or resynchronization therapy. Exclusion of patients with other proarrhythmogenic comorbidities is another potential advantage of our cohort. Its homogeneity is also reflected in the consistency of the severity of HF quantitatively expressed by the degree of systolic dysfunction of the left ventricle. Thus, in the light of our results, left ventricle ejection fraction remains the only clinical quantitative parameter used for selection of candidates for the primary prevention of SCD.

The long-term follow-up of patients in this dataset provides some interesting clinical observations: Only less than 12% of patients were smokers, quite in contrast with studies with higher proportion of smokers (Lellouche et al., 2007; Porthan et al., 2013). We anticipate a strong psychological impact of the circumstances arising from the diagnostic and treatment process in patients with coronary heart disease and HF, which may have resulted in smoking cessation. However, it is also possible that patients concealed smoking out of an (unfounded) fear of refusing to provide costly treatment. Smoking in our cohort did not affect overall mortality. Such a "smoker's paradox" is a well-known phenomenon in the population of patients with HF (Fonarow et al., 2008). However, recent analyses consider this paradox to be the result of a statistical bias in the impact of smoking in a population with many risk factors (Doi et al., 2019). Similarly, our results (difference in BMI in groups by overall mortality + 1.64 kg/m^2 in the group of surviving patients, 95% CI for the difference between means 0.34–2.94) agree with the known "obesity paradox" (Padwal et al., 2013). Systolic and diastolic blood pressure values indicate a good control of arterial hypertension in the monitored population, which however, may be caused by the phenomenon of "decapitated hypertension" in HF patients. The higher risk of death in patients with diabetes is consistent with the trend of their higher mortality in large population-based studies (Raghavan et al., 2019). It is clinically very interesting to find that lower glomerular filtration rate (GFR) is already a significant predictor of overall mortality with minimal renal impairment (KDIGO category G2 with normal or only minimally elevated serum creatinine). Considering large meta-analyses (van der Velde et al., 2011), both overall and cardiovascular mortality increased in proportion to renal impairment starting with GFR of 60 ml/min and lower. The median GFR in our group of deceased patients was 71.9 ml/min (IQR 54.3–88.0), which indicates a very significant effect of renal function on the prognosis of patients in our population.

The significant association of male gender with higher proportion of appropriate ICD interventions is nowadays a well-known phenomenon (Sticherling et al., 2018; Santangeli et al., 2010), and in the context with similar gender mortality suggest a smaller impact of sudden cardiac death on overall survival in women in this population. Greenlee et al. (2018) analyzed ICD treatment in patients from larger registries (a total of 2,540 ICD recipients) in the primary prevention of SCD and found that more than two-thirds of patients never received ICD-mediated intervention while more than three quarters of patients never received an appropriate therapy (ICD intervention triggered by ventricular tachycardia or ventricular fibrillation). However, the median follow-up in the mentioned work was less than two and a half years, while in our work more than 5 years. Almost 40% of patients received appropriate treatment in our cohort, and the median time to the first appropriate intervention was less than 2 years (23 months). Such a number of patients with appropriate ICD intervention indicates a very precise selection of candidates for primary preventive implantation of ICD at participating implantation center. Consistent with this finding is the fact that approximately 10% of our patients had inappropriate interventions, which is significantly less compared to the latter work (12% at half follow-up), probably mainly due to explicit elimination of patients with atrial fibrillation. This is in line with several clinical studies that have not confirmed the original intuitive hypothesis that the use of dual-chamber ICDs will reduce inappropriate interventions as well as overall mortality, as systems with added atrial electrode can better differentiate ventricular from supraventricular tachyarrhythmias. The preference for dual-chamber ICDs did not lead to a reduction in the rate of inappropriate treatment, and also was associated with a higher risk of peri- and post procedural complications and the need for earlier replacement of the generator (Theuns et al., 2008; Lee et al., 2010; Peterson et al., 2013; Defaye et al., 2017).

Limitations of the Study

As there is no uniform methodology for measuring the TpTe interval, procedure of any method described so far will always limit the investigation of the subject interval in relation to clinical outcomes. Because the study intervals were measured for each patient only at the beginning of the follow-up (changes in intervals over time are not captured), it is not statistically possible to describe direct relationships between the observed characteristics and outcomes, but "only" differences in the characteristics in the selected groups of patients.

The evaluation of an appropriate ICD intervention as a surrogate of the SCD is very often discussed. This is related to the knowledge acquired from the monitoring data from the ICD, which very convincingly prove that even malignant ventricular tachyarrhythmia (including ventricular fibrillation) can terminate spontaneously. This is in contrast to the "traditional" perception of these arrhythmias as "irreversible" and lethally ending without therapeutic intervention. Therefore, the extrapolation of appropriate ICD interventions as an exact measure of the incidence of SCD cannot be fully accepted, but it is a clinically meaningful approximation.

Other relative limitations include the retrospective monocentric design of the study, as well as the absence of randomization, assessment of infarct location, and separate monitoring of arrhythmic mortality.

CONCLUSION

The results of our retrospective study with long-term follow-up of post-MI patients with heart failure undergoing ICD implantation for primary prevention do not suggest any significant association

of electrocardiographic parameters reflecting transmural dispersion of ventricular repolarization (TpTe, TpTec) with overall and arrhythmia-free survival. Differences in some known clinical prognostic factors associated with overall survival in this population were found.

DATA AVAILABILITY STATEMENT

The data analyzed in this study is subject to the following licenses/restrictions: The dataset is copyright protected by ownership of The National Institute of Cardiovascular Diseases, Bratislava, Slovakia. Requests to access these datasets should be directed to RH, robert.hatala@nusch.sk.

ETHICS STATEMENT

The studies involving human participants were reviewed and approved by the Etická komisia NÚSCH, a.s., Bratislava. The patients/participants provided their written informed consent to participate in this study.

AUTHOR CONTRIBUTIONS

PMi contributed to the design, methodology, dataset, statistical analyses, and interpretation of the manuscript. SH contributed to the dataset and the intervals measurements. MS contributed to the design, manuscript, and the revision. PMa contributed to the methodology and devices implantation. IW contributed to the statistical analyses and interpretation. ST contributed to the dataset. AB contributed to the design and methodology. OB contributed to the dataset. RH contributed to the design, methodology, manuscript, and revision. All authors contributed to the article and approved the submitted version.

FUNDING

Submission funding grant was received from Slovak Heart Rhythm Association.

REFERENCES

Antzelevitch, C. (2010). M cells in the human heart. *Circ. Res.* 106, 815–817. doi: 10.1161/circresaha.109.216226

Antzelevitch, C., Sicouri, S., Litovsky, S., Lukas, A., Krishnan, S., Di Diego, J., et al. (1991). Heterogeneity within the ventricular wall. Electrophysiology and pharmacology of epicardial, endocardial, and M cells. *Circ. Res.* 69, 1427–1449. doi: 10.1161/01.res.69.6.1427

Bazett, H. C. (1920). An analysis of the time-relations of electrocardiograms. *Heart* 7, 353–370.

Defaye, P., Boveda, S., Klug, D., Beganton, F., Piot, O., Narayanan, K., et al. (2017). Dual- vs. single-chamber defibrillators for primary prevention of sudden cardiac death: long-term follow-up of the défibrillateur automatique implantable—prévention primaire registry. *EP Europace* 19, 1478–1484. doi: 10.1093/europace/euw230

Doi, S., Islam, N., Sulaiman, K., Alsheikh-Ali, A., Singh, R., Al-Qahtani, A., et al. (2019). Demystifying smoker's paradox: a propensity score–weighted analysis in patients hospitalized with acute heart failure. *J. Am. Heart Assoc.* 8:e013056. doi: 10.1161/jaha.119.013056

Drouin, E., Charpentier, F., Gauthier, C., Laurent, K., and Le Marec, H. (1995). Electrophysiologic characteristics of cells spanning the left ventricular wall of human heart: evidence for presence of M cells. *J. Am. Coll. Cardiol.* 26, 185–192. doi: 10.1016/0735-1097(95)00167-x

Fonarow, G., Abraham, W., Albert, N., Stough, W., Gheorghiade, M., Greenberg, B., et al. (2008). A smoker's paradox in patients hospitalized for heart failure: findings from OPTIMIZE-HF. *Eur. Heart J.* 29, 1983–1991. doi: 10.1093/eurheartj/ehn210

García-Pérez, L., Pinilla-Domínguez, P., García-Quintana, A., Caballero-Dorta, E., García-García, F., Linertová, R., et al. (2014). Economic evaluations of implantable cardioverter defibrillators: a systematic review. *Eur. J. Health. Econ.* 16, 879–893. doi: 10.1007/s10198-014-0637-x

Goldenberg, I., Moss, A., and Zareba, W. (2006). QT interval: how to measure it and what is "normal". *J. Cardiovasc. Electrophysiol.* 17, 333–336. doi: 10.1111/j.1540-8167.2006.00408.x

Greenlee, R., Go, A., Peterson, P., Cassidy-Bushrow, A., Gaber, C., Garcia-Montilla, R., et al. (2018). Device therapies among patients receiving primary prevention implantable cardioverter-defibrillators in the cardiovascular research network. *J. Am. Heart Assoc.* 7:e008292. doi: 10.1161/jaha.117.008292

Gupta, P., Patel, C., Patel, H., Narayanaswamy, S., Malhotra, B., Green, J., et al. (2008). Tp-e/QT ratio as an index of arrhythmogenesis. *J. Electrocardiol.* 41, 567–574. doi: 10.1016/j.jelectrocard.2008.07.016

Haarmark, C., Hansen, P., Vedel-Larsen, E., Haahr Pedersen, S., Graff, C., Andersen, M., et al. (2009). The prognostic value of the Tpeak-Tend interval in patients undergoing primary percutaneous coronary intervention for ST-segment elevation myocardial infarction. *J. Electrocardiol.* 42, 555–560. doi: 10.1016/j.jelectrocard.2009.06.009

Lee, D., Krahn, A., Healey, J., Birnie, D., Crystal, E., Dorian, P., et al. (2010). Evaluation of early complications related to de novo cardioverter defibrillator implantation. *J. Am. Coll. Cardiol.* 55, 774–782. doi: 10.1016/j.jacc.2009.11.029

Lellouche, N., De Diego, C., Akopyan, G., Boyle, N., Mahajan, A., Cesario, D., et al. (2007). Changes and predictive value of dispersion of repolarization parameters for appropriate therapy in patients with biventricular implantable cardioverter-defibrillators. *Heart Rhythm* 4, 1274–1283. doi: 10.1016/j.hrthm.2007.06.012

Letsas, K., Weber, R., Astheimer, K., Kalusche, D., and Arentz, T. (2009). Tpeak-Tend interval and Tpeak-Tend/QT ratio as markers of ventricular tachycardia inducibility in subjects with Brugada ECG phenotype. *Europace* 12, 271–274. doi: 10.1093/europace/eup357

Malik, M., Huikuri, H., Lombardi, F., Schmidt, G., Verrier, R., and Zabel, M. (2019). Is the Tpeak-Tend interval as a measure of repolarization heterogeneity dead or just seriously wounded? *Heart Rhythm* 16, 952–953. doi: 10.1016/j.hrthm.2019.01.015

Morin, D., Saad, M., Shams, O., Owen, J., Xue, J., Abi-Samra, F., et al. (2012). Relationships between the T-peak to T-end interval, ventricular tachyarrhythmia, and death in left ventricular systolic dysfunction. *Europace* 14, 1172–1179. doi: 10.1093/europace/eur426

Olde Nordkamp, L., Postema, P., Knops, R., van Dijk, N., Limpens, J., Wilde, A., et al. (2016). Implantable cardioverter-defibrillator harm in young patients with inherited arrhythmia syndromes: a systematic review and meta-analysis of inappropriate shocks and complications. *Heart Rhythm* 13, 443–454. doi: 10.1016/j.hrthm.2015.09.010

Padwal, R., McAlister, F., McMurray, J., Cowie, M., Rich, M., Pocock, S., et al. (2013). The obesity paradox in heart failure patients with preserved versus reduced ejection fraction: a meta-analysis of individual patient data. *Int. J. Obes.* 38, 1110–1114. doi: 10.1038/ijo.2013.203

Peterson, P., Varosy, P., Heidenreich, P., Wang, Y., Dewland, T., Curtis, J., et al. (2013). Association of single- vs dual-chamber ICDs with mortality,

readmissions, and complications among patients receiving an ICD for primary prevention. *JAMA* 309:2025. doi: 10.1001/jama.2013.4982

Porthan, K., Viitasalo, M., Toivonen, L., Havulinna, A., Jula, A., Tikkanen, J., et al. (2013). Predictive value of electrocardiographic T-wave morphology parameters and T-wave peak to T-wave end interval for sudden cardiac death in the general population. *Circ. Arrhythm. Electrophysiol.* 6, 690–696. doi: 10.1161/circep.113.000356

Raghavan, S., Vassy, J., Ho, Y., Song, R., Gagnon, D., Cho, K., et al. (2019). Diabetes mellitus–related all-cause and cardiovascular mortality in a national cohort of adults. *J. Am. Heart Assoc.* 8:e011295. doi: 10.1161/jaha.118.011295

Rosenthal, T., Masvidal, D., Abi Samra, F., Bernard, M., Khatib, S., Polin, G., et al. (2017). Optimal method of measuring the T-peak to T-end interval for risk stratification in primary prevention. *EP Europace* 20, 698–705. doi: 10.1093/europace/euw430

Rosenthal, T., Stahls, P., Abi Samra, F., Bernard, M., Khatib, S., Polin, G., et al. (2015). T-peak to T-end interval for prediction of ventricular tachyarrhythmia and mortality in a primary prevention population with systolic cardiomyopathy. *Heart Rhythm* 12, 1789–1797. doi: 10.1016/j.hrthm.2015.04.035

Santangeli, P., Pelargonio, G., Dello Russo, A., Casella, M., Bisceglia, C., Bartoletti, S., et al. (2010). Gender differences in clinical outcome and primary prevention defibrillator benefit in patients with severe left ventricular dysfunction: a systematic review and meta-analysis. *Heart Rhythm* 7, 876–882. doi: 10.1016/j.hrthm.2010.03.042

Shimizu, W., and Antzelevitch, C. (1998). Cellular basis for the ECG features of the LQT1 form of the long-QT syndrome. *Circulation* 98, 2314–2322. doi: 10.1161/01.cir.98.21.2314

Sicouri, S., and Antzelevitch, C. (1991). A subpopulation of cells with unique electrophysiological properties in the deep subepicardium of the canine ventricle. The M cell. *Circ. Res.* 68, 1729–1741. doi: 10.1161/01.res.68.6.1729

Smetana, P., Schmidt, A., Zabel, M., Hnatkova, K., Franz, M., Huber, K., et al. (2011). Assessment of repolarization heterogeneity for prediction of mortality in cardiovascular disease: peak to the end of the T wave interval and nondipolar repolarization components. *J. Electrocardiol.* 44, 301–308. doi: 10.1016/j.jelectrocard.2011.03.004

Srinivasan, N., Orini, M., Providencia, R., Simon, R., Lowe, M., Segal, O., et al. (2019). Differences in the upslope of the precordial body surface ECG T wave reflect right to left dispersion of repolarization in the intact human heart. *Heart Rhythm* 16, 943–951. doi: 10.1016/j.hrthm.2018.12.006

Sticherling, C., Arendacka, B., Svendsen, J. H., Wijers, S., Friede, T., Stockinger, J., et al. (2018). Sex differences in outcomes of primary prevention implantable cardioverter-defibrillator therapy: combined registry data from eleven European countries. *Europace* 20, 963–970. doi: 10.1093/europace/eux176

Strömberg, A., Fluur, C., Miller, J., Chung, M., Moser, D., and Thylén, I. (2014). ICD recipients' understanding of ethical issues, ICD function, and practical consequences of withdrawing the ICD in the end-of-life. *Pacing Clin. Electrophysiol.* 37, 834–842. doi: 10.1111/pace.12353

Theuns, D., Rivero-Ayerza, M., Boersma, E., and Jordaens, L. (2008). Prevention of inappropriate therapy in implantable defibrillators: a meta-analysis of clinical trials comparing single-chamber and dual-chamber arrhythmia discrimination algorithms. *Int. J. Cardiol.* 125, 352–357. doi: 10.1016/j.ijcard.2007.02.041

Turagam, M., Velagapudi, P., and Kocheril, G. A. (2013). Standardization of QRS duration measurement and LBBB criteria in CRT trials and clinical practice. *Curr. Cardiol. Rev.* 9, 20–23. doi: 10.2174/1573403138050 76269

van der Velde, M., Matsushita, K., Coresh, J., Astor, B., Woodward, M., Levey, A., et al. (2011). Lower estimated glomerular filtration rate and higher albuminuria are associated with all-cause and cardiovascular mortality. A collaborative meta-analysis of high-risk population cohorts. *Kidney Int.* 79, 1341–1352. doi: 10.1038/ki.2010.536

Watanabe, N., Kobayashi, Y., Tanno, K., Miyoshi, F., Asano, T., Kawamura, M., et al. (2004). Transmural dispersion of repolarization and ventricular tachyarrhythmias. *J. Electrocardiol.* 37, 191–200. doi: 10.1016/j.jelectrocard.2004.02.002

Yan, G., Wu, Y., Liu, T., Wang, J., Marinchak, R., and Kowey, P. (2001). Phase 2 early afterdepolarization as a trigger of polymorphic ventricular tachycardia in acquired long-QT syndrome. *Circulation* 103, 2851–2856. doi: 10.1161/01.cir.103.23.2851

Yılmaz, M. (2017). A novel electrocardiographic enigma: the measurement technique, interpretation of the Tp-e/QT ratio and its diagnostic use in making clinical decisions. *Int. J. Curr. Med. Pharm. Res.* 3, 2827–2832. doi: 10.24327/23956429.ijcmpr20170348

Conflict of Interest: The authors declare that the research was conducted in the absence of any commercial or financial relationships that could be construed as a potential conflict of interest.

The handling editor declared a past co-authorship with two of the authors MS and RH.

frontiers in Physiology

BRIEF RESEARCH REPORT
published: 03 September 2020
doi: 10.3389/fphys.2020.00953

Temporal Variability in Electrocardiographic Indices in Subjects With Brugada Patterns

Sharen Lee[1], Jiandong Zhou[2], Tong Liu[3], Konstantinos P. Letsas[4], Sandeep S. Hothi[5], Vassilios S. Vassiliou[6], Guoliang Li[7], Adrian Baranchuk[8], Raymond W. Sy[9,10], Dong Chang[11], Qingpeng Zhang[2] and Gary Tse[3,11]**

[1] Laboratory of Cardiovascular Physiology, Li Ka Shing Institute of Health Sciences, Hong Kong, China, [2] School of Data Science, City University of Hong Kong, Hong Kong, China, [3] Tianjin Key Laboratory of Ionic-Molecular Function of Cardiovascular Disease, Department of Cardiology, Tianjin Institute of Cardiology, Second Hospital of Tianjin Medical University, Tianjin, China, [4] Second Department of Cardiology, Laboratory of Cardiac Electrophysiology, Evangelismos General Hospital of Athens, Athens, Greece, [5] Heart and Lung Centre, New Cross Hospital, Wolverhampton, United Kingdom, [6] Norwich Medical School, University of East Anglia, Faculty of Medicine, Imperial College London, London, United Kingdom, [7] Arrhythmia Unit, Department of Cardiovascular Medicine, First Affiliated Hospital of Xi'an Jiaotong University, Xi'an, China, [8] Division of Cardiology, Kingston General Hospital, Queen's University, Kingston, ON, Canada, [9] Sydney Medical School, University of Sydney, Sydney, NSW, Australia, [10] Department of Cardiology, Royal Prince Alfred Hospital, University of Sydney, Sydney, NSW, Australia, [11] Xiamen Cardiovascular Hospital, Xiamen University, Xiamen, China

OPEN ACCESS

Edited by:
Ruben Coronel, University of Amsterdam, Netherlands

Reviewed by:
Michelle M. Monasky, IRCCS Policlinico San Donato, Italy
Dan Hu, Renmin Hospital of Wuhan University, China

***Correspondence:**
Qingpeng Zhang
qingpeng.zhang@cityu.edu.hk
Gary Tse
gary.tse@doctors.org.uk; garytse86@gmail.com

Specialty section:
This article was submitted to Cardiac Electrophysiology, a section of the journal Frontiers in Physiology

Received: *06 April 2020*
Accepted: *15 July 2020*
Published: *03 September 2020*

Citation:
Lee S, Zhou J, Liu T, Letsas KP, Hothi SS, Vassiliou VS, Li G, Baranchuk A, Sy RW, Chang D, Zhang Q and Tse G (2020) Temporal Variability in Electrocardiographic Indices in Subjects With Brugada Patterns. Front. Physiol. 11:953. doi: 10.3389/fphys.2020.00953

Introduction: Patients with Brugada electrocardiographic (ECG) patterns have differing levels of arrhythmic risk. We hypothesized that temporal variations in certain ECG markers may provide additional value for risk stratification. The present study evaluated the relationship between temporal variability of ECG markers and arrhythmic outcomes in patients with a Brugada pattern ECG. Comparisons were made between low-risk asymptomatic subjects versus high-risk symptomatic patients with a history of syncope, ventricular tachycardia (VT) or ventricular fibrillation (VF).

Methods: A total of 81 patients presenting with Brugada patterns were recruited. Serial ECGs and electronic health records from January 2004 to April 2019 were analyzed. Temporal variability of QRS interval, J point-T_{peak} interval (JTp), T_{peak}-T_{end} interval (Tp-e), and ST elevation (STe) in precordial leads V1-3, in addition to RR-interval from lead II, was assessed using standard deviation and difference between maximum and minimum values over the serial ECGs.

Results: Patients presenting with type 1 Brugada ECG pattern initially had significantly higher variability in JTp from lead V2 (SD: 33.5 ± 13.8 vs. 25.2 ± 11.5 ms, $P = 0.009$; max-min: 98.6 ± 46.2 vs. 78.3 ± 47.6 ms, $P = 0.047$) and ST elevation in lead V1 (0.117 ± 0.122 vs. 0.053 ± 0.030 mV; $P = 0.004$). Significantly higher variability in Tp-e interval measured from lead V3 was observed in the VT/VF group compared to the syncope and asymptomatic groups (SD: 20.5 ± 8.5 vs. 16.6 ± 7.3 and 14.7 ± 9.8 ms; $P = 0.044$; max-min: 70.2 ± 28.9 vs. 56.3 ± 29.0 and 43.5 ± 28.5 ms; $P = 0.011$).

Conclusion: Temporal variability in ECG indices may provide additional value for risk stratification in patients with Brugada pattern.

Keywords: Brugada, temporal, variability, repolarization, ECG

INTRODUCTION

Brugada syndrome (BrS) is an ion channelopathy which results in characteristic electrocardiographic (ECG) changes and predisposes patients with increased risk of ventricular tachycardia (VT), ventricular fibrillation (VF), and sudden cardiac death (SCD). The stratification of SCD risk is influenced by many factors, primarily the ECG pattern and symptoms presented (Gourraud et al., 2017). Syncope, VT and VF are deemed as strong predictors of SCD, while asymptomatic patients are considered to be of relatively low risk (Sieira et al., 2016). ECG markers are being explored for early identification of high-risk patients before they become symptomatic (Asvestas et al., 2018).

The spatial dispersion of different ECG indices for risk stratification has been well-explored. However, little analysis has been performed on their temporal variability. A recent study has reported significant temporal variability in indices measured from serial ECGs, with greater variability in patients with type 1 pattern (Castro Hevia et al., 2019). In the past, temporal variability in ECG indices has been simply attributed to the recognized dynamicity in Brugada ECG pattern (BrP) (Bayes de Luna et al., 2012). The recent demonstration of the difference in temporal variability between patient subgroups (Gray et al., 2017) inspired our interest to examine the potential use of temporal variability concerning risk stratification. Hence, the present study aims to examine the difference in temporal variability of ECG markers for risk stratification between low-risk asymptomatic patients, and high-risk symptomatic patients with a history of syncope, VT, or VF.

METHODS

Patient Selection and Electrocardiographic Measurement

This study received Ethics Approval from The Joint Chinese University of Hong Kong – New Territories East Cluster Clinical Research Ethics Committee (CREC Ref. No.: 2019.338). Institutional board approval was obtained and waived the need for patient consent in this retrospective study. The present single-center cohort consists of patients who visited the Prince of Wales Hospital, Hong Kong, China from the 1st of January, 2004 to the 1st of April, 2019 with electrocardiogram showing type 1 (cove-shaped) or type 2 (saddle-shaped) Brugada patterns. Patients with zero or one electronically documented ECG were excluded. Discrete ECGs throughout the follow-up duration were analyzed. The following ECG indices for leads V1, V2, and V3 from 12-lead ECG were measured using Philips ECGVue (standard edition): (1) QRS interval; (2) J point-T_{peak} interval (J-Tp, interval from J point to the peak of T wave); (3) T_{peak}-T_{end} interval (Tp-e, interval from the peak to the end of T wave returning to baseline); and (4) ST elevation (STe). RR interval was measured from lead II. ECGs were excluded if (1) artefacts were present in leads V1-3; (2) QRS complex and T waves were unidentifiable; and (3) the rhythm was paced.

The patient history was reviewed to identify the presence of syncope, VT and VF. The cohort was divided into three groups based on symptoms documented during follow-up: (1) asymptomatic, (2) syncope, and (3) VT/VF. Patients who presented with both syncope and VT/VF were included in both groups. Patients who presented with type 1 Brugada ECG, and those who did not, were also compared. The average and temporal dispersion of individual ECG indices were calculated. Temporal dispersion was calculated by two methods: (1) maximum – minimum (max-min) value of the index; and (2) standard deviation (SD) of the index over the series of ECG taken.

Statistical Analysis

Statistical analysis was performed using Stata MP 13. Statistical significance is defined as P-value <0.05. Intergroup differences were compared by Kruskal-Wallis' two-way ANOVA and Fisher's exact test for continuous and discrete variables, respectively. Pairwise comparison was performed for indices with significant intergroup differences by repeating the Kruskal-Wallis two-way ANOVA. Intra- and inter-observer agreement was assessed by the same investigator 4 weeks apart, and by a second investigator (**Supplementary Material**). by one-way mixed-effects individual, and two-way random-effects average absolute-agreement intraclass correlation coefficient (ICC), respectively ($0 < ICC < 0.4$ = poor; $0.4 < ICC < 0.59$ = fair; $0.6 < ICC < 0.74$ = good; $0.75 < ICC < 1.00$ = excellent) (Cicchetti, 1994).

RESULTS

After excluding patients with fewer than two ECG records, the cohort comprised 81 patients (initially type 1 = 35.8%, median follow-up period = 1281 days, interquartile range of follow-up period = 2571 days, 1150 ECGs analyzed, female = 8.6%, age of first BrP = 52.5 ± 1.85, age interquartile range = 24.0 years). All patients were Han Chinese and 79 of the 81 subjects were probands. The remaining two patients were identified from family screening. The age of first BrP and patient sex of the subgroups did not differ significantly (**Supplementary Table 1**). Both intra- and inter-observer agreement achieved fair to excellent quality (ICC > 0.4; **Supplementary Tables 2**, **3**).

Electrocardiographic indices were compared between patients with an initial type 1 pattern and those who had non-type 1 patterns (**Table 1**). The initial type 1 group displayed significantly longer lead V3 QRS interval (P = 0.021), shorter lead V3 JTp (P = 0.011), and greater lead V1 ST elevation (P = 0.000) compared to the non-type 1 group. They also showed significantly greater temporal dispersion for both lead V2 JTp (P-value: SD = 0.009, max-min = 0.047) and lead V1 ST elevation (P-value: SD = 0.004, max-min = 0.001).

Subsequent analyses were conducted by comparing ECG indices between asymptomatic patients (n = 39), patients with syncope (n = 38), and patients with VT/VF (n = 13) group. Within the syncope and VT/VF subgroups, five and two patients in the respective groups were initially asymptomatic, and developed syncope or VT/VF over the course of follow-up. A significant increase in variability was found in Tp-e measured form lead V3 under both standard deviation (P = 0.044) and maximum –

TABLE 1 | ECG biomarkers for initial type 1 vs. non-type 1 patterns.

	Overall (*n* = 81)	Non-type 1 (*n* = 52)	Type 1 (*n* = 29)	*P*-value
Average				
RR	863 ± 112	880 ± 118	833 ± 95.2	0.096
QRSV1	104 ± 13.5	102 ± 13.4	107 ± 13.3	0.085
QRSV2	110 ± 15.0	108 ± 15.8	113 ± 13.1	0.127
QRSV3	111 ± 14.8	108 ± 15.6	115 ± 12.4	**0.021**
JTpV1	202 ± 26.7	203 ± 29.4	201 ± 21.2	0.436
JTpV2	181 ± 25.9	181 ± 26.2	180 ± 25.9	0.825
JTpV3	175 ± 23.9	180 ± 24.7	166 ± 19.9	**0.011**
TpeV1	83.7 ± 15.4	82.6 ± 14.6	85.6 ± 16.7	0.640
TpeV2	101 ± 14.5	102 ± 14.5	101 ± 14.8	0.598
TpeV3	105 ± 14.6	106 ± 13.3	103 ± 16.8	0.220
STeV1	0.146 ± 0.143	0.101 ± 0.081	0.227 ± 0.189	**0.000**
STeV2	0.297 ± 0.159	0.277 ± 0.139	0.334 ± 0.187	0.285
STeV3	0.138 ± 0.080	0.133 ± 0.071	0.149 ± 0.096	0.910
Dispersion: SD				
RR	86.6 ± 40.4	84.8 ± 43.3	89.9 ± 35.3	0.509
QRSV1	12.1 ± 8.03	11.0 ± 6.12	14.1 ± 10.5	0.241
QRSV2	14.6 ± 9.73	14.2 ± 10.1	15.2 ± 9.24	0.503
QRSV3	10.9 ± 4.73	10.4 ± 4.80	11.9 ± 4.55	0.138
JTpV1	23.7 ± 13.3	25.3 ± 14.1	20.9 ± 11.4	0.215
JTpV2	28.2 ± 12.9	25.2 ± 11.5	33.5 ± 13.8	**0.009**
JTpV3	21.4 ± 13.1	20.7 ± 10.9	22.6 ± 16.5	0.922
TpeV1	17.3 ± 7.59	18.1 ± 8.25	15.9 ± 6.11	0.428
TpeV2	20.6 ± 10.2	19.2 ± 9.31	23.2 ± 11.4	0.126
TpeV3	16.0 ± 8.83	15.2 ± 6.80	17.4 ± 11.6	0.828
STeV1	0.076 ± 0.082	0.053 ± 0.030	0.117 ± 0.122	**0.004**
STeV2	0.127 ± 0.087	0.123 ± 0.089	0.135 ± 0.084	0.419
STeV3	0.070 ± 0.050	0.065 ± 0.052	0.079 ± 0.046	0.159
Dispersion: Max-Min				
RR	277 ± 155	274 ± 163	280 ± 144	0.863
QRSV1	39.7 ± 28.5	35.7 ± 25.6	46.8 ± 32.2	0.153
QRSV2	46.6 ± 31.5	43.0 ± 28.5	53.0 ± 35.8	0.268
QRSV3	34.8 ± 20.4	33.1 ± 20.5	37.8 ± 20.3	0.339
JTpV1	75.5 ± 45.3	78.8 ± 46.7	69.4 ± 42.8	0.342
JTpV2	85.6 ± 47.9	78.3 ± 47.6	98.6 ± 46.2	**0.047**
JTpV3	66.1 ± 44.6	63.6 ± 38.9	70.5 ± 53.8	0.957
TpeV1	53.8 ± 27.1	55.6 ± 29.2	50.6 ± 23.0	0.509
TpeV2	63.5 ± 35.5	58.2 ± 33.1	73.0 ± 38.2	0.081
TpeV3	50.8 ± 29.2	48.4 ± 27.3	55.0 ± 32.4	0.454
STeV1	0.210 ± 0.225	0.146 ± 0.123	0.324 ± 0.310	**0.001**
STeV2	0.367 ± 0.267	0.338 ± 0.251	0.417 ± 0.292	0.204
STeV3	0.191 ± 0.145	0.175 ± 0.138	0.221 ± 0.154	0.239

Units in milliseconds or millivolts. Variables with P < 0.05 are shown in bold text.

TABLE 2 | ECG biomarkers categorized based on symptoms.

	Asymptomatic (*n* = 39)	Syncope (*n* = 38)	VT/VF (*n* = 13)	*P*-value
Average				
RR	870 ± 104	857 ± 126	835 ± 103	0.564
QRSV1	105 ± 13.8	103 ± 13.8	106 ± 17.5	0.712
QRSV2	109 ± 15.4	111 ± 15.5	115 ± 17.1	0.631
QRSV3	111 ± 15.6	111 ± 14.9	114 ± 16.1	0.873
JTpV1	200 ± 30.2	205 ± 23.3	203 ± 27.2	0.841
JTpV2	191 ± 27.6	182 ± 25.2	177 ± 31.8	0.706
JTpV3	173 ± 23.0	179 ± 24.8	168 ± 31.9	0.185
TpeV1	86.7 ± 17.5	80.4 ± 12.7	86.7 ± 15.1	0.203
TpeV2	105 ± 16.6	97.8 ± 12.1	100 ± 9.73	0.121
TpeV3	108 ± 15.2	102 ± 14.2	108 ± 10.3	0.193
STeV1	0.135 ± 0.132	0.164 ± 0.159	0.168 ± 0.159	0.922
STeV2	0.326 ± 0.168	0.269 ± 0.145	0.254 ± 0.153	0.111
STeV3	0.160 ± 0.090	0.120 ± 0.066	0.097 ± 0.051	**0.017**
Dispersion: SD				
RR	85.0 ± 46.0	88.0 ± 36.1	74.4 ± 29.8	0.417
QRSV1	13.2 ± 9.9	11.2 ± 5.4	13.9 ± 6.37	0.487
QRSV2	13.5 ± 9.9	16.3 ± 9.8	12.4 ± 6.6	0.259
QRSV3	10.9 ± 5.0	11.4 ± 4.6	9.58 ± 3.6	0.397
JTpV1	23.7 ± 13.5	24.7 ± 13.6	21.4 ± 7.6	0.876
JTpV2	30.5 ± 15.5	25.9 ± 9.6	26.6 ± 9.7	0.598
JTpV3	23.3 ± 16.3	20.1 ± 9.4	19.4 ± 10.1	0.731
TpeV1	17.7 ± 8.90	17.2 ± 6.5	16.5 ± 5.8	0.929
TpeV2	20.9 ± 12.0	20.3 ± 8.5	21.4 ± 6.6	0.725
TpeV3	14.7 ± 9.8	16.6 ± 7.3	20.5 ± 8.5	**0.044**
STeV1	0.073 ± 0.065	0.082 ± 0.100	0.065 ± 0.041	0.984
STeV2	0.134 ± 0.090	0.122 ± 0.086	0.118 ± 0.074	0.778
STeV3	0.081 ± 0.061	0.061 ± 0.037	0.064 ± 0.039	0.201
Dispersion: Max-Min				
RR	251 ± 163	300 ± 153	288 ± 118	0.125
QRSV1	40.6 ± 32.3	40.0 ± 25.1	49.1 ± 26.2	0.467
QRSV2	39.5 ± 29.9	55.6 ± 32.5	47.9 ± 27.4	0.077
QRSV3	31.8 ± 20.2	38.9 ± 21.0	37.1 ± 20.8	0.270
JTpV1	69.8 ± 43.1	83.7 ± 48.4	77.5 ± 34.1	0.460
JTpV2	83.5 ± 51.1	87.7 ± 46.5	95.8 ± 47.2	0.638
JTpV3	66.0 ± 52.8	67.3 ± 37.2	71.8 ± 45.6	0.565
TpeV1	50.6 ± 27.8	57.7 ± 27.6	58.4 ± 23.0	0.535
TpeV2	57.2 ± 33.4	69.6 ± 37.6	80.9 ± 37.9	0.080
TpeV3	43.5 ± 28.5	56.3 ± 29.0	70.2 ± 28.9	**0.011**
STeV1	0.182 ± 0.150	0.250 ± 0.287	0.238 ± 0.218	0.835
STeV2	0.349 ± 0.236	0.289 ± 0.306	0.400 ± 0.277	0.894
STeV3	0.215 ± 0.160	0.174 ± 0.133	0.208 ± 0.171	0.405

Units in milliseconds or millivolts. Variables with P < 0.05 are shown in bold text.

minimum ($P = 0.011$) calculations, as shown in **Table 2**. Under further pairwise comparison, VT/VF group had significantly greater temporal dispersion in comparison to the asymptomatic group with both standard deviation ($P = 0.021$) and maximum – minimum ($P = 0.007$) methods, and to the syncope group under maximum- minimum ($P = 0.046$) calculation. Furthermore, the average extent of STe in lead V3 is significantly higher in VT/VF group in comparison to both the syncope ($P = 0.039$) and the asymptomatic group ($P = 0.010$) under pairwise comparison.

DISCUSSION

The present study demonstrates that increased temporal variability in Tp-e is found in patients with Brugada pattern of

higher SCD risk. Tp-e has been used to quantify the transmural dispersion of ventricular repolarization and used in BrS risk-stratification (Xia et al., 2005; Tse et al., 2018a). Increased transmural dispersion prolongs ventricular repolarization, which can lead to re-entry in phase 2 and subsequently ventricular tachyarrhythmia (Yan and Antzelevitch, 1999). Although the dynamicity of the Brugada pattern is well known, the significance of temporal variability in the risk stratification of BrS patients has not been fully explored (Viskin et al., 2018). The significant temporal variability in Tp-e amongst the high-risk arrhythmic group suggests the presence of a temporal variation in the transmural repolarization dispersion, and increased ventricular repolarization instability may explain the marked increase SCD risk in the symptomatic group. The fluctuations in the extent of transmural dispersion are further supported by the insignificant difference in Tp-e, and the dynamic manifestation of Brugada ECG pattern (Antzelevitch et al., 2005). Differing with the study by Castro Hevia et al. (2019), significant temporal variability was not noted in QRS duration in the present study, which might be attributed to the difference in calculation methodology. The significant intergroup differences in the average value of ECG indices is due to the diverse electrocardiographic pattern.

Although the diagnosis of Brugada syndrome focuses on the characteristic ECG pattern in leads V1 and V2, the present study demonstrates that lead V3 can also be useful in risk stratification. Information from lead V3 is often considered to be redundant in the clinical diagnosis of Brugada syndrome since it is less sensitive than leads V1-2 for Brugada ECG changes (Govindan et al., 2010). However, the present findings suggest that lead V3 might be able to provide insights into risk stratification through its sensitivity for ECG variability, and for which further research is needed to explore its clinical value in variability detection. It has been reported that Tp-e is longest in V3 when measured in children, possibly due to a higher number of M cells distributed in the interventricular septum (Bieganowska et al., 2013). The difference in temporal variability across the leads highlights the heterogeneity in ventricular repolarization of Brugada patients. Further research on the spatiotemporal dispersion of ECG indices is needed to elucidate the dynamicity in Brugada pattern.

The insignificant difference between the asymptomatic and syncope groups could be explained by the exact etiology of syncope. It has been reported that whilst patients presenting with unexplained syncope and a positive electrophysiological study are at high risk for arrhythmia, those with neurally mediated syncope share a similar prognosis to asymptomatic patients (Giustetto et al., 2017). Furthermore, there is growing evidence for similar genetic mutations to be present in both epilepsy and BrS. Syncope of such potential non-cardiogenic origins is unlikely to be affected by temporal variability of cardiac conduction and repolarisation, which might explain the insignificant results (Parisi et al., 2013; Tiron et al., 2015).

To reduce bias in ECG analysis, automatic measurements by the ECG machine can be applied. However, a comparison should be made against manual measurements to confirm accuracy in the detection of different ECG features, for example, the J point in Brugada ECGs. Future studies should further evaluate the use of automatic measurements in all ECG parameters analyzed in the present study and assess the clinical applications of the ECG parameters, particularly Tp-e. Whilst clinical studies have demonstrated that prolonged Tp-e reflects the presence of a resolved, temporary, arrhythmogenic substrate in patients with acute myocardial infarction, and predicts mortality for these patients, further research is required to explore its applicability in outcome prediction for spontaneous arrhythmia due to a channelopathy (Haarmark et al., 2009; Elitok et al., 2015).

Strengths and Limitations

There are several notable strengths of the present study. Firstly, a comprehensive analysis of different ECG features has been performed, with 3–50 ECGs measured per patient, and a total of more than 1000 ECGs analyzed. This extended previous studies using only single ECG measurements at baseline (Tse et al., 2018b; Lee et al., 2020). Moreover, there is good inter and intra-observer variability, as reflected by the intra-class coefficient. Several limitations should also be noted for the present study. First, the cohort is small and from a single center, hence findings should be externally validated and tested in a separate larger cohort in the future. Gender differences were not explored in the present study due to the limited number of female patients ($n = 7$). Since the majority of the patients were distributed in the middle ages (median age of first Brugada BrP onset = 53.0 years, interquartile range = 20.0 years), in addition to the relatively small cohort, the age differences were not examined. Unfortunately, only two patients undergone genetic testing in the present cohort, hence their genetic status cannot be commented upon. Moreover, the retrospective nature of the present study is susceptible to the bias inherent to such analyses. Besides, the sensitivity of the caliper used in measurement is limited by its one-decimal-place display, which results in a larger error in measuring small values, such as STe. The intervals between serial ECGs taken is variable between patients, and within a single patient, with more ECGs taken when the patients are less stable. Therefore, the ECG indices measured may tend to reflect a state of instability Errors may also be introduced in view of different operators undertaking the ECGs on different days. Furthermore, the relatively short follow-up duration limits the predictive value of the ECG parameters found toward patient life expectancy.

CONCLUSION

The present study demonstrates the presence of increased temporal variability in Tp-e amongst high-risk BrS patients, which illustrates a potential role for the analysis of serial changes in the surface ECG in the prognostic workup of BrS. Further research into the spatiotemporal dispersion of Brugada ECG patterns is need to gain insights into the dynamicity of Brugada electrophysiological changes.

DATA AVAILABILITY STATEMENT

The anonymized dataset and relevant materials have been made publicly available at Zenodo and can be accessed here:

https://zenodo.org/record/3351892; https://zenodo.org/record/3266172; and https://zenodo.org/record/3266179.

ETHICS STATEMENT

The studies involving human participants were reviewed and approved by The Joint Chinese University of Hong Kong – New Territories East Cluster Clinical Research Ethics Committee (The Joint CUHK-NTEC CREC). Written informed consent for participation was not required for this study in accordance with the national legislation and the institutional requirements.

AUTHOR CONTRIBUTIONS

SL and GT contributed to the study conception, data acquisition, database building, statistical analysis, manuscript drafting, and manuscript revision. All authors contributed to the data interpretation, statistical analysis, and manuscript revision.

FUNDING

This study was supported by the Research Grants Council of Hong Kong (T32-102/14-N to QZ), the Research Foundation of Major Science and Technology Projects of Tianjin Municipal Science and Technology Bureau (18ZXRHSY00180 to TL), and the National Natural Science Foundation of China (NSFC: 71972164 and 71972164 to TL).

SUPPLEMENTARY MATERIAL

The Supplementary Material for this article can be found online at: https://www.frontiersin.org/articles/10.3389/fphys.2020.00953/full#supplementary-material

REFERENCES

Antzelevitch, C., Brugada, P., Brugada, J., and Brugada, R. (2005). Brugada syndrome: from cell to bedside. *Curr. Probl. Cardiol.* 30, 9–54.

Asvestas, D., Tse, G., Baranchuk, A., Bazoukis, G., Liu, T., Saplaouras, A., et al. (2018). High risk electrocardiographic markers in Brugada syndrome. *Int. J. Cardiol. Heart Vasc.* 18, 58–64.

Bayes de Luna, A., Brugada, J., Baranchuk, A., Borggrefe, M., Breithardt, G., Goldwasser, D., et al. (2012). Current electrocardiographic criteria for diagnosis of brugada pattern: a consensus report. *J. Electrocardiol.* 45, 433–442.

Bieganowska, K., Sawicka-Parobczyk, M., Bieganowski, M., and Piskorski, J. (2013). Tpeak -tend interval in 12-lead electrocardiogram of healthy children and adolescents tpeak -tend interval in childhood. *Ann. Noninvas. Electrocardiol.* 18, 344–351.

Castro Hevia, J., Dorantes Sanchez, M., Martinez Lopez, F., Castaneda Chirino, O., Falcon Rodriguez, R., Puga Bravo, M., et al. (2019). Multiple serial ECGs aid with the diagnosis and prognosis of Brugada syndrome. *Int. J. Cardiol.* 277, 130–135.

Cicchetti, D. V. (1994). Guidelines, criteria, and rules of thumb for evaluating normed and standardized assessment instruments in psychology. *Psychol. Assess.* 6, 284–290.

Elitok, A., Ikitimur, B., Onur, I., Oz, F., Emet, S., Karaayvaz, E. B., et al. (2015). The relationship between T-wave peak-to end interval and ST segment recovery on intracoronary ECG during primary PCI. *Eur. Rev. Med. Pharmacol. Sci.* 19, 1086–1091.

Giustetto, C., Cerrato, N., Ruffino, E., Gribaudo, E., Scrocco, C., Barbonaglia, L., et al. (2017). Etiological diagnosis, prognostic significance and role of electrophysiological study in patients with Brugada ECG and syncope. *Int. J. Cardiol.* 241, 188–193.

Gourraud, J. B., Barc, J., Thollet, A., Le Marec, H., and Probst, V. (2017). Brugada syndrome: Diagnosis, risk stratification and management. *Arch. Cardiovasc. Dis.* 110, 188–195.

Govindan, M., Batchvarov, V. N., Raju, H., Shanmugam, N., Bizrah, M., Bastiaenen, R., et al. (2010). Utility of high and standard right precordial leads during ajmaline testing for the diagnosis of Brugada syndrome. *Heart* 96, 1904–1908.

Gray, B., Kirby, A., Kabunga, P., Freedman, S. B., Yeates, L., Kanthan, A., et al. (2017). Twelve-lead ambulatory electrocardiographic monitoring in Brugada syndrome: potential diagnostic and prognostic implications. *Heart Rhythm* 14, 866–874.

Haarmark, C., Hansen, P. R., Vedel-Larsen, E., Pedersen, S. H., Graff, C., Andersen, M. P., et al. (2009). The prognostic value of the Tpeak-Tend interval in patients undergoing primary percutaneous coronary intervention for ST-segment elevation myocardial infarction. *J. Electrocardiol.* 42, 555–560.

Lee, S., Li, K. H. C., Zhou, J., Leung, K. S. K., Lai, R. W. C., Li, G., et al. (2020). Outcomes in brugada syndrome patients with implantable cardioverter-defibrillators: insights from the sglt2 registry. *Front. Physiol.* 11:204. doi: 10.3389/fphys.2020.00204

Parisi, P., Oliva, A., Coll Vidal, M., Partemi, S., Campuzano, O., Iglesias, A., et al. (2013). Coexistence of epilepsy and Brugada syndrome in a family with SCN5A mutation. *Epilepsy Res.* 105, 415–418.

Sieira, J., Dendramis, G., and Brugada, P. (2016). Pathogenesis and management of Brugada syndrome. *Nat. Rev. Cardiol.* 13, 744–756.

Tiron, C., Campuzano, O., Perez-Serra, A., Mademont, I., Coll, M., Allegue, C., et al. (2015). Further evidence of the association between LQT syndrome and epilepsy in a family with KCNQ1 pathogenic variant. *Seizure* 25, 65–67.

Tse, G., Gong, M., Li, C. K. H., Leung, K. S. K., Georgopoulos, S., Bazoukis, G., et al. (2018a). Tpeak-Tend, Tpeak-Tend/QT ratio and Tpeak-Tend dispersion for risk stratification in Brugada Syndrome: A systematic review and meta-analysis. *J. Arrhythm.* 34, 587–597.

Tse, G., Li, K. H. C., Li, G., Liu, T., Bazoukis, G., Wong, W. T., et al. (2018b). Higher dispersion measures of conduction and repolarization in type 1 compared to non-type 1 Brugada syndrome patients: an electrocardiographic study from a single center. *Front. Cardiovasc. Med.* 5:132. doi: 10.3389/fphys.2020.00132

Viskin, S., Hochstadt, A., and Rosso, R. (2018). Type-I paradox of Brugada syndrome. *J. Am. Heart Assoc.* 7:e009298. doi: 10.1161/JAHA.118.009298

Xia, Y., Liang, Y., Kongstad, O., Holm, M., Olsson, B., and Yuan, S. (2005). Tpeak-Tend interval as an index of global dispersion of ventricular repolarization: evaluations using monophasic action potential mapping of the epi- and endocardium in swine. *J. Interv. Card. Electrophysiol.* 14, 79–87.

Yan, G. X., and Antzelevitch, C. (1999). Cellular basis for the Brugada syndrome and other mechanisms of arrhythmogenesis associated with ST-segment elevation. *Circulation* 100, 1660–1666.

Conflict of Interest: The authors declare that the research was conducted in the absence of any commercial or financial relationships that could be construed as a potential conflict of interest.

frontiers in Physiology

ORIGINAL RESEARCH
published: 18 September 2020
doi: 10.3389/fphys.2020.567383

Identification of Drug-Induced Multichannel Block and Proarrhythmic Risk in Humans Using Continuous T Vector Velocity Effect Profiles Derived From Surface Electrocardiograms

Werner Bystricky[1], Christoph Maier[1,2], Gary Gintant[3], Dennis Bergau[1] and David Carter[1]**

[1] Clinical Pharmacology and Pharmacometrics, AbbVie, Inc., North Chicago, IL, United States, [2] Department of Medical Informatics, Heilbronn University, Heilbronn, Germany, [3] Integrated Sciences and Technology, AbbVie, Inc., North Chicago, IL, United States

OPEN ACCESS

Edited by:
Ruben Coronel, University of Amsterdam, Netherlands

Reviewed by:
Daniel M. Johnson, The Open University, United Kingdom
Balazs Horvath, University of Debrecen, Hungary

***Correspondence:**
Werner Bystricky
werner.bystricky@abbvie.com
David Carter
david.carter@abbvie.com

Specialty section:
This article was submitted to Cardiac Electrophysiology, a section of the journal Frontiers in Physiology

Received: *29 May 2020*
Accepted: *27 August 2020*
Published: *18 September 2020*

Citation:
Bystricky W, Maier C, Gintant G, Bergau D and Carter D (2020) Identification of Drug-Induced Multichannel Block and Proarrhythmic Risk in Humans Using Continuous T Vector Velocity Effect Profiles Derived From Surface Electrocardiograms. Front. Physiol. 11:567383. doi: 10.3389/fphys.2020.567383

We present continuous T vector velocity (TVV) effect profiles as a new method for identifying drug effects on cardiac ventricular repolarization. TVV measures the temporal change in the myocardial action potential distribution during repolarization. The T vector dynamics were measured as the time required to reach p percent of the total T vector trajectory length, denoted as Tr(p), with p in {1, ..., 100%}. The Tr(p) values were individually corrected for heart rate at each trajectory length percentage p. Drug effects were measured by evaluating the placebo corrected changes from baseline of Tr(p)c jointly for all p using functional mixed effects models. The p-dependent model parameters were implemented as cubic splines, providing continuous drug effect profiles along the entire ventricular repolarization process. The effect profile distributions were approximated by bootstrap simulations. We applied this TVV-based analysis approach to ECGs available from three published studies that were conducted in the CiPA context. These studies assessed the effect of 10 drugs and drug combinations with different ion channel blocking properties on myocardial repolarization in a total of 104 healthy volunteers. TVV analysis revealed that blockade of outward potassium currents alone presents an effect profile signature of continuous accumulation of delay throughout the entire repolarization interval. In contrast, block of inward sodium or calcium currents involves acceleration, which accumulates during early repolarization. The balance of blocking inward versus outward currents was reflected in the percentage p_{zero} of the T vector trajectory length where accelerated repolarization transitioned to delayed repolarization. Binary classification using a threshold p_{zero} = 43% separated predominant hERG channel blocking drugs with potentially higher proarrhythmic risk (moxifloxacin, dofetilide, quinidine, chloroquine) from multichannel blocking drugs with low proarrhythmic risk (ranolazine, verapamil, lopinavir/ritonavir) with sensitivity 0.99 and specificity 0.97. The TVV-based effect profile provides a detailed view of drug

effects throughout the entire ventricular repolarization interval. It enables the evaluation of drug-induced blocks of multiple cardiac repolarization currents from clinical ECGs. The proposed p_{zero} parameter enhances identification of the proarrhythmic risk of a drug beyond QT prolongation, and therefore constitutes an important tool for cardiac arrhythmia risk assessment.

Keywords: cardiac safety, TVV, CiPA, QT prolongation, J-Tpeak interval, ion channel block, ventricular repolarization

INTRODUCTION

The implementation of the ICH E14 (ICH, 2005a) and S7B (ICH, 2005b) guidelines in 2005 represented a turning point in regulatory practices for drug approval. Their release was in response to cases of sudden cardiac death reported in the preceding decade, which resulted in withdrawal of several drugs from the market. The guidelines were inspired by the insight that a block of the hERG/IKr ion current delays ventricular repolarization and creates an electrophysiological environment that favors the development of the rare ventricular arrhythmia torsade de pointes (TdP) (Haverkamp et al., 2000). In the surface ECG, the most obvious effect of hERG/IKr-block is delayed repolarization manifested as prolongation of the QTc interval. Consequently, clinical guidance set the focus on this feature, and up to the present, careful monitoring of the QT interval remains an essential part in the drug approval process.

This change in regulatory practices was highly effective in preventing the approval of new drugs with unexpected cardiotoxic effects (Sager et al., 2014). However, QT prolongation turned out to be a relatively non-specific predictor of TdP proarrhythmia (Hondeghem, 2008) and could potentially terminate the development of promising compounds unnecessarily (Roden, 2004). Further research has revealed that simultaneous block of other ion channels, especially the late sodium and the L-type calcium channel, can attenuate the proarrhythmic effects of pure hERG/IKr block despite the presence of QT-prolongation (Redfern et al., 2003; Martin et al., 2004).

Recognizing the role of multiple ion currents in defining drug effects on repolarization, the comprehensive *in vitro* proarrhythmia assay (CiPA) initiative was launched in 2013 (Sager et al., 2014) with the mission to "engineer an assay for assessment of the proarrhythmic potential of new drugs that has improved specificity compared with the hERG assay plus Thorough QT study" (CiPA, 2020). The CiPA initiative is comprised of four components (Gintant et al., 2016), three of which are preclinical tests: (1) voltage-clamp based assessment of blocks in seven cardiac ion channels, (2) an *in silico* modeling approach based on modifications (Dutta et al., 2017) of the O'Hara-Rudy ventricular myocyte model (O'Hara et al., 2011) to simulate the effects of expected ion channel blocks onto the action potential on a cellular level, and (3) the use of human induced pluripotent stem cell-derived cardiomyocytes to confirm predicted effects *in vitro*.

For a list of 28 drugs, the proarrhythmic potential was ranked (high – intermediate – low) according to known properties (Gintant et al., 2016), and their ion-channel effects were thoroughly characterized (Crumb et al., 2016). The qNet metric (Dutta et al., 2017) was suggested as a surrogate for proarrhythmia, based on quantification of the balance of charge transport over four essential inward and outward currents, as obtained from the cellular action potential (AP) simulation. The qNet metric demonstrated excellent performance for separating the set of CiPA drugs into the risk categories (Li et al., 2019).

Besides the CiPA context, an advantage of human *in silico* drug trials over animal studies in predicting cardiotoxicity of 62 compounds was demonstrated (Passini et al., 2017). Simpler approaches compared to qNet suggested to only consider the net difference in block between depolarizing and repolarizing currents (Bnet) (Mistry, 2018; Han et al., 2019). More complex approaches extend the cellular simulation to multiple scales up to the level of the whole heart in three dimensions (Zemzemi et al., 2013; Okada et al., 2015; Hwang et al., 2019; Yang et al., 2020) and combine simulation with machine learning techniques to assess the arrhythmogenic risk of drugs (Sahli-Costabal et al., 2020). Others start directly from a chemical drug representation to predict potential cardiotoxic effects, e.g., by means of deep artificial neural networks (Cai et al., 2019).

Despite the impressive findings obtained from *in silico* and *in vitro* models, there are discrepancies between model predictions and experimental observations, in particular for multichannel blocking drugs (Britton et al., 2017). For *in vitro* models, results depend on the experimental protocol, and quality standards as well as experimental conditions need to be taken into account (Ridder et al., 2020). Consequently, the fourth CiPA component stipulates the complementary use of early, intensive clinical ECG monitoring to assess cardiac effects in humans, to confirm model predictions and to identify potential unanticipated threats.

In this context, research continues to find more specific clinical ECG biomarkers of a drug's proarrhythmic risk (Vicente et al., 2015). Most approaches focus on the ST-T region of the ECG as it corresponds to cardiac repolarization. A principal distinction is possible between methods targeting representative beat characteristics versus dynamic beat-to-beat aspects of repolarization. Beat-to-beat QT-interval variability was introduced as a marker of temporal lability of repolarization linked to arrhythmic susceptibility (Berger et al., 1997), and various algorithms and markers exist (Baumert et al., 2016). Alternative approaches assess QT interval dynamics by grouping QT according to heart rate (Fossa and Zhou, 2010), and suggest characterization

of electrocardiographic restitution by quantifying QT-TQ-interval relationship (Fossa, 2017). Finally, T-wave alternans analysis represents an important dynamic technique quantifying the occurrence of a specific type of modulation of T-wave morphology or amplitude. Its electrophysiological basis is well-understood (Verrier et al., 2011), and the phenomenon is causally linked to arrhythmogenic risk (Verrier and Malik, 2013). However, application of these dynamic techniques requires ECG data sequences of sufficient length. Moreover, their utilization has largely concentrated on arrhythmic risk stratification of patients under well-defined disease conditions. Comprehensive studies exploring their performance in pro-arrhythmic risk assessment of drugs are still missing.

In the group of approaches addressing static properties of repolarization, candidate features (Brennan and Tarassenko, 2012) have included morphological ECG properties like notching, flattening or asymmetry of the T-wave (Graff et al., 2009), as well as vectorcardiographic biomarkers like QRS-T angle (Acar et al., 1999), and early and late repolarization duration (Couderc, 2009). In a comprehensive series of three CiPA ECG studies (Johannesen et al., 2014; Johannesen et al., 2016; Vicente et al., 2019), the J-T_{peak}c interval was identified as the most suitable biomarker to separate multi-channel blocking drugs with low proarrhythmic risk from predominant hERG blockers with high proarrhythmic risk (sensitivity 0.82, specificity 0.77) (Vicente et al., 2016). Approaches to identify the T-wave peak in a more reproducible and stable way have been suggested (Hnatkova et al., 2019). Recently, we presented a TVV-based analysis approach as a new method for electrocardiographic repolarization assessment and demonstrated that it outperforms J-T_{peak}c as a biomarker for identification of multi-channel blocking drugs (Bystricky et al., 2019).

The rationale for this TVV approach may be outlined as follows: the T vector at a certain point in time during repolarization reflects the spatial gradients of the action potentials distributed over the entire myocardium as recorded from the body surface ECG. Any change of the T vector with time reflects a change of the myocardial potential distribution. Thus, the T vector trajectory between the J-point (the end of depolarization) and the end of the T wave is a three-dimensional descriptor of the state transition of the myocardial action potentials during repolarization. TVV denotes the velocity at which the T vector moves along the T vector trajectory, thus representing myocardial potential dynamics. The action potential dynamics of a single myocardial cell are determined by complex interactions of currents flowing across multiple ion channels that can be described in terms of a set of mathematical differential equations (O'Hara et al., 2011; Dutta et al., 2017; Tomek et al., 2019). Drugs affecting multiple ion channels will impact the repolarization dynamics at different times during the action potential. We hypothesize that drug-induced changes throughout the time course of repolarization will be reflected in the TVV along the T vector trajectory.

The purpose of our current study is to present an extension of the TVV methodology which allows for continuous quantification of changes in the temporal dynamics over the entire phase of repolarization. We apply this method to the published data from all three CiPA ECG studies in order to provide reference results for these publicly available data sets and corroborate our suggested interpretation with additional support. Finally, we illustrate the potential of TVV analysis by showing that a scalar biomarker p_{zero}, extracted from the TVV drug effect profile, can separate predominant hERG channel blocking drugs with potentially higher proarrhythmic risk from multichannel blocking drugs with low proarrhythmic risk with excellent performance.

MATERIALS AND METHODS

Study Data

We used de-identified data from the three CiPA ECG studies that are publicly available from PhysioNet (Goldberger et al., 2000).

The first study (Study A, ECGRDVQ) (Johannesen et al., 2014) was a randomized, double-blind, 5-period crossover clinical trial with 22 healthy subjects. Its aim was to investigate whether multichannel blocking drugs with different potentials for blocking potassium, late sodium, and calcium currents can be differentiated by their effect on the ECG. In the morning of each 24 h treatment period, all subjects received a single dose of one of the drugs dofetilide (500 μg), quinidine sulfate (400 mg), ranolazine (1,500 mg), verapamil hydrochloride (120 mg), or placebo. Triplicate 10-s resting ECGs were recorded, and serum PK samples were taken at 16 pre-defined time-points (pre-dose and 0.5, 1, 1.5, 2, 2.5, 3, 3.5, 4, 5, 6, 7, 8, 12, 14, 24 h post-dose). The washout period between treatments was 7 days (for further details see, Johannesen et al., 2014).

The second study (Study B, ECGDMMLD) (Johannesen et al., 2016) was a randomized, double-blinded, 5-period crossover clinical trial in 22 healthy subjects. It addressed the electrophysiological responses to hERG/IKr current blocking drugs with and without the addition of blockade of either late sodium or L-type calcium current blocking drugs. The 5 treatment periods included dofetilide alone, mexiletine without and with dofetilide, lidocaine without and with dofetilide, moxifloxacin without and with diltiazem, and placebo. In each period, subjects were dosed three times per day, in the morning (hour 0), afternoon (hour 4) and evening (hour 9.5) as described in **Table 1**. Serum PK samples were taken after each dosing, and triplicate 10-s resting ECGs were recorded at four timepoints at 30 min intervals after each dosing event. For details see (Johannesen et al., 2016).

The third study (Study C, CiPA) (Vicente et al., 2019) was designed as a prospective, small sample size CiPA validation study to assess the effect of multi-ion channel-blocking drugs on ECG parameters. It consisted of two parts:

- Part 1 was a double-blind, randomized, placebo-controlled, one period, parallel designed study to assess the effect of three balanced blockers (ranolazine, verapamil, and lopinavir + ritonavir), one predominant hERG blocker (chloroquine), and one placebo on the QTc and J-T_{peak}c

TABLE 1 | Dosing schema for study B, modified from Johannesen et al. (2016).

Treatment period	Morning dose	Afternoon dose	Evening dose
Placebo (Pla)	Pla	Pla	Pla
Dofetilide (Dof)	Pla	Dof	Dof
Mexiletine (Mex) + Dofetilide	Mex	Mex + Dof	Mex + Dof
Lidocaine (Lid) + Dofetilide	Lid	Lid + Dof	Lid + Dof
Moxifloxacin (Mox) + Diltiazem (Dil)	Mox	Mox	Mox + Dil

intervals in 50 healthy subjects. The four drugs and placebo were administered to 10 subjects in one period of three consecutive days to achieve low and high drug exposure.

- Part 2 was a double-blind, randomized, two-period crossover designed study to assess the effect of hERG block (dofetilide) versus calcium block (diltiazem) on the QTc and J-T_{peak}c intervals in 10 healthy subjects. In the dofetilide alone period, subjects received dofetilide on days 1 and 3. In the diltiazem + dofetilide period, subjects received diltiazem alone on days 1 and 2, and diltiazem + dofetilide on day 3.

In both parts, triplicate ECGs and PK samples were taken at multiple timepoints during the 3 days.

Details about the time courses of the drug plasma concentrations during the treatment phases of all three studies are given in the **Supplementary File S2**.

ECG Processing

All ECG files were analyzed with eECG/ABBIOS (AbbVie, Inc.'s proprietary, validated, ECG analysis system) in a semi-automated manner. ECGs were reviewed to identify artifacts, abnormal heartbeats, and unreliable automated annotations. All normal beats with acceptable annotations were used in the analysis. ECGs of concern were manually reviewed to identify and annotate a minimum of 3 heartbeats per ECG with T-waves unaffected by artifacts, and consistently placed T annotations. To ensure consistent placement of T annotations, reviewing was performed unblinded with respect to the subject and timepoint. 6 ECGs out of 5232 in Study A, 3 ECGs out of 4211 in Study B, and 0 ECG out of 5749 in Study C were not included in the analysis due to bad signal quality.

For each ECG, the 12 lead signals were adjusted to the isoelectric lines (defined by the median amplitude of the PQ interval and interpolated between the heart beats by a cubic spline), low-pass filtered (bidirectional Bessel filter with 36 Hz), and exported as an annotated ECG file in HL7 format (aECG) with 500 Hz sampling frequency, including the P, Q, J, and Tend annotations. The aECG files were loaded into, and further processed using the R (RCoreTeam, 2020) and the Julia (Bezanson et al., 2020) systems.

The time course of the three-dimensional T vector in a beat was calculated by means of the inverse Dower transformation (Dower et al., 1980).

Derivation of T Vector Trajectory Duration Curves

The T vector dynamics was measured for each normal heartbeat as the time required to reach p percent of the total T vector trajectory length, denoted as Tr(p) and referred to in our manuscript as trajectory (time) quantile p, with p in {1, 2, . . ., 100%}.

In order to exclude possible late depolarization effects, the beginning of the T vector trajectory was determined as the J-point plus 20 ms. The T vector trajectory was determined as described in Bystricky et al. (2019). The trajectory quantiles for an ECG were, individually for each p, calculated as average of the beat related Tr(p) values.

To visualize the repolarization dynamic of an ECG, we aligned the Tr(p) values in a trajectory duration curve (**Figure 1B**), where the relative distance covered along the T vector trajectory (**Figure 1A**) is displayed on the y axis (in % from top to bottom) and the corresponding duration in milliseconds is shown along the x axis.

Assuming a power law dependency of Tr(p) from the heart rate of the form $Tr(p) \sim \beta_p RR^{\alpha_p}$ with RR as the average beat interval of an ECG in seconds, we determined the heart rate correction exponents α_p for each trajectory length percentage p by fitting a linear mixed effects model of the form

$$\log(Tr(p)) = \log(\beta_p) + \alpha_p \log(RR) + \varepsilon$$

to all drug free data of studies A, B, and C with subject as random effect for the intercept $\log(\beta_p)$ and slope α_p (R method lme4::lmer). The heart rate corrected trajectory quantiles for an ECG were calculated as

$$Tr(p)c = Tr(p)/RR^{\alpha_p}$$

We determined the average trajectory duration curve under placebo condition in study A by fitting the mixed effects model

$$Tr(p)c_i = \theta_0(p) + \eta_i(p)$$

for a given trajectory length percentage p with $\theta_0(p)$ as fixed effect and $\eta_i(p)$ as random effect for subject i. To visualize drug induced changes to the trajectory duration curve, we modeled the trajectory quantiles under quinidine treatment in study A for the individual trajectory length percentages p by the following mixed effects exposure response model:

$$Tr(p)c_{i,k} = (\theta_0(p) + \eta_{0,i}(p)) + (\theta_1(p) + \eta_{1,i}(p)) \times C_{i,k}$$

$C_{i,k}$ is the drug concentration for subject i at time k; $\theta_0(p)$ and $\theta_1(p)$ are the fixed effects;$\eta_{0,i}(p)$, $\eta_{1,i}(p)$ are the random effects for subject i. The trajectory duration curve under quinidine was calculated as the model predictions for the individual *p*-values at the c_{max} quinidine concentration.

Calculation of Drug Effects on Tr(p)c

The drug effects on the individual Tr(p)c parameters were assessed by modeling the placebo corrected change from baseline, where Tr(p)c was calculated as the average value from the

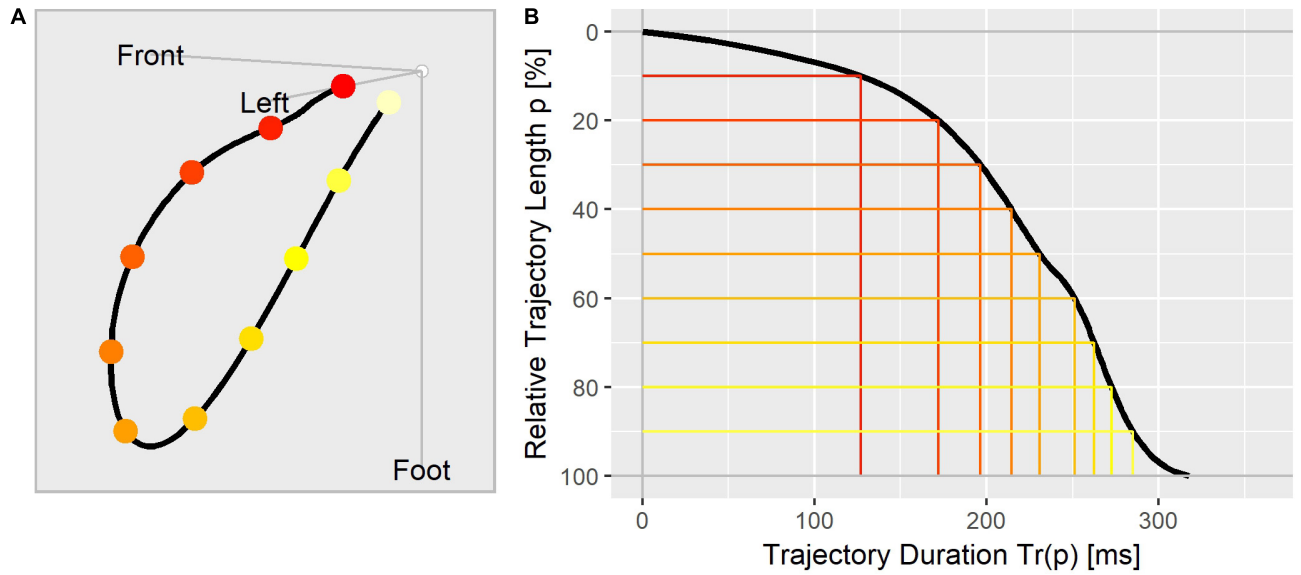

FIGURE 1 | (A) The T vector trajectory displayed in the body's physical orientation, divided into 10 equally long segments and colored from red (J-point) to yellow (T_{end}). **(B)** T vector trajectory duration curve indicating the elapsed time Tr(p) (x-axis) at which the corresponding percentage of the trajectory length (y-axis) is reached. The colored lines correspond to the trajectory points as marked in **(A)**.

replicate ECGs for the given subject and timepoint. Given the different designs in studies A, B, and C, the following mixed effects models were used.

Study A

We used a mixed effects exposure response model for describing the placebo corrected change from baseline of Tr(p)c with linear dependency on the drug concentration:

$$\Delta\Delta Tr(p)c_{ik} = (\theta_0(p) + \eta_{0,i}(p)) + (\theta_1(p) + \eta_{1,i}(p)) \times C_{ik}$$

$\Delta\Delta Tr(p)c_{ik}$ is the placebo corrected change from baseline of Tr(p)c for subject i at time k; $\theta_0(p)$ and $_{\theta_1(p)}$ are the fixed effect parameters for intercept and slope; $\eta_{0,i}(p)$ and $\eta_{1,i}(p)$ are the subject specific random effect parameters for intercept and slope; C_{ik} is the drug concentration for subject i at time k.

Study B

We measured the drug effects for the morning, afternoon, and evening dosing phases as the average of the placebo corrected change from baseline Tr(p)c values using the mixed effects model:

$$\Delta\Delta Tr(p)c_{ik} = \theta(p) + \eta_i(p)$$

$\Delta\Delta Tr(p)c_{ik}$ is the placebo corrected change from baseline of Tr(p)c for subject i at time k within the given dosing phase; $\theta(p)$ is the fixed effect parameter denoting the average drug effect; $\eta_i(p)$ is the subject specific random effect parameter.

Study C

Given the parallel design in the study part 1, we determined the drug effect profiles by modeling the changes from baseline Tr(p)c data according to Garnett et al. (2018) using the following mixed effects exposure response approach:

$$\Delta Tr(p)c_{ijk} = (\theta_0(p) + \eta_{0,i}(p)) + \theta_1(p)TRT_j + \sum_{\iota}(\theta_{2,\iota}(p) + \eta_{2,i,\iota}(p)) \times c_{ijk,\iota} + \theta_3(p)NT_k + \theta_4(p)(Tr(p)c_{i,j=0} - \overline{Tr(p)C_0})$$

$\Delta Tr(p)c_{ijk}$ is the change from baseline of Tr(p)c for subject i under treatment j at time k; $\theta_0(p)$ is the fixed effect population mean intercept in the absence of a treatment effect; $\eta_{0,i}(p)$ is the subject-specific random effect for the intercept; $\theta_1(p)$ is the fixed effect associated with treatment TRT_j (j = 0 for placebo, j = 1 for the active drug); $\theta_{2,\iota}(p)$ and $\eta_{2,i,\iota}(p)$ are the fixed and random effects for the slope with respect to the concentration $C_{ijk,\iota}$ of drug l (two drugs were used for the combination of dofetilide and diltiazem only); $\theta_3(p)$ is the fixed effect associated with the nominal timepointNT_k; $\theta_4(p)$ is the fixed effect associated with baseline $Tr(p)c_{i,j=0}$; $\overline{Tr(p)c_0}$ is the overall mean of all baseline Tr(p)c values.

The placebo corrected change from baseline effect for drug l with concentration C_ι on Tr(p)c was calculated as

$$\Delta\Delta Tr(p)c = \widehat{\theta_1(p)} + \sum_{\iota}\widehat{\theta_{2,\iota}(p)} \times C_\iota$$

where $\widehat{\theta\ldots(p)}$ denotes the estimated parameter.

Derivation of Continuous Drug Effect Profiles

To describe the effect of a drug continuously over the entire repolarization process, we combined the individual models for

the trajectory length percentages $p = 1, 2, \ldots, 100$ from above into one single functional mixed effects model, where the p-dependent model parameters were parametrized by polynomial splines with degree 3 (R method splines::bs). The spline's degree of smoothing along the p range is determined by the knots, defining the spline basis functions. We used equidistantly spaced knots with boundaries $p = 1$ and $p = 100$. Since the computational effort for fitting the functional model depends on the model complexity and of the number of knots, we used for the models in study A 8 knots, 16 knots for the models in study B, and 12 knots for the models in study C. Further details about the functional modeling approach are given in the **Supplementary File S3**.

A continuous drug effect profile was defined as the predicted $\Delta\Delta Tr(p)c$ for representative drug concentrations along the T vector trajectory between the length percentages $p = 1\%$ and $p = 100\%$. It describes how a drug accelerates or delays the repolarization process by measuring the drug-induced change of the time that it takes to reach a certain percentage of the total T vector trajectory length.

We used a non-parametric two-step bootstrapping simulation approach to determine the distribution of the effect profiles with subject as primary unit for resampling. The resampled subject data were then bootstrapped with ECG as secondary unit for resampling. For a given trajectory length percentage p, the predicted $\Delta\Delta Tr(p)c$ value was determined as the median bootstrap simulation value, and the two-sided 90% confidence band was determined as the 5 and 95% quantiles of the bootstrap simulation values. The functional models were fitted using the Julia package MixedModels (Bates et al., 2020) on a high-performance Linux cluster. Fitting the most complex functional model (combined treatment of lopinavir + ritonavir in study C with 406 model parameters and 50000 records) took approximately 1 h. Thus, we choose the number of bootstrap simulation steps as $N = 4000$ in the studies A and B, and 1000 in study C.

Determination of p_{zero}

Typically for multi-channel blocking drugs, the effect profiles are negative in the early repolarization phase (indicating accelerated repolarization) and positive in the late repolarization phase (indicating delayed repolarization). In order to describe the effective degree of balance of multiple channel blocks in one single number, we defined p_{zero} as the largest trajectory length percentage p where the effect profile changes its sign from negative to positive. Thus, effect profiles where all $\Delta\Delta$Tr(p)c values are negative were assigned a p_{zero} value of 100%, and effect profiles with all $\Delta\Delta$Tr(p)c values being positive were assigned a p_{zero} value of 1%. The distribution of p_{zero} was approximated using the bootstrap simulated effect profiles.

Classification of Predominant hERG Channel Blocking Drugs Versus Multichannel Blocking Drugs

We used p_{zero} as separation criterion to classify predominant hERG channel blocking drugs versus multichannel blocking drugs. We determined the classification performance for various threshold values in terms of sensitivity and specificity, using 1000 bootstrap samples of p_{zero} per drug. The thresholds were selected based on visual inspection of the distribution.

RESULTS

Heart Rate Correction for Tr(p)

The heart rate correction exponent α for the 100% trajectory quantile Tr(100) was estimated as 0.4437 (*SE*: 0.0119). α increased continuously with decreasing p, reaching a maximum of 1.0597 (*SE*: 0.0501) for the 6% trajectory quantile Tr(6), see **Figure 2**. The heart rate correction exponents for the individual percentages p are given in the **Supplementary File S1**. Note that for Tr(100), α lies between the heart rate correction exponents for the QT interval according to the Bazett formula (exponent = 0.5) and the Fridericia formula (exponent = 1/3).

T Vector Trajectories

Figure 3 displays the T vector trajectories and the (heart rate corrected) trajectory duration curves from three subjects in study A during a day under placebo and under quinidine treatment. The T vector trajectories under placebo reflect the diurnal variability within each subject. Following quinidine administration, the T vector trajectories are highly altered, with the manner of change varying between individuals. The T vector duration curves under placebo are well-aligned within the subjects. Following quinidine administration, the trajectory duration curves are strongly affected, such that the early part of the trajectory is passed faster, and the later part is delayed with strongest changes at about 2 h post-dosing.

The population average trajectory duration curves for placebo and quinidine at 1754 ng/mL plasma concentration are displayed in panel A of **Figure 4**, revealing an acceleration effect of quinidine in the initial 40% of the trajectory length and an average delay of about 50 ms at the end of repolarization. The related continuous quinidine effect profile measuring the placebo corrected change from baseline is displayed in panel B of

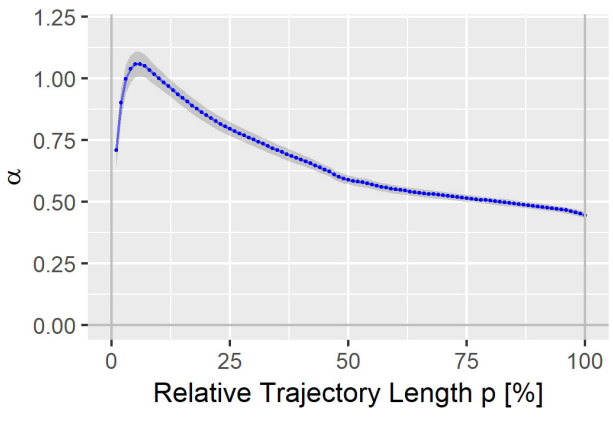

FIGURE 2 | Heart rate correction exponent α for the T vector trajectory quantiles Tr(p). The gray band denotes α ± standard error.

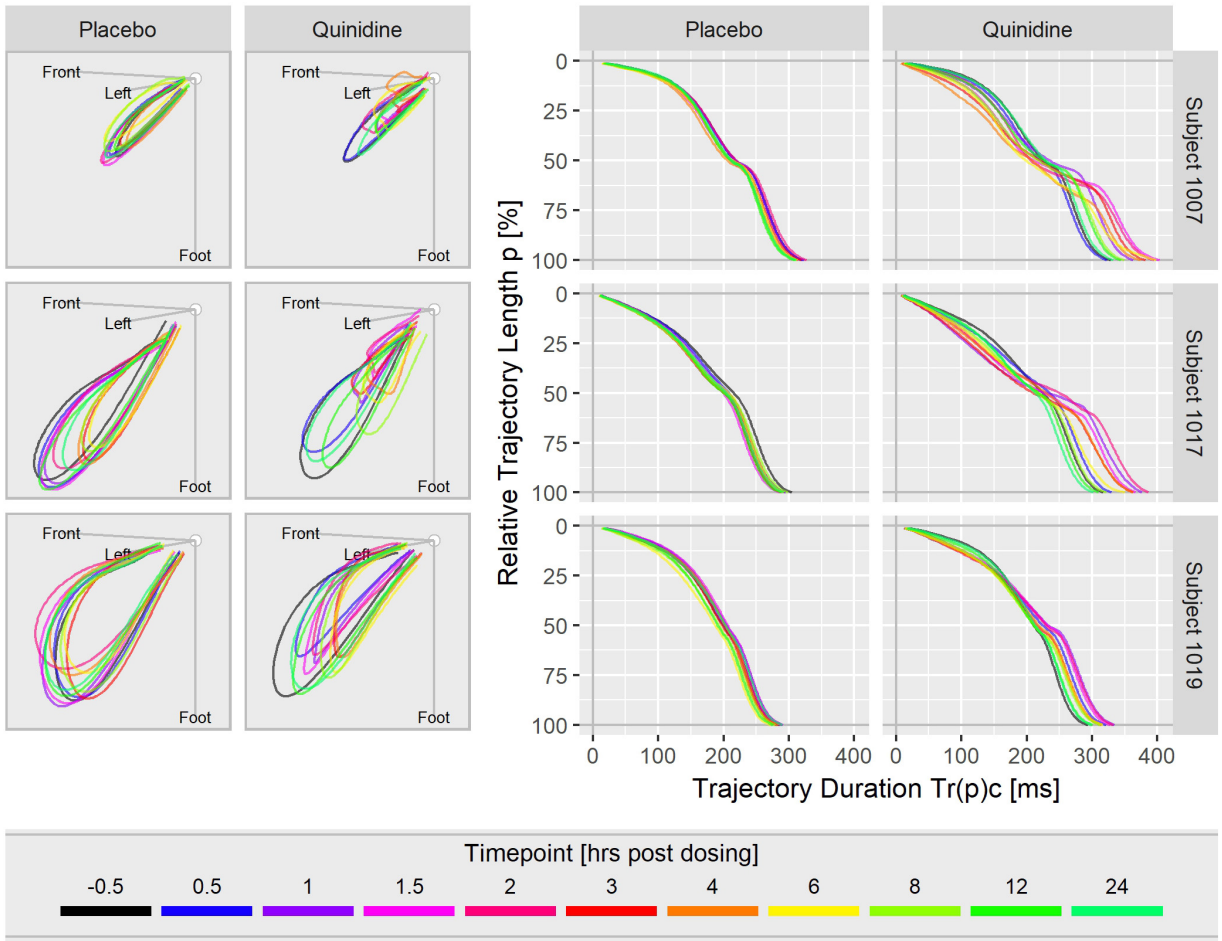

FIGURE 3 | T vector trajectories (left) and heart rate corrected trajectory duration curves (right) from three subjects under placebo and under quinidine treatment during a day. The colored timepoints denote the time in hours post-dosing. Quinidine maximum concentrations were 2130 ng/mL for subject 1007, 1100 ng/mL for subject 1017, 1680 ng/mL for subject 1019.

Figure 4. Gray lines represent bootstrap simulated effect profile samples, and the red lines denote the median and the 5 and 95% quantiles of the simulated effect profiles.

As can be seen in the trajectory duration curve for placebo, it takes about $2/3^{rd}$ of the J-T_{end} interval (Tr(50)c = 200 ms compared to Tr(100)c = 300 ms) to reach 50% of the entire trajectory length. A drug effect profile describes how the drug impacts the times it takes the heart vector to move along the T vector trajectory. Thus, negative $\Delta\Delta$Tr(p)c values (inflected to the left in **Figure 4B**) indicate accelerated repolarization, positive $\Delta\Delta$Tr(p)c values (inflected to the right in **Figure 4B**) indicate delayed repolarization. The effect on the 100% trajectory quantile Tr(100)c represents the drug effect on the J-T_{end} interval (corrected for heart rate).

Drug Effect Profiles in Studies A, B, and C

The drug effect profiles for the various treatment conditions in the three studies are displayed in the **Figures 5**–**7**. For studies A and C, the effect profiles show the predicted drug effects at the corresponding Cmax drug concentrations, with Cmax as the geometric mean of the subject's maximum drug concentrations. Furthermore, the prediction of the exposure response models at zero concentration (the so-called intercept) is displayed. An intercept significantly different from zero may indicate violation of the assumption about linear dependency of the drug effect on the drug concentration. For study B, the effect profiles show the drug effects at the average drug concentrations during the three treatment periods (morning, afternoon and evening). Details about the drug concentrations are further described in the appendices.

The dofetilide effect profile could be evaluated under four different conditions: in study A (**Figure 5A**), study B at afternoon and at evening (**Figure 6A**), and in study C (**Figure 7F**). All dofetilide effect profiles show up with similar shapes, characterized by an accelerated repolarization in the initial 20% of the T vector trajectory length and a continuously increased repolarization delay, with a final delay being roughly proportional to the given drug concentration.

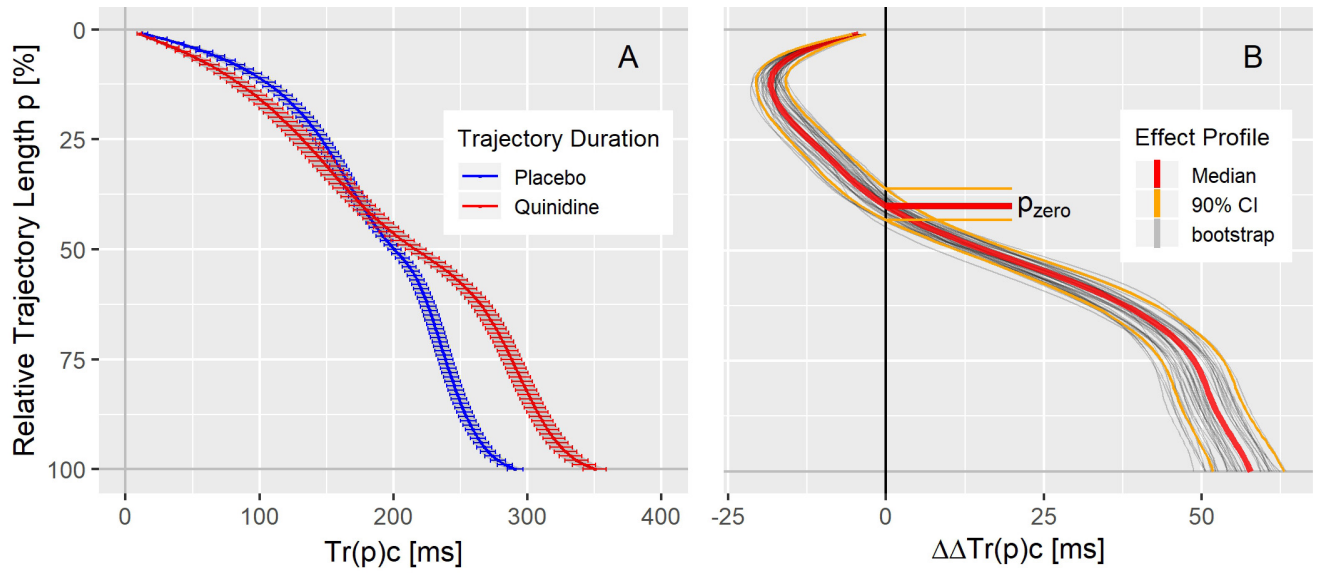

FIGURE 4 | (A) Average population T vector trajectory duration curves corrected for heart rate Tr(p)c in study A under placebo (blue) and quinidine (red) calculated for the plasma concentration of 1754 ng/mL with two-sided 90% confidence intervals. **(B)** Quinidine effect profile, showing the placebo corrected change from baseline Tr(p)c. The red lines denote the median, and the orange lines the 90% coverage of the bootstrap simulated continuous effect profiles. Gray lines are a subset of individual bootstrap simulations. The distribution of the zero-transition percentage p_{zero} of the simulated effect profiles (median: 5 and 95% quantile) is indicated by the horizontal lines.

The ranolazine effect profile was determined in study A (**Figure 5C**) and study C (**Figure 7B**). Both profiles show accelerated repolarization within the initial 50% of the T vector trajectory length, and delay through the end of repolarization. ΔΔTr(100)c was predicted in study A with 2043 ng/mL ranolazine concentration as 7.8 [5.8 to 9.8] ms; in study C with 3047 ng/mL concentration, the effect on ΔΔTr(100)c was 18.7 [13.0 to 24.6] ms.

Quinidine (in study A, **Figure 5B**) and chloroquine (in study C, **Figure 7A**) showed pronounced acceleration during the initial T vector trajectory length, and a strong delay through the end of repolarization. The ΔΔTr(100)c effect was 57.8 [51.7 to 63.2] ms for quinidine, and 38.4 [33.3 to 44.3] ms for chloroquine.

An even more pronounced acceleration during the initial 2/3rd of the T vector trajectory length was observed for the drug combination of lopinavir plus ritonavir (**Figure 7C**) with maximum accelerated repolarization at the 45% trajectory length percentage of ΔΔTr(45)c = −23.5 [−29.0 to −15.2] ms. In the further course of the repolarization, however, there was a delay which ended in a ΔΔTr(100)c value of 9.1 [3.3 to 14.6] ms.

In study A, verapamil caused a minor delay at the end of repolarization with ΔΔTr(100)c = 1.3 [−1.4 to 4.0] ms at a concentration of 114 ng/mL (**Figure 5D**). In study C, the predicted ΔΔTr(100)c at the concentration of 377 ng/mL was 13.3 [7.9 to 19.5] ms (**Figure 7D**). The effect profiles for both cases showed a small but clear acceleration during the first T vector trajectory half. The maximum acceleration in study A was observed for ΔΔTr(20)c with −5.1 [−7.1 to −2.9] ms; in study C the maximum acceleration was observed for ΔΔTr(16)c with −8.0 [15.6 to −1.2] ms.

In study B, both mexiletine (**Figure 6B**) and lidocaine (**Figure 6C**) shortened the J-T_{end} interval, indicated by the ΔΔTr(100)c value of −8.0 [−9.5 to −6.3] ms for mexiletine at an average concentration of 618 ng/mL and by −4.6 [−6.6 to −2.6] ms for lidocaine at an average concentration of 1034 ng/mL. These acceleration effects were generated within the first 50% of the T vector trajectory length and retained about constant through the end of repolarization. When mexiletine (**Figure 6B**) and lidocaine (**Figure 6C**) were combined with dofetilide in the afternoon and evening treatment phases, acceleration persisted during the initial repolarization. From about 40% of the length of the T vector trajectory the repolarization was delayed.

The moxifloxacin effect on repolarization was assessed in the morning and afternoon phases of study B where the effect profiles showed a continuously growing delay without any indication for acceleration (**Figure 6D**). The additional evening administration of diltiazem resulted in accelerated repolarization during the initial 40% of the T vector trajectory length while leaving the final J-T_{end} prolongation nearly unchanged compared to the afternoon.

Diltiazem was also assessed in study C. Here, the pure diltiazem effect profile showed a slight, continuously increasing delay, ending in a ΔΔTr(100)c value of 6.8 [3.0 to 10.8] ms for the Cmax concentration of 151 ng/mL (**Figure 7E**). The combination of diltiazem with dofetilide produced an effect profile with pronounced acceleration during the first 40% of the T vector trajectory length and showing large variability in the amount of acceleration (**Figure 7G**). Notably, the diltiazem Cmax concentrations differed considerably between the eight subjects enrolled in this treatment (from 165 to 1089 ng/mL).

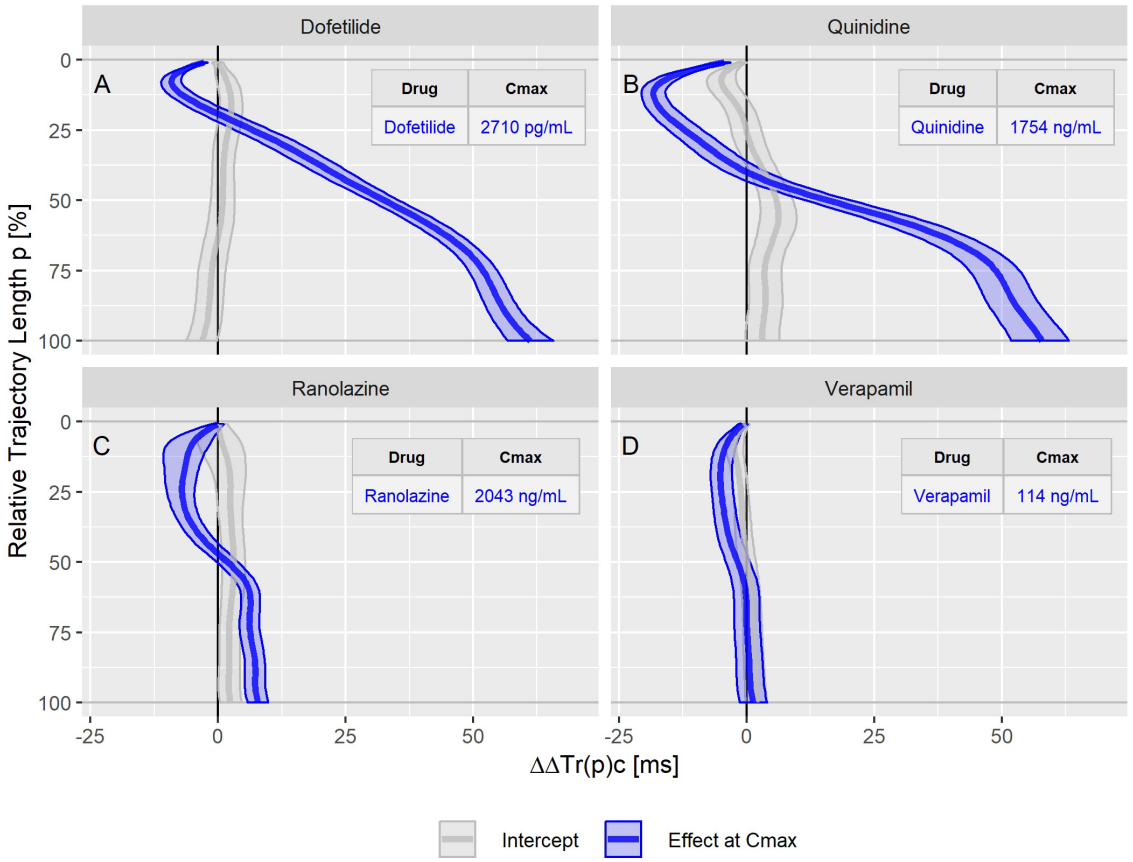

FIGURE 5 | Continuous drug effect profile estimates with 90% confidence bands for the drugs dofetilide **(A)**, quinidine **(B)**, ranolazine **(C)**, and verapamil **(D)** in study A. The blue bands denote the estimated drug effect at the drug's maximum plasma concentration (Cmax). The gray bands are the model prediction at zero drug concentration.

Classification of Predominant hERG Channel Blocking Drugs Versus Multichannel Blocking Drugs

Moxifloxacin, dofetilide, chloroquine, and quinidine were considered as predominant hERG channel blocking drugs with potentially higher proarrhythmic risk, while ranolazine, verapamil and the combination of lopinavir + ritonavir were considered multichannel blocking drugs with a low proarrhythmic risk (Gintant et al., 2016; Vicente et al., 2019). Mexiletine and lidocaine were not included since they did not prolong the J-T_{end} interval at all. Diltiazem was not included since the observed acceleration tendency during early repolarization when combined with moxifloxacin (**Figure 6**) or dofetilide (**Figure 8**) was not visible in the pure diltiazem effect profile (**Figure 7**). This may indicate limitations of the given model for this compound.

Figure 8 displays the bootstrap simulated common distribution of two repolarization characteristics for the mentioned drugs: the x-axis denotes the drug induced J-T_{end} prolongation measured by $\Delta\Delta$Tr(100)c, and the y-axis denotes the p_{zero} value, that is the percentage of the T vector trajectory length where accelerated repolarization reverts to delayed repolarization. Dofetilide was assessed under four treatment conditions what generated four distinct dofetilide data clouds, reflecting the different drug concentrations. Ranolazine, moxifloxacin, and verapamil were assessed under two treatment conditions each. Thus, two distinct data clouds can be identified for each of these drugs. Notably, the y-levels of the dofetilide, ranolazine, and moxifloxacin data clouds are quite similar for the given drug, indicating independence of p_{zero} from the drug concentrations.

A threshold value of 43% for p_{zero} separated the predominant hERG channel blocking drugs with potentially higher proarrhythmic risk from the multichannel blocking drugs having a low proarrhythmic risk with a sensitivity of 0.99 and a specificity of 0.97.

DISCUSSION

The T vector reflects the entire myocardial potential distribution at a given moment during repolarization as seen from the body surface ECG. The single-cell myocardial action potential itself is an expression of a complex dynamic process modulated by multiple ion channels and other biological

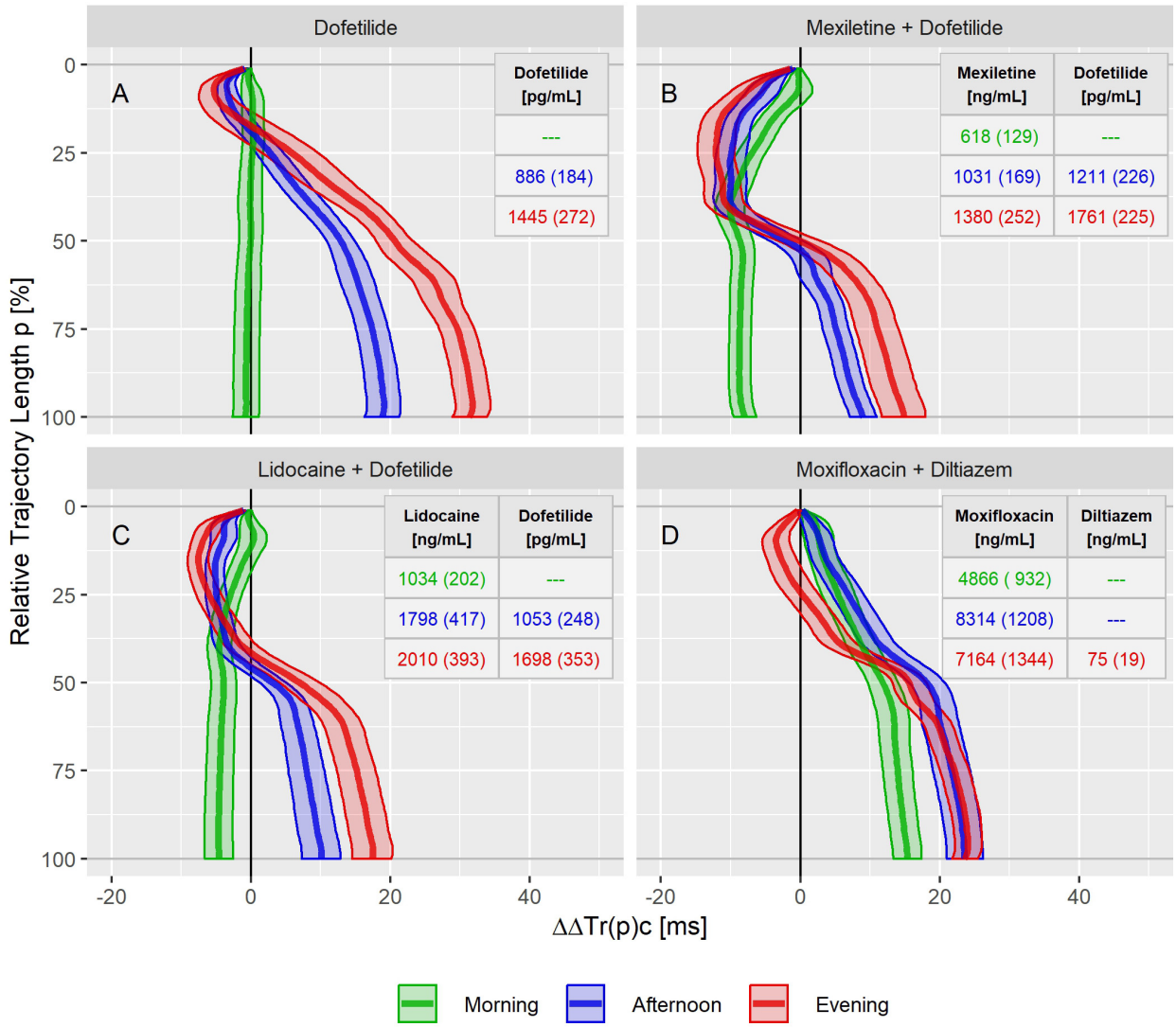

FIGURE 6 | Continuous drug effect profile estimates with 90% confidence bands for dofetilide **(A)**, mexiletine plus dofetilide **(B)**, lidocaine plus dofetilide **(C)**, and moxifloxacin plus diltiazem **(D)** at the three treatment timepoints in study B. Numbers denote the drug's average (standard deviation) plasma concentration within the timepoints.

factors (Nerbonne and Kass, 2005). On the scale of the entire heart, the myocardial potential distribution at a certain time during repolarization is generated by myocytes with different action potential characteristics (e.g., sub-endocardial, sub-epicardial, mid-myocardium cells) being activated at different times during the heart's depolarization process. Acknowledging that the details of the mapping from the collection of single cardiomyocyte action potentials to the whole-organ T vector are beyond our competence, our only assumption is that the temporal progression of the myocardial potential distribution is reflected in the temporal progression of the T vector. Hence, we consider the TVV, the velocity with which the T vector moves along the T vector loop, as an electrocardiographic measure of the repolarization dynamic.

Our results demonstrate that drugs inhibiting myocardial ion channels affect repolarization dynamics in a consistent way which can be quantified by TVV analysis. The signatures extracted from the TVV drug effect profiles allow an estimation of how strongly depolarizing and repolarizing ion currents are blocked by a drug. And finally, they allow highly accurate separation of drugs with potentially higher proarrhythmic risk from drugs with low proarrhythmic risk in the data sets available for the current study.

Ion Channel Blocks as Reflected in the Continuous Effect Profile

In this study, we describe ventricular repolarization dynamics in terms of the T vector trajectory duration curve, and we introduce continuous drug effect profiles as a new method for measuring drug effects on the repolarization dynamics throughout the entire

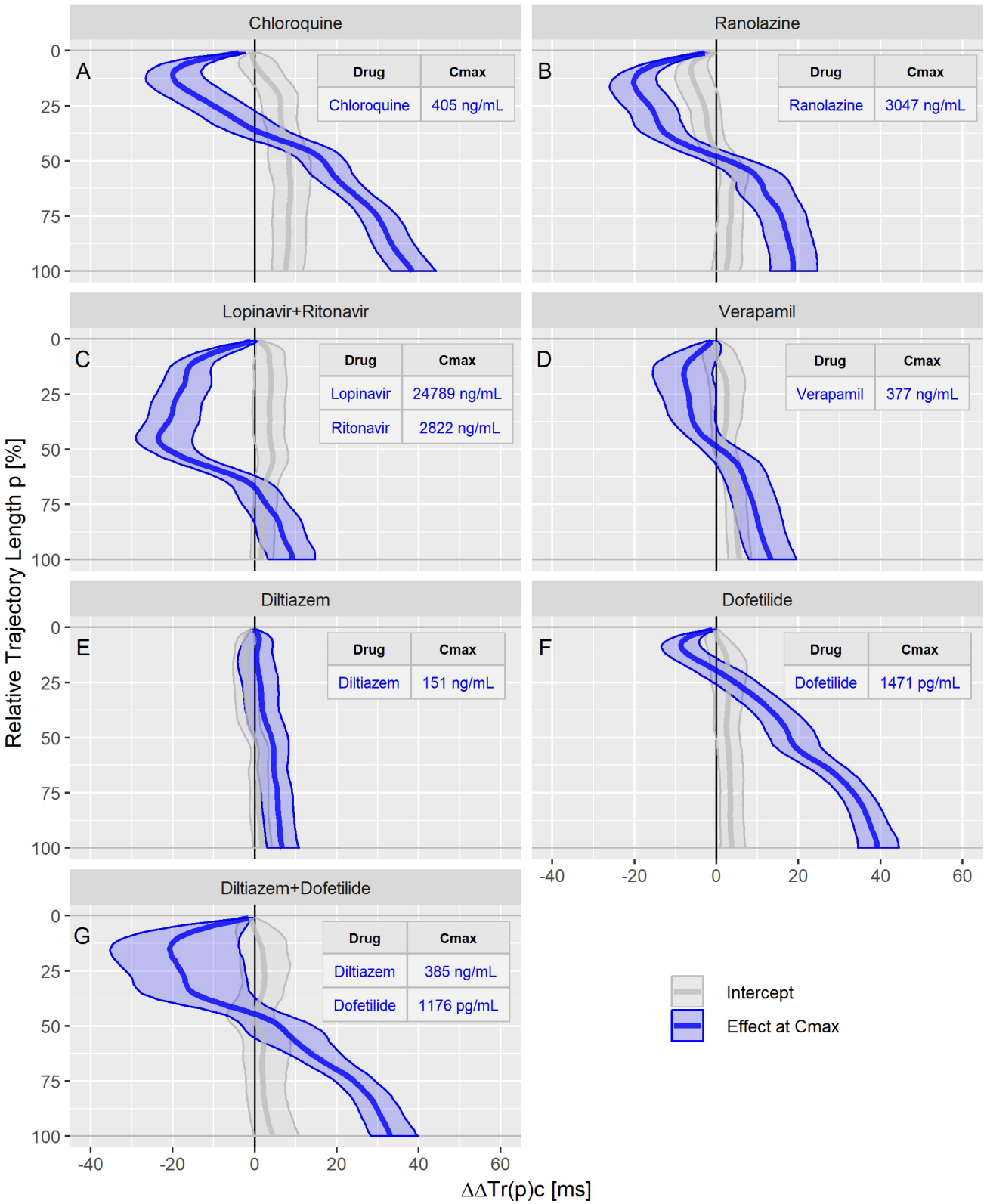

FIGURE 7 | Continuous drug effect profile estimates with 90% confidence bands for chloroquine **(A)**, ranolazine **(B)**, lopinavir plus ritonavir **(C)**, verapamil **(D)**, diltiazem **(E)**, dofetilide **(F)**, and diltiazem plus dofetilide **(G)** in study C. The blue bands denote the estimated drug effect for the drug's maximum plasma concentration (Cmax). The gray bands are the model prediction at zero drug concentration.

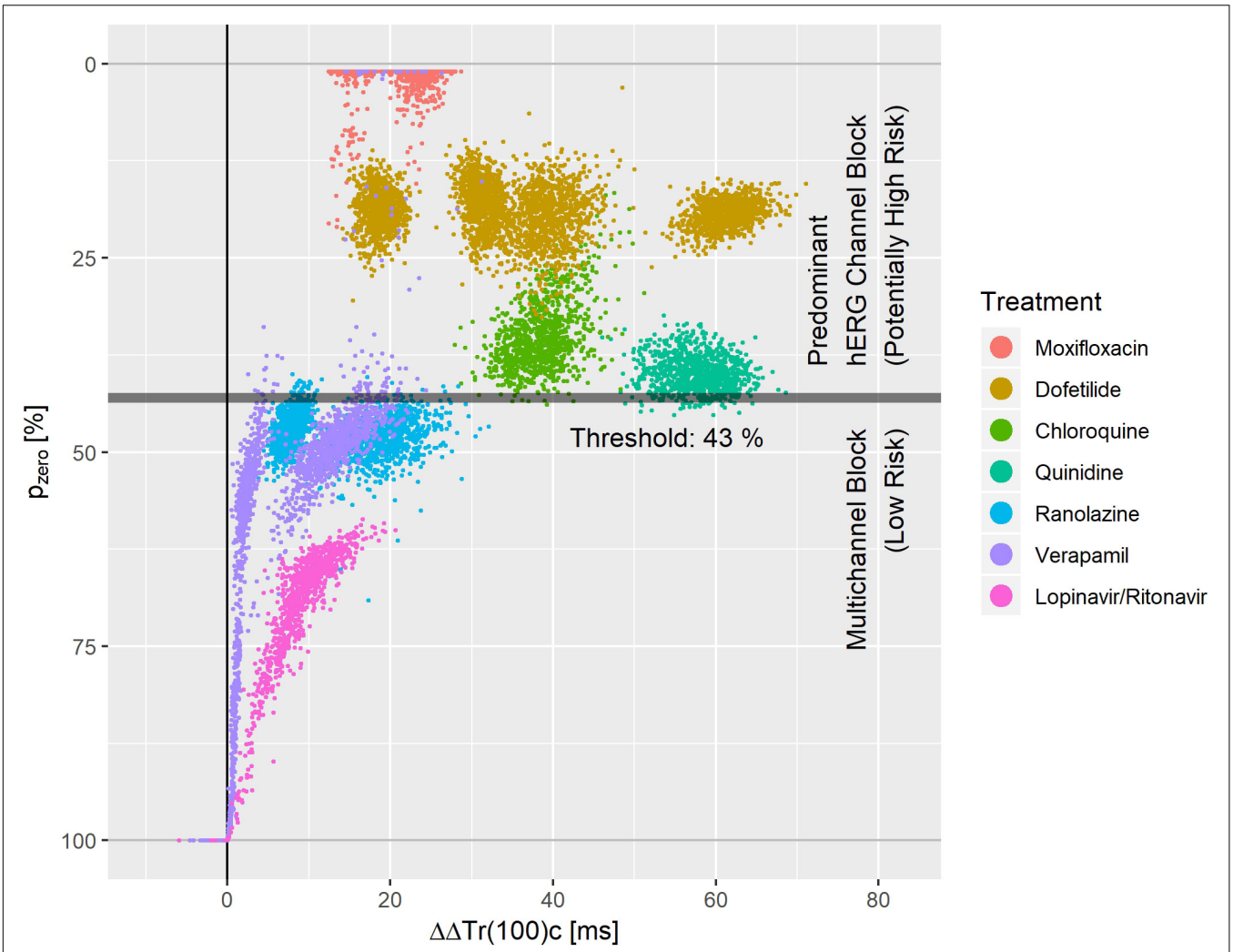

FIGURE 8 | Bootstrap simulated common distribution of p_{zero} (the effect profile's zero-transition percentage p) and ΔΔTr(100)c (the drug-induced the J-T_{end} prolongation) for predominant hERG channel blocking drugs with potentially higher proarrhythmic risk and multichannel blocking drugs with low proarrhythmic risk.

ventricular repolarization phase as seen in the J-T_{end} interval of the surface ECG.

Figure 3 shows that the T vector trajectories themselves differ very much between subjects and are modulated by cofactors like diurnal variations. Quinidine furthermore affects the trajectory shape and increases trajectory variability. Therefore, it is remarkable that the T vector trajectory duration curves are well-aligned within a given subject under placebo conditions, indicating that the repolarization dynamic follows a subject-specific pattern that is quite constant under normal conditions. For quinidine, we observe a consistent pattern such that the initial 40% of the T vector trajectories are passed faster while the remaining trajectory course is increasingly delayed (**Figure 3**). This quinidine effect on the cardiac repolarization dynamic in the entire population is quantitatively represented in the continuous effect profile as shown in **Figure 4**. Our results suggest that the repolarization dynamics and their drug induced changes are less affected by intra and inter-individual confounding factors compared to classical T waveform morphology characteristics. Placing emphasis on the quantification of relative changes in the timing of repolarization appears to contribute to accentuation and more consistent emergence of the drug effect. This held true not only for quinidine but also for all other drugs considered in this study.

This general effect profile pattern, characterized by early acceleration and late delay, was observed for all drugs that block both, the inward late sodium and L-type calcium currents, and the outward potassium currents (quinidine, ranolazine, chloroquine, lopinavir+ritonavir, verapamil). Interestingly, dofetilide as a predominant hERG blocker, also showed a slight but consistent and pronounced acceleration during the initial 20% of the trajectory length (see **Figures 5A**, **6A**, **7F**), whereas the effect profile of moxifloxacin showed delayed repolarization along the entire trajectory in both investigated conditions (**Figure 6D**). One explanation for this observed acceleration could be that although *in vitro* experiments report only a very

minor blocking of inward currents by dofetilide (Crumb et al., 2016), TVV analysis is based on *in vivo* measurements, which may also reveal drug effects that reflect more complex ion flow interactions.

Drugs predominantly blocking the late sodium channel (mexiletine – **Figure 6B**, lidocaine – **Figure 6C**) showed effect profiles reflecting continuous acceleration during the initial 40% of the trajectories. In the following trajectory section, the accumulated level of acceleration is merely maintained. Furthermore, combining mexiletine or lidocaine with dofetilide (**Figures 6B,C**) showed a slightly intensified acceleration during the initial trajectory, which then was compensated by the increasing delay along the further trajectory caused by dofetilide's potassium channel block.

Diltiazem, a calcium antagonist, administered together with moxifloxacin (**Figure 6D**) shifted the pure moxifloxacin effect profile to the left in the initial half of the trajectory, indicating an acceleration effect by diltiazem. Coadministration of diltiazem plus dofetilide (**Figure 7G**) created a similar acceleration pattern. However, pure diltiazem did generate a slight but continuously increasing delay over the entire trajectory (**Figure 7E**). Since the effective diltiazem concentration under single drug condition was between the diltiazem concentrations under the combination with moxifloxacin, respectively dofetilide, the diltiazem concentration cannot explain this somehow contradicting effect.

Our results strongly suggest that the observed acceleration of repolarization reflects a blocking of depolarizing inward ion currents (positive inward charge transfer), while the delay of repolarization reflects a blocking of repolarizing currents (outward transfer of positive charge). This interpretation is supported by the timing of activation of the L-type calcium and the late sodium currents early during ventricular repolarization, compared with the peak of the hERG/IKr current occurring during terminal repolarization of the action potential (Nerbonne and Kass, 2005). We assume that the physiologic activation sequence of the ion channels is preserved by the mapping of the cardiac action potentials onto the ECG. Hence, the observation that accelerations emerged at the lower percentages of the trajectory length (**Figures 5**–**7**) is in accordance with the expectation from physiology. Likewise, it fits in the picture that if such acceleration is counteracted by concurrent block of the hERG/IKr-channel, the related reduction of acceleration – and eventually reversion to a delay – becomes particularly evident around the mid-range trajectory length percentages between p = 40% and p = 60%. Here, we generally observed the strongest accumulation rate of delay for multichannel blocking drugs or drug combinations (**Figures 5**–**7**). Note that this corresponds to the region around the peak of the T-wave as discussed in Section "Relation of TVV to QT and J-Tpeak."

We think that the suggested TVV analysis approach provides a new perspective on repolarization dynamics, linking body surface measurements to cellular electrophysiological effects. We observe that effect profiles from different compounds generally differ in shape and magnitude, while effect profiles of the same compound exhibit stable morphologies over studies (with magnitude scaling related to differences in plasma concentration). Likewise, effect profiles of different drugs inhibiting the same channels to a comparable extent show similar signatures in their effect profiles. This makes us optimistic that the suggested drug effect profiles may turn out in the future to represent a characteristic fingerprint of a drug's specific ion channel blocking properties and/or extent of proarrhythmic risk. They may even contain more interpretable information about the ion channels involved. Instead of presenting additional details that could possibly support this idea, but would still remain speculative, we would like to offer collaboration to scientific groups specialized in modeling electrophysiology at different scales from the ion channel level over the cellular to the organ and ECG level to verify the TVV observations using existing models.

TVV and Risk Assessment

We measured the level of balance between blockage of depolarizing and repolarizing ion flow by the p_{zero} parameter, that is the T vector trajectory length percentage where acceleration transitions to delay. A threshold value of p_{zero} = 43% separated predominant hERG channel blocking drugs with potentially higher proarrhythmic risk (moxifloxacin, dofetilide, quinidine, chloroquine) from multichannel blocking drugs with low proarrhythmic risk (ranolazine, verapamil, lopinavir+ritonavir) with sensitivity 0.99 and specificity of 0.97. This is superior to the separation performance reported for J-T_{peak}c (Vicente et al., 2016) or for the 40% T vector trajectory duration quantile Tr40c (Bystricky et al., 2019). Tr40c describes the drug-induced change of time to reach 40% of the T vector trajectory length. In contrast, the parameter p_{zero} presented here describes the length fraction of the trajectory where the repolarization process is accelerated. Both parameters are correlated, but in our opinion the new parameter p_{zero} better quantifies the balance of multichannel blocks.

We would like to point out that both mexiletine and lidocaine would be correctly identified as 'low risk' compounds using p_{zero} = 43% as threshold. They were omitted from **Figure 8**, since both drugs had negative $\Delta\Delta$Tr(100)c values with p_{zero} = 100%.

Multiple clusters from the same drug in **Figure 8** arise from differences in plasma concentration. For most of the drugs with sufficiently pronounced (>10 ms) prolongation of J-T_{end}, the distribution of p_{zero} was almost independent from the J-T_{end} prolongation. This shows that p_{zero} provides substantial information about a possible proarrhythmic risk, which goes beyond QTc.

For a multi-channel blocking drug, the ratio of the strengths of the blockade can change with the drug concentration. Hence, we would expect that p_{zero} may also vary, at least for extreme concentrations. We should therefore assume that more complex separation rules are required when considering additional drugs and extended concentration ranges. Moreover, there is no reason to suppose that lower values of p_{zero} would necessarily correspond to higher proarrhythmic risk. The lower values of p_{zero} observed for moxifloxacin in **Figure 8** compared, for example, to dofetilide do not mean that moxifloxacin would indicate a higher propensity for arrhythmia

than dofetilide. Rather, there may exist ranges of p_{zero} that reflect potentially critical electrophysiological lability. Again, only the analysis of more compounds will help to shed light on this question.

Finally, the proarrhythmic risk of a drug may depend on factors specific to the individual. A risk assessment is therefore not always conclusive and can be controversial, as with moxifloxacin (Liu et al., 2017; Goto et al., 2020; Yang et al., 2020).

Relation of TVV to QT and J-T_{peak}

Our TVV-based analysis approach targets the J-T_{end} interval, excluding the QRS complex, i.e., the heart's depolarization process. Therefore, the measured drug-induced change of QTc should be equal to the measured change of Tr(100)c for drugs that do not affect depolarization (the used heart rate correction methods may cause some slight differences between the measurements). For drugs that prolong depolarization, such as chloroquine (Vicente et al., 2019), the observed changes in Tr(100)c will be accordingly smaller than the observed changes in QTc.

The J-T_{peak} interval was corrected for heart rate in the referenced studies A, B and C, similar to the way we corrected heart rate for the trajectory quantiles Tr(p) in our analyses. The heart rate correction exponent for J-T_{peak} was 0.58 (Johannesen et al., 2014), which is similar to the heart rate correction exponent that we identify for the 50 to 55% trajectory length percentages (**Figure 2**).

The T_{peak} was typically observed to be between 50 and 60% of the T vector trajectory length (Bystricky et al., 2019). This means that the T vector trajectory path up to the point with largest distance from the origin is slightly longer than the trajectory path back to depolarization (visible in **Figure 1**). Thus, the observed drug effects reflected in the J-T_{peak}c parameter (the main parameter of interest in the studies A, B, and C) might be compared with the drug effect profile sections between 50 and 60% of the trajectory length. In study C, named CiPA Phase I ECG Biomarker Validation Study, the prespecified primary endpoint was to show that balanced ion channel-blocking drugs that prolong QTcF would not prolong J-T_{end}c defined by an upper bound of the two-sided 90% confidence interval of $\Delta\Delta$J-T_{end}c < 10 ms at C_{max} (Vicente et al., 2019). This primary endpoint was met for verapamil and lopinavir/ritonavir but was slightly missed by ranolazine (the upper bound of the 90% confidence interval of $\Delta\Delta$J-T_{peak}c for ranolazine was 12.0 ms). As can be seen in **Figure 7**, the upper bound of the two-sided 90% confidence band of ranolazine's effect profile passes the 10 ms at about 50% of the trajectory length. Also, study C reported a negative slope for $\Delta\Delta$J-T_{peak}c in the exposure-response analysis of lopinavir/ritonavir. This corresponds to the negative effect profile at p between 50 and 60% for lopinavir+ritonavir in **Figure 7**. Finally, the informative value of the measured $\Delta\Delta$J-T_{peak}c change for chloroquine was put into question by the authors of study C due to a positive intercept observed in the exposure-response model for chloroquine. This type of non-proportionality was also observed in our analysis, visible in the intercept band for chloroquine in **Figure 7**, being significantly larger than zero from about $p = 20$ to 100%.

These observations indicate consistency between the TVV analysis and the J-T_{peak}c analyses observed in studies A, B, and C. However, we think that the major information characterizing balanced ion channel-blocking drugs is represented over the entire repolarization phase captured in the effect profile, but which is missed to some extent by looking at only one point in time (T_{peak}). From a method perspective, providing the effect profile in a continuous fashion constitutes a substantial extension to our previous work (Bystricky et al., 2019). The latter described the effect profile using 10 separate mixed-effects models each associated with a fixed relative trajectory position. Thus, the repolarization period was discretized at 10 equidistant trajectory length percentages. In contrast, the approach presented here rests on a continuous approximation of the effect profile using a number of B-splines. A single mixed-effects model depending on the parameters of this approximation permits estimation of the entire effect profile. This way, the number of free parameters is independent of the sampling density of the effect profile, and dependencies between the trajectory percentages are inherently considered. We are confident that further advantages of this continuous assessment will be demonstrable with more data covering additional compounds becoming available in the future.

Limitations

Overreading of the ECG annotations was done in an unblinded fashion, but all attempts were made to prevent bias related to drug or drug concentration.

Typically, the applicability of regression models should be evaluated by thoroughly examining the properties of the estimated model parameters and the residuals (Garnett et al., 2018). The functional extension of the mixed effects models used in our analyses adds an additional layer of complexity to the models, making model verification challenging. We therefore regard the proposed functional regression analysis approach, which to our knowledge has been described for the first time in the context of ECG modeling, as a method that requires further scrutiny.

The performance of p_{zero} in separating proarrhythmic drugs from drugs with low proarrhythmic risk was evaluated based on a retrospective analysis of a limited number of drugs used in the three CiPA studies. It will be necessary to study other drugs with known proarrhythmic risk to get an understanding of the generalizability of this method and to propose standard, quantifiable, and reproducible thresholds of concern across a larger and more diverse input dataset.

In addition, it will be necessary to evaluate drugs that specifically affect depolarization to learn how this may influence the drug's TVV effect profile and p_{zero}.

The TVV analysis presented here explores repolarization on a global beat level, not taking into account beat-to-beat variability of repolarization. Acknowledging that beat-to-beat dynamic aspects play a crucial role in the pathway to arrhythmia, extending the TVV analysis for capturing beat-to-beat dynamics may possibly improve proarrhythmic risk assessment given that data of sufficient length is available.

CONCLUSION

The TVV-based analysis approach provides new and detailed insights into the repolarization dynamics measured clinically. It links ECG characteristics to cellular electrophysiological effects of multiple ion currents that define repolarization. We have demonstrated that the TVV-derived drug effect profile reveals important information about a drug's proarrhythmic risk.

DATA AVAILABILITY STATEMENT

Publicly available datasets were analyzed in this study which can be found here: https://www.physionet.org/content/ecgrdvq/1.0.0/, https://www.physionet.org/content/ecgdmmld/1.0.0/, and https://www.physionet.org/content/ecgcipa/1.0.0/.

ETHICS STATEMENT

The studies involving human participants were reviewed and approved by US Food and Drug Administration (FDA) Research Involving Human Subjects Committee and the local institutional review board. All participants gave written informed consent.

AUTHOR CONTRIBUTIONS

WB and CM developed the TVV analysis method. WB analyzed the data. DC supervised this study. All authors contributed to the discussion and prepared the manuscript.

FUNDING

The analysis presented was funded by AbbVie. AbbVie contributed to the design, research, and interpretation of data, writing, reviewing, and approving the publication. GG, DB, and DC are employees of AbbVie and may hold stock. WB and CM are consultants for AbbVie.

ACKNOWLEDGMENTS

Our work is completely based on the impressive groundwork of the teams led by David Strauss and supported by the U.S. Food and Drug Administration, CiPA, the Cardiac Safety Research Consortium and the International Consortium for Innovation and Quality in Pharmaceutical Development. It was the published studies A, B, and C with the combination of different compounds that made it possible for us to develop this new TVV analysis approach and the continuous drug effect profiles. We would very much appreciate the availability of many more study data in the public to give the scientific community the opportunity to develop new approaches that the authors may not have originally considered. We also want to thank our AbbVie colleagues Kent Kamradt, Panagiotis Flevaris, and Patrick Welsh for valuable discussion and review of the manuscript.

SUPPLEMENTARY MATERIAL

The Supplementary Material for this article can be found online at: https://www.frontiersin.org/articles/10.3389/fphys.2020.567383/full#supplementary-material

REFERENCES

Acar, B., Yi, G., Hnatkova, K., and Malik, M. (1999). Spatial, temporal and wavefront direction characteristics of 12-lead T-wave morphology. *Med. Biol. Eng. Comput.* 37, 574–584. doi: 10.1007/BF02513351

Bates, D., Alday, P., Kleinschmidt, D., Calderón, J. B. S., Noack, A., Kelman, T., et al. (2020). *JuliaStats/MixedModels.jl: v2*.3.0.

Baumert, M., Porta, A., Vos, M. A., Malik, M., Couderc, J.-P., Laguna, P., et al. (2016). QT interval variability in body surface ECG: measurement, physiological basis, and clinical value: position statement and consensus guidance endorsed by the European Heart Rhythm Association jointly with the ESC Working Group on Cardiac Cellular Electrophysiology. *Europace* 18, 925–944. doi: 10.1093/europace/euv405

Berger, R. D., Kasper, E. K., Baughman, K. L., Marban, E., Calkins, H., and Tomaselli, G. F. (1997). Beat-to-beat QT interval variability: novel evidence for repolarization lability in ischemic and nonischemic dilated cardiomyopathy. *Circulation* 96, 1557–1565. doi: 10.1161/01.cir.96.5.1557

Bezanson, J., Karpinski, S., Viral, B., and Shah, V. B. (2020). *The Julia Programming Language: A Fresh Approach to Technical Computing*. Available online at: https://julialang.org (accessed March 20, 2020).

Brennan, T. P., and Tarassenko, L. (2012). Review of T-wave morphology-based biomarkers of ventricular repolarisation using the surface electrocardiogram. *Biomed. Signal Process. Control* 7, 278–284. doi: 10.1016/j.bspc.2011.05.010

Britton, O. J., Abi-Gerges, N., Page, G., Ghetti, A., Miller, P. E., and Rodriguez, B. (2017). Quantitative comparison of effects of dofetilide, sotalol, quinidine, and verapamil between human ex vivo trabeculae and in silico ventricular models incorporating inter-individual action potential variability. *Front. Physiol.* 8:597. doi: 10.3389/fphys.2017.00597

Bystricky, W., Maier, C., Gintant, G., Bergau, D., Kamradt, K., Welsh, P., et al. (2019). T vector velocity: a new ECG biomarker for identifying drug effects on cardiac ventricular repolarization. *PLoS One* 14:e0204712. doi: 10.1371/journal.pone.0204712

Cai, C., Guo, P., Zhou, Y., Zhou, J., Wang, Q., Zhang, F., et al. (2019). Deep learning-based prediction of drug-induced cardiotoxicity. *J. Chem. Inform. Model.* 59, 1073–1084. doi: 10.1021/acs.jcim.8b00769

CiPA (2020). *The CiPA Project Homepage*. Available online at: https://cipaproject.org/about-cipa/ (accessed March 20, 2020).

Couderc, J.-P. (2009). Measurement and regulation of cardiac ventricular repolarization: from the QT interval to repolarization morphology. *Philos. Trans. Ser. A Math. Phys. Eng. Sci.* 367, 1283–1299. doi: 10.1098/rsta.2008.0284

Crumb, W. J., Vicente, J., Johannesen, L., and Strauss, D. G. (2016). An evaluation of 30 clinical drugs against the comprehensive in vitro proarrhythmia assay (CiPA) proposed ion channel panel. *J. Pharmacol. Toxicol. Methods* 81, 251–262. doi: 10.1016/j.vascn.2016.03.009

Dower, G. E., Machado, H. B., and Osborne, J. A. (1980). On deriving the electrocardiogram from vectoradiographic leads. *Clinical Cardiology* 3, 87–95. doi: 10.1002/clc.1980.3.2.87

Dutta, S., Chang, K. C., Beattie, K. A., Sheng, J., Tran, P. N., Wu, W. W., et al. (2017). Optimization of an in silico cardiac cell model for proarrhythmia risk assessment. *Front. Physiol.* 8:616. doi: 10.3389/fphys.2017.00616

Fossa, A. A. (2017). Beat-to-beat ECG restitution: a review and proposal for a new biomarker to assess cardiac stress and ventricular tachyarrhythmia vulnerability. *Ann. Noninvas. Electrocardiol.* 22:e12460. doi: 10.1111/anec.12460

Fossa, A. A., and Zhou, M. (2010). Assessing QT prolongation and electrocardiography restitution using a beat-to-beat method. *Cardiol. J.* 17, 230–243.

Garnett, C., Bonate, P. L., Dang, Q., Ferber, G., Huang, D., Liu, J., et al. (2018). Scientific white paper on concentration-QTc modeling. *J. Pharmacokinet. Pharmacodyn.* 45, 383–397. doi: 10.1007/s10928-017-9558-5

Gintant, G., Sager, P. T., and Stockbridge, N. (2016). Evolution of strategies to improve preclinical cardiac safety testing. *Nat. Rev. Drug Discov.* 15, 457–471. doi: 10.1038/nrd.2015.34

Goldberger, A. L., Amaral, L. A., Glass, L., Hausdorff, J. M., Ivanov, P. C., Mark, R. G., et al. (2000). PhysioBank, PhysioToolkit, and PhysioNet: components of a new research resource for complex physiologic signals. *Circulation* 101, E215–E220.

Goto, A., Sakamoto, K., Hagiwara-Nagasawa, M., Kambayashi, R., Chiba, K., Nunoi, Y., et al. (2020). In vivo analysis of the effects of intravenously as well as orally administered moxifloxacin on the pharmacokinetic and electrocardiographic variables along with its torsadogenic action in the chronic atrioventricular block cynomolgus monkeys. *J. Pharmacol. Sci.* 143, 272–280. doi: 10.1016/j.jphs.2020.05.006

Graff, C., Matz, J., Christensen, E. B., Andersen, M. P., Kanters, J. K., Toft, E., et al. (2009). Quantitative analysis of T-wave morphology increases confidence in drug-induced cardiac repolarization abnormalities: evidence from the investigational IKr inhibitor Lu 35-138. *J. Clin. Pharmacol.* 49, 1331–1342. doi: 10.1177/0091270009344853

Han, S., Han, S., Kim, K.-S., Lee, H.-A., and Yim, D.-S. (2019). Usefulness of Bnet, a simple linear metric in discerning Torsades De pointes risks in 28 CiPA drugs. *Front. Pharmacol.* 10:1419. doi: 10.3389/fphar.2019.01419

Haverkamp, W., Breithardt, G., Camm, A. J., Janse, M. J., Rosen, M. R., Antzelevitch, C., et al. (2000). The potential for QT prolongation and pro-arrhythmia by non-anti-arrhythmic drugs: clinical and regulatory implications. Report on a Policy Conference of the European Society of Cardiology. *Cardiovasc. Res.* 47, 219–233. doi: 10.1016/s0008-6363(00)00119-x

Hnatkova, K., Vicente, J., Johannesen, L., Garnett, C., Strauss, D. G., Stockbridge, N., et al. (2019). Detection of T Wave peak for serial comparisons of JTp interval. *Front. Physiol.* 10:934. doi: 10.3389/fphys.2019.00934

Hondeghem, L. M. (2008). QT prolongation is an unreliable predictor of ventricular arrhythmia. *Heart Rhythm.* 5, 1210–1212. doi: 10.1016/j.hrthm.2008.05.006

Hwang, M., Han, S., Park, M. C., Leem, C. H., Shim, E. B., and Yim, D.-S. (2019). Three-dimensional heart model-based screening of proarrhythmic potential by in silico simulation of action potential and electrocardiograms. *Front. Physiol.* 10:1139. doi: 10.3389/fphys.2019.01139

ICH (2005a). *The Clinical Evaluation of QT/QTc Interval Prolongation and Proarrhythmic Potential for Non-Antiarrhythmic Drugs*. Geneva: *ICH*.

ICH (2005b). *The non-Clinical Evaluation of the Potential for Delayed Ventricular Repolarization (QT Interval Prolongation) by Human Pharmaceuticals S7B*. Geneva: *ICH*.

Johannesen, L., Vicente, J., Mason, J. W., Erato, C., Sanabria, C., Waite-Labott, K., et al. (2016). Late sodium current block for drug-induced long QT syndrome: results from a prospective clinical trial. *Clin. Pharmacol. Therapeut.* 99, 214–223. doi: 10.1002/cpt.205

Johannesen, L., Vicente, J., Mason, J. W., Sanabria, C., Waite-Labott, K., Hong, M., et al. (2014). Differentiating drug-induced multichannel block on the electrocardiogram: randomized study of dofetilide, quinidine, ranolazine, and verapamil. *Clin. Pharmacol. Therapeut.* 96, 549–558. doi: 10.1038/clpt.2014.155

Li, Z., Ridder, B. J., Han, X., Wu, W. W., Sheng, J., Tran, P. N., et al. (2019). Assessment of an in silico mechanistic model for proarrhythmia risk prediction under the CiPA initiative. *Clin. Pharmacol. Therapeut.* 105, 466–475. doi: 10.1002/cpt.1184

Liu, X., Ma, J., Huang, L., Zhu, W., Yuan, P., Wan, R., et al. (2017). Fluoroquinolones increase the risk of serious arrhythmias: a systematic review and meta-analysis. *Medicine* 96:e8273. doi: 10.1097/MD.0000000000008273

Martin, R. L., McDermott, J. S., Salmen, H. J., Palmatier, J., Cox, B. F., and Gintant, G. A. (2004). The utility of hERG and repolarization assays in evaluating delayed cardiac repolarization: influence of multi-channel block. *J. Cardiovasc. Pharmacol.* 43, 81–90. doi: 10.1080/01926230500431376

Mistry, H. B. (2018). Complex versus simple models: ion-channel cardiac toxicity prediction. *PeerJ* 6:e4352. doi: 10.7717/peerj.4352

Nerbonne, J. M., and Kass, R. S. (2005). Molecular physiology of cardiac repolarization. *Physiol. Rev.* 85, 1205–1253. doi: 10.1152/physrev.00002.2005

O'Hara, T., Virág, L., Varró, A., and Rudy, Y. (2011). Simulation of the undiseased human cardiac ventricular action potential: model formulation and experimental validation. *PLoS Comput. Biol.* 7:e1002061. doi: 10.1371/journal.pcbi.1002061

Okada, J.-I., Yoshinaga, T., Kurokawa, J., Washio, T., Furukawa, T., Sawada, K., et al. (2015). Screening system for drug-induced arrhythmogenic risk combining a patch clamp and heart simulator. *Sci. Adv.* 1:e1400142. doi: 10.1126/sciadv.1400142

Passini, E., Britton, O. J., Lu, H. R., Rohrbacher, J., Hermans, A. N., Gallacher, D. J., et al. (2017). Human in silico drug trials demonstrate higher accuracy than animal models in predicting clinical pro-arrhythmic cardiotoxicity. *Front. Physiol.* 8:668. doi: 10.3389/fphys.2017.00668

RCoreTeam (2020). *R: A Language and Environment for Statistical Computing*. Vienna: R Foundation for Statistical Computing.

Redfern, W. S., Carlsson, L., Davis, A. S., Lynch, W. G., MacKenzie, I., Palethorpe, S., et al. (2003). Relationships between preclinical cardiac electrophysiology, clinical QT interval prolongation and torsade de pointes for a broad range of drugs: evidence for a provisional safety margin in drug development. *Cardiovasc. Res.* 58, 32–45. doi: 10.1016/s0008-6363(02)00846-5

Ridder, B. J., Leishman, D. J., Bridgland-Taylor, M., Samieegohar, M., Han, X., Wu, W. W., et al. (2020). A systematic strategy for estimating hERG block potency and its implications in a new cardiac safety paradigm. *Toxicol. Appl. Pharmacol.* 394:114961. doi: 10.1016/j.taap.2020.114961

Roden, D. M. (2004). Drug-induced prolongation of the QT interval. *N. Engl. J. Med.* 350, 1013–1022. doi: 10.1056/NEJMra032426

Sager, P. T., Gintant, G., Turner, J. R., Pettit, S., and Stockbridge, N. (2014). Rechanneling the cardiac proarrhythmia safety paradigm: a meeting report from the Cardiac Safety Research Consortium. *Am. Heart J.* 167, 292–300. doi: 10.1016/j.ahj.2013.11.004

Sahli-Costabal, F., Seo, K., Ashley, E., and Kuhl, E. (2020). Classifying drugs by their arrhythmogenic risk using machine learning. *Biophys. J.* 118, 1165–1176. doi: 10.1016/j.bpj.2020.01.012

Tomek, J., Bueno-Orovio, A., Passini, E., Zhou, X., Minchole, A., Britton, O., et al. (2019). Development, calibration, and validation of a novel human ventricular myocyte model in health, disease, and drug block. *eLife* 8:e48890. doi: 10.7554/eLife.48890

Verrier, R. L., Klingenheben, T., Malik, M., El-Sherif, N., Exner, D. V., Hohnloser, S. H., et al. (2011). Microvolt T-wave alternans physiological basis, methods of measurement, and clinical utility–consensus guideline by international society for holter and noninvasive electrocardiology. *J. Am. Coll. Cardiol.* 58, 1309–1324. doi: 10.1016/j.jacc.2011.06.029

Verrier, R. L., and Malik, M. (2013). Electrophysiology of T-wave alternans: mechanisms and pharmacologic influences. *J. Electrocardiol.* 46, 580–584. doi: 10.1016/j.jelectrocard.2013.07.003

Vicente, J., Johannesen, L., Hosseini, M., Mason, J. W., Sager, P. T., Pueyo, E., et al. (2016). Electrocardiographic biomarkers for detection of drug-induced late sodium current block. *PLoS One* 11:e0163619. doi: 10.1371/journal.pone.0163619

Vicente, J., Johannesen, L., Mason, J. W., Crumb, W. J., Pueyo, E., Stockbridge, N., et al. (2015). Comprehensive T wave morphology assessment in a randomized clinical study of dofetilide, quinidine, ranolazine, and verapamil. *J. Am. Heart Assoc.* 4:e001615. doi: 10.1161/JAHA.114.001615

Vicente, J., Zusterzeel, R., Johannesen, L., Ochoa-Jimenez, R., Mason, J. W., Sanabria, C., et al. (2019). Assessment of multi-ion channel block in a Phase I randomized study design: results of the CiPA Phase I ECG biomarker validation study. *Clin. Pharmacol. Therapeut.* 105, 943–953. doi: 10.1002/cpt.1303

Yang, P.-C., DeMarco, K. R., Aghasafari, P., Jeng, M.-T., Dawson, J. R. D., Bekker, S., et al. (2020). A Computational pipeline to predict cardiotoxicity: from the atom to the rhythm. *Circ. Res.* 126, 947–964. doi: 10.1161/CIRCRESAHA.119.316404

Zemzemi, N., Bernabeu, M. O., Saiz, J., Cooper, J., Pathmanathan, P., Mirams, G. R., et al. (2013). Computational assessment of drug-induced effects on the electrocardiogram: from ion channel to body surface potentials. *Br. J. Pharmacol.* 168, 718–733. doi: 10.1111/j.1476-5381.2012.02200.x

Conflict of Interest: GG, DB, and DC were employed by AbbVie. WB and CM were working as consultant for AbbVie.

frontiers in Physiology

ORIGINAL RESEARCH
published: 23 September 2020
doi: 10.3389/fphys.2020.554838

Insights Into the Spatiotemporal Patterns of Complexity of Ventricular Fibrillation by Multilead Analysis of Body Surface Potential Maps

Marianna Meo[1,2,3], Arnaud Denis[1,4], Frédéric Sacher[1,4], Josselin Duchâteau[1,2,3,4], Ghassen Cheniti[1,4], Stéphane Puyo[1,4], Laura Bear[1,2,3], Pierre Jaïs[1,2,3,4], Mélèze Hocini[1,2,3,4], Michel Haïssaguerre[1,2,3,4], Olivier Bernus[1,2,3] and Rémi Dubois[1,2,3]*

[1] Institute of Electrophysiology and Heart Modeling (IHU Liryc), Foundation Bordeaux University, Bordeaux, France, [2] Centre de Recherche Cardio-Thoracique de Bordeaux, U1045, University of Bordeaux, Bordeaux, France, [3] Centre de Recherche Cardio-Thoracique de Bordeaux, U1045, Institut National de la Santé et de la Recherche Médicale, Bordeaux, France, [4] Electrophysiology and Ablation Unit, Bordeaux University Hospital, Bordeaux, France

OPEN ACCESS

Edited by:
Marek Malik,
Imperial College London,
United Kingdom

Reviewed by:
Elena Tolkacheva,
University of Minnesota Twin Cities,
United States
Michael Liu,
University of California, Los Angeles,
United States

***Correspondence:**
Marianna Meo
marianna.meo@ihu-liryc.fr;
mariannameo@gmail.com

Specialty section:
This article was submitted to Cardiac Electrophysiology, a section of the journal Frontiers in Physiology

Received: 23 April 2020
Accepted: 12 August 2020
Published: 23 September 2020

Citation:
Meo M, Denis A, Sacher F, Duchâteau J, Cheniti G, Puyo S, Bear L, Jaïs P, Hocini M, Haïssaguerre M, Bernus O and Dubois R (2020) Insights Into the Spatiotemporal Patterns of Complexity of Ventricular Fibrillation by Multilead Analysis of Body Surface Potential Maps. Front. Physiol. 11:554838. doi: 10.3389/fphys.2020.554838

Background: Ventricular fibrillation (VF) is the main cause of sudden cardiac death, but its mechanisms are still unclear. We propose a noninvasive approach to describe the progression of VF complexity from body surface potential maps (BSPMs).

Methods: We mapped 252 VF episodes (16 ± 10 s) with a 252-electrode vest in 110 patients (89 male, 47 ± 18 years): 50 terminated spontaneously, otherwise by electrical cardioversion (DCC). Changes in complexity were assessed between the onset ("VF start") and the end ("VF end") of VF by the nondipolar component index (NDI_{BSPM}), measuring the fraction of energy nonpreserved by an equivalent 3D dipole from BSPMs. Higher NDI reflected lower VF organization. We also examined other standard body surface markers of VF dynamics, including fibrillatory wave amplitude (A_{BSPM}), surface cycle length ($BsCL_{BSPM}$) and Shannon entropy ($ShEn_{BSPM}$). Differences between patients with and without structural heart diseases (SHD, 32 vs. NSHD, 78) were also tested at those stages. Electrocardiographic features were validated with simultaneous endocardium cycle length (CL) in a subset of 30 patients.

Results: All BSPM markers measure an increase in electrical complexity during VF ($p < 0.0001$), and more significantly in NSHD patients. Complexity is significantly higher at the end of sustained VF episodes requiring DCC. Intraepisode intracardiac CL shortening (VF start 197 ± 24 vs. VF end 169 ± 20 ms; $p < 0.0001$) correlates with an increase in NDI, and decline in surface CL, f-wave amplitude, and entropy ($p < 0.0001$). In SHD patients VF is initially more complex than in NSHD patients (NDI_{BSPM}, $p = 0.0007$; $ShEn_{BSPM}$, $p < 0.0001$), with moderately slower ($BsCL_{BSPM}$, $p = 0.06$), low-amplitude f-waves (A_{BSPM}, $p < 0.0001$). In this population, lower NDI ($p = 0.004$) and slower surface CL ($p = 0.008$) at early stage of VF predict self-termination. In the NSHD group, a more abrupt increase in VF complexity is quantified by all BSPM parameters during sustained VF ($p < 0.0001$), whereas arrhythmia

evolution is stable during self-terminating episodes, hinting at additional mechanisms driving VF dynamics.

Conclusion: Multilead BSPM analysis underlines distinct degrees of VF complexity based on substrate characteristics.

Keywords: ventricular fibrillation, complexity, body surface potential maps, singular value decomposition, sudden cardiac death, electrocardiology, structural diseases, ventricular fibrillation mechanisms

INTRODUCTION

Sudden cardiac death is a major health problem worldwide accounting for 8% to 12% of all deaths (Hayashi et al., 2015), with global annual incidence rates between 50 and 100 per 100,000 cases (Fishman et al., 2010).

Ventricular fibrillation is the most serious heart rhythm disturbance and the main cause of SCD (Priori et al., 2015). Early studies interpreted the apparently chaotic and random activation of the myocardium during VF as totally disorganized (Moe et al., 1964). Later, the development of multielectrode (Rogers et al., 1999) and optical mapping (Park and Gray, 2015) techniques for the analysis of the electrical activation of the myocardium has enabled a more detailed evaluation of the electrical substrate of the arrhythmia, and both multiple wavelet and mother rotor hypotheses have been thought to be involved in VF initiation and maintenance (Jalife, 2000; Weiss et al., 2005). However, despite such advances, the mechanisms underlying this electrical disorder are still controversial. Yet, a quantitative assessment of VF organization may help understanding which factors determine the onset, perpetuation, and cessation of this arrhythmia (Such-Miquel et al., 2013), and be clinically relevant in the outline of more effective strategies for defibrillation and resuscitation, and the prediction of shock timings and success.

There is an increasing interest in BSPM technologies to noninvasively measure cardiac potentials with higher spatial resolution compared with standard 12-lead ECG. Indeed, subtle anomalies underlying VF may be missed by current imaging technologies, and rather bring a specific electrical signature, which may be critical in the treatment of patients with structurally normal hearts (Cheniti et al., 2018). However, a few studies have attempted a detailed analysis of the complexity of VF from multiple electrodes on body surface, due to the impossibility to quickly attach large sets of leads to a patient and acquire intraepisode recordings (Fitz-Clarke et al., 2006). Accordingly, most of the metrics currently used to describe VF from ECG are mainly determined from isolated leads, e.g., dominant frequency (Eftestøl et al., 2000) or entropy (Chicote et al., 2016), and a few multilead approaches have been developed (Clayton et al., 1995; Fitz-Clarke et al., 2006). Furthermore, to our knowledge, none of these works has clearly elucidated whether and how surface electrical patterns of VF may reflect underlying mechanisms.

Motivated by all these elements, this study aims put forward a multilead methodology to noninvasively describe spatiotemporal progression of VF and investigate how complexity patterns evolve in the presence/absence of SHDs.

Abbreviations: BSPM, body surface potential mapping; CL, cycle length; DCC, electrical cardioversion; DCM, dilated cardiomyopathy; ECG, electrocardiogram; ERP, early repolarization pattern; ERS, early repolarization syndrome; HCM, hypertrophic cardiomyopathy; IQR, interquartile range; LVD, left ventricular dysfunction; NDI, Nondipolar Component Index; NSHD, no structural heart disease(s); OHCM, obstructive hypertrophic cardiomyopathy; ROC, receiver operating characteristic; SCD, sudden cardiac death; SHDs, structural heart disease(s); SVD, singular value decomposition; VF, ventricular fibrillation; VT, ventricular tachycardia.

MATERIALS AND METHODS

VF Population

This study included 110 patients (89 male, 47 ± 18 years) enrolled for VF ablation. As in Haïssaguerre et al. (2018), SHDs were screened by echocardiography and delayed gadolinium-enhanced magnetic resonance imaging in 32 patients, whereas the remaining subjects (78) presented no structural alterations (NSHD). Pharmacological testing was performed by injecting ajmaline or catecholamine (adrenaline and isoprenaline) to diagnose patients with Brugada syndrome, long QT, and catecholaminergic polymorphic VT, respectively. This study was carried out in accordance with the recommendations of the protocol CARRY, ID-RCB: 2015-A00401-48, *Comité de Protection des Personnes Sud-Ouest et Outre Mer III* (ClinicalTrial.gov number: NCT02647749). It was approved by the Institutional Clinical Research and Ethics Committee and all subjects gave written informed consent in accordance with the Declaration of Helsinki. Baseline information for this patients' cohort are detailed in **Table 1**.

Noninvasive Mapping of VF and BSPM Preprocessing

A mean of 2.3 ± 2.1 spontaneous or induced VF episodes/patient were mapped with a 252-electrode vest (CardioInsight, Medtronic, MN, United States) at a sampling rate of 1 kHz before ablation, with a total of 177 episodes recorded in the NSHD group, and 75 episodes from the SHD group. Mean duration of VF was 18 ± 10 s. In keeping with current guidelines (Al-Khatib et al., 2017), VF was defined as rapid, grossly irregular electrical activity with marked variability in electrocardiographic waveform, and cycle length (CL) < 200 ms. VF rhythms have been reviewed and annotated by expert electrophysiologists. As in Haïssaguerre et al. (2018), the duration of VF episodes was dependent on the time-to-charge of the external defibrillator before shock delivery. The longer this waiting time, the longer the duration of the recorded episode, which was then labeled as "Sustained VF" if shock was delivered. Conversely, episodes with spontaneous reversion of VF to sinus rhythm

TABLE 1 | Clinical characteristics of the VF population.

	SHD (n = 32)	NSHD (n = 78)	p-value
Sex, male (n)	26	63	**<0.0001**
Age, mean ± std (years)	58 ± 18	41 ± 18	**<0.0001**
Pathology subtype (n) (no. male)	Ischemic VF 15 (13)	Brugada syndrome 29 (28)	
	HCM 9 (7)	Idiopathic VF 25 (17)	
	DCM 3 (2)	ERS 8 (6)	
	VT 3 (2)	ERP 6 (6)	
	OHCM 1 (1)	Brugada syndrome and ERP 4 (4)	
	LVD 1 (1)	Torsade de pointe 4 (1)	
		Long QT syndrome 1 (0)	
		Catecholaminergic VT 1 (1)	

DCM, dilated cardiomyopathy; ERP, early repolarization pattern; ERS, early repolarization syndrome; HCM, hypertrophic cardiomyopathy; LVD, left ventricular dysfunction; OHCM, obstructive hypertrophic cardiomyopathy; std, standard deviation; VT, ventricular tachycardia; p-values in boldface are statistically significant vs. "SHD". For each pathology subtype, the number of male patients is reported between brackets.

before the cardioversion (DCC) discharge were referred to as "self-terminating VF." Baseline wander was suppressed by the median estimation method (Sörnmo and Laguna, 2005). Body surface potentials were arranged as a $L \times N$ matrix $\mathbf{Y} = \left[\mathbf{y}(1) \ldots \mathbf{y}(N)\right] \in \Re^{L \times N}$, where $L = 252$ is the number of BSPM electrodes, and N the number of time samples. Signal quality was assessed by visual inspection, and too noisy electrode recordings were discarded if required, therefore in some patients we may have $L < 252$.

Electrophysiological Study and Ablation

Electroanatomical mapping (CARTO system, Biosense Webster, CA, United States) was performed as in Haïssaguerre et al. (2018). Briefly, a transseptal or retroaortic approach was adopted to access the endocardial left ventricle and a subxyphosternal approach to access into the pericardial space. Decapolar and multispline (Pentaray, Biosense Webster, CA, United States) catheters were used for endocardial and epicardial exploration, respectively. Intracardiac electrograms were recorded and stored by a computer-based digital amplifier/recorder system (Labsystem Pro, Bard Electrophysiology). VF was induced by programmed stimulation from one of the ventricles (mainly the right one), if required. Endocardial VF CLs were measured mainly in the right ventricle. After mapping, VF ablation was subsequently performed with an irrigated-tip catheter as in Haïssaguerre et al. (2018) and targeted ventricular sites with abnormal electrograms and driver activities estimated by ECG imaging.

Novel Multilead Methodology to Measure VF Complexity

Previous research has shown that ventricular repolarization could be effectively described in an orthogonal 3D space and that higher-order components reflected T-wave spatial heterogeneities, representing an arrhythmogenic substrate (De Ambroggi et al., 1997; Priori et al., 1997; Malik et al., 2000). Similar approaches have also been applied to the quantification of QRS dispersion and prediction of sudden death (Peters et al., 1999; Turrini et al., 2001). Moving from the theoretical basis in Di Marco et al. (2012), Meo et al. (2017) and Meo et al. (2018), we measured spatiotemporal organization of VF using the nondipolar component index (NDI), namely, the fraction of signal energy that is not captured by a 3D dipolar approximation of body surface cardiac activity. However, unlike those studies, we were more interested in determining the temporal evolution of VF complexity rather than its static characteristics. Accordingly, the input BSPMs were divided in 500-ms windows. Each multilead signal frame was then mean-centered and projected on a 3D subspace estimated by SVD:

$$\mathbf{Y}^{(s)} = \mathbf{U}\mathbf{S}\mathbf{V}^{\mathrm{T}}$$

With $\mathbf{U}$ and $\mathbf{V}$ standing for the left and right singular vectors of $\mathbf{Y}^{(s)}$, respectively, and the diagonal matrix $\mathbf{S}$ containing the singular values σ_ℓ, $\ell = 1, \ldots, L$. In line with the mathematical formulation proposed by Meo et al. (2018), NDI was computed as:

$$\mathrm{NDI}_{BSPM} = 100 \cdot \left(1 - \frac{\sum_{\ell=1}^{3} \sigma_\ell^2}{\sum_{\ell=1}^{L} \sigma_\ell^2}\right)$$

under the hypothesis that more organized VF patterns could be properly described by a 3D cardiac dipole and yield lower NDI values, whereas more variable and unpredictable waveforms (both in time and across leads) would be less likely to be accurately described by this model, thus they will be associated with higher NDI values. With regard to the choice of the frame duration, the proposed value was selected as a trade-off between the amount of input information and SVD applicability, as we needed to accurately capture spatiotemporal variability properties of signal patterns from least two to three fibrillatory cycles, while preserving data stationarity within the BSPM frame and obtaining reliable measures (Meo et al., 2018). Since endocardial CL in our validation subset ranged between 150 and 250 ms, our choice proved to be suitable. The effect of tuning parameters on SVD-derived features has been more systematically tested in previous works (Meo et al., 2013a).

Other Body Surface Markers of VF Electrical Complexity and Dynamics

Organization of VF and its time evolution have also been assessed by other signal parameters reported in literature and conventionally computed from single-lead ECG.

Fibrillatory wave (f-wave) is known to be predictive of successful defibrillation shocks (Strohmenger et al., 2001) in patients with cardiac arrest, and its decline in time reflects increasing intracellular electrical decoupling with VF progression (Caldwell et al., 2012). Accordingly, this parameter was computed from each electrode using a custom approach based on the interpolation of signal local extrema through polynomial envelopes (Meo et al., 2013b, 2018). The output amplitude index was the median value over all electrodes and denoted A_{BSPM}.

The same method also served as a preliminary step for the assessment of body surface VFCL, as faster activations typically correlate with duration of VF and are less likely to be terminated by defibrillation (Strohmenger et al., 2001). As in Meo et al. (2018), signal local maxima were detected by a derivative-threshold algorithm, and the median of CLs between 90 and 250 ms was computed over all BSPM leads (body surface VFCL, denoted as $BsCL_{BSPM}$), to reject the influence of false peaks.

Finally, complexity of VF has also been quantified by a nonlinear index, i.e., Shannon entropy, under the hypothesis that less regular and repetitive patterns are characterized higher uncertainty in a statistical sense. We assume that lower values of the index render more predictable times series. Entropy-based indices are widely used to detect VF rhythms (Hajeb-Mohammadalipour et al., 2018) and predict defibrillation outcome (Chicote et al., 2016). The ability of this parameter to identify rotational activities in atrial fibrillation patients has also been demonstrated (Ganesan et al., 2013). To account for contributions from all BSPM recordings, Shannon entropy has been determined with histogram bin width set at 0.01 mV, and the median $ShEn_{BSPM}$ over all electrodes has been assumed as a marker for VF complexity.

We also investigated the scalability of BSPM-derived features to 12-lead ECG for a potential application of VF complexity analysis in a larger clinical scenario. For this purpose, each of the aforementioned parameters has been also computed from an equivalent ECG obtained from a subset of BSPM electrodes at the locations of standard leads and denoted NDI_{ECG12}, A_{ECG12}, $BsCL_{ECG12}$, and $ShEn_{ECG12}$, respectively. A summary of all body surface descriptors of VF progression is reported in **Table 2**.

Time Analysis of VF Electrical Complexity in Relation to Its Termination Mode and Mechanisms

To explore VF progression over its entire duration in detail and evaluate the ability of signal indices to track intra-episode changes in complexity, each of the presented BSPM- and ECG-metrics has been assessed in consecutive 500-ms frames, so as to obtain only one curve for each index to be straightforwardly compared with the simultaneous time evolution of the multielectrode body surface signals.

On the other hand, to systematically validate the ability of these indices to describe VF complexity in a statistical framework, all body surface parameters have been assessed at specific time frames in all recordings, i.e., at the beginning ("VF start") and at the end of the VF episode ("VF end"), thus returning one scalar value per VF stage to be then used for subsequent statistical analyses. The selection of the lower bound of the "VF start" window depended on VF initiation mode. Specifically, in case of spontaneous VF, the beginning of the "VF start" frame was taken in correspondence to the onset of the second VF beat. When VF was externally induced, the 4-s signal portion starting at the second VF beat after the last stimulation spike was considered instead. On the contrary, the choice of the "VF end" starting time was related to VF cessation mechanisms, based on the definition of "sustained VF" and "self-terminating VF" from section "Noninvasive Mapping of VF and BSPM Preprocessing." To examine the dynamics of late VF in the "sustained VF" set, signal features were computed from the "VF end" frame over the last 4 s of the recording with stable isoelectric line before DCC discharge. Conversely, in the "self-terminating VF" group, the terminal "VF end" window covered the last 4 s of VF before rhythm transition. This scheme enabled a rigorous statistical comparison between signal features at different and easily identifiable time points of VF based on the criteria described above, which were the same for all recordings.

As in Meo et al. (2017), each of these episode portions was assumed equal to 4 s, in order to account for a sufficient number of fibrillatory cycles and increase statistical confidence for signal features' assessment. This choice is also in keeping with previous studies about human VF (Clayton et al., 1995; Haïssaguerre et al., 2018), demonstrating that abrupt changes in VF complexity usually occur within the first 4 to 5 s of arrhythmia, with significant CL acceleration and increased electrogram fragmentation. In the light of this, too short recordings (less than 8 s) were discarded from our analysis. For the same reason, we decided to compare only signal indices from the initial and the terminal 4-s portions of VF, and not to include further intermediate frames between the two of them, as in some

TABLE 2 | Summary of all BSPM markers of VF dynamics used in this study.

BSPM index	Signal property	Mathematical definition and references	Hypothesis
NDI_{BSPM} [%]	Surface f-wave multielectrode spatial complexity	The ratio of the sum of the fourth-to-last SVD eigenvalues to the sum of all eigenvalues (Di Marco et al., 2012; Meo et al., 2018)	More disorganized VF is less accurately described by a 3D dipole (higher NDI_{BSPM})
A_{BSPM} [mV]	Surface f-wave amplitude	Median of single-lead f-wave amplitudes, computed as the temporal average of the difference between upper and lower envelopes, obtained by polynomial interpolation of signal local extrema (Meo et al., 2013b)	Lower surface f-wave amplitude reflects more complex VF (lower A_{BSPM})
$BsCL_{BSPM}$ [ms]	Surface f-wave cycle length	Median of single-lead f-wave cycle lengths, computed as the mean temporal distance between consecutive local signal maxima (Meo et al., 2013b, 2018)	Higher VF complexity is associated with faster fibrillatory activities on body surface (lower $BsCL_{BSPM}$)
$ShEn_{BSPM}$ [a.u.]	Surface f-wave regularity	Expected value of f-wave amplitude self-information (i.e., negative logarithm of f-wave amplitude probability density function) (Chicote et al., 2016; Hajeb-Mohammadalipour et al., 2018)	Less regular and repetitive signal patterns describe more disorganized VF (higher $ShEn_{BSPM}$)

The same definitions apply to parameters derived from the equivalent 12-lead ECG (with subscript "BSPM" replaced by "ECG12"); a.u., arbitrary units.

recordings it was not possible to extract signal segments with the same duration prior to feature extraction.

At each of the aforementioned VF stages, we investigated whether and how VF termination mode affects body surface complexity. Accordingly, differences between "self-terminating VF" and "sustained VF" were tested at the onset ("VF start") and at the end ("VF end") of all episodes. To evaluate the impact of structural alterations on VF electrical patterns, unmatched comparisons were performed between SHD and NSHD patients during early ("VF start") and late VF ("VF end"). Furthermore, to incorporate the information about VF cessation modality, differences between "self-terminating VF" and "sustained VF" were tested at the onset ("VF start") and at the end ("VF end") of the episode in each patients' population (SHD and NSHD groups).

Finally, to validate the ability of body surface indices to detect temporal changes in VF dynamics, we analyzed a subset of 30 patients, for whom a measure of intracardiac CL was available at the beginning and at the end of VF. In all subjects, an intraepisode acceleration was observed, thus confirming a complexification of the arrhythmia at the level of the tissue. Accordingly, we used this information to investigate whether this transition from early organization ("Organized") to subsequent disorganization of VF ("Disorganized") could be captured by the proposed body surface markers, which were therefore computed at both stages of the episode.

Statistical Analysis

Continuous variables in tables were expressed as mean ± standard deviation, while categorical variables were reported as counting and percentages. Lilliefors test was preliminarily applied to all parameters to verify their distribution. If data followed a Gaussian distributed distribution, intergroup differences were checked by an unpaired Student's *t*-test with Welch's correction for unequal group variances and sizes. In the other cases, a Wilcoxon's rank sum test was performed. Chi-squared test was applied to categorical variables. Specifically, these tests were performed at the onset ("VF start") and the end ("VF end") of VF to investigate the link between electrical characteristics and mechanism complexity (i.e., SHD vs. NSHD patients), as well as their relation with VF termination mode ("self-terminating VF" vs. "sustained VF"). Statistical tests were considered significant if $p < 0.05$. Changes in body surface indices between the onset and the offset of VF ("VF start" vs. "VF end") were assessed by a paired Student's *t*-test from normally distributed parameters or nonparametric Wilcoxon signed-rank test otherwise. Parameters in the boxplots are displayed as median with interquartile range (IQR).

The same analysis was applied to the subset of patients presented in section "Other Body Surface Markers of VF Electrical Complexity and Dynamics" to validate intraepisode changes in VF dynamics ("Organized" vs. "Disorganized") from body surface markers as matched with intracardiac CL. Furthermore, transitions from "Organized" to "Disorganized" VF were precisely determined from every signal feature by the receiver operating characteristics curve (ROC) analysis. Specifically, numerical thresholds for these transitions were computed as the cutoff values, which simultaneously maximized the sensitivity (Sens: rate of correct predictions of "Disorganized" VF) and the specificity (Spec: rate of correct predictions of "Organized" VF) of the classifier, thus providing the best discrimination between "Organized" and "Disorganized" stages of VF. This approach allowed us to automatically determine a unique threshold optimized over the entire database and cope with interpatient and intrapatient variability of signal indices. Classifiers' performance was quantified by the values of sensitivity and specificity associated with the optimal cutoff, as well as the area under the ROC curve (AUC).

RESULTS

VF Mapping

Overall, VF was successfully induced in 51 out of 75 episodes in SHD patients (68%), and 130 out of 177 episodes in the NSHD group (74%), with no differences between the two populations ($p = 0.38$). In the remaining cases, it occurred spontaneously, also with similar rates in both patients' groups. VF was shorter in NSHD (14 ± 8 s) than SHD patients (19 ± 13 s, $p = 0.003$), regardless of its termination mode. Spontaneous cessation of VF prior to shock delivery was observed in 37 out of 177 episodes (21%) in patients with structurally normal hearts, and 13 out of 75 (17%) episodes in the other population, with no significant intergroup differences ($p = 0.38$). Time to self-termination of VF was slightly longer in SHD (14 ± 9 s) than in NSHD patients (9 ± 6 s, $p = 0.04$). On the other hand, VF was terminated by DCC in 60 out of 75 cases (20 ± 13 s) and 140 out of 177 cases (16 ± 8 s) in SHD and NSHD subjects, respectively, also with similar intragroup proportions ($p = 0.88$) and duration ($p = 0.06$). In both groups, sustained VF cases were more numerous than the self-terminating ones ($p < 0.0001$) and required DCC. Furthermore, shocked episodes were longer than those terminating spontaneously both in the SHD ($p = 0.04$) and NSHD ($p < 0.0001$) subjects. At least one episode of VF was mapped in each patient, with comparable proportions between the two groups (SHD 2.3 ± 1.9 vs. NSHD 2.3 ± 2.2 episodes/patient, $p = 0.52$).

BSPM-Based Analysis of Electrical Complexity Dynamics

An overall increase in VF complexity over time is underlined by all BSPM markers ($p < 0.0001$). At early stage, organized VF is measured by low NDI (VF start 1.9 ± 1.4% vs. VF end 3.4 ± 2.4%), amplitude voltage A_{BSPM} is high (0.5 ± 0.3 vs. 0.3 ± 0.2 mV), and slow activities are measured by long $BsCL_{BSPM}$ (166 ± 21 vs. 154 ± 22 ms) in the entire dataset. An unexpected, albeit significant, trend of $ShEn_{BSPM}$ is observed in the entire dataset, with a decrease in time from 6.6 ± 0.5 to 6.2 ± 0.6, in contrast with our initial hypothesis.

As shown in **Figure 1A**, at the onset of VF, none of these indices can significantly distinguish between sustained and self-terminating VF, while at the end of DCC-shocked episodes complexity is significantly higher, and amplitude and entropy appear reduced, with faster oscillations than in case

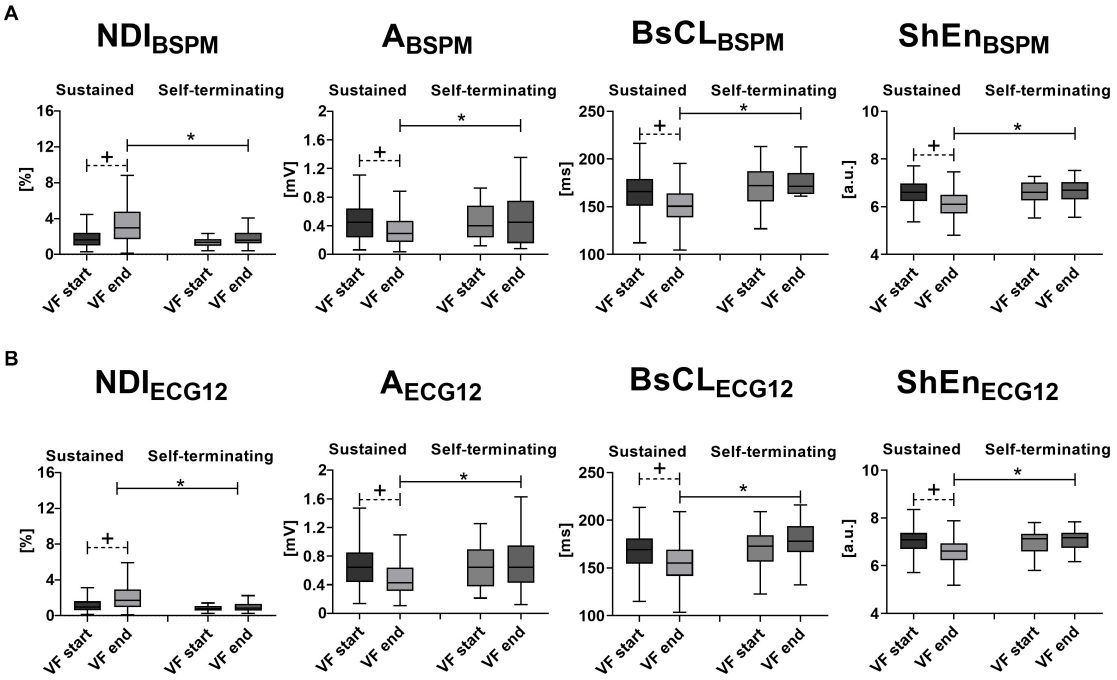

FIGURE 1 | Body surface signal features' time evolution and VF termination: statistical analysis of intraepisode changes ("VF start" vs. "VF end," matched p value) in VF organization for a specific VF termination mode, and evaluation of differences between "Sustained VF" and "Self-terminating VF" at each episode phase (unmatched p-value) using body surface signal features. **(A)** BSPM-derived metrics of VF dynamics (from left to right): NDI_{BSPM}, A_{BSPM}, $BsCL_{BSPM}$, and $ShEn_{BSPM}$. **(B)** ECG-derived metrics of VF dynamics (from left to right): NDI_{ECG12}, A_{ECG12}, $BsCL_{ECG12}$, and $ShEn_{ECG12}$. Parameters in the boxplots are displayed as median with IQR. $^{+}p < 0.05$ vs. VF start (matched comparison, dashed line); $^{*}p < 0.05$ vs. sustained VF (unmatched comparisons, continuous line); a.u., arbitrary units.

of spontaneous termination ($p < 0.0001$). Furthermore, time evolution of sustained VF is characterized by more complex and variable waveforms, which are significantly captured by all BSPM markers. By contrast, self-terminating VF results in more regular and simple patterns and a stable trend in signal features. After removing outliers identified by the Grubb's test (with significance taken for $p < 0.05$), a modest increasing correlation between the length to self-termination from VF onset and NDI_{BSPM} fold change from "VF start" to "VF end" is observed in our database (Pearson' correlation coefficient $R = 0.56$, $p = 0.003$), while the other BSPM features do not exhibit any significant correlation.

Temporal increase in body surface complexity is also corroborated by a decrease in intracardiac CL (Organized 197 ± 24 ms vs. Disorganized 169 ± 20 ms; $p < 0.0001$) in the validation subset introduced in section "Other Body Surface Markers of VF Electrical Complexity and Dynamics," as confirmed by the outcome of the paired analysis and ROC assessment in **Table 3** ($p < 0.0001$ for all BSPM parameters, except for A_{BSPM}, $p = 0.0003$).

Late disorganization of VF is accurately assessed according to the statistical tests and ROC analysis of signal indices, although the ratio between sensitivity and specificity is slightly unbalanced for NDI_{BSPM} and $ShEn_{BSPM}$. Also, $BsCL_{BSPM}$ sensitivity is relatively poor than for other parameters.

To gain deeper insights into the ability of these indices to describe VF dynamics, equivalent ECGs extracted from BSPMs from a representative example for each VF termination mode are shown in **Figure 2**, as well as the time evolution of all body surface markers and the thresholds returned by the ROC analysis.

Concerning the sustained VF episode in **Figure 2A** (left), from the NDI index even short transients of organization/disorganization can be detected using optimized thresholds (**Figure 2B**). The timing of irreversible disorganization before cardioversion (approximately 6 s from the onset) can be can promptly identified from body surface

TABLE 3 | Statistical analysis of intraepisode changes in VF organization from body surface signal analysis of VF episodes with simultaneous invasive measure of VF CL.

	Organized	Disorganized	p-value	AUC	Sens	Spec
NDI_{BSPM} [%]	1.2 ± 0.7	2.5 ± 1.9	**<0.0001**	78	90	57
NDI_{ECG12} [%]	0.8 ± 0.5	1.8 ± 1.3	**<0.0001**	79	77	70
A_{BSPM} [mV]	0.6 ± 0.2	0.3 ± 0.2	**0.0003**	70	77	60
A_{ECG12} [mV]	0.8 ± 0.3	0.6 ± 0.3	**0.001**	71	67	77
$BsCL_{BSPM}$ [ms]	179 ± 20	162 ± 16	**<0.0001**	77	53	93
$BsCL_{ECG12}$ [ms]	178 ± 16	160 ± 18	**<0.0001**	79	73	80
$ShEn_{BSPM}$ [a.u.]	6.9 ± 0.4	6.3 ± 0.5	**<0.0001**	79	80	67
$ShEn_{ECG12}$ [a.u.]	7.1 ± 0.4	6.7 ± 0.5	**<0.0001**	76	70	77

All BSPM- and ECG-derived metrics are reported as mean ± standard deviation; p-values in boldface are statistically significant vs. "organized." AUC, area under curve; Sens, sensitivity; Spec, specificity; a.u., arbitrary units.

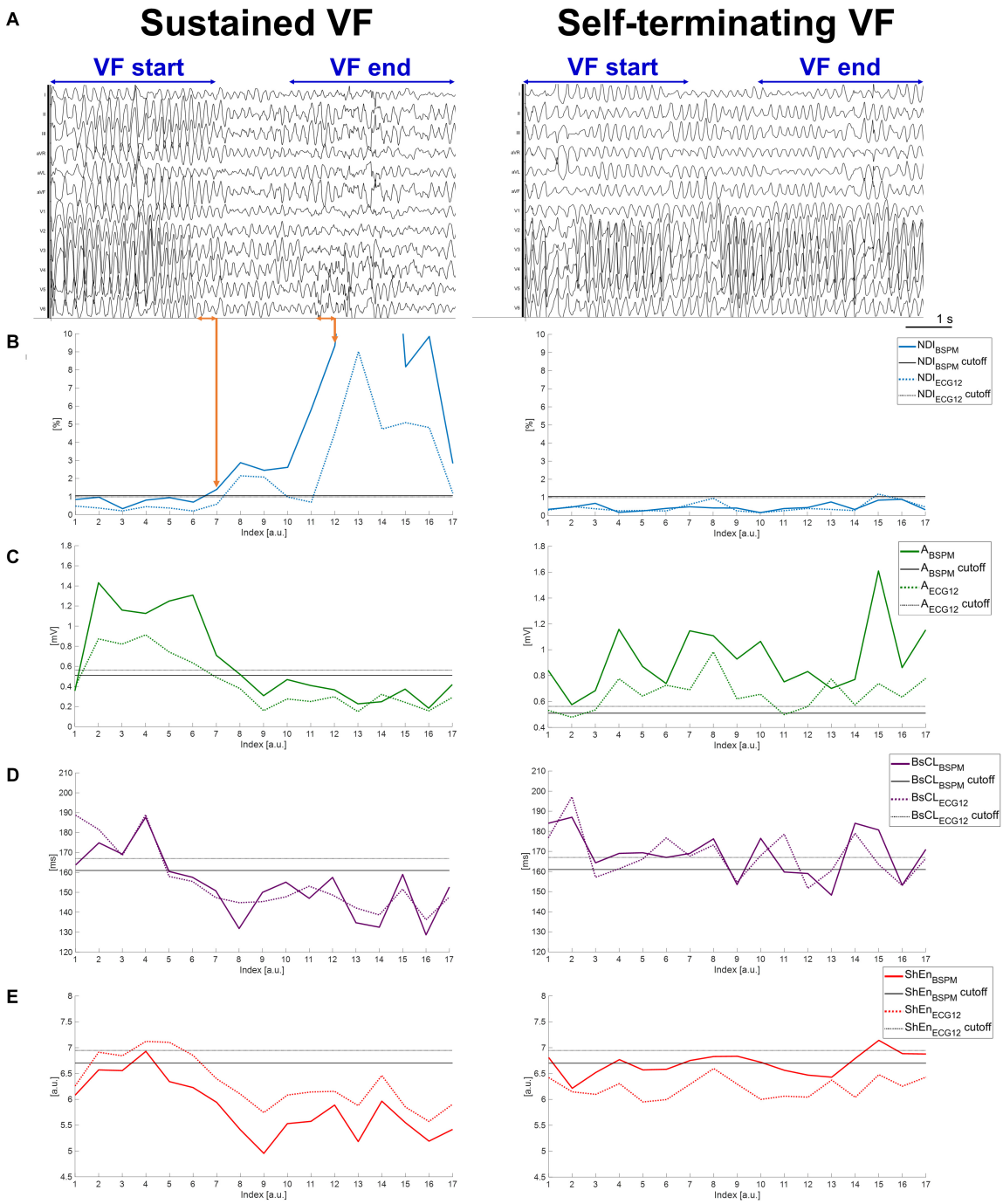

FIGURE 2 | Temporal dynamics of sustained and self-terminating VF and body surface metrics of complexity. **(A)** A representative equivalent 12-lead ECG computed from measured BSPMs during an episode of sustained VF (left side of the panel) and during self-terminating VF (right side). Only signals recorded during VF episodes matching the criteria described in section "Noninvasive Mapping of VF and BSPM Preprocessing" and "Time Analysis of VF Electrical Complexity in Relation to Its Termination Mode and Mechanisms" were exported from the mapping system for subsequent quantitative analysis, i.e., those in the time frame between the first time sample of the "VF start" window (i.e., at the onset of the second VF beat of spontaneous or induced events), and the last time sample of the "VF end" window (i.e., before DCC shock for sustained VF, or before transition to sinus rhythm for self-terminating VF). The "VF start" and "VF end" time frames used for signal feature statistical analysis are indicated on the top of the ECGs for each episode. Each curve value is associated with VF patterns from the previous 500-ms frame on surface signals over the entire duration of the episode. The most abrupt pattern changes during sustained VF are indicated by orange arrows. **(B)** Time evolution of NDI_{BSPM} and NDI_{ECG12}. **(C)** Time evolution of A_{BSPM} and A_{ECG12}. **(D)** Time evolution of $BsCL_{BSPM}$ and $BsCL_{ECG12}$. **(E)** Time evolution of $ShEn_{ECG12}$ and $ShEn_{ECG12}$. Continuous and dotted line curves are associated with signal features derived from BSPMs and equivalent ECGs, respectively. Colored lines represent the temporal trend of parameter, with each point describing VF dynamics in the previous 500-ms signal frame. Horizontal continuous (dotted) black lines are the thresholds output by ROC analysis of each BSPM (ECG) index, validated by comparison with the intracardiac CL.

(in less than 3 s), with more pronounced differences between the beginning and the end of the episode underlined by the BSPM-derived index (a difference of one order of NDI magnitude) rather than the 12-lead counterpart. On the other hand, in case of spontaneous termination of VF as in **Figure 2A** (right), the range of values covered by the NDI parameter over time is less broad (**Figure 2B**, right), and always below the ROC thresholds determined from the validation set. Similar dynamics and timings can be retrieved by descriptors of f-wave amplitude in **Figure 2C** (left) for the shocked episode, and again more marked changes from the onset can be better appreciated from BSPMs rather than ECG. In contrast, both A_{BSPM} and A_{ECG12} parameters are characterized by a stable evolution when VF terminates with no external intervention **Figure 2C** (right). Similar considerations can be done for body surface CL in **Figure 2D** regardless of the termination mode, although the trend of indices computed using different lead configurations are slightly different at certain time frames. These differences are more evident during DCC-terminated (**Figure 2D**, left) rather than nonsustained VF (right). Unlike the other parameters, the timing of disorganization of shocked VF in **Figure 2E** (left) seems to be better explained by Shannon entropy from ECG rather than BSPM. In contrast, during self-terminating VF (**Figure 2E**, right), $ShEn_{BSPM}$ curve crosses the ROC cutoff several times, and $ShEn_{ECG12}$ is always below its corresponding threshold, i.e., indicating spurious increased complexity.

Relation Between Electrical Complexity of VF From BSPMs and Structural Alterations of the Myocardium

As underlined by the statistical analysis of BSPM metrics in **Figure 3A**, according to NDI, in SHD patients VF is initially more complex than in NSHD patients ($p = 0.0007$). Similarly, f-wave amplitude is slightly lower in patients with structural alterations ($p < 0.0001$), with moderately slower cycles ($p = 0.06$). Entropy is also lower at early stage of VF in these patients ($p < 0.0001$). In both populations, there is a strong increase in electrical complexity with progression of VF ($p < 0.0001$). At the end of the episode, marked intergroup differences in amplitude and entropy are still preserved ($p < 0.0001$). In contrast, body surface CL ($p = 0.06$) and NDI ($p = 0.54$) are comparable at the end of VF in both datasets.

In the presence of structural abnormalities, lower complexity at baseline is assessed by lower NDI ($p = 0.004$, **Figure 4A**, left) and slower surface CL ($p = 0.008$, **Figure 4C**, left) from BSPMs, which are associated with spontaneous cessation of VF and have a stable evolution during the episode. In contrast, amplitude (**Figure 4B**, left) and entropy-based (**Figure 4D**, left)

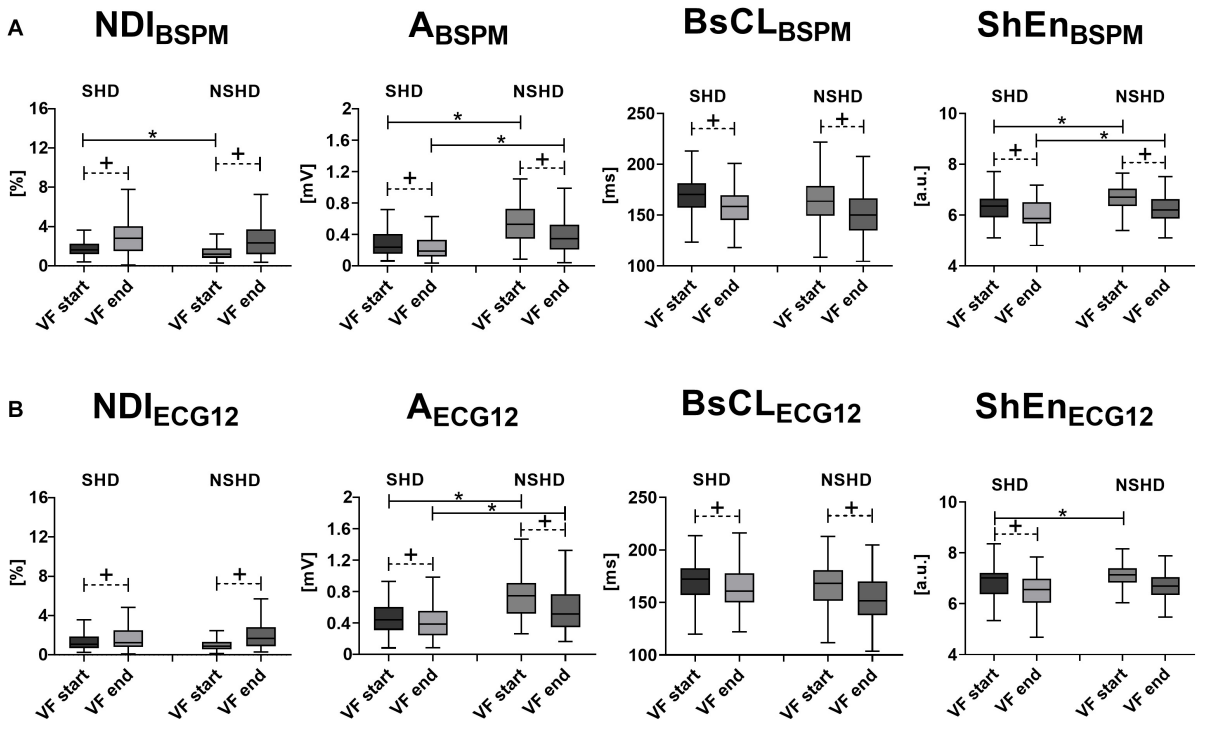

FIGURE 3 | Body surface electrical complexity and structural abnormalities during VF. Statistical analysis of intraepisode changes ("VF start" vs. "VF end," matched *p*-value) in VF organization in SHD and NSHD patients and assessment of intergroup differences at the starting and the offset of the episode (unmatched *p*-value) using body surface signal features. **(A)** BSPM-derived metrics of VF dynamics (from left to right): NDI_{BSPM}, A_{BSPM}, $BsCL_{BSPM}$ and $ShEn_{BSPM}$. **(B)** ECG-derived metrics of VF dynamics (from left to right): NDI_{ECG12}, A_{ECG12}, $BsCL_{ECG12}$ and $ShEn_{ECG12}$. Parameters in the boxplots are displayed as median with IQR. $^{+}p < 0.05$ vs. VF start (matched comparison, dashed line); $^{*}p < 0.05$ vs. sustained VF (unmatched comparisons, continuous line); a.u., arbitrary units.

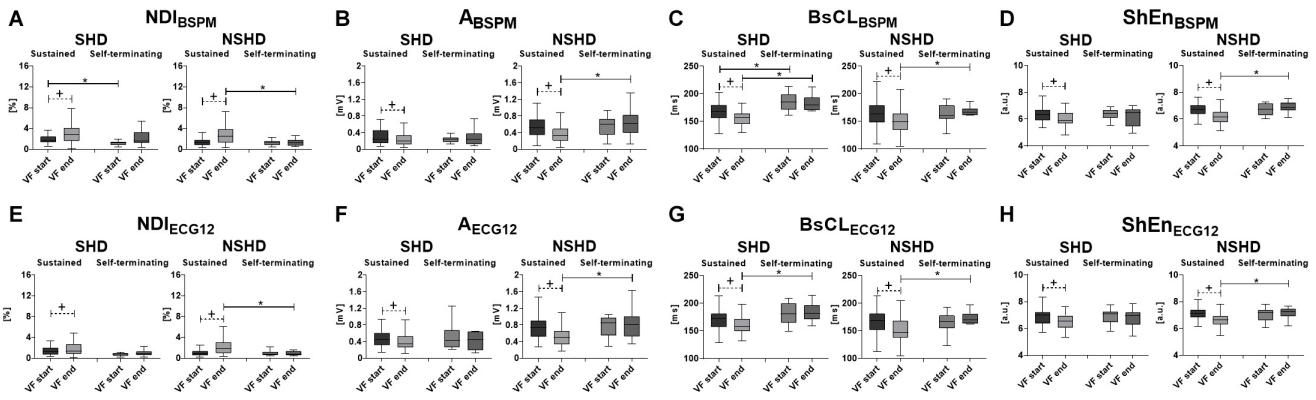

FIGURE 4 | Body surface electrical complexity in relation with mode of termination of VF and structural abnormalities. Statistical analysis of intraepisode changes ("VF start" vs. "VF end," matched p-value) in VF dynamics in SHD (left side of each panel) and NSHD (right side) patients and differences between sustained and self-terminating VF at the starting and the offset of the episode (unmatched p-value) using BSPM- and ECG-derived parameters: **(A)** NDI_{BSPM}; **(B)** A_{BSPM}; **(C)** $BsCL_{BSPM}$; **(D)** $ShEn_{BSPM}$; **(E)** NDI_{ECG12}; **(F)** A_{ECG12}; **(G)** $BsCL_{ECG12}$; **(H)** $ShEn_{ECG12}$. Parameters in the boxplots are displayed as median with IQR. $^{+}p < 0.05$ vs. VF start (matched comparison, dashed line); $^{*}p < 0.05$ vs. sustained VF (unmatched comparisons, continuous line); a.u., arbitrary units.

indices do not exhibit any significant correlation with VF self-termination ($p = 0.98$ and $p = 0.82$, respectively). On the other hand, sustained VF is characterized by a significant increase in electrical disorganization and outlined by all BSPM markers. At the end of the episode, all indices are comparable, regardless of the termination mode, but cycles are still faster in patients undergoing DCC ($p = 0.002$).

In patients with structurally intact hearts (NSHD, **Figures 4A–D**, right side of the panels), self-termination of VF cannot be assessed by BSPM markers at the onset of VF, as complexity is comparable in shocked and self-terminating episodes. However, unlike the SHD group, during sustained VF a sharper increase in electrical complexity (**Figure 4A**, right), with progressive decrease in f-wave amplitude (**Figure 4B**, right), surface CL (**Figure 4C**, right) and entropy (**Figure 4D**, right), is underlined by all parameters ($p < 0.0001$). Furthermore, VF is more disorganized at the end of episodes requiring DCC than those terminating with no external intervention (NDI_{BSPM}, $p = 0.0095$), with low-voltage (A_{BSPM}, $p = 0.002$), fast oscillations ($BsCL_{BSPM}$ $p = 0.004$).

Comparison With 12-Lead ECG-Derived Metrics

As previously explained, the BSPM descriptors of VF dynamics introduced in section "Materials and Methods" have also been computed from an equivalent standard ECG to verify whether it is possible to derive similar information about VF progression from a reduced number of electrodes.

As for BSPM parameters, all ECG-derived indices highlight increased VF complexity, a decline in f-wave amplitude, and CL shortening between the beginning (VF start, NDI_{ECG12}: $1.3 \pm 1.0\%$; A_{ECG12}: 0.7 ± 0.3 mV; $BsCL_{ECG12}$: 168 ± 22 ms; $ShEn_{ECG12}$: 7.0 ± 0.5) and the end of the episode (VF end, NDI_{ECG12}: $1.9 \pm 1.5\%$; A_{ECG12}: 0.5 ± 0.3 mV$BsCL_{ECG12}$: 158 ± 23 ms; $ShEn_{ECG12}$: 6.6 ± 0.6, $p < 0.0001$).

Similarly, at the beginning of VF, there are no significant differences between sustained and self-terminating episodes (**Figures 1A,B**). In keeping with BSPM analysis, sustained VF is associated with an intraepisode increase in complexity NDI_{ECG12}, a reduction in f-wave amplitude A_{ECG12} and entropy $ShEn_{ECG12}$, and a CL shortening according to $BsCL_{ECG12}$ ($p < 0.0001$). On the other hand, ECG parameters do not change significantly between the beginning and the end of self-terminating VF. Again, we find a moderate correlation between NDI_{ECG12} fold change and length to episode self-termination (Pearson's correlation coefficient $R = 0.44$, $p = 0.03$), as opposed to other ECG features. In addition, unlike cases of spontaneous termination, late sustained VF is more disorganized, as outlined by higher NDI_{ECG12} ($p = 0.0003$) and lower $ShEn_{ECG12}$ ($p < 0.0001$), with faster fibrillatory patterns ($BsCL_{ECG12}$, $p < 0.0001$) and smaller wave deflections (A_{ECG12}, $p = 0.009$).

Changes in VF dynamics are correctly captured by ECG metrics and validated by simultaneous measure of intracardiac CL ($p < 0.0001$ for all ECG indices, except for A_{ECG12}, $p = 0.001$). As shown in **Table 3**, organized and disorganized stages of VF can be accurately identified, and prediction performance still appears satisfactory when a reduced number of leads is considered. A more careful inspection of the temporal evolution of each ECG feature in **Figure 2** reveals that ECG-derived metrics overall follow quite well their BSPM counterparts, and they can identify the timing of VF disorganization during shocked episodes, while showing a stable evolution in case of self-termination. However, differences between the onset and the end of VF according to ECG indices are usually less pronounced that those highlighted from BSPMs. Once again, NDI_{ECG12} and A_{ECG12} can capture small changes in VF temporal patterns and their trends are similar to those computed from BSPMs. The CL index $BsCL_{ECG12}$ often exhibits a different evolution compared with $BsCL_{BSPM}$, but disorganization timing can be still captured within the first seconds of VF. On the contrary, the resolution of $ShEn_{ECG12}$ is

overall lower than the other indices and ROC thresholds are not optimal in all patients.

In contrast with BSPM analysis, at the onset of VF differences between populations with different structural characteristics are not captured by all parameters (**Figure 3B**). Specifically, NDI_{ECG12} is comparable in both sets at baseline ($p = 0.07$), and fibrillatory activities have similar cycles ($p = 0.13$). In contrast, in patients with normal hearts higher initial organization is rendered by lower entropy ($p = 0.002$), and f-wave amplitude is higher ($p < 0.0001$) than in SHD subjects. Both groups exhibit a significant intraepisode increase in complexity, a reduction in f-wave amplitude, and surface CL shortening, although more modest in patients with structural abnormalities and compared with BSPM-derived trends. When VF terminates, ECG markers enhance similar behaviors to BSPM indices, i.e., low voltage oscillations ($p < 0.0001$), but slow cycles in SHD patients ($p = 0.002$). On the contrary, both NDI_{ECG12} and $ShEn_{ECG12}$ do not account for the effect of structural alterations at the end of VF ($p = 0.27$ and $p = 0.09$, respectively).

The relation between VF termination mode and structural alterations has also been investigated from ECG, and the results of this analysis are reported in **Figures 4E–H**. Unlike their BSPM counterpart, ECG-based indices cannot significantly predict self-termination of VF in the SHD population, as there were no differences between nonsustained and sustained VF events at baseline. In SHD patients, episodes of sustained VF are still associated with an increase in electrical complexity (**Figure 4E**, left) and decline in amplitude of the fibrillatory patterns with time (**Figure 4F**, left), although with a more blunted dynamics (NDI_{ECG12} and A_{ECG12}, $p = 0.005$). ECG feature trend is again stable in case of spontaneous termination, with no significant changes in all parameters between the onset and the end of VF in the SHD group. Differences between sustained and self-terminating episodes in terms of surface CL (**Figure 4F**, left, $p = 0.0008$) are preserved during late VF. In the NSHD group, ECG markers of VF organization highlight similar patterns to those obtained by BSPM analysis. According to all ECG parameters, differences in body surface complexity between sustained and non-sustained episodes clearly appear only later in time ("VF end"), whereas at the onset of VF ("VF start") ECG features are comparable in both datasets. As for BSPM indices, a strong reduction in electrical organization (i.e., with an increase in NDI, **Figure 4E**, right), f-wave amplitude (**Figure 4F**, right), CL (**Figure 4G**, right) and entropy (**Figure 4G**, right) can be observed during sustained VF exclusively ($p < 0.0001$).

DISCUSSION

This study put forward a noninvasive methodology to explore and measure the complexity of VF by analyzing body surface cardiac potentials at multiple locations and finer spatial resolution. To our knowledge, this is the first report that explicitly and noninvasively investigates the link between patterns of electrical complexity of VF and myocardial structural alterations in a large cohort of patients using a multilead signal processing approach.

Temporal Evolution of Electrocardiographic Markers of VF Organization

As in Tovar and Jones (2000), Haïssaguerre et al. (2018), and Robson et al. (2018), overall we observed a sharp transition from early organization to late disorganization of electrical patterns of VF, due to the progressive and rapid metabolic deterioration of myocardial tissue, which drastically reduces the probability of survival to cardiac arrest and defibrillation success (Brown et al., 1989; Winkle et al., 1990). In our database, these changes could be captured from body surface signal analysis within a few seconds after the onset of VF (usually less than four), and they were validated with simultaneous measure of endocardial CL in a subset of patients. Furthermore, the dynamics of VF could be tracked in high detail, and the contribution of signals from multiple electrodes could be effectively summarized into one curve per parameter, thus easing the inspection of the fibrillatory patterns.

When information about VF termination mode was included as a fixed effect into the statistical analysis, distinct dynamic behaviors were underlined by body surface signal processing. All electrocardiographic parameters described stable fibrillatory patterns during self-terminating VF, as confirmed by previous invasive studies (Mäkikallio et al., 2002; Cismaru et al., 2013), whereas a strong increase in electrical complexity characterized episodes requiring DCC, despite comparable degrees of complexity at baseline.

Temporal increase in NDI assessed by SVD significantly correlated with progressive disorganization of VF with time. Several studies have confirmed the prognostic value of SVD-based analysis of body surface cardiac electrical activity. SVD of T-wave from surface ECG has been successfully applied to assess physiological and pathological properties of ventricular repolarization (Priori et al., 1997; Malik et al., 2000), under the hypothesis that increased dispersion of the electrical recovery would have been less accurately modeled by a 3D dipole. The study presented in Meo et al. (2018) moved from similar assumptions to measure the complexity of atrial fibrillation and use this information to guide ablation therapy. Our findings confirm the applicability of this methodology to cardiac signals during VF, and activation patterns can be reliably quantified by NDI from body surface.

In our VF population, f-wave amplitude decreased with progression of VF, in line with (Caldwell et al., 2012). As surface ECG can be regarded as the sum of all of the underlying myocardial electrical fields, the level of organization of the VF waveform relates to the organization of the myocardial elements in relation to each other. Local electrical vectors will increasingly oppose each other, thereby reducing the electrical voltage as measured at a global level (Wltkowskl et al., 1998; Balderston et al., 2018). Nevertheless, amplitude-related measures of VF complexity should be examined with caution, as their values can be affected by other factors not related to the arrhythmia itself, such as body size and cardiac axis (Ng and Goldberger, 2014). Furthermore, not only pairwise comparisons between intraepisode amplitude measures may be hampered by sudden

changes in contact quality of the recording electrodes, but also the intrinsic variability of amplitude values from patient to patient may affect the reliability of this metric alone with respect to the interpretation of VF dynamics.

As in Cismaru et al. (2013), surface VFCL prolonged between the onset and the end of self-terminating VF, while it decreased during sustained VF. VFCL from body surface potentials can provide an assessment of temporal changes in the properties of cellular substrate during VF (Patwardhan et al., 2000), and it is used as a predictor of defibrillation outcome (Strohmenger et al., 2001). Unlike previous works, surface CL was computed through a peak detection-based algorithm rather than a frequency domain approach (e.g., dominant frequency from Fourier transform), as stationarity is a fundamental assumption of the Fourier transform, thus spectral analysis may fail to capture the dynamical nature of VF (Cheng et al., 2012).

We expected entropy to increase with VF progression, as in Hajeb-Mohammadalipour et al. (2018). Yet, in some studies low values of several entropy-based metrics have also been measured even from ECG rhythms requiring external DCC (Chicote et al., 2016; Oh et al., 2017), and, more generally, during specific pathological conditions, such as congestive heart failure (Acharya et al., 2017). This apparent contradiction can be potentially explained by two reasons: (1) some entropy indices (e.g., Shannon entropy) are signal amplitude-dependent, thus even in presence of extremely regular patterns (such as sinus rhythm) they may not correctly capture signal regularity, if voltage is too low (Oh et al., 2017); (2) prior to entropy assessment, ECG signals can be preprocessed using different approaches [e.g., wavelet transform (Acharya et al., 2015; Oh et al., 2017)] in order to enhance specific patterns, therefore in some contexts results may differ from those obtained from raw data and make a direct comparison more difficult. Because in our implementation the entropy index suffered from poor temporal resolution, and it was often unable to track subtle intraepisode changes in VF progression, special attention should be paid to the interpretation of quantitative results in our database.

Electrical Complexity and Structural Cardiac Diseases

VF mechanisms are still poorly understood, thus hampering the development of suitable therapeutic strategies and arrhythmia management. Despite the apparent lack of synchrony and coordination of the fibrillatory process, several studies have confirmed that there is indeed a high degree of temporal and spatial organization in the fibrillating tissue (Gray et al., 1998). Nonetheless, we still lack tools to characterize VF electrical activation patterns and capture subtle changes both in time and space across the myocardium. Our research demonstrates that organization of VF can be measured from body surface, and that it accounts not only for the electrical properties of the myocardium, but also for those of the structural substrate.

SHD patients globally exhibited higher complexity than those with normal hearts at early stage of VF. Specifically, in this group lower f-wave amplitude and slower surface CL have been measured from body surface potentials, which is in line with previous research on ischemic VF, although the leading mechanisms have not been clearly elucidated yet (Bradley et al., 2011; Caldwell et al., 2012). The amount of nondipolar components as quantified by NDI was also initially higher in the SHD population, suggesting that structural substrate also contributes to electrical organization and cannot be accurately modeled in a 3D space. Although VF was initially more organized in the NSHD group, in these patients the temporal increase in VF complexity was more pronounced, rapid, and abrupt than in those with structural alterations, whereas in the SHD group structural substrate seems to have a dampening effect on VF electrical perpetuation and make it evolve more gradually. Indeed, during late VF the influence of structure appears less relevant, as BSPM complexity was comparable in both groups. The modalities according to which electrical-related factors may overdrive structural alterations with progression of VF are not clear though, and deeper insights may be provided by phase mapping (Umapathy et al., 2010; Robson et al., 2018).

Importantly, increased baseline complexity of VF as resulting from the combination of structural and non-structural alterations was found to be associated with sustained VF episodes from SHD patients, and it prompted DCC performance to terminate the arrhythmia. More precisely, slow fibrillatory activities at baseline predicted spontaneous termination of VF, as confirmed invasively by Muñoz et al. (2009). Increased electrical disorganization at the beginning of VF was also quantified by a higher amount of nondipolar content (i.e., higher NDI), which is known to be associated with significant arrhythmic complications in a multitude of pathological conditions (Priori et al., 1997; Malik et al., 2000). However, to our knowledge, our research is the first application of NDI as a noninvasive tool to predict VF termination mode in the first seconds of the arrhythmia, thus opening meaningful perspectives into the understanding and management of VF. Similarly, the descriptive accuracy of f-wave amplitude and entropy has not been systematically assessed yet in this framework, and our report demonstrates that both parameters are poor descriptors of VF self-termination at baseline in all SHD patients. The role of amplitude-based metrics from surface ECG in the characterization of ischemic VF has been questioned (Caldwell et al., 2012), therefore any evidence provided by these parameters should be investigated in more detail.

In patients with structurally normal hearts, VF had a similar evolution to the SHD group depending on its termination mode, although intraepisode changes in body surface complexity were characterized by a faster and sharper evolution than in the presence of structural diseases. All electrocardiographic features exhibited similar trends, in keeping with previous research (Cismaru et al., 2013). However, it is worth to note that differences between sustained and self-terminating episodes according to all BSPM parameters arose only during late VF (i.e., approximately 10 s after arrhythmia onset in the NSHD group), hinting at potential additional mechanisms driving VF dynamics beyond structural substrates in this population. Also in this case, a correlation of BSPM-derived indices with the distribution of VF drivers (Haïssaguerre et al., 2018) would be

desirable to better characterize the electrophysiological causes of VF in these patients.

What Can Be Inferred From Standard ECG?

As mentioned in section "Other Body Surface Markers of VF Electrical Complexity and Dynamics," all BSPM features have also been computed from an equivalent standard ECG to investigate the scalability of our findings to the 12-lead configuration, which is more easily available in clinical centers. Overall, our results show that the characterization of VF dynamics is still preserved by the alternative signal features, although transitions in electrical organization appear less exacerbated by ECG indices during sustained VF compared to their BSPM counterparts. The reduced spatial resolution had a significant impact on features' computation in SHD patients, for whom the ability of certain indices (i.e., surface CL and NDI) to predict self-termination of VF at baseline was lost. This evidence confirms the benefits from a multilead signal processing approach, as the analysis of multiple electrodes may help: (1) increasing the statistical confidence of body surface measures; (2) compensating the lack of information from standard leads in case of electrode displacement, poor signal quality, etc., which would be otherwise impossible to derive and (3) capturing cardiac electrical activity at multiple angles and orientations that are not generally accounted for by standard ECG configurations. With regard to that, the use of posterior leads has proven to be useful in the localization of premature contractions from the outflow tracts in Zhang et al. (2017), and nonstandard systems (e.g., the 15-lead ECG) should be generally considered in patients who also present inferior and suspected posterior myocardial infarction (Steg et al., 2012). Finally, multielectrode potential mapping may be simultaneously used with other techniques (for instance, electrocardiographic imaging) to identify diseased ventricular sites, which may induce threatening arrhythmias, thus combining BSPM timing information with trigger spatial location. This would provide added benefit for patients with apparently normal hearts, but with microstructural alterations that are often misdetected by current imaging techniques (Haïssaguerre et al., 2018).

Limitations and Perspectives

The limited number of noninvasive signal processing approaches to measure VF complexity from literature made the comparison between BSPM parameters more challenging. The studies mentioned in our report have been performed in a large variety of experimental frameworks and using different models, thus evidence from the state of the art appeared sometimes controversial. However, our findings are in line with previous research about human VF, and they have been corroborated by invasive measures, thus increasing the confidence of our conclusions.

To validate surface signal assessment, we used endocardial CL as a reference, since it is conventionally regarded in clinics as a good marker of electrical activation rate at the level of the tissue. However, for ethical reasons, it was not possible to explore the mechanisms of VF maintenance at a higher resolution in this clinical scenario. In Meo et al. (2020), we have tried (at least partially) to address this question, and we have shown that in explanted porcine hearts NDI can identify more heterogeneous repolarization substrates, with uneven spatial distribution of epicardial CL and reentrant drivers from ventricular sites with different repolarization timings. Further investigation is needed to translate these findings from our experimental model to clinical patients, and to test additional hypotheses to explain all the pathologies encountered across our dataset.

No specific gender-related differences in VF dynamics were found in our dataset based on surface signal analysis. Overall, we observed that VF progression was comparable both in male and female patients according to all parameters, independently of the lead configuration. Further investigation is needed to elucidate the mechanisms underlying potential inter-gender differences in subpopulations from our dataset and link them to other risk factors.

Our patients' cohort has been split into two macro-categories (i.e., SHD vs. NSHD), although each group includes patients with different pathologies and electrocardiographic manifestations. This choice is motivated not only by the will to investigate the impact of structural alterations in a more general framework, but also by the reduced number of VF recordings in certain categories (even one or two for certain diseases), which hampers the generalization of certain findings. The inclusion of additional signal recordings in those categories in a future study may allow for the assessment of more specific patient-related electrical signatures during VF.

Body surface markers of VF complexity were not correlated with defibrillation shock outcome, as it goes beyond the scope of this research. Indeed, while the use of hundreds of electrodes is not considered feasible when prompt defibrillation is required for out-of-hospital cardiac arrest, our analysis of VF in a controlled environment proved the descriptive value of multilead electrocardiographic markers and the possibility to extract valuable information about VF complexity using electrical signals only, with very short duration and no need for other information about the patient (e.g., clinical history, anatomy, etc.). In future, we may potentially try to incorporate other noninvasive markers (e.g., ventricular volumes from echocardiography, scar and fibrosis distribution from magnetic resonance imaging, etc.) to verify whether they can provide any additional information beyond electrical markers.

Importantly, some of our findings could be retrieved from standard ECG as well, thus opening promising perspectives to the analysis of VF from body surface in a larger clinical s cenario. Nonetheless, as discussed in section "What Can Be Inferred from Standard ECG?", some important differences between BSPM and ECG features were observed, in particular at the onset of VF, i.e., the impossibility to predict self-termination of VF in patients with structural anomalies from the standard leads, and using a higher number of electrodes may also offer additional insights in the spatial localization of triggering mechanisms. Therefore, future research may try to compensate them, e.g., by introducing novel signal features, or designing alternative ECG lead placement configurations, and/or with a different number of electrodes at specific locations.

With regard to that, alternative multilead setups with an intermediate number of electrodes between BSPM and ECG could not be straightforwardly tested. Indeed, for some of the reasons presented in section "Noninvasive Mapping of VF and BSPM Preprocessing", in certain patients cardiac potentials could not be recorded over the entire set of electrodes (28% of VF episodes, with between 236 and 251 electrodes used). Most of these electrodes were localized in the lower section of the vest, thus comparison with ECG was still feasible in all patients, but a comparison of signal features from nonstandard electrodes was not implementable in a unified framework. For this purpose, in future the use of computational models may help evaluating the robustness of signal indices to different electrode locations and easily varying the number of recording channels while keeping comparable and controlled testing conditions.

Our investigation merely aimed to globally assess progression of VF from body surface, but driving mechanisms of the arrhythmia and their spatial distribution over the ventricles have not been described. As pointed out in section "Discussion," correlating BSPM metrics with phase mapping analysis may help addressing some unanswered questions and may be attempted in future. At this stage, we showed that body surface mapping can precociously help identifying patients with abnormal electrical disorganization at the onset of VF, who can be therefore subsequently inspected in more detail through more invasive approaches.

CONCLUSION

We developed a noninvasive multilead signal processing framework to measure VF complexity, track its temporal evolution and assess the relation between myocardial electrical characteristics and structural substrate. The main findings outlined by our investigation can be summarized as follows:

a. Sustained VF is characterized by an early, sharp increase in electrical complexity, with quick deterioration within the first few seconds from the onset. Conversely, self-terminating VF exhibits a stable evolution throughout the duration of the episode, which can be timeously predicted as well. These different dynamic behaviors hint at distinct mechanisms underlying the perpetuation of the arrhythmia with time.
b. While the termination mode similarly affects VF evolution in all patients regardless of the structural substrate properties, in patients with apparently normal hearts VF is more organized at baseline, but electrophysiological degeneration into sustained forms is more rapid and severe than in those with structural diseases, as myocardial alterations contribute to dampen and slow down VF dynamics. These elements suggest that while structural determinants for VF evolution play a more relevant role at early stage of the arrhythmia, late VF is dominated by alternative driving mechanisms accelerating its deterioration.
c. The combination of structural and electrophysiological substrate characteristics influences the timing of the transition from early organization to late disorganization of VF, and this information may help optimizing defibrillation shock timing and waveforms, thus improving current strategies for VF treatment and opening a perspective toward personalized therapy of this arrhythmia.
d. These distinct patterns of VF complexity can be described in detail by our approach using electrical signals only, and the spatial content of multielectrode BSPMs can be condensed into a few parameters, thus easing visualization and interpretation of VF dynamics from surface cardiac potentials.
e. Some of these results can be retrieved by our approach from the 12-lead ECG as well, thus broadening its applicability to a wider clinical scenario, when high-resolution BSPM systems are not available. Nevertheless, particular attention should be paid to patients without apparent structural hearts diseases, as in these subjects the ECG-based assessment of VF complexity from a lower number of electrodes may be less accurate at early stage of VF compared to the full BSPM configuration and lead to potential misinterpretation of the arrhythmic patterns.

Overall, our signal processing methodology provides relevant insights into the understanding and the management of VF patients.

DATA AVAILABILITY STATEMENT

Due to the nature of this research, participants of this study did not agree for their data to be shared publicly, so the raw data supporting the conclusions of this article is not publicly available. Requests to access the datasets should be directed to MiH, michel.haissaguerre@chu-bordeaux.fr.

ETHICS STATEMENT

The studies involving human participants were reviewed and approved by Comité de Protection des Personnes Sud-Ouest et Outre Mer III and Institutional Clinical Research and Ethics Committee. The patients/participants provided their written informed consent to participate in this study.

AUTHOR CONTRIBUTIONS

All authors have significantly contributed to this work. MM conceived and designed the study, implemented the signal processing methods, analyzed and interpreted the results, and drafted the manuscript. AD, FS, JD, and GC performed VF ablation procedures and helped analyzing clinical data. SP acquired clinical BSPM recordings. PJ, MéH, and MiH supervised clinical data acquisition and helped assessing algorithm performance. LB and OB provided further contributions to the interpretation of the results. RD contributed

to the conception of the study, provided feedback about the implementation of the methods and the interpretation of the results, and revised the manuscript.

FUNDING

This study was supported by the French Government as part of the "Investments of the Future" program managed by the National Agency Research (ANR-10-IAHU04-LIRYC), the European Research Council (FP7/2007–2013 grant agreement number 322886, SYMPHONY), and the Leducq Foundation (RHYTHM network).

ACKNOWLEDGMENTS

The research presented in this manuscript extends a study presented to computing in cardiology 2017 Conference and Heart Rhythm Society 2018 and 2019 Conferences.

REFERENCES

Acharya, U. R., Fujita, H., Sudarshan, V. K., Oh, S. L., Adam, M., Tan, J. H., et al. (2017). Automated characterization of coronary artery disease, myocardial infarction, and congestive heart failure using contourlet and shearlet transforms of electrocardiogram signal. *Knowl. Based Syst.* 132, 156–166. doi: 10.1016/j.knosys.2017.06.026

Acharya, U. R., Fujita, H., Sudarshan, V. K., Sree, V. S., Eugene, L. W. J., Ghista, D. N., et al. (2015). An integrated index for detection of Sudden Cardiac Death using discrete wavelet transform and nonlinear features. *Knowl. Based Syst.* 83, 149–158. doi: 10.1016/j.knosys.2015.03.015

Al-Khatib, S. M., Stevenson, W. G., Ackerman, M. J., Bryant, W. J., Callans, D. J., Curtis, A. B., et al. (2017). AHA/ACC/HRS guideline for management of patients with ventricular arrhythmias and the prevention of sudden cardiac death: executive summary. *Circulation* 138, e210–e271. doi: 10.1161/CIR.0000000000000549

Balderston, J. R., Gertz, Z. M., Ellenbogen, K. A., Schaaf, K. P., and Ornato, J. P. (2018). Association between ventricular fibrillation amplitude immediately prior to defibrillation and defibrillation success in out-of-hospital cardiac arrest. *Am. Heart J.* 201, 72–76. doi: 10.1016/j.ahj.2018.04.002

Bradley, C. P., Clayton, R. H., Nash, M. P., Mourad, A., Hayward, M., Paterson, D. J., et al. (2011). Human ventricular fibrillation during global ischemia and reperfusion: paradoxical changes in activation rate and wavefront complexity. *Circulation* 4, 684–691. doi: 10.1161/circep.110.961284

Brown, C. G., Dzwonczyk, R., Werman, H. A., and Hamlin, R. L. (1989). Estimating the duration of ventricular fibrillation. *Ann. Emerg. Med.* 18, 1181–1185. doi: 10.1016/s0196-0644(89)80056-3

Caldwell, J. C., Burton, F. L., Cobbe, S. M., and Smith, G. L. (2012). Amplitude changes during ventricular fibrillation: a mechanistic insight. *Front. Physiol.* 3:147. doi: 10.3389/fphys.2012.00147

Cheng, K. A., Dosdall, D. J., Li, L., Rogers, J. M., Ideker, R. E., Huang, J., et al. (2012). Evolution of activation patterns during long-duration ventricular fibrillation in pigs. *Am. J. Physiol. Heart Circ. Physiol.* 302, 992–1002. doi: 10.1152/ajpheart.00419.2011

Cheniti, G., Vlachos, K., Meo, M., Puyo, S., Thompson, N., Denis, A., et al. (2018). Mapping and ablation of idiopathic ventricular fibrillation. *Front. Cardiovasc. Med.* 5:123. doi: 10.3389/fcvm.2018.00123

Chicote, B., Irusta, U., Alcaraz, R., Rieta, J. J., Aramendi, E., Isasi, I., et al. (2016). Application of entropy-based features to predict defibrillation outcome in cardiac arrest. *Entropy* 18, 1–17. doi: 10.3390/e18090313

Cismaru, G., Brembilla-Perrot, B., Pauriah, M., Zinzius, P. Y., Sellal, J. M., Schwartz, J., et al. (2013). Cycle length characteristics differentiating non-sustained from self-terminating ventricular fibrillation in Brugada syndrome. *Europace* 15, 1313–1318. doi: 10.1093/europace/eut023

Clayton, R. H., Murray, A., and Campbell, R. W. F. (1995). Analysis of the body surface ECG measured in independent leads during ventricular fibrillation in humans. *PACE Pacing Clin. Electrophysiol.* 18, 1876–1881. doi: 10.1111/j.1540-8159.1995.tb03835.x

De Ambroggi, L., Aimè, E., Ceriotti, C., Rovida, M., and Negroni, S. (1997). Mapping of ventricular repolarization potentials in patients with arrhythmogenic right ventricular dysplasia: principal component analysis of the ST-T waves. *Circulation* 96, 4314–4318. doi: 10.1161/01.cir.96.12.4314

Di Marco, L. Y., Bourke, J. P., and Langley, P. (2012). Spatial complexity and spectral distribution variability of atrial activity in surface ECG recordings of atrial fibrillation. *Med. Biol. Eng. Comput.* 50, 439–446. doi: 10.1007/s11517-012-0878-8

Eftestøl, T., Sunde, K., Aase, S. O., Husøy, J. H., and Steen, P. A. (2000). Predicting outcome of defibrillation by spectral characterization and nonparametric classification of ventricular fibrillation in patients with out-of-hospital cardiac arrest. *Circulation* 102, 1523–1529. doi: 10.1161/01.cir.102.13.1523

Fishman, G. I., Chugh, S. S., Dimarco, J. P., Albert, C. M., Anderson, M. E., Bonow, R. O., et al. (2010). Sudden cardiac death prediction and prevention: report from a national heart, lung, and blood institute and heart rhythm society workshop. *Circulation* 122, 2335–2348. doi: 10.1161/CIRCULATIONAHA.110.976092

Fitz-Clarke, J. R., Sapp, J. L., Warren, J. W., Clements, J. C., and Horáček, B. M. (2006). Body surface potential mapping and computer simulation of human ventricular fibrillation. *Comput. Cardiol.* 33, 397–400.

Ganesan, A. N., Kuklik, P., Lau, D. H., Brooks, A. G., Baumert, M., Lim, W. W., et al. (2013). Bipolar electrogram Shannon entropy at sites of rotational activation implications for ablation of atrial fibrillation. *Circulation* 6, 48–57. doi: 10.1161/circep.112.976654

Gray, R. A., Pertsov, A. M., and Jalife, J. (1998). Spatial and temporal organization during cardiac fibrillation. *Nature* 392, 75–78. doi: 10.1038/32164

Haïssaguerre, M., Hocini, M., Cheniti, G., Duchateau, J., Sacher, F., Puyo, S., et al. (2018). Localized structural alterations underlying a subset of unexplained sudden cardiac death. *Circulation* 11:e006120. doi: 10.1161/CIRCEP.117.006120

Hajeb-Mohammadalipour, S., Ahmadi, M., Shahghadami, R., and Chon, K. H. (2018). Automated method for discrimination of arrhythmias using time, frequency, and nonlinear features of electrocardiogram signals. *Sensors* 18:2090. doi: 10.3390/s18072090

Hayashi, M., Shimizu, W., and Albert, C. M. (2015). The spectrum of epidemiology underlying sudden cardiac death. *Circ. Res.* 116, 1887–1906. doi: 10.1161/circresaha.116.304521

Jalife, J. (2000). Ventricular fibrillation: mechanisms of initiation and maintenance. *Annu. Rev. Physiol.* 62, 25–50. doi: 10.1146/annurev.physiol.62.1.25

Mäkikallio, T. H., Huikuri, H. V., Myerburg, R. J., Seppänen, T., Kloosterman, M., Interian, A., et al. (2002). Differences in the activation patterns between sustained and self-terminating episodes of human ventricular fibrillation. *Ann. Med.* 34, 130–135. doi: 10.1080/07853890252953527

Malik, M., Acar, B., Gang, Y. I., Yap, Y. G., Hnatkova, K., and John Camm, A. (2000). QT dispersion does not represent electrocardiographic interlead heterogeneity of ventricular repolarization. *J. Cardiovasc. Electrophysiol.* 11, 835–843. doi: 10.1111/j.1540-8167.2000.tb00061.x

Meo, M., Bear, L. R., Abell, E., Cluitmans, M., Jaïs, P., Hocini, M., et al. (2020). *Noninvasive Tracking of Repolarization Gradients as a Substrate for Ventricular Fibrillation*. San Diego, CA: Heart Rhythm Society Congress, 383–476.

Meo, M., Pambrun, T., Derval, N., Dumas-Pomier, C., Puyo, S., Duchâteau, J., et al. (2018). Noninvasive assessment of atrial fibrillation complexity in relation to ablation characteristics and outcome. *Front. Physiol.* 9:929. doi: 10.3389/fphys.2018.00929

Meo, M., Potse, M., Puyo, S., Bear, L., Hocini, M., Häissaguerre, M., et al. (2017). "Non-invasive assessment of spatiotemporal organization of ventricular fibrillation through principal component analysis," in *Proceedings of the Computing in Cardiology* (Rennes: IEEE). doi: 10.22489/CinC.2017.101-051

Meo, M., Zarzoso, V., Meste, O., Latcu, D. G., and Saoudi, N. (2013a). Catheter ablation outcome prediction in persistent atrial fibrillation using weighted

principal component analysis. *Biomed. Signal Process. Control.* 8, 958–968. doi: 10.1016/j.bspc.2013.02.002

Meo, M., Zarzoso, V., Meste, O., Latcu, D. G., and Saoudi, N. (2013b). Spatial variability of the 12-lead surface ECG as a tool for noninvasive prediction of catheter ablation outcome in persistent atrial fibrillation. *IEEE Trans. Biomed. Eng.* 60, 20–27. doi: 10.1109/tbme.2012.2220639

Moe, G. K., Abildskov, J., and Han, J. (1964). *Factors Responsible for the Initiation and Maintenance of Ventricular Fibrillation. Sudden Cardiac Death*. New York, NY: Grune & Stratton.

Muñoz, J. J. S., Álvarez, J. L. R., Alberola, A. G., Carrión, J. R., Everss, E., Ortiz, M., et al. (2009). Spectral analysis of sustained and non-sustained ventricular fibrillation in patients with an implantable cardioverter-defibrillator. *Rev. Española Cardiol.* 62, 690–693. doi: 10.1016/S1885-5857(09)72234-0

Ng, J., and Goldberger, J. J. (2014). The ups and downs of ventricular fibrillation waveforms. *J. Am. College Cardiol.* 64, 1370–1372. doi: 10.1016/j.jacc.2014.07.953

Oh, S. L., Hagiwara, Y., Adam, M., Sudarshan, V. K., Koh, J. E., Tan, J. H., et al. (2017). Shockable versus nonshockable life-threatening ventricular arrhythmias using dwt and nonlinear features of ECG signals. *J. Mech. Med. Biol.* 17:1740004. doi: 10.1142/s0219519417400048

Park, S. A., and Gray, R. A. (2015). Optical mapping of ventricular fibrillation dynamics. *Membr. Potential Imaging Nerv. Syst. Heart* 313–342. doi: 10.1007/978-3-319-17641-3_13

Patwardhan, A., Moghe, S., Wang, K. E., and Leonelli, F. (2000). Frequency modulation within electrocardiograms during ventricular fibrillation. *Am. J. Physiol. Heart Circ. Physiol.* 279, 825–835.

Peters, S., Peters, H., and Thierfelder, L. (1999). Risk stratification of sudden cardiac death and malignant ventricular arrhythmias in right ventricular dysplasia-cardiomyopathy. *Int. J. Cardiol.* 71, 243–250. doi: 10.1016/s0167-5273(99)00142-4

Priori, S. G., Blomström-Lundqvist, C., Mazzanti, A., Blom, N., Borggrefe, M., Camm, J., et al. (2015). ESC Guidelines for the management of patients with ventricular arrhythmias and the prevention of sudden cardiac death. *Eur. Heart J.* 36, 2793–2867.

Priori, S. G., Mortara, D. W., Napolitano, C., Diehl, L., Paganini, V., Cantù, F., et al. (1997). Evaluation of the spatial aspects of T-wave complexity in the long-QT syndrome. *Circulation* 96, 3006–3012. doi: 10.1161/01.cir.96.9.3006

Robson, J., Aram, P., Nash, M. P., Bradley, C. P., Hayward, M., Paterson, D. J., et al. (2018). Spatio-temporal organization during ventricular fibrillation in the human heart. *Ann. Biomed. Eng.* 46, 864–876. doi: 10.1007/s10439-018-2007-9

Rogers, J. M., Huang, J., Smith, W. M., and Ideker, R. E. (1999). Incidence, evolution, and spatial distribution of functional reentry during ventricular fibrillation in pigs. *Circ. Res.* 84, 945–954. doi: 10.1161/01.res.84.8.945

Sörnmo, L., and Laguna, P. (2005). *Bioelectrical Signal Processing in Cardiac and Neurological Applications*. Amsterdam: Elsevier.

Steg, P. G., James, S. K., Atar, D., Badano, L. P., Lundqvist, C. B., Borger, M. A., et al. (2012). ESC Guidelines for the management of acute myocardial infarction in patients presenting with ST-segment elevation. *Eur. Heart J.* 33, 2569–2619.

Strohmenger, H. U., Eftestol, T., Sunde, K., Wenzel, V., Mair, M., Ulmer, H., et al. (2001). The predictive value of ventricular fibrillation electrocardiogram signal frequency and amplitude variables in patients with out-of-hospital cardiac arrest. *Anesth. Analgesia* 93, 1428–1433. doi: 10.1097/00000539-200112000-00016

Such-Miquel, L., Chorro, F. J., Guerrero, J., Trapero, I., Brines, L., Zarzoso, M., et al. (2013). Evaluation of the complexity of myocardial activation during ventricular fibrillation. An experimental study. *Rev. Esp. Cardiol.* 66, 177–184. doi: 10.1016/j.rec.2012.08.012

Tovar, O. H., and Jones, J. L. (2000). Electrophysiological deterioration during long-duration ventricular fibrillation. *Circulation* 102, 2886–2891. doi: 10.1161/01.cir.102.23.2886

Turrini, P., Corrado, D., Basso, C., Nava, A., Bauce, B., and Thiene, G. (2001). Dispersion of ventricular depolarization-repolarization. *Circulation* 103, 3075–3080. doi: 10.1161/01.cir.103.25.3075

Umapathy, K., Nair, K., Masse, S., Krishnan, S., Rogers, J., Nash, M. P., et al. (2010). Phase mapping of cardiac fibrillation. *Circulation* 3, 105–114.

Weiss, J. N., Qu, Z., Chen, P. S., Lin, S. F., Karagueuzian, H. S., Hayashi, H., et al. (2005). The dynamics of cardiac fibrillation. *Circulation* 112, 1232–1240.

Winkle, R. A., Mead, R. H., Ruder, M. A., Smith, N. A., Buch, W. S., and Gaudiani, V. A. (1990). Effect of duration of ventricular fibrillation on defibrillation efficacy in humans. *Circulation* 81, 1477–1481. doi: 10.1161/01.cir.81.5.1477

Wltkowskl, F. X., Leon, L. J., Penkoske, P. A., Giles, W. R., Spano, M. L., Dltto, W. L., et al. (1998). Spatiotemporal evolution of ventricular fibrillation. *Nature* 392, 78–82. doi: 10.1038/32170

Zhang, F., Hamon, D., Fang, Z., Xu, Y., Yang, B., Ju, W., et al. (2017). Value of a posterior electrocardiographic lead for localization of ventricular outflow tract arrhythmias: the V4/V8 ratio. *JACC Clin. Electrophysiol.* 3, 678–686. doi: 10.1016/j.jacep.2016.12.018

Conflict of Interest: The authors declare that the research was conducted in the absence of any commercial or financial relationships that could be construed as a potential conflict of interest.

frontiers in Physiology

ORIGINAL RESEARCH
published: 30 September 2020
doi: 10.3389/fphys.2020.568021

Contribution of Depolarization and Repolarization Changes to J-Wave Generation and Ventricular Fibrillation in Ischemia

Alena S. Tsvetkova[1], Jan E. Azarov[1,2,3], Olesya G. Bernikova[1], Alexey O. Ovechkin[1,4], Marina A. Vaykshnorayte[1], Marina M. Demidova[2,5] and Pyotr G. Platonov[2,6]*

[1]Department of Cardiac Physiology, Institute of Physiology, Komi Science Center, Ural Branch, Russian Academy of Sciences, Syktyvkar, Russia, [2]Department of Cardiology, Clinical Sciences, Lund University, Lund, Sweden, [3]Department of Biochemistry and Physiology, Institute of Medicine, Pitirim Sorokin Syktyvkar State University, Syktyvkar, Russia, [4]Department of Therapy, Institute of Medicine, Pitirim Sorokin Syktyvkar State University, Syktyvkar, Russia, [5]V. A. Almazov National Medical Research Center, Saint Petersburg, Russia, [6]Arrhythmia Clinic, Skåne University Hospital, Lund, Sweden

Background: Activation delay in ischemic myocardium has been found to contribute to J-wave appearance and to predict ventricular fibrillation (VF) in experimental myocardial infarction. However, the role of ischemia-related repolarization abnormalities in J-wave generation remains unclear.

Objectives: The objective of our study was to assess a contribution of myocardial repolarization changes to J-wave generation in the body surface ECG and VF in a porcine acute myocardial infarction model.

Methods: In 22 anesthetized pigs, myocardial ischemia was induced by occlusion of the left anterior descending coronary artery (LAD, n = 14) and right coronary artery (RCA, n = 8). Body surface ECGs were recorded simultaneously with intramyocardial unipolar electrograms led from flexible electrodes positioned across the left ventricular (LV) wall, interventricular septum (IVS), and right ventricular (RV) wall at apical, middle and basal levels of the ventricles (a total of 48 leads). Local activation times (ATs) and activation-repolarization intervals (ARIs, differences between dV/dt maximum during T-wave and dV/dt minimum during QRS) were measured.

Results: J-waves appeared in left precordial leads (in 11 out of 14 animals with LAD occlusion) and right precordial leads (in six out of eight animals with RCA occlusion). During ischemic exposure, ATs prolonged, and the activation delay was associated with J-wave development (OR = 1.108 95% CI 1.072–1.144; $p < 0.001$) and VF incidence (OR = 1.039 95% CI 1.008–1.072; $p = 0.015$). ARIs shortened in the ischemic regions (in the IVS under LAD-occlusion and the lateral RV base under RCA-occlusion). The difference between maximal ARI in normal zones and ARI in the ischemic zones (ΔARI) was associated with J-wave appearance (OR = 1.025 95% CI 1.016–1.033, $p < 0.001$) independently of AT delay in multivariate logistic regression analysis.

Conclusions: Both AT delay and increase of ΔARIs contributed to the development of J-wave in body surface ECG. However, only AT delay was associated with VF occurrence.

Keywords: ischemia, J-wave, ventricular fibrillation, activation time, repolarization, ECG

OPEN ACCESS

Edited by:
Ruben Coronel, University of Amsterdam, Netherlands

Reviewed by:
Richard David Walton, Université de Bordeaux, France
Mark Potse, Inria Bordeaux - Sud-Ouest Research Centre, France

****Correspondence:***
Jan E. Azarov
j.azarov@gmail.com

Specialty section:
This article was submitted to Cardiac Electrophysiology, a section of the journal Frontiers in Physiology

Received: *31 May 2020*
Accepted: *14 September 2020*
Published: *30 September 2020*

Citation:
Tsvetkova AS, Azarov JE, Bernikova OG, Ovechkin AO, Vaykshnorayte MA, Demidova MM and Platonov PG (2020) Contribution of Depolarization and Repolarization Changes to J-Wave Generation and Ventricular Fibrillation in Ischemia. Front. Physiol. 11:568021. doi: 10.3389/fphys.2020.568021

INTRODUCTION

The presence of J-wave in ECG once considered a benign phenomenon (Mehta et al., 1999) was subsequently admitted to be a predictor of idiopathic malignant ventricular tachyarrhythmias (Haissaguerre et al., 2008). J-wave appearance was also found to suggest an increased risk for ventricular tachycardia or fibrillation in acute myocardial infarction (Jastrzebski and Kukla, 2009; Naruse et al., 2012; Sato et al., 2012). During dynamic ECG observation in an experimental acute myocardial infarction model, development of J-waves preceded episodes of ventricular fibrillation (VF; Demidova et al., 2014).

Explanation for J-wave generation remains equivocal. An alternative name for this phenomenon, an early repolarization pattern, suggests an essential role of certain repolarization distinctions in its development. Indeed, in isolated myocardial preparations J-wave was demonstrated to be a manifestation of a transmural potential difference resulting from variation in spike-and-dome morphology of action potentials across the ventricular wall (Yan and Antzelevitch, 1996). A number of agents that can increase or reduce this variation, accordingly modify manifestation of the early repolarization pattern (Antzelevitch and Yan, 2010).

Development of J-waves can be also seen in depolarization disturbances. J-wave appearance in patients with non-compact cardiomyopathy, as well as in patients with arrhythmogenic right ventricular dysplasia/cardiomyopathy (ARVD/C) characterized by changes in depolarization suggests that there are alternative, including depolarization-related mechanisms of its formation (Peters and Selbig, 2008; Caliskan et al., 2012). Myocardial ischemia presents another setting where J-wave formation can result from depolarization slowing. A conduction block-related mechanism could be responsible for J-wave augmentation with cycle length shortening in acute myocardial infarction patients (Nakayama et al., 2013, 2019). Recently, in an *in vivo* model of acute myocardial infarction, we directly demonstrated an association between activation delay in the ischemic myocardium, J-wave, and VF occurrence (Azarov et al., 2019). However, a role, if any, of repolarization abnormalities in these phenomena in ischemia has not yet been tested.

The objective of the present study was to assess an association between myocardial repolarization changes and J-wave appearance in body surface ECG and VF incidence in a porcine acute myocardial infarction model.

MATERIALS AND METHODS

Experiments were performed in 22 domestic pigs (30–45 kg body weight) purchased from a local producer. The study conformed to the *Guide for the Care and Use of Laboratory Animals, 8th Edition* published by the National Academies Press (United States) 2011, the guidelines from Directive 2010/63/EU of the European Parliament on the protection of animals used for scientific purposes and was approved by the Ethical Committee of the Institute of Physiology of the Komi Science Centre, Ural Branch of Russian Academy of Sciences. Experimental procedures were described earlier (Azarov et al., 2019). Briefly, the animals were anesthetized with zoletil (Virbac S.A., Carros, France, 10–15 mg/kg, i.m.), xylazine (Interchemie, Castenray, Netherlands, 0.5 mg/kg, i.m.), and propofol (Norbrook Laboratories Ltd., UK, 1 mg/kg, i.v.), intubated and mechanically ventilated. The heart was accessed *via* a midsternal incision.

Data Registration

Coronary occlusion was induced by ligation of the left anterior descending coronary artery (LAD, n = 14) or right coronary artery (RCA, n = 8). Three flexible plunge electrodes (16 lead terminals each) were placed in the anterior portion of the left ventricle (LV), interventricular septum (IVS), and right ventricle (RV) at apical, middle, and basal levels (**Figure 1**). The filaments of the flexible plunge electrodes were pulled through ventricular walls with a taper point surgical needle. Positions of electrodes were selected so as to comprise both expected ischemic and expected nonischemic areas (**Figure 1**, panel **A**). The electrodes were fabricated with isolated 70-μm copper wires, fixed with a knot on a 0.8-mm vicryl filament. Lead terminals on the electrode filament were equally spaced, with an interelectrode distance of 5.0 mm (electrode filament length 75 mm) for the basal and middle levels and 3.5 mm (electrode filament length 52.5 mm) for the apical level (**Figure 1**, panel **B**).

After electrode and ligature placement, the chest was reclosed, and the heart was allowed to stabilize for 30 min. Recordings were done at baseline and at 1, 2.5, 5, 10, 15, 20, 25, 30, 35, and 40 min of coronary occlusion. Unipolar intramyocardial electrograms were recorded in parallel with 12 standard ECG leads and additional right precordial leads (**Figure 2**, panel **A**) by means of a custom-designed system (16 bits; bandwidth 0.05–1,000 Hz; sampling rate 4,000 Hz). **Figure 3** gives an example of raw signals recorded in baseline and during LAD occlusion from the lead terminals located on the same electrode filament passing through the ventricular walls and cavities at the middle level.

The animals were euthanized under deep anesthesia by an intravenous potassium chloride injection either at the end of ischemic episode or immediately after VF development. The hearts were excised, and localization of ischemic zone (area at risk) was assessed by staining with Evans blue dye (Sigma-Aldrich GmbH, Germany), which was injected into the coronary arteries with LAD or RCA ligature tightened (**Figure 1**, panel **C**). Depths and positions of the electrodes in each heart were determined by cutting the stained heart at three levels parallel to planes of introduction of the electrode filaments. The leads located in the cavities of the ventricles and/or in the pericardial cavity were excluded from analysis.

Data Processing

In each intramyocardial lead, local activation time (AT) and end of repolarization time (RT) were measured from the body surface QRS onset to instants of a dV/dt minimum during QRS-complex and dV/dt maximum during T-wave, respectively; activation-repolarization interval (ARI) was calculated as a difference

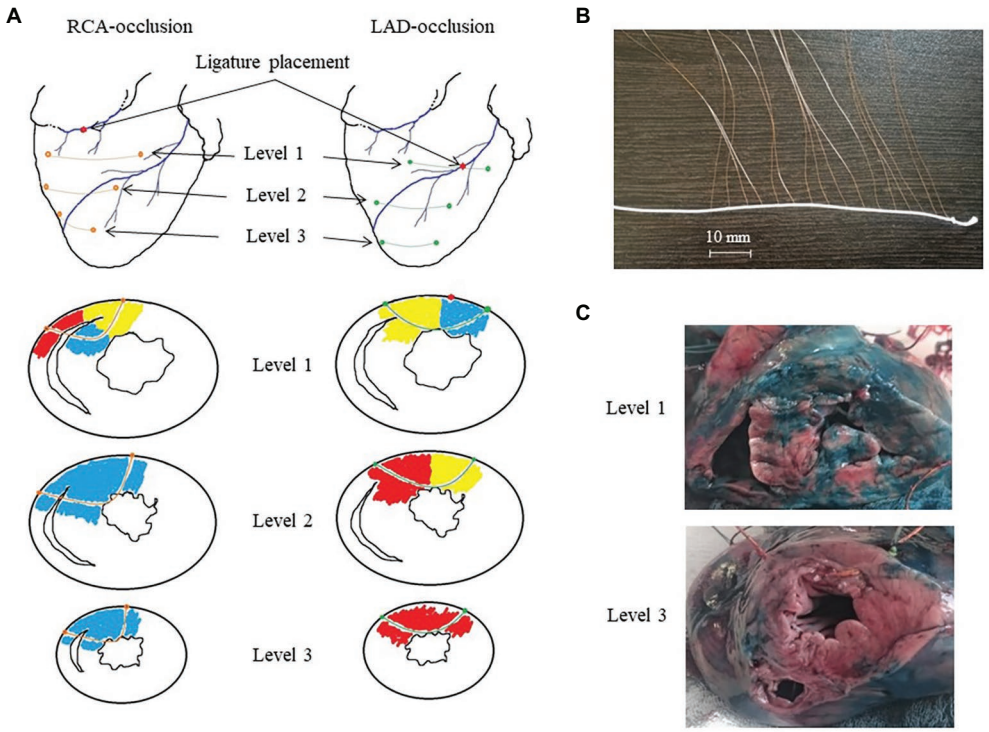

FIGURE 1 | Intramyocardial recordings with flexible plunge electrodes. Panel **A**: scheme of ligature and flexible plunge electrodes placement in respect to ischemic (red), border (yellow) and normal (blue) myocardium under right coronary artery (RCA)- and left anterior descending artery (LAD)-occlusions on basal (level 1), middle (level 2) and apical (level 3) levels. Panel **B**: a photograph of a flexible plunge electrode. See an electrode filament (white thread), lead cooper wires fixed on the thread with knots with insulation removed at the knots (lead terminals). The interelectrode spacing was 5.0 mm for the basal and middle levels and 3.5 mm for the apical level. Panel **C**: photographs of porcine heart cross-cuts after the experiment with LAD occlusion after staining with Evans blue dye at the basal (level 1) and apical (level 3) levels. See mostly stained myocardium (except posterior IVS portion) at the level 1 and unstained (ischemic) myocardium at the level 3. Also, see a visible electrode filament passing through the anterior wall at the level 3 photograph.

between RT and AT (Millar et al., 1985; Haws and Lux, 1990; Coronel et al., 2006). J wave was considered present in the body surface ECGs, if it was manifested in at least two contiguous leads as notching or slurring of terminal R-wave below 50% of its height (Macfarlane et al., 2015).

A major challenge of the present study was that in the setting *in vivo* we could not utilize classical measurements of action potentials in a way performed by Yan and Antzelevitch (1996). We approached this problem as follows. A "repolarization-related" electromotive force responsible for J-wave generation is expected to develop as a difference in plateau potentials between normal and ischemic regions. The cause of this difference is apparently a drastic change in action potential morphology in the ischemic region (often referred to as "triangulation"). We assumed that the difference in the plateau potentials between the normal and ischemic regions could be reasonably estimated as a difference in local repolarization durations between these regions, which can be obtained from intramyocardial unipolar electrograms. Thus, to meet the stated objective, we tested as potential predictors a maximal AT value throughout all intramyocardial leads (AT max) and a difference between the maximal ARI throughout all intramyocardial leads and the average ARI observed in the ischemic region (ΔARI).

Statistical Analysis

Data are expressed as medians and interquartile intervals. Statistical analysis was performed with the SPSS package (IBM SPSS Statistics 23). According to the Kolmogorov-Smirnov normality test, either parametric (two-way ANOVA with Dunnett *post-hoc* test) or nonparametric (Wilcoxon and Fridman tests) were used for repeated measurements. Comparisons between different groups of animals were done with Student's t-test or with the Mann-Whitney test. Uni- and multi-variate logistic regression analyses were used to test for a possible relationship between intramural ATs and ARIs with appearance of J-waves on the surface ECG and VF. The differences were considered significant at $p < 0.05$.

RESULTS

J-Wave and VF Incidence

The body surface ECGs demonstrated no J-wave pattern in any leads at baseline. J-waves developed approximately in three quarters of pigs (11 out of 14 in the LAD group and six out of eight in the RCA group; **Figure 2**). J-waves were observed either steadily (nine and four animals in LAD and RCA group,

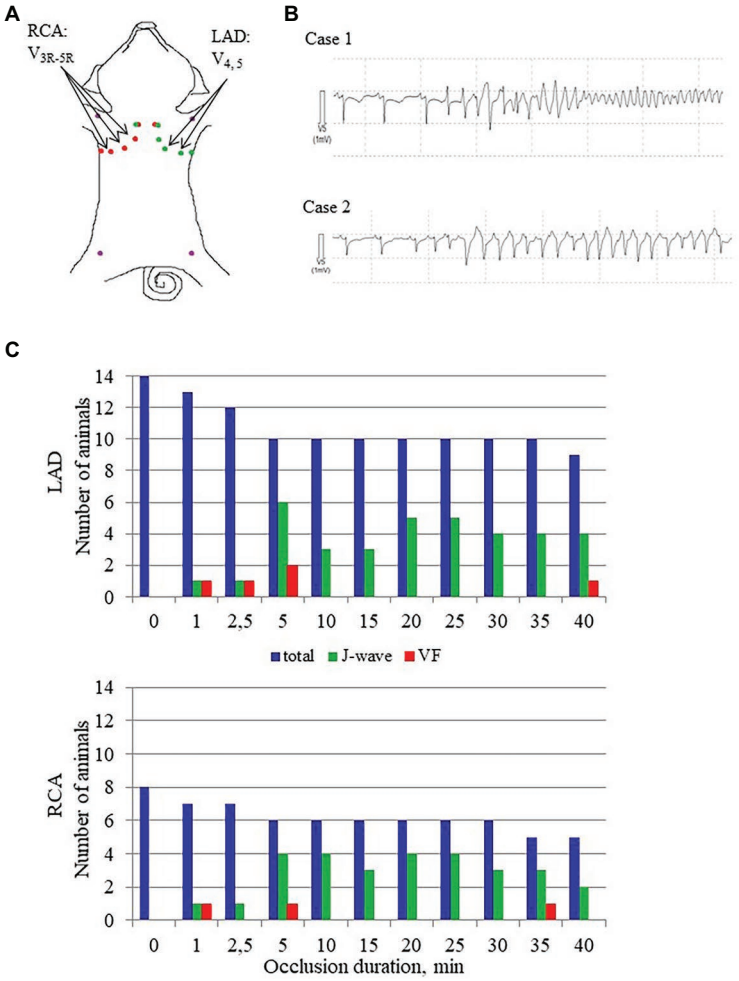

FIGURE 2 | J-wave and VF incidence. Panel **A** shows distribution of body surface leads for ECG recording in conditions of LAD and RCA occlusions. Arrows indicate leads where J-waves were consistently observed in LAD and RCA occlusions. Panel **B** shows typical cases of malignant ventricular tachyarrhythmias development *via* polymorphic tachycardia (case 1), which sometimes started with irregular beats with similar QRS morphology (case 2). Panel **C** shows J-wave and ventricular fibrillation (VF) incidence during LAD (top) and RCA (bottom) occlusions. The height of the bars corresponds to numbers of animals having J-waves in ECG, numbers of animals experiencing VF at a given time-point along with a total number of animals under observation by a given time-point. Note that the total number of animals decrease as the animals were euthanized after development of VF.

respectively) or transiently (two animals in each group) in the period after 2.5–5 min until the end of ischemic exposure. Under LAD occlusion, J-waves were mostly observed in leads V_4–V_5 and aVL. Under RCA occlusion, J-waves could be found in leads V1–V2 among the standard 12 leads, but mostly in additional right-sided and elevated precordial leads. Top tracings in **Figure 4** give examples of J-wave formation at the 5th and 25th min of ischemic exposure. Morphological characteristics of J-waves were not constant during occlusion. There could be slur to notch transformation (**Figure 4**) or dynamical changes of its amplitude and duration (**Figure 5**). Eight pigs (five out of 14 in the LAD group and three out of eight in the RCA group) experienced VF, after which the animals were euthanized. J-wave development preceded six out of eight (75%) VF episodes but was not a significant predictor of VF (OR 1.20 95% CI 0.17–8.66, p = 0.857). The most common type of VF initiation (**Figure 2**, panel **B**) was through polymorphic tachycardia (case 1), which in some animals sometimes started with irregular beats with similar QRS morphology (case 2). VF developed mostly during the first 5 min of coronary occlusion (**Figure 2**, panel **C**).

AT Dynamics

In the baseline state, ATs were relatively uniform throughout ventricular myocardium, and AT max was usually observed in the basal regions. During ischemic exposure, AT max was found in the ischemic or border areas according to location of occlusion (LAD or RCA). The ischemic regions were a middle part of IVS and a base of the lateral RV wall in LAD and RCA groups, respectively. During occlusion of both arteries, AT max similarly increased in a biphasic manner with two maxima at approximately 5 and 20–30 min of ischemic episode.

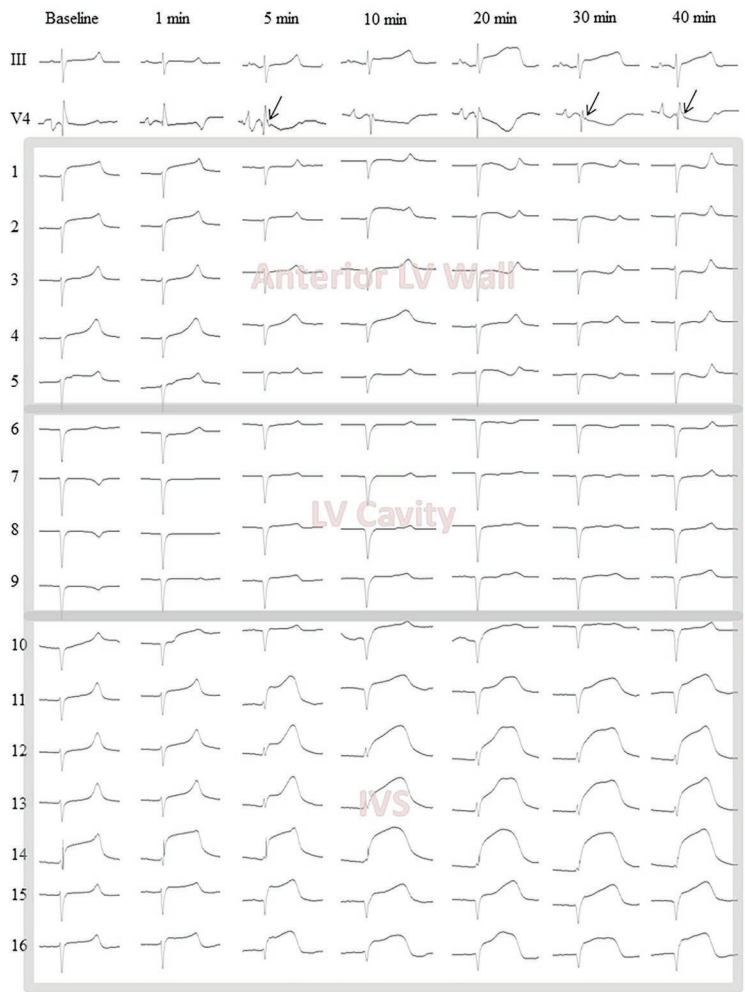

FIGURE 3 | Representative body surface lead III and V4 electrocardiograms along with intramyocardial electrograms (1–16) from the middle level flexible plunge electrode in baseline and during LAD occlusion. Arrows indicate J-waves arising during occlusion in the lead V4. Leads 1–4 are located in the LV anterior wall from epicardium (1) to endocardium (4). See slight ST-segment elevation at baseline confirming a contact of the leads with myocardial tissue. Lead 5 is located at the very endocardial surface of the LV. See unstable signals (ST-segment) at baseline and 1 min likely due to mechanical artifacts caused by moving endocardial structures. Leads 6–9 are located in the LV cavity. See QS waveform of the QRS complexes and absence of dynamics during occlusion. These signals are subject to exclusion at a data processing step. Lead 10 is located at the very left endocardial surface of interventricular septum (IVS). See features similar to those of the lead five. Leads 11–16 are located in the IVS subject to ischemic insult. See dynamical changes of the QRST complex during occlusion. The lead 14 demonstrates significant ST-segment elevation at baseline due to mechanical injury. However, the ischemia-related changes are also visible in the lead 14.

Figure 5 gives an example of the biphasic change of AT in the same lead located in the ischemic zone. It can be seen that the extent of AT prolongation is higher in the earlier phase. Similarly, AT max is longest at 3–5 min (**Figure 6**). In the animals that survived until the end of occlusion (it means that these animals did not experience VF), quite a similar dynamics of AT max was found, though the magnitude of maxima were lower (compare panels **A,B** in **Figure 6**). In LAD occlusion, the AT max tended to be higher than in RCA occlusion, but the differences did not reach statistical significance. Irrespectively of occlusion duration, AT max observed simultaneously with J-wave in the body surface ECG was significantly longer than AT max not associated with J-wave on surface ECG [49 (IQR 39–63) vs. 34 (IQR 31–39) ms, $p = 0.001$, respectively, **Figure 6**, panels **C,D**]. **Figure 5** shows that the body surface J-wave developed when AT in the ischemic zone significantly prolonged and disappeared when AT transiently recovered. In univariate logistic regression analysis, AT max was associated with J-wave development both in LAD (OR = 1.118 95% CI 1.072–1.165; $p < 0.001$) and RCA (OR = 1.051 95% CI 1.008–1.098; $p < 0.020$) occlusions. In a whole group (LAD + RCA occlusion, $n = 22$), AT max was associated with both J-wave (OR = 1.108 95% CI 1.072–1.144; $p < 0.001$) and VF (OR = 1.039 95% CI 1.008–1.072; $p = 0.015$) incidence. In the animals that survived until the end of occlusion (nine in LAD and six in the RCA group of animals without VF), univariate analysis also showed that AT max was associated with J-wave development in LAD (OR = 1.115 95% CI

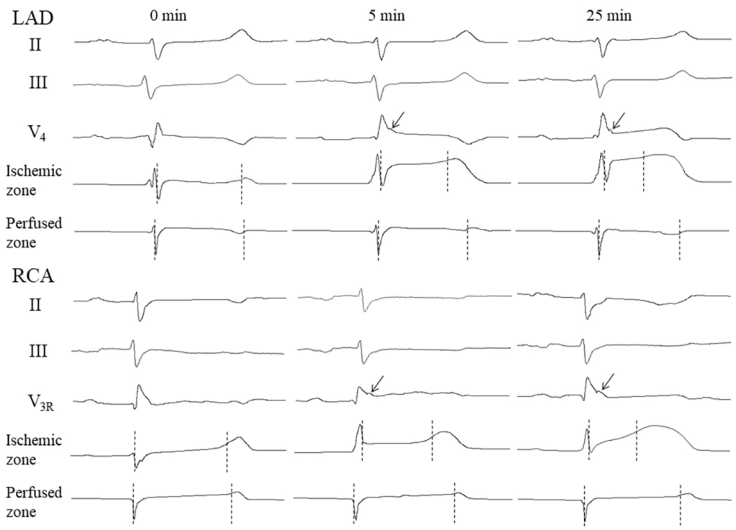

FIGURE 4 | Representative ECGs and intramyocardial electrograms from perfused and ischemic regions at baseline, and at early and late periods of coronary occlusion. Vertical markers show activation time (AT) and repolarization time (RT) instants. Arrows point to J-waves. See activation-repolarization interval (ARI) shortening in the ischemic zone at the 5th and 25th min vs. ARI no changing at the same time-points in the perfused zone.

1.063–1.168; $p < 0.001$; $n = 9$), RCA (OR = 1.089 95% CI 1.014–1.171; $p = 0.020$; $n = 6$) occlusions, and in the whole No-VF group (LAD + RCA, $n = 15$; OR = 1.100 95% CI 1.062–1.139; $p < 0.001$; $n = 15$).

ARI Dynamics

Durations of maximal ARIs (consistently observed in the nonischemic zones) demonstrated no significant changes in comparison with baseline in both LAD and RCA groups (**Figure 7**, panels **A,B**). By the end of ischemic exposure, significant shortening of ARIs was observed in these regions [223 (IQR 222–236) ms at 40th min of LAD occlusion vs. 307 (IQR 302–323) in baseline, $p = 0.003$; and 213 (IQR 157–287) ms at 40th min of RCA occlusion vs. 253 (IQR 186–316) ms in baseline, $p = 0.030$].

ARI distribution in the myocardium in baseline was not uniform. Median ARIs in the RV base were shorter, than those in the LV base [253 (IQR 186–316) ms vs. 302 (259–316) ms, respectively; $p < 0.001$]. At the apical level, ARIs did not differ between RV and LV [261 (IQR 182–357) ms and 283 (212–323) ms, respectively; $p = 0.377$]. Multiple comparisons of ARIs at each time-point during ischemia vs. baseline showed different dynamics in the LAD and RCA groups (**Figure 7**, panels **A,B**). The former demonstrated significant shortening mostly at the beginning of occlusion. In contrast, RCA ligation induced less pronounced changes in the affected region. At the very beginning, there was even moderate ARI increase in several animals. However, ischemia-related shortening progressively increased up to the end of RCA occlusion. As a result, ΔARI developed during the ischemic episodes. As displayed in **Figure 8**, panel **A**, dynamics of ΔARI differed for two occlusion sites. In LAD occlusion, a dramatic increase of ΔARI was observed during first 5 min with subsequent partial restoration till the end of ischemic exposure. In RCA occlusion, ΔARI progressively increased during the whole episode, but the extent of ΔARI increase was less than in LAD occlusion.

Irrespectively of the infarct-related artery, ΔARI was significantly higher in the presence of J-waves in the body surface ECGs [97 (IQR 71–155) vs. 49 (IQR 29–97) ms, $p = 0.001$, respectively, **Figure 8**, panel **C**]. **Figure 5** shows that J-wave development corresponded to the shortest ARIs in the ischemic zone resulting in increased ΔARI. In univariate logistic regression analysis, ΔARI was associated with J-wave development both in LAD (OR = 1.029 95% CI 1.018–1.040; $p < 0.001$, $n = 14$) and RCA (OR = 1.019 95% CI 1.005–1.034; $p = 0.008$, $n = 8$) groups. In the combined group (LAD + RCA), ΔARI was also associated with J-wave occurrence (OR = 1.025 95% CI 1.016–1.033, $p < 0.001$, $n = 22$) but not with VF (OR = 1.007 95% CI 0.994–1.020, $p = 0.313$). The similar dynamics of ΔARI was shown in the animals survived the entire 40 min period of occlusion (**Figure 8**, panels **B,D**). In these animals, ΔARI was also associated with J-wave appearance in LAD (OR = 1.030 95% CI 1.017–1.043; $p < 0.001$, $n = 9$), RCA (OR = 1.018 95% CI 1.004–1.033; $p = 0.013$, $n = 6$), and combined LAD + RCA (OR = 1.024 95% CI 1.015–1.032, $p < 0.001$, $n = 15$) groups.

In multivariate logistic regression analysis, it was shown that both AT max and ΔARI (i.e., the activation delay in the ischemic zone and the difference between the maximal ARI and ARI in the ischemic zone) were independent predictors (OR = 1.078 95% CI 1.040–1.118, $p < 0.001$ and OR = 1.016 95% CI 1.007–1.025, $p = 0.001$, respectively, $n = 15$) of J-wave appearance on ECG during coronary occlusion of both localizations. A scatter plot in **Figure 9** displays a relationship between AT prolongation and ARI shortening in the ischemic zone in respect to baseline (time-point 0)

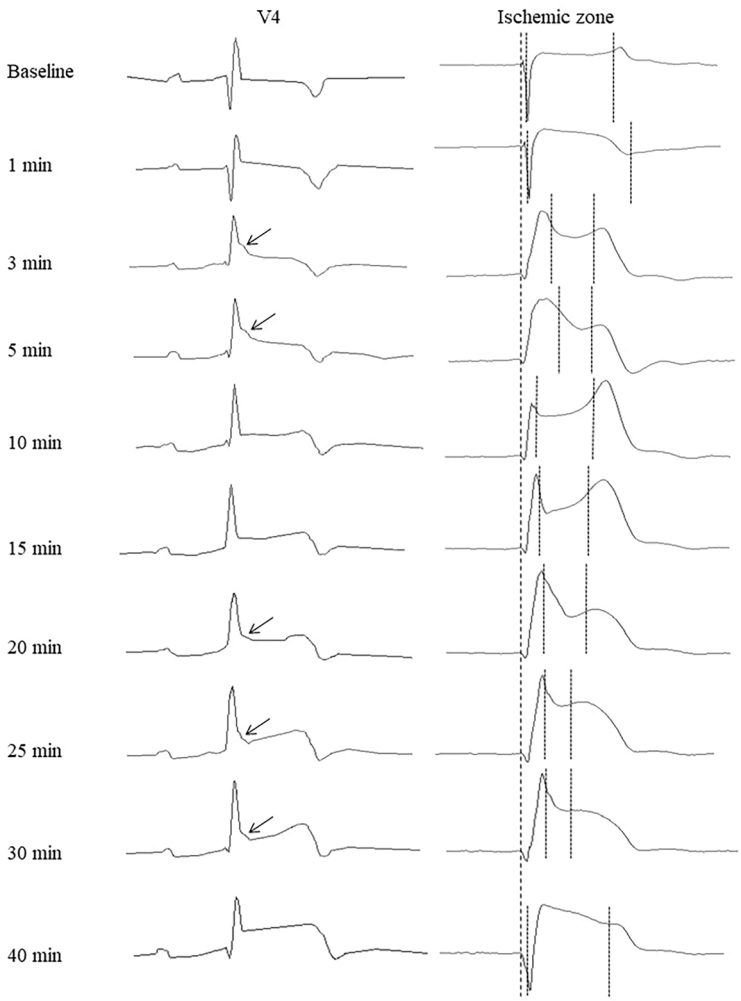

FIGURE 5 | Representative precordial electrocardiograms and unipolar electrograms demonstrating J-wave formation during LAD occlusion. Arrows indicate J-waves in the lead V4 electrocardiograms. Thick dotted lines indicate a QRS onset in cardiac signals serving as a reference time-point for measurements of activation times and end of repolarization times (thin dotted lines). See correlation between J-wave development and marked prolongation of activation time and/or shortening of end of repolarization time.

and demonstrates that J-waves were not observed in cases when ARI prolonged in the affected region (Chi-square 16.7, $p < 0.001$). These cases are indicated by blue circles in a domain of negative ARI shortening (that means ARI prolongation). Collectively, these findings suggest independent contribution to J-wave generation from depolarization and repolarization changes.

DISCUSSION

In the present study, we demonstrated that in experimental ischemia J-wave development was associated with the activation delay and increased difference in repolarization durations between normal and ischemic regions. These relationships were similar in conditions where either left or right ventricular myocardium was predominantly affected, except for the expected differences in the leads where J-waves were observed. The activation delay, but not repolarization abnormalities was associated with VF.

Appearance of J-waves in the body surface ECG is considered as a marker of arrhythmic risk. Despite a high interest, the origin of this phenomenon observed in quite different conditions remains unclear, and both depolarization- and repolarization-related mechanisms are under discussion (Haïssaguerre et al., 2019). Myocardial ischemia provides a setting with increased risk for fatal ventricular tachyarrhythmia caused by severe electrophysiological changes in the myocardium. These changes can be loosely categorized (similarly to the mechanisms of J-wave generation) as related to depolarization and repolarization disorders. The former basically concerns conduction slowing (Kleber et al., 1986) caused by inactivation of sodium channels (Kleber and Rudy, 2004) and gap junctions uncoupling (De Groot and Coronel, 2004), and the latter is largely concerned with action potential duration shortening

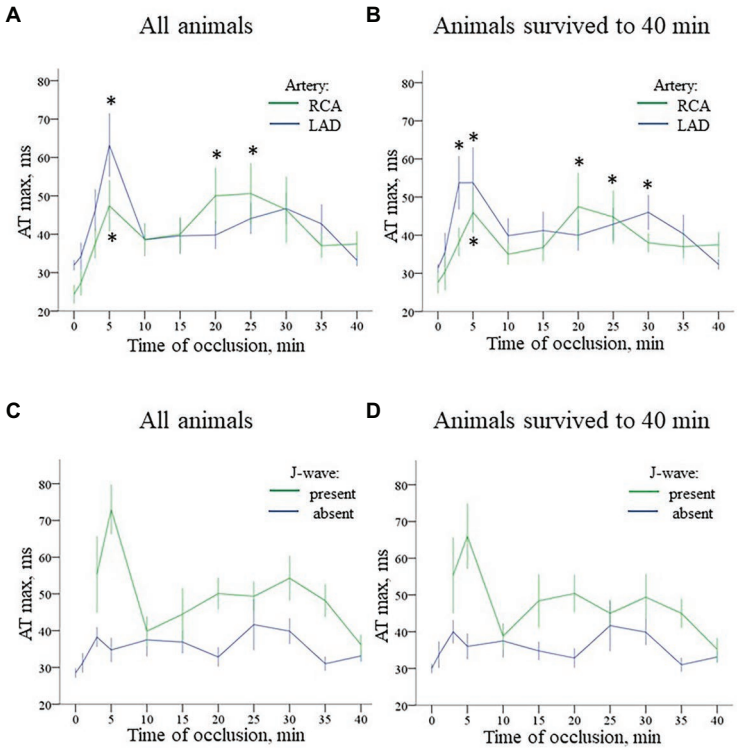

FIGURE 6 | Time-course of evolution AT max (Mean ± SEM) during coronary occlusion in all animals (panels **A,C**) and in the animals that survived until the 40th min of occlusion and experiencing no ventricular fibrillation (VF; panels **B,D**). Panel **A** shows AT max changes during LAD (n = 14) and RCA (n = 8) occlusion. See quite similar dynamics with early and delayed peaks of AT prolongation in both groups. Panel **B** shows analogous AT max changes in animals that survived until the 40th min of ischemia (i.e., experiencing no VF) during LAD (n = 9) and RCA (n = 6) occlusion. See that though AT max prolongation is lower in the no-VF group, the overall dynamics of AT max changes is similar to that in all animals displayed in panel **A**. Panel **C** presents comparison of AT max for the cases with and without J-waves in the body surface ECG in the combined group (LAD and RCA occlusion together, n = 22). Panel **D** shows analogous data for the animals that survived until the 40th min of occlusion (n = 15). $^{*}p < 0.05$ vs. baseline (ANOVA, *post-hoc* Dunnet test).

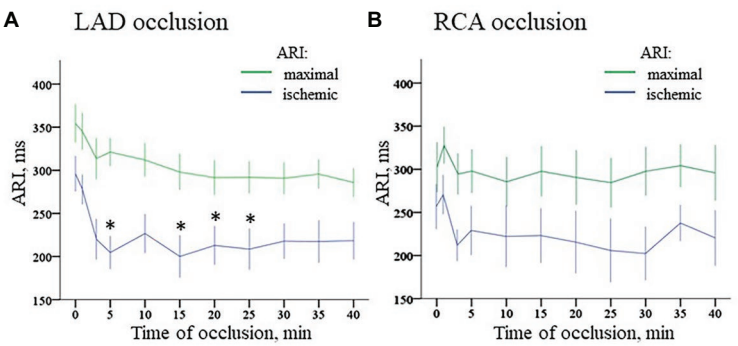

FIGURE 7 | Dynamics of ischemic and maximal ARI changes during coronary occlusion. Panel **A** displays changes in ARIs in the ischemic zone (middle part of IVS) and maximal ARIs observed in the normal myocardium during LAD occlusion. Similarly, panel **B** displays changes of ARIs in the ischemic zone [base of lateral right ventricular (RV) wall] and maximal ARIs observed in the normal myocardium during RCA occlusion. $^{*}p < 0.05$ vs. baseline (ANOVA, *post-hoc* Dunnet test).

induced largely by activation of $I_{K(ATP)}$ current among other causes (Shaw and Rudy, 1997; Carmeliet, 1999).

Theoretically, generation of J-wave should be based on a potential difference arising between ventricular regions shortly after the QRS-complex with the region proximal to the lead to be positively charged (i.e., less depolarized). This condition is met under ischemia when the activation wave is slowly spreading toward a positive lead terminal across the ischemic area. Similarly, J-wave appeared under inhibition of sodium current (Meijborg et al., 2016). In the previous study (Azarov et al., 2019),

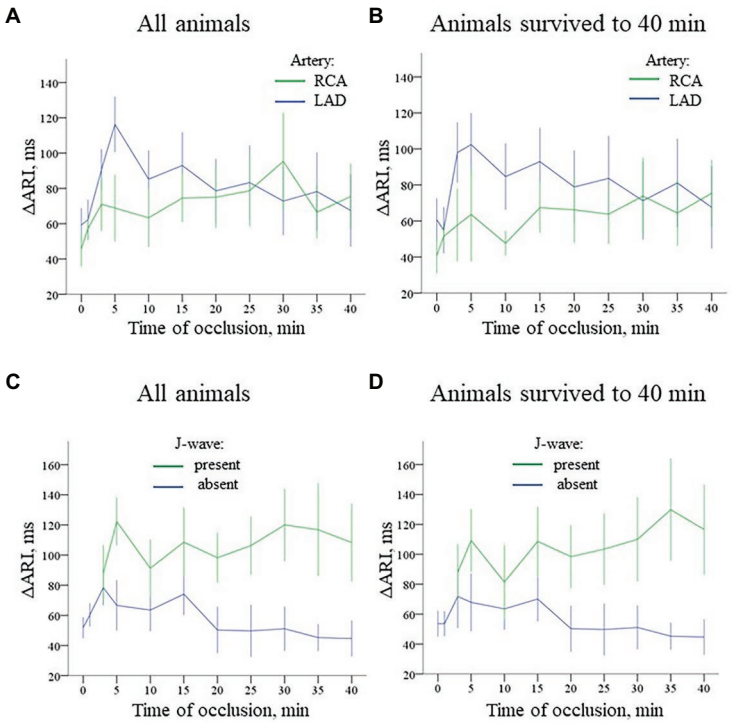

FIGURE 8 | Time-course of evolution of ΔARI (Mean ± SEM) during coronary occlusion in all animals (panels **A,C**) and in the animals that survived until the 40th min of occlusion and experiencing no VF (panels **B,D**). Data are presented similarly to **Figure 6**. Panel **A** ΔARI changes during LAD (n = 14) and RCA (n = 8) occlusion. See different ΔARI dynamics in two groups caused by different patterns of ARI changes in the ischemic regions depicted in **Figure 7**. Panel **B** ΔARI changes in the animals that survived until the 40th min of ischemia (i.e., experiencing no VF) during LAD (n = 9) and RCA (n = 6) occlusion. Panel **C** Comparison of ΔARI for the cases with and without J-waves in the body surface ECG in the combined group (LAD and RCA occlusion together, n = 22). Panel **D** shows analogous data for the animals that survived until the 40th min of occlusion (n = 15).

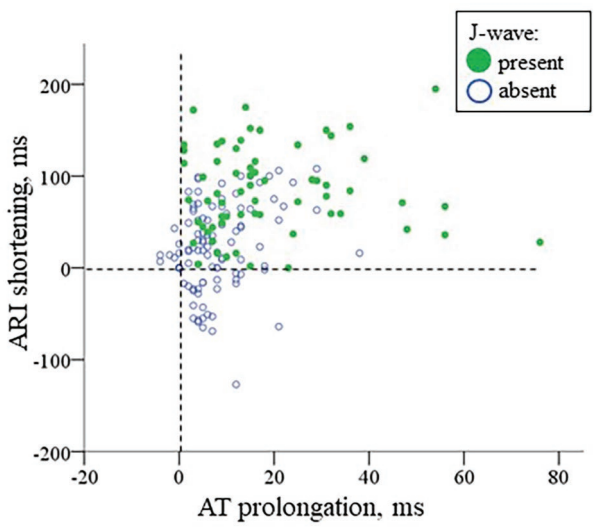

FIGURE 9 | A scatter plot for AT prolongation vs. ARI shortening in the ischemic region in respect to baseline values for cases with and without J-waves in the body surface ECG in the combined group (LAD and RCA occlusion together, n = 22). The negative values indicate AT shortening or ARI prolongation, respectively.

we directly showed an association between activation delay in the ischemic myocardium and J-wave development in the precordial leads. Clinical data (Nakayama et al., 2013, 2019) also suggest that conduction delay facilitates formation of J-waves in patients with myocardial ischemia.

Similarly to the condition of delayed depolarization, less depolarized myocardium can be found in conditions of accelerated phase 1 repolarization. Such mechanism of J-wave generation was demonstrated in ventricular wedge preparations when intrinsic transmural difference in spike-and-dome morphology of action potentials is increased due to variation in I_{to} current density (Yan and Antzelevitch, 1996; Koncz et al., 2014). In the ischemic cardiac tissue, action potential repolarization shortens and loses a plateau phase (Shaw and Rudy, 1997; Carmeliet, 1999). Apparent manifestation of these changes resembles the phase 1 acceleration and together with the delayed activation can produce overlapping electric fields resulting in J-waves (Bacharova et al., 2013; Bacharova and Halkias, 2016). However, our present study is, to our knowledge, the first to report a direct association between ischemia-induced shortening of repolarization and J-wave formation in the body surface ECG.

The repolarization-related predictor of J-wave development used in our present study was the difference between the "ischemic" (i.e., shortest) ARI and ARI in the normal myocardium.

Using this parameter, we assumed that the greater was this duration difference, the greater was the potential difference between these regions, and therefore the greater was the electric field responsible for J-wave development. Interestingly, we observed much less ΔARI in RCA occlusion, whereas dynamics of ATs were quite similar in the RV and LV ischemic areas under RCA and LAD occlusion, respectively. Though the different repolarization responses to ischemia cannot be explained directly by the data obtained, this observation is consistent with the findings of Pandit et al. (2011) demonstrating a larger $I_{K(ATP)}$ current in the LV as compared to the RV. Moreover, ARIs in the RV base were shorter in baseline and probably had less repolarization reserve. Anyway, the ΔARI parameter was an independent predictor of J-wave appearance both in uni- and multi-variate (together with activation delay) analysis, both in LAD- and RCA-occlusion groups separately as well as in combination.

The interest to J-waves as a distinct ECG phenomenon is well-understood taking into account its potential use as a predictor of fatal ventricular arrhythmias. However, it was pointed out that not every ever observed J-wave necessarily predicts ventricular fibrillation or sudden cardiac death (Bourier et al., 2018; Demidova et al., 2019). Our previous (Azarov et al., 2019) and present studies demonstrated that both repolarization- and depolarization-related mechanisms are involved in J-wave generation in the ischemic conditions. However, only activation delay is associated with VF incidence. Furthermore, a threshold for activation delay needed for VF development is higher than for J-wave generation. These data imply that only deeply affected individuals demonstrating J-waves would suffer from VF.

Thus, in the open chest model of myocardial infarction, repolarization abnormalities expressed as a difference in ARIs between the normal and ischemic myocardium contributed to J-waves formation together with activation delay, but did not predict VF occurrence, which was associated only with activation slowing.

Limitations

Estimation of action potential duration as ARI obtained from the *in vivo* recorded myocardial electrograms can be considered as reliably validated (Millar et al., 1985; Haws and Lux, 1990; Coronel et al., 2006). However, the action potential phase 1 repolarization supposedly related to generation of J-wave occurs "within an ARI" and could not be recorded directly. To evaluate repolarization abnormalities in this period, we assumed that the well-known triangularization of the action potential in the ischemic myocardium is expressed in changes of ARIs. This approach presents a main limitation for this work and warrants cautious interpretation of the results. However, the data obtained in the ischemic porcine myocardium (Coronel et al., 1992) suggest a correlation between changes in action potential shape and duration, whereas the latter could be estimated from the unipolar intramyocardial electrograms.

Ischemic conditions impose additional limitations on interpretation of measured ARIs since morphology of action potentials is significantly altered under ischemia. However, ARI measurements and analysis are still feasible in such settings (Ejima et al., 1998). Moreover, we did not attempt to determine exact action potential durations which might have been underestimated in assessments with the aid of ARI in hypoxic myocardium. Our goal was only to attain an indirect evaluation of changes of action potential morphology supposedly responsible for J-wave generation, and such evaluation, if done cautiously, can be considered reasonable.

DATA AVAILABILITY STATEMENT

The raw data supporting the conclusions of this article will be made available by the authors, without undue reservation.

ETHICS STATEMENT

The animal study was reviewed and approved by the Ethical Committee of the Institute of Physiology of the Komi Science Centre, Ural Branch of Russian Academy of Sciences.

AUTHOR CONTRIBUTIONS

AT, JA, OB, AO, MD, and PP contributed to the design. AT, JA, OB, AO, MV, and MD contributed to the experiments. AT, JA, AO, and MV contributed to the data analysis. AT and JA drafted the article. All authors contributed to the article and approved the submitted version.

FUNDING

The study was supported by Russian Science Foundation (RSF 18-15-00309 to JA, AT, and OB), The Swedish Heart Lung Foundation (#20180222 to MD and #20180444 to PP), donation funds at Skåne University Hospital, and governmental funding of clinical research within Swedish healthcare system (ALF #46702).

REFERENCES

Antzelevitch, C., and Yan, G. X. (2010). J wave syndromes. *Heart Rhythm* 7, 549–558. doi: 10.1016/j.hrthm.2009.12.006

Azarov, J. E., Ovechkin, A. O., Vaykshnorayte, M. A., Demidova, M. M., and Platonov, P. G. (2019). Prolongation of the activation time in ischemic myocardium is associated with J-wave generation in ECG and ventricular fibrillation. *Sci. Rep.* 9:12202. doi: 10.1038/s41598-019-48710-3

Bacharova, L., and Halkias, I. (2016). The identification of the QRS complex offset in the presence of ST segment deviation. *J. Electrocardiol.* 49, 977–979. doi: 10.1016/j.jelectrocard.2016.07.028

Bacharova, L., Szathmary, V., and Mateasik, A. (2013). QRS complex and ST segment manifestations of ventricular ischemia: the effect of regional slowing of ventricular activation. *J. Electrocardiol.* 46, 497–504. doi: 10.1016/j.jelectrocard.2013.08.016

Bourier, F., Denis, A., Cheniti, G., Lam, A., Vlachos, K., Takigawa, M., et al. (2018). Early repolarization syndrome: diagnostic and therapeutic approach. *Front Cardiovasc. Med.* 5:169. doi: 10.3389/fcvm.2018.00169

Caliskan, K., Ujvari, B., Bauernfeind, T., Theuns, D. A., Van Domburg, R. T., Akca, F., et al. (2012). The prevalence of early repolarization in patients with noncompaction cardiomyopathy presenting with malignant ventricular arrhythmias. *J. Cardiovasc. Electrophysiol.* 23, 938–944. doi: 10.1111/j.1540-8167.2012.02325.x

Carmeliet, E. (1999). Cardiac ionic currents and acute ischemia: from channels to arrhythmias. *Physiol. Rev.* 79, 917–1017.

Coronel, R., de Bakker, J. M. T., Wilms-Schopman, F. J. G., Opthof, T., Linnenbank, A. C., Belterman, C. N., et al. (2006). Monophasic action potentials and activation recovery intervals as measures of ventricular action potential duration: experimental evidence to resolve some controversies. *Heart Rhythm* 3, 1043–1050. doi: 10.1016/j.hrthm.2006.05.027

Coronel, R., Wilms-Schopman, F. J., Opthof, T., Cinca, J., Fiolet, J. W., and Janse, M. J. (1992). Reperfusion arrhythmias in isolated perfused pig hearts. Inhomogeneities in extracellular potassium, ST and TQ potentials, and transmembrane action potentials. *Circ. Res.* 71, 1131–1142.

De Groot, J., and Coronel, R. (2004). Acute ischemia-induced gap junctional uncoupling and arrhythmogenesis. *Cardiovasc. Res.* 62, 323–334. doi: 10.1016/j.cardiores.2004.01.033

Demidova, M. M., Carlson, J., Erlinge, D., and Platonov, P. (2019). Early repolarization pattern on ECG recorded prior to the acute coronary event does not predict ventricular fibrillation during ST-elevation myocardial infarction. *Heart Rhythm* 17, 629–636. doi: 10.1016/j.hrthm.2019.11.011

Demidova, M. M., Martin-Yebra, A., van der Pals, J., Koul, S., Erlinge, D., Laguna, P., et al. (2014). Transient and rapid QRS-widening associated with a J-wave pattern predicts impending ventricular fibrillation in experimental myocardial infarction. *Heart Rhythm* 11, 1195–1201. doi: 10.1016/j.hrthm.2014.03.048

Ejima, J., Martin, D., Engle, C., Sherman, Z., Kunimoto, S., and Gettes, L. S. (1998). Ability of activation recovery intervals to assess action potential duration during acute no-flow ischemia in the in situ porcine heart. *J. Cardiovasc. Electrophysiol.* 9, 832–844.

Haissaguerre, M., Derval, N., Sacher, F., Jesel, L., Deisenhofer, I., de Roy, L., et al. (2008). Sudden cardiac arrest associated with early repolarization. *N. Engl. J. Med.* 358, 2016–2023. doi: 10.1056/NEJMoa071968

Haïssaguerre, M., Nademanee, K., Hocini, M., Cheniti, G., Duchateau, J., Frontera, A., et al. (2019). Depolarization versus repolarization abnormality underlying inferolateral J-wave syndromes: new concepts in sudden cardiac death with apparently normal hearts. *Heart Rhythm* 16, 781–790. doi: 10.1016/j.hrthm.2018.10.040

Haws, C. W., and Lux, R. L. (1990). Correlation between in vivo transmembrane action potential durations and activation-recovery intervals from electrograms. Effects of interventions that alter repolarization time. *Circulation* 81, 281–288.

Jastrzebski, M., and Kukla, P. (2009). Ischemic J wave: novel risk marker for ventricular fibrillation? *Heart Rhythm* 6, 829–835. doi: 10.1016/j.hrthm.2009.02.036

Kleber, A. G., Janse, M. J., Wilms-Schopmann, F. J., Wilde, A. A., and Coronel, R. (1986). Changes in conduction velocity during acute ischemia in ventricular myocardium of the isolated porcine heart. *Circulation* 73, 189–198. doi: 10.1161/01.cir.73.1.189

Kleber, A. G., and Rudy, Y. (2004). Basic mechanisms of cardiac impulse propagation and associated arrhythmias. *Physiol. Rev.* 84, 431–488. doi: 10.1152/physrev.00025.2003

Koncz, I., Gurabi, Z., Patocskai, B., Panama, B. K., Szel, T., Hu, D., et al. (2014). Mechanisms underlying the development of the electrocardiographic and arrhythmic manifestations of early repolarization syndrome. *J. Mol. Cell. Cardiol.* 68, 20–28. doi: 10.1016/j.yjmcc.2013.12.012

Macfarlane, P. W., Antzelevitch, C., Haissaguerre, M., Huikuri, H. V., Potse, M., Rosso, R., et al. (2015). The early repolarization pattern: a consensus paper. *J. Am. Coll. Cardiol.* 66, 470–477. doi: 10.1016/j.jacc.2015.05.033

Mehta, M., Jain, A. C., and Mehta, A. (1999). Early repolarization. *Clin. Cardiol.* 22, 59–65.

Meijborg, V. M. F., Potse, M., Conrath, C. E., Belterman, C. N. W., De Bakker, J. M. T., and Coronel, R. (2016). Reduced sodium current in the lateral ventricular wall induces inferolateral J-waves. *Front. Physiol.* 7:365. doi: 10.3389/fphys.2016.00365

Millar, C. K., Kralios, F. A., and Lux, R. L. (1985). Correlation between refractory periods and activation-recovery intervals from electrograms: effects of rate and adrenergic interventions. *Circulation* 72, 1372–1379.

Nakayama, M., Sato, M., Kitazawa, H., Saito, A., Ikeda, Y., Fujita, S., et al. (2013). J-waves in patients with an acute ST-elevation myocardial infarction who underwent successful percutaneous coronary intervention: prevalence, pathogenesis, and clinical implication. *Europace* 15, 109–115. doi: 10.1093/europace/eus259

Nakayama, M., Satomi, K., Yuhara, M., Uchiyama, T., Aizawa, Y., and Aizawa, Y. (2019). Conduction delay-induced J-wave augmentation in patients with coronary heart disease. *Am. J. Cardiol.* 123, 1262–1266. doi: 10.1016/j.amjcard.2019.01.015

Naruse, Y., Tada, H., Harimura, Y., Hayashi, M., Noguchi, Y., Sato, A., et al. (2012). Early repolarization is an independent predictor of occurrences of ventricular fibrillation in the very early phase of acute myocardial infarction. *Circ. Arrhythm. Electrophysiol.* 5, 506–513. doi: 10.1161/CIRCEP.111.966952

Pandit, S. V., Kaur, K., Zlochiver, S., Noujaim, S. F., Furspan, P., Mironov, S., et al. (2011). Left-to-right ventricular differences in IKATP underlie epicardial repolarization gradient during global ischemia. *Heart Rhythm* 8, 1732–1739. doi: 10.1016/j.hrthm.2011.06.028

Peters, S., and Selbig, D. (2008). Early repolarization phenomenon in arrhythmogenic right ventricular dysplasia-cardiomyopathy and sudden cardiac arrest due to ventricular fibrillation. *Europace* 10, 1447–1449. doi: 10.1093/europace/eun279

Sato, A., Tanabe, Y., Chinushi, M., Hayashi, Y., Yoshida, T., Ito, E., et al. (2012). Analysis of J waves during myocardial ischaemia. *Europace* 14, 715–723. doi: 10.1093/europace/eur323

Shaw, R., and Rudy, Y. (1997). Electrophysiologic effects of acute myocardial ischemia: a theoretical study of altered cell excitability and action potential duration. *Cardiovasc. Res.* 35, 256–272.

Yan, G. X., and Antzelevitch, C. (1996). Cellular basis for the electrocardiographic J wave. *Circulation* 93, 372–379.

Conflict of Interest: The authors declare that the research was conducted in the absence of any commercial or financial relationships that could be construed as a potential conflict of interest.

frontiers in Physiology

ORIGINAL RESEARCH
published: 09 November 2020
doi: 10.3389/fphys.2020.578173

Augmented Oscillations in QT Interval Duration Predict Mortality Post Myocardial Infarction Independent of Heart Rate

Fatima J. El-Hamad[1], Safa Y. Bonabi[2], Alexander Müller[3], Alexander Steger[3], Georg Schmidt[3] and Mathias Baumert[1]**

[1] School of Electrical and Electronic Engineering, The University of Adelaide, Adelaide, SA, Australia, [2] School of Electronic and Telecommunications Engineering, RMIT University, Melbourne, VIC, Australia, [3] Internal Medicine I Department, Technical University of Munich, Munich, Germany

Objective: This study seeks to decompose QT variability (QTV) into physiological sources and assess their role for risk stratification in patients post myocardial infarction (MI). We hypothesize that the magnitude of QTV that cannot be explained by heart rate or respiration carries important prognostic information.

Background: Elevated beat-to-beat QTV is predictive of cardiac mortality, but the underlying mechanisms, and hence its interpretation, remain opaque.

Methods: We decomposed the QTV of 895 patients post MI into contributions by heart rate, respiration, and unexplained sources.

Results: Cox proportional hazard analysis demonstrates that augmented oscillations in QTV and their level of dissociation from heart rate are associated with a higher 5-year mortality rate (18.4% vs. 4.7%, $p < 0.0001$). In patients with left ventricular ejection fraction (LVEF) > 35%, a higher QTV risk score was associated with a significantly higher 5-year mortality rate (16% vs. 4%, $p < 0.0001$). In patients with a GRACE score $\geq$ 120, a higher QTV risk score was associated with a significantly higher 5-year mortality (25% vs. 11%, $p < 0.001$).

Conclusion: Augmented oscillations in QTV and discordance from heart rate, possibly indicative of excessive sympathetic outflow to the ventricular myocardium, predict high risk in patients post MI independent from established risk markers.

Clinical Trial Registration: www.ClinicalTrials.gov, identifier NCT00196274.

Keywords: repolarization variability, risk stratification, sudden death, myocardial infarction, autoregressive model, cardiovascular disease

OPEN ACCESS

Edited by:
Ruben Coronel, University of Amsterdam, Netherlands

Reviewed by:
Peter Taggart, University College London, United Kingdom
Celestino Sardu, Second University of Naples, Italy

****Correspondence:***
Mathias Baumert
mathias.baumert@adelaide.edu.au
Fatima J. El-Hamad
fatima.el-hamad@adelaide.edu.au

Specialty section:
This article was submitted to Cardiac Electrophysiology, a section of the journal Frontiers in Physiology

Received: *30 June 2020*
Accepted: *16 October 2020*
Published: *09 November 2020*

Citation:
El-Hamad FJ, Bonabi SY, Müller A, Steger A, Schmidt G and Baumert M (2020) Augmented Oscillations in QT Interval Duration Predict Mortality Post Myocardial Infarction Independent of Heart Rate. Front. Physiol. 11:578173. doi: 10.3389/fphys.2020.578173

INTRODUCTION

Myocardial infarction (MI) is the most common cause of sudden cardiac death (SCD); over 80% of fatal arrhythmias are caused by structural coronary arterial abnormalities and their consequences (Huikuri et al., 2001). Prediction of SCD currently poses a clinical challenge and identification of high-risk patients needs to be considerably improved (Myerburg, 2001).

Autonomic dysfunction and electrical instability are key factors predisposing MI patients to ventricular tachycardia and ventricular fibrillation and consequent SCD (Schwartz et al., 1992; Liew, 2010; Wellens et al., 2014). Indices of ventricular repolarization lability, such as QT variability (QTV), have attracted considerable interest in the area of risk stratification as they allow for a non-invasive investigation of the autonomic nervous system influence on the ventricular myocardium and the lability of the ventricular repolarization process (Myerburg, 2001; Wellens et al., 2014). Measures of QTV (QTVI, SDQT) are increased post MI and their prognostic value has been demonstrated in several studies (Wellens et al., 2014; Baumert et al., 2016a). QTV was increased in six out of the 12-lead ECG recording of patients with recent MI even after covarying for low T wave amplitude (Hasan et al., 2013) and in post MI patients with reduced LVEF compared to those with preserved LVEF and those with uncomplicated coronary heart disease (Sosnowski et al., 2002). QTV was also increased in coronary disease patients with old MI when compared to those without MI (Yao et al., 2019). QTVI has been shown to be predictive of SCD and all-cause mortality in patients with LVEF between 35% and 40% (Piccirillo et al., 2007). In 24-h Holter recordings of patients with acute MI, QT/RR variability ratio was found to be predictive of all-cause mortality independent of other established risk markers (Jensen et al., 2005).

Beat-to-beat fluctuations in the QT interval (representing the variability of the repolarization process) are the result of a complex process that involves multiple physiological mechanisms. The rate adaptation of the QT interval constitutes a large fraction of QTV in the normal heart (El-Hamad et al., 2015; Baumert et al., 2016b). Respiration also influences QTV indirectly through respiratory sinus arrhythmia (Sutherland et al., 1983; Baumert et al., 2016b). Furthermore, ventricular repolarization is directly influenced by the autonomic nervous system (Merri et al., 1993) via the dense innervation of sympathetic nerves into the ventricular myocardium, contributing to rate-independent QTV (Hall, 2011). Hence, in the compromised heart, excessive sympathetic outflow might initiate lethal ventricular arrhythmias (Ng, 2016).

In the context of MI, few studies report on the rate-independent component of repolarization variability. Zhu et al. (2008) found that repolarization variability independent of heart rate was increased in MI patients compared to age-matched healthy subjects, while the rate-dependent component was not different between the two groups. Others found no difference in the percentage of RR-dependent RT interval variability between MI patients and age-matched healthy subjects (Lombardi et al., 1998). Comparing MI patients with reduced LVEF to those with preserved LVEF and to another group with coronary artery disease but no MI, Sosnowski et al. (2002) reported an increase in overall RT variability and specifically an increase in its HF power, suggesting an important role for respiration. They also observed an uncorrelation between RR and RT interval variability in MI patients with depressed LVEF compared to the other two groups.

There are only few reports on QTV's individual components in patients post MI, and none on their individual role in risk stratification post MI. In this study, we hypothesize that the component of QTV that cannot be explained by heart rate or respiration, possibly reflecting sympathetic influences on the ventricles, carries important prognostic information. To test this hypothesis, we decomposed QTV into three components (hart rate dependent, respiratory dependent, and independent component) and assessed their individual roles in risk stratification in patients post MI.

MATERIALS AND METHODS

Study Cohort

We analyzed high-resolution ECG recorded previously for cardiac risk stratification post MI (Barthel et al., 2013). A total of 941 MI survivors were enrolled between March 2000 and May 2005. Acute MI was diagnosed based on at least two of the following findings: typical chest pain lasting $\geq$ 20 min, creatine kinase above twice the upper normal limit of the respective laboratory, and admission ST-segment elevation $\geq$ 0.1 mV in at least two contiguous limb leads or $\geq$ 0.2 mV in at least two contiguous precordial leads (Bernard et al., 1979). Eligible patients had survived acute MI less than four weeks before recruitment, they were aged 80 years or less, had sinus rhythm, and did not meet the criteria for secondary prophylactic implantation of implantable cardioverter defibrillator before hospital discharge. A total of 32 patients did not pass the initial screening due to atrial fibrillation (Sinnecker et al., 2015).

The main outcome measure was total mortality during a follow-up period of 5 years (once every 6 months), where the last follow-up was performed in May 2010. The study was conducted at the hospital of the Technische Universität München, the German Heart Centre, and the Klinikum Rechts der Isar, both in Munich, Germany. The study protocol was approved by the local ethics committee, and written consent from patients was obtained.

Measurements

ECG (Porti System, TMS, Netherlands) and thoracic respiratory signals (piezoelectric thoracic sensor; Pro-Tech, United States) were recorded at 1.6 kHz for 30 min in each patient within 2 weeks of index MI. Patients were studied in the morning in the supine position without interruption of their normal medication regimen. The GRACE score, including the age of the patient, a history of past heart failure, a history of past MI, serum creatinine at admission, the cardiac biomarker status at admission, systolic blood pressure at admission, the pulse at admission, ST-deviation at admission, and in-hospital percutaneous coronary intervention, was selected for predicting the long-term prognosis (Eagle et al., 2004). Details of other recorded signals can be found elsewhere (Barthel et al., 2013).

Data Pre-processing

All ECG signals were visually inspected for signal quality; recordings with poorly defined T wave were excluded from the analysis based on subjective assessment. Beat-to-beat heart period (RR) and beat-to-beat Q peak to T end interval (QT) were obtained from all ECGs. We used an automated template-based

algorithm that tracks QT changes beat by beat with high accuracy and robust to noise (Schmidt et al., 2014). The QT interval was automatically determined on the template beat using a slope method and manually adjusted if necessary.

The thoracic respiratory signal was sampled at the occurrence of the R-peak in the ECG signal to obtain beat-to-beat values of respiration. All beat-to-beat series (RR, QT, respiration) were visually inspected to select stationary segments of around 350 consecutive beats. All selected RR segments were then visually validated against the ECG to identify QRS detection errors and irregular heart rhythms. Recordings with RR segments consisting of more than 10% ventricular or supraventricular ectopic beats (EBs) were excluded from the analysis, while ectopic beats were mathematically interpolated in recordings with less than 10% EBs using the spline interpolation method. QT, RR and respiration time series were detrended using the smoothness priors method (Tarvainen et al., 2002) comprising a time-varying finite-impulse response high-pass filter with a corner frequency of 0.04Hz. The detrended data segments were normalized to zero mean and unit variance for power spectral analysis.

Model-Based QTV Analysis

Power contribution analysis was performed to decompose QTV into heart period dependent, respiratory dependent and unexplained contributions.

We employed a linear autoregressive model with two external inputs (ARXX) to decompose QT variability (Baselli et al., 1997). We chose an open-loop structure, where the rhythm sources generating the three signals are assumed uncorrelated, which allows the decomposition of QTV power into contributions by the different inputs. Thus, the autoregressive model was defined as:

$$A_1(z)\ QT(i) = B_1(z)\ RR(i) + B_2(z)\ Resp(i) + e_{QT}(i) \quad (1)$$

Equation (1) describes QTV as a function of its own past, past and present values of heart period (RR) and respiration (Resp) and a noise source that represents actual noise and rhythms originating from sources not accounted for in the model. Heart period was modeled as autoregressive model with respiration as an external input, while respiration was modeled as a separate autoregressive process. Details of the mathematical models and their parameters are described elsewhere (Baselli et al., 1997; El-Hamad et al., 2015).

The Akaike information criterion (Akaike, 1974) was used to select the model order of the multivariate autoregressive process from the range 6 to 12. Model parameters were estimated using the least squares method. Resulting models were validated by assessing the correlation between model residuals and whiteness of model noise sources (Porta et al., 1998; El-Hamad et al., 2015).

The following variables were computed:

- QT_{mean}–average QT interval (in ms).
- QT_c–rate-corrected average QT interval, using Bazett's formula (in ms).
- QTV_{total}–variance of beat-to-beat QT intervals (in ms^2).
- $QTV_{respiration}$–variance of beat-to-beat QT intervals related to respiration (in %).
- QTV_{RR}–variance of beat-to-beat QT intervals related to heart period (in %).
- $QTV_{unexplained}$–variance of beat-to-beat QT intervals independent from heart period and respiration (in %).

Statistics

Univariate Cox regression analysis was performed on each demographic variable to assess its predictive value for mortality; expressed as hazard ratios (HR) with 95% confidence intervals (CI). To test whether the characteristics of patients who were excluded from analysis were significantly different from those in the final study cohort, we compared both groups using the two-sample Wilcoxon test and the chi-squared test for continuous and categorical variables, respectively.

The predictive value of the different QT variability measures was assessed using univariate Cox regression analysis. The significant predictors resulting from the univariate analysis were then included in a multivariable Cox regression analysis with the stepAIC method (Hothorn and Lausen, 2003). The linear predictor model resulting from the multivariate cox regression analysis is termed 'QTV risk score' which includes QTV measures which were found to contribute independently to risk prediction. The optimal cut-off for the QTV risk score was calculated by the Maximally Selected Rank Statistics (Hothorn and Lausen, 2003; Lausen et al., 2004). We chose the maximum of the log-rank statistics with at least 90% of the observations in group 1 and no more than 90% of the observations in group 1 as constraints. To assess the additive predictive value of the QTV risk score beyond established clinical risk markers, we performed multivariable Cox regression analysis using the QTV risk score as well as a model consisting of the following clinical predictor variables: GRACE score, LVEF, presence of diabetes, chronic obstructive pulmonary disease and expiration-triggered respiratory sinus arrhythmia. Kaplan–Meier survival curves were computed for the QTV risk score and for subgroup analysis based on LVEF $\leq$ 35% and GRACE $\geq$ 120 points. A p-value < 0.05 was considered significant. All statistics were performed with R (R Core Team, 2014).

RESULTS

Data Pre-processing Results

Out of 941 recordings, we excluded 20 from the analysis due to poor signal quality. After manually selecting stationary segments of QT, RR and respiration, another 26 recordings were excluded due to the high percentage of irregular heartbeats (more than 10% ventricular or supraventricular ectopic beats; or bigeminus rhythm). Of the 895 patients included in the analysis, 62 died during the follow-up period. **Table 1** shows the clinical characteristics and demographics for subjects included in the final analysis compared to those excluded from the analysis. Mortality was higher in the group of excluded patients (10 deaths). On average, those patients were significantly older, had a higher GRACE score and had a lower estimated glomerular filtration rate (**Table 1**).

TABLE 1 | Patient demographics and hazard ratios of the entire study population as well as the comparison of characteristics of included versus excluded patients.

Variables	Study population (*n* = 941)	Hazard Ratio* (99% CI)	*p*-value	Included patients (*n* = 895)	Excluded patients (*n* = 46)	Included versus excluded (*p*-value)
Age (years), median (IQR)	60.9 (51.6–68.8)	1.09 (1.06–1.12)	<0.001	60.7 (51.5–68.6)	66.6 (58.9–73.1)	0.004
Females, *n* (%)	182 (19.3)	1.22 (0.67–2.21)	0.52	173 (19.3)	9 (19.6)	1.00
Diabetes mellitus, *n* (%)	184 (19.6)	2.72 (1.63–4.53)	<0.001	176 (19.7)	8 (17.4)	0.85
History of previous MI, *n* (%)	90 (9.6)	3.34 (1.87–5.97)	<0.001	84 (9.4)	6 (13)	0.57
Hypertension, *n* (%)	682 (72.5)	1.58 (0.84–2.96)	0.16	652 (72.8)	30 (65.2)	0.34
Smoking, *n* (%)	488 (51.9)	0.88 (0.54–1.45)	0.62	461 (51.5)	27 (58.7)	0.42
COPD, *n* (%)	39 (4.1)	3.85 (1.83–8.08)	<0.001	37 (4.1)	2 (4.3)	1
CK max (U/l), median (IQR)	1302 (646–2460)	1 (1–1)	0.89	1316 (648–2475)	1106 (599–2040)	0.64
LVEF (%), median (IQR)	53 (45–60)	0.95 (0.94–0.97)	<0.001	53 (45–60)	51.5 (38–58.75)	0.23
MI localization						
Anterior, *n* (%)	391 (41.5)	1.08 (0.65–1.78)	0.77	375 (41.9)	16 (34.8)	0.42
Posterior, *n* (%)	435 (46.2)	0.79 (0.47–1.31)	0.36	409 (45.7)	26 (56.5)	0.2
Lateral, *n* (%)	102 (10.8)	1.62 (0.83–3.18)	0.17	98 (10.9)	4 (8.7)	0.81
Unclassified, *n* (%)	12 (1.3)	0 (0–Inf)	0.996	12 (1.3)	0 (0 0)	0.91
BMI (kg/m^2), median (IQR)	26.6 (24.5–29.1)	1.02 (0.96–1.09)	0.52	26.6 (24.5–29.0)	25.1 (24.1–28.7)	0.26
Serum creatinine (mg/dL), median (IQR)	1.1 (0.9–1.3)	1.77 (1.46–2.15)	<0.001	1.1 (0.9–1.3)	1.1 (1–1.3)	0.29
Cardiogenic shock/CPR, *n* (%)	41 (4.4)	0.81 (0.2–3.32)	0.77	36 (4)	5 (10.9)	0.07
Intervention						
PCI, *n* (%)	878 (93.3)	0.65 (0.28–1.51)	0.31	835 (93.3)	43 (93.5)	1
Thrombolysis, *n* (%)	14 (1.5)	0 (0–Inf)	0.996	14 (1.6)	0 (0 0)	0.82
CABG, *n* (%)	6 (0.6)	3.36 (0.47–24.22)	0.23	5 (0.6)	1 (2.2)	0.7
No revascularization possible, *n* (%)	43 (4.6)	1.91 (0.77–4.77)	0.16	41 (4.6)	2 (4.3)	1
Aspirin, *n* (%)	913 (97)	0.56 (0.18–1.78)	0.33	869 (97.1)	44 (95.7)	0.91
Clopidogrel, *n* (%)	920 (97.8)	0.4 (0.13–1.29)	0.13	876 (97.9)	44 (95.7)	0.63
Beta-blockers, *n* (%)	897 (95.3)	0.67 (0.24–1.84)	0.43	854 (95.4)	43 (93.5)	0.8
ACE-inhibitors, *n* (%)	885 (94)	0.56 (0.24–1.31)	0.18	842 (94.1)	43 (93.5)	1
Statins, *n* (%)	879 (93.4)	0.52 (0.24–1.14)	0.1	837 (93.5)	42 (91.3)	0.78
Diuretics, *n* (%)	415 (44.1)	2.11 (1.26–3.51)	0.004	388 (43.4)	27 (58.7)	0.06
GRACE score	110.2 (93.4–25.8)	1.04 (1.03–1.05)	<0.001	109.3 (92.5–125.4)	121.7 (109.9–136.0)	0.001
eGFR Counahan Barratt	71.9 (62.4–82.7)	0.97 (0.95–0.98)	<0.001	72.2 (62.4–83.1)	67.6 (54.7–75.4)	0.02

*ACE, angiotensin-converting enzyme; BMI, body mass index; CABG, coronary artery bypass graft; CK, serum creatine kinase; COPD, chronic obstructive pulmonary disease; CPR, cardiopulmonary resuscitation; IQR, inter-quartile range; LVEF, left ventricular ejection fraction; MI, myocardial infarction; PCI, percutaneous coronary intervention. *Hazard ratio refers to risk of total mortality.*

Model-Based QTV Analysis Results

The average QT interval and rate-corrected QT interval were 425.7 ± 44.8 ms and 432.6 ± 39.7 ms, respectively. The variance of beat-to-beat fluctuations in QT interval was 10.4 ± 24.7 ms^2 on average.

Figure 1 shows the relative contribution of RR and respiration to total QTV in survivors, and non-survivors averaged across all patients. While the absolute value of the RR and respiration contribution is higher for non-survivors due to the overall increase in QT power in that group, the relative contribution of RR and respiration to QTV is decreased in non-survivors as demonstrated by the pie charts. The QT power independent of RR and respiration is increased and exhibits a clear peak in the low-frequency band.

Figure 2 shows the Kaplan–Meier curves for QTV and its individual components. An increase in QTV and QTV independent of RR and respiration was associated with increased risk of mortality (QTV:16.8% vs. 5.5%, $p < 0.001$; QTV independent:15.2% vs. 5.5%, $p < 0.001$). On the other hand, the 5-year mortality rate was higher for patients with reduced RR and respiratory contributions to QTV (13.5% vs. 4.8%, $p < 0.001$; 11% vs. 5.7%, $p = 0.003$, respectively).

Cox Regression Analysis

In univariate Cox regression analysis (**Table 2**), all QT variables were significantly associated with mortality except for $QTV_{respiration}$. Multivariable stepwise Cox regression analysis of QT variables identified the increase in QTV_{total} and $QTV_{unexplained}$ as significant predictors of mortality in addition to QT_c prolongation (**Table 2**). A linear predictor score (termed QTV risk score) was calculated from a linear combination of these significant predictors.

Analysis of deviance demonstrated the added value of QTV_{total} and $QTV_{unexplained}$ to the model when compared to a model with QT_c alone ($\chi^2 = 12.2$, $p = 0.002$). Using stepwise multivariable cox regression, we explored whether the

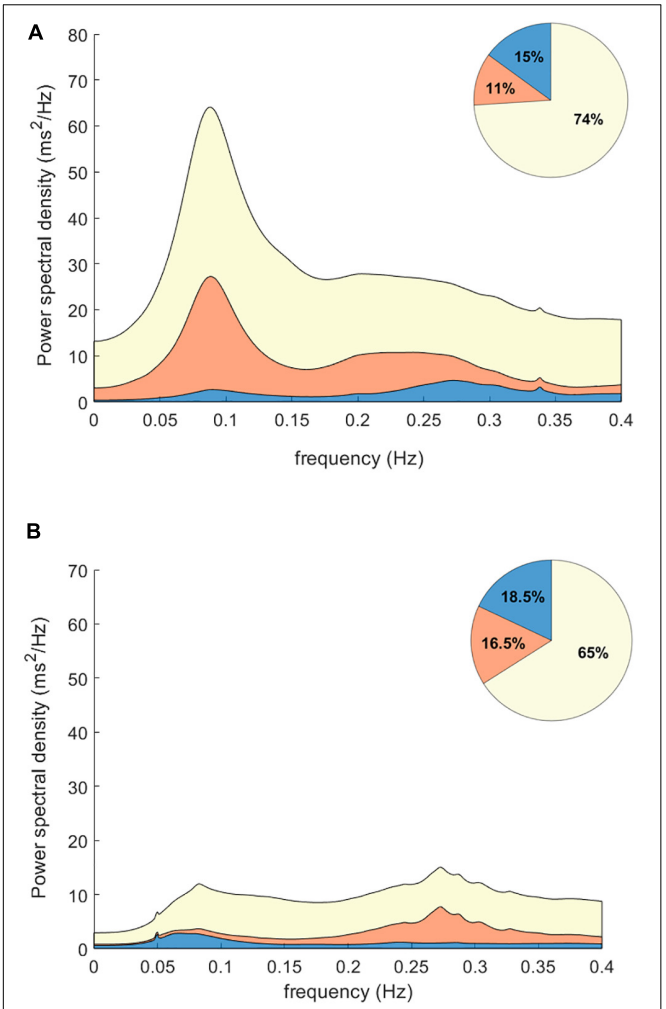

FIGURE 1 | Power contributions to QT interval variability. Plots show the spectrograms averaged for non-survivors **(A)** and survivors **(B)** post MI. The relative contribution of RR interval variability is shown in blue; the contribution of respiration is shown in orange. While the absolute value of the RR (blue) and respiration (orange) contributions are higher for non-survivors due to the overall increase in QTV in that group, the relative contribution of RR and respiration to QT power is decreased in non-survivors as shown in the pie charts. Notably, the QT power independent of RR and respiration (yellow) is increased and exhibits a clear peak in the low-frequency band.

QTV risk score adds predictive value to a model consisting of the following clinical predictor variables (model details can be found in **Table 3**): GRACE score, LVEF, presence of diabetes, chronic obstructive pulmonary disease and expiration-triggered respiratory sinus arrhythmia. Here, the QTV risk score added significant predictive value with an HR = 1.73 (1.23–2.51), $p = 0.002$ (**Table 4**).

Kaplan–Meier curves of the dichotomized QTV risk score are shown in **Figure 3**. The 5-year mortality rate for patients with a high QTV risk score was significantly higher compared to those with a lower QTV risk score (18.4% vs. 4.7%, $p = 2.92 \times 10^{-9}$).

The cohort was divided into subgroups based on LVEF. In the group with LVEF > 35%, the 5-year mortality risk was significantly higher for patients who had a high QTV risk score (16% vs. 4%, $p = 1.19 \times 10^{-7}$). The QTV risk score was also marginally predictive of mortality in patients with LVEF ≤ 35% (**Figure 4**).

In a subgroup of patients with GRACE score ≥ 120, patients with a higher QTV risk score had a significantly higher 5-year mortality risk compared to those with lower QTV risk score in the same group (25% vs. 11%, $p = 0.0009$) (**Figure 5**).

DISCUSSION

Our study demonstrates that heart rate-independent mechanisms play a dominant role in creating excessive QTV observed in MI patients with increased mortality risk. The novel QTV risk score yields improved risk stratification within a subgroup of MI patients who already display traditional risk markers (GRACE score ≥ 120). It can also identify vulnerable patients in patient groups with normal to moderate LVEF (LVEF > 35%).

Repolarization lability can trigger malignant arrhythmias and subsequent SCD in patients post MI (Liew, 2010). QTV was found to be elevated during ischemic episodes compared to non-ischemic episodes (Murabayashi et al., 2002). We found that QTV is elevated in non-surviving MI patients when compared to those who survived.

Previously, simple QTV metrics were combined with conventional risk markers to identify MI patients at high risk of mortality (Jensen et al., 2005; Piccirillo et al., 2007). Here, we sought to decompose QTV into its physiological sources and assessed their individual role in risk stratification. We found that the relative contribution of RR interval variability to QTV was reduced in non-survivors, indicating attenuated rate-adaptation of the QT interval. This attenuation of the QT-RR relationship has also been found in MI patients with reduced LVEF when compared to those with coronary artery disease but no MI (Sosnowski et al., 2002). Others found no difference in the RR dependent component of QTV when comparing MI patients to healthy subjects (Lombardi et al., 1998; Zhu et al., 2008). These aggregate results suggest that the attenuation in QT-RR relationship is only prevalent in high-risk patients rather than in all patients post MI. Possibly, the attenuation is linked to increased sympathetic activation (Zaza et al., 1991; Porta et al., 2010; El-Hamad et al., 2015). Holter recordings showed substantial predictive value of attenuated rate-adaptation of the QT interval for SCD in MI patients (Hintze et al., 2002; Chevalier et al., 2003).

In our study, the respiratory contribution to QTV did not play a significant role in predicting patients at risk in the univariate model (**Table 2**). Hence, we considered a simplified model without respiration. It's predictive performance was comparable to the original model (data not shown), suggesting that recording of respiration is not necessary. Contrary to our findings, others have reported an increase in high frequency of RT interval variability in patients with reduced LVEF compared to those with

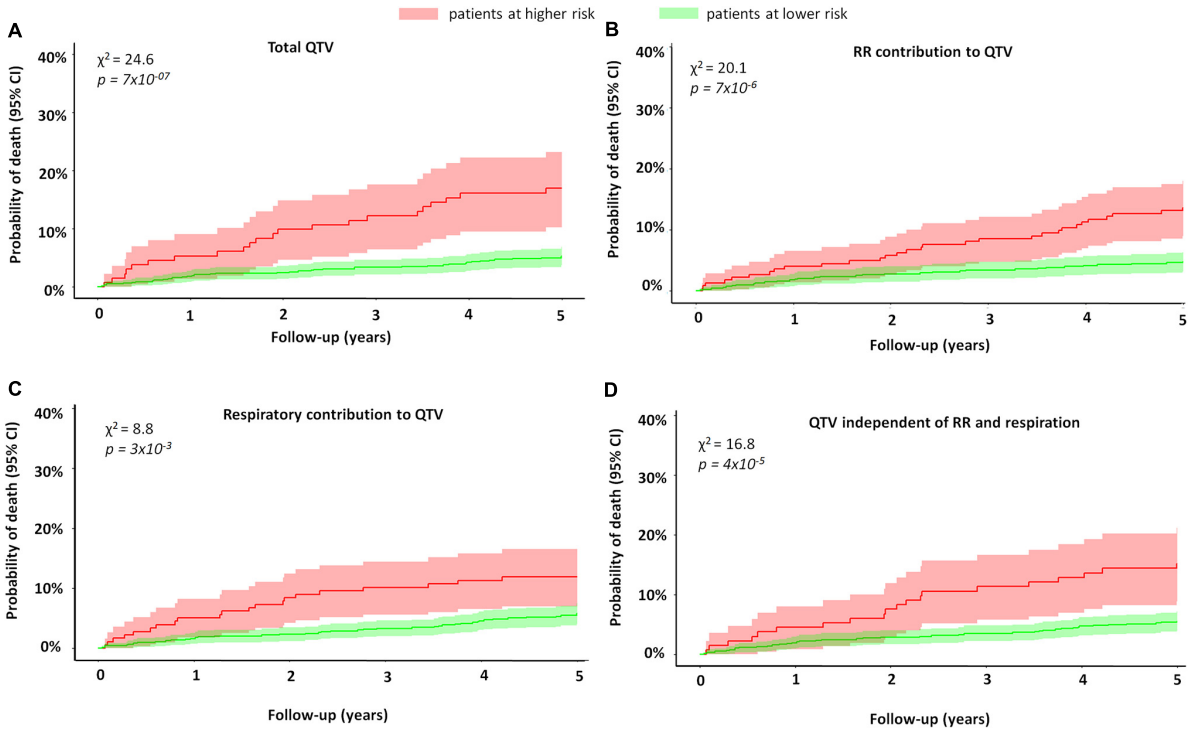

FIGURE 2 | Mortality of MI patients stratified by QTV and its components. The figure shows the Kaplan–Meier curves of MI patients stratified by **(A)** total QT variability, **(B)** percentage of RR contribution to QTV, **(C)** percentage of respiratory contribution to QTV, and **(D)** percentage of QTV independent of RR and respiration. The red curve represents patients at higher risk, while the green curve represents those with lower risk. Patients with higher QTV had a higher risk of mortality compared to those with lower QTV (16.8% vs. 5.5%, $p < 0.001$). Patients with higher QTV independent of RR and respiration also had a higher 5-year mortality rate (15.2% vs. 5.5%, $p < 0.001$). Finally, the 5-year mortality rate was higher for patients with reduced RR and respiratory contributions to QTV (13.5% vs. 4.8%; 11% vs. 5.7%, respectively). The figure demonstrates the univariate predictive value of QTV and its components is risk stratification.

preserved LVEF or with coronary artery disease but no MI (Sosnowski et al., 2002).

The portion of QTV that cannot be explained by rate-adaptation or respiration-related mechanisms was increased in patients who died during the follow-up period (**Table 2**). In healthy subjects, the unexplained fraction of QTV has been previously shown to correlate with an increase in sympathetic tone during tilt (Porta et al., 2010; El-Hamad et al., 2015) and is augmented in post-MI patients compared to healthy subjects (Zhu et al., 2008).

The pathophysiological mechanisms that increase overall QTV and QTV independent of heart period and respiration and contribute to mortality risk are not fully understood. By design, our study does not facilitate the direct interpretation of the QTV component independent of heart rate and respiration. However, the spectral component of QTV that is independent of RR and respiration exhibits a clear peak in the low-frequency (LF; 0.04-0.15 Hz) region that is elevated in the non-survivors, as shown in **Figure 1**. It is well-known that sympathetic nerve activity oscillates at the LF rhythm, creating Traube–Hering–Mayer waves in arterial blood pressure that coincide with oscillations in RR variability. Sympathetic nerve activity modulates the relationship between

TABLE 2 | Univariate and multivariable Cox regression analysis of QT variables.

Variable	Univariate		Multivariable (All variables in)	
	Hazard ratio (95%)	*p*-value	Hazard ratio (95%)	*p*-value
QT_c (ms)	1.01 (1.01–1.02)	<0.001	1.010 (1.01–1.03)	0.001
QTV_{total} (ms^2)	1.01 (1.006–1.014)	<0.001	1.005 (1.00–1.01)	0.08
$QTV_{respiration}$ (%)	0.99 (0.97–1.005)	0.168	-	-
QTV_{RR} (%)	0.96 (0.94–0.99)	0.004	-	-
$QTV_{unexplained}$ (%)	1.03 (1.01–1.045)	0.001	1.024 (1.01–1.04)	0.004

TABLE 3 | Multivariable Cox regression analysis of clinical risk markers.

Variable	Hazard ratio (±SE)	*p*-value
GRACE score	1.04 (±0.006)	<0.001
ETA	0.79 (±0.04)	<0.001
LVEF	0.97 (±0.01)	0.007
Diabetes	1.72 (±0.27)	0.047
COPD	2.19 (±0.39)	0.044

GRACE, global registry of acute coronary event; ETA, expiration triggered arrhythmia; LVEE, left ventricular ejection fraction; COPD, chronic obstructive pulmonary disease.

TABLE 4 | Hazard ratios and 95% confidence intervals of the clinical and QTV models in the multivariable cox regression analysis.

Variables	Hazard ratio[a] (95% CI)	*p*-value
Clinical model[b]	2.45(2.2–3.3)	<0.001
QTV risk score[c]	1.73 (1.23–2.51)	0.002

[a] *Hazard ratio refers to the risk of total mortality.*
[b] *Model details in* ***Table 3****.*
[c] *Model details in* ***Table 2****.*

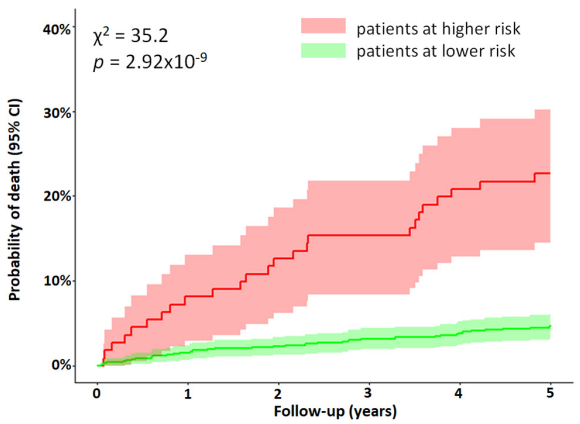

FIGURE 3 | Mortality of MI patients stratified by the QTV risk score. Kaplan–Meier curves were obtained from the dichotomized multivariable Cox regression model. The red curve represents patients above the cut off value (0.626), while the green curve represents all other patients. Difference between the two curves was tested using the log-rank test ($\chi^2 = 35.2$, $p = 2.92\times10^{-9}$). The figure demonstrates the predictive value of an increase in QTV risk score for identifying patients with a higher risk of mortality post MI.

repolarization and cycle length in the LF band (Zaza et al., 1991). It also contributes directly to the magnitude of QTV by affecting L-type channel Ca^{2+} current and the slow delayed rectifier potassium current in ventricular myocytes. Nerve sprouting (Zhou et al., 2004) and sympathetic hyperinnervation following acute MI can create electrical instability, where augmented sympathetic activity can lead to malignant ventricular arrhythmias (Cao et al., 2000). Other studies suggest that systemic inflammation post-MI could contribute at least in part to the increase in QTV (Tseng et al., 2012). Since the severity and prognosis of myocardial infarction are highly dependent on the size and location of the infarcted tissue, affecting the extent of spatial repolarization heterogeneity (Hiromoto et al., 2006), QTV independent of heart rate and respiration may also be affected by the characteristics of the damaged substrate.

Markers of an abnormal substrate or structural heart disease are some of the most common risk factors for SCD, and reduced LVEF is currently considered the most important marker for risk stratification (Wellens et al., 2014). Current international guidelines for implantable cardioverter defibrillator implantation for primary prevention are predominantly based on LVEF (O'Gara et al., 2013; Priori et al., 2015). However, the majority of SCDs occur in patients with preserved LVEF (LVEF > 30%) (Buxton et al., 2007; Wellens et al., 2014). Therefore, the identification of high-risk patients in this cohort is critical.

Several markers of electrical instability and autonomic tone, such as heart rate variability, heart rate turbulence, T wave alternans, and QTV index, have been associated with increased risk of SCD in post MI patients with preserved LVEF (Piccirillo et al., 2007; Gatzoulis et al., 2019). In this group of patients, we found that a higher QTV risk score is associated with a four times higher risk of mortality compared to those with lower values of QTV risk score. Gatzoulis et al. (2019) reported that patients with preserved LVEF who display at least one ECG-derived non-invasive risk factor were at higher risk of SCD. As QTV reflects

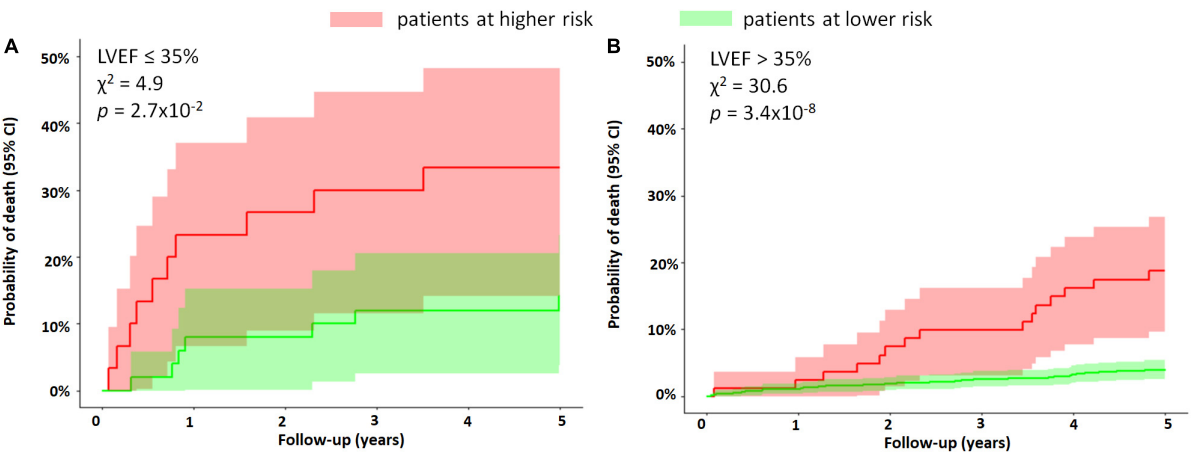

FIGURE 4 | Subgroup analysis based on LVEF. The figure shows the Kaplan–Meier curves of MI patients stratified by the QTV risk score for subgroups with **(A)** LVEF ≤ 35% and **(B)** LVEF > 35%. The 5-year mortality rate was significantly higher in patients with LVEF > 35% who had a high QTV risk score (16% vs. 4%, $p = 1.19\times10^{-7}$). The QTV risk score was only marginally predictive of mortality in patients with LVEF ≤ 35%. The figure demonstrates the ability of the QTV risk score to further stratify a subgroup at high risk in the group with LVEF > 35%.

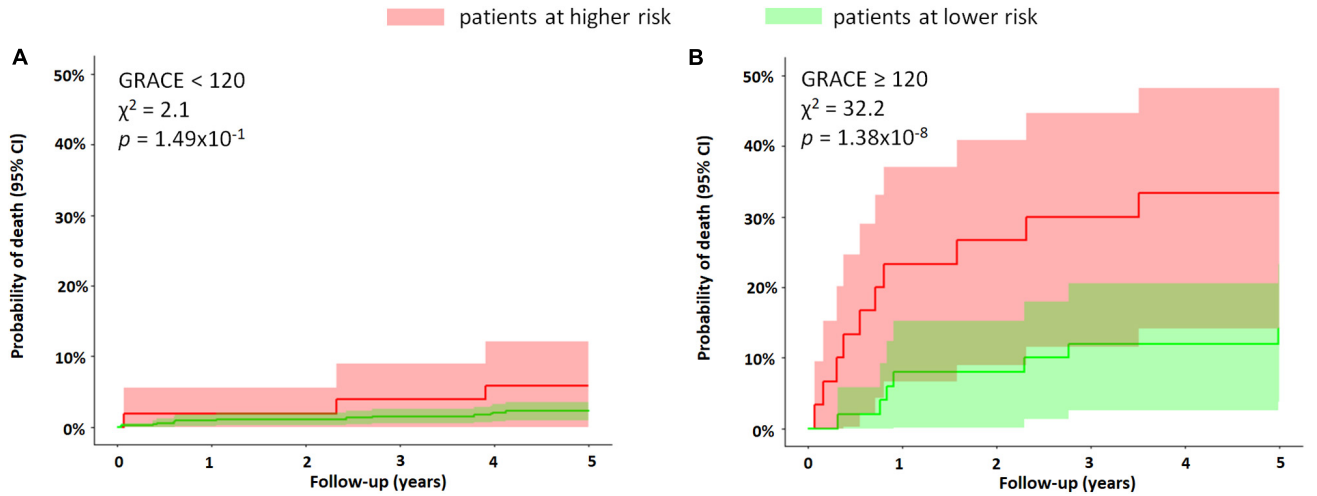

FIGURE 5 | Subgroup analysis based on GRACE score. The figure shows the Kaplan–Meier curves of MI patients stratified by the QTV risk score for subgroups with **(A)** GRACE score < 120 and **(B)** GRACE score ≥ 120. The QTV risk score was significantly predictive of mortality only in patients with a score ≥ 120, where the 5-year mortality rate was 25% versus 11%, p = 0.0009. The figure demonstrates the ability of the QTV risk score to further stratify a subgroup with a higher risk in the high-risk cohort (GRACE ≥ 120).

lability of the ventricular repolarization process, a higher QTV risk score could identify patients more susceptible to ventricular arrhythmia.

The QTV risk score was only marginally predictive in the group with reduced LVEF. This could be explained by the fact that patients with reduced LVEF have a higher competing risk of death from heart failure than other modes of death when compared to patients with preserved LVEF (Hall et al., 2018). The GRACE score is a hospital discharge risk score shown to be predictive of mortality in patients with acute coronary syndrome. It combines multiple prognostic factors such as age, history of heart failure and MI, and heart rate (Tang et al., 2007). Patients with a GRACE score ≥ 120 are considered to be at high risk. In our study, the QTV risk score was able to identify a subgroup of patients at higher risk within the subgroup of high-risk patients identified by a GRACE score ≥ 120.

Our study has several limitations. Current guidelines recommend using 12-lead ECG screening for specific high-risk patients (Priori et al., 2015); we used single-lead ECG in favor of lower complexity and cost. By choosing the lead with the largest T wave and the lowest noise, we obtained a reasonably good approximation of the global repolarization duration. However, potentially valuable information on the repolarization dispersion across leads could not be assessed. Although we used high-resolution ECG, conventional ECG sampled at > 300 Hz is sufficient for QTV analysis (Baumert et al., 2016a). Patients were studied at rest, and while autonomous nervous system provocation tests tend to increase the predictive power of ECG markers, their practical use in patients is limited due to the complexity of tests (Wellens et al., 2014). Stationary segments of heart period, QT interval and respiratory time series were present in all recordings as judged by visual assessment. Fully automated methods should be considered in the future for a more rigorous assessment. The 5-year mortality rate in our cohort was low, and hence, the identified groups with increased mortality may be small. This may have impacted our analysis by possibly reducing its statistical power and broadening the confidence intervals of the Kaplan–Meier curves, as seen in **Figures 3–5**. Accurate identification of specific patients at risk based on QTV alone might be challenging. Patients who were not in sinus rhythm were excluded from the analysis, which introduced a mortality bias. We did not systematically measure serum creatine kinase-muscle/brain and troponin levels. Since the study enrollment, improved treatments for MI have become clinically available (e.g., improved stents and antithrombotic drugs) that may have affected our findings. Our follow-up protocol did not include data collection on change in patient characteristics and therapy adherence. The primary study endpoint was all-cause mortality. Future studies should validate our findings on data from a different cohort stratifying for cardiovascular mortality, in particular, SCD.

CONCLUSION

In conclusion, the QTV risk score might help stratify high-risk patients that already display traditional risk markers and identify patients at higher risk of mortality, albeit their preserved LVEF. The implementation of risk stratification strategies to predict risk in patients with preserved LVEF requires the use of a combination of several risk markers. New stratification strategies which can be translated into daily clinical practice are necessary to stratify patients with moderate and normal LVEF yet are at higher risk of SCD. The QTV risk score is a non-invasive risk marker that can be easily incorporated into daily clinical practice. However, the prognostic value of the QTV risk score needs to be prospectively validated on other cohorts, and further investigation into its utility for specifically predicting SCD is required.

DATA AVAILABILITY STATEMENT

The data presented in this article are not readily available. Data access requests should be emailed to author Georg Schmidt directly.

ETHICS STATEMENT

The studies involving human participants were reviewed and approved by the ethics committees at the hospital of the Technische Universität München, the German Heart Centre, and the Klinikum Rechts der Isar, both in Munich, Germany. The patients/participants provided their written informed consent to participate in this study.

AUTHOR CONTRIBUTIONS

FE-H was responsible for the conception, modeling, analysis, and interpretation of data; for drafting of the manuscript and revising it critically for important intellectual content; and for the final approval of the manuscript submitted. SB was responsible for the processing and analysis of data; for revising the manuscript critically for important intellectual content; and for the final approval of the manuscript submitted. AM was responsible for the analysis and interpretation of data; for drafting of the manuscript; and for the final approval of the manuscript submitted. AS was responsible for the conception, design, and analysis of the data; for revising the manuscript critically for important intellectual content; and for the final approval of the manuscript submitted. GS was responsible for the conception, design, analysis, and interpretation of data; for revising the manuscript critically for important intellectual content; and for the final approval of the manuscript submitted. MB was responsible for the conception, design, and interpretation of data; for drafting of the manuscript and revising it critically for important intellectual content; and for the final approval of the manuscript submitted. All authors contributed to the article and approved the submitted version.

FUNDING

The study was partly funded by a Fellowship from the Australian Research Council, Australian Capital Territory, Australia (ARC DP 110102049). This work was supported by the Bundesministerium für Bildung, Wissenschaft, Forschung und Technologie (13N/7073/7), the Kommission für Klinische Forschung, the Deutsche Forschungsgemeinschaft (SFB 386), the British Heart Foundation (FS/10/038), and the NIHR Biomedical Research Centre Scheme. These sponsors had no role in the study design, data collection, data analysis, data interpretation, or writing of the report.

REFERENCES

Akaike, H. (1974). A new look at the statistical model identification. *IEEE. Trans. Automat. Contr.* 19, 716–723. doi: 10.1109/TAC.1974.1100705

Barthel, P., Wensel, R., Bauer, A., Müller, A., Wolf, P., Ulm, K., et al. (2013). Respiratory rate predicts outcome after acute myocardial infarction: a prospective cohort study. *Eur. Heart J.* 34, 1644–1650. doi: 10.1093/eurheartj/ehs420

Baselli, G., Porta, A., Rimoldi, O., Pagani, M., and Cerutti, S. (1997). Spectral decomposition in multichannel recordings based on multivariate parametric identification. *IEEE. Trans. Biomed. Eng.* 44, 1092–1101. doi: 10.1109/10.641336

Baumert, M., Porta, A., Vos, M. A., Malik, M., Couderc, J.-P., Laguna, P., et al. (2016a). QT interval variability in body surface ECG: measurement, physiological basis, and clinical value: position statement and consensus guidance endorsed by the European heart rhythm association jointly with the ESC working group on cardiac cellular electrophysiology. *Europace* 18, 925–944. doi: 10.1093/europace/euv405

Baumert, M., Schmidt, M., Zaunseder, S., and Porta, A. (2016b). Effects of ECG sampling rate on QT interval variability measurement. *Biomed. Signal Process. Contr.* 25, 159–164. doi: 10.1016/j.bspc.2015.11.011

Bernard, E., Corday, E., Eliasch, H., Gonin, A., Haiti, R., Nikolaeva, L. F., et al. (1979). Nomenclature and criteria for diagnosis of ischemic heart disease. report of the joint international society and federation of Cardiology/World health organization task force on standardization of clinical nomenclature. *Circulation* 59, 607–609. doi: 10.1161/01.CIR.59.3.607

Buxton, A. E., Lee, K. L., Hafley, G. E., Pires, L. A., Fisher, J. D., Gold, M. R., et al. (2007). Limitations of ejection fraction for prediction of sudden death risk in patients with coronary artery disease: lessons from the MUSTT study. *J. Am. Coll. Cardiol.* 50, 1150–1157. doi: 10.1016/j.jacc.2007.04.095

Cao, J.-M., Fishbein, M. C., Han, J. B., Lai, W. W., Lai, A. C., Wu, T.-J., et al. (2000). Relationship between regional cardiac hyperinnervation and ventricular Arrhythmia. *Circulation* 101, 1960–1969. doi: 10.1161/01.cir.101.16.1960

Chevalier, P., Burri, H., Adeleine, P., Kirkorian, G., Lopez, M., Leizorovicz, A., et al. (2003). QT dynamicity and sudden death after myocardial infarction. *J. Cardiovasc. Electrophysiol.* 14, 227–233. doi: 10.1046/j.1540-8167.2003.02431.x

Eagle, K. A., Lim, M. J., Dabbous, O. H., Pieper, K. S., Goldberg, R. J., Van de Werf, F., et al. (2004). A validated prediction model for all forms of acute coronary syndrome: estimating the risk of 6-month postdischarge death in an international registry. *JAMA* 291, 2727–2733. doi: 10.1001/jama.291.22.2727

El-Hamad, F., Lambert, E., Abbott, D., and Baumert, M. (2015). Relation between QT interval variability and muscle sympathetic nerve activity in normal subjects. *Am. J. Physiol. Heart Circ. Physiol.* 309, H1218–H1224. doi: 10.1152/ajpheart.00230.2015

Gatzoulis, K. A., Tsiachris, D., Arsenos, P., Antoniou, C. K., Dilaveris, P., Sideris, S., et al. (2019). Arrhythmic risk stratification in post-myocardial infarction patients with preserved ejection fraction: the PRESERVE EF study. *Eur. Heart J.* 40, 2940–2949. doi: 10.1093/eurheartj/ehz260

Hall, J. E. (2011). *Guyton and Hall Textbook of Medical Physiology*. Philadelphia, PA: Saunders Elsevier.

Hall, T. S., von Lueder, T. G., Zannad, F., Rossignol, P., Duarte, K., Chouihed, T., et al. (2018). Relationship between left ventricular ejection fraction and mortality after myocardial infarction complicated by heart failure or left ventricular dysfunction. *Int. J. Cardiol.* 272, 260–266. doi: 10.1016/j.ijcard.2018.07.137

Hasan, M. A., Abbott, D., and Baumert, M. (2013). Beat-to-beat QT interval variability and T-wave amplitude in patients with myocardial infarction. *Physiol. Meas.* 34, 1075–1083. doi: 10.1088/0967-3334/34/9/1075

Hintze, U., Vach, W., Burchardt, H., Videbæk, J., and Møller, M. (2002). QT interval dynamics predict mortality in high-risk patients after myocardial infarction. *Scand. Cardiovasc. J.* 36, 276–281. doi: 10.1080/140174302320774474

Hiromoto, K., Shimizu, H., Mine, T., Masuyama, T., and Ohyanagi, M. (2006). Correlation between beat-to-Beat QT interval variability and impaired left ventricular function in patients with previous myocardial infarction. *Ann. Noninvasive. Electrocardiol.* 11, 299–305. doi: 10.1111/j.1542-474X.2006.00121.x

Hothorn, T., and Lausen, B. (2003). On the exact distribution of maximally selected rank statistics. *Comput. Stat. Data Anal.* 43, 121–137. doi: 10.1016/s0167-9473(02)00225-6

Huikuri, H. V., Castellanos, A., and Myerburg, R. J. (2001). Sudden death due to cardiac arrhythmias. *N. Engl. J. Med.* 345, 1473–1482. doi: 10.1056/NEJMra000650

Jensen, B. T., Abildstrom, S. Z., Larroude, C. E., Agner, E., Torp-Pedersen, C., Nyvad, O., et al. (2005). QT dynamics in risk stratification after myocardial infarction. *Heart Rhythm.* 2, 357–364.

Lausen, B., Hothorn, T., Bretz, F., and Schumacher, M. (2004). Assessment of optimal selected prognostic factors. *Biom. J.* 46, 364–374. doi: 10.1002/bimj.200310030

Liew, R. (2010). Prediction of sudden arrhythmic death following acute myocardial infarction. *Heart* 96, 1086–1094. doi: 10.1136/hrt.2010.194407

Lombardi, F., Colombo, A., Porta, A., Baselli, G., Cerutti, S., and Fiorentini, C. (1998). Assessment of the coupling between rtapex and rr interval as an index of temporal dispersion of ventricular repolarization. *Pacing Clin. Electrophysiol.* 21, 2396–2400. doi: 10.1111/j.1540-8159.1998.tb01189.x

Merri, M., Alberti, M., and Moss, A. J. (1993). Dynamic analysis of ventricular repolarization duration from 24-hour Holter recordings. *IEEE. Trans. Biomed. Eng.* 40, 1219–1225. doi: 10.1109/10.250577

Murabayashi, T., Fetics, B., Kass, D., Nevo, E., Gramatikov, B., and Berger, R. D. (2002). Beat-to-beat QT interval variability associated with acute myocardial ischemia. *J. Electrocardiol.* 35, 19–25. doi: 10.1054/jelc.2002.30250

Myerburg, R. J. (2001). Sudden cardiac death: exploring the limits of our knowledge. *J. Cardiovasc. Electrophysiol.* 12, 369–381. doi: 10.1046/j.1540-8167.2001.00369.x

Ng, G. A. (2016). Neuro-cardiac interaction in malignant ventricular arrhythmia and sudden cardiac death. *Auton. Neurosci.* 199, 66–79. doi: 10.1016/j.autneu.2016.07.001

O'Gara, P. T., Kushner, F. G., Ascheim, D. D., Casey, D. E., Chung, M. K., de Lemos, J. A., et al. (2013). 2013 ACCF/AHA guideline for the management of ST-Elevation myocardial infarction: a report of the american college of cardiology foundation/american heart association task force on practice guidelines. *Circulation* 127, e362–e425. doi: 10.1161/CIR.0b013e3182742cf6

Piccirillo, G., Magrì, D., Matera, S., Magnanti, M., Torrini, A., Pasquazzi, E., et al. (2007). QT variability strongly predicts sudden cardiac death in asymptomatic subjects with mild or moderate left ventricular systolic dysfunction: a prospective study. *Eur. Heart J.* 28, 1344–1350. doi: 10.1093/eurheartj/ehl367

Porta, A., Baselli, G., Caiani, E., Malliani, A., Lombardi, F., and Cerutti, S. (1998). Quantifying electrocardiogram RT-RR variability interactions. *Med. Biol. Eng. Comput.* 36, 27–34. doi: 10.1007/bf02522854

Porta, A., Tobaldini, E., Gnecchi-Ruscone, T., and Montano, N. (2010). RT variability unrelated to heart period and respiration progressively increases during graded head-up tilt. *Am. J. Physiol. Heart Circ. Physiol.* 298, 1406–1414.

Priori, S. G., Blomström-Lundqvist, C., Mazzanti, A., Blom, N., Borggrefe, M., Camm, J., et al. (2015). 2015 ESC Guidelines for the management of patients with ventricular arrhythmias and the prevention of sudden cardiac death the task force for the management of patients with ventricular arrhythmias and the prevention of sudden cardiac death of the European Society of Cardiology (ESC)endorsed by: Association for European Paediatric and Congenital Cardiology (AEPC). *Eur. Heart J.* 36, 2793–2867. doi: 10.1093/eurheartj/ehv316

R Core Team. (2014). R: A language and environment for statistical computing. *R Foundation for Statistical Computing*, Vienna. Available online at: http://www.R-project.org

Schmidt, M., Baumert, M., Porta, A., Malberg, H., and Zaunseder, S. (2014). Two-Dimensional warping for one-dimensional signals: conceptual framework and application to ECG processing. *IEEE. Trans. Sign. Process.* 62, 5577–5588. doi: 10.1109/TSP.2014.2354313

Schwartz, P. J., La Rovere, M. T., and Vanoli, E. (1992). Autonomic nervous system and sudden cardiac death. experimental basis and clinical observations for post-myocardial infarction risk stratification. *Circulation* 85, I77–I91.

Sinnecker, D., Barthel, P., Huster, K. M., Müller, A., Gebhardt, J., Dommasch, M., et al. (2015). Force–interval relationship predicts mortality in survivors of myocardial infarction with atrial fibrillation. *Int. J. Cardiol.* 182, 315–320. doi: 10.1016/j.ijcard.2015.01.018

Sosnowski, M., Czyz, Z., and Tendera, M. (2002). Time and frequency analysis of beat-to-beat R-T interval variability in patients with ischaemic left ventricular dysfunction providing evidence for non-neural control of ventricular repolarisation. *Eur. J. Heart Fail.* 4, 737–743. doi: 10.1016/s1388-9842(02)00167-168

Sutherland, D. J., McPherson, D. D., Spencer, C. A., Armstrong, C. S., Horacek, B. M., and Montague, T. J. (1983). Effects of posture and respiration on body surface electrocardiogram. *Am. J. Cardiol.* 52, 595–600. doi: 10.1016/0002-9149(83)90033-4

Tang, E. W., Wong, C.-K., and Herbison, P. (2007). Global Registry of Acute Coronary Events (GRACE) hospital discharge risk score accurately predicts long-term mortality post acute coronary syndrome. *Am. Heart J.* 153, 29–35. doi: 10.1016/j.ahj.2006.10.004

Tarvainen, M. P., Ranta-aho, P. O., and Karjalainen, P. A. (2002). An advanced detrending method with application to HRV analysis. *IEEE. Trans. Biomed. Eng.* 49, 172–175. doi: 10.1109/10.979357

Tseng, Z. H., Secemsky, E. A., Dowdy, D., Vittinghoff, E., Moyers, B., Wong, J. K., et al. (2012). Sudden cardiac death in patients with human immunodeficiency virus infection. *J. Am. Coll. Cardiol.* 59, 1891–1896. doi: 10.1016/j.jacc.2012.02.024

Wellens, H. J. J., Schwartz, P. J., Lindemans, F. W., Buxton, A. E., Goldberger, J. J., Hohnloser, S. H., et al. (2014). Risk stratification for sudden cardiac death: current status and challenges for the future. *Eur. Heart J.* 35, 1642–1651. doi: 10.1093/eurheartj/ehu176

Yao, L., Li, P., Liu, C., Hou, Y., Yan, C., Li, L., et al. (2019). Comparison of QT interval variability of coronary patients without myocardial infarction with that of patients with old myocardial infarction. *Comput. Biol. Med.* 113:103396. doi: 10.1016/j.compbiomed.2019.103396

Zaza, A., Malfatto, G., and Schwartz, P. J. (1991). Sympathetic modulation of the relation between ventricular repolarization and cycle length. *Circ. Res.* 68, 1191–1203. doi: 10.1161/01.res.68.5.1191

Zhou, S., Chen, L. S., Miyauchi, Y., Miyauchi, M., Kar, S., Kangavari, S., et al. (2004). Mechanisms of cardiac nerve sprouting after myocardial infarction in dogs. *Circ. Res.* 95, 76–83. doi: 10.1161/01.RES.0000133678.22968.e3

Zhu, Y., Lee, P. J., Pan, J., and Lardin, H. A. (2008). The relationship between ventricular repolarization duration and RR interval in normal subjects and patients with myocardial infarction. *Cardiology* 111, 209–218. doi: 10.1159/000121607

Conflict of Interest: The authors declare that the research was conducted in the absence of any commercial or financial relationships that could be construed as a potential conflict of interest.

frontiers in Physiology

ORIGINAL RESEARCH
published: 05 February 2021
doi: 10.3389/fphys.2020.578059

Electrocardiographic Risk Markers of Cardiac Death: Gender Differences in the General Population

Mira Anette E. Haukilahti[1], Tuomas V. Kenttä[1], Jani T. Tikkanen[1], Olli Anttonen[2], Aapo L. Aro[3], Tuomas Kerola[2], Antti Eranti[4], Arttu Holkeri[3], Harri Rissanen[5], Markku Heliövaara[5], Paul Knekt[5], M. Juhani Junttila[1] and Heikki V. Huikuri[1]*

[1] Research Unit of Internal Medicine, Medical Research Center Oulu, University of Oulu and University Hospital of Oulu, Oulu, Finland, [2] Department of Internal Medicine, Päijät-Häme Central Hospital, Lahti, Finland, [3] Division of Cardiology, Heart and Lung Center, University of Helsinki and Helsinki University Hospital, Helsinki, Finland, [4] Heart Center, Central Hospital of North Karelia, Joensuu, Finland, [5] Department of Public Health Solutions, Finnish National Institute for Health and Welfare (THL), Helsinki, Finland

OPEN ACCESS

Edited by:
Ruben Coronel, University of Amsterdam, Netherlands

Reviewed by:
Marina Cerrone, New York University School of Medicine, United States
Hassan Khan, New York University, United States

***Correspondence:**
Mira Anette E. Haukilahti
anette.haukilahti@student.oulu.fi

Specialty section:
This article was submitted to Cardiac Electrophysiology, a section of the journal Frontiers in Physiology

Received: *30 June 2020*
Accepted: *21 December 2020*
Published: *05 February 2021*

Citation:
Haukilahti MAE, Kenttä TV, Tikkanen JT, Anttonen O, Aro AL, Kerola T, Eranti A, Holkeri A, Rissanen H, Heliövaara M, Knekt P, Junttila MJ and Huikuri HV (2021) Electrocardiographic Risk Markers of Cardiac Death: Gender Differences in the General Population. Front. Physiol. 11:578059. doi: 10.3389/fphys.2020.578059

Background: Cardiac death is one of the leading causes of death and sudden cardiac death (SCD) is estimated to cause approximately 50% of cardiac deaths. Men have a higher cardiac mortality than women. Consequently, the mechanisms and risk markers of cardiac mortality are not as well defined in women as they are in men.

Aim: The aim of the study was to assess the prognostic value and possible gender differences of SCD risk markers of standard 12-lead electrocardiogram in three large general population samples.

Methods: The standard 12-lead electrocardiographic (ECG) markers were analyzed from three different Finnish general population samples including total of 20,310 subjects (49.9% women, mean age 44.8 ± 8.7 years). The primary endpoint was cardiac death, and SCD and all-cause mortality were secondary endpoints. The interaction effect between women and men was assessed for each ECG variable.

Results: During the follow-up (7.7 ± 1.2 years), a total of 883 deaths occurred (24.5% women, $p < 0.001$). There were 296 cardiac deaths (13.9% women, $p < 0.001$) and 149 SCDs (14.8% women, $p < 0.001$). Among those who had died due to cardiac cause, women had more often a normal electrocardiogram compared to men (39.0 vs. 27.5%, $p = 0.132$). After adjustments with common cardiovascular risk factors and the population sample, the following ECG variables predicted the primary endpoint in men: left ventricular hypertrophy (LVH) with strain pattern ($p < 0.001$), QRS duration > 110 ms ($p < 0.001$), inferior or lateral T-wave inversion ($p < 0.001$) and inferolateral early repolarization ($p = 0.033$). In women none of the variables remained significant predictors of cardiac death in multivariable analysis, but LVH, QTc ≥ 490 ms and T-wave inversions predicted SCD ($p < 0.047$ and 0.033, respectively). In the interaction analysis, LVH

(HR: 2.4; 95% CI: 1.2–4.9; p = 0.014) was stronger predictor of primary endpoint in women than in men.

Conclusion: Several standard ECG variables provide independent information on the risk of cardiac mortality in men but not in women. LVH and T-wave inversions predict SCD also in women.

Keywords: gender differences, ECG, sudden cardiac death, cardiac death, left ventricular hypertrophy, prolonged QRS, T wave inversion

INTRODUCTION

Cardiovascular disease (CVD) remains the leading cause of death worldwide both in women and men, despite of the overall reduction in CVD mortality (Naghavi et al., 2015; Maffei et al., 2019). The death rates for CVD have declined 22% from 2005 to 2015 (Benjamin et al., 2018), but they seem now to be again increasing among US women, probably due to obesity epidemic (Mosca et al., 2011). Even though the first female-specific recommendation for prevention of CVD was published by American Heart Association in 1995 (Mosca et al., 1999), the erroneous perception that women are protected against CVD is still strong (Sciomer et al., 2018). Traditional Framingham risk factors for CVD have shown to increase the risk of cardiac mortality in both genders (Greenland et al., 2003) even though the impact of classical risk factors for CVD are likely to also differ among men and women (Maffei et al., 2019). In addition, there are many risk factors unique for women associating to reproductive capability and pregnancy, and the development of CVD in women may correlate with some specific events occurring in their reproductive history (Maffei et al., 2019).

Supplementing the traditional risk assessment with electrocardiographic (ECG) risk markers drawn from standard 12-lead electrocardiogram might assist in detecting subclinical changes in cardiac structure and function in previously asymptomatic subjects. These subjects with elevated risk for CVD could then be referred to risk reduction therapies (O'Malley and Redberg, 2012). In previous literature, ST-segment depression, T-wave inversion, ECG signs of left ventricular hypertrophy (LVH) including strain and premature ventricular contractions have been associated with 2–10-fold risk for coronary artery disease (CAD) events (Chou et al., 2011) and combined cardiovascular events (Jørgensen et al., 2014) among asymptomatic subjects. In addition, recent studies have shown that prolonged QRS duration (Aro et al., 2011), certain patterns of early repolarization (Tikkanen et al., 2009; Junttila et al., 2014) and fragmented QRS complex predict cardiac mortality (Terho et al., 2014). Studies evaluating screening for the risk of cardiac mortality using resting electrocardiogram, focusing especially on gender differences in general populations, are sparse (Holkeri et al., 2020). In the future the lack of awareness of the high CVD risk among certain subgroups of women must be overcome, and better sex-specific risk assessment tools for cardiovascular mortality needs to be developed. The aim of the current study was to assess the prognostic value of ECG risk markers for cardiac mortality but also for SCD and all-cause mortality in three large general population samples and conceive possible gender differences in the prognostic value of these markers.

Abbreviations: BMI, body mass index; CAD, coronary artery disease; CI, confidence interval; CVD, cardiovascular disease; ECG, electrocardiographic; ER, early repolarization; fQRS, fragmented QRS complex; HR, hazard ratio; LVH, left ventricular hypertrophy; SCD, sudden cardiac death; SD, standard deviation.

MATERIALS AND METHODS

Patient Populations

Standard 12-lead ECGs were analyzed from 20,310 participants (49.9% women, mean age 44.8 ± 8.7 years) of the Coronary Heart Disease Study of the Finnish Mobile Clinic Health Examination Survey (N = 10,807), the Mini-Finland Health Survey (N = 5,143) and the Health 2000 Health Examination Survey (N = 4,360). All three studies are general population-based surveys of middle-aged subjects including the approximately similar number of women and men from different geographical areas in Finland. The studies were conducted in different eras by Social Insurance Institution and National Institution for Health and Welfare. Flowchart in **Figure 1** represents the final study population.

The Finnish Mobile Clinic Health Examination Survey (1966–1972)

The Coronary Heart Disease Study of the Finnish Mobile Clinic Health Examination Survey consists total of 10,957 subjects aged 30–61 years. The study was carried out between 1966 and 1972 in 4 different geographical areas in Finland. The details of the study population have been described previously (Reunanen et al., 1983). The study subjects underwent recording of standard 12-lead resting electrocardiogram, measurement of blood pressure and body mass index (BMI), and completed a questionnaire regarding their health behavior, known diseases and medications. After excluding 53 subjects with unreadable electrocardiogram and subjects with bundle branch blocks, 10,807 subjects were included in the present study (47.8% female, mean age 44.0 ± 8.5 years).

The Mini-Finland Health Survey (1978–1980)

The Mini-Finland Health Survey was conducted between 1978 and 1980, and the primary study population of 8,000 subjects aged ≥ 30 years and was representative of the Finnish population at the time. Out of these subjects, 7,217 participated in similar health examinations and measurements as in Mobile Clinic Study above. The detailed descriptions of the study protocol have been

FIGURE 1 | A flowchart of the patient populations.

published elsewhere (Knekt et al., 2017). In the current study, subjects older than 61 years were excluded to standardize the study samples. After exclusion, a total of 5,143 subjects (52.2% female, mean age 44.6 ± 9.2 years) remained in the final study population sample.

The Health 2000 Survey (2000–2001)

The Health 2000 Health Examination Survey was carried out between 2000 and 2001. The primary study population contained a representative sample of 8,028 adults between ages 30 and 80. The baseline examinations were conducted on 6,345 subjects and after excluding unreadable electrocardiograms 6,305 subjects remained (54.6% female, mean age 51.5 ± 12.8 years). The details of study population have been described previously (Heistaro, 2020). In the current study, subjects over 61 years old were excluded to standardize the study samples. After exclusions, a total of 4,360 subjects (52.3% female, mean age 45.5 ± 8.4 years) remained in the final study population sample.

Electrocardiography

The standard resting 12-lead electrocardiograms were recorded at paper speed of 50 mm/s and calibration of 10 mm/mV at study baseline. QRS duration and QT interval were measured from leads II or V5. QRS duration was considered prolonged if it was ≥ 110 ms. Heart rate correction for the QT interval was performed with Bazett's formula. The presence of early repolarization ≥ 0.1 mV with horizontal or descending ST segment and fragmented QRS were assessed as described previously (Tikkanen et al., 2009; Terho et al., 2014). Early repolarization was classified inferolateral if there were ≥ 2 slurred or notched J-point elevations ≥ 0.1 mV in inferior (II, III, aVF) or lateral (I, aVL, V4–V6) leads. ST segment was classified as horizontal or descending if it was under 0.1 mV 100 ms after the end of the QRS complex. Fragmented QRS complexes were classified by coronary artery regions as anterior (V1–V3), inferior or lateral if there were ≥ 2 fragmented QRS complexes within the region. Similarly, inferolateral T-wave inversions were classified by coronary artery regions as inferior or lateral if T-wave amplitude was < −0.1 mV in ≥ 2 contiguous leads in the same region. The Sokolow-Lyon criteria was used for grading electrocardiographic LVH, i.e., if the sum of S wave amplitude in V1 and R wave amplitude in V5/V6 (whichever larger) was ≥35 mm, electrocardiogram was graded as positive for LVH. By LVH with repolarization abnormalities we refer to ECG sign of LVH observed with inferior or lateral T-wave inversions. Any ECG abnormality variable indicated the presence of at least one of the following ECG risk markers: QRS duration ≥ 110 ms, QTc ≥ 450 ms in men, or ≥470 ms in women, presence of ECG signs of LVH, T-wave inversion, inferolateral ER or fQRS. Prevalence and risks for endpoints of any other ECG abnormality

was not assessed in this study. Subjects with a bundle branch block were excluded from the final study population.

Follow-Up and Endpoints

In the Coronary Heart Disease Study of the Finnish Mobile Clinic Health Examination Survey, baseline measurements were performed 1966-1972. The participants were followed for 30 ± 11 years until the end of year 2007. In the Mini-Finland Study the baseline measurements were performed 1978–1980 and participants were followed for 24.0 ± 10.6 years from the baseline examinations until the end of 2011. The baseline measurements of the Health 2000 Study were carried out in 2000 and 2001. The mean follow-up time was 8.8 ± 1.1 years until the end of January 2009. In the present analyses the follow-up time was limited to 8 years in all analyses to clarify the role of electrocardiography in the risk assessment since the cardiovascular risk profile could ultimately change during a longer follow-up period.

The primary endpoint of the study was cardiac death and the secondary endpoints were sudden cardiac death and death from any cause. The causes of death were determined using nationwide health registers; Causes of Death Register maintained by Statistics Finland. The quality and validity of these registers has been well established (Rapola et al., 1997). Death of cardiac cause was defined using International Classification of Disease code of cause of death representing the codes I20–I25 in the International Classification of Diseases 10. A committee of qualified and experienced cardiologists unaware of the ECG analysis reviewed all the cardiac deaths. They evaluated each case by using the death certificates and hospital records. Definition used for SCD is based on definitions presented in Cardiac Arrhythmia Pilot Study and has been described earlier in detail (Greene et al., 1989; Tikkanen et al., 2009). In addition, death was classified as SCD if the event was unwitnessed yet lacking the evidence of other cause of death. All three studies were approved by the local ethics committees and followed the guidelines of The Declaration of Helsinki.

Statistical Analyses

All continuous variables are presented as mean ± standard deviation (SD) and categorical variables as number of cases with prevalence among the study population in brackets. When comparing the categorial variables between groups of interest the Pearson Chi-Square test was used. Similarly, Student's *t*-test was used when comparing continuous variables. Cox proportional hazards model was used to calculate hazard ratios (HR) and their 95% confidence intervals (CI) in the pooled data. In multivariable analysis, variables were adjusted by age, smoking, diabetes, CAD, BMI, cholesterol, systolic blood pressure, heart rate, and the population sample. The statistical significance of the interaction effect between gender and prognostic value of each ECG variable was tested using the Cox regression analysis. In addition, Cox regression was applied separately for each cohort and the subsequent results were analyzed via random effects meta-analysis model in order to get the pooled hazard ratios and heterogeneity analyses (Cochrane's Q). For Cochranes Q, $P < 0.1$ was considered to represent statistically significant heterogeneity between populations. All statistical analyses were performed using Statistical Package for Social Studies version 26.0 (IBM SPSS Statistics) and R version 3.6.3 (R Foundation for Statistical Computing, Vienna, Austria.). We considered p-value of < 0.05 as statistically significant.

RESULTS

The standard 12-lead ECG markers were analyzed from 20,310 subjects (49.9% women, mean age 44.8 ± 8.7 years). Characteristics of the study population are represented in **Table 1**. On average women were slightly older at the time of baseline measurements in comparison to men, and they also had higher heart rate and longer QTc duration than men. Men had longer QRS complexes than women. There were considerably more smokers among men than in women in each study population combined, and men also had on average higher prevalence of diabetes mellitus. Prevalence for each end point were considerably higher among male subjects in comparison to female subjects. Approximately two fifth of the subjects who experienced cardiac death (40.6%, $N = 317$, $p < 0.001$) or SCD (40.0%, $N = 120$, $p < 0.001$) had CAD. The proportion of CAD was expectedly higher among male victims: 44.7 vs. 33.2% for men and women, (respectively) among subjects with cardiac death ($p < 0.001$), and 43.8 vs. 28.4% among victims of SCD ($p < 0.001$).

During the follow-up of 7.7 ± 1.2 years, a total of 296 cardiac deaths occurred of which 13.9% were among female subjects ($N = 41$, $p < 0.001$). The prevalence of different ECG markers is represented in **Table 2**. At least one ECG abnormality was present in 61.0% of the female victims of cardiac death. Only prevalence of fQRS was higher among women than in men, though the number of cases was so low that no statistically significant differences in the prevalence of ECG abnormalities between genders were detected. LVH with and without repolarization abnormalities, QTc prolongation > 470 ms and inferior or lateral T-wave inversions associated with the relative risk for cardiac death among women in univariate model but did not remain statistically significant after adjustments with age, smoking, diabetes, CAD, BMI, cholesterol, systolic blood pressure, heart rate, and the study sample (**Table 2**). Only extremely prolonged QTc time associated with higher risk for cardiac death among women than in men, but this ECG marker was found only from one woman. In random effects meta-analysis any of the ECG abnormalities were not statistically significant in women. However, statistically significant interaction effect was observed between gender and prognostic value of LVH (**Table 3**), and it provided stronger prognostic value for cardiac death in women than in men.

Among male subjects who had died for cardiac causes at least one ECG abnormality was present in 72.5%. The prevalence of each ECG variable, excluding fQRS, was slightly higher among male cardiac death victims in comparison to female cardiac death victims. Among men prolonged QRS duration, LVH with strain changes, inferior or lateral T-wave inversions and inferolateral ER predicted the occurrence of cardiac death in multivariate model (**Table 2**). In random effects meta-analysis prolonged QRS [HR: 3.0 (95% CI: 1.7–5.2, $P < 0.001$), Cochrane Q-value: 1.1

TABLE 1 | The baseline characteristics of each population sample.

	Finnish mobile clinic health examination survey, *N* = 10,807		Mini-finland health survey, *N* = 5,143		Health 2000 examination survey, *N* = 4,360	
	Female *N* = 5,167	**Male *N* = 5,640**	**Female *N* = 2,686**	**Male *N* = 2,457**	**Female *N* = 2,282**	**Male *N* = 2,078**
Continuous variables	**Mean ± SD**	**Mean ± SD**	**Mean ± SD**	**Mean ± SD**	**Mean ± SD**	**Mean ± SD**
Age (years)	44.3 ± 8.4	43.7 ± 8.5	44.9 ± 9.3	44.4 ± 9.1	45.4 ± 8.5	45.6 ± 8.4
BMI (kg/m^2)	26.2 ± 4.4	25.6 ± 3.3	25.5 ± 4.5	25.8 ± 3.5	26.1 ± 5.0	27.0 ± 4.2
Systolic blood pressure (mmHg)	138.1 ± 23.5	138.7 ± 19.5	137.9 ± 20.9	139.8 ± 18.2	125.9 ± 18.4	131.6 ± 16.6
Cholesterol (mmol/l)	6.5 ± 1.3	6.5 ± 1.3	3.9 ± 1.1	4.5 ± 1.3	5.7 ± 1.1	6.0 ± 1.1
QRS duration (ms)	84.8 ± 7.0	88.4 ± 7.8	82.6 ± 7.8	89.4 ± 8.8	86.5 ± 8.4	95.5 ± 10.1
QTc (ms)	415.2 ± 26.2	401.7 ± 27.1	419.5 ± 23.7	405.3 ± 23.8	416.9 ± 15.9	410.9 ± 15.6
Heart rate (1/min)	79.6 ± 15.5	72.0 ± 14.2	69.0 ± 12.7	64.7 ± 12.8	63.8 ± 10.3	62.3 ± 11.1
Categorial variables	**N (%)**	**N (%)**	**N (%)**	**N (%)**	**N (%)**	**N (%)**
QRS ≥ 110 ms	7 (0.1%)	59 (1.0%)	6 (0.2%)	42 (1.7%)	13 (0.6%)	166 (8.0%)
QTc ≥ 470 ms (W)/ ≥ 450 ms (M)	107 (2.1%)	232 (4.1%)	51 (1.9%)	75 (3.1%)	17 (0.7%)	31 (1.5%)
QTc ≥ 490 ms	16 (0.3%)	14 (0.2%)	14 (0.5%)	5 (0.2%)	2 (0.1%)	1 (0.0%)
LVH	1,058 (20.5%)	2,465 (43.8%)	139 (5.2%)	467 (19.0%)	76 (3.3%)	275 (13.2%)
LVH + T-wave inversion	6 (0.1%)	26 (0.5%)	8 (0.3%)	20 (0.8%)	3 (0.1%)	2 (0.1%)
Inferior or lateral T-wave inversion	29 (0.6%)	45 (0.8%)	31 (1.2%)	36 (1.5%)	6 (0.3%)	7 (0.3%)
Inferolateral ER	224 (4.3%)	406 (7.2%)	361 (13.4%)	472 (19.2%)	35 (1.5%)	130 (6.3%)
Lateral ER	111 (2.2%)	151 (2.8%)	194 (7.2%)	183 (7.4%)	28 (1.2%)	101 (4.9%)
Inferior ER	114 (2.3%)	270 (4.9%)	174 (6.5%)	313 (12.7%)	10 (0.4%)	50 (2.4%)
Inferolateral ER + horizontal/ descending ST-segment	175 (3.4%)	225 (4.1%)	238 (8.9%)	295 (12.0%)	22 (1.0%)	56 (2.7%)
Any fQRS	778 (15.2%)	1,196 (21.4%)	465 (17.3%)	418 (17.0%)	1,324 (58.2%)	1,392 (68.6%)
Lateral fQRS	30 (0.7%)	52 (1.2%)	48 (1.8%)	48 (2.0%)	818 (36.0%)	1,050 (51.7%)
Inferior fQRS	650 (13.0%)	1,062 (19.5%)	375 (14.0%)	327 (13.3%)	701 (30.8%)	592 (29.2%)
Anterior fQRS	141 (3.1%)	173 (3.8%)	65 (2.4%)	68 (2.8%)	163 (7.2%)	146 (7.2%)
Smoking	680 (13.2%)	2,990 (53.0%)	431 (16.0%)	964 (39.2%)	502 (22.1%)	653 (31.5%)
Diabetes	82 (1.6%)	111 (2.0%)	58 (2.2%)	90 (3.7%)	54 (2.4%)	103 (5.0%)
CAD	753 (14.6%)	714 (12.7%)	110 (4.1%)	156 (6.3%)	13 (0.6%)	56 (2.7%)
Cardiac death	22 (0.4%)	154 (2.7%)	12 (0.4%)	73 (3.0%)	7 (0.3%)	28 (1.3%)
Sudden cardiac death	12 (0.2%)	73 (1.3%)	6 (0.2%)	26 (1.1%)	4 (0.2%)	28 (1.4%)
All-cause mortality	115 (2.2%)	408 (7.2%)	63 (2.3%)	174 (7.1%)	38 (1.7%)	85 (4.1%)

For categorical variables values are presented as number of cases within genders and corresponding percentage within brackets. Continuous values are presented as mean with standard deviation (SD) below to it. Underlined values differed statistically significantly ($p < 0.05$) between genders. BMI, body mass index; CAD, coronary artery disease; SD, standard deviation.

($P = 0.582$)] and inferior or lateral T-wave inversion [HR: 3.8 (95% CI: 2.0–7.0, $P < 0.001$), Cochrane *Q*-value: 2.5 ($P = 0.293$)] remained statistically significant in competing risks regression multivariable model and associated with cardiac death, as well as any ECG abnormality [HR: 1.6 (95% CI: 1.0–2.4, $P = 0.035$), Cochrane *Q*-value: 3.0 ($P = 0.229$)].

The prognostic value of ECG variables for SCD and all-cause mortality are shown in **Tables 4**, **5**. T-wave inversions, extremely prolonged QTc and LVH remained statistically significant predictors for SCD in multivariable analysis both in women and in men. In men, T-wave inversion [HR: 3.2 (95% CI: 1.7–6.1, $P = 0.001$), Cochrane *Q*-value: 1.9 ($P = 0.386$)] and LVH [HR: 1.6 (95% CI: 1.1–2.4, $P = 0.025$), Cochrane *Q*-value: 0.158 ($P = 0.924$)] remained statistically significant risk factors for SCD also in random effect meta-analysis as did any ECG abnormality [HR: 1.7 (95% CI: 1.1–2.7, $P = 0.011$), Cochrane *Q*-value: 0.630 ($P = 0.730$)] and prolonged QRS duration [HR: 3.4 (95% CI: 1.8–6.4, $P < 0.001$), Cochrane *Q*-value: 1.1 ($P = 0.573$)]. Any of the ECG variables were not statistically significant among women in random effect meta-analysis, and no statistically

TABLE 2 | The gender differences in the prevalence and risks for cardiac death of each ECG risk marker with 8 years follow-up time.

	Women, *N* = 41					**Men, *N* = 255**				
	Unadjusted			**Adjusted**		**Unadjusted**			**Adjusted**	
	N (%)	**HR (95% CI)**	***P*-value**	**HR (95% CI)**	***P*-value**	**N (%)**	**HR (95% CI)**	***P*-value**	**HR (95% CI)**	***P*-value**
Any ECG abnormality	25 (61.0%)	**2.2 (1.2–4.2)**	**0.012**	1.6 (0.80–3.1)	0.185	182 (72.5%)	**1.7 (1.3–2.2)**	**<0.001**	**1.6 (1.2–2.1)**	**0.002**
QRS ≥ 110 ms	0 (0.0%)	No events		No events		14 (5.5%)	**2.2 (1.3–3.8)**	**0.004**	**3.1 (1.8–5.3)**	**<0.001**
QTc ≥ 470 ms (W)/ ≥ 450 ms (M)	3 (7.3%)	**4.6 (1.4–14.9)**	**0.011**	3.2 (0.95–10.9)	0.061	23 (9.2%)	**3.1 (2.0–4.7)**	**<0.001**	1.3 (0.80–2.0)	0.306
QTc ≥ 490 ms	**1 (2.4%)**	**8.0 (1.1–58.1)**	**0.040**	**9.4 (1.2–71.7)**	**0.031**	1 (0.4%)	2.5 (0.35–17.9)	0.357	1.4 (0.19–10.2)	0.737
LVH	13 (31.7%)	**3.3 (1.7–6.3)**	**<0.001**	1.8 (0.79–3.9)	0.167	97 (38.2%)	**1.4 (1.1–1.7)**	**<0.019**	1.2 (0.90–1.6)	0.209
LVH + T-wave inversion	2 (4.9%)	**38.5 (9.3–159.4)**	**<0.001**	3.2 (0.40–25.3)	0.275	13 (5.1%)	**17.0 (9.7–29.8)**	**<0.001**	**3.4 (1.9–6.2)**	**<0.001**
Inferior or lateral T-wave inversion	3 (7.3%)	**12.9 (4.0–41.7)**	**<0.001**	2.0 (0.47–8.8)	0.341	26 (10.2%)	**17.8 (11.8–26.7)**	**<0.001**	**4.3 (2.8–6.7)**	**<0.001**
Inferolateral ER	2 (4.9%)	0.79 (0.19–3.3)	0.748	0.64 (0.15–2.7)	0.542	31 (12.2%)	1.3 (0.87–1.8)	0.218	1.1 (0.78–1.7)	0.438
Lateral ER	1 (2.4%)	0.74 (0.10–5.4)	0.766	0.54 (0.07–4.1)	0.553	11 (4.4%)	1.0 (0.55–1.8)	0.978	1.0 (0.56–1.9)	0.904
Inferior ER	1 (2.5%)	0.84 (0.12–6.1)	0.859	0.77 (0.10–5.8)	0.799	22 (8.8%)	1.5 (0.94–2.3)	0.091	1.3 (0.80–2.0)	0.326
Inferolateral ER + horizontal/ descending ST-segment	2 (4.9%)	1.2 (0.28–4.8)	0.847	1.6 (0.38–6.9)	0.511	19 (7.6%)	1.4 (0.86–2.2)	0.192	**1.7 (1.0–2.7)**	**0.033**
Any fQRS	14 (34.1%)	1.5 (0.80–2.9)	0.197	1.6 (0.78–3.3)	0.197	77 (31.0%)	1.1 (0.81–1.4)	0.685	1.3 (0.97–1.7)	0.079
Lateral fQRS	6 (16.2%)	1.8 (0.77–4.4)	0.171	2.4 (0.64–9.3)	0.188	25 (11.5%)	0.88 (0.56–1.3)	0.537	1.7 (0.99–3.0)	0.054
Inferior fQRS	8 (20.0%)	1.2 (0.55–2.6)	0.641	1.1 (0.49–2.6)	0.777	50 (20.8%)	1.1 (0.77–1.4)	0.725	1.2 (0.86–1.62)	0.300
Anterior fQRS	3 (8.3%)	2.2 (0.69–7.3)	0.181	2.3 (0.69–7.7)	0.175	13 (6.0%)	1.4 (0.82–2.5)	0.195	1.3 (0.70–2.2)	0.464

CI, confidence interval; ER, early repolarization; fQRS, fragmented QRS; HR, hazard ratio; LVH, left ventricular hypertrophy. Results are adjusted by age, smoking, diabetes, CAD, BMI, cholesterol, systolic blood pressure, heart rate, and the study sample. Statistically significant values $p < 0.05$ are written in bold.

TABLE 3 | The interaction effect between sex and the prognostic value of each ECG variable.

	Women vs. Men								
	Cardiac death			**SCD**			**All-cause mortality**		
	HR	**95% CI**	***P*-value**	**HR**	**95% CI**	***P*-value**	**HR**	**95% CI**	***P*-value**
Any ECG abnormality	1.3	0.67–2.6	0.419	1.4	0.51–3.7	0.532	**1.7**	**1.2–2.3**	**0.001**
QRS ≥ 110 ms	No events in women			No events in women			1.2	0.16–8.8	0.868
QTc ≥ 470 ms (W)/ ≥ 450 ms (M)	1.5	0.43–5.2	0.530	2.0	0.42–9.8	0.384	0.91	0.44–1.9	0.914
QTc ≥ 490 ms	0.32	0.02–5.2	0.420	0.33	0.02–5.4	0.437	1.9	0.39–9.7	0.420
Inferior or lateral T-wave inversion	0.72	0.21–2.5	0.600	0.92	0.19–4.4	0.913	0.81	0.40–1.7	0.561
LVH	**2.4**	**1.2–4.9**	**0.014**	2.5	0.99–6.4	0.053	**1.7**	**1.2–2.4**	**0.003**
LVH + T-wave inversion	2.2	0.48–10.1	0.311	1.6	0.20–13.8	0.649	2.3	0.95–5.4	0.064
Inferolateral ER	0.63	0.14–2.7	0.531	0.85	0.10–6.9	0.877	1.6	0.98–2.6	0.059
Lateral ER	0.73	0.09–5.8	0.768		No events		**3.1**	**1.6–5.7**	**<0.001**
Inferior ER	1.1	0.13–8.9	0.938	0.93	0.09–9.2	0.949	0.73	0.31–1.7	0.482
Inferolateral ER + horizontal/ descending ST-segment	0.84	0.19–3.8	0.821	1.3	0.15–11.2	0.824	1.2	0.65–2.2	0.548
Any fQRS	1.4	0.72–2.9	0.301	1.0	0.40–2.8	0.923	**1.6**	**1.1–2.2**	**0.009**
Lateral fQRS	2.1	0.79–5.5	0.133	0.71	0.97–2.6	0.064	**1.8**	**1.1–3.0**	**0.014**
Inferior fQRS	1.1	0.49–2.6	0.764	1.1	0.33–3.4	0.919	0.82	no events	0.986
Anterior fQRS	1.5	0.42–5.7	0.514	0.97	0.11–8.6	0.980	**1.8**	0.35–1.9	0.647

Interactions between gender and ECG risk markers were assessed using Cox regression analysis.
CI , confidence interval; ER, early repolarization; fQRS, fragmented QRS; HR, hazard ratio; LVH, left ventricular hypertrophy; SCD, sudden cardiac death. HR, hazard ratio. Statistically significant values ($p < 0.05$) are written in bold.

TABLE 4 | The gender differences in the prevalence and risks for sudden cardiac death of each ECG risk marker with 8 years follow-up time.

	Women, *N* = 22					Men, *N* = 127				
	Unadjusted			Adjusted		Unadjusted			Adjusted	
	N (%)	HR (95% CI)	*P*-value	HR (95%CI)	*P*-value	N (%)	HR (95% CI)	*P*-value	HR (95% CI)	*P*-value
Any ECG abnormality	15 (68.2%)	**3.1 (1.3–7.5)**	**0.014**	2.3 (0.90–5.8)	0.084	98 (77.8%)	**2.2 (1.5–3.4)**	**<0.001**	**1.9 (1.3–2.9)**	**0.003**
QRS ≥ 110 ms	0 (0.0%)	No events		No events		11 (8.7%)	**3.6 (1.9–6.7)**	**<0.001**	**3.7 (1.9–7.0)**	**<0.001**
QTc ≥ 470 ms (W)/ ≥ 450 ms (M)	2 (9.1%)	**5.8 (1.4–24.9)**	**0.018**	4.2 (0.93–19.0)	0.063	11 (8.7%)	**2.9 (1.5–5.3)**	**0.001**	1.3 (0.67–2.5)	0.437
QTc ≥ 490 ms	**1 (4.5%)**	**15.2 (2.0–113.2)**	**0.008**	**14.8 (1.8–119.1)**	**0.011**	1 (0.8%)	4.9 (0.69–35.3)	0.112	**2.4 (1.0–5.4)**	**0.039**
Inferior or lateral T-wave inversion	2 (9.1%)	**16.3 (3.8–69.8)**	**<0.001**	**5.4 (1.1–25.6)**	**0.033**	13 (10.2%)	**17.5 (9.9–31.1)**	**<0.001**	**4.6 (2.5–8.5)**	**<0.001**
LVH	8 (36.4%)	**4.0 (1.7–9.6)**	**0.002**	**2.8 (1.0–7.8)**	**0.047**	53 (42.1%)	**1.6 (1.1–2.3)**	**0.010**	**1.7 (1.2–2.6)**	**0.008**
LVH + T-wave inversion	1 (4.5%)	**36.1 (4.8–268.3)**	**<0.001**	8.0 (0.88–71.9)	0.064	8 (6.3%)	**21.0 (10.3–43.1)**	**<0.001**	**5.3 (2.4–11.4)**	**<0.001**
Inferolateral ER	1 (4.5%)	0.74 (0.10–5.5)	0.765	0.61 (0.08–4.8)	0.639	11 (8.7%)	0.87 (0.47–1.6)	0.651	0.90 (0.48–1.7)	0.732
Lateral ER	0 (0.0%)	No events		No events		1 (0.8%)	0.18 (0.03–1.3)	0.084	0.20 (0.03–1.4)	0.104
Inferior ER	1 (4.5%)	1.6 (0.21–11.5)	0.668	1.6 (0.20–12.6)	0.658	11 (8.7%)	1.4 (0.77–2.6)	0.261	1.5 (0.78–2.8)	0.239
Inferolateral ER + horizontal/ descending ST-segment	1 (4.5%)	1.1 (0.14–7.9)	0.949	1.5 (0.20–11.4)	0.699	6 (4.8%)	0.83 (0.37–1.9)	0.663	1.1 (0.48–2.5)	0.819
Any fQRS	7 (31.8%)	1.4 (0.56–3.4)	0.485	1.4 (0.52–3.7)	0.504	43 (35.8%)	1.3 (0.90–1.9)	0.154	1.3 (0.84–1.9)	0.270
Lateral fQRS	2 (10.5%)	1.1 (0.26–4.8)	0.880	0.98 (0.16–6.1)	0.986	20 (19.0%)	1.6 (0.97–2.6)	0.064	1.7 (0.86–3.3)	0.127
Inferior fQRS	4 (18.2%)	1.1 (0.36–3.2)	0.904	1.1 (0.36–3.2)	0.906	23 (20.0%)	1.0 (0.64–1.6)	0.984	1.0 (0.66–1.6)	0.866
Anterior fQRS	1 (5.3%)	1.4 (0.18–10.3)	0.760	1.3 (0.16–9.7)	0.828	6 (5.9%)	1.4 (0.62–3.2)	0.417	1.1 (0.48–2.5)	0.815

CI, confidence interval; ER, early repolarization; fQRS, fragmented QRS; HR, hazard ratio; LVH, left ventricular hypertrophy. Results are adjusted by age, smoking, diabetes, CAD, BMI, cholesterol, systolic blood pressure, heart rate, and the study sample. Statistically significant values ($p < 0.05$) are written in bold.

significant interaction between gender and the ECG variables were seen for SCD. LVH, prolonged QRS duration and any ECG abnormality associated with moderately higher risk of SCD among subjects with prior CAD. LVH with repolarization abnormalities and T wave inversions associated with considerably higher risk among SCD victims without prior CAD but number of cases was substantially low. Differences among SCD victims with and without prior CAD are represented in **Table 6**. For all-cause mortality statistically significant interactions between gender and LVH, lateral ER, total and lateral fQRS as well as any ECG abnormality were seen, the abnormalities having greater prognostic value in women than in men.

DISCUSSION

In the current study, the gender differences in the prevalence and prognostic value of different ECG markers were studied in a large middle-aged general population, and many differences between men and women were found. The prevalence of all endpoints was considerably higher in men than in women. Women had more often a normal electrocardiogram compared to men. Electrocardiographic LVH seemed to have different prognostic value between middle-aged men and women.

The prevalence of all endpoints in the current study were considerably higher among men which is in line with the previous reports (Kannel et al., 1998; Albert et al., 2003; Haukilahti et al., 2019). The risk of CAD increases considerably with age among both genders (Jousilahti et al., 1999). Approximately 40% of the subjects with cardiac death or SCD had CAD, and the relatively low proportion of CAD can be largely explained with the mean age of the study population. The proportion of CAD was expectedly higher among male subjects with cardiac endpoint. Both CAD (Airaksinen et al., 2016) and SCD (Kannel et al., 1998) have been shown to occur approximately 10 years later in women than in men. However, the prevalence of CVD among women has been reported to equal that of men with advancing age (Maffei et al., 2019). In addition, the prevalence of any vascular disease has been shown to be higher with each decade of life, and each additional decade of life approximately doubles the risk of vascular disease (Savji et al., 2013).

The presence of any ECG abnormality was significantly more commonly found among male subjects who had experienced cardiac death in comparison to their female counterparts. Two fifths of the female cardiac death victims did not have any prior ECG abnormalities while approximately a quarter of the male victims had a normal electrocardiogram. The difference in the proportion of normal electrocardiograms narrowed in SCD victims, yet the gender difference still existed.

In the present study, ECG signs of LVH was found to be more prevalent among men who had experienced cardiac death, yet the overall number of subjects with ECG sign of LVH was low in both

TABLE 5 | The gender differences in the prevalence and risks for all-cause mortality of each ECG risk marker with 8 years follow-up time.

	Women, *N* = 216					**Men, *N* = 667**				
	Unadjusted			**Adjusted**		**Unadjusted**			**Adjusted**	
	N (%)	**HR (95% CI)**	***P*-value**	**HR (95% CI)**	***P*-value**	**N (%)**	**HR (95% CI)**	***P*-value**	**HR (95% CI)**	***P*-value**
Any ECG abnormality	131 (60.9%)	**2.2 (1.7–2.9)**	**<0.001**	**1.8 (1.4–2.4)**	**<0.001**	445 (67.5%)	**1.3 (1.1–1.6)**	**0.001**	**1.2 (1.0–1.5)**	**0.012**
QRS ≥ 110 ms	**1 (0.5%)**	1.8 (0.26–13.0)	0.548	1.7 (0.24–12.1)	0.601	**26 (3.9%)**	**1.5 (1.0–2.3)**	**0.032**	**1.9 (1.3–2.8)**	**0.002**
QTc ≥ 470 ms (W)/ ≥ 450 ms (M)	**9 (4.2%)**	**2.5 (1.3–4.9)**	**0.006**	1.6 (0.81–3.1)	0.182	**55 (8.4%)**	**2.8 (2.1–3.6)**	**<0.001**	1.3 (0.96–1.7)	0.090
QTc ≥ 490 ms	2 (0.9%)	3.0 (0.74–12.0)	0.123	1.7 (0.42–7.1)	0.444	**6 (0.9%)**	**5.8 (2.6–12.9)**	**<0.001**	**2.4 (1.0–5.4)**	**0.039**
Inferior or lateral T-wave inversion	10 (4.6%)	**7.9 (4.2–14.9)**	**<0.001**	**2.7 (1.4–5.5)**	**0.005**	39 (5.8%)	**9.7 (7.0–13.4)**	**<0.001**	**3.1 (2.2–4.4)**	**<0.001**
LVH	**50 (23.1%)**	**4.0 (1.7–9.6)**	**0.002**	**1.5 (1.0–2.1)**	**0.032**	**239 (36.0%)**	**1.6 (1.1–2.3)**	**0.010**	1.1 (0.91–1.3)	0.369
LVH + T-wave inversion	7 (3.2%)	**24.9 (11.7–52.8)**	**<0.001**	**7.4 (3.1–17.3)**	**<0.001**	22 (3.3%)	**10.8 (7.1–16.5)**	**<0.001**	**3.0 (1.9–4.8)**	**<0.001**
Inferolateral ER	23 (10.6%)	**1.8 (1.2–2.8)**	**0.006**	1.5 (0.98–2.4)	0.062	74 (11.1%)	1.1 (0.90–1.5)	0.283	1.1 (0.84–1.4)	0.543
Lateral ER	**18 (8.3%)**	**2.7 (1.7–4.4)**	**<0.001**	**2.1 (1.3–3.5)**	**0.003**	**25 (3.9%)**	0.88 (0.59–1.3)	0.521	0.92 (0.61–1.4)	0.673
Inferior ER	**6 (2.9%)**	0.96 (0.43–2.2)	0.917	0.84 (0.37–1.9)	0.674	**52 (8.0%)**	1.3 (0.98–1.7)	0.067	1.2 (1.90–1.6)	0.227
Inferolateral ER + horizontal/ descending ST-segment	14 (6.5%)	1.6 (0.90–2.7)	0.111	**1.8 (1.0–3.1)**	**0.039**	47 (7.2%)	1.3 (0.96–1.7)	0.098	**1.5 (1.1–2.1)**	**0.007**
Any fQRS	71 (27.5%)	**1.5 (1.1–1.9)**	**0.010**	**1.5 (1.1–2.1)**	**0.007**	187 (28.5%)	0.94 (0.79–1.1)	0.448	1.1 (0.91–1.3)	0.374
Lateral fQRS	27 (14.2%)	**1.6 (1.0–2.4)**	**0.029**	**2.0 (1.1–3.4)**	**0.017**	66 (11.3%)	0.86 (0.67–1.1)	0.256	**1.5 (1.1–2.1)**	**0.025**
Inferior fQRS	50 (23.5%)	**1.5 (1.1–2.0)**	**0.016**	**1.5 (1.1–2.1)**	**0.018**	127 (19.7%)	0.99 (0.81–1.2)	0.897	1.1 (0.87–1.3)	0.582
Anterior fQRS	7 (3.7%)	0.94 (0.44–2.0)	0.866	0.94 (0.44–2.0)	0.881	28 (4.8%)	1.1 (0.78–1.7)	0.494	1.1 (0.72–1.6)	0.763

CI, confidence interval; ER, early repolarization; fQRS, fragmented QRS; HR, hazard ratio; LVH, left ventricular hypertrophy. Statistically significant values ($p < 0.05$) are written in bold. Results are adjusted by age, smoking, diabetes, CAD, BMI, cholesterol, systolic blood pressure, heart rate, and the study sample.

genders leading to lack of statistical power in the multivariate model. However, in the gender interaction analysis the prognostic value of LVH for cardiac death and all-cause mortality was stronger in women than in men. The risk of cardiovascular events among asymptomatic subjects is 1.6-fold in subjects with LVH, and slightly higher among women than in men (Chou et al., 2011). Previously, LVH has also been associated with the risk of cardiovascular mortality (Prineas et al., 2001). In a study by Desai et al. (2012), the risk of cardiovascular mortality was over eightfold among women without clinical CVD but the presence of ECG sign of LVH defined by criteria of Sokolow-Lyon, and nearly fivefold in men. In addition, the risk of adverse outcomes was found to be higher in each subgroup and among both genders if LVH co-existed with repolarization abnormalities. Previously, in a large middle aged general population cohort the ECG sign of LVH observed with strain pattern was associated with over sixfold risk for CAD event in white men and over twofold risk in black women (Machado et al., 2006). In a current study the general population sample was even larger than in those two studies with similar kind of findings. In the present study LVH with inferolateral T wave inversion associated with increased relative risk for cardiac death in men, yet the number of cases was limited. Previously, T-wave inversions and changes in ST segment with ECH LVH are associated with more severe LVH and elevated risk of adverse outcomes (Hancock et al., 2009; Rautaharju et al., 2009; Bang et al., 2014).

Prolonged QRS duration is a well-known marker of adverse prognosis in subjects with cardiac disease (Kashani and Barold, 2005; Schinkel et al., 2009) but also in the general population (Aro et al., 2011). However, the previous literature on sex differences in prognostic value of QRS prolongation is sparse. In the current study, prolonged QRS duration was more prevalent among male subjects who experienced cardiac death and it was associated with higher relative risk for cardiac death among men than among women. Other known risk factors for cardiovascular events are changes in ST segment and T-wave (Chou et al., 2011). In the current study we did not assess ST segment changes alone. T-wave inversions were slightly more commonly found among women than in men who had experienced cardiac death, yet they remained statistically significant in a multivariate model for this endpoint only among men. Previously T-wave abnormalities have been associated with 1.6–2.1 -fold risk for CAD in the general population (Machado et al., 2006; Chou et al., 2011) and inferolateral T-wave inversions also to increased risk for cardiac death and SCD (Aro et al., 2012; Laukkanen et al., 2014). However, the information of gender differences in prognostic value of T wave inversions is sparse. In a current study, T-wave inversions and LVH remained significant predictors of SCD in multivariable analysis also in women. No gender interaction was seen in any of the variables as predictors of SCD. These data show that ECG may be even better independent predictor

TABLE 6 | Differences in the prevalence and risks for sudden cardiac death among subjects with and without previous coronary artery disease.

	SCD victims without prior CAD, *N* = 93					**SCD victims with prior CAD, *N* = 56**				
		Unadjusted		**Adjusted**			**Unadjusted**		**Adjusted**	
	N (%)	**HR (95% CI)**	***P*-value**	**HR (95%CI)**	***P*-value**	**N (%)**	**HR (95% CI)**	***P*-value**	**HR (95% CI)**	***P*-value**
Any ECG abnormality	66 (71.7%)	**2.5 (1.6–3.9)**	**<0.001**	**1.9 (1.2–3.0)**	**0.009**	47 (83.9%)	**4.0 (2.0–8.2)**	**<0.001**	**3.6 (1.7–7.4)**	**0.001**
QRS ≥ 110 ms	**6 (6.5%)**	**5.0 (2.2–11.3)**	**<0.001**	**3.7 (1.6–8.7)**	**0.002**	**5 (8.9%)**	**5.5 (2.2–13.9)**	**<0.001**	**7.5 (2.8–19.7)**	**<0.001**
QTc ≥ 470 ms (W)/ ≥ 450 ms (M)	6 (6.5%)	**3.1 (1.4–7.2)**	**0.007**	1.7 (0.71–4.0)	0.233	7 (12.5%)	**2.4 (1.1–5.3)**	**0.031**	2.0 (0.88–4.7)	0.098
QTc ≥ 490 ms	1 (1.1%)	5.0 (0.69–35.7)	0.111	3.0 (0.40–21.9)	0.286	1 (1.8%)	4.0 (0.56–29.1)	0.168	4.0 (0.51–32.1)	0.188
Inferior or lateral T-wave inversion	7 (7.5%)	**27.5 (12.7–59.4)**	**<0.001**	**15.8 (6.8–36.7**)	**<0.001**	8 (14.3%)	**3.7 (1.7–7.8)**	**0.001**	**2.8 (1.3–6.1)**	**0.009**
LVH	32 (34.4%)	**2.0 (1.3–3.1)**	**0.002**	**1.9 (1.2–3.1)**	**0.009**	29 (52.7%)	**2.3 (1.4–3.9)**	**0.002**	**2.7 (1.5–4.8)**	**0.001**
LVH + T-wave inversion	**2 (2.2%)**	**25.0 (6.1–101.4)**	**<0.001**	**9.3 (2.1–41.1)**	**0.003**	**7 (12.7%)**	**8.0 (3.6–17.7)**	**<0.001**	**6.1 (2.5–14.6)**	**<0.001**
Inferolateral ER	6 (6.5%)	0.81 (0.35–1.8)	0.615	0.82 (0.35–1.9)	0.644	6 (10.7%)	1.2 (0.53–2.9)	0.623	1.2 (0.49–2.7)	0.748
Lateral ER	1 (1.1%)	0.28 (0.04–2.0)	0.201	0.29 (0.04–2.1)	0.224	0 (0.0%)	No events		No events	
Inferior ER	6 (6.5%)	1.5 (0.64–3.3)	0.367	1.5 (0.65–3.5)	0.333	6 (10.7%)	2.1 (0.88–4.8)	0.096	1.8 (0.75–4.3)	0.188
Inferolateral ER + horizontal/ descending ST-segment	4 (4.3%)	0.88 (0.32–2.4)	0.793	1.3 (0.47–3.5)	0.629	3 (5.4%)	1.0 (0.33–3.3)	0.940	1.1 (0.34–3.5)	0.897
Any fQRS	33 (36.7%)	1.5 (0.97–2.3)	0.072	1.2 (0.74–2.0)	0.437	17 (32.7%)	1.8 (0.99–3.2)	0.053	1.5 (0.82–2.7)	0.195
Lateral fQRS	17 (20.2%)	**1.9 (1.1–3.3)**	**0.017**	1.5 (0.71–3.0)	0.307	5 (12.5%)	**2.9 (1.1–7.5)**	**0.025**	2.7 (0.96–7.8)	0.059
Inferior fQRS	15 (16.9%)	0.88 (0.50–1.5)	0.645	0.83 (0.48–1.5)	0.523	12 (25.0%)	1.7 (0.90–3.3)	0.101	1.6 (0.81–3.0)	0.190
Anterior fQRS	5 (6.0%)	1.5 (0.62–3.8)	0.349	1.3 (0.53–3.3)	0.541	2 (5.3%)	1.1 (0.26–4.4)	0.930	0.77 (0.18–3.2)	0.716

CAD, coronary artery disease; CI, confidence interval; ER, early repolarization; fQRS, fragmented QRS; HR, hazard ratio; LVH, left ventricular hypertrophy. Results are adjusted by age, smoking, diabetes, CAD, BMI, cholesterol, systolic blood pressure, heart rate, medication for hypertension and the study sample. Statistically significant values ($p < 0.05$) are written in bold.

of more specific modes of death, such as SCD, in women. Cardiac death can be due to many different mechanisms, which may explain why it is not well predicted by standard ECG, especially in women.

We pooled the data from three different population samples, because the event rates in single samples are relatively low in women. This is an obvious limitation of the study. The study populations represent the Finnish general population from different decades and treatments for cardiac diseases have developed dramatically during the follow-up period. On this account all results might not be completely transferable to current decade even though a quarter of the population was studied in the twenty-first century. It is also possible that the health behavior has changed considerably during the decades. However, the populations were quite homogenous in terms of cardiovascular risk factors. The lack of other ethnicities may also be considered as a limitation of our study. Regarding the ECG variables determined in this study, standard QTc limits for men and women were used (Rautaharju et al., 2009), but there is no uniformly accepted gender-specific limits for QRS duration, even though there is a subtle difference in QRS duration between men and women. Therefore, QRS > 110 ms was used as a cut-off point in the study and the selected cut off point in the study and the selected cut off point was based on one large retrospective register study (Desai et al., 2006). In addition, LVH could have been more definitely diagnosed by echocardiography, which was not available at the start of the collection of these populations. However, recently ECG LVH has supposed to be at least partly distinct entity from echocardiographic LVH (Aro and Chugh, 2016) and also to be independently prognostic for cardiovascular mortality and morbidity with similar level as LVH diagnosed by magnetic resonance imaging (Bacharova et al., 2015). To our knowledge, this is the largest study which has been conducted to determine the prevalence and prognostic significance of multiple ECG variants for cardiac mortality, SCD and all-cause mortality in the middle-aged general population. Still, the event rate in SCD, especially among women, remains low due to the nature of SCD which causes challenges in obtaining enough statistical power when performing gender stratified analysis.

In conclusion, we studied the impact of gender on the prevalence and prognostic value of different ECG markers in a large middle-aged general population. All mortality endpoints were more commonly found among male subjects. The prevalence of all ECG variables apart from fQRS was higher among men in comparison to women. Based on this study, electrocardiographic LVH has a slightly different prognostic value between middle-aged men and women, with more pronounced prognostic value for cardiac death among women. Similarly, T-wave inversions, prolonged QRS duration

and inferolateral ER were associated with increased risk of cardiac death only among men.

DATA AVAILABILITY STATEMENT

Publicly available datasets were analyzed in this study. This data can be found here: https://thl.fi/.

ETHICS STATEMENT

The studies involving human participants were reviewed and approved by the Ethics Committee of Northern Ostrobothnia Hospital District. Written informed consent for participation was not required for this study in accordance with the national legislation and the institutional requirements.

AUTHOR CONTRIBUTIONS

HH and MH: conceptualization. AE, AH, MH, PK, HR, MJ, TK, JT, AA, and OA: data curation. MH and TK: investigation, methodology, and visualization. HH and MJ: project administration and supervision. TK: software. MH: writing—original draft. TK, HH, MJ, AE, AH, PK, HR, JT, AA, and OA: writing—review and editing. All authors contributed to the article and approved the submitted version.

ACKNOWLEDGMENTS

We thank the Juho Vainio Foundation, The Maud Kuistila Memorial Foundation, The Finnish Medical Foundation, Finnish Foundation for Cardiovascular Research, The Paulo Foundation, Aarne Koskelo Foundation, and Päivikki and Sakari Sohlberg Foundation.

REFERENCES

Airaksinen, J., Aalto-Setälä, K., Hartikainen, J., Huikuri, H., Laine, M., Lommi, J., et al. (2016). *Kardiogia: Sepelvaltimotaudin Vaaratekijät ja Ateroskleroosi*, 3rd Edn. Helsinki: Duodecim.

Albert, C. M., Chae, C. U., Grodstein, F., Rose, L. M., Rexrode, K. M., Ruskin, J. N., et al. (2003). Prospective study of sudden cardiac death among women in the United States. *Circulation* 107, 2096–2101. doi: 10.1161/01.CIR.0000065223.21530.11

Aro, A. L., Anttonen, O., Tikkanen, J. T., Junttila, M. J., Kerola, T., Rissanen, H. A., et al. (2011). Intraventricular conduction delay in a standard 12-lead electrocardiogram as a predictor of mortality in the general population. *Circ. Arrhythm Electrophysiol.* 4, 704–710. doi: 10.1161/CIRCEP.111.963561

Aro, A. L., Anttonen, O., Tikkanen, J. T., Junttila, M. J., Kerola, T., Rissanen, H. A., et al. (2012). Prevalence and prognostic significance of T-Wave inversions in right precordial leads of a 12-lead electrocardiogram in the middle-aged subjects. *Circulation* 125, 2572–2577. doi: 10.1161/CIRCULATIONAHA.112.098681

Aro, A. L., and Chugh, S. S. (2016). Clinical diagnosis of electrical versus anatomic left ventricular hypertrophy. *Circ. Arrhythmia Electrophysiol.* 9:e003629. doi: 10.1161/CIRCEP.115.003629

Bacharova, L., Chen, H., Estes, E. H., Mateasik, A., Bluemke, D. A., Lima, J. A., et al. (2015). Determinants of discrepancies in detection and comparison of the prognostic significance of left ventricular hypertrophy by electrocardiogram and cardiac magnetic resonance imaging. *Am. J. Cardiol.* 115, 515–522. doi: 10.1016/j.amjcard.2014.11.037

Bang, C. N., Devereux, R. B., and Okin, P. M. (2014). Regression of electrocardiographic left ventricular hypertrophy or strain is associated with lower incidence of cardiovascular morbidity and mortality in hypertensive patients independent of blood pressure reduction - A LIFE review. *J. Electrocardiol.* 47, 630–635. doi: 10.1016/j.jelectrocard.2014.07.003

Benjamin, E. J., Virani, S. S., Callaway, C. W., Chamberlain, A. M., Chang, A. R., Cheng, S., et al. (2018). Heart disease and stroke statistics – 2018 update: a report from the American Heart Association. *Circulation* 137, E67–E492. doi: 10.1161/CIR.0000000000000558

Chou, R., Arora, B., Dana, T., Fu, R., Walker, M., and Humphrey, L. (2011). Screening asymptomatic adults with resting or exercise electrocardiography: a review of the evidence for the U.S. Preventive Services Task Force. *Ann. Intern. Med.* 155, 375–385. doi: 10.7326/0003-4819-155-6-201109200-00006

Desai, A. D., Yaw, T. S., Yamazaki, T., Kaykha, A., Chun, S., and Froelicher, V. F. (2006). Prognostic significance of quantitative QRS duration. *Am. J. Med.* 119, 600–606. doi: 10.1016/j.amjmed.2005.08.028

Desai, C. S., Ning, H., and Lloyd-Jones, D. M. (2012). Competing cardiovascular outcomes associated with electrocardiographic left ventricular hypertrophy: the atherosclerosis risk in communities study. *Heart* 98, 330–334. doi: 10.1136/heartjnl-2011-300819

Greene, H. L., Richardson, D. W., Barker, A. H., Roden, D. M., Capone, R. J., Echt, D. S., et al. (1989). Classification of deaths after myocardial infarction as arrhythmic or nonarrhythmic (The Cardiac Arrhythmia Pilot Study). *Am. J. Cardiol.* 63, 1–6. doi: 10.1016/0002-9149(89)91065-5

Greenland, P., Knoll, M. D., Stamler, J., Neaton, J. D., Dyer, A. R., Garside, D. B., et al. (2003). Major risk factors as antecedents of fatal and nonfatal coronary heart disease events. *J. Am. Med. Assoc.* 290, 891–897. doi: 10.1001/jama.290.7.891

Hancock, E. W., Deal, B. J., Mirvis, D. M., Okin, P., Kligfield, P., and Gettes, L. S. (2009). AHA/ACCF/HRS recommendations for the standardization and interpretation of the electrocardiogram. Part V: electrocardiogram changes associated with cardiac chamber hypertrophy a scientific statement from the American Heart Association electrocardiography and arrhythmias committee, council on clinical cardiology; the American College of Cardiology foundation; and the heart rhythm society. *J. Am. Coll. Cardiol.* 53, 992–1002. doi: 10.1016/j.jacc.2008.12.015

Haukilahti, M. A. E., Holmström, L., Vähätalo, J., Kenttä, T., Tikkanen, J., Pakanen, L., et al. (2019). Sudden cardiac death in women. *Circulation* 139, 1012–1021. doi: 10.1161/CIRCULATIONAHA.118.037702

Heistaro, S. (2020). *Methodology Report : Health 2000 Survey. Publications of the National Public Health Institute B26/2008*. Available online at: http://www.julkari.fi/handle/10024/78185 (accessed May 30, 2020)

Holkeri, A., Eranti, A., Haukilahti, M. A. E., Kerola, T., Kenttä, T. V., Tikkanen, J. T., et al. (2020). Impact of age and sex on the long-term prognosis associated with early repolarization in the general population. *Heart Rhythm* 17, 621–628. doi: 10.1016/j.hrthm.2019.10.026

Jørgensen, P. G., Jensen, J. S., Marott, J. L., Jensen, G. B., Appleyard, M., and Mogelvang, R. (2014). Electrocardiographic changes improve risk prediction in asymptomatic persons age 65 years or above without cardiovascular disease. *J. Am. Coll. Cardiol.* 64, 898–906. doi: 10.1016/j.jacc.2014.05.050

Jousilahti, P., Vartiainen, E., Tuomilehto, J., and Puska, P. (1999). Sex, age, cardiovascular risk factors, and coronary heart disease: a prospective follow-up study of 14 786 middle-aged men and women in Finland. *Circulation* 99, 1165–1172. doi: 10.1161/01.CIR.99.9.1165

Junttila, M. J., Tikkanen, J. T., Kenttä, T., Anttonen, O., Aro, A. L., Porthan, K., et al. (2014). Early repolarization as a predictor of arrhythmic and nonarrhythmic cardiac events in middle-aged subjects. *Heart Rhythm* 11, 1701–1706. doi: 10.1016/j.hrthm.2014.05.024

Kannel, W. B., Wilson, P. W., D'Agostino, R. B., and Cobb, J. (1998). Sudden coronary death in women. *Am. Heart J.* 136, 205–212. doi: 10.1053/hj.1998.v136.90226

Kashani, A., and Barold, S. S. (2005). Significance of QRS complex duration in patients with heart failure. *J. Am. Coll. Cardiol.* 46, 2183–2192. doi: 10.1016/j.jacc.2005.01.071

Knekt, P., Rissanen, H., Järvinen, R., and Heliövaara, M. (2017). Cohort profile: the finnish mobile clinic health surveys FMC, FMCF and MFS. *Int. J. Epidemiol.* 46, 1760i–1761i. doi: 10.1093/ije/dyx092

Laukkanen, J. A., Di Angelantonio, E., Khan, H., Kurl, S., Ronkainen, K., and Rautaharju, P. (2014). T-wave inversion, QRS duration, and QRS/T angle as electrocardiographic predictors of the risk for sudden cardiac death. *Am. J. Cardiol.* 113, 1178–1183. doi: 10.1016/j.amjcard.2013.12.026

Machado, D. B., Crow, R. S., Boland, L. L., Hannan, P. J., Taylor, H. A., and Folsom, A. R. (2006). Electrocardiographic findings and incident coronary heart disease among participants in the atherosclerosis risk in communities (ARIC) study. *Am. J. Cardiol.* 97, 1176–1181. doi: 10.1016/j.amjcard.2005.11.036

Maffei, S., Guiducci, L., Cugusi, L., Cadeddu, C., Deidda, M., Gallina, S., et al. (2019). Women-specific predictors of cardiovascular disease risk – new paradigms. *Int. J. Cardiol.* 286, 190–197. doi: 10.1016/j.ijcard.2019.02.005

Mosca, L., Benjamin, E. J., Berra, K., Bezanson, J. L., Dolor, R. J., Lloyd-Jones, D. M., et al. (2011). Effectiveness-based guidelines for the prevention of cardiovascular disease in women-2011 update: a guideline from the American Heart Association. *Circulation* 123, 1243–1262. doi: 10.1161/CIR.0b013e31820faaf8

Mosca, L., Grundy, S. M., Judelson, D., King, K., Limacher, M., Oparil, S., et al. (1999). Guide to preventive cardiology for women. *Circulation* 99, 2480–2484. doi: 10.1161/01.CIR.99.18.2480

Naghavi, M., Wang, H., Lozano, R., Davis, A., Liang, X., Zhou, M., et al. (2015). Global, regional, and national age-sex specific all-cause and cause-specific mortality for 240 causes of death, 1990-2013: a systematic analysis for the Global Burden of Disease study 2013. *Lancet* 385, 117–171. doi: 10.1016/S0140-6736(14)61682-2

O'Malley, P. G., and Redberg, R. F. (2012). Risk refinement, reclassification, and treatment thresholds in primary prevention of cardiovascular disease. *Arch. Intern. Med.* 170, 1602–1603. doi: 10.1001/archinternmed.2010.327

Prineas, R. J., Rautaharju, P. M., Grandits, G., and Crow, R. (2001). Independent risk for cardiovascular disease predicted by modified continuous score electrocardiographic criteria for 6-year incidence and regression of left ventricular hypertrophy among clinically disease free men: 16-Year follow-up for the multiple risk factor intervention trial. *J. Electrocardiol.* 34, 91–101. doi: 10.1054/jelc.2001.23360

Rapola, J. M., Virtamo, J., Korhonen, P., Haapakoski, J., Hartman, A. M., Edwards, B. K., et al. (1997). Validity of diagnoses of major coronary events in national registers of hospital diagnoses and deaths in Finland. *Eur. J. Epidemiol.* 13, 133–138. doi: 10.1023/A:1007380408729

Rautaharju, P. M., Surawicz, B., and Gettes, L. S. (2009). AHA/ACCF/HRS recommendations for the standardization and interpretation of the electrocardiogram. Part IV: the ST segment, T and U waves, and the QT interval a scientific statement from the American Heart Association electrocardiography and arrhythmias Co. *J. Am. Coll. Cardiol.* 53, 982–991. doi: 10.1016/j.jacc.2008.12.014

Reunanen, A., Aromaa, A., Pyörälä, K., Punsar, S., Maatela, J., and Knekt, P. (1983). The social insurance institution's coronary heart disease study. Baseline data and 5-year mortality experience. *Acta Med. Scand. Suppl.* 673, 1–120.

Savji, N., Rockman, C. B., Skolnick, A. H., Guo, Y., Adelman, M. A., Riles, T., et al. (2013). Association between advanced age and vascular disease in different arterial territories: a population database of over 3.6 million subjects. *J. Am. Coll. Cardiol.* 61, 1736–1743. doi: 10.1016/j.jacc.2013.01.054

Schinkel, A. F. L., Elhendy, A., van Domburg, R. T., Biagini, E., Rizzello, V., Veltman, C. E., et al. (2009). Prognostic significance of QRS duration in patients with suspected coronary artery disease referred for noninvasive evaluation of myocardial ischemia. *Am. J. Cardiol.* 104, 1490–1493. doi: 10.1016/j.amjcard.2009.07.012

Sciomer, S., Moscucci, F., Dessalvi, C. C., Deidda, M., and Mercuro, G. (2018). Gender differences in cardiology: is it time for new guidelines? *J. Cardiovasc. Med. (Hagerstown)* 19, 685–688. doi: 10.2459/JCM.0000000000000719

Terho, H. K., Tikkanen, J. T., Junttila, J. M., Anttonen, O., Kenttä, T. V., Aro, A. L., et al. (2014). Prevalence and prognostic significance of fragmented QRS complex in middle-aged subjects with and without clinical or electrocardiographic evidence of cardiac disease. *Am. J. Cardiol.* 114, 141–147. doi: 10.1016/j.amjcard.2014.03.066

Tikkanen, J. T., Anttonen, O., Junttila, M. J., Aro, A. L., Kerola, T., Rissanen, H. A., et al. (2009). Long-term outcome associated with early repolarization on electrocardiography. *N. Engl. J. Med.* 361, 2529–2537. doi: 10.1056/NEJMoa0907589

Conflict of Interest: The authors declare that the research was conducted in the absence of any commercial or financial relationships that could be construed as a potential conflict of interest.

Advantages of publishing in Frontiers

OPEN ACCESS
Articles are free to read for greatest visibility and readership

FAST PUBLICATION
Around 90 days from submission to decision

HIGH QUALITY PEER-REVIEW
Rigorous, collaborative, and constructive peer-review

TRANSPARENT PEER-REVIEW
Editors and reviewers acknowledged by name on published articles

Frontiers
Avenue du Tribunal-Fédéral 34
1005 Lausanne | Switzerland

Visit us: www.frontiersin.org
Contact us: frontiersin.org/about/contact

REPRODUCIBILITY OF RESEARCH
Support open data and methods to enhance research reproducibility

DIGITAL PUBLISHING
Articles designed for optimal readership across devices

FOLLOW US
@frontiersin

IMPACT METRICS
Advanced article metrics track visibility across digital media

EXTENSIVE PROMOTION
Marketing and promotion of impactful research

LOOP RESEARCH NETWORK
Our network increases your article's readership